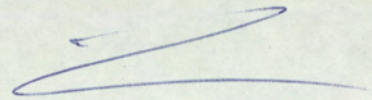


This thesis is dedicated to my parents,  
without whose love, help and sacrifice my  
objectives could never have been realised.

Malcolm Hawleyford

A large, stylized handwritten flourish or signature mark in blue ink, consisting of a long horizontal line with a curved underline and a small loop at the end.

APPLICATION OF DELTA-MODULATION TO TELEVISION SYSTEMS

THESIS  
621.397222 HAO  
-4.JUL72 152308

Malcolm John Hawksford

Thesis for the degree of Doctor of Philosophy

The University of Aston in Birmingham

April 1972

SUMMARY

Digital methods of pulse modulation are being widely applied in the transmission of information over communication networks. The thesis is primarily concerned with one specific class of pulse modulation called delta-modulation. In its basic form, delta-modulation represents the simplest and most economical method of digitally encoding analogue signals.

The thesis discusses delta-modulation from a theoretical and practical viewpoint. A mathematical model is presented which permits a comprehensive understanding of the processes of delta-modulation. The model can readily be extended to other forms of digital pulse modulation and is therefore presented as a general method of analysing digital-encoding systems. The theory develops the design requirements of a delta-modulator and indicates methods of improving the encoding performance.

The thesis describes a family of digital encoding systems for colour television. These systems are discussed in relation to chromaticity. Finally, a particular system is described, for which an experimental model was built and tested. This system transmitted the chrominance information during the line blanking period. The experimental model functioned satisfactorily in real time with encoding rates ranging from 50 MHz to 100 MHz. At these pulse rates, subjective assessment of the system was favourable.

Contents.

Title.

Summary.

**Contents.**

List of Symbols.

Chapter 1: Research Objectives.

Chapter 2: Pulse and Pulse Coding Techniques.

2.1..... Digital communication.

2.2..... Fundamentals of delta-modulation.

2.3..... Delta-sigma modulation.

2.4..... Hybrid delta / delta-sigma modulation and its application to pre-emphasis and de-emphasis networks.

2.5..... Pulse code modulation and its relation to delta-modulation.

2.6..... General methods of producing delta-modulator and delta-sigma modulator encoders.

2.7..... Analogue networks in the closed loop of delta-modulators and delta-sigma modulators.

2.8..... Non-recursive digital filter as passive, finite-memory, feedback network of a delta-modulator.

2.9..... Up / down counter and digital to analogue converter to synthesise ideal single-integrator response.

2.10... An approximate noise analysis for single-integration delta-modulation.

Chapter 3: Analogue Modelling of Digital Systems.

3.1... Introduction to concept of analogue modelling for delta-modulation.

- 3.2..... Definition of basic model with assumptions.
- 3.3..... Analytical verification of delta-modulator model, single carrier system.
- 3.4..... Analytical verification of delta-modulator model, double carrier.
- 3.5..... Extension of deltamodem model to RC integrator in the analogue feedback network.
- 3.6..... Extension of deltamodem model to second-order feedback network.
- 3.7..... Generalised model to include slope overload.
- 3.8..... Extension of model to P.C.M.
- Chapter 4: Analysis of Deltamodulator and F.C.M. systems using model equivalent.
- 4.1..... Direct analysis of delta-modulator and P.C.M. systems for sinusoidal inputs, with extension to general periodic functions.
- 4.2..... Direct analysis of delta-modulation system for ramp and sine wave input signals.
- 4.3..... Direct analysis of delta-modulation system for ramp input.
- 4.4..... High-band delta-modulation with low-frequency deviation, with application to spectral analysis of delta-modulation and P.C.M. systems.
- 4.5..... Analytical determination of a P.P.M. waveform from a phase-modulated carrier.
- 4.6..... Application of high-band delta-modulation and analytical determination of P.P.M. signal to general spectral analysis.

- 4.7.... Model with generalised feedback and observations of stability of delta-modulators.
- Chapter 5: Adaptive Delta-modulation with Pulse Grouping Techniques.
- 5.1.... Introduction to pulse grouping.
- 5.2.... Determination of threshold level of an  $N^{\text{th}}$  order pulse group, for delta-sigma modulation.
- 5.3.... Suppressed-carrier delta-modulation.
- 5.4.... Basic adaptive system for delta-modulation.
- 5.5.... Instantaneous non-linear delta-modulation.
- Chapter 6: Basic Fundamentals of Television Systems.
- 6.1.... Picture structure and bandwidth requirements.
- 6.2.... Spacial and temporal identity.
- 6.3.... The video signal.
- 6.4.... Gamma correction.
- Chapter 7: Fundamentals of Colour with Application to Television.
- 7.1.... Introduction.
- 7.2.... Trichromatic visual model.
- 7.3.... Colour-matching functions.
- 7.4.... Chromaticity triangle.
- 7.5.... Fundamentals of colorimetry applied to colour television.
- 7.6.... The principle of constant luminance.
- 7.7.... Colour difference signals.
- 7.8.... Systematic representation of chromaticity changes on the chromaticity diagram.
- Chapter 8: Colour Encoding Systems.
- 8.1.... Introduction.

- 8.2.... The P.A.L. encoded system.
- 8.3.... Classification of basic digital-encoding techniques primarily for encoding colour-signals using delta-sigma modulation.
- 8.4.... Multi-channel realisation through time-division multiplexing, (t.d.m.).
- 8.5.... Pulse-compression in digital encoder for colour television systems.
- 8.6.... High-frequency averaging of two or three simultaneous, multiplexed signals.
- 8.7.... Chrominance band-limiting of  $E_R$ ,  $E_G$ ,  $E_B$  signals.
- 8.8.... Baseband encoding of video signals for modulating three simultaneous delta-sigma modulators, each channel being full bandwidth and symmetrical. (System group A1).
- 8.9.... Three channel encoding systems using two symmetrical t.d.m. channels and one low-bandwidth auxilliary channel. (System group A2).
- 8.10... Two-channel encoding using two symmetrical t.d.m. signals and reduced vertical chrominance resolution. (System group B1).
- 8.11... Two channel system using a single wide-bandwidth channel with auxilliary low-bandwidth channel. (C.I.S.S.), (System group B2).
- Chapter 9: Instrumentation of Digital Encoding System for Colour Television Signals.
- 9.1.... Introduction to 'Chrominance in Synchs. System', (C.I.S.S.).

- 9.2.... The analogue encoder.
  - 9.3.... The digital control system.
  - 9.4.... Delta-sigma modulators and demodulators.
  - 9.5.... Analogue decoder system.
  - 9.6.... Chopped filtering of luminance  
and chrominance signals.
- Chapter 10: Computer Programming and Comparative  
Simulation.
- 10.1... Deltamodem model and delta-modulator  
comparative simulation.
  - 10.2... Delta-modulator simulation using a non-  
recursive filter to approximate the  
response of a RC integrator.
  - 10.3... Simulation of instantaneous , non-linear  
delta-modulator.
  - 10.4... Delta-modulator simulation to determine  
pulse group relationships to the slope  
of the modulating signal.
  - 10.5... Computer instantaneous adaptation results.
- Chapter 11: Experimental results.
- 11.1... Objective waveform tests and results.
  - 11.2... Objective picture tests and results.
  - 11.3... Subjective tests and results.
- Chapter 12: Conclusions.
- 12.1... Theoretical analysis of digital encoding.
  - 12.2... Design of delta-modulators.
  - 12.3... Adaptive delta-modulation.
  - 12.4... Computer simulation.

- 12.5... Digital and analogue signal encoding  
for colour television.
- 12.6... Experimentation and subjective assessment  
of C.I.S.S.
- 12.7... Assessment of research and future objectives.

Acknowledgements.

References.\*

Appendix 1: Analogue circuitry.

Appendix 2: Digital Circuitry.

Appendix 3: Chrominance and delay system.

Appendix 4: Active filter for Chrominance demodulation.

Supporting Paper: Exact model for delta-modulation  
processes.

\* Where a reference is applicable to a discussion,  
it is listed in brackets after the section sub-  
heading.

---

CAPTIONS

- Fig. 1-1. Basic areas and system sections described and analysed in thesis.
- Fig. 2-1. General delta-modulator system.
- Fig. 2-2. Pulse coding sequence of a perfect integrator store delta-modulator.
- Fig. 2-3. Integration networks.
- (a) RC active integrator with finite gain amplifier.
  - (b) Equivalent network of Fig. 2-3 (a).
  - (c) d.c. gain determined by negative feedback loop.
- Fig. 2-4. Calculation model of step height for RC integration network.
- Fig. 2-5. (a) Ideal second-order system with predictive loop.
- Fig. 2-5. (b) Passive approximation to second-order system.
- Fig. 2-6. Predictive process applied to local store output.
- Fig. 2-7. (a) Delta-sigma modulator formed by integrating input to delta-modulator.
- Fig. 2-7. (b) Delta-sigma modulator by transposition of the integrators of Fig. 2-7(a) to the forward path of the delta-modulator control loop.
- Fig. 2-8. Hybrid delta-modulator.
- Fig. 2-9. Hybrid delta-modulator with external pre-emphasis and de-emphasis networks.
- Fig. 2-10. Pulse-amplitude modulation.
- Fig. 2-11. Quantisation of P.A.M. signal and allocation of binary numbering to quantisation levels.
- Fig. 2-12. Extraction of quantised P.A.M. from quantised delta-modulated signal.

- Fig. 2-13. Non-optimum pulses in analogue network, closed-loop delta-modulator.
- (a) Damped rise and fall.
- (b) Underdamped rise and fall.
- Fig. 2-14. (a) Delta-modulator with lumped-loop delay.
- Fig. 2-14. (b) Effects of delay time on pulse generation.
- Fig. 2-15. Basic single-integration delta-sigma modulator.
- Fig. 2-16. Ideal basic integrator.
- Fig. 2-17. Three current source, push-pull integrator.
- Fig. 2-18. Non-recursive filter used in the feedback path of a delta-modulator to simulate analogue store.
- Fig. 2-19. Linear delay-line equivalent of digital non-recursive filter.
- Fig. 2-20. Relation of coefficients  $a_N$  to normalised impulse response of RC filter.
- Fig. 2-21. Digital store delta-modulator using up/down counter and digital-to-analogue converter.
- Fig. 2-22. Probability distribution and density function assumed for quantisation error signal.
- Fig. 2-23. Quantisation error function with linear interpolation between sample peaks.
- Fig. 2-24. Delta-error pulse to triangular-error pulse converter.
- Fig. 2-25. Four basic triangular waveforms.
- Fig. 2-26. Waveform assisting mean-power calculation.
- Fig. 2-27. One-sided distribution of  $\left(\frac{\sin x}{x}\right)^4$  against  $x$  up to first zero.
- Fig. 2-28. Assumed power distribution.
- Fig. 3-1. Generalised delta-modulation.
- Fig. 3-2. Generalised model for delta-modulation and delta-sigma modulation.

- Fig. 3-3. Deltamodem model waveforms.
- Fig. 3-4. Double-carrier model of delta-modulator.
- Fig. 3-5. Double-carrier model of delta-modulator.
- Fig. 3-6.  $(1/P)$  pulse duration (from delta pulse) generator.
- Fig. 3-7. Idling pattern for pulses of height  $V$  and duration  $(1/P)$  when integrated by a RC network.
- Fig. 3-8. (a) Equivalent active network of RC integrator.
- Fig. 3-8. (b) RC integration with equivalent network in the feedback path of a delta-modulator.
- Fig. 3-9. (a) Equivalent RC integrator delta-modulator using ideal phase-control model with external feedback path.
- Fig. 3-9. (b) Extension of model to delta-sigma modulation.
- Fig. 3-10. Alternative equivalent networks of a double-integration delta-modulator.
- (A) General form of delta-modulator with predictive loop.
- (B) Identical network to (A) but rearranged to expose ideal single-integrator delta-modulator.
- Fig. 3-11. Equivalent model for second-order delta-modulator.
- (A) Rearranged second-order delta-modulator.
- (B) Equivalent model network derived from (A).
- (C) Final rearranged equivalent model of second-order delta-modulator.
- Fig. 3-12. Derivation of decoder network for second-order model.
- (A) Decoding network derived from equivalent model system.
- (B) Rearrangement of (A) demonstrating that decoding network is equivalent to second-order system.
- Fig. 3-13. (A) Double-integration delta-modulator with prediction.
- (B) Model equivalent of (A).

- Fig. 3-14. Illustration of optimum and non-optimum integration.
- Fig. 3-15. Double carrier model simulating double-integration delta-modulator, without time quantisation of output pulses.
- Fig. 3-16. Slope-overload function required for deltamodem model.
- Fig. 3-17. Basic slope limiter required for deltamodem model.
- Fig. 3-18. Double carrier P.C.M. model.
- Fig. 4-1. Pulse grouping of periodic pulse sequence.
- Fig. 4-2. Standard pulse generator.
- Fig. 4-3. Location of  $t_R$  by binary slot division.
- Fig. 4-4. High-band to low-band conversion through sampling, for odd  $b$ .
- Fig. 4-5. High-band to low-band conversion through sampling, for even  $b$ .
- Fig. 4-6. Flow chart of model systems for generating the P.A.M. signals of delta-modulation and pulse code modulation.
- Fig. 4-7. Conversion of  $x(t)$  to P.P.M. waveform  $f_P(t)$ .
- (A) Mathematical functions and waveforms of conversion.
- (B) System diagram of conversion process.
- Fig. 4-8. Calculation procedure for high-band delta-modulator using high-band phase modulator and the pulse converter of Fig. 4-7.
- Fig. 4-9. Idling delta-modulator.
- Fig. 4-10. Idling pattern controlled by lumped-loop delay.
- Fig. 4-11. Half cycle production of idling pattern.
- Fig. 4-12. Time delay and phase delay at a frequency,  $f$ .
- Fig. 4-13. (1/P) duration hold network.

- Fig. 4-14. Three examples of phase delay for the fundamental frequency component of the  
 ....1010....  
 idling pattern.
- Fig. 4-15. Variation of  $\phi_T(f)$  against frequency,  $f$ .
- Fig. 4-16. Variation of  $\phi_1(f)$  against frequency,  $f$ .
- Fig. 4-17. Modified second-order system for investigating low-frequency stability.
- (A) Second-order phase-control model indicating probable signal delay.
- (B) Linear, low-frequency equivalent model with maximum signal delay of  $(1/P)$ .
- Fig. 5-1. Pulse-group frequency of occurrence functions for d.c. input signals applied to delta-sigma modulator.
- Fig. 5-2. Pulse group detection of order  $N$  with examples of detection of 1, 2, 3, 4, 5, order positive pulse groupings.
- Fig. 5-3. First-order pulse groupings with integration.
- Fig. 5-4. Change of phase of idling pattern with level of  $S_2(t)$ .
- Fig. 5-5. 'Full-wave' rectification using 1st order pulse groupings.
- Fig. 5-6. Adaptive control of delta-sigma modulator with external control network.
- (A) Encoder.
- (B) Decoder.
- Fig. 5-7. Variation of the modulus of  $A_M(f)$ , for constant values of  $\lambda$ , with signal frequency,  $f$ .
- Fig. 5-8. Instantaneous adaptive delta-sigma modulator, using single integration.
- Fig. 5-9. Process of second-order adaptive companding.

- Fig. 6-1. Simple linear scan line structure.
- Fig. 6-2. Two interlaced fields forming a single picture scan.
- Fig. 6-3. Synchronisation pulses and synchronisation parameters.
- Fig. 6-4. C.C.I.R., 625 line-standard, luminance signal.
- Fig. 7-1. (a) Indirect determination of probable sensitivity curves of a human eye.
- Fig. 7-1. (b) Curves of sensitivity determined from bleaching of pigments of the human retina.
- Fig. 7-2. Colour triangle for g, r, coordinates in r, g, b system.
- Fig. 7-3. Position of  $(C_1)$ ,  $(C_2)$ ,  $(C_M)$ , on chromaticity diagram.
- Fig. 7-4. (u), (v), (w), chromaticity coordinate system.
- Fig. 7-5. Colour triangle formed by stimuli  $(C_R)$ ,  $(C_G)$ ,  $(S_C)$ .
- Fig. 7-6. Chromaticity diagram showing location of (R), (G), (B),  $(C_R)$ ,  $(S_C)$ ,  $(C_B)$  and ratios  $\frac{E_R - E_L}{E_L}$ ,  $\frac{E_B - E_L}{E_L}$  on (u), (v), (w) diagram.
- Fig. 8-1. Vector presentation of chrominance with respect to phase and amplitude of the subcarrier of the quadrature modulation process.
- Fig. 8-2. (a) Symmetrical, three channel t.d.m. system.
- Fig. 8-2. (b) Symmetrical, two channel t.d.m. system.
- Fig. 8-3. Chrominance pulse compression system.
- Fig. 8-4. Luminance error coupling to enhance luminance encoding performance in exchange for chrominance encoding accuracy.
- Fig. 8-5. High-frequency addition network to limit chrominance resolution and make equal the high-frequency components of the video signals of  $E_R$ ,  $E_G$ ,  $E_B$ .
- Fig. 8-6. Chromaticity diagram for proposed three-channel system, using  $A_{3n}$ ,  $B_{3n}$ ,  $C_{3n}$ .
- Fig. 8-7. Sequential multiplexing for reducing 3 channels to 2 channels.

- Fig. 9-8. Chromaticity diagram for C.I.S.S., having channels  $A_{2n}$ ,  $B_{2an}$ ,  $C_{2an}$ , displayed on u, v, w chart.
- Fig. 9-1. Basic encoding, modulation and decoding systems used in C.I.S.S. simulation.
- Fig. 9-2. Differential summing amplifier.
- Fig. 9-3. The summing amplifier for generating  $A_{2n}$ .
- Fig. 9-4. Signal matrixing to form  $A_{2n}$ ,  $-A_{2n}$ ,  $B_{2an}$ ,  $-B_{2an}$ ,  $C_{2an}$ ,  $-C_{2an}$  from signals  $E_R$ ,  $E_G$ ,  $E_B$ .
- Fig. 9-5. Black level clamp network.
- Fig. 9-6. Multiplex switcher for chrominance and luminance channels.
- Fig. 9-7. Line-drive amplifier for luminance and chrominance channels, with pre-emphasis network.
- Fig. 9-7. (a) Pre-emphasis and de-emphasis characteristics for luminance and chrominance channels.
- Fig. 9-8. Complete analogue encoder (excluding digital control).
- Fig. 9-9. Digital control system.
- Fig. 9-10.(a) Encoder B.l.c. generation.
- Fig. 9-10.(b) Decoder B.l.c. generation.
- Fig. 9-11. Counter for multiplex control.
- Fig. 9-12. Production of  $C_{c1}$ ,  $C_{c2}$ ,  $C_{c3}$ ,  $C_{c4}$  from equations (9-18), (9-19), (9-20).
- Fig. 9-13. Switch and mode storage logic. (Applicable for luminance and chrominance channels).
- Fig. 9-14. Clock inversion, clock and synch. distribution.
- Fig. 9-15. Luminance multiplex logic and synch. pulses.
- Fig. 9-16. Indicator-lamp circuit showing logic inputs.
- Fig. 9-17. Pulse control system for decoder.
- Fig. 9-18. Motorola ÷ 5 logic for MECL 3 system.

- Fig. 9-19. (a) Chrominance delta-sigma modulator.
- Fig. 9-19. (b) Luminance delta-sigma modulator with 2nd order pulse grouping.
- Fig. 9-20. Luminance channel decoder.
- Fig. 9-21. Primary chrominance decoding.
- Fig. 9-22. Chrominance channel delay, sum and difference.
- Fig. 9-23. Final signal matrixing.
- Fig. 9-24. Luminance and chrominance chopped filters.
- Fig. 10-1. (a) Symmetrical idling pattern with p.s.z.c.'s correctly placed for symmetrical error.
- Fig. 10-1. (b) Carrier advanced by  $\pi/2$  due to input of just less than 0.5, assuming initial conditions as in Fig. 10-1 (a).
- Fig. 10-1. (c) Carrier retarded by  $\pi/2$  due to input of just greater than -0.5, assuming initial conditions as in Fig. 10-1(a).
- Fig. 10-2. Adaptive delta-modulator presented for computation.
- Fig. 10-3. Signal to quantisation noise ratios for a delta-modulator against frequency with  $D^*$  as parameter and clock pulse rate constant. The delta-modulator has second and third order adaptation. prf. = 50,  $H[0] = 0$ ,  $H[1] = 0.2$ .
- Fig. 10-4. Signal to quantisation noise ratios for a delta-modulator against frequency with  $D^*$  as parameter and clock rate constant. The delta-modulator has second and third-order adaptation. prf. = 50,  $H[2] = 0.4$ ,  $H[3] = 0.6$ .
- Fig. 10-5. Signal to quantisation noise ratios for a delta-modulator against frequency with  $D^*$  as parameter and clock rate constant. The delta-modulator has second- and third-order adaptation. prf. = 50,  $H[4] = 0.8$ ,  $H[5] = 1.0$ .

- Fig. 10-6. Signal to quantisation noise ratios for a delta-modulator against frequency with  $D^*$  as parameter and clock pulse rate constant. The delta-modulator has second and third-order adaptation. prf. = 100,  $H[0] = 0$ ,  $H[1] = 0.2$ .
- Fig. 10-7. Signal to quantisation noise ratios for a delta-modulator against frequency with  $D^*$  as parameter and clock pulse rate constant. The delta-modulator has second and third-order adaptation. prf. = 100,  $H[2] = 0.4$ ,  $H[3] = 0.6$ .
- Fig. 10-8. Signal to quantisation noise ratios for a delta-modulator against frequency with  $D^*$  as parameter and clock pulse rate constant. The delta-modulator has second and third-order adaptation. prf. = 100,  $H[4] = 0.8$ ,  $H[5] = 1.0$ .
- Fig. 10-9. Signal to quantisation noise ratios for a delta-modulator against frequency with  $D^*$  as parameter and clock pulse rate constant. The delta-modulator has second-order only adaptation. prf. = 100,  $H[0] = 0$ ,  $H[1] = 0.2$ .
- Fig. 10-10. Signal to quantisation noise ratios for a delta-modulator against frequency with  $D^*$  as parameter and clock pulse rate constant. The delta-modulator has second-order only adaptation. prf. = 100,  $H[2] = 0.4$ ,  $H[3] = 0.6$ .
- Fig. 10-11. Signal to quantisation noise ratios for a delta-modulator against frequency with  $D^*$  as parameter and clock pulse rate constant. The delta-modulator has second-order only adaptation. prf. = 100,  $H[4] = 0.8$ ,  $H[5] = 1.0$ .

\*  $D$ , normalised modulating signal, single sine wave.

- Fig. 10-12. Signal to quantisation noise ratios against modulating signal showing constant frequency contours. Clock frequencies of 50 and 100 units. No adaptation applied to single-integration delta-modulator.
- Fig. 10-13. Signal to quantisation noise ratios against modulation depth for single-integration delta-modulator with second-order only adaptation. (Clock pulse rate constant at 100 units.) Contours of constant frequency.
- Fig. 10-14. Signal to quantisation noise ratios against modulation depth for single integration delta-modulation with second and third-order adaptation. (Clock pulse rates 50 and 100 units.) Contours of constant frequency.
- Fig. 11-1 to Fig. 11-7. System test waveforms and performance record.  
(See page 426 for list of sub-captions).
- Fig. 11-8. (a) Ramp input to C.I.S.S., luminance drive only, delta-sigma modulations switched out.
- Fig. 11-8. (b) Ramp input to C.I.S.S., luminance drive only, delta-sigma modulators switched in (encoding rate (100MHz)).
- Fig. 11-9. (a) Through C.I.S.S., delta-sigma modulators switched out.
- Fig. 11-9. (b) Through C.I.S.S., delta-sigma modulators switched in, encoding rate 100 MHz.
- Fig. 11-9. (c) Through C.I.S.S., delta-sigma modulators switched in, encoding rate 50 MHz.
- Fig. 11-9. (d) Through C.I.S.S., delta-sigma modulators switched in, encoding rate 18→25 MHz.
- Fig. 11-10.(a) Through C.I.S.S., delta-sigma modulators switched out.

- Fig. 11-10.(b) Through C.I.S.S., delta-sigma modulators switched in,  
encoding rate 100 MHz.
- Fig. 11-10.(c) Through C.I.S.S., delta-sigma modulators switched in,  
encoding rate 50 MHz.
- Fig. 11-10.(d) Through C.I.S.S., delta-sigma modulators switched in,  
encoding rate 18→25 MHz.
- Fig. 11-11.(a) Through C.I.S.S., delta-sigma modulators switched out.
- Fig. 11-11.(b) Through C.I.S.S., delta-sigma modulators switched in,  
encoding rate 100 MHz.
- Fig. 11-11.(c) Through C.I.S.S., delta-sigma modulators switched in,  
encoding rate 50 MHz.
- Fig. 11-11.(d) Through C.I.S.S., delta-sigma modulators switched in,  
encoding rate 18→25 MHz.
- Fig. 11-12.(a) Through C.I.S.S., delta-sigma modulators switched out.
- Fig. 11-12.(b) Through C.I.S.S., delta-sigma modulators switched in,  
encoding rate 100 MHz.
- Fig. 11-12.(c) Through C.I.S.S., delta-sigma modulators switched in,  
encoding rate 50 MHz.
- Fig. 11-12.(d) Through C.I.S.S., delta-sigma modulators switched in,  
encoding rate 18→25 MHz.
- Fig. 11-13.(a) Through C.I.S.S., delta-sigma modulators switched out.
- Fig. 11-13.(b) Through C.I.S.S., delta-sigma modulators switched in,  
encoding rate 100 MHz.
- Fig. 11-13.(c) Through C.I.S.S., delta-sigma modulators switched in,  
encoding rate 50 MHz.
- Fig. 11-13.(d) Through C.I.S.S., delta-sigma modulators switched in,  
encoding rate 18→25 MHz.
- Fig. 11-14.(a) Through C.I.S.S., delta-sigma modulators switched in,  
encoding rate 50 MHz.

- Fig. 11-14.(b) Through C.I.S.S., delta-sigma modulators switched in, encoding rate 18→25 MHz.
- Fig. 11-15.(a) Through C.I.S.S., delta-sigma modulators switched in, encoding rate 50 MHz.
- Fig. 11-15.(b) Through C.I.S.S., delta-sigma modulators switched in, encoding rate 18→25 MHz.
- Fig. 11-16.(a) Through C.I.S.S., delta-sigma modulators switched in, encoding rate 50 MHz.
- Fig. 11-16 (b) Through C.I.S.S., delta-sigma modulators switched in, encoding rate 18→25 MHz.
- Fig. 11-17 (a) Through C.I.S.S., delta-sigma modulators switched in, encoding rate 50 MHz.
- Fig. 11-17.(b) Through C.I.S.S., delta-sigma modulators switched in, encoding rate 18→25 MHz.
- Fig. 11-18. Results of subjective tests, encoding rate 100 MHz.
- Fig. 11-19. Results of subjective tests, encoding rate of 50 MHz.

Captions for diagrams of appendices.

- Fig. A1-1. Basic encoder matrixing amplifier.
- Fig. A1-2. High-gain, high-frequency amplifier module with no d.c. shift control.
- Fig. A1-3. High-gain, high-frequency amplifier module with d.c. shift control.
- Fig. A1-4. High-gain, high-frequency line driver and delay-line driver amplifier, with d.c. shift.
- Fig. A1-5. Differential input/output amplifier for sum and difference channels.
- Fig. A1-6. Unity-gain amplifier for Butterworth filters.
- Fig. A2-1. Synchronisation pulse separator and clock source.
- Fig. A2-2. B.l.c. generator for encoder, including FET drive.

- Fig. A2-3. Initial set-up and clock detector.
- Fig. A2-4. FET gate drive stage.
- Fig. A3-1. Specification of DL-20 delay line.
- Fig. A3-2 (a) Crystal oscillator.
- Fig. A3-2. (b) Waveform squaring circuit.
- Fig. A3-3. Delay-line modulator.
- Fig. A3-4. (a) Demodulator switching generator.
- Fig. A3-4. (b) Balanced product de-modulator.
- Fig. A4-1. Sixth-order Butterworth filter.

- $A$ , gain of amplifier.  
 $a$ , function defined on page 24 .  
 $a_1$ , coefficient.  
 $A_2$ , video signal of two channel t.d.m. system.  
 $A_{2n}$ , normalised video signal of two channel t.d.m. system.  
 $(A_{2n})$ , trichromatic stimulus corresponding to  $A_{2n}$ .  
 $A_{2q}$ , luminance quantisation noise in C.I.S.S.  
 $A_3, A_3', A_{3H}, A_{3n}$ , video signals of three channel t.d.m. system.  
 $A_{32}, A_{32}', A_{32n}$ , video signals of three channel t.d.m. system using auxiliary channel.  
 $A_{3q}$ , quantisation noise contribution of  $A_{3r}$ .  
 $A_{3r}$ , received video signal of three channel t.d.m. system.  
 $A_{Da}(f)$ , transfer function of adaptive filter in decoder.  
 $A_{dc}$ , chrominance de-emphasis transfer function.  
 $A_d(f), A_D(f)$ , transfer function of double integrator network.  
 $A_{dl}$ , luminance de-emphasis transfer function.  
 $A(f), A(s)$ , linear transfer functions in feedback loop of delta-modulator.  
 $A_G(f)$ , transfer function in feedback path of generalised delta-modulator.  
 $A_I$ , transfer function of active integrator.  
 $A_{Ma}(f)$ , transfer function of adaptive filter in encoder.  
 $a_N$ ,  $N^{\text{th}}$  coefficient of non-recursive filter.  
 $A_r$ , aspect ratio of display.  
 $A_S(f)$ , transfer function of single integrator.  
 $A_x(f)$ , spectrum of phase modulated function  $x(f)$ .  
 $B$ , blue channel response proportional to  $\beta_0$ .  
 $(B)$ , blue stimulus in trichromatic system.  
 $b$ , function defined on page 24 .

- $b$ , positive integer.
- $b, b_1, b_2, b_m$ , blue chromaticity coordinates on (R), (G), (B) colour triangle.
- $b_1$ , coefficient.
- $B_2$ , video signal of two channel t.d.m. system.
- $B_{2an}$ , normalised chrominance signal of C.I.S.S.
- $(B_{2an})$ , trichromatic stimulus corresponding to  $B_{2an}$ .
- $B_{2n}$ , normalised video signal of two channel t.d.m. system.
- $B_{2q}$ , chrominance quantisation noise in C.I.S.S.
- $B_3, B_3', B_{3H}, B_{3R}$ , video signals of three channel t.d.m. system.
- $B_{32}, B_{32}', B_{32n}$ , video signals of three channel t.d.m. system using auxiliary channel.
- $B_{3q}$ , quantisation noise contribution of  $B_{3r}$ .
- $B_{3r}$ , received video signal of three channel t.d.m. system.
- $B_C$ , blue tristimulus value in (R),(G), (B) system.
- $B_{C1}$ , primary chrominance B.l.c. pulse.
- $B_{C2}$ , secondary chrominance B.l.c. pulse.
- $B_{e1}$ , B.l.c. pulse of encoder.
- $(B_L)$ , blue trichromatic stimulus, units are of luminance.
- $B_{\ell+}, B_{\ell-}$ , luminance decoder B.l.c. pulses.
- $\bar{B}_\lambda, \bar{B}_{\lambda N}$ , number of units of blue stimulus required in colour match to produce one unit of a colour of wavelength  $\lambda$  or  $\lambda N$ .
- $C$ , capacitance.
- $(C)$ , colour on colour triangle.
- $c$ , function defined on page 24 .
- $c$ , number of digits in binary word.
- $C_1, \dots, C_N$ , capacitor values.
- $(C_1), (C_2), (C_M)$ , resultant colours on colour triangle.
- $C_{2an}$ , normalised chrominance signal of C.I.S.S.
- $(C_{2an})$ , trichromatic stimulus corresponding to  $C_{2an}$ .

- $C_3, C_3', C_{3H}, C_{3R}$ , video signals of three channel t.d.m. system.
- $C_{3a}, C_{3an}$ , auxiliary chrominance signal of two channel t.d.m. system with auxiliary channel.
- $C_{3q}$ , quantisation noise contribution of  $C_{3r}$ ,
- $C_{3r}$ , received video signal of three channel t.d.m. system.
- $(C_B)$ , trichromatic stimulus corresponding to a signal  $D_B$ .
- $C_{C1}, C_{C2}, C_{C3}, C_{C4}$ , multiplex control pulses used in encoder.
- $C_{D1}, C_{D2}, C_{DD1}, C_{DD2}$ , multiplex control pulses used in decoder.
- $(C_{GB})$ , a colour that is a mixture of green and blue only.
- $(C_I)$ , trichromatic stimulus corresponding to the  $E_I$  signal of N.T.S.C.
- $(C_L)$ , colour on colour triangle measured in luminance units.
- $C_{\ell 1}, C_{\ell 2}$ , clock pulses.
- $(C_Q)$ , trichromatic stimulus corresponding to the  $E_Q$  signal of N.T.S.C.
- $(C_R)$ , trichromatic stimulus corresponding to a signal  $D_R$ .
- $(C_{RG})$ , a colour that is a mixture of red and green only.
- $C_t$ , clock detection signal.
- $c(t)$ , comparator output of delta-modulator.
- $D, D_2, D_{2,3}$  amplitude of modulating signal applied to digital modulator.
- $D_B, D_G, D_R$ , blue, green and red colour-difference signals.
- $D_C$ , slope of ramp input to delta-modulator.
- $D_d(t)$ , modulating signal applied to second-order delta-modulator.
- $\bar{D}_f$ , maximum amplitude of sine wave of frequency  $f$ , required to fully load a delta-modulator.
- $D(f)$ , Fourier Transform of  $D(t)$ .
- $D_L(S)$ , Laplace Transform of  $D_L(t)$ .

$D_L(t)$ ,	output of slope limiter.
$D_m(t)$ ,	demodulated output signal of second-order delta-modulator.
$D(S)$ ,	Laplace Transform of $D(t)$ .
$D(t)$ ,	modulating signal applied to single-integrator delta-modulator.
$e_1, e_2$ ,	see page 327 for definition.
$E_2$ ,	quantisation error signal at $(N + 2)$ sample, after a non-optimum error comparison at the $(N + 1)$ sample.
$E_B, E_G, E_R$ ,	blue, green and red electrical signals proportional to $B_C, G_C, R_C$ .
$E_{Bd}, E_{Gd}, E_{Rd}$ ,	blue, green and red signals at output of decoder.
$E_I, E_Q$ ,	colour-difference signals of N.T.S.C. system.
$E_{i1}, E_{i2}$ ,	see page 327 for definition.
$E_L$ ,	luminance signal.
$E'_L$ ,	gamma corrected luminance signal.
$E_{LH}, E_{BH}, E_{GH}, E_{RH}$ ,	) see page 282 for definition.
$E_{LL}, E_{BL}, E_{GL}, E_{RL}$ ,	
$E_{NC}, E_{(N+1)C}$ ,	composite P.A.L. signal on lines $N, (N + 1)$ .
$E_{O1}, E_{O2}$ ,	see page 327 for definition.
$E_u, E_v$ ,	weighted chrominance signals of P.A.L. system, related to $D_B, D_R$ and used to modulate the subcarrier.
$E_\lambda$ ,	luminance or energy distribution of wavelengths of light defining a colour (C).
$f, f_o$ ,	frequency.
$f_o$ ,	fundamental frequency component of phase-modulated pulse waveform.
$F_B(f)$ ,	Basic pulse spectrum of the delta pulse sequence of duration $2 K_o/P$ .
$F_{C1}, F_{C2}$ ,	chrominance mode of operation store, output signals.
$f(f)$ ,	Fourier Transform of $f(t)$ .

$f_{hs}$ ,	horizontal spatial bandwidth.
$f_K$ ,	assumed upper-frequency limit of the power spectrum $P_T(f_0)$ .
$f_L$ ,	line repetition frequency.
$F_{L1}, F_{L2}$ ,	luminance mode of operation store, output signals.
$f_m$ ,	frequency of modulating signal.
$f_N$ ,	frequency of occurrence of $N^{\text{th}}$ order pulse group.
$f_P(f)$ ,	Fourier Transform of $f_P(t)$ .
$F_{P2}(f)$ ,	spectrum of $P_2(t)$ , when in delta-pulse format.
$f_P(t)$ ,	P.P.M. waveform derived from $f(t)$ .
$F_R(f)$ ,	spectrum generated by all $R^{\text{th}}$ pulses.
$f_S$ ,	sampling rate of the P.A.M. system.
$f_{S1}$ ,	spatial bandwidth.
$f_{SC}$ ,	subcarrier frequency.
$f_S(t)$ ,	delta-pulse sifting function.
$F_S(f)$ ,	spectrum of standard-pulse waveform.
$f(t)$ ,	phase-modulated square wave.
$F_T(f)$ ,	total spectrum obtained by superposition of all $F_R(f)$ spectra.
$f_u$ ,	bandwidth of base-band signal.
$f_v$ ,	bandwidth of scanning signal.
$f_{vS}$ ,	vertical spatial frequency.
$f_x$ ,	bandwidth of pulse function $P_x(t)$ .
$G$ ,	green channel response proportional to $\gamma$ .
$G$ ,	constant, attenuation factor.
$(G)$ ,	green stimulus in trichromatic system.
$g, g_1, g_2, g_m$ ,	green chromaticity coordinates on (R),(G),(B) colour triangle.

$G_C$ ,	green tristimulus value in (R), (G), (B) system.
$G_H$ ,	value of G calculated with hold network.
$(G_L)$ ,	green trichromatic stimulus, units are of luminance.
$G_{+(N)}$ ,	$N^{\text{th}}$ order, positive pulse group.
$G_{-(N)}$ ,	$N^{\text{th}}$ order, negative pulse group.
$G_T$ ,	value of G calculated without hold network.
$\bar{g}_\lambda, \bar{g}_{\lambda N}$ ,	number of units of green stimulus required in colour match to produce one unit of a colour of wavelength $\lambda$ or $\lambda N$ .
$h$ ,	quantisation step height of delta-modulator store output,
$H'$ ,	comparator reference level, (high).
$h_1, h_2$ ,	consecutive values of $q(t)$ at sampling instants $\frac{N}{P}$ , $\frac{(N+1)}{P}$ .
$h(f)$ ,	transfer function of store in feedback path of delta-modulator.
$h_1(f), h_2(f)$ ,	transfer functions of hybrid delta-modulator.
$h \{ \dots \}$ ,	operating function of store in feedback of delta-modulator.
$h_p(f)$ ,	pre-emphasis transfer function in hybrid delta-modulator.
$I$ ,	current.
$i$ ,	time varying current.
$i_c$ ,	current proportional to quantisation error in a delta-sigma modulator.
$I_{C+}, I_{C-}$ ,	possible values of $i_c$ when $M(t) = 0$ , depending whether $P(t) = 1$ or $0$ .
$I_K, I_S$ ,	constant-current sources.
$I_m$ ,	constant of proportionality, which forms the modulating current in the current-steered integrator, when $M(t) = 0$ .
$I_P$ ,	two state current, whose value depends upon $P(t)$ .

$\bar{I}_P$ ,	maximum value of $I_P$ .
$j$	$(-1)^{1/2}$ .
$K$ ,	constant of proportionality.
$k, k_n$ ,	multiplying factors.
$K_0$ ,	number of pulses forming fundamental sequence in phase-modulation process, when excited by a single-sine wave.
$K_1$ ,	(assumed) slope of power spectrum.
$k_1, k_2$ ,	constants in C.I.S.S. chrominance signals.
$K_C$ ,	clock inverter switch.
$k_m$ ,	amplitude weighting of $M^{\text{th}}$ pulse.
$L$ ,	integer,
$l$ ,	red channel luminosity coefficient.
$L'$ ,	comparator reference level, (low).
$L_1, L_2, L_C, L_M$ ,	luminance values.
$L_B, L_G, L_R$ ,	photometric luminances of $(B_L), (G_L), (R_L)$ .
$L_{C1}, L_{C2}$ ,	luminance multiplex control pulses, encoder.
$L_D, L_{DD}$ ,	luminance multiplex control pulses, decoder.
$L_h$ ,	picture width.
$L_v$ ,	picture height.
$L \{ \dots \}$ ,	operating function of comparator and one-bit store in the forward path of a delta-modulator.
$M, M_1$ ,	integers.
$m$ ,	green channel luminosity coefficient.
$M_1, M_2$ ,	mixture proportions of colour.
$\bar{M}_1$ ,	Laplace Transform of output of differentiator in slope limiter, Fig. 3-17.
$\bar{M}_2$ ,	Laplace Transform of amplified error signal in slope limiter, Fig. 3-17.

$M(f)$ ,	Fourier Transform of $M(t)$ .	(28)
$M_L$ ,	lamp indicator logic input.	
$M_N$ ,	number of integer phase rotations of $x_N(t)$ .	
$m(N)$ ,	threshold level of $N^{\text{th}}$ order pulse group, (referred to delta-sigma modulator's input signal).	
$M_P$ ,	number of integer-phase rotations of $x_P(t)$ .	
$M_S$ ,	number of stages in shift register of non- recursive filter.	
$M(t)$ ,	modulating signal applied to delta-sigma modulator.	
$N, \bar{N}$ ,	integers.	
$n$ ,	blue channel, luminosity coefficient.	
$N_1$ ,	number of lines in a picture.	
$N_a$ ,	integer factor by which chrominance digit rate is reduced compared with luminance channel digit rate.	
$N_c$ ,	logic function.	
$N_L$ ,	lamp logic input.	
$N_{N1}$ ,	number of negative pulses in delta-modulator process from zero time to $N^{\text{th}}$ sample.	
$N_{N2}$ ,	number of negative pulses in deltamodem model process from zero time to $N^{\text{th}}$ sample.	
$N_P$ ,	total quantisation power in frequency range $-f_u$ to $+f_u$ .	
$N_{P1}$ ,	number of positive pulses in delta-modulator process from zero time to $N^{\text{th}}$ sample.	
$N_{P2}$ ,	number of positive pulses in deltamodem model process from zero time to $N^{\text{th}}$ sample.	
$P$ ,	pulse repetition rate.	
$P_D(q)$ ,	probability distribution function of quanti- sation error.	

$P(f)$ ,	Fourier Transform of $P(t)$ .
$P_1(f)$ ,	Fourier Transform of $P_1(t)$ .
$P_{\text{PCM}}(t)$ ,	pulse waveform of P.C.M. system.
$P_r$ ,	picture repetition rate.
$P_T(f_o)$ ,	power spectrum of quantisation noise in single-integrator delta-modulator.
$P(t)$ ,	time domain pulse function.
$P_1(t)$ ,	output pulse waveform of delta-modulator.
$P_1'(t), P_2'(t)$ ,	pulses at remote receiver corresponding to $P_1(t), P_2(t)$ and including error pulses.
$P_2(t)$ ,	pulse-output waveform of deltamodem model.
$P_x(t)$ ,	band-limited pulse function in the time domain.
$Q$ ,	integer.
$Q_1, \dots, Q_N$ ,	output of up/down counter of digital store delta-modulator.
$q(f)$ ,	Fourier Transform of $q(t)$ ,
$q_p(t)$ ,	quantisation error signal of P.C.M. system.
$q_s(f)$ ,	Fourier Transform of $q_s(t)$ .
$q_s(t)$ ,	quantisation error-signal of delta-sigma modulator.
$q(t)$ ,	quantisation error signal of delta-modulator.
$R$ ,	resistance, (where appropriate).
$R$ ,	red channel response proportional to $\rho_o$ .
$R, R'$ ,	integers.
$(R)$ ,	red stimulus in trichromatic system.
$R_1, \dots, R_N$ ,	resistor values.
$r, r_1, r_2, r_m$ ,	red chromaticity coordinates on $(R), (G), (B)$ colour triangle.
$R_a$ ,	number of pulses in active line period to be compressed into line blanking period.

$R_c$ ,	red tristimulus value in (R), (G), (B) system.
$R_c$ ,	P.C.M. signal range using a c-digit word with uniform quantisation level spacing.
$(RC), (R_1, C_1)$ ,	time constants.
$(RC)_F$ ,	time constant of integrator for finite-pulse integrator.
$(RC)_S$ ,	time constant of integrator for delta-pulse integrator.
$R_{C1}, R_{C2}$ ,	'reset' inputs to chrominance mode store.
$(R_L)$ ,	red trichromatic stimulus, units are of luminance.
$r_\lambda, r_{\lambda N}$ ,	units of red stimulus required in colour match to produce one unit of a colour of wavelength $\lambda$ or $\lambda N$ .
$s$ ,	slope of straight line of chromaticity diagram.
$s$ ,	complex number in Laplace Transform.
$S_1(f)$ ,	Fourier Transform of $S_1(t)$ .
$S_1(t)$ ,	local stored output signal of delta-modulator.
$S_1'(t)$ ,	remotely generated signal corresponding to the local signal $S_1(t)$ .
$S_2(t)$ ,	integrated waveform of $P_2(t)$ .
$S_{22}(t)$ ,	output of second-order network.
$(S_C), (S_{CL})$ ,	equal energy reference white stimulus, (suffix L indicates luminance units).
$S_{C1}, S_{C2}$ ,	'set' input to chrominance mode.
$s_f$ ,	scaling factor.
$S_{F1}, S_{F2}, S_{F3}, S_{F4}$ ,	mode selector switches.
$S_H(t)$ ,	integrated pulse waveform of high-band delta-modulator.
$S_p$ ,	signal power of sinusoidal modulation signal.

$S_{PCM}(f)$ ,	Fourier Transform of $S_{PCM}(t)$ .
$S_{PCM}(t)$ ,	quantised P.A.M. signal of P.C.M. system.
$S_{RC}(t)$ ,	impulse response of RC integrator.
$S_{RC}(t, M_S)$ ,	truncated impulse response of RC integrator, synthesised by a digital, non-recursive filter.
$s_y$ ,	multiplex-clock synchronisation pulse.
$t$ ,	time.
$T_1, T_2$ ,	time constants in double-integrator loop.
$T_c$ ,	tristimulus values required to equal reference white, ( $S_c$ ).
$T_{cd}$ ,	time constant of chrominance de-emphasis network.
$T_D$ ,	excess loop delay time.
$T_e(f)$ ,	transfer function of triangular waveform converter.
$T(f)$ ,	time delay as a function of frequency.
$T_H(f)$ ,	zero-order hold transfer function.
$t_K$ ,	time of $K^{\text{th}}$ pulse.
$T_L(f)$ ,	transfer function of line drivers, (pre-emphasis function).
$T_{Ld}$ ,	time constant of luminance de-emphasis network.
$t_M$ ,	time of $M^{\text{th}}$ pulse.
$t_N$ ,	time of $N^{\text{th}}$ pulse.
$T_{P100}(f)$ ,	transfer function of 100% clock pulse duration, hold network.
$t_R$ ,	time of $R^{\text{th}}$ pulse.
$u$ ,	chromaticity coordinate in (U), (V), (W) system.
(U),	trichromatic stimulus of uniform chrominance, colour triangle.
$V$ ,	amplitude of pulse.
(V),	trichromatic stimulus of uniform chrominance, colour triangle.

$v$ ,	chromaticity coordinate of (U), (V), (W) system.
$V_c$ ,	initial voltage on capacitor used in RC integrator.
$v_c$ ,	capacitor voltage formed by integrating $i_c$ .
$V_{in}$ ,	input to RC integrator.
$V_o$ ,	integrated output of RC integrator.
(W),	reference white on (R), (G), (B) colour triangle.
(W),	trichromatic stimulus of uniform-chromaticity colour triangle.
$w$ ,	chromaticity coordinate of (U), (V), (W) system.
$X$ ,	amplitude of $x(t)$ .
$x$ ,	instantaneous angle, radians.
$x$ ,	line-blanking duration.
$X_C$ ,	output of counter in chrominance logic.
$X_D$ ,	data input of counter in chrominance logic.
$x(t)$ ,	phase-modulated cosine wave.
$x_N(t)$ ,	phase-modulated carrier in double-carrier model, setting position of negative pulses.
$x_P(t)$ ,	phase-modulated carrier in double-carrier model, setting position of positive pulses.
$y$ ,	line duration.
$y_1$ ,	general parameter in exponential process.
$Y_C$ ,	output of counter in chrominance logic.
$Y_D$ ,	data input of counter in chrominance logic.
$Z$ ,	positive integer such that the solution for $K_o$ is the lowest positive integer.
$Z_1$ ,	impedance.
$\beta$ ,	blue sensitivity curve of eye.
$\beta_o$ ,	particular blue response generated by an object.
$\beta_G$ ,	blue response generated by green stimulus.

$\gamma,$	gamma coefficient.
$\gamma,$	green sensitivity curve of eye.
$\gamma_o,$	particular green response generated by an object.
$\gamma_B,$	green response generated by blue stimulus.
$\gamma_R,$	green response generated by red stimulus.
$\Delta l,$	spacing of black and white dots on picture.
$\Delta l_m,$	minimum dot spacing that system can reproduce, (picture element spacing).
$\Delta E_{LN}, \Delta E_{BN}, \Delta E_{GN}, \Delta E_{KN},$	instantaneous transmission impairments.
$\delta t,$	small positive time increment.
$\Delta V_C,$	change of capacitor voltage measured across capacitor of an RC integrator.
$\delta(t - \frac{M}{P}),$	dirac delta pulse generated at time $t = \frac{M}{P}.$
$\delta w,$	weighting of delta-pulse.
$\epsilon(N),$	a number related to an $N^{\text{th}}$ order pulse group allowing the representation of fractional cycles of f.m. carrier.
$\epsilon_p,$	excess pulses available in line-blanking period.
$\theta,$	angle, radians.
$\lambda,$	constant for normalisation of chrominance signals in C.I.S.S.
$\lambda, \lambda_N,$	wavelength of light.
$\lambda,$	control signal in adaptive loop.
$\rho,$	red sensitivity curve of eye.
$\rho_o,$	particular red response generated by an object.
$\rho_B,$	red response generated by blue stimulus.
$\rho_D(q),$	probability density function of quantisation error.
$\rho_G,$	red response generated by green stimulus.

$\sigma$ ,	constant of proportionality.
$\phi$ ,	excess phase of phase-modulator in delta-modem model process.
$\phi(t)$ ,	phase function related to $P(t)$ .
$\phi(f)$ ,	phase function of triangular function in generalised delta-modulator.
$\phi_D(f)$ ,	phase function of double-integrator network.
$\phi_H(f)$ ,	phase function of hold network.
$\phi_N$ ,	excess phase of $x_N(t)$ .
$\phi_P$ ,	excess phase of $x_P(t)$ .
$\phi_T(f)$ ,	total phase function, including store transfer function and zero-hold transfer function.
$\omega_m$ ,	angular frequency of modulating signal.

LIST OF COMPUTER PROGRAMME SYMBOLSSection 10-1

	$D_s(t)$ , shifted input signal.
Real variables:	AI, modulating signal.
	K, ratio of modulating signal frequency to clock frequency.
	K1, parameter relating modulation depth to modulating signal frequency.
	L, incremental-step parameter.
	M, phase-modulated carrier.
	M1, temporary store for preceding value of M.
	N, time-increment parameter.
	S, modulation depth.
	WM, modulating signal frequency.
	WM1, redundant parameter.
	X, temporary error signal.
Integer variables:	PO, p.s.z.c. local store.
	PRF, clock frequency.
	R, incremental-step parameter.
Arrays:	A[1:1000], modulating signal store.
	C[1:1000], error-signal store for deltamodem model.
	C1[1:1000], error-signal store for delta-modulator.
	D[1:1000], demodulated-signal store for deltamodem model.
	D1[1:1000], demodulated-signal store for delta-modulator.
	P[1:1000], output-pulse sequence of deltamodem model.
	P1[1:1000], output-pulse sequence of delta-modulator.

Section 10-2

Realvariables: AI, modulating signal.  
E, error signal.  
F, demodulated output signal.  
K, ratio of modulating signal frequency to  
clock frequency.  
K1, 0.9 K.  
S, redundant variable.  
WM, modulating signal frequency.

Integer  
variables: L, incremental-step parameter.  
PRF, clock frequency.  
R, incremental-step parameter.

Arrays: C[0:250], digital-filter coefficients.  
P[0:1000], output-pulse sequence store.

Section 10-3

Real variables: D, modulating signal.

DD, sum of the squares of D.

F, modulating signal frequency.

P, clock frequency.

S, modulation-depth parameter.

W1, angular frequency of modulating signal  
divided by clock frequency.

W2,  $10/(\text{LN}(10))$ .

W3, temporary loop store for s.

Integer  
variables: G, incremental-step parameter.

M, incremental-step parameter.

R, incremental-step parameter.

Arrays: DC[0:10], sum of the squares of the error signal.

H[0:10], parameter controlling adaptation.

I1[0:10], demodulated signal.

I<sub>2</sub>, I<sub>21</sub>[0:10] sum of pulse-group output signals (allowing  
introduction of second-order integration).

SN[0:10], signal to quantisation-noise ratio.

PO, P1, P2, P3, P4,  
P5, [0:10], shift-register store of output pulse sequence  
for pulse grouping.

PL1, PL2, PL3, PL4,  
PL5, [0:10], pulse grouping store for 1st, 2nd, 3rd, 4th  
and 5th order pulse groups.

PLX[0:10], sum of pulse-group output signals.

Section 10-4

Real variables: D, modulating signal.

E1, E2, E3, E4, sum of the squares of the error signals of 1st, 2nd, 3rd, 4th order pulse groups.

K1, K2, K3, K4, frequency of occurrence of 1st, 2nd, 3rd and 4th order pulse groups over range of samples.

M, slope of modulating signal (ramp).

Integer variables: A, number of samples in average.

C, parameter controlling magnitude of A.

L, 100 M.

P0, P1, P2, P3,

P4, consecutive pulses stored for pulse group detection.

R, incremental-step parameter.

S, sum of zero-order pulse groups (+1 for positive pulse group, -1 for negative pulse group).

X1, X2, X3, X4, as S, but applied to 1st, 2nd, 3rd and 4th order pulse groups.

## Arrays:

Y1, Y2, Y3,

Y4[1:100], true modulating signal levels for calculating error signals of decoded 1st, 2nd, 3rd and 4th order pulse group detectors.

Present day technology has produced complex devices<sup>1</sup> capable of response times of less than one nanosecond (certain devices respond even faster). It is therefore possible to extend already known techniques and also apply new theories to signals of much higher frequencies. An example is the digital encoding of colour television signals. The thesis is concerned with a specific class of digital encoding called delta-modulation and applies this basic system to television processing. The thesis structure is shown in Fig. 1-1.

A full description of delta-modulation is given in Chapter 2. Delta modulation, in its basic form, represents the simplest type of analogue to digital encoder. Delta-modulation first appeared under a French patent in 1946<sup>2</sup> and later in 1948<sup>3</sup>. The first paper discussing the principles of delta-modulation appeared in September 1951<sup>4</sup> written in Dutch and March 1952<sup>4</sup> in English. A later paper in November 1952<sup>5</sup> by De Jager gave the first fully technical discussion of delta-modulation. This paper discussed both single and double-integration modulators and gave an elementary discussion of predictive stabilisation. Approximate expressions were also developed for both single and double-integration modulators.

Although the delta-modulator is the simplest of digital encoders, it is extremely complex to analyse mathematically. Various sophisticated attempts<sup>6,7,8,9</sup> have been made to analyse the process, but these are generally statistical analyses. The papers describe the two basic forms of noise, slope-overload noise and granular noise.

In television systems, however, slope overload can be minimised since the exact signal excursion is defined. Methods of analysing delta-modulation using frequency analysis<sup>10</sup> have been attempted but lead to extremely complex expressions.

A paper by J.B. O'Neal<sup>11</sup> determines an absolute bound for the signal to quantisation noise ratios for digital encoding systems. However, in this paper the expression for signal to quantisation noise for delta-modulation is empirical; thus it may be somewhat suspect. The results, however, suggest that for a bandwidth-to-pulse-rate ratio of less than  $\approx 14.5$  then delta-modulation is superior to P.C.M. Further comparisons between P.C.M. and delta-modulation are given by Zetterberg<sup>12</sup>. The bound to the signal to quantisation noise determined by O'Neal<sup>11</sup> does not depend on any of the redundancies found in television systems. Thus using the properties of inter-line and inter-field correlation could yield superior results.

A recent paper by Iwersen<sup>13</sup> with later experimental investigation by Laane<sup>14</sup> gave a detailed analysis for the power spectrum of a single-integration delta-modulator. A novel feature of these two papers is the realisation that the integrator step heights are asymmetrical (rising step height not equal to falling step height). The authors show that this asymmetry is equivalent to a ramp or staircase input being superimposed on the modulating signal. The papers analyse and demonstrate the power spectrum for idle-channel noise, sine-wave modulation and broad-bandwidth input with this assumed asymmetry. Theory and practice show that for encoding low-level signals this asymmetry in integrator step height is advantageous. Advantage of this asymmetry was taken in developing a practical encoder<sup>15</sup>. These papers also observe that with sinusoidal modulation, phase-modulation components are generated. This fact is in

agreement with the author's own theory presented in Chapter 3. The effects of asymmetric step height (i.e. equivalent ramp input) are discussed in Chapter 4. The papers indicate that when simple modulating signals are applied to a delta-modulator, the power spectrum is not equivalent to a broad-band spectrum, thus certain simple theories will be grossly in error.

Although the signal to quantisation noise ratios are of importance when considering digital encoding systems, the results can be extremely misleading<sup>11,19</sup>. With basic delta-modulation, which generally represents a redundant form of encoding but with good noise immunity, the quantisation noise generated has correlation with the modulating signal. Thus the subjective effect of a particular distribution may not be as objectionable as an equivalent amount of gaussian noise<sup>11</sup>. One of the objectives of the thesis has been not to be influenced too deeply by analyses of delta-modulation presented to date. The aim has been to investigate the properties of delta-modulation in terms of encoding television signals and to consider a variety of methods for encoding colour information. It is appreciated that the main advantage of the delta-modulator as an analogue to digital encoder is its simplicity. The network requires only a few components and could readily be adapted to integrated-circuit techniques<sup>15, 16</sup>.

In the thesis, considerable detail is given to the requirements of the encoder and various arrangements of encoder are described. The emphasis at all times is on application to the encoding of wide-bandwidth signals. On the theoretical side delta-modulation is analysed in terms of the spectra of the output pulse waveform. This task has been somewhat simplified by the development of an equivalent model to delta-modulation. The equivalent model also

gives much useful information on the stability of the modulator. A description will not be given at this stage as each section of Fig. 1-1 is dealt with in detail. Further detail can be found about delta-modulation in standard text books<sup>18,19</sup>.

A further application of single-integration delta-modulation is in encoding of P.C.M.<sup>20,21,22</sup>. Thus, although delta-modulation in its basic form may not be adequate in terms of efficiency, it does produce a useful means of generating P.C.M. In Chapter 4 the quantisation-noise analysis of delta-modulation is extended to P.C.M. The theory described and developed is therefore adequate for analysing a range of digital encoding systems. Various modifications<sup>20,21</sup> of the delta-modulator encoder are described for multiplexing several signals into a common pulse waveform. It is the author's opinion, however, that such strategy would tend to inferior encoding, since the basic delta-modulator would be required to operate at the full channel bit rate. Further, the addition of analogue multiplexing as well as multiplexing of the memories required for each channel would save little compared with independent encoders and one digital multiplexing switch.

A major modification of delta-modulation is delta-sigma modulation<sup>23, 24</sup>. A full discussion of this system is given in Chapter 2. The advantage of delta-sigma modulation for the transmission of video signals<sup>24</sup> has been realised and experiments were carried out using a tunnel diode in both a delta-modulator<sup>25</sup> and a delta-sigma modulator<sup>24</sup>. Operating frequencies of up to 100 MHz were obtained with the delta-modulator, where the signal to quantisation noise was stated to be 42 db. A circuit<sup>25</sup> using experimental U.H.F. transistors was stated to achieve 39 db, using a 40 MHz bit rate.

This figure was obtained from the maximum possible signal amplitude that would just overload the modulator compared to the quantisation-noise power generated by a 50 Hz modulating signal. For this low-frequency signal the quantisation-noise power was stated to be independent of the signal amplitude. The main disadvantage of the tunnel-diode circuit is the low-voltage pulse output obtained (0.2 volts).

A second major modification of delta-modulation and delta-sigma modulation is to have an adaptive step height. Adaptive systems have been developed in two basic categories, instantaneous adaptation and syllabic adaptation<sup>28,29,30,31</sup>. Many of the syllabic type of encoder described are only suitable for low-quality speech applications. In these systems, the integrator (or pulse) step height changes according to the envelope or syllabic characteristics of speech; thus these systems are totally unsuitable for television applications. Very little use, if any, has been made of noise masking effects. Noise masking is based on the premise that if a signal of sufficient amplitude exists in a particular band, then that signal will mask the noise components in that bandwidth. However, noise outside the band will not necessarily be masked.

Audio-frequency noise reduction systems based on noise masking have been extensively developed by Dolby Laboratories Inc.<sup>26,27</sup>. Although little technical information has been produced to date on the system developed by this company, noise reduction over the audio spectrum of between ten and fifteen decibels can be achieved. Such systems used with any channel introducing noise would produce a considerable improvement. The author feels that the theory of noise masking applies also to our visual senses and that similar noise reduction techniques can be applied to video. A simple system

outline is given in Chapter 5.

With delta-modulation, the signal-to-quantisation noise ratio improves with decreasing signal frequency, assuming ideal integration. Thus, assuming the pulse rate for encoding is sufficiently high, then it is only necessary to mask the high-frequency quantisation-noise components of the base-band signal. This leads to the concept of adaptive pre-emphasis networks and complementary de-emphasis networks. The main disadvantage of most syllabic and instantaneous delta-modulation is the introduction of further instrumentation in the feedback loop, thus limiting the performance when considering pulse rates sufficiently high for encoding video signals. Chapter 5 discusses a modified approach to both instantaneous and non-instantaneous adaptive modulation, suitable for high pulse rates.

Two papers by Winkler<sup>32,33</sup>, describe an original form of adaptation. The integrated output waveform rises exponentially rather than linearly, with a corresponding improvement in step-response performance. The method has been used for facsimile transmissions where three pulses per picture element were used. Results are claimed to be comparable to six or seven bit P.C.M. The system is necessarily less tolerant of transmission errors than delta-modulation. A simpler adaptive system<sup>34</sup>, using exponential adaptation but with only a one-bit memory is described by Jayant. This system realises a limited improvement in performance; however, the adaptive system is stated to be suitable for video-frequency transmission.

Many different methods are available for improving the coding performance of delta-modulators. However, when considering television systems not using specialised bandwidth reduction techniques, many of the systems are complex to design due to the high frequencies

involved. Thus, only simple modifications which do not detract from the basic simplicity of the delta-modulator are considered in this thesis.

The objectives of the investigation were primarily to develop encoding principles for television signals and to develop an adequate theory for the delta-modulator. This has resulted in a family of encoding methods each with particular characteristics. A system having particularly favourable characteristics was designed and constructed and subjective and objective measurements are presented. At various stages in the development, computer programming was applied to obtain exact solutions to particular problems to enable fuller understanding.

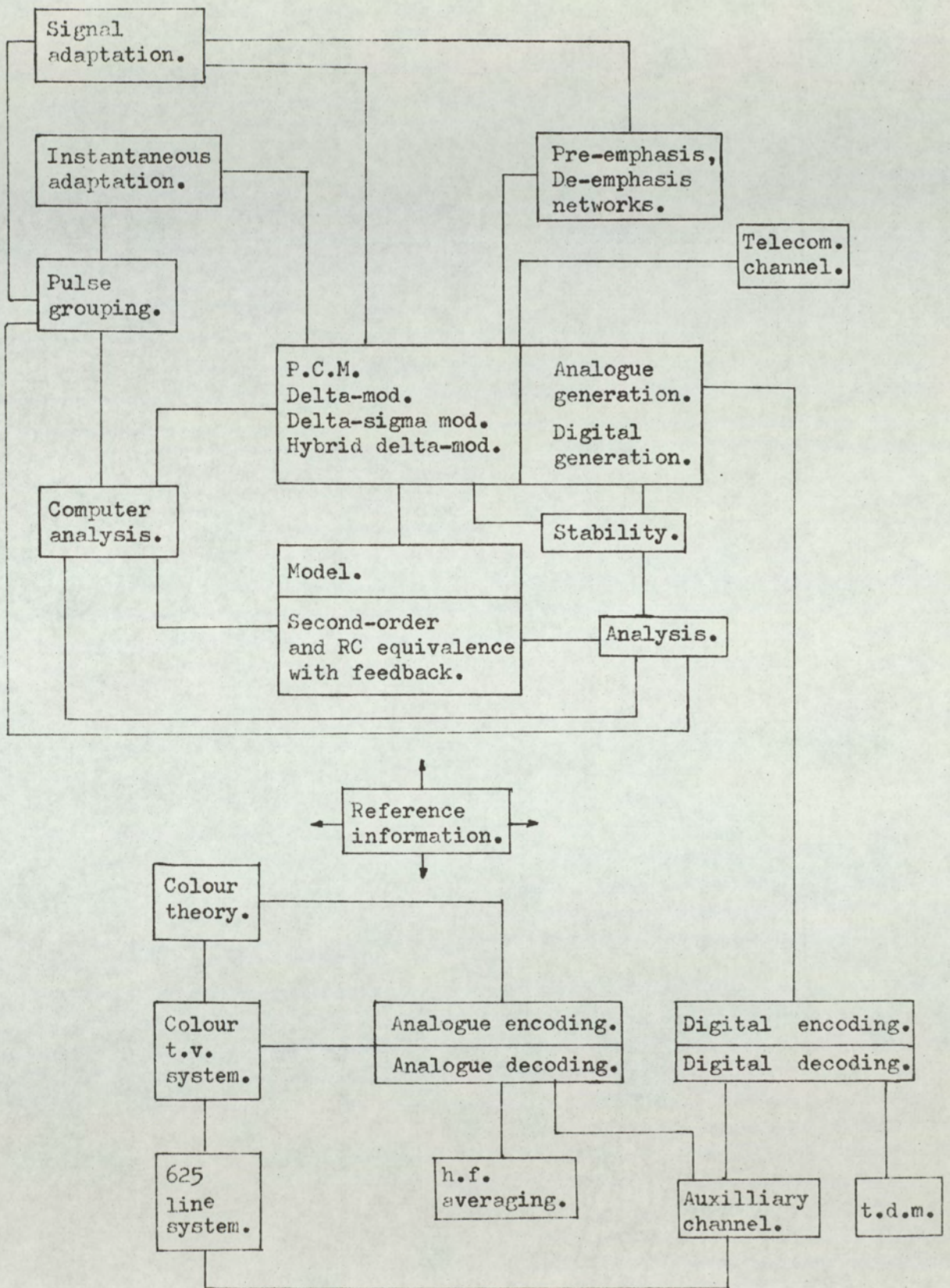


Fig.1-1. Basic areas and system sections described and analysed in the thesis,

## 2.1 Digital Communication . (18, 35)

When an analogue signal is transmitted over a communications network, inevitable signal impairment will result. Such impairment is due to attenuation and phase distortions, both linear and non-linear, reflection and accumulated noise. In certain special cases these defects can be minimised by careful equalisation of the channel; however, such strategy can only be limited in application and permanent signal degradation will result. Present communication systems require high performance links capable of operating under adverse conditions.

The digital channel is a system capable of meeting many of these requirements. Before describing its properties, a basic definition of a digital channel will be given. A digital communication channel has the properties of only recognising a signal at equally spaced, discrete intervals in time and the nature of the signal is such that only discrete signal levels are detectable. In the present discussion and the systems to be described, these levels will be restricted to two definable signal levels. Thus, the term 'digital channel' will infer a binary, digital channel; the two levels are designated 'one' and 'zero'. The data input for the digital channel takes the form of a pulse waveform, where the rate of pulses (including both '1's and '0's) is constant at all time and is referred to as the bit rate, digit rate or transmission rate. Since a binary, digital channel is

considered, each pulse must have an amplitude limited to one of two defined levels. Thus, the digital system has only a single, discretely variable, parameter, the pulse amplitude. Hence digital communication is concerned with the efficient allocation of pulse amplitudes at each sample instant in order that information can be transmitted.

One of the essential features of a digital channel is that it has the capability of information retrieval, even when the signal has been impaired by distortion and noise. When the impaired signal is received, it is known that at the equally spaced sampling instants, the signal is at one of two signal levels. Thus, providing the level is identifiable, a new signal pulse can be generated and inserted in place of the impaired pulse. The process is termed regeneration and is a basic feature of a digital channel which depends on the signal to noise-power ratio of the channel. As the transmitted signal becomes more noisy, the probability of an error in the regeneration process becomes greater. When the channel is a landline, the effect may be minimised by frequent regeneration, before the recognition error probability becomes too great. However, regeneration is not used on transmission channels using radio links because this would require the signal to be demodulated at each repeater to provide the base-band digital signal for regeneration. Such a process is obviously not desirable. It is usual in these cases, to modulate the pulse waveform onto a carrier, the modulation process having inherent noise immunity; examples are frequency and phase modulation.

Digital channels allow for time division multiplexing of signal sources with efficient elimination of cross-channel interference. This feature, of course, is not unique to digital communication, but the signal presentation allows for efficient and accurate processing and transmission of t.d.m. signals. This feature is extremely important when considering the encoding of television colour signals. A colour television system requires three basic channels to define the image. When these signals are in analogue form, on separate channels, they are extremely sensitive to imbalance and line distortions, in fact, an imbalance as low as 0.1db can be detected by the eye. Hence, in analogue form, precision circuits and transmission lines are necessary to maintain the required colorimetric balance. By encoding the signals in digital form, the signal balance is no longer a function of the transmission line and lower quality transmission may be acceptable.

Modern communications require information storage facilities and the ability to handle general data. This can readily be achieved with a digital signal. The digitally - encoded analogue signal can easily be applied to digital computers for processing and control, from which valuable data can readily be obtained.

In a digital channel, it is necessary to know how many pulses-per-second can be transmitted in a finite bandwidth, so that each pulse can be optimally detected for decoding or regeneration and to obtain a measure of the required signal power.

Let the pulse sequence be a series of delta pulses, where the weighting is  $k_m$  for the  $M^{\text{th}}$  sample. In this particular case of a binary, digital channel,  $k_m$  can have one of two values.

The pulse sequence is represented by the infinite series:

$$P(t) = \sum_{M=-\infty}^{+\infty} k_m \cdot \delta\left(t - \frac{M}{P}\right), \quad \dots(2.1)$$

where,  $P(t)$  is the time-domain pulse function.

$P$  the pulse repetition rate.

$M$  an integer.

The Fourier Transform is given by:

$$P(f) = \sum_{M=-\infty}^{+\infty} k_m \cdot e^{-j2\pi f \cdot \frac{M}{P}}, \quad \dots(2.2)$$

Bandlimiting the pulse function to a frequency  $f_x$ , the time domain response of the band-limited function is given by the Inverse Fourier Transform:

$$P_x(t) = \int_{-f_x}^{+f_x} \sum_{M=-\infty}^{+\infty} k_m \cdot e^{-j2\pi f \cdot \frac{M}{P}} \cdot df \quad \dots(2.3)$$

By integrating equation (2.3) and rearranging, it can be shown that:

$$P_x(t) = 2f_x \sum_{M=-\infty}^{+\infty} k_m \left[ \frac{\text{Sin}\{2\pi f_x (t - \frac{M}{P})\}}{\{2\pi f_x (t - \frac{M}{P})\}} \right] \quad \dots(2.4)$$

Consider the  $M^{\text{th}}$  pulse; this pulse may be detected without crosstalk from adjacent pulses at times ( $t = \frac{M}{P}$ ), providing that the zeroes of the remaining pulses formed by the  $(\text{Sin } x)/x$  function, coincide with the peak of the  $k_m$  pulse. For this condition:

$$P = 2.f_x \quad \dots(2.5)$$

If  $P < 2.f_x$ , then further filtering will realise the ideal condition, whereas if  $P > 2.f_x$ , permanent inter-pulse crosstalk occurs. Thus, it may be concluded that in a bandwidth  $(P/2)\text{Hz.}$ , a pulse rate of  $P(\text{P.P.S.})$  may be propagated without interference between adjacent pulses and that under these conditions the ideal signalling pulse has a shape defined by:

$$\text{Signalling Pulse Shape} = \left[ \frac{\text{Sin}\{\pi.P.t\}}{\{\pi.P.t\}} \right] \quad \dots(2.6)$$

This result, equation (2.6), is not physically realisable. However, a close approximation is possible by careful filtering; this requires excess bandwidth. Hence in a practical situation,  $P < 2.f_x$  and bandwidth redundancy is introduced by relaxing the system design.

It is evident from observation of the digital communication channel, that in a given time period only a finite amount of information can be transmitted. This is a limitation of the system. Consider an analogue channel. If in the analogue system no noise were present, then at every instant, assuming initially an infinite bandwidth, an infinite number of levels could be transmitted. This condition is never realised in practice. Most systems and all systems for sound and video transmission have a finite base - bandwidth; thus above a frequency  $f_u$ , zero energy exists. Also, either noise is present which limits the number of levels of signal which can accurately be defined, or in

a system a certain level of noise is possible which will not generate obvious impairment.

If a certain background noise is permissible and the signal is band-limited, then an analogue signal can be encoded into a digital pulse sequence, suitable for transmission over a digital channel. The system for converting an analogue signal into a digital signal is called an 'analogue to digital converter'. The reverse system is called a 'digital to analogue converter'. Section 2.2. considers how analogue to digital conversion is achieved by delta-modulation; section 2.3 explains a delta-sigma modulator, digital encoder and finally, section 2.5 explains pulse-code-modulation (P.C.M.).

In all the digital encoders, an analogue signal can, theoretically, convey information at an infinite rate. However, the digital channel can convey information only at a finite rate. Thus, the digital process will modify the analogue signal. The distortion introduced by pulse coding is referred to as 'quantisation distortion' or 'quantisation noise' and is fundamental to all digital encoding systems.

## 2.2 Fundamentals of delta-modulation. (5, 36, 37, 38)

Delta-Modulation is a method of encoding a digital signal to convey information contained in an analogue modulating signal. The digital modulation process is based on making a sequence of two state decisions at the digit rate of the encoder. The decisions are such that the pulse sequence directly conveys information about the analogue signal. Thus if the spectrum of the pulse sequence were analysed, it would be a function of the base-band modulating signal spectrum.

Delta-Modulation ( $\Delta M$ ) is related to the inter-sample differences of the modulating signal and thus encodes the first derivative of the modulating signal. Since the modulation process is formed by a two-state decision at each sampling point, it is necessary to observe and store past information about the signal in order that the dynamic range may be extended to more than two levels.

The basic modulator is shown in 2-1(a). It consists of a system that makes two-level decisions, the decisions being based on a comparison of the present value of analogue signal with a stored signal. After a decision is made, the local store is updated accordingly. It will be shown that the characteristics of the store control the bounds of the modulating signal.

The operation of the delta-modulator is as follows. The modulating signal  $D(t)$  is compared with the locally stored signal  $S_1(t)$  to generate a difference signal  $q(t)$ . The comparator gives an output  $c(t)$  such that,

$$\begin{aligned} q(t) &> 0, & c(t) &= 1, \\ q(t) &< 0, & c(t) &= -1, \end{aligned}$$

The comparator output  $c(t)$  is then sampled by a clock pulse and held for a duration of the clock period. The held pulse then forms the pulse sequence  $P_1(t)$ . The store network is updated by the transmission pulse in readiness for the next comparison at the following sequential sample.

Thus, the modulator generates a local signal  $S_1(t)$  which at each sample instant approximates to the analogue modulating signal  $D(t)$ . The quantisation error is therefore  $q(t)$ , where,

$$q(t) = D(t) - S_1(t), \dots (2.7)$$

The signal  $S_1(t)$  can be transmitted to a remote receiver by propagating the pulse sequence  $P_1(t)$  down a digital transmission channel. At the receiver  $S_1(t)$  can be reconstructed by an identical store to that in the encoder. Finally, as shown in Fig. 2-11(b), the quantised signal  $S_1(t)$  is band-limited to exclude frequency components outside the range of the modulating signal.

In practice, the store may be any network that permits efficient encoding and produces a stable feedback network.

The validity of the decoding system may be established as follows,

Let:

$$S_1(t) = h \{P_1(t)\} \dots (2.8)$$

$$P_1(t) = L \{q(t)\} \dots (2.9)$$

where  $h$  and  $L$  are operating functions. From equations (2.7), (2.8), (2.9),

$$D(t) = h \{P_1(t)\} + L^{-1}\{P_1(t)\} \dots (2-10)$$

where  $L^{-1}$  represents the inverse function of  $L$ . However, this operation is non-reciprocal and completely indeterminate; thus it represents an error for which no better approximation can be found. Hence,  $S_1(t)$  is the best approximation to  $D(t)$  that can be realised for a given system.

In practice, the remotely decoded signal  $S_1'(t)$  will not track  $S_1(t)$ , the local decoded signal, exactly. This is due to two basic reasons. Firstly, transmissions errors are always probable, however small the probability, when noise is introduced in the transmission channel. Secondly, the initial conditions on the local and remote stores will in general be different. The two system failings may be minimised by frequent accurate regeneration, before channel noise increases the error probability to a too great a level, and by limiting the store to a finite memory. Thus transmission errors and incorrect initial conditions are only transient.

The simplest, reliable store is an arithmetic accumulator, the output of which changes a fixed amount at each sample, the change being either a positive or a negative increment, depending upon the polarity of the modulator output pulse,  $P_1(t)$ .

Analytically, this system can be realised by letting the output pulse sequence be a series of positive and negative Dirac impulses or delta pulses. The store is then a perfect integrator. The output of the store is thus a

series of positive and negative step functions. Fig. 2-2 illustrates a basic coding sequence of a delta-modulator with a perfect-integrator store, the step height of which is,  $h$ , and the clock rate is  $P$ , (p.p.s.).

The modulation process is said to be in a non-overload condition when at each sampling instant,

$$- h < q(t) < + h$$

This condition is violated when the signal slope,  $\frac{d}{dt} D(t)$  is greater than the attainable output slope of the store, the modulator is then said to be in a condition of slope overload.

With the modulation process illustrated in Fig. 2-1, the quantisation error is measured just after the occurrence of a sample, that is once the store has been updated. Thus the time  $t_N$  for this measurement, is defined as,

$$t_N = \frac{N}{P} + \delta t \quad \left| \quad \text{LIM } \delta t \rightarrow 0 \quad \dots (2-11).$$

where  $N$  is the  $N^{\text{th}}$  sample.

In a practical delta-modulator, pulses of finite duration and amplitude are used, each pulse being arranged so that the leading edge coincides with the delta sample; the duration is generally the clock-pulse period,  $(1/P)$ .

Consider the response of a finite pulse of amplitude  $V$  and duration  $(1/P)$  in comparison to a delta pulse, under an integration process. For the two pulses to generate equivalent responses when used in a delta-modulator, then the integrated responses prior to the next sampling instant must be identical. For this condition, with a single-integration store, the area under the delta pulse and the finite pulse must be identical. Thus, if the weighting of the  $\delta$  pulse sequence is  $\delta\omega$ , then,

$$\text{Area of Finite Pulse} = V \cdot \frac{1}{P},$$

$$\text{Area of } \delta \text{ Pulse} = \delta\omega,$$

$$\text{therefore } V = P \cdot \delta\omega, \dots (2-12).$$

However, if the time constants used in the delta pulse integrator and finite pulse, integrator are different say,  $(RC)_S$ , and  $(RC)_F$ , then for both pulses to generate the same step height,

$$(RC)_F = \frac{V}{P\delta\omega} \cdot (RC)_S \dots (2-13).$$

The effect of using a finite-pulse duration of one clock interval, with a perfect integration store, is to delay the integrated value by one clock period. Thus the error for the  $N^{\text{th}}$  sample is measured as,

$$q\left(\frac{N}{P}\right) = D\left(\frac{N}{P}\right) - S_1\left(\frac{N+1}{P}\right), \dots (2-14).$$

Thus, the step height,  $h$ , is only realised after integrating over the duration of the pulse. For analytical reasons, the delta pulse systems will usually be considered, as this has the minimum of system parameters.

If, in a delta-modulation process with perfect integration, the quantisation levels are rigorously defined, then certain observations can be made about the system waveforms. For convenience, the step height has been normalised to '1' and the quantisation levels arranged, arbitrarily, to be integer values. Fig. 2-2 then reveals that on even samples, the store output signal,  $S_1(t)$  is at even quantisation levels and at odd samples  $S_1(t)$  is on odd quantisation levels. This result is of importance when considering delta-modulation to P.C.M. transformations.

For values of  $p(t)$  which lie between the limits of

a quantisation level and an adjacent level, the output pulse pattern is unaffected and the idling pattern is generated at the modulator output. The idling pattern can be represented as ...010101.... The system therefore exhibits a threshold of coding, such that the modulation signal,  $D(t)$ , must exceed a quantisation level in order to excite a change in the output-pulse sequence. It is possible under the idling condition, that the long-term mean of the quantisation error signal,  $q(t)$ , is non-zero. The introduction of a second-order system can detect this non-zero condition and correspondingly **reduce** the coding threshold to a lower value.

It has been stated that infinite memory in the feedback path of the delta-modulator and in the remote decoding network, is undesirable, because long-term accumulation of errors results in poor low-frequency stability. It is usual to introduce low-frequency roll-off in the integrator response to minimise these difficulties. Fig. (2-3a) illustrates an operational integrator and Fig. (2-3b) shows the equivalent network of this configuration. In practice, the finite-gain amplifier would be formed from a very high-gain amplifier with d.c. feedback applied. Such a network is shown in Fig.(2-3c),

In the networks of Fig. (2-3), all the integrators exhibit low-frequency roll-off due to the finite amplifier gain. Thus, even when an operational amplifier is employed as an integrator, the system appears as a RC integrator with a cascaded gain element. Assuming the amplifiers to have a gain  $A$ , but perfect in terms of bandwidth and input and output impedance, then:

$$A_I(f) = -A \cdot \left\{ \frac{1}{(1 + j 2\pi f(1 + A)(R_1 C_1))} \right\}, \dots (2-15)$$

In delta-modulation, the slope-overload characteristic of the delta-modulator is, in general, frequency dependent. The frequency-selective network for the practical, single-integration store may be considered a RC integration network, as described by equation (2-15). Perfect integration is realised when  $A \rightarrow \infty$ . To determine the maximum amplitude of a sine wave  $\overline{D}_f$  of frequency  $f$ , that fully loads a RC integrator delta-modulator:

For this calculation, a sinusoidal excitation is applied, and the relationship between its peak amplitude and frequency determined. This then determines the shape of the Fourier Transform of a general modulating function that will optimally load the modulator.

A RC integrator, modifies the step height of the store depending upon the relative position of store output  $S_1(t)$  in the system dynamic range. Since the step height changes with  $S_1(t)$ , the slope overload criterion also depends upon  $S_1(t)$ .

In the calculation, pulses of amplitude  $V$  and duration  $1/P$ , where  $P$  is the clock-rate, are considered. The results are therefore of practical use. To determine the step-height, the change in capacitor voltage,  $\Delta V_c$ , over a clock period ( $1/P$ ), is calculated, assuming an initial capacitor voltage  $V_c$ . The time interval is taken from  $\frac{N}{P}$  to  $\frac{(N+1)}{P}$ . The calculation is performed for a positive-voltage pulse, but is also applicable for negative pulses due to system symmetry. Fig. 2-4 illustrates the basis of

the initial calculation, where the RC integrator has a time constant of value RC.

The change in capacitor voltage  $\Delta V_c$ , is given by

$$\Delta V_c = \frac{1}{C} \cdot \int_{\frac{N}{P}}^{\frac{(N+1)}{P}} I \cdot dt, \quad \dots(2-16)$$

The current I in the capacitor over the time interval is identical to the resistor current, assuming no loading. Hence,

$$I = \frac{V - (V_c + \Delta V_c)}{R}, \quad \dots(2-17)$$

Eliminating I between equations (2-16) and (2-17)

$$\Delta V_c = \frac{1}{(RC)} \cdot \int_{\frac{N}{P}}^{\frac{(N+1)}{P}} \{V - (V_c + \Delta V_c)\} dt,$$

Rearranging the integration

$$\int_0^{\Delta V_c} \frac{d(\Delta V_c)}{\{V - (V_c + \Delta V_c)\}} = \frac{1}{(RC)} \int_{\frac{N}{P}}^{\frac{(N+1)}{P}} dt,$$

Hence, integrating and rearranging,

$$\Delta V_c = \{1 - e^{-1/(P.R.C.)}\} (V - V_c), \quad \dots(2-18)$$

The slope of the delta-modulator output  $S_1(t)$ , over the time interval  $\frac{N}{P}$  to  $\frac{(N+1)}{P}$ , when  $S_1(\frac{N}{P}) = V_c$  is given by

$$\left. \frac{d}{dt} S_1(t) \right|_{V_c} = \frac{\Delta V_c}{\left\{ \frac{(N+1)}{P} - \frac{N}{P} \right\}} = P \cdot \Delta V_c$$

Thus, substituting for  $\Delta V_c$  from equation (2-18),

$$\left. \frac{d}{dt} S_1(t) \right|_{V_c} = P.(V-V_c). (1-e^{-1/(P.R.C.)}), \dots(2-19)$$

If the quantisation error exceeds a maximum of one quantisation step, then the modulator is in a condition of slope overload. This condition occurs if the modulating signal slope exceeds the local store slope defined by equation (2-19).

Let the sinusoidal modulating signal of frequency  $f$  be given by

$$D(t) = \overline{D}_f \cdot \text{Sin}(2\pi ft), \dots(2-20)$$

where,  $D(t)$ , is the modulating signal.

$\overline{D}_f$ , the maximum amplitude of  $D(t)$  that can be encoded at a frequency  $f$  without slope overload.

$f$ , the modulating frequency.

The first time derivative of  $D(t)$  is given by

$$\frac{d}{dt} D(t) = (2\pi f). \overline{D}_f \cdot \text{Cos}(2\pi ft), \dots(2-21)$$

When the maximum-amplitude signal is applied to the deltamodulator, the condition for no slope overload is

$$\left. \frac{d}{dt} D(t) \right|_{V_c} = \left. \frac{d}{dt} S_1(t) \right|_{V_c} \dots(2-22)$$

where  $V_c$  is the value of  $S_1(t)$  where the condition for slope overload is limiting, and  $\overline{D}_f$  is set so that there is only one solution of the equation per half cycle, considering the positive increments of step height. A similar solution is obtained for negative increments in the negative cycle of the modulating signal due to system symmetry.

Substituting for  $D(t)$  and  $S_1(t)$  from equations (2-19) and (2-21) in equation (2-22), gives

$$P.(V - V_c). (1 - e^{-1/(PRC)}) = (2\pi f). \overline{D}_f. \text{Cos}(2\pi ft),$$

Providing slope overload does not occur, then from equation (2-14),

$$V_c = \overline{D}_f. \text{Sin}(2\pi ft) + q(t),$$

where  $q(t)$  is within  $\pm \Delta V_c$ .

Hence, eliminating  $V_c$ ,

$$\begin{aligned} P.(V - \overline{D}_f. \text{Sin}(2\pi ft) - q(t)). (1 - e^{-1/(PRC)}), \\ = (2\pi f). \overline{D}_f. \text{Cos}(2\pi ft), \end{aligned}$$

$$\begin{aligned} \text{Therefore, } P.(V - q(t)). (1 - e^{-1/(PRC)}) - P.\overline{D}_f. \text{Sin}(2\pi ft). (1 - e^{-1/(PRC)}), \\ = (2\pi f). \overline{D}_f. \text{Cos}(2\pi ft), \quad \dots(2-23) \end{aligned}$$

-----  
 Rewriting equation (2-23) as

$$a + b. \text{Sin}\theta = c. \text{Cos}\theta, \quad \dots(2-24)$$

$$\text{where, } a = P.(V - q(t)). (1 - e^{-1/(PRC)}),$$

$$b = -P.\overline{D}_f. (1 - e^{-1/(PRC)}),$$

$$c = (2\pi f). \overline{D}_f,$$

$$\theta = (2\pi ft),$$

Squaring equation (24)

$$(a^2 + 2ab \text{Sin}\theta + b^2 \text{Sin}^2\theta) = c^2(1 - \text{Sin}^2\theta)$$

$$\text{Therefore, } (b^2 + c^2). \text{Sin}^2\theta + 2ab \text{Sin}\theta + (a^2 - c^2) = 0$$

The condition for a single solution of  $\sin\theta$  is  

$$\{2ab\}^2 = 4.(b^2+c^2).(a^2-c^2)$$

Hence, simplifying,

$$c^2(a^2-b^2-c^2) = 0,$$

therefore,  $c = 0,$

or,  $a^2-b^2-c^2 = 0,$  .....(2-25)

$c=0$  is not a realistic condition; thus for a single solution of  $\sin\theta$ , using the quadratic solution,

$$\sin\theta = \frac{-a.b}{(b^2+c^2)}, \quad \text{.....(2-26)}$$

-----  
 Substituting for a, b, c in equation (2-25),

$$\{P.(V-q(t)).(1-e^{-1/(PRC)})\}^2 - \{P.\overline{D}_f.(1-e^{-1/(PRC)})\}^2$$

$$- \{(2\pi f).\overline{D}_f\}^2 = 0,$$

Solving for  $\overline{D}_f$  and taking square roots,

$$\overline{D}_f = \frac{\{V - q(t)\}}{\left[ 1 + \frac{(2\pi f)^2}{P^2(1-e^{-1/(PRC)})^2} \right]^{\frac{1}{2}}}, \quad \text{.....(2-27)}$$

Since  $-\Delta V_c < q(t) < \Delta V_c$ , there is a tolerance on  $\overline{D}_f$  which can cause slope overload. Since in general, the coding pattern repeats only after many cycles of modulating signal, for constant  $\overline{D}_f$ ,  $f$  and  $P$ , slope overload may just occur on certain cycles. Thus to ensure that slope overload can never occur, put,

$$q(t) = \Delta V_c \left| \begin{array}{l} \\ V_c \end{array} \right| ,$$

Hence, equation (2-27) becomes,

$$\overline{D}_f = \frac{\{V - \Delta V_c\}}{\left[1 + \frac{(2\pi f)^2}{p^2 \{1 - e^{-1/(PRC)}\}^2}\right]^{\frac{1}{2}}}, \quad \dots(2-28)$$

To determine  $\Delta V_c$  at  $S_1(t) = V_c$ , substitute for a, b, c,  $\theta$  in equation (2-26). Hence,

$$\sin(2\pi ft) = \frac{\left[p^2 \cdot \overline{D}_f \cdot (V - q(t)) \cdot (1 - e^{-1/(PRC)})^2\right]}{\left[p^2 \cdot \overline{D}_f^2 (1 - e^{-1/(PRC)})^2 + \overline{D}_f^2 (2\pi f)^2\right]}$$

$$\text{Now, } V_c = \overline{D}_f \cdot \sin(2\pi ft) + q(t),$$

Substituting for  $\sin(2\pi ft)$ ,

Therefore,

$$V_c = \left[ \frac{p^2 (V - q(t)) (1 - e^{-1/(PRC)})^2}{p^2 (1 - e^{-1/(PRC)})^2 + (2\pi f)^2} \right] + q(t).$$

Since  $\Delta V_c$  is a second-order effect, it is reasonable to neglect  $q(t)$  in the expression for  $V_c$ .

Thus

$$V_c \approx \left[ \frac{V}{1 + \frac{(2\pi f)^2}{p^2 \{1 - e^{-1/(PRC)}\}^2}} \right]$$

Substituting for  $V_c$  in equation (2-18),

$$\Delta V_c = V \cdot \left[ 1 - \frac{1}{\left[ 1 + \frac{(2\pi f)^2}{P^2 \cdot \{1 - e^{-1/(PRC)}\}^2} \right]} \right] \cdot (1 - e^{-1/(PRC)}),$$

.....(2-29)

Equation (2-29) calculates the quantisation step at the point verging on slope overload, and thus represents the maximum margin on equation (2-28) to prevent slope overload.

Consider now an approximate form of equation (2-28).

$$\begin{aligned} & \text{Expanding, } P^2 \cdot \{1 - e^{-1/(PRC)}\}^2 \\ & P^2 \{1 - 2 \cdot e^{-1/(PRC)} + e^{-2/(PRC)}\} \\ & = P^2 \left\{ 1 - 2 \left( 1 - \frac{1}{(PRC)} + \frac{1}{(PRC)^2 \cdot 2} - \frac{1}{(PRC)^3 \cdot 6} + \dots \right) \right. \\ & \quad \left. + \left( 1 - \frac{2}{(PRC)} + \frac{4}{(PRC)^2 \cdot 2} - \frac{8}{(PRC)^3 \cdot 6} + \dots \right) \right\} \\ & = P^2 \left\{ \frac{1}{(PRC)^2} - \frac{1}{(PRC)^3} + \frac{7}{(PRC)^4 \cdot 12} - \dots \right\} \end{aligned}$$

In a practical modulator,  $RC < 10^{-6}$

$$P \approx 100 \cdot 10^6 \text{ (P.P.S.)}$$

therefore,  $PRC > 100$ ,

$$\text{Hence, } P^2 \cdot \{1 - e^{-1/(PRC)}\}^2 \approx \frac{1}{RC},$$

Substituting the above expression in equation (2-28) gives:

$$\frac{\overline{D}_f}{(V - \Delta V_c)} = \frac{1}{\{1 + (2\pi fRC)^2\}^{\frac{1}{2}}} \quad \dots(2-30)$$

Equation (2-30) represents a practical solution for the slope-overload condition, for a single sine wave of frequency  $f$ .

Equation (2-30) shows that the slope-overload characteristic of the dltamodulator is identical to the gain characteristic of a passive, RC integrator. The signal magnitude of the overload characteristic is obtained by applying a sine-wave input of magnitude  $V$  (Volts) and sweeping the frequency of the sine-wave over the base-band frequency range of the delta-modulator. The amplitude,  $V$  (volts), of the sine wave applied is equal to the pulse amplitude,  $V$  (volts), of the output pulse waveform of the delta modulator. This process may be applied for any transfer function that is introduced into the feedback network. Thus, to optimise the loading of a dltamodulator it is necessary to develop a transfer function that matches the power spectrum of the modulating signal. However, to realise optimum performance for the dltamodulator, a hybrid system is required. This is discussed in section 2.4. The limiting factor on the transfer function in the closed loop of the dltamodulator is the stability criterion of the system.

For modulating signals that are high in frequency compared with the low-frequency turnover of the integrating network, or in systems where the integrating network is a perfect integrator, then equation (2-30) becomes

$$\overline{D}_f \left| \begin{array}{l} = \\ f \gg \frac{1}{2\pi(RC)} \end{array} \right. = V \cdot \frac{(RC)}{(2\pi f)}, \quad \dots(2-31)$$

A delta-modulator feedback loop allows the introduction of a second-order network, which within limits, can produce a stable system with an increased dynamic range. Observations of stability will be considered in a later chapter, but in general two cascaded integrators with a predictive loop can generate a stable system. Fig. 2.5A illustrates an ideal second-order system and Fig. 2.5B is a passive approximation to the ideal.

The transfer function  $A_d(f)$  of the ideal second-order system of Fig. 2.5A, is given by,

$$A_d(f) = \frac{-1}{(2\pi f)^2 \cdot T_1 T_2} + \frac{G}{j(2\pi f) T_1}$$

Therefore

$$A_d(f) = \frac{-1}{(2\pi f) \cdot T_1} \left\{ \frac{1}{(2\pi f) T_2} + j \cdot G \right\}, \quad \dots(2-32)$$

If the pulse height of the delta-modulator is,  $V$ , then the slope overload characteristic, for a sine wave of frequency  $f$  is,

$$\overline{D}_f = V \cdot \left[ \frac{1}{(2\pi f) T_1} \cdot \left\{ \frac{1}{(2\pi f T_2)^2} + G^2 \right\}^{\frac{1}{2}} \right] \quad \dots(2-33)$$

It is found with a double-integration network, that when making a comparison at the  $N^{\text{th}}$  sample, it is necessary to predict linearly the store output one clock period in advance, and use this predicted value in the

comparison procedure. The prediction is locally applied to each sample. Consider the case where a sample is to occur at time  $\frac{N}{P}$  and the predicted value of store output is required at time  $\frac{(N+1)}{P}$ .

Fig. 2.6 illustrates the behaviour of the store output  $S_1(t)$ .

The store output at time  $\frac{N}{P}$  without prediction is  $S_1(\frac{N}{P})$ , but the predicted value  $S_1(\frac{N}{P}) \Big|_{\text{Predicted}}$  is required.

The predicted value assumes that  $S_1(t)$  continues to change over the interval  $N$  to  $(N+1)$  in a similar way to its change over the interval  $(N-1)$  to  $N$ . Therefore, there is no discontinuity at time  $(N/P)$  when considering the predicted value of  $S_1(t)$ .

Applying Taylor's expansions over the interval  $\frac{N}{P}$  to  $\frac{(N+1)}{P}$ , gives

$$S_1(\frac{N}{P}) \Big|_{\text{Predicted}} = S_1(\frac{N}{P}) + \frac{1}{P} \cdot S'(\frac{N}{P}) + \frac{1}{2 \cdot P^2} \cdot S''(\frac{N}{P}),$$

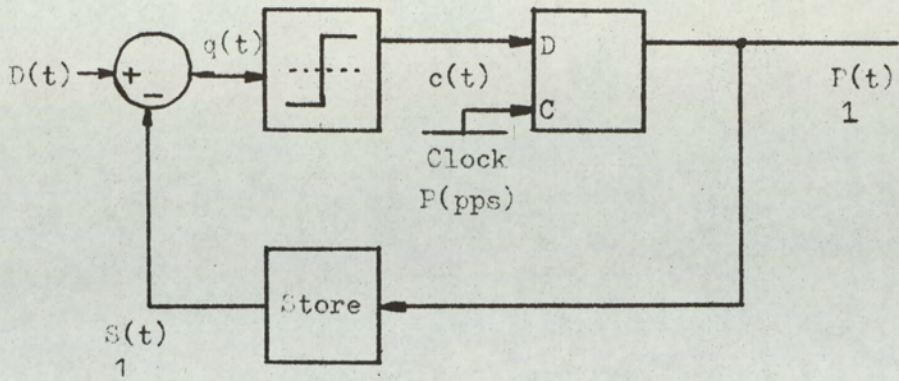
Since linear prediction produces a stable system, the second derivative term may be neglected, as it is a small quantity for a finite pulse and zero for a delta pulse.

Hence in the network shown in Fig. (2.5A),

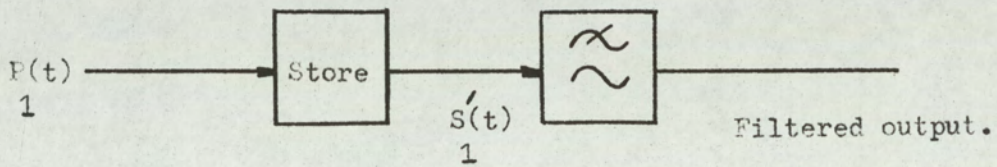
$$G = \frac{1}{P \cdot T_2} \dots (2-34).$$

The problem of stability depends upon the transfer function of the network in the closed loop of the dltamodulator and the type of pulse applied to the

transfer function. However, in most of the literature,  
the above predictive assumption produces an efficient  
encoder.



(a) Encoder.



(b) Decoder.

Fig.2-1. General delta-modulator system.

Quantisation levels.

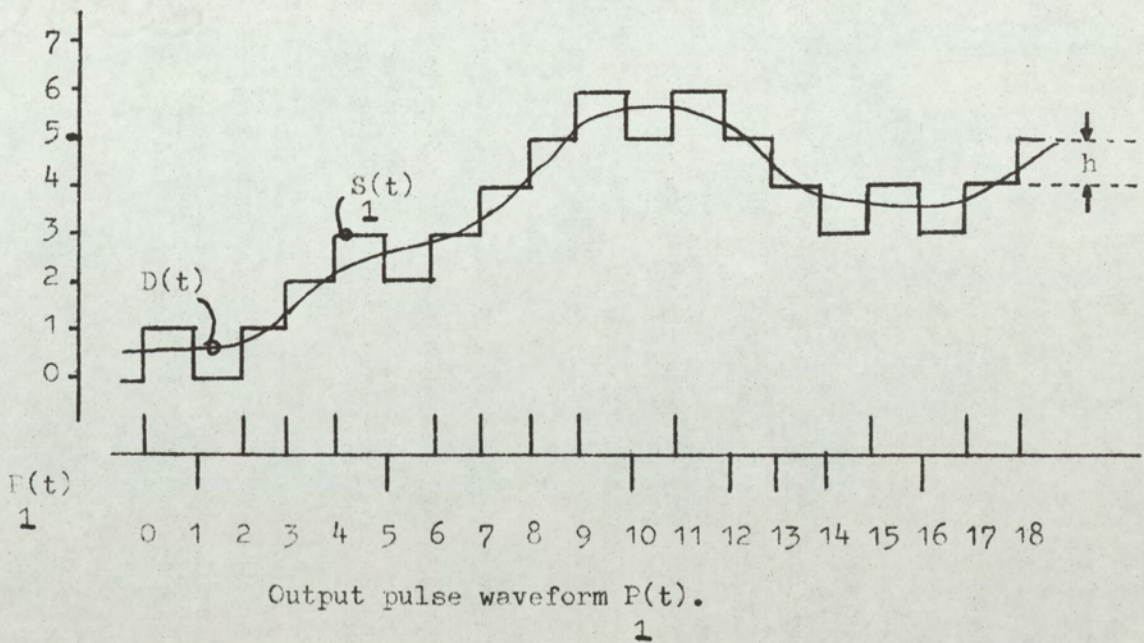
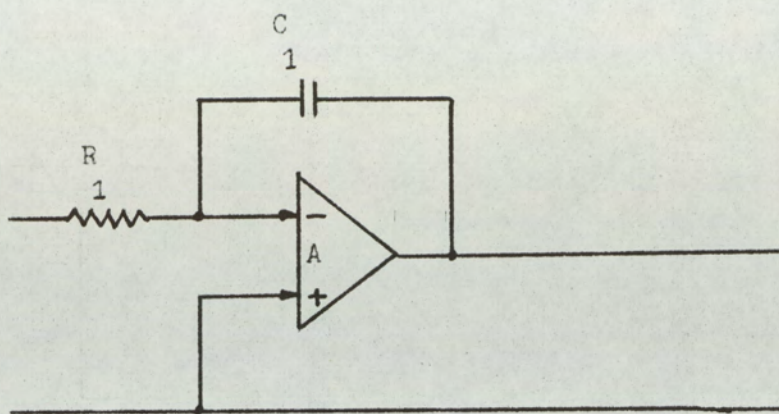
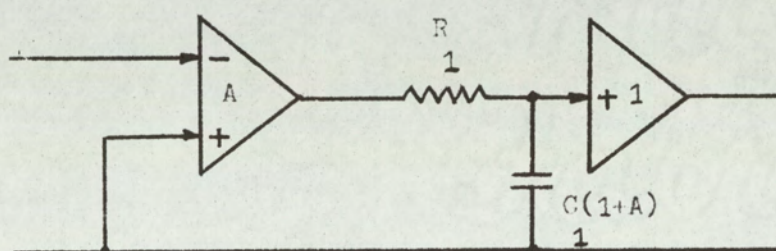


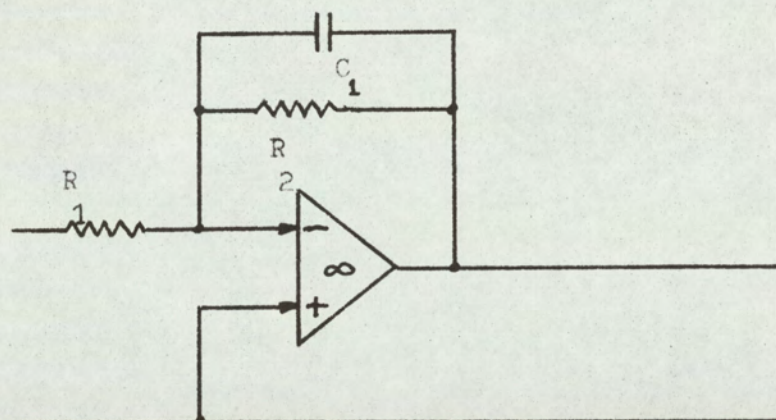
Fig.2-2. Pulse coding sequence of a perfect integrator store delta-modulator.



(a).



(b).

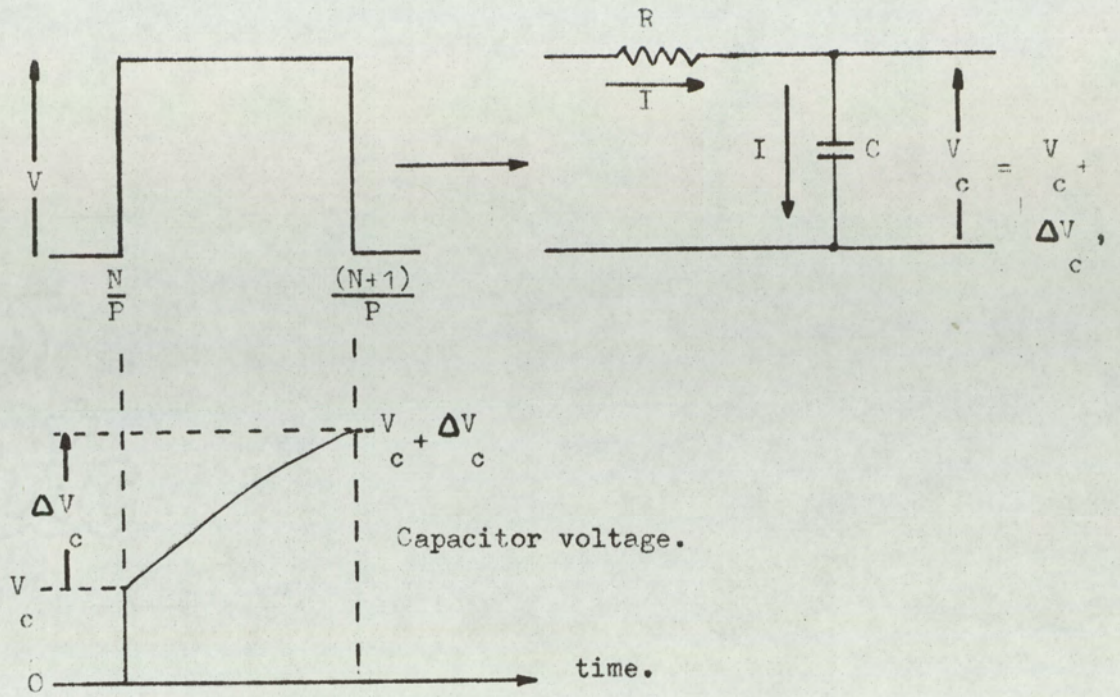


$$A = \frac{R}{R} \frac{2}{1}$$

(c).

Fig.2-3. Integration networks.

- (a) RC active integrator with finite gain amplifier.
- (b) Equivalent network of Fig.2-3(a).
- (c) d.c. gain determined by negative feedback loop.



- $V$  pulse amplitude.
- $(1/P)$  pulse duration.
- $RC$  time constant of RC integrator.
- $\Delta V_c$  change in integrator output over time interval  $\frac{N}{P}$  to  $\frac{(N+1)}{P}$ , when initial voltage at time  $\frac{N}{P}$  is  $V_c$ .
- $V_c$  initial integrator voltage at time  $\frac{N}{P}$ .
- $I$  resistor and capacitor current over clock period.

Fig.2-4. Calculation model of step height for RC integration network.

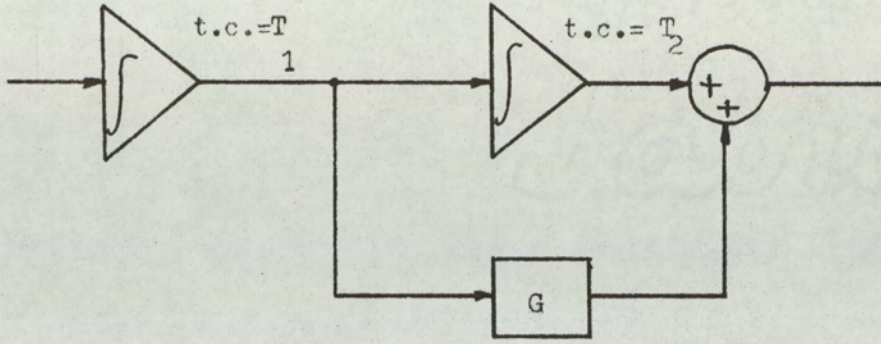


Fig.2-5(a).

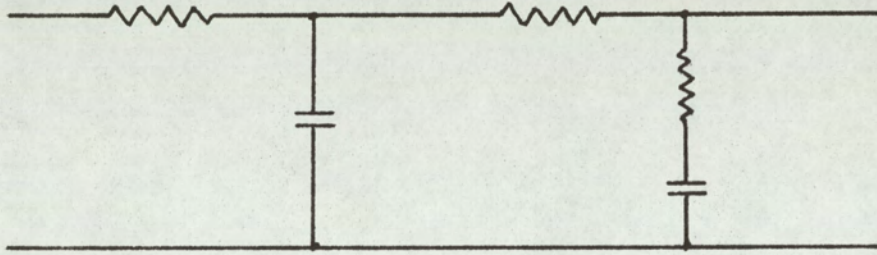


Fig.2-5(b).

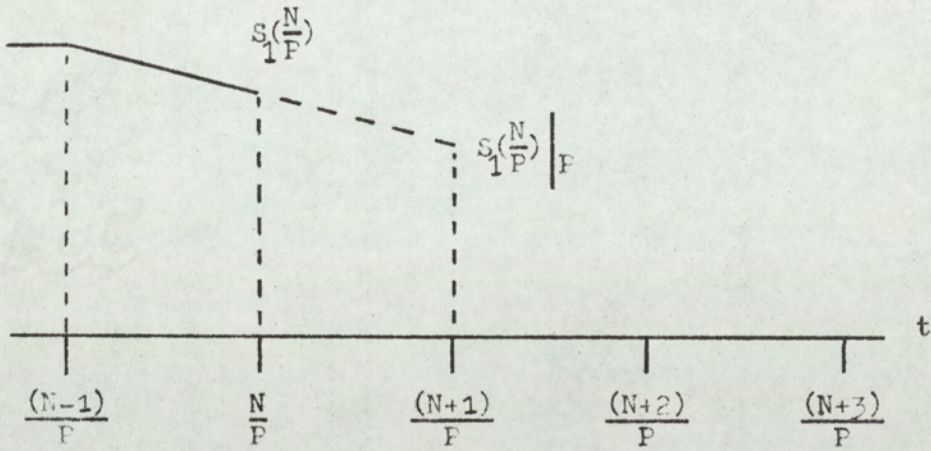


Fig.2-6.

Fig.2-5(a). Ideal second-order system with predictive loop.

Fig.2-5(b). Passive approximation to second-order system.

Fig.2-6. Predictive process applied to local store output.

2.3 DELTA-SIGMA-MODULATION. ( $\Delta\Sigma M$ ) (23, 24)

By introducing a linear transfer function in the input signal path, it is possible to generate an output pulse waveform  $P_1(t)$  which contains, directly, the spectrum of the modulating signal,  $M(t)$ . Such a modulator is termed a delta-sigma-modulator,  $\Delta\Sigma M$ .

Let the store in the feedback path of a delta-modulator have a general linear transfer function  $h(f)$ . Let us analyse the delta-modulator variables in terms of their Fourier Transforms, where,

$$D(f) = F\{D(t)\}, \quad \dots(2-35)$$

$$S_1(f) = F\{S_1(t)\}, \quad \dots(2-36)$$

$$P_1(f) = F\{P_1(t)\}, \quad \dots(2-37)$$

$$q(f) = F\{q(t)\}, \quad \dots(2-38)$$

$$M(f) = F\{M(t)\}, \quad \dots(2-39)$$

Substituting for  $D(t)$ ,  $S_1(t)$  and  $q(t)$  from equations (2-35), (2-36), (2-38) in equation (2-7), gives:

$$q(f) = D(f) - S_1(f)$$

$$\text{But } S_1(f) = h(f) \cdot P_1(f)$$

Therefore,

$$P_1(f) = \{h(f)\}^{-1} \cdot D(f) - \{h(f)\}^{-1} \cdot q(f),$$

$$\text{Put } M(f) = \{h(f)\}^{-1} \cdot D(f) \quad \dots(2-40)$$

Therefore,

$$P_1(f) = M(f) - \{h(f)\}^{-1} \cdot q(f) \quad \dots(2-41)$$

When a transfer function  $h(f)$  is introduced in the input signal path to a delta-modulator, equations

(2-40) and (2-41) show that the output pulse sequence is directly related to the modulating signal. However, the quantisation noise is now frequency dependant. Thus, if  $q(f)$  is the quantisation noise spectrum for the delta-modulator and  $q_s(f)$  the quantisation noise spectrum for the delta-sigma modulator, then

$$q_s(f) = \frac{q(f)}{h(f)}, \quad \dots(2-42)$$

The conversion of delta-modulation to delta-sigma-modulation is thus seen as a transposition of the linear demodulation network, prior to final filtering, to the input-signal path of the delta-modulator.

Equation (2-41) demonstrates that the delta-sigma modulator is realised by inverting the transfer function  $h(f)$  in the forward path of a modulator loop. Fig. 2-7 illustrates the formation of a delta-sigma modulator network.

The delta-sigma modulator has certain advantages over delta-modulation these are as follows:

- a) The  $\Delta\Sigma$  is capable of transmitting a d.c. signal, since decoding only requires a low-pass filter.
- b) Transmission errors are not accumulated, and only generate a transient response, this response depending upon the low-pass filter.
- c) The output voltage swing of the integrator is limited by the feedback action; in practice, it is only a fraction of a volt, oscillating about the comparator threshold level. Thus, the modulator is not limited by the finite dynamic range of active integrators.

- d) Only a single transfer function is required in the modulation process. Also, the transfer function in the decoder is eliminated, further simplifying the process and eliminating the need for accurately matching two networks to prevent amplitude and phase distortion.
- e) The gain/frequency response is constant. The peak amplitude of the 100% pulses generated by the modulator set the peak amplitude of the modulating signal,  $M(t)$ , at all frequencies in the modulating base-band. In this system, however, the threshold of coding becomes coarser as the modulating frequency increases. This is due to the modification of the noise structure shown in equation (2-42); the quantisation noise rising at the higher signal frequencies.

It will be shown that the deltasigma modulator has many advantageous features when applied to the encoding of video signals. Also, the modulator lends itself more readily to instrumentation, especially when high pulse rates are required.

The stability criteria of a  $\Delta\Sigma M$  are identical to that of a  $\Delta M$ , since the closed loop contains the same transfer function. It is also possible to introduce the second-order network in the forward path, this still being represented by  $h(f)$ .

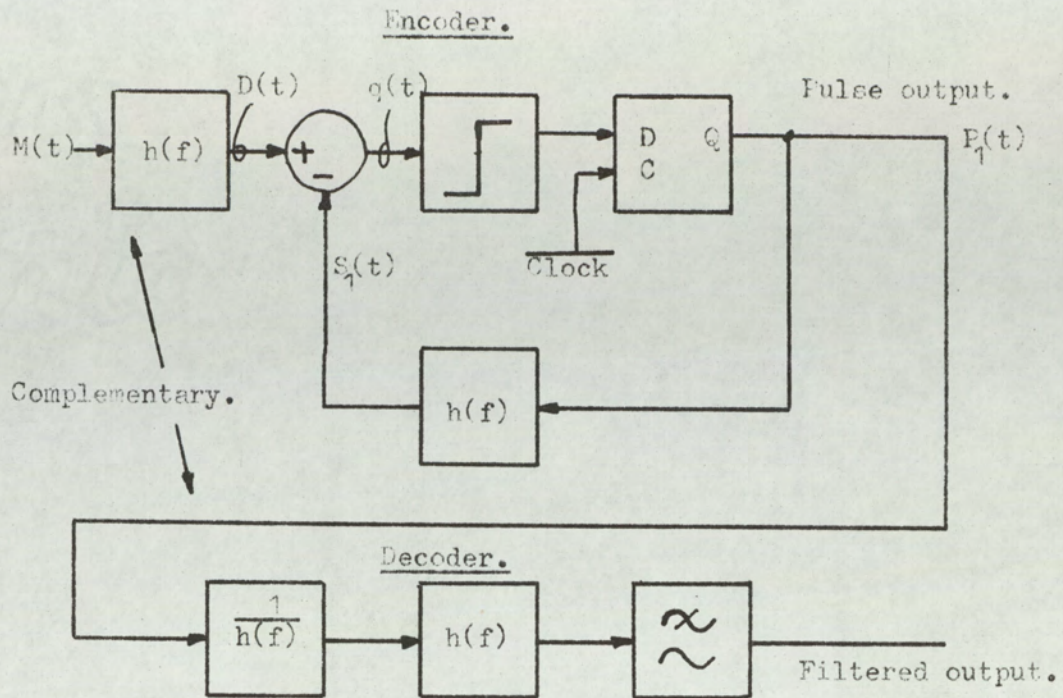


Fig.2-7(a).

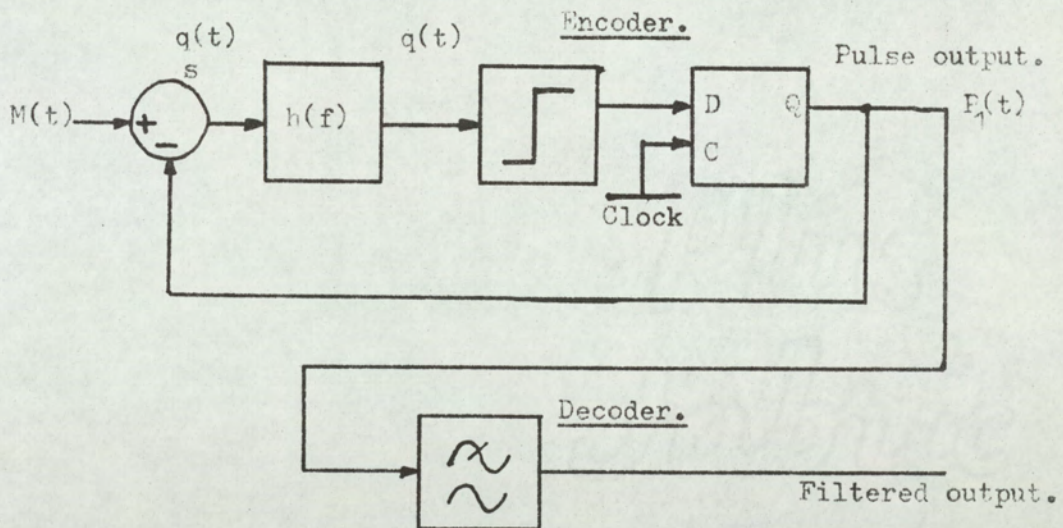


Fig.2-7(b).

Fig.2-7(a). Delta-sigma modulator formed by integrating input to delta-modulator.

Fig.2-7(b). Delta-sigma modulator by transposition of the integrators of Fig.2-7(a) to the forward path of the delta-modulator control loop.

2.4 Hybrid delta/delta-sigma modulation and its application to pre-emphasis and de-emphasis networks.

Signals generated by a particular signal source can generally be represented by a characteristic amplitude/frequency characteristic. It is desirable to match the power distribution of the modulating signal to the overload/frequency power distribution of the delta-modulator, so that the optimum signal to quantisation noise ratio may be realised.

The strategy for optimisation can be achieved by two methods. The first allows for the modification of the delta-modulator overload characteristic. This, within certain bounds, may be obtained by modification of the transfer function in the feedback loop, without degrading the inherent signal to quantisation noise ratio of the delta-modulator.

Consider the general pulse modulator of Fig. 2.8. It will be termed a hybrid delta-modulator.

In the hybrid delta-modulator, the demodulation network is derived from the network in the feedback path,  $h_1(f)$ . Thus, the modulating signal applied to the hybrid delta-modulator is pre-emphasised by the transfer function  $\{h_1(f)\}^{-1}$ .

To maintain stability, and realise the optimum signal to quantisation noise ratio, then

$$h_1(f) \cdot h_2(f) = h(f) \quad \dots(2-43)$$

where,  $h_1(f)$ , is the transfer function in the feedback path.

$h_2(f)$ , is the transfer function in the forward path.

$h(f)$ , is the closed loop transfer function to realise the optimum signal to quantisation noise of a given system, yet maintaining stability.

In certain circumstances, the transfer function  $h_2(f)$  may be omitted. This, however, usually results in a degraded signal to quantisation noise ratio. An example is the single RC integrator in the feedback loop. The performance of this modulator may be considerably improved by the addition of a transfer function  $h_2(f)$ , such that the total closed loop transfer function is a double integrator with predictive loop.

The second method of pre-emphasis is to introduce an external matching filter network to modify the modulating signal and the inverse network to de-emphasise the decoded signal, as shown in Fig. 2.9. This method is to be preferred with high speed modulators, since only certain circuit configurations operate satisfactorily.

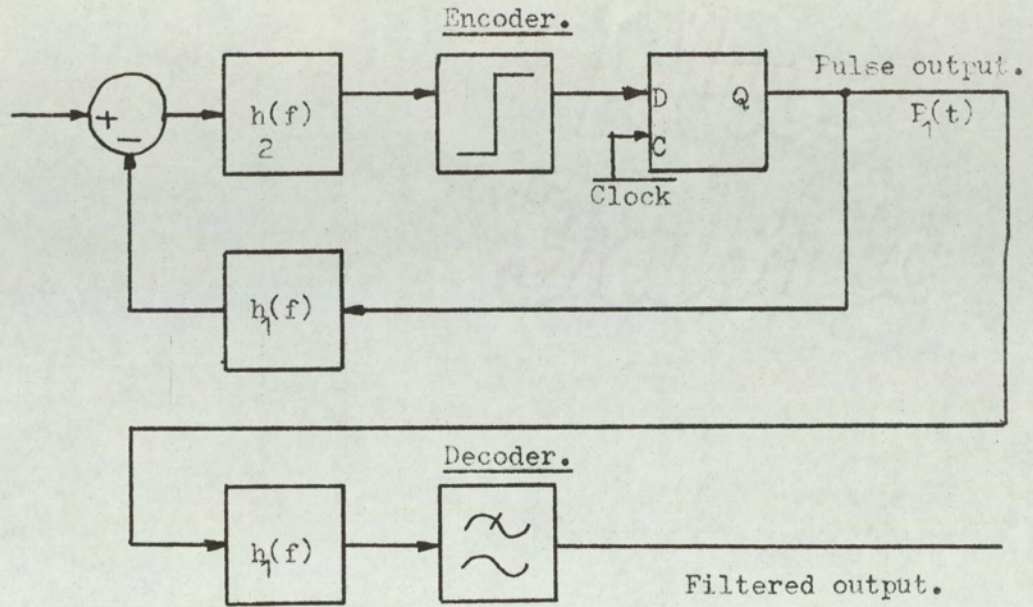


Fig.2-8. Hybrid delta-modulator.

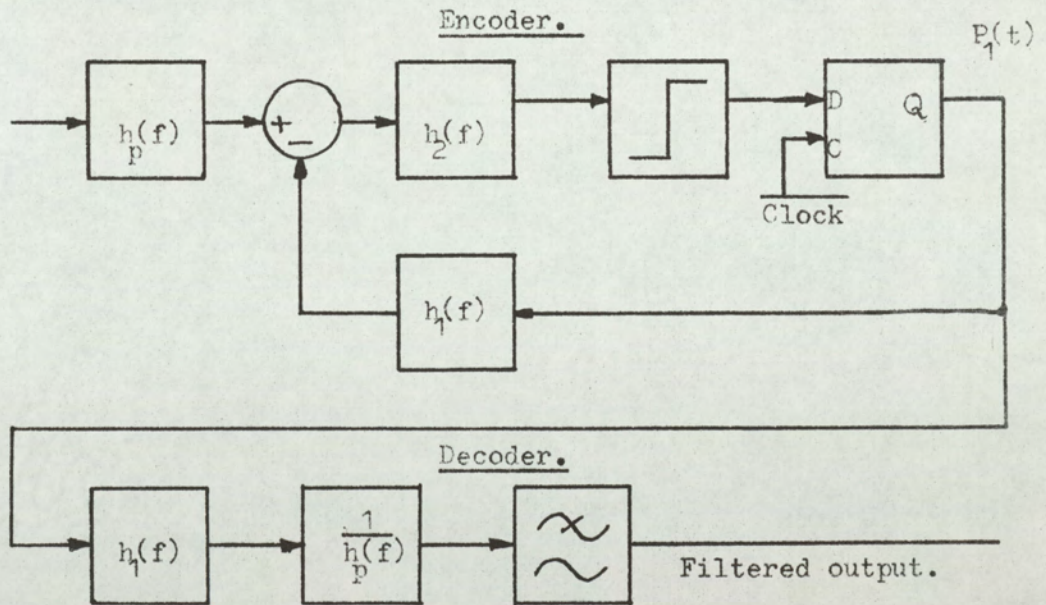


Fig.2-9. Hybrid delta-modulator with external pre-emphasis and de-emphasis networks.

2.5 Pulse code modulation and its relationship to delta-modulation. (12, 22, 39, 40, 41, 42)

Pulse Code Modulation, (P.C.M.), is a method of digitally encoding analogue signals. The Sampling Theorem states that a bandlimited signal can be completely defined by a series of samples occurring at a rate exceeding twice the highest frequency component in the modulating signal baseband. A sampled analogue signal is termed a pulse-amplitude modulated signal. Fig. 2.10 illustrates the construction of a P.A.M. waveform and shows the form of the resultant Fourier Transform. In this system, the sampling function is a sequence of delta pulses, the sample values shown represent the weightings of these pulses.

Since a digital channel can convey information only at a finite rate, it is necessary to restrict the information of each sample pulse in the P.A.M. system. The amplitude signal range of the P.A.M. system, is divided into a set of finite levels, which will be considered to be of equal spacings. At each sample, the P.A.M. signal is compared with the discrete levels and approximated to the nearest level. Such a process, as described in section 2.1, is termed quantisation; it results, through the approximation, in quantisation error. It is possible to allocate a number to each quantisation level; thus the analogue modulating signal is reduced to a sequence of numbers. In the system under discussion, the array of numbers will be presented in a binary form. Fig. 2.11 illustrates a simple four-level P.C.M. system.

In Fig. 2.11, if  $f_s$  is the sampling rate of the P.A.M. system, the quantised signal may be represented by a sequence of binary numbers occurring at a rate  $f_s$ . The binary number may be directly represented by a two-level digital signal, hence,

$$P_{PCM}(t) = \begin{matrix} \vdots & 0 & 0 & \vdots & 1 & 0 & \vdots & 1 & 0 & \vdots & 0 & 1 & \vdots & 1 & 1 & \vdots & 1 & 0 \\ \vdots & & & \vdots & & \\ \frac{N}{f_s} & & & \frac{(N+1)}{f_s} & & & \frac{(N+2)}{f_s} & & & \frac{(N+3)}{f_s} & & & \frac{(N+4)}{f_s} & & & \frac{(N+5)}{f_s} & & \end{matrix}$$

where  $P_{PCM}(t)$  is the pulse waveform of the P.C.M. signal.

By suitable synchronisation of the pulse waveform, the binary numbers can be identified at the receiver and the quantised P.A.M. signal reconstructed.

In the present section, the relationship of the quantised P.A.M. signal to the quantised output of a delta-modulator will be considered. In section 2.6, a method of generating a P.C.M. binary encoded pulse waveform is outlined, using a digital delta-modulator.

For discussion, the uniform quantisation levels of the P.C.M. system are assumed spaced at intervals of value 2 units. Since the quantisation process approximates each P.A.M. sample to the nearest quantisation level, the instantaneous quantisation error  $q_p(t)$  lies within the range:

$$-1 \leq q_p(t) \leq 1,$$

In the sampling process for generating P.C.M., the samples are equally spaced and occur at a rate  $f_s$ , where

$$f_s \geq 2.f_u,$$

where,  $f_u$ , is the upper frequency bound to the baseband

modulating signal.

Consider now the quantised output of a perfect single-integration delta-modulator, where the step height is uniform and normalised to a value of unity. The initial condition of the integrator is set so that each quantisation level is at an integer value. The modulator is assumed to generate delta pulses at the output; thus the integrator level changes in unit steps. For this system, the instantaneous quantisation error, assuming no slope overload, is given by  $q(t)$ , where

$$-1 \leq q(t) \leq 1,$$

An initial observation is that the error signals of both P.C.M. and delta-modulator have the same tolerance, when the parameters are defined as above. In the quantised P.A.M. system, the quantised signal values are always an even integer value. However, in the delta-modulation system, the quantised output is only at even levels on even samples, (see section 2.2 and Fig. 2.2). If the following conditions are satisfied:

- a) the delta-modulation sampling rate  $P$  is made an even positive integer multiple of the P.A.M. sampling rate  $f_s$ .
- b) The modulating signal to the delta-modulator and quantised, P.A.M. system is identical.
- c) The delta-modulator sampling rate and P.A.M. sampling rates are phased so that the samples of P.A.M. coincide with even samples of the delta-modulator.

Then the two quantised signals are at the same quantisation level at the P.A.M. sampling instant. This process is illustrated in Fig. 2.12.

The method of producing the quantised P.A.M. signal using a perfect-integrator delta-modulator only applies when the delta-modulator sampling rate is sufficiently high that the delta-modulator can encode, without slope overload, the full signal range of the P.C.M. system at the highest frequency  $f_u$ . Thus, there is a minimum delta-modulation pulse rate that can be used. However, any integer multiple above this minimum rate may be used.

There are two conditions for determining the minimum delta-modulation sampling rate,  $P$ . The first condition is that  $P$  is a positive, even, integer multiple of the P.A.M. sampling rate  $f_s$ .

$$\text{i.e. } P = (2N).f_s \quad \dots(2.44)$$

where,  $P$ , is the delta-modulator sampling (clock) rate.

$N$ , is a positive integer.

$f_s$ , is the P.A.M. sampling rate.

To determine the second condition, let each quantised P.A.M. sample be represented by a  $C$ -digit binary code. Hence if the interval between adjacent quantisation levels is 2 units, the P.C.M. signal range  $R_c$  for a  $C$ -digit code is,

$$\begin{aligned} R_c &= 2 \cdot 2^c \\ \text{Therefore, } R_c &= 2 \cdot 2^{(c+1)} \quad \dots(2.45) \end{aligned}$$

The worst-case sinusoidal modulating signal is where the amplitude of the sine wave is  $R_c/2$  and its frequency is  $f_u$ , the upper frequency limit.

Hence, the modulating signal  $D(t)$  is given by:

$$D(t) = \frac{R_c}{2} \cdot \sin(2\pi f_u t)$$

Therefore,

$$D(t) = 2^c \cdot \sin(2\pi f_u t) \quad \dots(2.46)$$

From equation (2.46), the maximum signal slope is:

$$\left. \frac{dD(t)}{dt} \right|_{\text{MAX}} = 2^c \cdot (2\pi f_u) \\ = 2 \cdot (c+1) \pi \cdot f_u, \quad \dots(2.47)$$

The delta-modulator must be able to encode the slope given by equation (2.47) without slope overload. Since the step height is unity, and the clock duration  $1/P$ , the maximum slope that can be encoded is  $P$ . Hence, from equation (2.47):

$$P = \{2 \cdot (c+1) \pi \cdot f_u\} \quad \dots(2.48)$$

Thus, to encode, without slope overload, the full dynamic range of the P.C.M. system, it is necessary that:

$$P \geq \{2^{(c+1)} \cdot \pi \cdot f_u\} \quad \dots(2.49)$$

This is the second condition for encoding the quantised P.A.M. signal with a delta-modulator. Hence from equations (2.49) and (2.44) eliminating  $P$ ,

$$N \geq 2^c \cdot \pi \cdot \left\{ \frac{f_u}{f_s} \right\} \quad \dots(2.50)$$

where  $N$  is a positive integer.

Mathematically, the quantised P.A.M. signal is extracted from the delta-modulated quantised output  $S_1(t)$  by sampling, with a  $\delta$  function, at a sampling rate  $f_s$ . If  $S_{PCM}(t)$  is the quantised P.A.M. signal of the P.C.M. system, then,

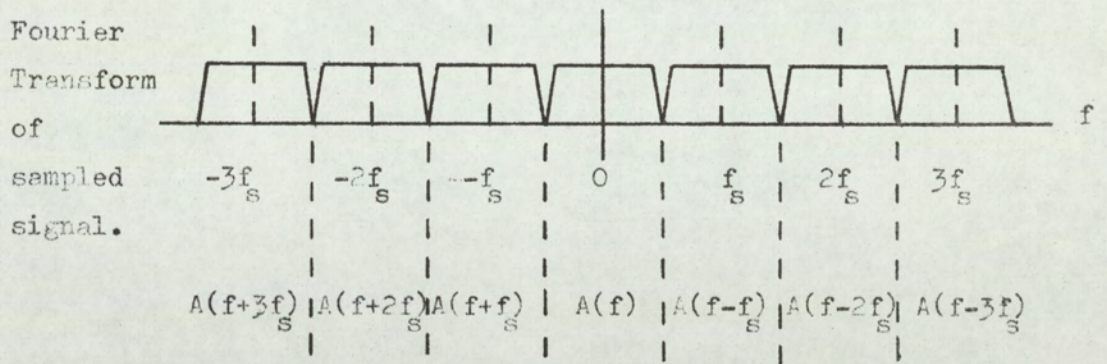
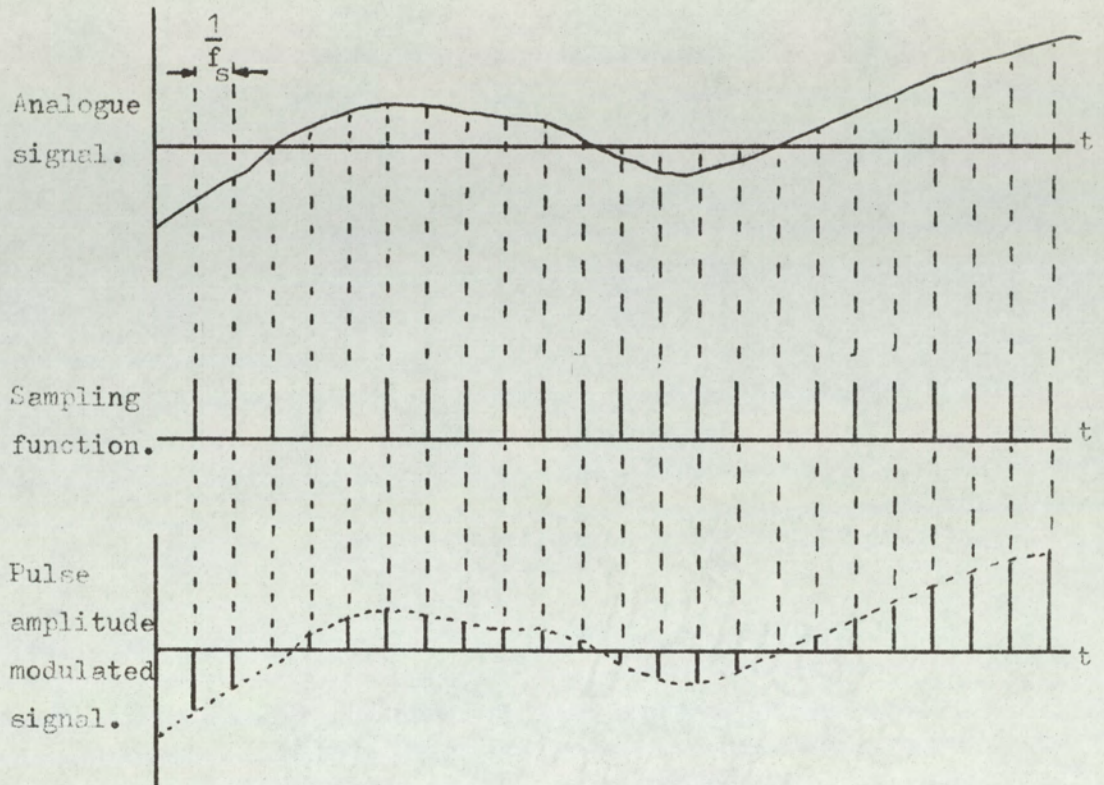
$$S_{PCM}(t) = S_1(t) \cdot \sum_{M_1=-\infty}^{+\infty} \delta\left(t - \frac{M_1}{f_s}\right) \quad \dots(2.51)$$

where  $M_1$  is an integer and the conditions discussed in this section enforced.

The frequency domain equivalent of equation (2.51) is,

$$S_{PCM}(f) = f_s \cdot \sum_{M_1=-\infty}^{+\infty} S_1(f - M_1 f_s) \quad \dots(2.52)$$

Thus, once the spectrum of  $S_1(t)$  is known, the P.C.M. spectrum can be calculated from the convolution in equation (2.52).



$A(f)$ ..... Base-band signal spectrum.

Fig.2-10. Pulse-amplitude modulation.

Quantisation levels.

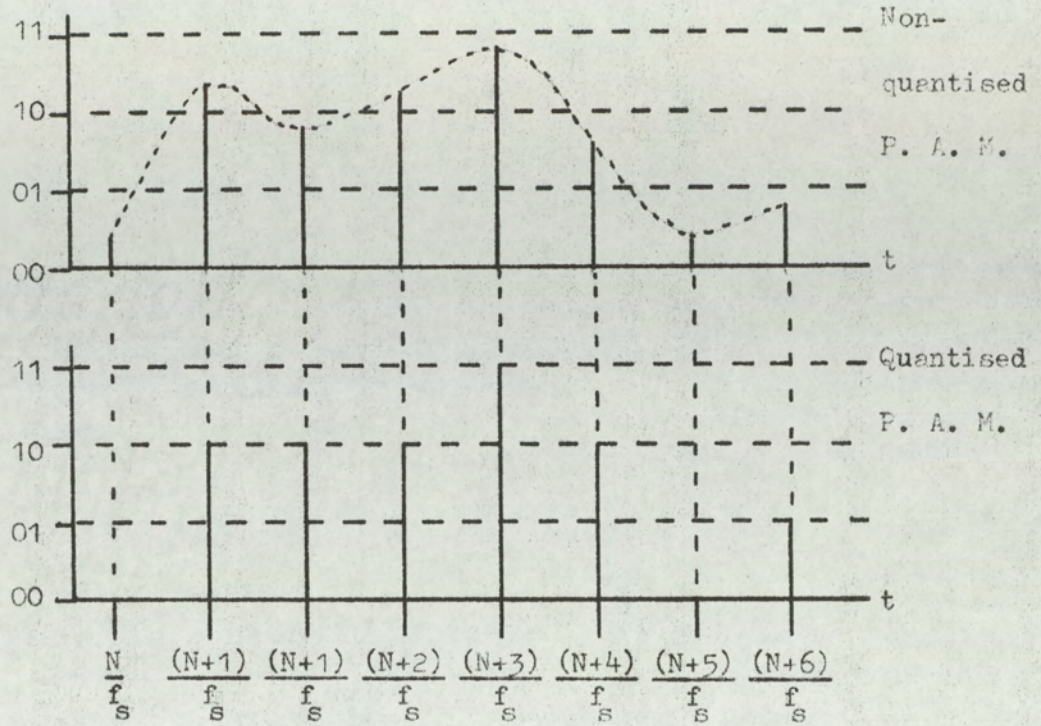


Fig.2-11 Quantisation of P.A.M. signal and allocation of binary numbering to quantisation levels.

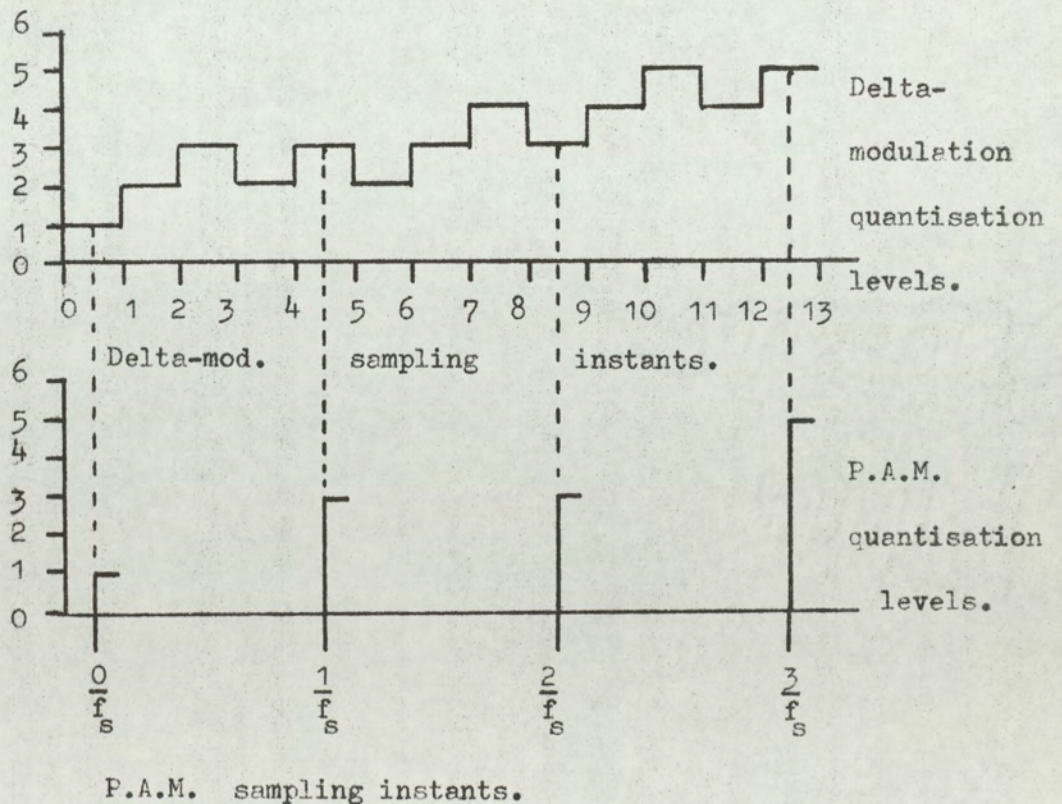


Fig.2-12. Extraction of quantised P.A.M. signal from quantised delta-modulated signal.

## 2.6 General methods of producing delta-modulator and delta-sigma modulator encoders.

There are five basic methods by which a delta-modulator digital-encoder pulse sequence may be generated:

1. Use of analogue networks in the closed loop of a delta-modulator.
2. Non-recursive filter to simulate a passive, finite-memory, feedback network.
3. Use of a logical up/down counter and digital to analogue converter in the feedback path.
4. Equivalent open-loop model, (this is the subject of chapter 3).
5. Digital computer simulation of delta-modulator encoding systems.

The above processes are closely related, since basically they perform the same functions; however, each has advantages and disadvantages. The following three sections are concerned with methods 1, 2 and 3 respectively. Method 4 is the subject of chapter 3. Method 5 is not discussed in this chapter, since this is a function of programming technique, where the program could simulate the methods 1, 2, 3, 4. Examples of computer simulation of adaptive delta-modulators are given in chapter 10.

2.7 Analogue networks in the closed loop of delta-modulators and delta-sigma modulators. (25, 43, 44)

With an analogue network in the forward or the feedback path of a delta-modulator, the encoding performance depends upon the modulator parameters. Such parameters are: precision of pulse generation, pulse jitter, noise, and loop delays caused by instrumentation defects and non-perfect components.

In a typical analogue feedback delta-modulator, the basic loop operations are:

1. Linear subtraction.
2. Signal comparison.
3. Single-bit storage and clocking.
4. Pulse generation.
5. Processing by transfer function.

The main sources of error in the modulator loop are threshold effects and response times of the comparator, together with the delay and finite rise-time of the one-digit clocked store. When signal comparisons are made near the threshold of the comparator, the comparator response time may be extremely slow, thus introducing considerable propagation delay. If the comparator exhibits hysteresis effects, this can also modify the response.

The rise and fall times of the one-digit store are also finite. Thus, when a sequence of, say, 'one' pulses is generated, the pulses containing the rising and falling

edges will have non-optimum weighting. This is illustrated in Fig. 2.13. The area under the first and fourth pulse can be seen to be in error; when they are applied to the transfer function, they will generate a non-optimum response. Two possible rise and fall-time waveforms are illustrated.

Because of the accumulated delays around the loop, due to the non-ideal network elements, to generate ideally a quantisation level requires a time greater than the sample duration. This delay produces an excess redundancy in the encoding process, which rises as the delay-time/sample period ratio increases.

Assume that the excess loop delay time is  $T_D$ . This delay may be inserted in the quantisation-error signal path. Fig. 2.14 shows such a modulator and indicates the basic limitations imposed by the comparator and loop delays. In this system, comparisons made at a time  $T_D$  or less before the  $(N+1)$ th sample will not be detected at the  $(N+1)$ th sample. Thus, the error signal rises to a value  $E_2$  at the  $(N+2)$ th sample and the quantisation error is greater than one step height. The excess error which can occur is approximately  $P.T_D$ . In practice, the excess error can take any value between zero and  $P.T_D$ . However, there is also a probability of the excess error occurring which depends on the ratio of  $T_D$  to  $1/P$ , i.e.  $P.T_D$ . Thus, for an excess loop delay time  $T_D$ , it is reasonable that:

$$\text{Excess error} = f(P.T_D), \quad \dots(2.53)$$

Hence, for efficient encoding with the analogue feedback network, the product  $P.T_D$  must be kept small. This excess delay becomes a severe problem when encoding video waveforms, since the sample duration is as small as 10 nanoseconds. Hence, with the analogue encoder, it is difficult to maintain efficient encoding at high speed.

The excess delay also limits the type of network that can be used in the closed loop, since stability problems arise. It will be shown that a single integrator with 100% duration pulses is just on the limit of stability, for efficient encoding, (see section 4.7).

Analogue memories, although susceptible to propagation delays inherent in the closed loop, have the basic advantage of simplicity. It is possible to use digital integrators in a delta-sigma modulator if the modulating signal is pre-processed by an integrator before delta-modulation. However, the d.c. stability will be poor if a high signal-to-noise ratio is required at low frequencies. A delta-sigma modulator can be approached digitally by the use of algorithmic expressions, but such processes, though accurate, are relatively slow with the present generation of digital computers.

Thus, the analogue encoder, shown in Fig. 2.15, offers an inexpensive practical modulator, where deviation from the ideal, though not desirable, may be acceptable.

Since the thesis concerns high-speed analogue-to-digital conversion for video applications, only single-integration networks are considered. This is because

higher-order systems introduce increased phase shift. This, together with inherent instrumental loop delays, makes the stability margin indeterminate and possibly erratic, leading to inferior encoding. Finite pulse rise times together with distributed stray capacitance in the modulator can also make performance unpredictable.

As the integration process tends towards a perfect integrator, the low-frequency encoding accuracy is improved and the modulator can respond to very low-frequency changes of small magnitude. The integration process can be approached from an operational amplifier network as described in relation to Fig. 2.3, A, B. However, such a system requires a high-frequency amplifier with high gain; this introduces its own characteristic defects, such as possible ringing and delay and so tends to introduce a higher-order response. An ideal integrator is shown in Fig. 2.16. This can be approximated in practice and designed to produce only a small delay.

In the delta-sigma modulator, the difference between modulating signal and pulse output signal is summed by the integrator, so that the sum of the differences is continually minimised by the action of the delta-modulator loop. If the current,  $i_c$ , is proportional to the difference signal  $\{M(t) - P_1(t)\}$ , then the capacitor voltage  $v_c$  represents the desired summation by continual integration.

The integrator of Fig. 2.16, produces an output voltage  $v_c$ , given by:

$$v_c = \int_{-\infty}^t i_c \cdot dt \quad \dots(2.54)$$

The integration process may be developed using basically three unidirectional current-sources, shown in Fig. 2.16, thus providing push-pull operation when charging the capacitor C. The value of C is chosen to be a compromise between the maximum voltage swing of the integrator and the threshold sensitivity of the comparator. In Fig. 2.17, one current source is switched on and off, corresponding to the state of the output of the delta-modulator; the other two produce the bi-directional modulating current required for integration.

Let:  $M(t)$ , be the normalised modulating signal of a delta-sigma modulator, such that,

$$|M(t)| \leq 1.$$

$I_p$ , current proportional to the state of the one-bit store, corresponding to  $P(t)$ , such that,

$$I_p = \bar{I}_p, \text{ when } P_1(t) = 1.$$

$$I_p = 0, \text{ when } P_1(t) = 0.$$

$I_m$ , is a constant of proportionality forming the mean current to be modulated by  $M(t)$ .

$I_k$ , is a constant current, since the total modulated current,  $\{M(t) \cdot I_m + I_k\} \geq 0$ .

$I_s$ , is a constant current to a sink to provide a push-pull current drive to the capacitor C.

The capacitor current,  $i_c$ , is thus:

$$i_c = \{M(t) \cdot I_m + I_k\} - I_p - I_s, \quad \dots(2.55)$$

When  $M(t)=0$ , the current  $i_c$  is equal and opposite depending on the state of  $I_p$ , i.e.:

$$I_p = \bar{I}_p, \quad \text{then } i_c = I_{c+},$$

$$I_p = 0, \quad \text{then } i_c = I_{c-},$$

and  $M(t)=0$  requires:

$$\{I_{c+}\} = -\{I_{c-}\},$$

Hence, equating  $(I_{c+})$  and  $-(I_{c-})$  in equation (2.55), when  $M(t)=0$ , gives:

$$(I_k - \bar{I}_p - I_s) = -(I_k - I_s)$$

Therefore,

$$(I_s - I_k) = \frac{\bar{I}_p}{2}, \quad \dots(2.56)$$

The absolute values of  $I_k$  and  $I_s$  are immaterial, providing that  $I_s$  and  $I_k$  are positive. However, their difference is given by equation (2.56). The condition  $I_k=0$  could be imposed, but this would require the circuits to operate linearly down to zero current and would leave no margin for drift.

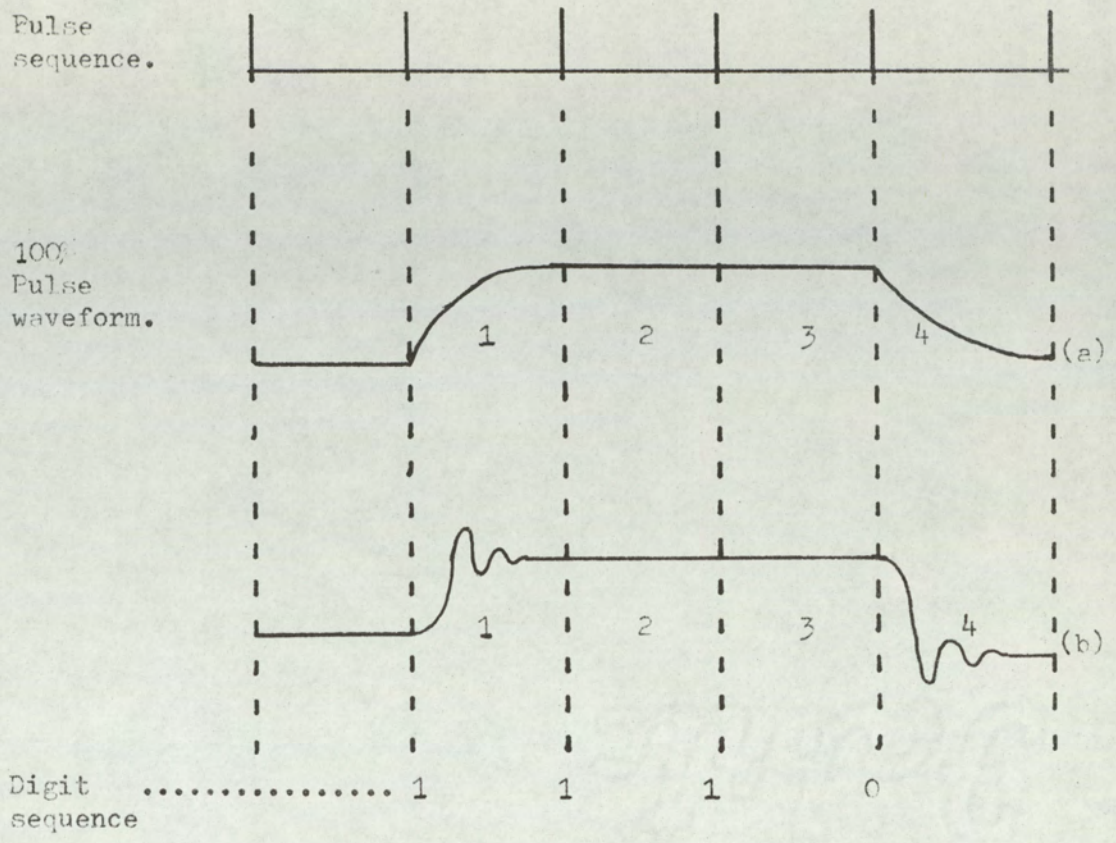


Fig.2-13. Non-optimum pulses in analogue network, closed-loop

delta-modulator.....(a) damped rise and fall,  
 (b) underdamped rise and fall.

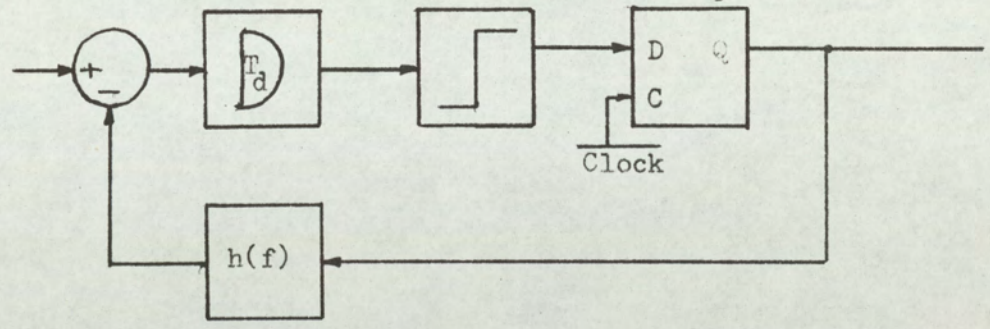


Fig.2-14(a).

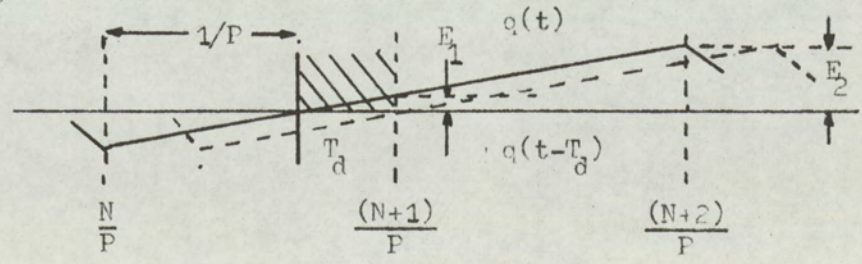


Fig.2-14(b).

Fig.2-14(a) Delta-modulator with lumped-loop delay.

Fig.2-14(b).Effects of delay time on pulse generation.

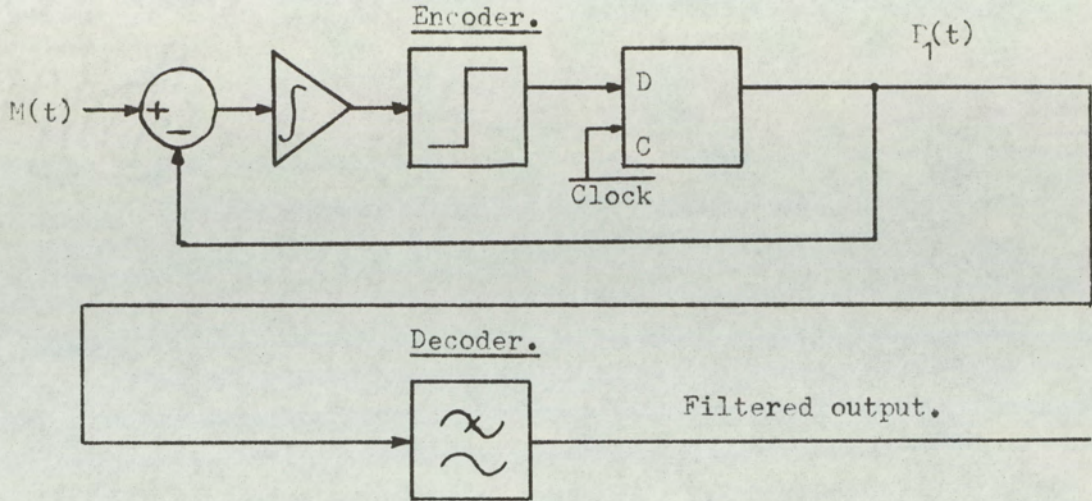


Fig.2-15. Basic single-integration delta-sigma modulator.

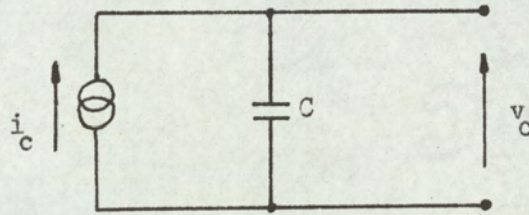


Fig.2-16. Ideal basic integrator.

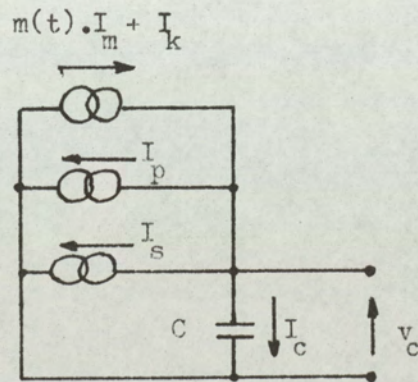


Fig.2-17. Three current source, push-pull integrator.

2.8 Non-recursive digital filter as passive, finite-memory feedback network of a delta-modulator.

From the discussion of section 2.7, it is evident that any system which minimises the effects of excess loop delay, will reduce the encoding error. In the analogue system, the computations are distributed over the whole sample period. However, the processes are basically arithmetical and for the single integrator, the same response can be generated with a digital accumulator. If a digital process is derived which generates the equivalent output voltage  $S_1(t)$  at each sample instant and the computational time is less than the sample duration, then switching transients have time to decay and a comparator with a finite response time can be used. Thus, the performance should be accurate and predictable. The second objective is to maintain this encoding accuracy when the sample interval is as small as ten nanoseconds. In digital systems, it is usually possible to design circuitry without capacitors; thus systems can be produced in integrated form.

The digital system to be discussed in this section is capable of extremely high pulse rates and uses a non-recursive filter to synthesise the store response. Fig. 2.18 illustrates the basic schematic of a non-recursive filter that is suitable for use in a delta-modulator.

The non-recursive filter consists of a simultaneously-clocked shift register. Each element of the register is

clocked at the pulse rate  $P$  (P.P.S.) of the delta-modulator. Thus the pulses produced at the output of the delta-modulator,  $P_1(t)$ , are stored as they are progressively shifted down the register at the system clock rate. Finally, the pulses are 'forgotten', when they have been shifted by the length of the register; hence the limited memory. Each stage of the register produces an output level, which remains constant over a period equal to the clock duration. The output signals of the shift register stages are weighted by coefficients and then summed to form the integrated signal  $S_1(t)$ . The magnitude of  $S_1(t)$  depends on the state of the register. By suitable choice of the weighting coefficients, the filter can produce a signal approximately equal to the sampled and held response of an analogue integrator. The operation of the delta-modulator is, in other ways, identical to the analogue system; the digital system replaces the analogue network.

The non-recursive filter can only synthesise responses that are convergent. The impulse response of an RC integrator is convergent and can therefore be synthesised. The number of elements in the register must be finite and consequently there is a truncation error. Providing that the RC response is simulated for a duration of  $5RC$ , then the truncation error is negligible. A basis for the determination of the coefficients in the filter may be established as follows:

The shift register in Fig. 2.18, is capable of propagating a two-level signal that changes at the delta-

modulator clock rate. The same signal distribution could be realised by propagating signal  $P_1(t)$  down linear delay lines, with incremented delays,  $\frac{1}{P}$ ,  $\frac{2}{P}$ ,  $\frac{3}{P}$ , etc.

The digital filter may therefore be calculated in terms of an array of linear delay lines, where the driving function is digital. Fig. 2.19 illustrates the proposed model.

The time response of the above filter to an input pulse sequence  $P_1(t)$  is defined at the sampling instant as:

$$S_1(t) = \sum_{N=0}^{M_s} a_N \cdot P_1\left(t - \frac{N}{P}\right), \quad \dots(2.57)$$

where,  $N$  and  $M_s$  are integers and  $M_s$  is the number of stages in the delay array.

$$\text{Let } P_1(t) = \delta(t),$$

$$\text{Therefore } S_1(t) = \sum_{N=0}^{M_s} a_N \cdot \delta\left(t - \frac{N}{P}\right), \quad \dots(2.58)$$

Equation (2.58) represents the sampled impulse response of the non-recursive filter. The impulse response of the passive RC network when the same magnitude impulse is applied to the input, is:

$$S_{RC}(t) = e^{-t/(RC)},$$

where,  $S_{RC}(t)$  is the impulse response. The signal  $S_{RC}(t)$  is evaluated only at the sampling instants. Thus when  $S_{RC}(t)$  is modulated by the delta sifting function:

$$S_{RC}(t) \Big|_{\text{SAMPLED}} = \sum_{N=0}^{\infty} e^{-N/(PRC)} \cdot \delta\left(t - \frac{N}{P}\right) \quad \dots(2.59)$$

Equating the coefficients of equations (2.58) and (2.59) and introducing a scaling factor ( $S_f$ ) gives:

$$a_N = (S_f) \cdot e^{-N/(PRC)} \quad \dots(2.60)$$

In the practical filter, the number of delay increments is finite,  $M_s$ ; thus there are only coefficients evaluated from equation (2.60) up to  $a_{M_s}$ . These coefficients are related to the impulse response of the RC integrator, as shown in Fig. 2.20.

The truncated response of the non-recursive filter is represented by:

$$S_{RC}(t, M_s) = \sum_{N=0}^{M_s} e^{-N/(PRC)} \cdot \delta(t - \frac{N}{P}), \quad \dots(2.61)$$

Since it is required that the impulse response of the network is convergent, the response contains only finite energy. Thus, as  $t \rightarrow \infty$ , mean square terms tend to zero. To obtain a figure of merit for the truncated response, the total error energy to total impulse-response energy ratio is calculated for a single impulse response.

The total impulse response energy obtained from equation (2.59), is:

$$\begin{aligned} \text{Total impulse response energy} &= \sum_{N=0}^{\infty} e^{-2N/(PRC)} \cdot \delta(t - \frac{N}{P}) \\ &= \frac{1}{\{1 - e^{-2/(PRC)}\}} \end{aligned}$$

The total error energy, when the impulse response is truncated after  $M_s$  terms is given by:

$$\text{Error energy} = \sum_{N=M_s}^{\infty} e^{-2N/(PRC)} \cdot \delta(t - \frac{N}{P})$$

$$= \sum_{N=0}^{\infty} e^{-2N/(PRC)} \cdot \delta\left(t - \frac{N}{P}\right) - \sum_{N=0}^{M_s} e^{-2N/(PRC)} \cdot \delta\left(t - \frac{N}{P}\right)$$

Therefore,

$$\text{Error energy} = \left[ \frac{1}{\{1 - e^{-2/(PRC)}\}} - \frac{e^{-2(M_s+1)/(PRC)}}{\{1 - e^{-2/(PRC)}\}} \right]$$

Therefore,

$$\frac{\text{Error energy}}{\text{Total energy}} \Bigg|_{\substack{\text{Impulse} \\ \text{Response}}} = \{1 - e^{-(2)(M_s+1)/(PRC)}\} \dots (2.62)$$

$$\text{Ideally, } \frac{2(M_s+1)}{P} \geq 5(RC),$$

Therefore,

$$M_s \geq \left\{ \frac{5 \cdot (PRC) - 1}{2} \right\}. \dots (2.63)$$

Using the criterion of condition (2.63), a large number of store elements in the shift register would result. Hence, for a practical system, a modified response with fewer storage elements would be necessary. The scope of this system approach is considerable as a method of generating high-speed delta-modulation.

The feasibility of the non-recursive filter has been checked by digital simulation on a computer. This is discussed in chapter 10.

The non-recursive filter allows a second-order response to be introduced without the inherent loop-delay problems. However, such procedures require considerable analysis, especially because of truncation errors. Moreover the truncation error must at all times be small in comparison to the step height, even on the extremes of the dynamic range.

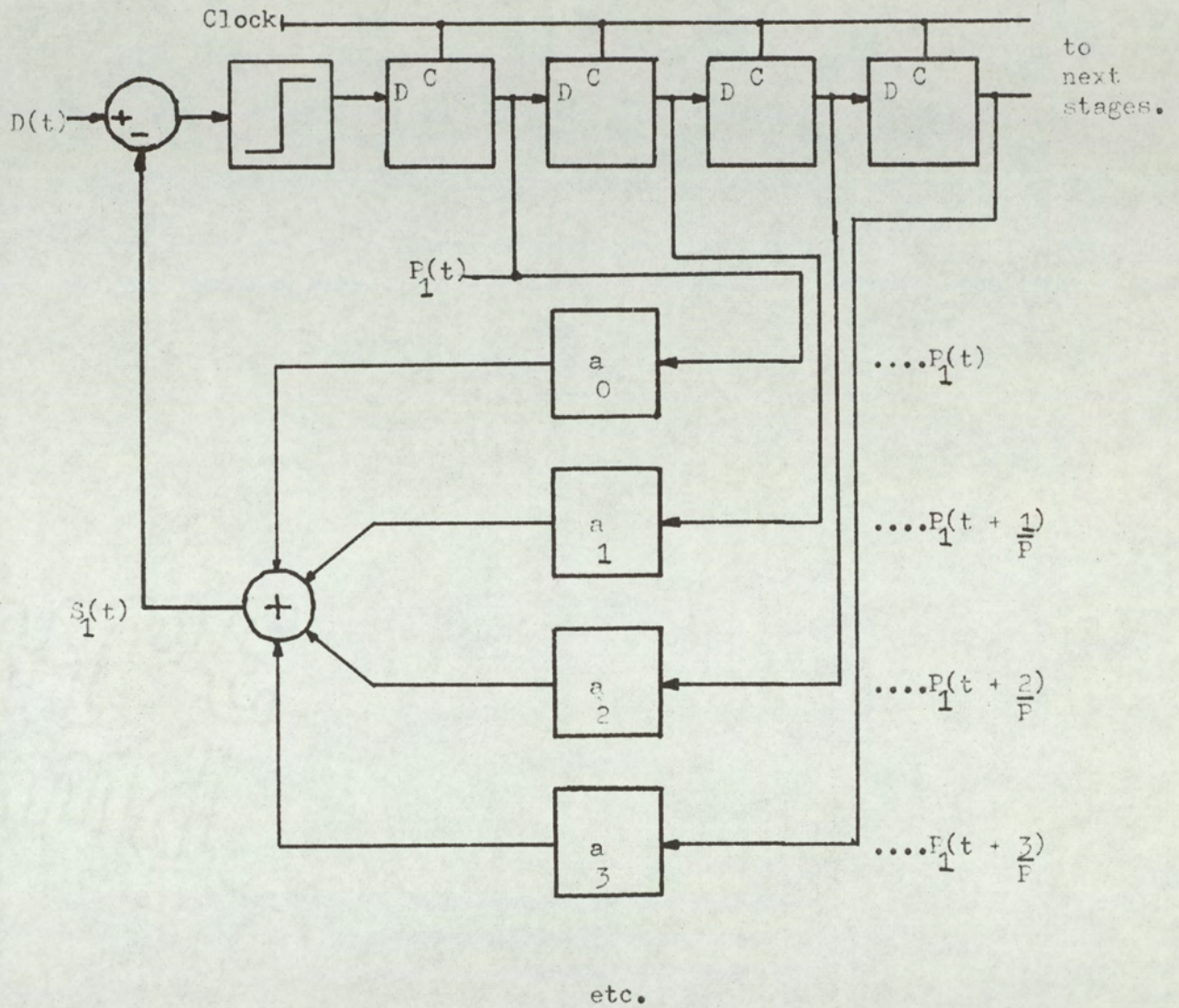


Fig.2-18. Non-recursive filter used in the feedback path of a delta-modulator to simulate analogue store.

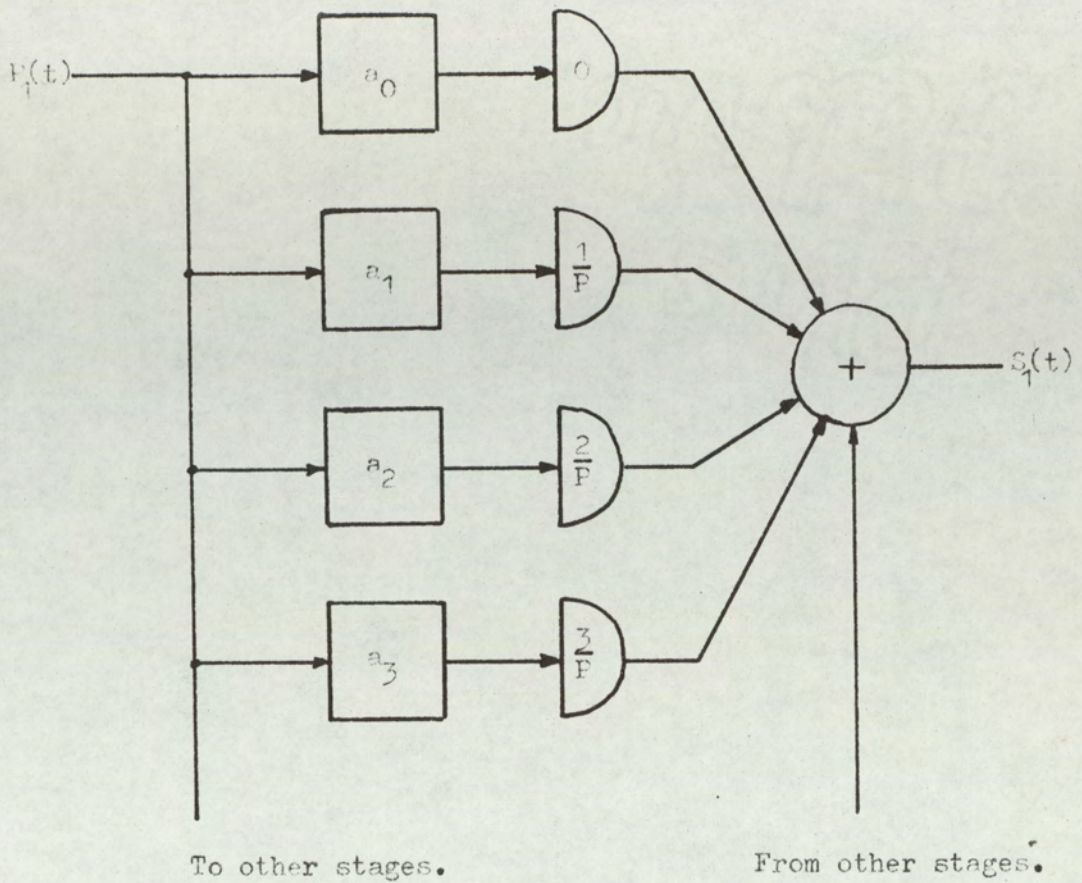


Fig.2-19 Linear delay-line equivalent of digital non-recursive filter.

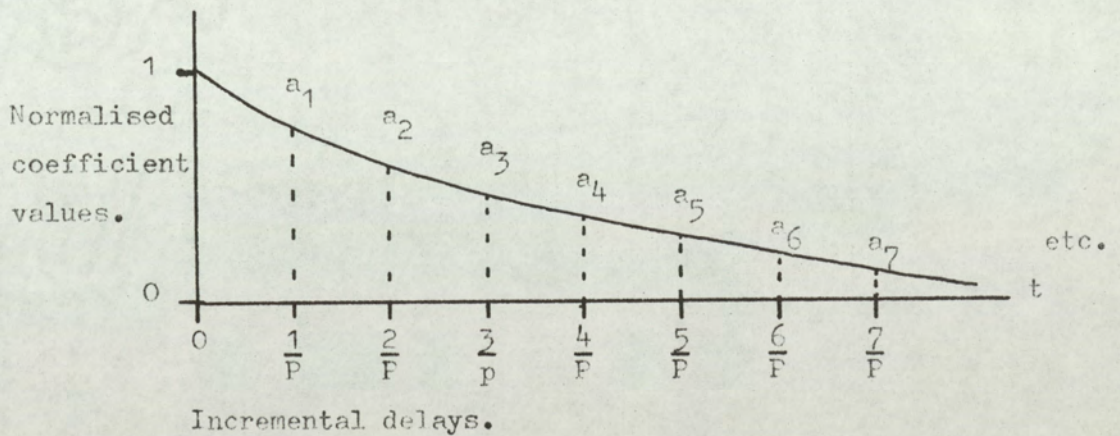


Fig.2-20 Relation of coefficients  $a_N$  to normalised impulse response of RC filter.

2.9 Up/down counter and digital to analogue converter to synthesise ideal single-integrator response.

An alternative digital method for generating delta-modulation pulse waveforms, is a system using an up/down counter and a digital-to-analogue converter in the feedback loop as shown in fig. 2.17. This method provides a more efficient store capacity, since it can operate on binary codes, thus requiring less circuitry. The system simulates a constant quantisation step modulator. However, because the store has finite capacity, the dynamic range is limited by the store capacity. Consequently, to extend the dynamic range, a greater store capacity is required.

In this system, the output pulse sequence is applied to the up/down counter, such that,

$$\begin{aligned} P_1(t) &= 1 && \text{Counter counts up on the clock.} \\ P_1(t) &= 0 && \text{Counter counts down on the clock.} \end{aligned}$$

The binary store output is converted by a high-speed digital to analogue converter to the integrated pulse output signal  $S_1(t)$ .

There are two basic methods in which the digital integrator may be connected into the loop of the delta-modulator. The comparator output can feed directly onto the up/down counter, to control the direction of the count at the clock pulse. However, the comparator cannot reach a final decision until the counter and digital to analogue

converter have reached their final state; only then can a decision be made as to the next count direction. Since the counter requires directional information in advance of the clock pulse, due to the logical function in the counter, a late comparator decision may not be detected in time for the next clock pulse; this is particularly likely in high speed systems.

Since the response of a one-digit store, typically a 'D' type bistable, is much faster than the input logic of an up/down counter, a single-bit store may be interposed between counter and comparator. The response of the one-bit store is fast and it produces the required pulse waveform  $P_1(t)$ , at its output. Its introduction also allows nearly a whole sampling period, under all conditions, for the up/down counter to reach a directional count decision.

The output,  $Q_1$ , of the one-bit store is applied to the digital-to-analogue converter and is given a weighting of 2 units, where the weighting of the least significant digit of the counter is 1 unit, the rest being scaled on a binary basis. This weighting of the one-bit store is necessary, since the counter direction always lags behind the one-bit store by a clock period. Thus when  $Q_1$  changes, the counter change at that instant is always opposite, thus to give a step height in the direction indicated by the one bit store, the weighting on  $Q_1$  is twice that of  $Q_2$ .

Thus assuming a normalised step height and that the  $Q$ 's take values of  $\pm 1$ , then:

$$S_1(t) = 2 \cdot Q_1 + 2^0 \cdot Q_2 + 2^1 \cdot Q_3 + 2^2 \cdot Q_4 + \dots + 2^{(N-2)} \cdot Q_N,$$

$$\text{i.e. } S_1(t) = 2 \cdot Q_1 + \sum_{N=2}^N Q_N \cdot 2^{(N-2)}, \quad \dots (2.64)$$

where,  $N$  is the number of parallel digit channels to the digital-to-analogue converter.

In this system, it is necessary to limit the count in the positive and negative directions to prevent the counter recirculating at the extremes of the dynamic range and thus producing an erroneous output. The method cannot realise the full potential of a delta-modulator due to the finite store capacity. However with sufficient stages, adequate low-frequency dynamic range is obtainable.

The method of encoding delta-modulation with this type of digital integrator may be applied to the encoding of a P.C.M. system. In section (2.5), the relationship between delta-modulation and P.C.M. was discussed. Since this encoder produces a binary number, delayed by one clock period, at each delta-modulation sample, this number may be sampled at the P.A.M. sampling rate, suitable for a P.C.M. system, and with the conditions of equation (2.50) enforced. Each sample is in the required digital format, and may be placed in a register and shifted into the digital channel over the next P.A.M. sample period. Hence, a P.C.M. encoder is realised.

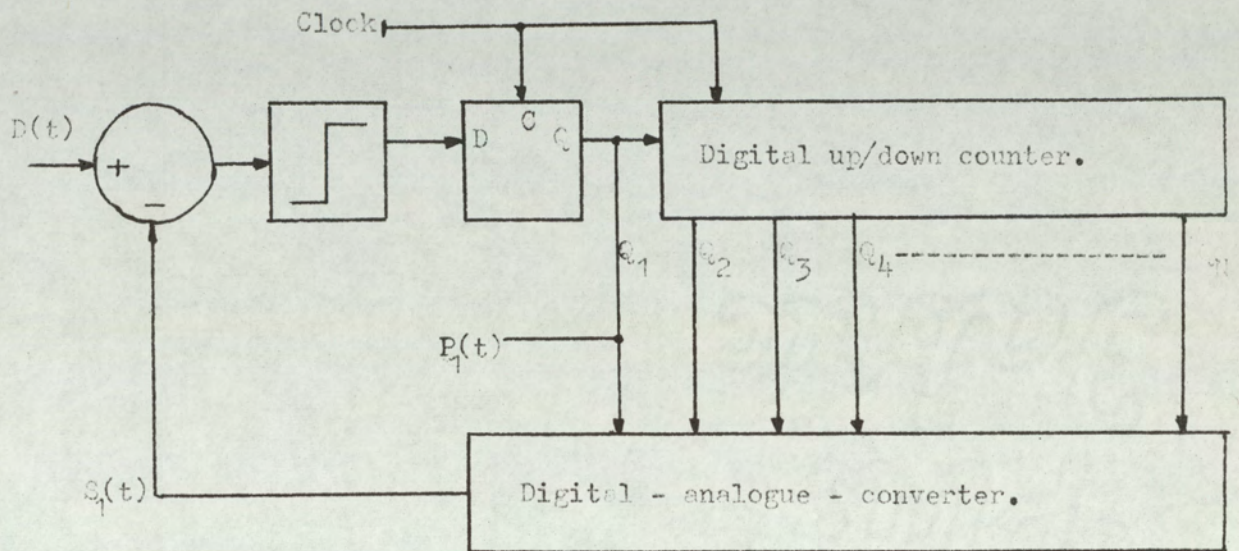


Fig.2-21.

Digital store delta-modulator using up/down counter and digital -to - analogue converter.

2.10 An approximate noise analysis for single integration delta-modulation. (8, 17, 19)

The quantisation error signal,  $q(t)$ , is defined as the difference between the modulation signal and the reconstructed signal. The point at which the quantisation error is measured depends upon whether the encoder pulse output is considered as a sequence of  $\delta$  pulses or as a sequence of finite amplitude and duration rectangular pulses. For the  $\delta$  pulse sequence, the error signal is measured at the instant just after sampling. Providing that there is perfect system operation with no effects from loop delay, then the error at this instant is within  $\pm h$  where  $h$  is the step height of the single-integration delta-modulator. This error voltage can be sifted from the encoder by the  $\delta$  sampling function, the phase of which is adjusted so that the sifting occurs at a time  $t_N$ , defined by equation (2.11). The error signal is therefore a sequence of weighted  $\delta$  pulses with a period of  $(1/P)$ , where  $P$  is the delta-modulator p.r.f. If the assumption is made that zero correlation exists between the modulating signal and the quantisation error signal, and that the value of each error pulse has equal probability over a range  $-h$  to  $+h$ , then it is possible to calculate a mean square value for the error pulses, in terms of its maximum value,  $h$ .

The probability distribution and density functions are therefore linear and of the form as shown in Fig. 2.22;

the functions are respectively  $P_D(q)$ ,  $P_D(q)$ .

For these functions

$$\text{mean} = \int_{-h}^{+h} \frac{x}{2h} \cdot dx = 0 \quad \dots(2.65)$$

$$\text{variance} = \int_{-h}^{+h} \frac{x^2}{2h} \cdot dx = \frac{h^2}{3} \quad \dots(2.66)$$

For a stationary process, the variance is equal to the mean square value of the pulse height distribution, thus

$$\text{mean square value} = \frac{h^2}{3} \quad \dots(2.67)$$

If a sequence of  $\delta$  pulses weighted by  $(h^2)/3$  is compared to the random quantisation error pulses, both sequences will generate the same power.

In a delta-modulator using 100% duration pulses and analogue single integration, the quantisation error waveform is nearly triangular, providing changes in signal slope over a sample period is small. Fig. 2.23 shows a weighted- $\delta$ -quantisation error-pulse waveform with the peaks of the error pulses joined by straight lines to form the error signal of the delta-modulator.

Consider a general sample interval  $\frac{N}{P}$  to  $\frac{(N+1)}{P}$ . The line joining the peaks of the  $\delta$  error pulses are shown at these samples as  $h_1$ ,  $h_2$ . The slope of the line is given by,

$$\begin{aligned} \text{Slope} \left| \begin{array}{l} \frac{(N+1)}{P} \\ \frac{N}{P} \end{array} \right. &= \left\{ \frac{h_2 - h_1}{\frac{(N+1)}{P} - \frac{N}{P}} \right\} \\ &= P \cdot (h_2 - h_1) \end{aligned}$$

A rectangular pulse of amplitude  $(h_2-h_1)$  and duration  $(1/P)$  when integrated with a time constant  $(1/P)$  would generate the required slope  $P.(h_2-h_1)$ .

Thus, by taking the difference between two adjacent  $\delta$  error pulses to give a  $\delta$  pulse of  $(h_2-h_1)$  weighting the difference pulse can be integrated with unit-time constant. By using a delay, a pulse of amplitude  $(h_2-h_1)$  and duration  $(1/P)$  is produced. The method is repeated for all adjacent points of error pulses, and the triangular error function obtained.

Fig. 2.24 shows a network that produces the triangular waveform by generating the linear inter-sample function for an input of error  $\delta$  functions.

The triangular converter has a transfer function  $T_e(f)$ , where,

$$\begin{aligned} T_e(f) &= \{1 - e^{-j2\pi f/P}\} \cdot \left\{ \frac{1}{j2\pi f} \right\} \cdot \{1 - e^{-j2\pi f/P}\} \left\{ \frac{P}{j2\pi f} \right\}, \\ &= \frac{-P}{4(\pi f)^2} \cdot \{1 - e^{-j2\pi f/P}\}, \end{aligned}$$

Therefore

$$T_e(f) = \frac{e^{-j\pi f/2P}}{P} \cdot \left\{ \frac{\text{Sin}(\pi f/P)}{(\pi f/P)} \right\}^2 \quad \dots(2.68)$$

$T_e(f)$  allows the frequency response of the noise to be determined when the quantisation error function assumes a triangular form.

The total mean power dissipated by the triangular waveform can be determined without integrating the power spectrum (obtained from a knowledge  $T_e(f)$  and the input quantisation error function).

Statistically it has been shown that the mean square value of quantisation error pulses is  $(h^2/3)$ . Thus, the

random-error sequence having an infinite range of values over  $-h$  to  $h$ , has been reduced to a random two-level sequence where the pulses are equally  $-h/\sqrt{3}$  or  $h/\sqrt{3}$ . The random two-level signal in terms of the triangular waveform, can generate four basic waveforms, each of which is equally probable. Fig. 2.25 illustrates these four basic waveform.

Assume that the triangular waveforms nos. 1 to 4 are equally probable when generated from a random two-level error function of value  $h/\sqrt{3}$  or  $-h/\sqrt{3}$ . The mean power in the triangular wave can be calculated using the above waveforms and the equi-probable distribution of the waveforms.

For the power evaluation, only two waveforms need be considered. Thus, the mean power can be calculated using the waveform shown in Fig. 2.29.

$$\text{mean power} = \frac{P}{2} \left[ \int_0^{1/P} \left( \frac{2h}{\sqrt{3}} P \cdot t - \frac{h}{\sqrt{3}} \right)^2 dt + \int_{1/P}^2 \left\{ \frac{h}{\sqrt{3}} \right\}^2 dt \right]$$

Therefore,

$$\text{mean power in triangular waveform} = \frac{2 \cdot h^2}{9} \quad \dots (2.69)$$

Now consider the power in the sequence of random  $\delta$  quantisation error pulses, i.e. the true error waveform. The mean square value of the error waveform is  $h^2/3$  and its repetition frequency is  $P$ . Thus,

$$\text{total mean power of random } \delta \text{ function} = P \cdot \frac{h^2}{3},$$

The power spectrum of the random sequence is given by  $P_T(f_0)$  and, since the random  $\delta$  sequence has a flat

energy distribution,

$$\text{then } P_T(f_0) = \frac{P \cdot h^2}{3} \cdot T_e(f_0) \cdot T_e^*(f_0) \cdot \delta(f - f_0).$$

Substituting for  $T_e(f_0)$  from equation (2.68) gives:

$$P_T(f_0) = \frac{h^2}{3 \cdot P} \cdot \left\{ \frac{\text{Sin}(\pi f/P)}{(\pi f/P)} \right\}^4 \cdot \delta(f - f_0). \quad \dots(2.70)$$

In equation (2.70) the power/frequency distribution, follows a form,  $\left\{ \frac{\text{Sin}x}{x} \right\}^4$ . This function is illustrated in Fig. (2.27).

In a typical application, a ratio of about 1:9 between highest modulating frequency and clock rate can be considered a maximum. Thus, the power density up to  $\pi/9$  can be represented to a good approximation by a line of slope  $K_1$ . By assuming a sharp cut off at a frequency  $f_k$  it is possible to represent the power spectrum by a trapezoidal distribution, for which the power density over the baseband frequencies is approximately that of the  $\left\{ \frac{\text{Sin}x}{x} \right\}^4$  distribution.

Since the one-sided power spectrum only is considered, the total power in the positive half is calculated from equation (2.69) as,  $\frac{1}{2} \cdot \left\{ \frac{2h^2}{9} \right\}$ .  
Therefore, Power in positive half of spectrum =  $\frac{h^2}{9}$ .

Assume this power to be contained in the trapezoidal distribution, the trapezoidal cut off frequency being  $f_k$  and the slope being  $K_1$ . Thus:

$$\frac{h^2}{9} = \frac{h^2}{3P} \left\{ \frac{1}{2} (1 + (1 - K_1 \cdot f_k) f_k) \right\},$$

Therefore,

$$f_k = \frac{1}{K_1} \left\{ 1 - \sqrt{1 - \frac{2K_1 P}{3}} \right\}, \quad \dots (2.71)a$$

$$\text{or, } f_k = \frac{P}{3} \quad \text{when } K_1 = 0 \quad \dots (2.71)b$$

It is sufficient to consider the case for  $K_1 = 0$  since the  $(\text{Sinx}/x)^4$  is approximately flat over the baseband regions.

If  $f_u$  is the upper frequency limit in the baseband, then Fig. 2.28 illustrates the approximate noise power distribution in the positive half of the power spectrum.

The total power in a band  $-f_u$  to  $+f_u$  is twice that of the power in the one-sided band as shown. Thus;

$$\begin{aligned} \text{Total noise power } N_p &= 2 \cdot \frac{f_u}{P} \cdot \frac{h^2 \cdot P}{3P \cdot 3}, \\ &= \frac{2}{3} \cdot \frac{f_u}{P} \cdot h^2, \end{aligned}$$

Consider the case of a single sine wave of amplitude  $\overline{D}_f$

$$\text{where, } D(t) = \overline{D}_f \cdot \text{Sin}(2\pi ft).$$

The maximum value of  $\overline{D}_f$  for a frequency  $f$  is

$$\left| \frac{dD(t)}{dt} \right|_{\text{MAX}} = \overline{D}_f \cdot 2\pi f = h \cdot P$$

$$\text{Therefore, } h = \frac{\overline{D}_f \cdot 2\pi f}{P}$$

$$\text{If } S_p \text{ is signal power, where } S_p = \frac{\overline{D}_f^2}{2}$$

$$\text{Then } h^2 = 8\pi^2 \frac{f^2}{P^2} \cdot S_p$$

$$\text{Hence, } \frac{S_P}{N_P} = \left\{ \frac{3}{16 \pi^2} \right\} \cdot \frac{P^3}{f \cdot f_u} \quad \dots(2.72)$$

Equation (2.72) is the value of signal power to quantisation error power. Here, a value of total noise power of  $\left(\frac{h^2}{4 \cdot 5}\right)$  was assumed for the triangular error function. The analysis assumes that the signal to quantisation noise ratio is evaluated for frequencies well above the (possible) low frequency turnover of the integrator. For signals in the region of turnover or below, the noise becomes signal dependant since the step height is modulated. Also the increasing step becomes different from the decreasing step for signals removed from the mid-dynamic range region.

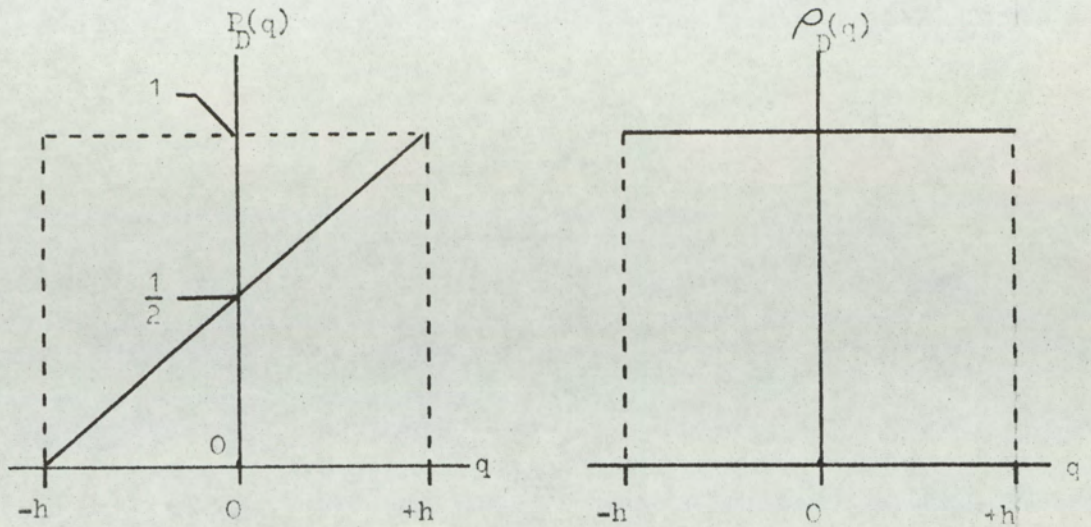


Fig.2-22. Probability distribution and density function assumed for quantisation error signal.

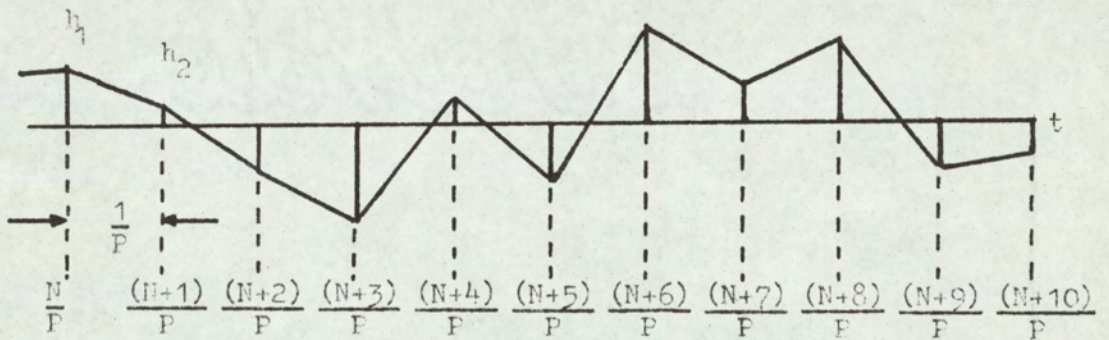


Fig.2-23. Quantisation error function with linear interpolation between sample peaks.

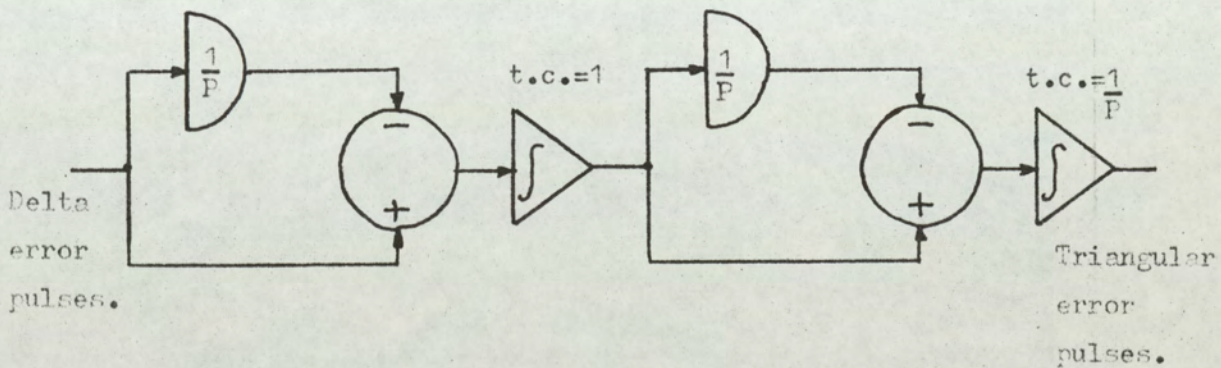


Fig.2.24. Delta-error pulse to triangular-error pulse converter.

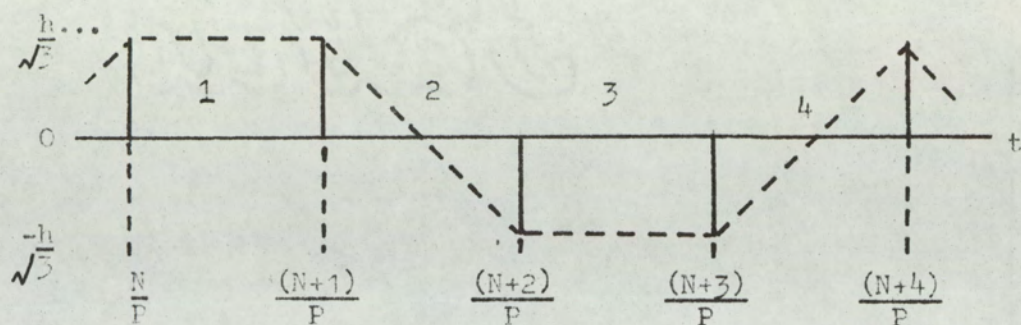


Fig.2.25. Four basic triangular waveforms.

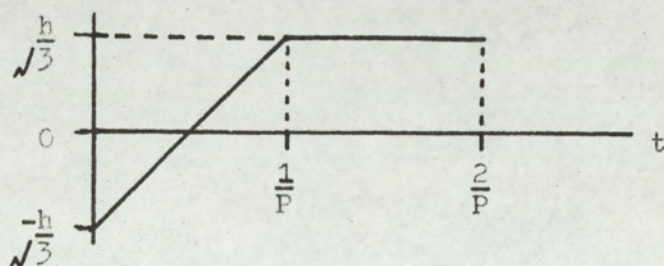


Fig.2.26. Waveform assisting mean-power calculation.

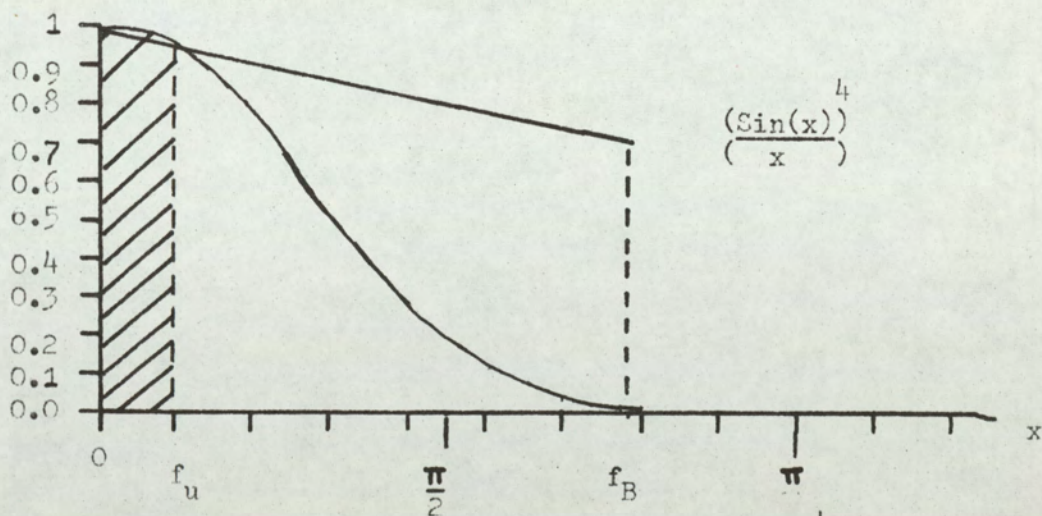


Fig.2.27. One-sided distribution of  $\left(\frac{\text{Sin}(x)}{x}\right)^4$  against  $x$  up to the first zero.

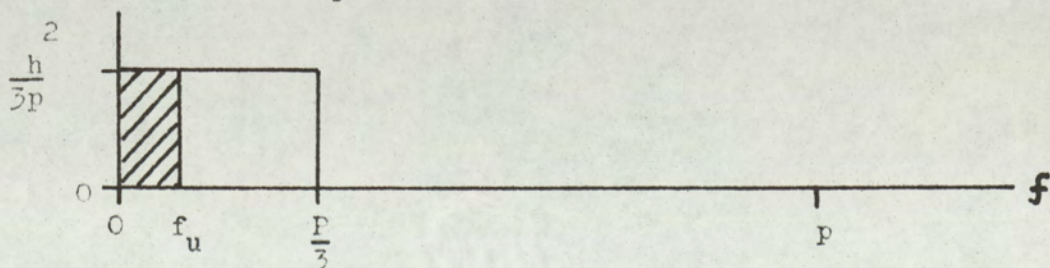


Fig.2.28. Assumed power distribution.

CHAPTER 3. ANALOGUE MODELLING OF DIGITAL SYSTEMS.

3.1 Introduction to concept of analogue modelling for delta-modulation. (4, 13, 14, 45, 46)

The concept of negative feedback has appeared to be a fundamental in digitally encoding an analogue signal using delta-modulation. In this system, decision making is judged on a direct comparison of a locally generated and stored signal with the analogue modulating signal. At each sample interval of the delta-modulator, a decision is made and the store updated accordingly. It will be shown that there is a class of store whose response can be exactly reproduced by an open-loop system. The open-loop model lends itself readily to analysis and will be shown to be applicable to several amplitude-quantised systems. In essence, the model transposes an amplitude-quantised system to a time-quantised system. In so doing, it reveals much detail about the noise structure of quantised systems.

Consider the operation of a single, ideal integrator, delta-modulator. For a constant level input, the output pulse waveform,  $P_1(t)$ , assumes the idling state, ...01010..., the repetition frequency of which is exactly one half the clock rate of the modulator, i.e.  $P/2$ . When the slope of the input signal increases positively, the rate of '1' pulses also increases. The rate of '1' pulses can increase until they occur at the clock rate  $P$ . Any further slope increase of the

modulating signal will not produce a further increase in pulse frequency; the modulator is then in a state of slope overload. The rate of '0' pulses for this modulating signal, however, falls from  $P/2$  to a limiting value, at slope overload, of zero. If the slope of the modulating signal is negative, then the converse applies. Thus the rate of '1' pulses decreases and the rate of '0' pulses increases. Therefore, the rate of '1' and '0' pulses is related to the slope of the modulating signal. In a delta-modulator, the position of '1' and '0' pulses are constrained to the clock sampling instants. Also, in a given time period the total number of '1' and '0' pulses is equal to the number of clock pulses in the period. This last constraint implies that, if the rate of '1' pulses increases, then the rate of '0' pulses must decrease, the sum of the two rates being a constant, i.e. the clock rate  $P$ .

It is possible to compare a delta-modulator to a phase modulator. A phase modulator is controlled by the rate of change of the modulating signal. With a constant level input, the output frequency is constant. As the slope of the modulating signal increases, the frequency of the phase modulator also increases. Similarly, for a negative slope the phase-modulator frequency decreases. For comparison, let the output frequency of the phase modulator be  $P/2$  for a constant-level modulating signal. It is apparent that the behaviour of the phase modulated carrier is similar to that of the rate of production of '1' pulses, since the frequency is also controlled by the slope of the modulating signal. To make the comparison

more rigorous, a reference point can be defined on the phase-modulated carrier. Initially it is assumed that the phase modulator modulates a sinusoidal carrier oscillating symmetrically about zero d.c. level. The reference point is defined as the zero crossing of the carrier having positive slope and will be referred to as 'the positive-slope-zero crossing', P.S.Z.C.

On comparison, the behaviour of '1' pulses of the delta-modulator can be seen to be very similar to the behaviour of P.S.Z.C.'s of the phase modulator, except that the position of the P.S.Z.C.'s is infinitely variable. The comparison becomes more accurate if the position of the P.S.Z.C.'s is restrained to specific time instants, such that their time positions coincide with the clock samples of a delta-modulator. The redistribution of the P.S.Z.C.'s introduces a time quantisation error.

It will be shown that, with suitable time quantisation of the P.S.Z.C.'s, a performance can be obtained identical to that of a delta-modulator. It was shown in section (2.5) that P.C.M. is closely related to delta-modulation. By using a similar comparison, it is possible to define a model which is capable of constructing the amplitude-quantised signals of a P.C.M. encoder/decoder system.

The delta-modulator, can be generalised to include RC integration and extended to include double-integration systems, though the latter requires the application of negative feedback. Finally, a practical implementation of the model is described and an application suggested for use in high-frequency delta-modulators.

In section (2.3) the relationship between delta-modulation and delta-sigma modulation was defined. A similar relationship can be defined for the model. By transposing the integrator in the model to the input, the system becomes frequency controlled. The frequency of the modulator is now related to the amplitude of the modulating signal. Thus, by replacing the phase modulator with a frequency modulator in the model, a delta-sigma model equivalent is produced.

A rigorous definition of the model will be described, together with a mathematical verification of equivalence.

### 3.2 Definition of basic model with assumptions.

Fig. 3.1 illustrates a general system for delta-modulation in which both a delta-modulator and delta-sigma-modulator are represented. The basis of the system is the central deltamodem which is capable of encoding an analogue signal using a single-integrator store, the integrator store also providing the local demodulated output, prior to final filtering.

With the switches  $SW_a$ ,  $SW_b$  in position 1, a delta-modulator is represented, while with the switches in position 2 a delta-sigma modulator is represented. It can be seen that both systems have a common modulator network; this is defined as the deltamodem. The integrators in the system are given a unit-time constant and the step height of  $S_1(t)$ , the store output, has a value 1. Hence, if the clock rate is  $P$ , then the maximum signal slope of  $D(t)$  is  $P$ .

The input to the delta-sigma modulator is defined  $M(t)$  where,

$$\left| \begin{array}{c} M(t) \\ \text{Max} \end{array} \right| = 1, \quad \dots(3.1)$$

For the sigma-entry signal to fully load the deltamodem, the signal  $D(t)$  must have a slope of  $P$  when  $M(t) = 1$ . Thus, since the integrator has a unit-time constant, the signal  $M(t)$  is multiplied by a factor  $P$ , to generate the required slope from the integrator output.

In a typical transmission system, the remote pulse signal  $P_1'(t)$  is not equal to the local pulse signal  $P_1(t)$  due to inevitable transmission errors. Thus, the model is only concerned with the local signal  $P_1(t)$  and the local store output  $S_1(t)$ .

Fig. 3.2 is the equivalent model of Fig. 3.1. The presentation is identical to the delta-modulator systems in that the switches  $SW_a$ ,  $SW_b$  select between the model for delta-modulation and the model for delta-sigma modulation. However, the deltamodem model equivalent is common to both the delta-entry and sigma-entry system. It is therefore only necessary to compare the deltamodem of Fig. 3.1 with the deltamodem model of Fig. 3.2.

In the theory it will be shown that  $P_1(t)$  corresponds to  $P_2(t)$  and  $S_1(t)$  corresponds to  $S_2(t)$ , the local signals of the pulse modulators.

The analysis is initially restricted to a single-integration system with delta pulse excitation, since this system can be shown to be fundamental to other variants of delta-modulation processes.

The proposed model for representing the deltamodem consists of the following functions:

- a) The input signal to the deltamodem model controls the phase of a sinusoidal carrier. The centre frequency, corresponding to a constant-level input, is set at exactly one half the delta-modulator clock rate  $P$ . The phase modulation is such that when the input signal slope extends to a magnitude

P, then the frequency deviation is  $P/2$ . This slope loading is consistent with a delta-modulator operating at clock rate P with a unit-step height, since for this system the maximum input slope is then P, after which slope overload occurs. The section is shown in Block A, Fig. 3.2.

- b) The phase-modulated carrier is converted to a naturally-sampled P.P.M. signal. This is achieved by two processes. First, the phase-modulated carrier P.S.Z.C.'s are detected, Block B of Fig. 3.2. The positions of the P.S.Z.C.'s then define the leading edge of a standard pulse which is generated by Block C of Fig. 3.2. The parameters of the standard pulse are such that the length is made equal to a clock period,  $1/P$  and the height is of magnitude 2 units. A d.c. level of unity magnitude is subtracted from the pulse waveform such that the resultant pulses swing from a level -1 to a level +1.
- c) The P.P.M. signal is now time quantised by "time-slotting". The time axis is divided into equally-spaced time slots of duration  $1/P$  occurring at a rate P, where P is the equivalent delta-modulator clock rate. If the leading edge of a standard pulse occurs within a time slot, then a '1' pulse is generated at the end of the time slot; if no leading edge occurs, then a '0' pulse is generated. Thus, a series of discrete pulses is generated. The method of deriving the time-quantised signal from a phase-modulated sinusoid is shown in Fig. 3.3.

The length of the standard pulse is made identical to the duration of a time slot; hence the length is  $1/P$ . If, now the leading edge of a standard pulse falls within a time slot, then the standard pulse is in a '1' state at the end of that time slot. The end of the time slot defines the sampling point in an equivalent delta-modulation process; thus the P.P.M. signal is sampled by a delta sampling pulse at this instant. If a standard pulse is present, then a  $+\delta$  output occurs. If no pulse is present, i.e. a leading edge has not occurred within the time slot, then the sample output is  $-\delta$ .

By these sub-systems, an output pulse waveform  $P_2(t)$  is generated which corresponds to the pulse waveform  $P_1(t)$ , where the position of the  $\delta$  sampling pulses coincide with the clock position of the delta-modulator.

Fig. 3.3. illustrates the processes of the delta-modem model.

To demonstrate equivalence, the following conditions and assumptions are imposed:

1. The integration processes are assumed ideal, so that there is no drift, and the step height is uniform over the operating dynamic range. This is valid, since digital integration can be performed to a high degree of accuracy. Also, it will be shown that the imperfect integrator response can be simulated by the perfect integrator with an external network.
2. In the delta-modulator of Fig. 3.1, the comparator performance is such that,

error signal  $> 0$ , comparator output high.

error signal  $< 0$ , comparator output low.

The comparator performance is considered perfect, having zero hysteresis and instant response time. Again in a digital system this can be achieved to a high degree of accuracy. In practice, however, comparator performance will be deficient and the self-correcting properties of the loop apply. It will be shown that with a storage time quantisation network the model has a similar correction procedure.

3. In the sampling process of the model of Fig. 1B, if the P.S.Z.C.'s coincide with the delta sampling function, then a '1' pulse appears at the output of the model. This condition is equivalent to the error being at its extreme negative value. The error, however, depends upon the relative position of the standard pulse with respect to the P.S.Z.C.; this will be assumed to coincide with the leading edge of the pulse and the theory developed accordingly. Variations on this positioning are considered later. (Chapter 10).
4. The initial conditions of the pulse summing integrators in both the model and the delta-modulator are set over the first time slot to a value 0.5. Thus,

$$S_1(t) = S_2(t) = 0.5,$$

for  $0 \leq t < 1/P$

The initial condition of the remaining integrators are set zero at  $t=0$ . It is also assumed that the input modulating signals to both model and delta-modulator are initially zero at  $t=0$ . Thus, at the

commencement of processing, the systems will not be overloaded.

5. At no time does the input signal exceed the overload condition. In a practical system the slope-overload conditions can be simulated, however, the analysis does not account for this condition.
6. If there are no errors in the transmission channel, then similar waveforms are present at the sending and receiving terminals of Fig. 3.1 and Fig. 3.2, i.e.:

$$S'_1(t) = S_1(t)$$

$$S'_2(t) = S_2(t)$$

Since in general this does not occur, the analysis is only concerned with the deltamodem and deltamodem model local signals  $S_1(t)$  and  $S_2(t)$ , prior to low-pass filtering. Thus transmission errors are of no concern to the equivalence of the system.

7. The time slot associated with  $N^{\text{th}}$  sample is defined over the interval,

$$\frac{(N-1)}{P} < t \leq \frac{N}{P},$$

8. In the theory, the pulse occurring at the origin is not included, only pulses from  $N=1$  are counted.

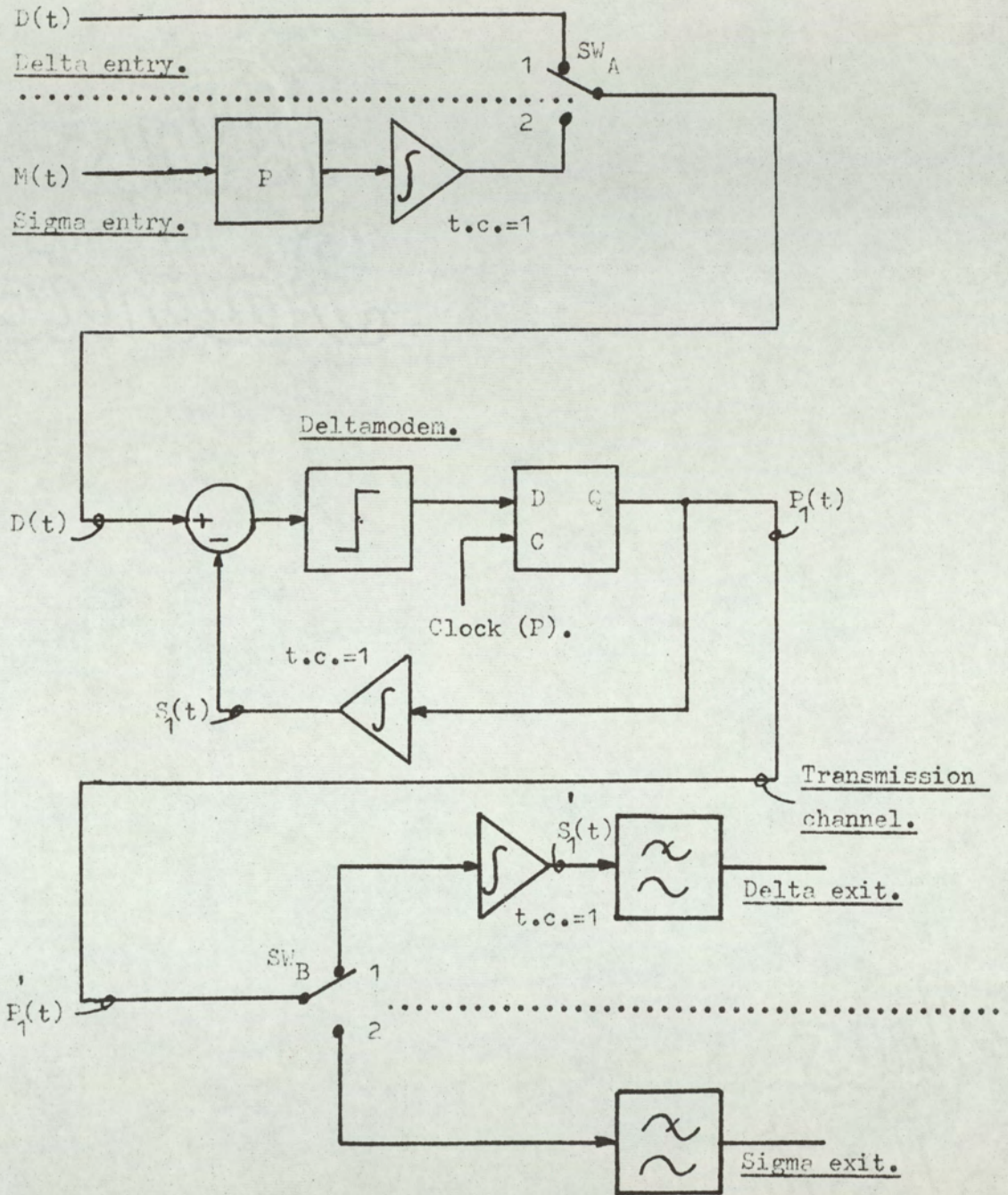


Fig.3.1. Generalised delta-modulation.

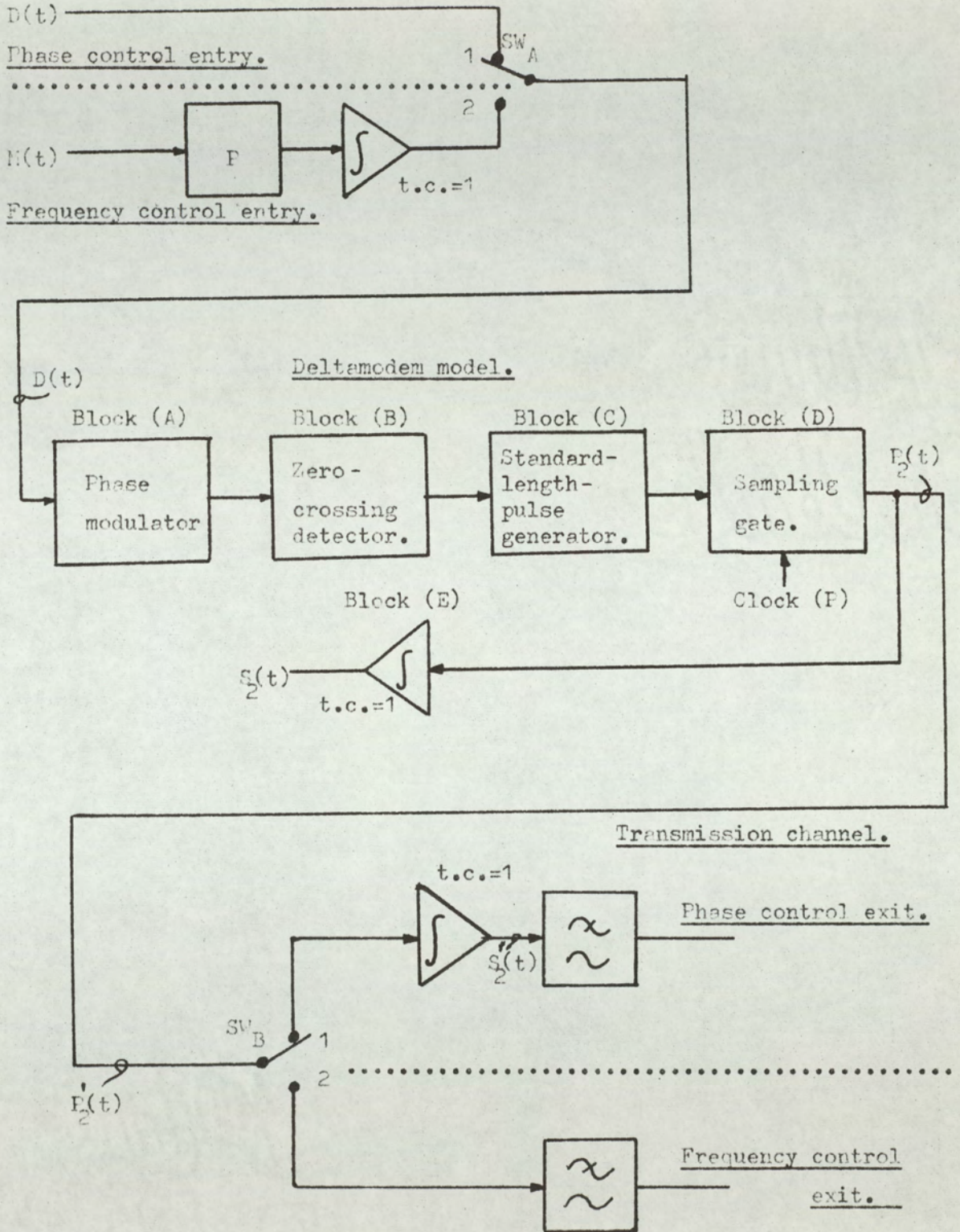
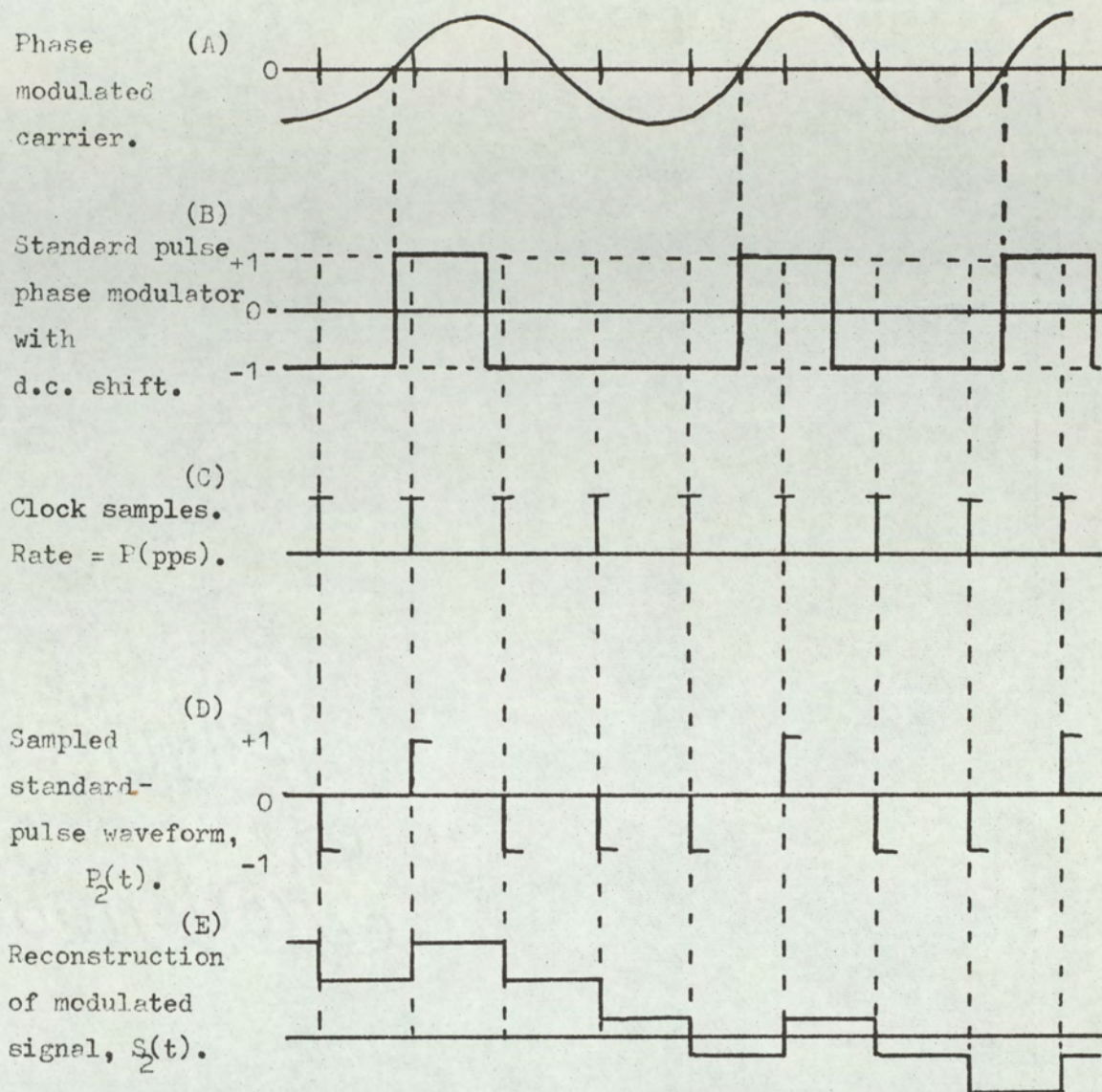


Fig.3-2. Generalised model for delta-modulation and delta-sigma modulation.



Trace (A).... P.P.M. signal formed from phase modulated sinusoid.

Trace (B).... P.P.M. with standard pulse of width  $(1/P)$  enabling time slotting of leading edge to the following clock sample position, where the clock rate is  $P$ (pps).

Trace (C).... Clock sample pulses.

Trace (D).... Time slotted P.P.M. signal corresponding to  $P_2(t)$ .

Trace (e).... Integrated waveform of  $P_2(t)$  generating  $S_2(t)$ .

Fig.(3-3). Delta Modem model waveforms.

### 3.3 Analytical verification of delta-modulator model, single-carrier system.

#### A. The deltamodem-feedback network

This system is described with reference to Fig.

3.1. In the deltamodem, the clock rate is  $P$  (P.P.S.) thus the sample spacing is  $1/P$  secs.

Consider the modulating signal at the  $N^{\text{th}}$  sample.

$$\text{i.e. } t = \frac{N}{P},$$

$$\text{Therefore } D(t) = D\left(\frac{N}{P}\right), \quad \dots(3.2)$$

Since the deltamodem at no time is driven into slope overload, then the store output  $S_1(t)$  lies within  $\pm$  one quantisation step of  $D(t)$ , at each sample instant. Thus,

$$S_1(t) = D(t) - q(t), \quad \dots(3.3)$$

$$\text{where, } -1 < q(t) < +1.$$

This assumes that the quantisation step is normalised to 1. That is, since  $P_1(t)$  is composed of a sequence of delta pulses, and since all integrators have unit time constants, then the changes of the integrator output  $S_1(t)$  at each sample instant are restricted to  $\pm 1$ .

Hence, at time  $t$ , where,  $t$  is defined by equation (2.11),

$$S_1\left(\frac{N}{P}\right) = D\left(\frac{N}{P}\right) - q\left(\frac{N}{P}\right), \quad \dots(3.4)$$

If at time  $\left(\frac{N}{P}\right)$ , there have been,

$N_{P1}$  positive pulses

$N_{N1}$  negative pulses

and  $N$  is the total number of pulses, then,

$$N = N_{P1} + N_{N1}, \quad \dots(3.5)$$

The initial condition on  $S_1(t)$ , during the first time slot is set at 0.5 units.

$$\text{Thus, } S_1(t) = 0.5,$$

$$\text{for } 0 < t \leq \frac{1}{P}.$$

By giving  $S_1(t)$  this initial condition, the idling pattern will oscillate symmetrically about a signal  $D(t) = 0$ .

Thus, at the  $N^{\text{th}}$  sample,  $S_1(t)$  is given by:

$$S_1\left(\frac{N}{P}\right) = N_{P1} - N_{N1} + 0.5,$$

Substituting for  $N_{N1}$  from equation (3.5).

$$\text{Therefore, } S_1\left(\frac{N}{P}\right) = 2 \cdot N_{P1} - N + 0.5, \quad \dots(3.6)$$

The production of a positive or negative pulse at the output of the modulator is considered at each sampling instant, such that the error remains within  $\pm 1$ . That is equation (3.6) is evaluated for all positive  $N$  such that equation (3.3) applies, the output pulse waveform  $P_1(t)$  is thus uniquely defined.

Expressed in this form, single-integration delta-modulation can be seen to be a controlled counting system, the count number being matched to the modulating signal.

Equation (3.6) also indicates that, since the clock rate is constant, knowledge of the position of positive pulses only, or negative pulses only, is required to define the reconstructed signal  $S_1(t)$ . Thus, either positive or

negative pulses only need be transmitted, providing information at the receiver about the clock is known, if regeneration is required.

The introduction of 100% output pulses in no way affects the theory, providing there is no extra loop delays inherent in the modulator. The only difference is that the error signal is now delayed by one clock period. This will not effect the decision-making system, since both  $\delta$  pulse system and 100% pulse system give the same information to the comparator at the instant of sampling.

#### B. The deltamodem model.

The Deltamodem Model is shown in Fig. 3.2. Block A, the first stage of the model, is a phase modulator; it modulates a cosine function of centre frequency  $P/2$ , where  $P$  is the deltamodem p.r.f.

A general expression for this modulated carrier is

$$x(t) = X \cdot \text{Cos}\{\pi \cdot P \cdot t + \phi(t)\}, \quad \dots(3.7)$$

where  $\phi(t)$  is a linear function of the modulating signal  $D(t)$ . Put,

$$\phi(t) = K \cdot D(t), \quad \dots(3.8)$$

The signal  $D(t)$  is constrained such that the frequency deviation does not exceed  $\pm 2\pi(P/2)$ . This restriction is in accordance with the slope-overload criterion. To keep the phase rotation of  $x(t)$  in equation (3.7) positive or zero, then

$$\left| \frac{d}{dt} \phi(t) \right|_{\text{MAX}} = \frac{P}{2} \cdot (2\pi), \quad \dots(3.9)$$

Substituting  $\phi(t)$  from equation (3.8),

$$\left| K \cdot \frac{d}{dt} D(t) \right|_{\text{MAX}} = \frac{P}{2} \cdot (2\pi), \quad \dots(3.10)$$

The maximum slope of  $D(t)$  is defined at the onset of slope overload, when the output pulse sequence of a delta-modulator is either all '1' pulses or all '0' pulses.

Thus, assuming unit step height and a clock rate of  $P$ .

$$\left| \frac{d}{dt} D(t) \right|_{\text{MAX}} = P, \quad \dots(3.11)$$

Thus substituting for  $D(t)$  from equation (3.10) in equation (3.11), gives,

$$\begin{aligned} \left| K \cdot \frac{d}{dt} P(t) \right|_{\text{MAX}} &= K \cdot \left| \frac{d}{dt} D(t) \right|_{\text{MAX}}, \\ &= K \cdot P, \\ &= \frac{P}{2} \cdot (2\pi), \end{aligned}$$

Hence  $K = \pi$ ,

Thus, substituting for  $K$  in equation (3.8) and then  $\phi(t)$  from equation (3.8) into equation (3.7), therefore  $x(t) = X \cdot \text{Cos}\{\pi(P \cdot t + D(t))\}$ ,  $\dots(3.12)$

The phase-modulated carrier is now converted to a naturally-sampled P.P.M. signal, by observing the P.S.Z.C.'s of  $x(t)$  which occur whenever the phase of  $x(t)$  passes through  $(2 \cdot M \cdot \pi - \frac{\pi}{2})$ , where  $M$  is a positive integer, being the  $M^{\text{th}}$  P.S.Z.C. from  $t=0$ .

At time  $t$ , defined by equation (2.11), let the number

of complete positive rotations of the phase of  $x(t)$  be  $M$  and let  $\phi$  be the excess phase at this instant. Then:

$$\phi + (2M\pi - \frac{\pi}{2}) = \pi.(P.t + D(t)), \quad \dots(3.13)$$

where,  $0 \leq \phi < 2\pi$ ,

At time  $t$ ,  $N$  samples have occurred. Thus, substituting from equation (2.11) in equation (3.13),

$$(\frac{\phi}{\pi}) + 2.M - 0.5 = P.(\frac{N}{P}) + D(\frac{N}{P}),$$

$$\text{Therefore } (2M - 0.5) + (\frac{\phi}{\pi}) = N + D(\frac{N}{P}), \quad \dots(3.14)$$

at time  $(N/P)$ , let,

$N_{P2}$ , positive pulses have occurred.

$N_{N2}$ , negative pulses have occurred.

Again, an initial condition is set on  $S_2(t)$  during the first time slot, to bring the model initially into alignment with the deltamodem. Thus, at time  $(N/P)$ :

$$S_2(\frac{N}{P}) = N_{P2} - N_{N2} + 0.5 \quad \dots(3.15)$$

$$\text{But, } N = N_{P2} + N_{N2} \quad \dots(3.16)$$

Since the pulses are confined to time slots, such that at time  $N/P$ ,  $N$  time slots have occurred and for each time slot a '1' or '0' forms the output, then equations (3.16) applies.

Substituting  $N_{N2}$  from equation (3.16) in equation (3.15),

$$S_2(\frac{N}{P}) = N_{P2} - (N - N_{P2}) + 0.5,$$

Therefore

$$S_2(\frac{N}{P}) = 2.N_{P2} - N + 0.5, \quad \dots(3.17)$$

In equation (3.14),  $M$  represents the number of positive rotations of the phase of  $x(t)$ , excluding the rotation in the  $N=0$  time slot. Since the system does not enter slope overload, all the rotations of the phase are detected and pass through the sampling process. Thus, since each rotation is represented by a positive pulse, then:

$$M = N_{P2} , \quad \dots(3.18)$$

Substituting from equation (3.18) in equation (3.14) and rearranging,

$$2 \cdot N_{P2} - N + 0.5 = D\left(\frac{N}{P}\right) - \left(\frac{\phi}{\pi}\right) + 1,$$

Thus, substituting in equation (3.17) gives:

$$S_2\left(\frac{N}{P}\right) = D\left(\frac{N}{P}\right) + \left(1 - \frac{\phi}{\pi}\right), \quad \dots(3.19)$$

The error term is  $\left(1 - \frac{\phi}{\pi}\right)$ ,

since  $0 \leq \phi < 2\pi$ ,

therefore  $0 \leq \frac{\phi}{\pi} < 2$ ,

and  $-1 \leq \left(1 - \frac{\phi}{\pi}\right) < 1$

Thus, equation (3.19) states that the accumulated output at the  $N^{\text{th}}$  sample is equal to the modulating signal to within an accuracy of  $\pm 1$ . This is identical to the deltamodem.

Since equation (19) holds for all integer values of  $N$ , the time-quantised P.S.Z.C.'s define a unique pulse pattern  $P_2(t)$ .

Hence, with the appropriate choice of initial

conditions for the model and deltamodulator integrator and of the initial condition of the phase-modulated carrier, then:

$$S_1\left(\frac{N}{P}\right) = S_2\left(\frac{N}{P}\right),$$

and consequently,

$$P_1\left(\frac{N}{P}\right) = P_2\left(\frac{N}{P}\right)$$

for  $N = 1, 2, 3, \dots$  etc.

Since the modulating signal  $D(t)$  and the accumulated signal in both processes are identical at each sampling instant, then the error signal is also identical. Consequently both systems generate the same noise structure.

Thus time-quantised pulse-phase modulation is in every way identical to delta-modulation with a single, perfect integrator, providing that the correct initial conditions are observed. It is also necessary that slope overload does not occur and the phase-modulator has a linear relationship between modulating-signal slope and carrier frequency.

If the switches  $SW_a$ ,  $SW_b$  in Fig. 3.1 and Fig. 3.2 are in position (2), an integrator is introduced at the input to both the deltamodem and the deltamodem model. A multiplier,  $P$ , is also introduced so that the magnitude of the input signal can be independent of the system parameters, i.e. if the clock rate is changed, the multiplier is also changed. In this system  $D(t)$  is given by,

$$D(t) = P \int_0^t M(t) dt \quad \dots(3.20)$$

where  $M(t)$  is normalised as detailed in equation (3.1).

The input  $M(t)$  now controls the frequency of the carrier  $x(t)$  instead of its phase. In the system of Fig. 3.1, the integrator converts the deltamodem from a delta-modulator to a delta-sigma modulator, and in the system of Fig. 3.2, the integrator and phase-modulator can be combined to form a frequency-modulator.

Thus, delta-modulation is equivalent to time quantised pulse-phase modulation and delta-sigma modulation is equivalent to time quantised pulse-frequency modulation.

### 3.4 Analytical verification of delta-modulation, double carrier

The analysis of section (3.3) can be considered from a modified view point. The analysis was basically concerned with the positioning of the P.S.Z.C.'s to form the positive pulse sequence of the waveform  $P_2(t)$ , the output of the deltamodem model. The behaviour of the negative pulses followed automatically, in that, if a P.S.Z.C. did not occur within a time slot, then the pulse inserted at the end of the time slot was a zero. Since, at each sampling instant, the sum of negative and positive pulses is equal to the number of samples, it is clear that if the positive pulse rate increases, the negative pulse rate must decrease accordingly, and vice versa.

The system can also be described by introducing a pair of phase-modulated carriers, the phase modulation being equal and opposite, thus two functions can be defined  $x_P(t)$  and  $x_N(t)$  which take the basic form of equation (3.12). i.e.

$$x_P(t) = X \cdot \text{Cos}\{\pi \cdot (P \cdot t + D(t))\} , \quad \dots(3.21)$$

$$\text{and } x_N(t) = X \cdot \text{Cos}\{\pi \cdot (P \cdot t - D(t) + 1)\} \quad \dots(3.22)$$

Fig. 3.4 illustrates these functions for the idling pattern where  $D(t) = 0$  and shows the P.S.Z.C.'s generating the positive and negative pulse sequence of the output of the deltamodem model,  $P_2(t)$ .

Consider the state of equations (3.21) and (3.22) at the  $N^{\text{th}}$  sample.

Let  $M_P$  be the rotations of the phase of  $x_P(t)$ , not including the pulse at the origin and  $M_N$  the rotation of the phase of  $x_N(t)$ .  $\phi_P$ ,  $\phi_N$  are the excess phase angles of time  $N/P$ .

Thus expressing the equations (3.21), (3.22) in the form of equation (3.13) gives;

$$\phi_P + (2 \cdot M_P \cdot \pi - \frac{\pi}{2}) = \pi \left( P \cdot \left( \frac{N}{P} \right) + D \left( \frac{N}{P} \right) \right),$$

Therefore,

$$(2M_P - 0.5) + \left( \frac{\phi_P}{\pi} \right) = N + D \left( \frac{N}{P} \right), \quad \dots(3.23)$$

For equation (3.22)

$$\phi_N + (2 \cdot M_N \cdot \pi - \frac{\pi}{2}) = \pi \cdot \left( P \cdot \left( \frac{N}{P} \right) - D \left( \frac{N}{P} \right) + 1 \right)$$

Therefore,

$$(2 \cdot M_N - 1.5) + \left( \frac{\phi_N}{\pi} \right) = N - D \left( \frac{N}{P} \right) \quad \dots(3.24)$$

Summing equation (3.23) and (3.24) gives,

$$2 \cdot (M_P + M_N) - 2 + \left( \frac{\phi_P + \phi_N}{\pi} \right) = 2 \cdot N$$

Therefore,

$$N = (M_P + M_N) + \left\{ \left( \frac{\phi_P + \phi_N}{2\pi} \right) - 1 \right\}, \quad \dots(3.25)$$

However,  $N$  is an integer, also  $M_P$  and  $M_N$  are integers, therefore,

$$N = M_P + M_N \quad \dots(3.26)$$

since  $0 < \phi_P, \phi_N < 2\pi$   
 $0 < (\phi_P + \phi_N) < 4\pi$   
 $0 < \left( \frac{\phi_P + \phi_N}{2\pi} \right) < 2$

Therefore,

$$-1 < \left\{ \left( \frac{\phi_P + \phi_N}{2\pi} \right) - 1 \right\} < 1.$$

Equation (3.26) is the only valid solution for equation (3.25) due to the restrictions of  $M_P$ ,  $M_N$  integer and the phase error term  $\left\{ \left( \frac{\phi_P + \phi_N}{2\pi} \right) - 1 \right\}$ .

Thus, it can be concluded,

$$(\phi_P + \phi_N) = 2\pi, \quad \dots(3.27)$$

Subtracting equation (3.24) from equation (3.23),

$$2.(M_P - M_N) + \left\{ \frac{\phi_P - \phi_N}{\pi} \right\} + 1.0 = 2.D\left(\frac{N}{P}\right),$$

Therefore,

$$(M_P - M_N) = D\left(\frac{N}{P}\right) - \left[ 0.5 + \left\{ \frac{\phi_P - \phi_N}{2\pi} \right\} \right], \quad \dots(3.28)$$

At the  $N^{\text{th}}$  sample,  $S_2\left(\frac{N}{P}\right)$  is given by equation (3.15), assuming the initial condition of 0.5 on  $S_2(t)$  during the zero time slot.

During sampling, the positive and negative pulses of the two carriers are repositioned in time, thus generating quantisation. However, assuming that slope overload does not occur, all pulses are detected by the sampling process and appear at the output,  $P_2(t)$ , with a slight time shift. Thus at the  $N^{\text{th}}$  sample:

$$N_{P2} = M_P,$$

$$N_{N2} = M_N,$$

Therefore

$$(M_P - M_N) = (N_{P2} - N_{N2}),$$

Substituting for  $(M_P - M_N)$  in equation (3.28) and

then for  $(N_{P2} - N_{N2})$  in equation (3.15), gives

$$S_2\left(\frac{N}{P}\right) = D\left(\frac{N}{P}\right) - \left[ 0.5 + \left\{ \frac{\phi_P - \phi_N}{2\pi} \right\} \right] + 0.5,$$

Therefore,

$$S_2\left(\frac{N}{P}\right) = D\left(\frac{N}{P}\right) - \left\{ \frac{\phi_P - \phi_N}{2\pi} \right\}.$$

Since,  $0 \leq \phi_P, \phi_N < 2\pi$ ,

Therefore,

$$-1 \leq \left\{ \frac{\phi_P - \phi_N}{2\pi} \right\} < +1.$$

Thus,

$$S_2\left(\frac{N}{P}\right) = D\left(\frac{N}{P}\right) - q\left(\frac{N}{P}\right), \quad \dots(3.30)$$

where,  $-1 \leq q\left(\frac{N}{P}\right) < 1$ ,

Thus, the delta-modulator can be represented by two phase-modulated carriers, the modulation signals of which are inverted to each phase modulator. A phase displacement of  $\pi$  is required to produce the correct idling pattern, since a delta-modulator has a single unstable mode of oscillation defined by the input signal, this will be discussed in section (4.7).

In the original delta-modulator model of section (3.3), the second inverted phase modulator was omitted; its effect on negative pulses was obtained by the action of equation (3.26), which was performed by the sampling process. The second model, section (3.4), completely describes the action of a single integrator delta-modulation, illustrating the nature of the reciprocating action between '1' pulses and '0' pulses.

Fig. 3.5 illustrates the complete model for the double-carrier system.

In Fig. 3.5, the only difference in the two channels is the standard pulse generator. For positive pulses, this generator produces a pulse of amplitude +1 and duration  $1/P$  and for negative pulses the other generator produces a pulse of height -1 and duration  $1/P$ .

In the system, only P.S.Z.C.'s were detected, for the negative-pulse channel, the  $\pi$  radian phase displacement for the idling pattern, could have been obtained by sensing the negative-slope zero crossings and keeping the two carriers in phase; the result would be otherwise identical.

If the models of section 3.3 and section 3.4 are required to produce a finite pulse of amplitude (say) 1 and duration  $1/P$ , then the pulse generator of Fig. 3.6 is applicable. The transfer function of the network is given in equation (3.30). This network is of great importance when considering the stability criteria for an analogue-feedback delta-modulator, since it introduces phase and amplitude effects.

A pulse generator for the output of a delta-modulator model, to provide interfacing with digital equipment is illustrated in Fig. 3.6. Its transfer function is,

$$T_{P100}(f) = \frac{1}{P} \cdot e^{-j\pi f/P} \frac{\text{Sin}\left(\frac{\pi f}{P}\right)}{\left(\frac{\pi f}{P}\right)}, \quad \dots(3.30A)$$

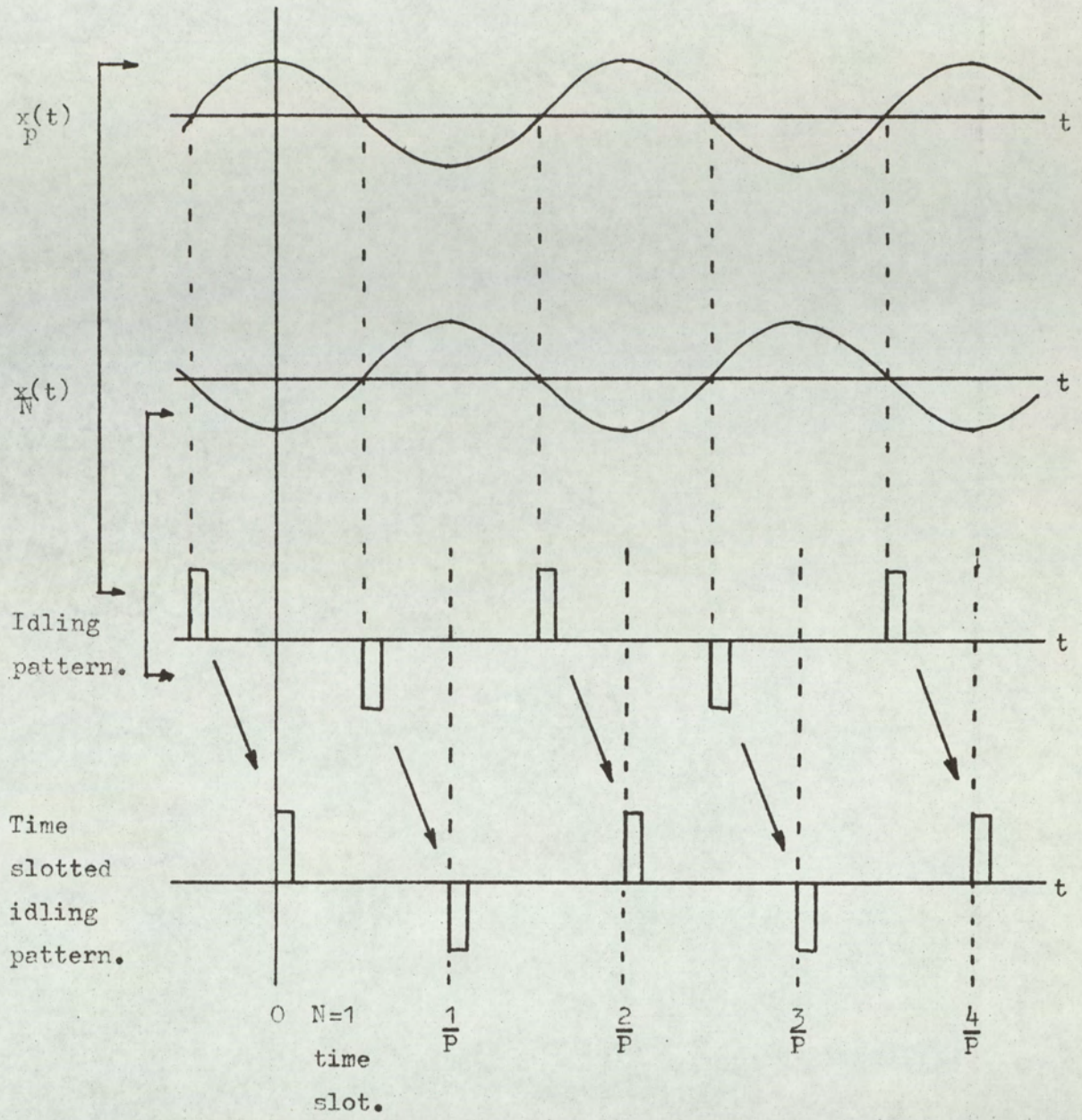


Fig.3-4. Double-carrier model of delta-modulator.

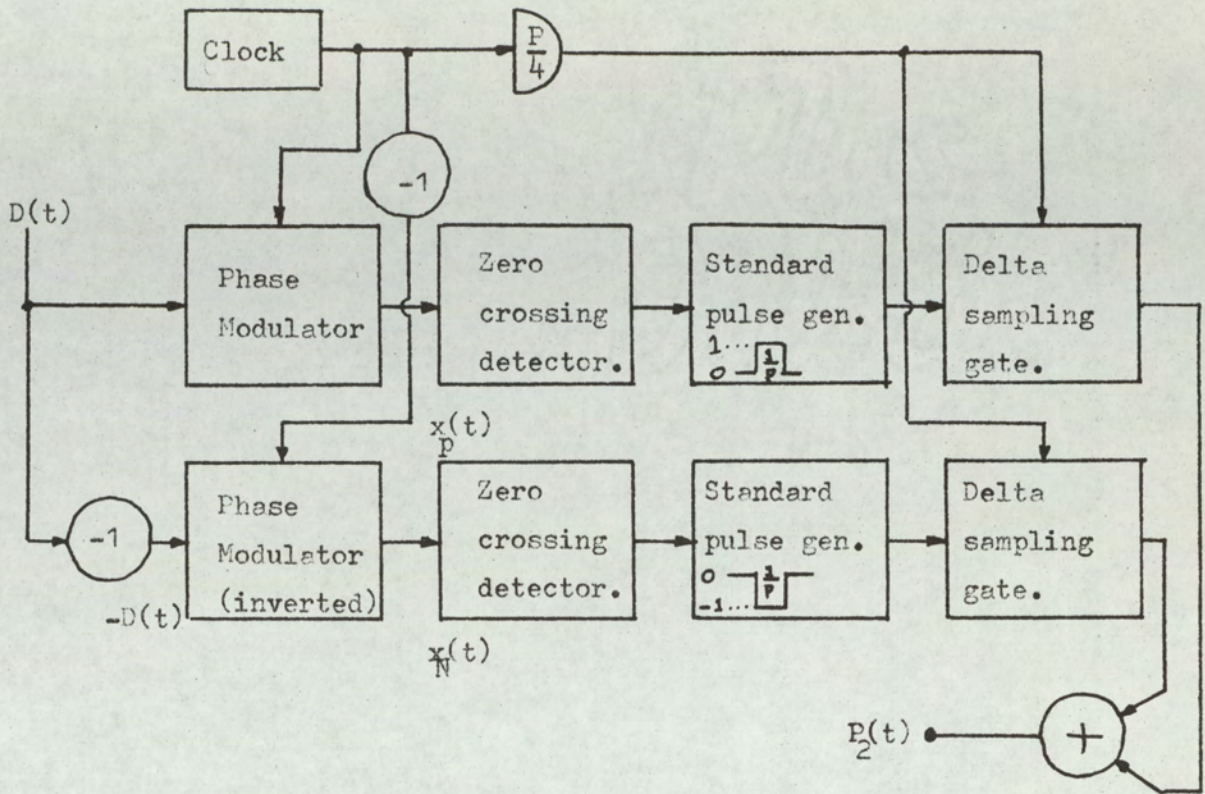


Fig.3-5. Double-carrier model of delta-modulator.

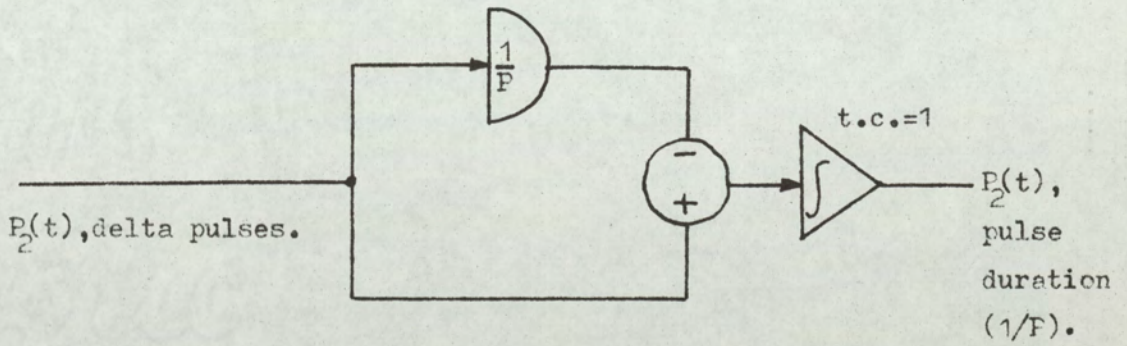


Fig.3-6 (1/P) pulse duration(generator).

### 3.5 Extension of deltamodem model to RC integrator in the analogue-feedback network.

The model, as described in sections (3.3) and (3.4), is only applicable to a perfect integrator driven by a delta-pulse sequence or equivalent train of finite pulses with an area equal to the delta pulse. However, in an analogue feedback delta-modulator, this condition can never be realised, even when a high-gain amplifier is used, since such devices have a finite gain at d.c. (In practice, clipping due to limited dynamic range will generally apply before RC integration effects can be observed.) Also, for integrator demodulation, a finite gain at d.c. is desirable to give immunity to long-term error accumulation, produced by incorrect pulse recognition at the receiver terminal. The latter effect is achieved to its best advantage by using hybrid delta-modulation as previously described. However, in practice, this is often not employed; thus further investigation of the model is warranted.

To generalise the model to RC integration, in the closed loop, it is necessary to define parameters to permit an equivalent realisation. The basic deltamodem model is retained in the form already described. The step height of the model is normalised to 'one unit' and the clock rate is  $P$ (p.p.s.). The delta-modulator with RC integration is arranged to have a symmetrical idling pattern of unit step height, when the input signal is zero. The delta-modulator has a multiplying factor

introduced in the network, such that changes in the RC time constant maintain the described idling pattern. Since the analogue system is usually operated with 100% pulses, i.e. duration  $1/P$ , the analysis will be appropriate to this system. However, other duration pulses, including delta pulses, can be used, though the multiplying factor would require modification. This in no way invalidates the theory.

The output pulses are of constant area, their amplitude is 1 unit and the duration  $1/P$  secs. Fig. 3.7 illustrates the symmetrical idling pattern of unit deviation when driven by the pulses described. Let the multiplier be  $V$ ; thus the pulses appear to be of amplitude  $V$  and duration  $(1/P)$ . Therefore,  $V$  represents the final aiming potential of the integrated pulse waveform. The integrator has a time constant  $RC$  secs.

The equation of the integrated idling pulse waveform over a clock period is of the form,

$$y_1 = a_1 \cdot e^{-t/RC} + b_1$$

Initial conditions,  $y_1 = -\frac{1}{2}$ ,  $t=0$ ,

therefore,  $-\frac{1}{2} = a_1 + b_1$

Final conditions,  $y_1 = \frac{1}{2}$ ,  $t = 1/P$ ,

therefore,  $\frac{1}{2} = a_1 \cdot e^{-1/PRC} + b_1$

Aiming potential,  $t \rightarrow \infty$ ,  $y_1 \rightarrow V$ .

$$V = b_1,$$

Eliminating  $a_1$  and  $b_1$ , gives

$$V = \frac{1}{2} \left[ \frac{1+e^{-1/(PRC)}}{1-e^{-1/(PRC)}} \right], \quad \dots(3.31)$$

Equation (3.31) gives the multiplier required in the feedback path to enable a unit amplitude idling pattern.

A RC integrator is represented by the equation,

$$V_o = \frac{1}{(R.C)} \int_0^t (V_{in} - V_o) dt, \quad \dots(3.32)$$

This has an equivalent network as shown in Fig. 3.8.

Using the network of Fig. 3.8a, derived from equation (3.32), together with the multiplier of (3.31) to normalise the idling pattern step height, the delta-modulator of Fig. 3.9 is evolved and is compared with an equivalent network.

The feedback network in the RC integrator and the network of the equivalent delta-modulator are identical. Thus, using Laplace, the feedback transfer functions may be equated,

$$\begin{aligned} \frac{P}{S} \cdot (A(s) + 1) &= V \cdot \left\{ \frac{1}{1+s(RC)} \right\}, \\ \text{Therefore } A(s) &= - \frac{1+s \left[ (RC) - \frac{V}{P} \right]}{(1+s(RC))}, \\ \text{Therefore } A(s) &= - \frac{1}{\{1+s(RC)\}} - \left[ 1 - \frac{V}{(PRC)} \right] \cdot \frac{s(RC)}{\{1+s(RC)\}} \\ &\dots(3.33) \end{aligned}$$

Consider the expansions of equation (3.31)

$$V = \frac{1}{2} \left[ \frac{1 + 1 + \left(\frac{-1}{\text{PRC}}\right) + \frac{1}{\sqrt{2}}\left(\frac{-1}{\text{PRC}}\right)^2 + \dots}{1 - 1 - \left(\frac{-1}{\text{PRC}}\right) - \frac{1}{\sqrt{2}}\left(\frac{-1}{\text{PRC}}\right) - \dots} \right] \quad \dots(3.34)$$

$$\text{In practice } (\text{PRC}) > 50, \quad \dots(3.35)$$

$$V \approx P(\text{RC})$$

$$\text{Therefore, } \frac{V}{(\text{PRC})} = 1 \quad \dots(3.36)$$

Substituting equation (3.36) in equation (3.33) gives,

$$A(s) = \frac{-1}{1+s(\text{RC})} \quad \dots(3.37)$$

The equivalent network of Fig. 3.8b can be represented by a single-integrator delta-modulator with perfect integration and unit-step height, with an external negative feedback loop completed by  $A(s)$ . Fig. 3.9 illustrates the delta-modulator and the equivalent model when  $A(s)$  is represented by equation Fig. (3.36).

RC integration is thus seen to be simulated by the ideal model when the system is closed by a positive-feedback loop which includes the RC integration network. Thus, at low frequencies, when the RC loop can exert full control, the information storage capacity is reduced, since the loop generates redundancy in feeding information back to the input. If the time constant is made small, such that equation (3.36) is violated, then the feedback network is seen by equation (3.33) to have a parallel differential network. However, in a practical situation, this would never arise.

The model for RC integration is readily extended to delta-sigma modulation. According to section (2.3), the delta-sigma modulator is realised by transposing the demodulator

integrator to the input signal path, combining the integrator with the integrator in the feedback path and introducing the integration process into the forward path. Fig. 3.9b illustrates the transformation.

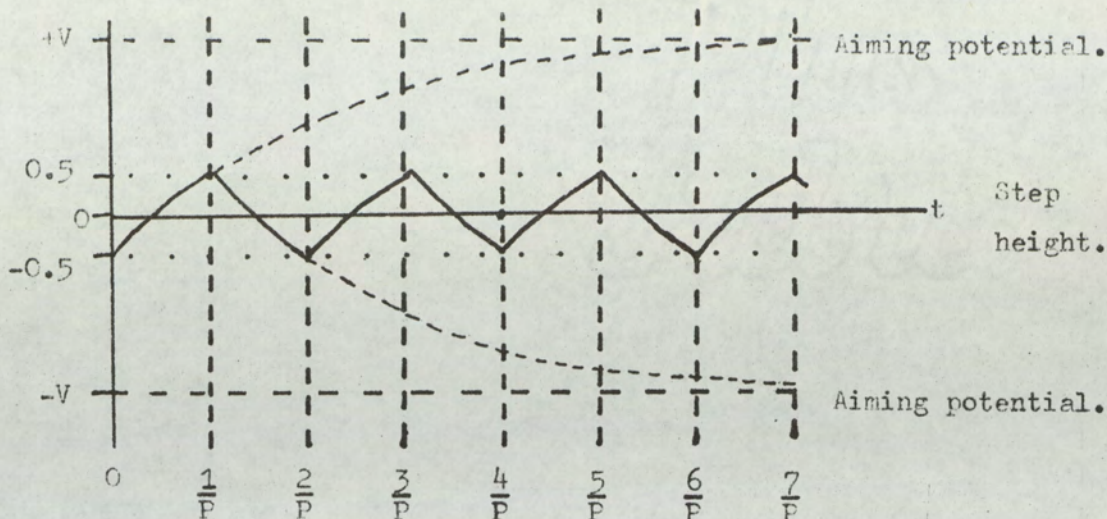


Fig.3-7. Idling pattern for pulses of height  $V$  and duration  $(1/P)$ , when integrated by a RC network.

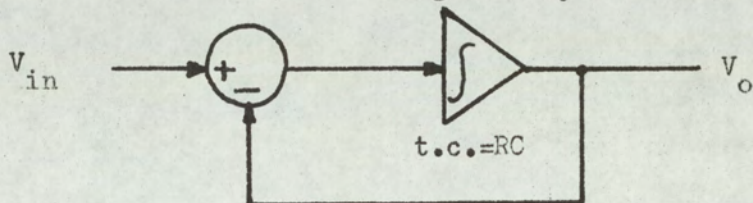


Fig.3-8(a). Equivalent active network of RC integrator.

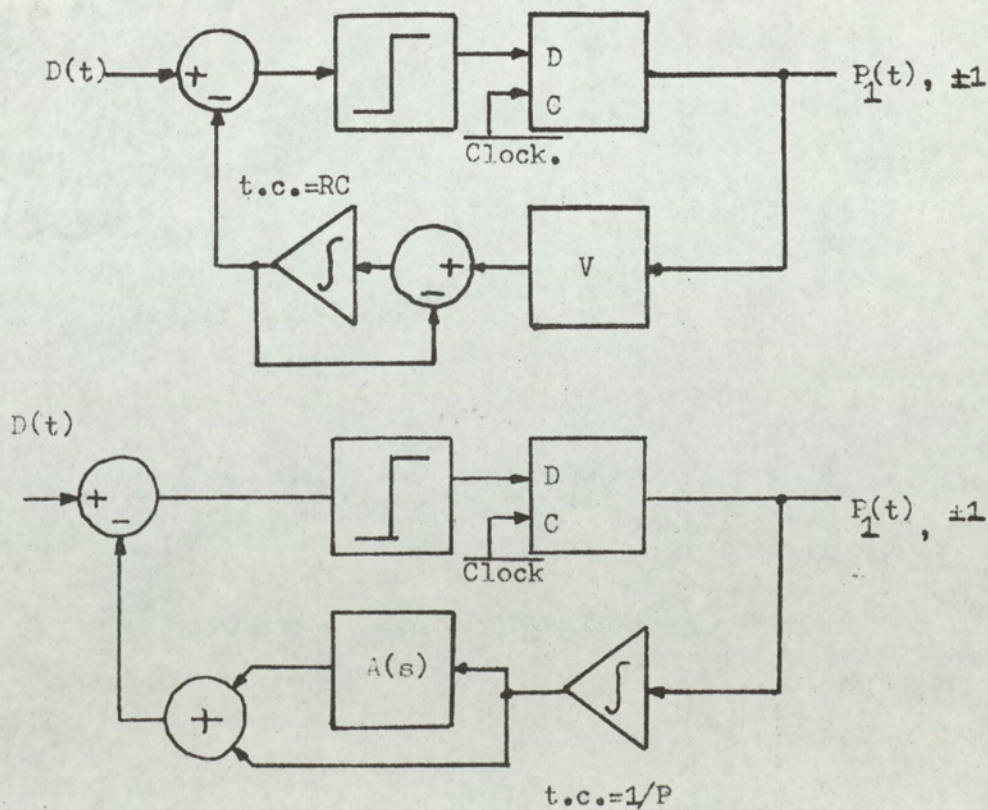
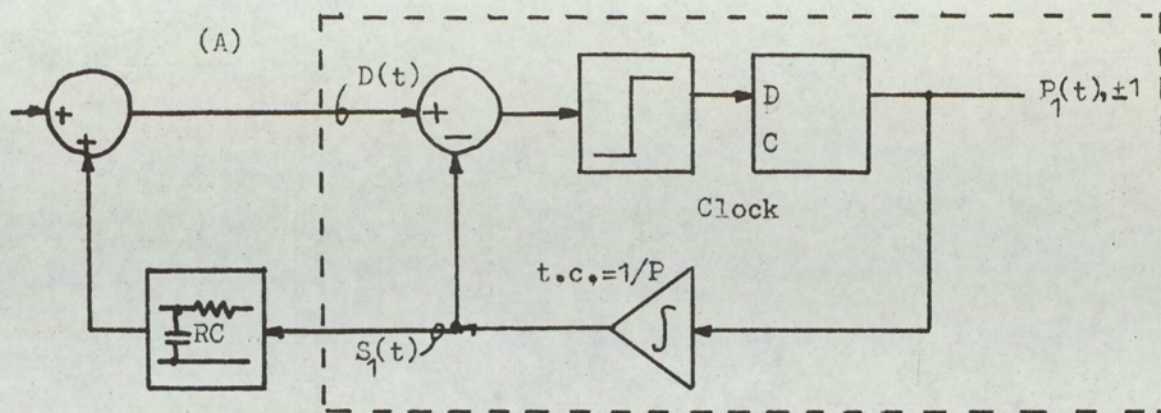
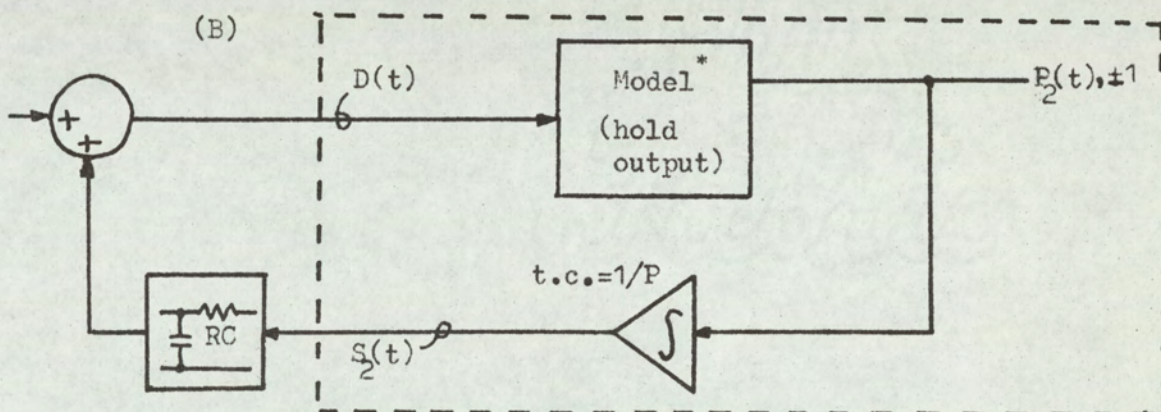


Fig.3-8(b). RC integration with equivalent network in the feedback path of a delta-modulator.



Positive feedback path.



Positive feedback path.

Fig.3-9.(a). Equivalent RC integrator delta-modulator using ideal phase-control model with external feedback path.

- (A). Rearranged RC integrator delta-modulator, defining perfect integrator delta-modulator with external positive feedback path.
- (B) As in (A) but phase-control model substituted for perfect single-integrator delta-modulator.

\* Hold network of duration  $(1/P)$  on output of model.

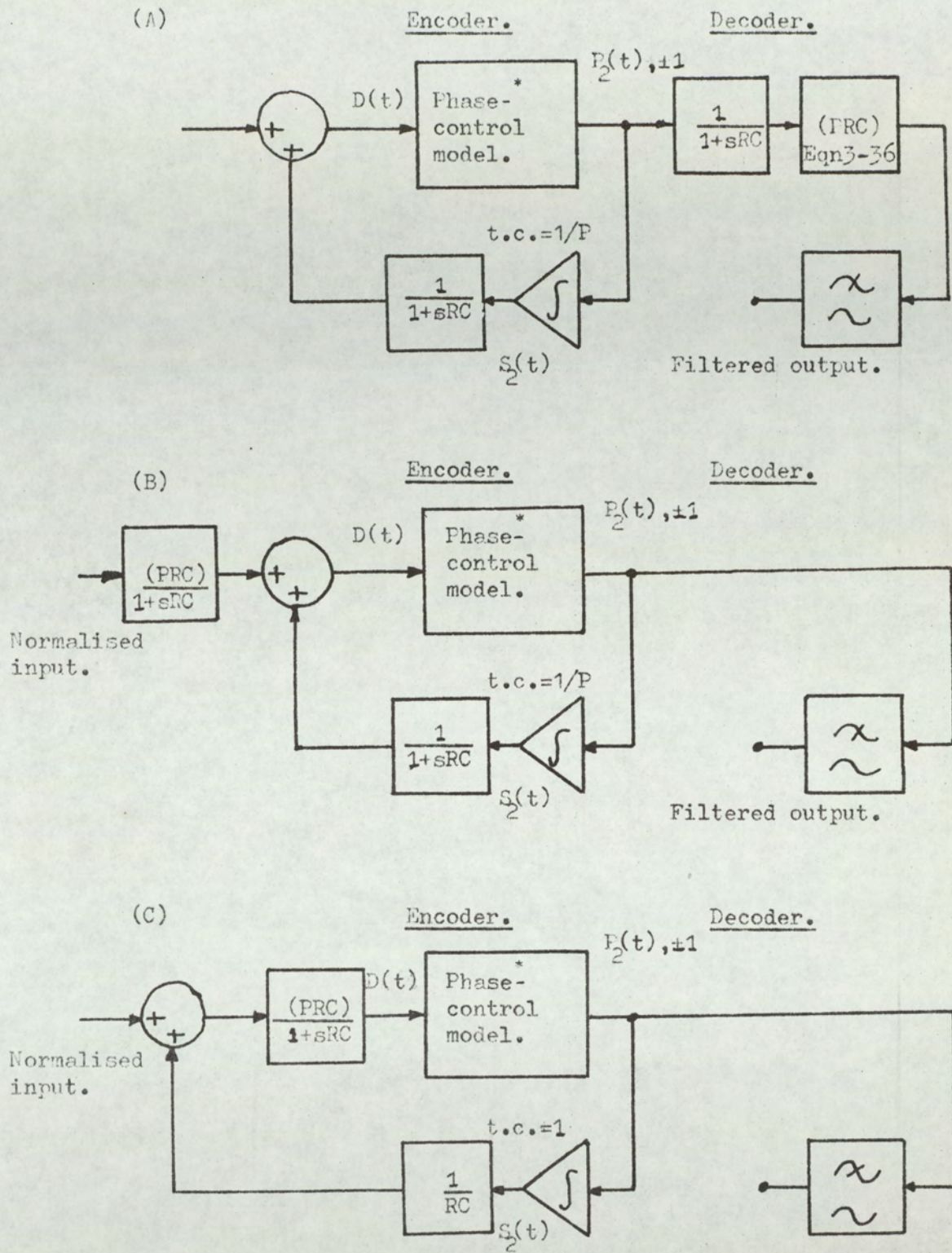


Fig.3-9(b). Extention of model to delta-sigma modulation.

- (A)...RC integrator model equivalent of delta-modulator.
- (B)...Transformation of linear decoding network to input.
- (C)...RC integration network positioned in forward path of control loop.

\* The phase-control model incorporates a hold network of duration  $(1/P)$  on the output.

### 3.6 Extension of deltamodem model to second-order feedback network.

The analogue model has so far been limited to a first-order system with single integration. It has been demonstrated that R.C. integration can also be simulated. These models have been characterised by an open-loop system, which has simulated a closed-loop non-linear network. It is necessary, however, to consider second-order systems in delta-modulation, as these demonstrate considerable noise improvement over the first-order system. Such systems are generally limited to double integration with prediction, when the output  $\delta$  pulses of a delta-modulator are processed by a zero-order hold.

Fig. 3.10 illustrates a second-order system with a predictive loop. The transfer function of the second network in the feedback path is generalised to  $A(f)$ .

For the second-order system shown in Fig. 3.10, a, b let  $D_d(t)$  be the system input signal.

$$\text{In both systems, } S_1(t) = \int_0^t P_1(t)dt, \quad \dots(3.38)$$

For system A,

$$q(t) = D_d(t) - \left\{ \frac{G}{T_1} S_1(t) + \frac{1}{T_1} A(S_1(t)) \right\}$$

For system B,

$$q(t) = D_d(t) - \left\{ \frac{G}{T_1} S_1(t) + \frac{A(S_1(t))}{G} \cdot \frac{G}{T_1} \right\}$$

Therefore,

$$q(t) = D_d(t) - \left\{ \frac{G}{T_1} S_1(t) + \frac{1}{T_1} A(S_1(t)) \right\}, \quad \dots(3.39)$$

i.e. both systems are equivalent.

Note,  $A(f)$  is a linear transfer function in the frequency domain.

$A(S_1(t))$  represents the time response of the network  $A(f)$  to a signal  $S_1(t)$ .

Fig. 3.11 illustrates a slightly modified version of Fig. 3.10b and compares the network with a model equivalent.

In Fig. 3.11, a, b,

$$D(t) = \frac{T_1}{G} \cdot \{D_d(t) - \frac{G}{T_1} A(S_2(t))\},$$

Therefore,

$$D(t) = \frac{T_1}{G} \cdot D_d(t) - A(S_2(t)), \quad \dots(3.40)$$

From equation (3.40) the final equivalent system, shown in Fig. 3.11c, is derived.

Fig. 3.11c, illustrates the final system equivalent. It can be seen that the effects of  $G$  and  $T_1$  effectively control the input loading and the magnitude of the second-order network.

Demodulation from the equivalent system is achieved as follows. Providing slope overload does not occur, then the signal  $S_2(t)$  tracks the input to the model  $D(t)$ , the phase-control system effectively acting as a signal differentiator. It is seen that the output of the second network  $A(f)/G$  is subtracted from the input signal (after scaling). Thus, to reconstruct the true signal, this component must be added back to the quantised signal  $S_2(t)$ . Let  $\frac{S_{22}(t)}{G}$  be the output of the second network

$\frac{A(f)}{G}$ , thus for modulation; i.e.  $S_{22}(t)$  is the output of the network  $A(f)$ .

$$D(t) = \frac{T_1}{G} \cdot D_d(t) - \frac{S_{22}(t)}{G},$$

$$\text{But, } S_2(t) = D(t) - q(t),$$

where  $q(t)$  is the quantisation noise of the single integration model.

$$\begin{aligned} \text{Thus, } \frac{S_{22}(t)}{G} &= \frac{T_1}{G} \cdot D_d(t) - D(t), \\ &= \frac{T_1}{G} \cdot D_d(t) - S_2(t) - q(t), \end{aligned}$$

Thus, the demodulated output  $D_m(t)$  is given by:

$$\begin{aligned} D_m(t) &= \left\{ \frac{T_1}{G} \cdot D_d(t) - S_2(t) - q(t) \right\} + S_2(t), \\ \text{i.e. } D_m(t) &= \frac{S_{22}(t)}{G} + S_2(t), \quad \dots(3.41) \end{aligned}$$

The demodulation process expressed in equation (3.41) is shown in Fig. 3.12. Two equivalent forms of network are illustrated, the second of which can be seen to be identical to the original network of Fig. 3.10a.

The quantisation noise  $q(t)$  is still generated on the basis of a single-integrator delta-modulator. However, the model modulating signal  $D(t)$  is now a much more complex function due to the components fed back from the output pulse waveform through the second-order network. This complexity tends to distribute the noise components more evenly across the frequency spectrum. Thus, noise powers calculated on a constant probability density function should be more accurate. The effect of the second-

order store is to increase the amplitude range over a single integrator. This enables more signal power to be encoded, with a resulting increase in signal to quantisation error ratio.

In the double-integration delta-modulator, the use of analogue integrators introduces constraints on the system. For example, at the output of the ideal model, a zero-order hold circuit is used to generate pulses, generally of duration  $1/P$ . This hold circuit obviously modifies the system response when a double-integration network is introduced. It thus introduces its own inherent characteristics to the modulator, which are not fundamental to delta-modulation.

Consider the delta-modulator of Fig. 3.13, with normalised integrator time constants.

When the delta-modulation process is not modified by the inherent properties of a zero-order hold circuit to produce finite pulses, and delta pulses are applied to the integration feedback network, then the operation is as follows:

Assume zero initial conditions at  $t=0$ , then at  $M^{\text{th}}$  sample,

$$s_2(t) = s_2\left(\frac{M}{P}\right) = \sum_{R=0}^M P_2\left(\frac{R}{P}\right), \quad \dots(3.42)$$

$$s_{22}(t) = s_{22}\left(\frac{M}{P}\right) = \sum_{N=0}^M s_2\left(\frac{N}{P}\right) = \sum_{N=0}^M \sum_{R=0}^M P_2\left(\frac{R}{P}\right), \quad \dots(3.43)$$

Equations (3.42) and (3.43) define the ideal operation of a delta-modulator system. In this case,  $S_{22}(t)$  is defined as the output of the second integrator. Fig. 3.14 illustrates the integration processes of,

- A. ideal delta-modulation
- B. realisation of ideal system with analogue network and delta pulses.
- C. non-optimum system using finite 100% pulses of unit area.

For the following discussion only the ideal system in Fig. 3.14A is considered, the computations being assumed instant on the evaluation of equations (3.42) and (3.43). Thus, the inherent deficiencies of the analogue networks, which are not a fundamental to delta-modulation can be ignored.

When the delta-modulator and delta-modulator model are operated in a non-overload condition,

$$D(t) = \frac{D_d(t)}{G} - \frac{1}{G} \cdot S_{22}(t),$$

Hence, at the  $M^{\text{th}}$  sample and applying equation (3.43),

$$D\left(\frac{M}{P}\right) = \frac{1}{G} \cdot D_d\left(\frac{M}{P}\right) - \frac{1}{G} \cdot \sum_{N=0}^M \sum_{R=0}^M P_2\left(\frac{R}{P}\right),$$

$$\text{but, } D\left(\frac{M}{P}\right) = S_2\left(\frac{M}{P}\right) + q\left(\frac{M}{P}\right)$$

Substituting for  $S_2\left(\frac{M}{P}\right)$  from equation (3.42) and then for  $D\left(\frac{M}{P}\right)$  above, gives,

$$\sum_{R=0}^M P_2\left(\frac{R}{N}\right) + q\left(\frac{M}{P}\right) = \frac{1}{G} D_d\left(\frac{M}{P}\right) - \frac{1}{G} \sum_{N=0}^M \sum_{R=0}^M P_2\left(\frac{R}{P}\right),$$

Therefore,

$$G \sum_{R=0}^M P_2\left(\frac{R}{P}\right) + \sum_{N=0}^M \sum_{R=0}^M P_2\left(\frac{R}{P}\right) = D_d\left(\frac{M}{P}\right) - q\left(\frac{M}{P}\right),$$

....(3.44)

Consider now the system shown in Fig. 3.15. This is the double-carrier model of section 3.4, but without time quantisation. The output is assumed to be a sequence of positive and negative delta pulses occurring at the respective P.S.Z.C.'s.

The analysis of section 3.4, states that, at the time  $(M/P)$ , the output  $S_2(M/P)$  is independent of whether the signal is time quantised or not. That is, the sum of the positive and negative pulses is the same whether they are directly phase modulated or phase modulated and redistributed to the nearest sample point in a time slot. This reasoning also applies to the double summation of  $S_{22}(M/P)$ , which is assumed to be calculated instantaneously.

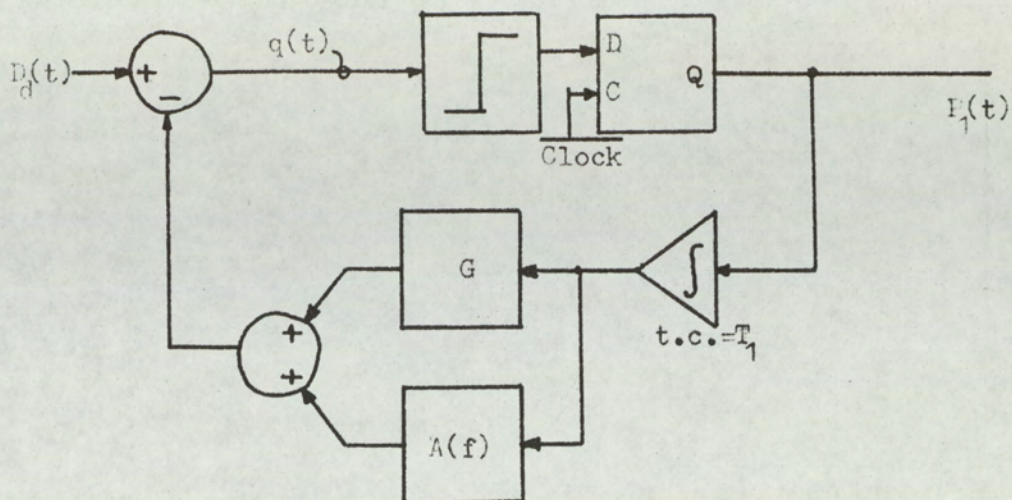
Thus, if the output pulses of the system in Fig. 3.15 are time quantised after feedback has been applied, the pulse waveform will be identical to that of a system where the feedback loop includes the time quantisation procedure. Hence, equation (3.44) applies to both the system in Fig. 3.15 and that in Fig. 3.13.

The basic problem of second-order systems can thus be compared with frequency and phase modulators, where demodulation is locally applied and fed into a feedback network to the modulator input. The delta-modulator should exhibit similar properties to such systems.

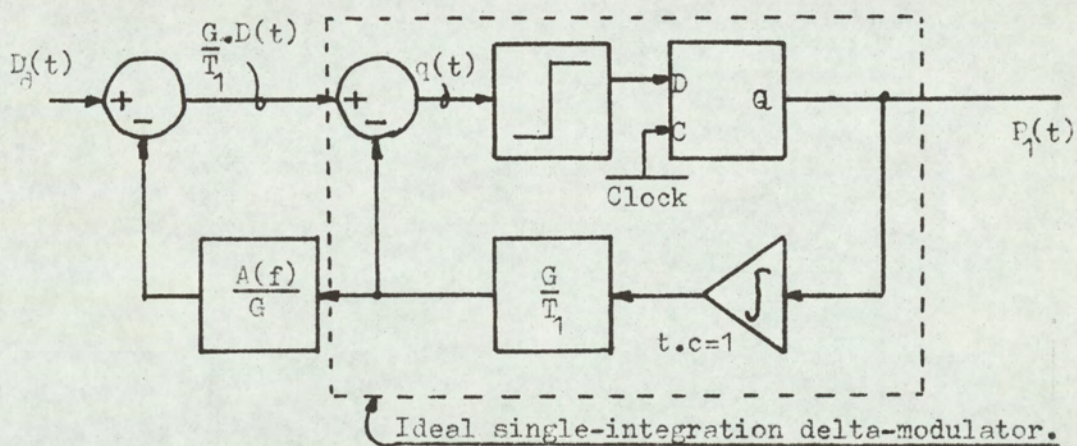
It is also important to realise that the model can only be used to simulate systems with a predictive loop due

to its finite forward gain. It is clear that if  $G \rightarrow 0$ , the system is unrealisable as an equivalent model network.

Equation (3.44) also represents a stability criterion. For any step input  $D_d(t)$ , a sequence of  $P_2(t)$  must be found such that, at each sample time, the summation on the left-hand side of the equation will converge to an error  $< \frac{1}{2}$ , represented by  $q(t)$ . It must be emphasised, however, that the introduction of zero-order hold and analogue circuits considerably modifies the system performance. To realise the ideal summation system, digital techniques are essential.



(A)



(B)

Fig.3-10. Alternative equivalent networks of a double-integration delta-modulator.

(A)...General form of delta-modulator with predictive loop.

(B)...Identical network to (A) but rearranged to expose ideal single-integrator delta-modulator.

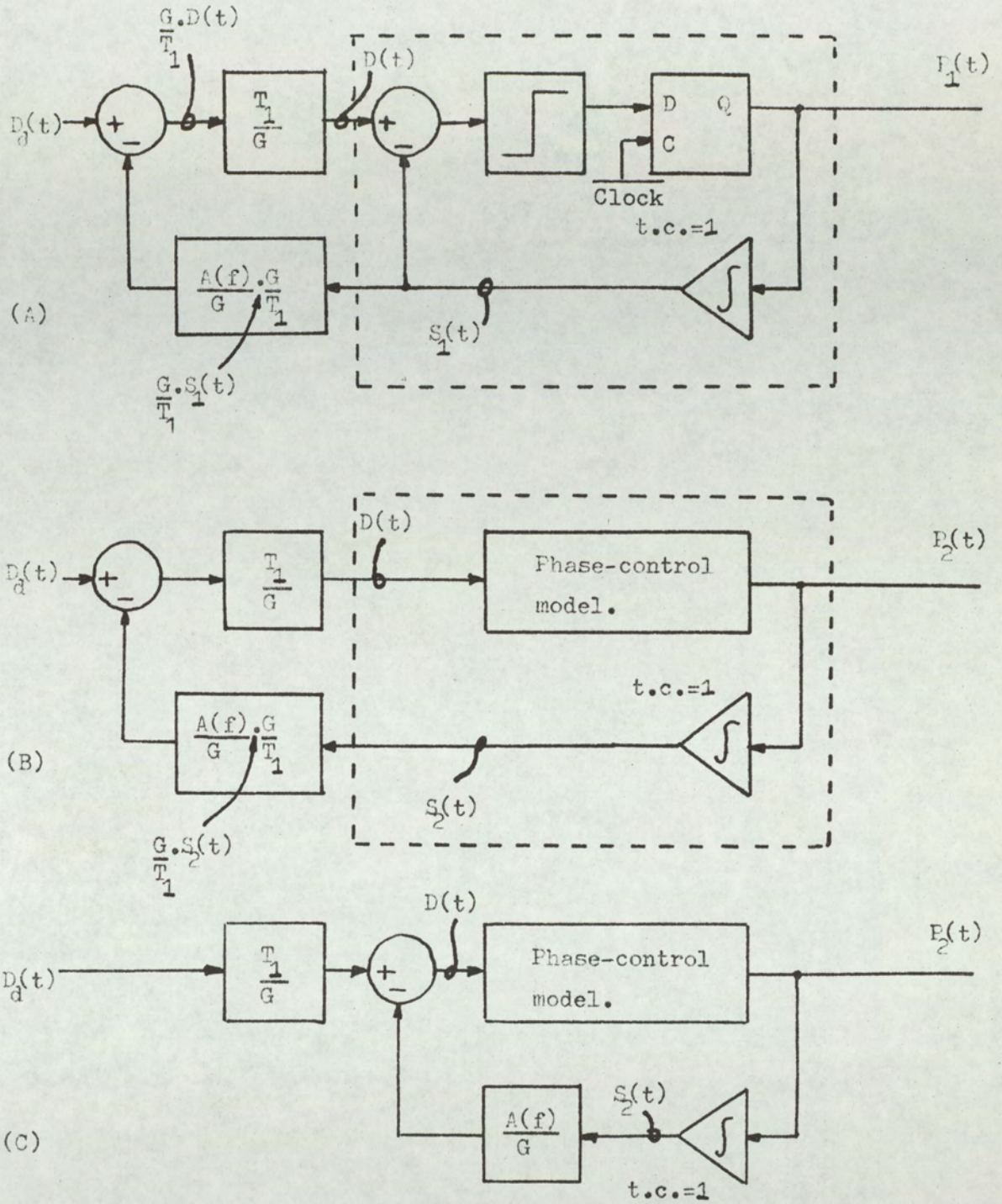


Fig.3-11. Equivalent model for second-order delta-modulator.

(A)...Rearranged second-order delta-modulator.

(B)...Equivalent model network derived from (A).

(C)...Final rearranged equivalent model of second-order delta-modulator.

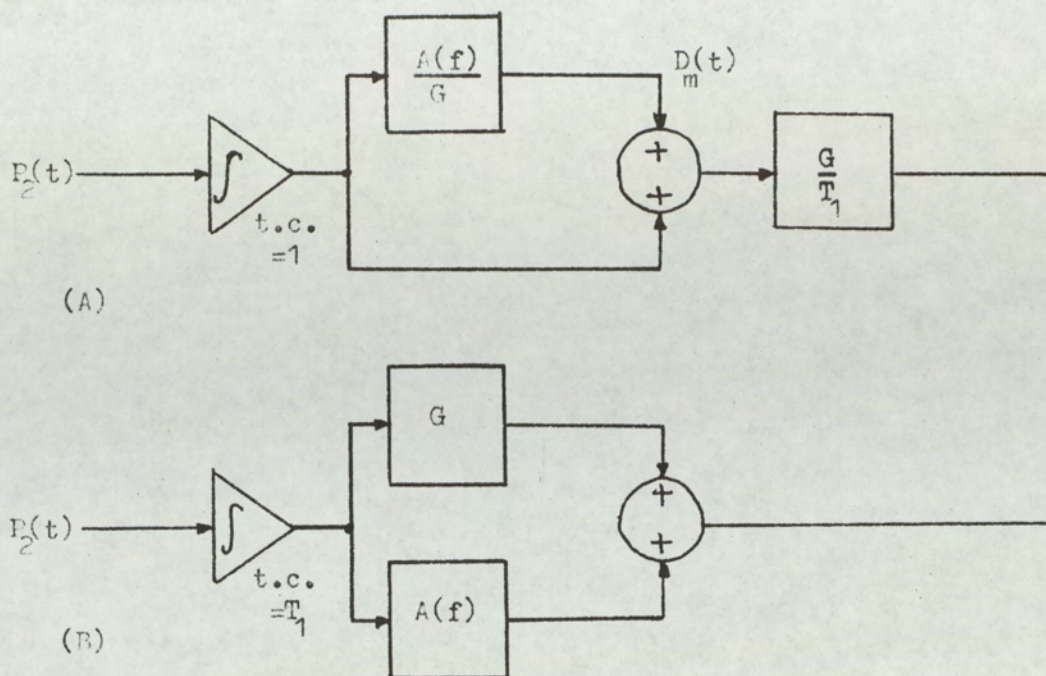


Fig.3-12. Derivation of decoder network for second-order model.

(A)... Decoding network derived from equivalent model system.

(B)... Rearrangement of (A) demonstrating that decoding network is equivalent to second-order system.

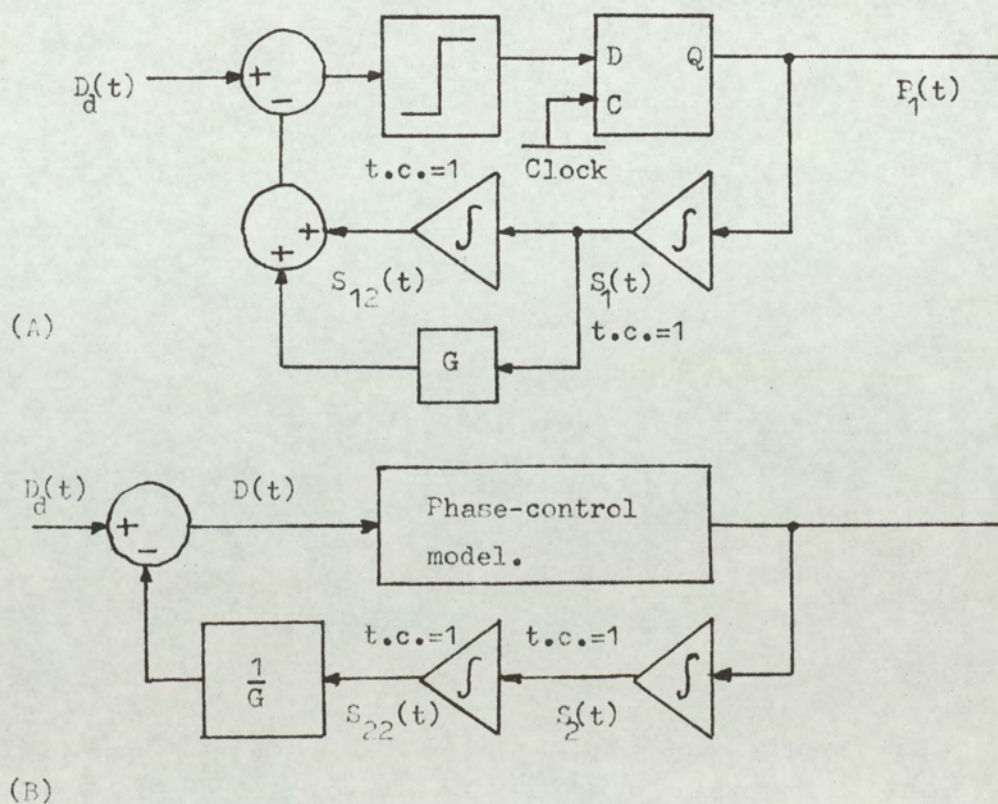


Fig.3-13. Double-integration delta-modulator with model equivalent.

(A)... Double-integration delta-modulator with prediction.

(B)... Model equivalent of (A).

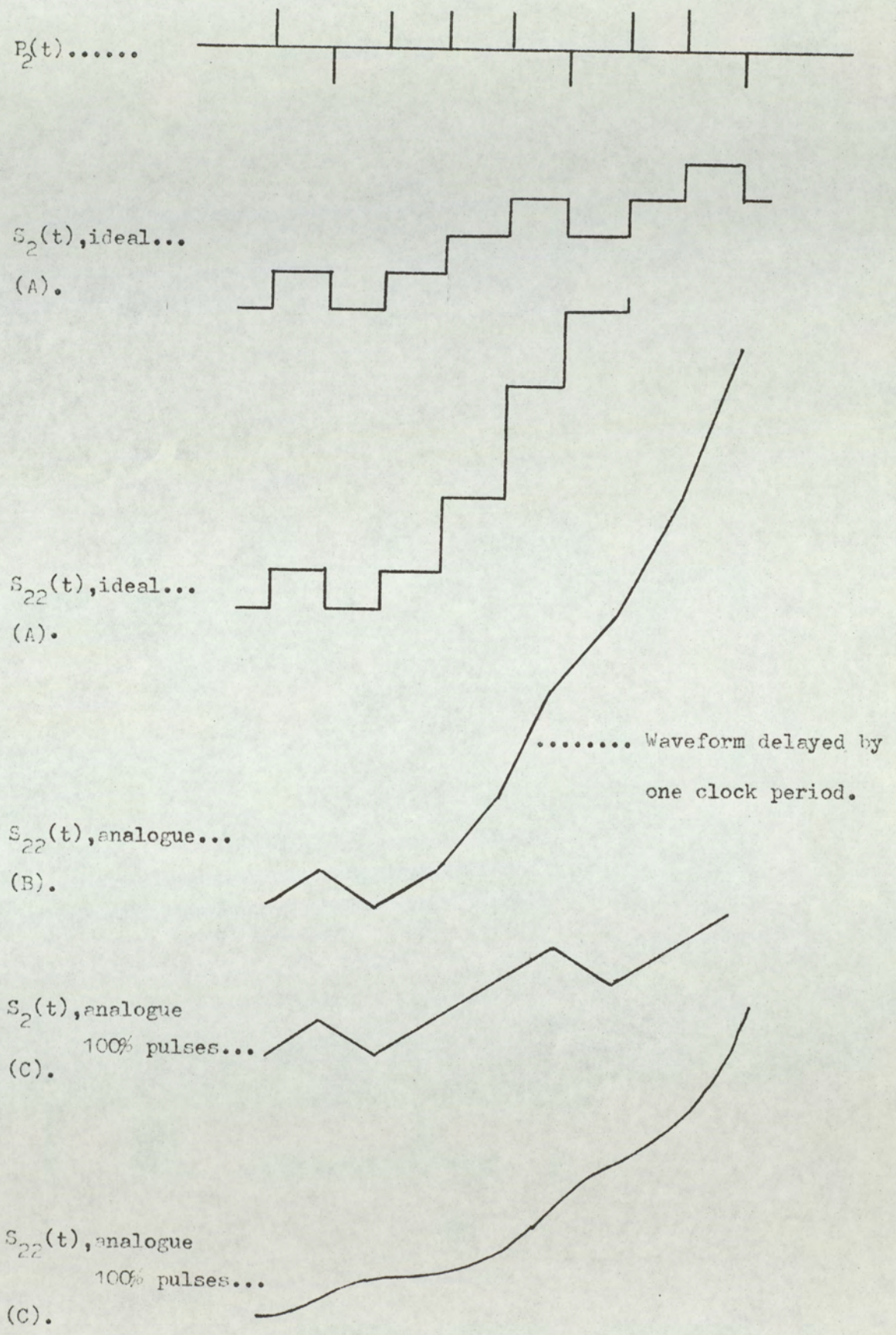


Fig.3-14. Illustration of optimum and non-optimum integration.

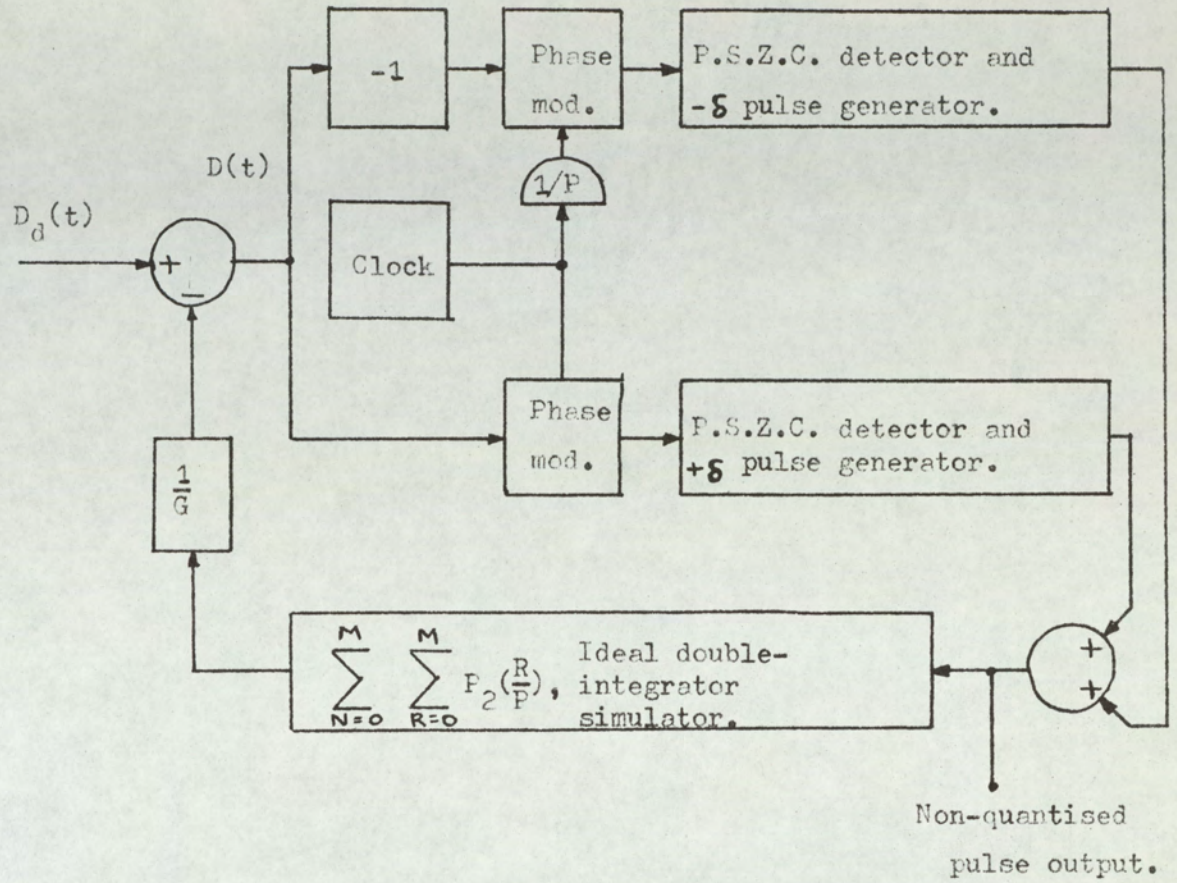


Fig.3-15. Double-carrier model simulating double-integration delta-modulator, without time quantisation of output pulses.

### 3.7 Generalised model to include slope overload.

The basic model is not capable of producing the slope-overload characteristic of delta-modulation. In a practical implementation, this concept can be introduced, but the structure is not readily analysed. The slope-overload condition does not occur in the single-integrator model providing that the modulating signal  $D(t)$  does not drive the phase modulator over a frequency deviation greater than  $\pm P/2$ , (where  $P$  is the system clock rate and  $P/2$  the centre frequency of the phase modulator). Thus, to prevent overload, the signal slope must be pre-distorted by special slope limiters. Such a modification to the signal slope will produce a reduction in the signal to quantisation-error noise ratio, even before digital modulation.

In a feedback delta-modulator, the slope limitation is more complex than can be achieved by a simple slope limiter. When a delta-modulator ceases to be in slope overload, the output level is the same as the input signal level (except for quantisation error). If simple slope limitation was applied to the modulating signal, this condition would no longer apply. Thus, the output of the slope limiter would not be equal to the input signal after slope limitation had occurred. The function of the slope limiter, which is to precede the deltamodem model, is illustrated in Fig. 3.16.

When the signal slope of  $D(t)$  is less than the overload limit, the transfer function of the slope limiter is 1. When the slope of  $D(t)$  exceeds the maximum slope

which the delta-modem can accept, the limiter maintains its output at the maximum slope. This value is maintained until the output of the slope limiter is equal to the input signal  $D(t)$ . A simple slope limiter would only maintain the output at maximum slope during the time when the signal slope was overloading the system. Thus, when the limiter ceased to limit, the output signal amplitude would generally not be equal to the modulating signal  $D(t)$ .

A basic practical limiter which meets the requirements of the delta-modulator is illustrated in Fig. 3.17.

Consider the transfer function during the linear region of the system. Applying Laplace and using the notation in Fig. 3.17, then,

For the integrator:

$$D_L(S) = \frac{1}{S}(\bar{M}_1 + \bar{M}_2)$$

but  $\bar{M}_1 = S \cdot D(S)$ , by differentiation

and  $\bar{M}_2 = A \cdot (D(S) - D_L(S))$ .

Therefore,  $D_L(S) = \frac{1}{S}(S \cdot D(S) + A \cdot D(S) - A \cdot D_L(S))$ ,

Rearranging,

$$D_L(S) \cdot \{A+S\} = D(S) \cdot \{A+S\},$$

Therefore,  $D_L(S) = D(S)$ .

thus,  $D_L(t) = D(t)$

If, however,  $D(t)$  exceeds the slope-overload condition, then the output of the differentiator causes the amplitude limiter to limit. In turn, the output of the integrator is a ramp of constant slope, the levels being adjusted to just hold the delta-modem at overload,

i.e. all 1 pulses or all 0 pulses as output. When  $D(t) \neq D_L(t)$  the amplified error signal  $\bar{M}_2$  is large thus maintaining the slope limiter in limitation.  $\bar{M}_2$  cannot become zero until the input and output are equal. Thus, slope limiting is held until  $D_L(t) = D(t)$ .

In the deltamodem model discussed, the maximum signal slope was  $P$ , which was equal to the clock rate (i.e. unit-step height in deltamodem). By making the integrator and differentiator of unit-time constant, the amplitude of limitation controls the signal slope. The amplitude limiter is assumed to have a unit-transfer function when it is not limiting.

It is interesting to note that the output of the phase-controlled model is identical to the modulating signal when on the limit of slope overload. That is, when  $D(t) = \pm P$ , then  $S_2(t) = \pm P$ , without quantisation error, assuming that the frequency components associated with the integrated pulse waveform are removed by low-pass filtering.

Thus, the error noise caused by slope limiting of the modulation signal may be added to the quantisation noise of the delta-modulator. This is because during slope overload only the slope limiter exhibits an error 'noise'. The noise analysis of the phase-control model becomes difficult under slope overload. However, if the modulating signal is periodic, each section of the modulating signal may be treated separately. That is, during the active region only the deltamodem produces error and during slope

limitation, only the slope limiter produces error. Thus the two error sources operate on a complementary basis, both adding to the total system noise.

Thus, preceding the deltamodem model by the network shown in Fig. 3.17, the slope overload condition of a delta-modulator can be simulated.

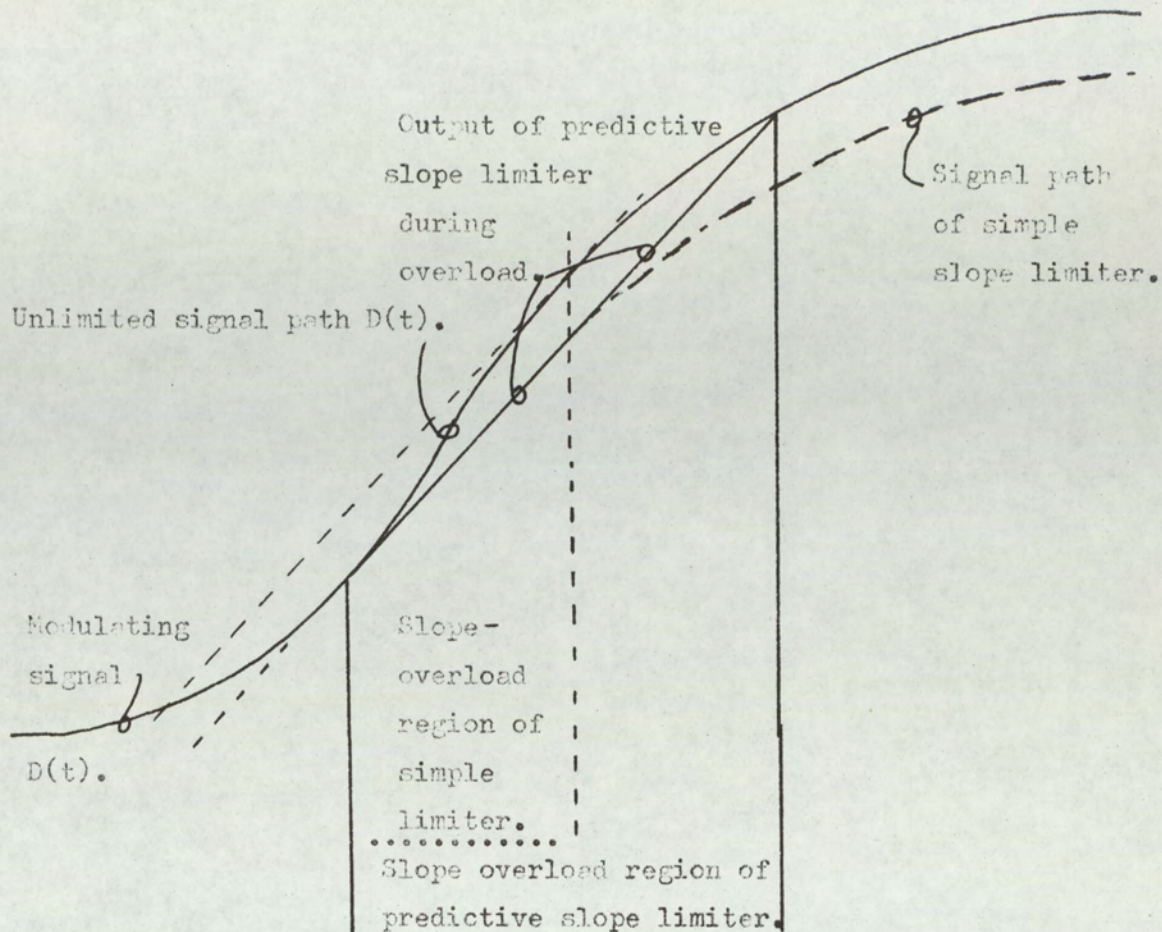


Fig.3-16. Slope-overload function required for deltamodem model.

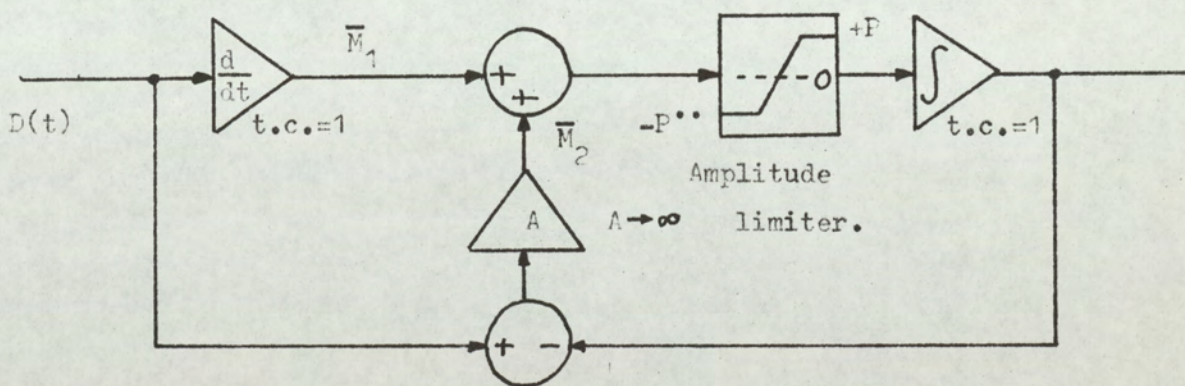


Fig.3-17. Basic slope limiter required for deltamodem model.

## 3.8 Extension of model to P.C.M. (21, 22)

In section (2.5) the relationship between delta-modulation and P.C.M. was discussed and equations (2.51) and (2.52) demonstrated the sampling principle formally. This method is also applicable to the deltamodem model, the parallel equations being determined by putting:

$$S_2(t) = S_1(t)$$

$$\text{hence, } S_{\text{PCM}}(t) = S_2(t) \cdot \sum_{M_1=-\infty}^{+\infty} \delta\left(t - \frac{M_1}{f_s}\right) \quad \dots(3.45)$$

$$S_{\text{PCM}}(f) = f_s \cdot \sum_{M_1=-\infty}^{+\infty} S_2(f - M_1 \cdot f_s) \quad \dots(3.46)$$

It is possible to formulate a P.C.M. model based almost exactly on the double-carrier model of section (3.4). Equation (3.30) states that the integrated output of the positively and negatively modulated, delta-pulse generators, evaluated at the  $N^{\text{th}}$  sample is within  $\pm 1$  of the modulating signal  $D(t)$ . The P.C.M. model is shown in Fig. 3.18.

Equation (3.25) states that after  $N$  clock periods, there will have been  $N$  positive and negative delta pulses. Thus, it can be concluded that if  $N$  is an even integer, then the integrated delta pulses are at an even level. If  $N$  is odd, then the integrator output is odd.

According to equation (2.44), the integrated waveform is sampled at a frequency  $f_s$ , where

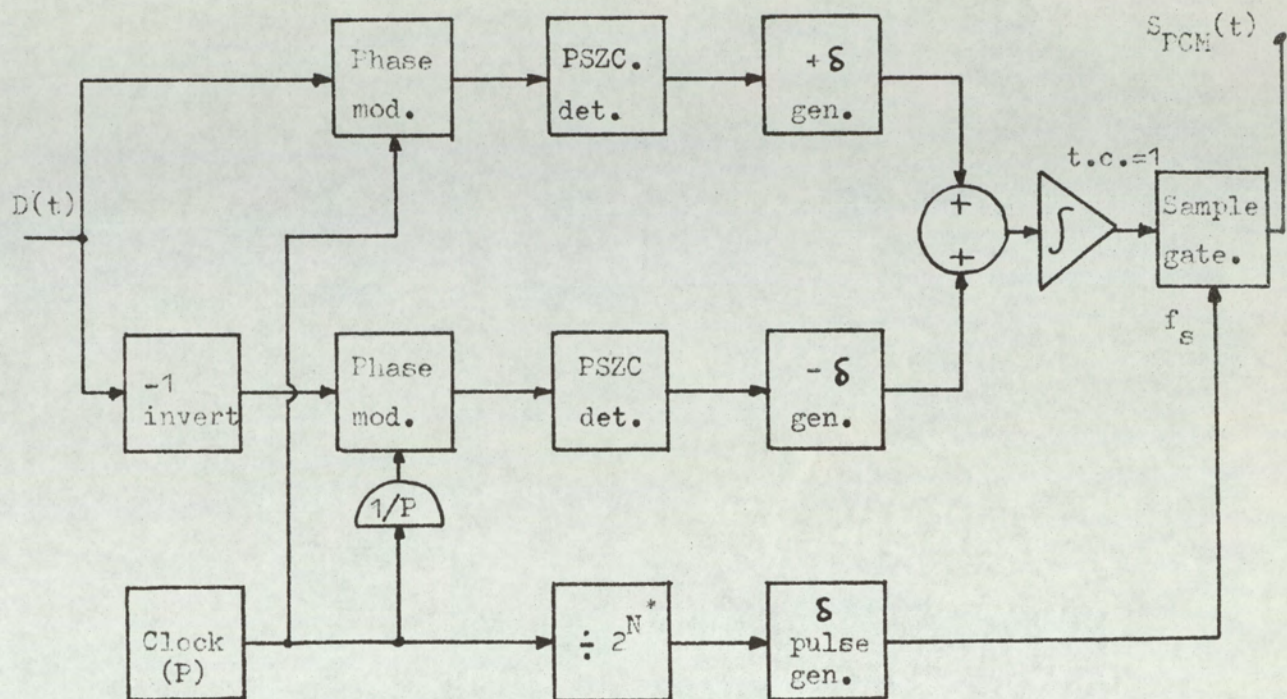
$$f_s = \frac{P}{2N}$$

i.e. Sampling period =  $\frac{2N}{P}$ ,

The restriction on  $N$  is defined by the conditions of equation (2.50).

Thus, using the model in Fig. 3.17, the standard pulse generator and delta-modulation sampling are eliminated, hence simplifying the spectral development of the quantised P.A.M. waveform.

In the model two phase modulators are used to develop  $x_P(t)$  and  $x_N(t)$ . At the P.S.Z.C.'s of  $x_P(t)$  a  $+\delta$  pulse is inserted and at the P.S.Z.C.'s of  $x_N(t)$  a  $-\delta$  pulse is inserted. The two pulse streams are algebraically added by integration using a unit time-constant integrator to form a unit-step function. After sampling at a rate  $f_s$ , the weighted delta-pulse samples of the quantised P.A.M. signal for the P.C.M. system are produced. Normally a sample-and-hold network of suitable duration would be introduced. Such a network is illustrated in the next chapter in Fig. 4.2.



\*  $N$  refers to Eqn.(2-50).

fig.3-18. Double-carrier P.C.M. model.

CHAPTER 4. ANALYSIS OF  $\Delta$ M and P.C.M. SYSTEMS USING  
MODEL EQUIVALENT.

4.1 Direct analysis of delta-modulation and P.C.M. systems for sinusoidal inputs, with extensions to general periodic functions. (13, 14)

The analysis presented is suitable for evaluation of the spectral components of a delta-modulator when excited by a sine-wave input. The analysis uses the phase-control model equivalent in developing the spectrum. The final equations are suitable for computer evaluation. The analysis is restricted to signals within the bound of slope overload.

A phase-modulated carrier is described by equation (4.1), where,

$$x(t) = X \cdot \text{Sin}\{\pi \cdot (P \cdot t + D(t))\}, \quad \dots(4.1)$$

where,  $x(t)$  is the phase-modulated sine wave.

$X$  the amplitude of the phase-modulated sine wave.

$P/2$  the centre frequency, where  $P$  is the equivalent  $\Delta$ M clock rate.

$D(t)$  the modulating input signal.

The P.S.Z.C.'s of  $x(t)$  occur when the phase of  $x(t)$  is multiples of  $2\pi$ .

Let  $t_m$  be the time of the  $M^{\text{th}}$  P.S.Z.C., measured from zero time.

Hence, considering the phase of  $x(t)$ ,

$$2\pi \cdot M = \pi \cdot \{P \cdot t_m + D(t_m)\},$$

$$\text{Therefore, } 2M = P.t_m + D(t_m), \quad \dots(4.2)$$

Consider a modulating signal,

$$D(t_m) = -D.\text{Sin}(\omega_m.t_m), \quad \dots(4.3)$$

Hence from equations (4.2) and (4.3),

$$2M = P.t_m - D.\text{Sin}(\omega_m.t_m), \quad \dots(4.4)$$

where,  $D$  is the amplitude of modulating signal,

$\omega_m$  is the angular frequency of modulating signal.

An equation of the form,

$$\psi = \phi - e.\text{Sin}(\phi),$$

has a solution for  $\phi$  as,

$$\phi = \psi + 2. \sum_{N=1}^{\infty} \frac{1}{N}.J_N(N.e).\text{Sin}(N.\psi),$$

Rearranging equation (4.4) gives,

$$\frac{2.M}{P}.\omega_m = \omega_m.t_m - \frac{D.\omega_m}{P}.\text{Sin}(\omega_m.t_m)$$

Hence, solving for  $(\omega_m.t_m)$ ,

$$\omega_m.t_m = \frac{2.M}{P}.\omega_m + 2. \sum_{N=1}^{\infty} \frac{1}{N}.J_N\left(\frac{N.D.\omega_m}{P}\right).\text{Sin}\left(\frac{N.2.M.\omega_m}{P}\right),$$

Therefore,

$$t_m = \frac{2.M}{P} + \frac{2}{\omega_m} \sum_{N=1}^{\infty} \frac{1}{N}.J_N\left(\frac{N.D.\omega_m}{P}\right).\text{Sin}\left(\frac{2.N.M.\omega_m}{P}\right),$$

.....(4.5)

Equation (4.5) gives the solution for the times of the P.S.Z.C. which depends upon the value of  $M$ . The times

are seen to be exact time positions occurring at half clock intervals, the positions of which are modulated in phase by the addition of the second term in equation (4.5).

The output of the phase modulator, after P.S.Z.C. detection, has a pulse generated of length  $1/P$ , which is initiated at each P.S.Z.C. The system output is thus a sequence of pulses, each pulse being allocated to a value of  $M$ . The range of  $M$  is assumed infinite for a periodic modulating signal, thus:

$$-\infty < M < \infty.$$

Since the input signal is periodic, a condition must be reached whereby the output pulse pattern repeats. Let the pulse pattern repeat after every  $K_0$  pulses of the idling patterns.

$$\text{Hence, at every } K_0^{\text{th}} \text{ pulse, } t_m = t_k \dots(4.6)$$

Since there is no d.c. component in the modulating signal, the total number of pulses that have occurred in the periodic pulse group must equal the number of pulses that would occur in an unmodulated sequence (i.e. idling pattern). Otherwise, **when** integrated, a d.c. shift would occur.

Hence,  $K_0$  pulses have occurred at a mean rate of  $P/2$  P.P.S. (Note that these pulses are the positive pulses only in the delta-modulator pulse waveform.)

$$\text{Therefore, } t_K = \frac{2 \cdot K_0}{P} \dots(4.7)$$

where  $t_K$  is the time duration of the pulse group.

$$\text{At time } t_K, \quad M = K_0 \dots(4.8)$$

Substituting for  $M$  and  $t_K$  from equations (4.7) and (4.8) into equation (4.5),

therefore,

$$t_K = \frac{2 \cdot K_o}{P} + \frac{2}{\omega_m} \cdot \sum_{N=1}^{\infty} \frac{1}{N} \cdot J_N \left( \frac{N \cdot D \cdot \omega_m}{P} \right) \cdot \sin \left( \frac{2 \cdot N \cdot K_o \cdot \omega_m}{P} \right)$$

$$= \frac{2K_o}{P},$$

Hence,

$$\frac{2}{\omega_m} \cdot \sum_{N=1}^{\infty} \frac{1}{N} \cdot J_N \left( \frac{N \cdot D \cdot \omega_m}{P} \right) \cdot \sin \left( \frac{2 \cdot N \cdot K_o \cdot \omega_m}{P} \right) = 0 \quad \dots (4.9)$$

i.e. for every  $K_o^{\text{th}}$  pulse, the phase modulation of the P.S.Z.C.'s is the same.

Equation (4.9) contains both zeroes of  $J_N(\dots)$  and zeroes of  $\sin(\dots)$ . However, the cycle of pulses depend only upon the frequency of the modulating signal; thus the selected zeroes must be independant of  $D$ . It is also necessary that an integral number of cycles of  $x(t)$  are chosen, since the reference is the P.S.Z.C. The choice of zeroes must reject those that occur at odd half cycles, i.e. the negative-slope zero crossings.

Thus, for the summation over the range  $N$  to be independant of values of  $D$ , up to slope overload, then:

$$\sin \left( \frac{2 \cdot N \cdot K_o \cdot \omega_m}{P} \right) = 0, \quad \text{for all } N.$$

For this condition and the conditions that the solution be selected at only even half cycles and independant of  $N$ .

$$\left( \frac{2 \cdot N \cdot K_o \cdot \omega_m}{P} \right) = N \cdot (Z \cdot 2\pi),$$

Simplifying,

$$\frac{K_0 \cdot \omega_m}{P} = \pi Z, \quad \dots(4.10)$$

Putting,  $\omega_m = 2 \cdot \pi \cdot f_m$  \dots(4.11)

Thus, from equations (4.10) and (4.11),

$$K_0 = Z \cdot \frac{P}{2 \cdot f_m} \quad \dots(4.12)$$

where,  $f_m$  is the modulating frequency.

$Z$  is a positive integer such that the solution of  $K_0$  is the lowest positive integer.

Since  $t_K$  represents the period of occurrence of the pulse pattern, then the fundamental-frequency component in the pulse waveform is  $f_0$ , where,

$$f_0 = \frac{1}{t_K} \quad \dots(4.13)$$

which, from equation (4.7) and (4.12), gives

$$f_0 = \frac{f_m}{Z} \quad \dots(4.14)$$

The theory states that after  $K_0$  pulses, the pulse pattern repeats. Thus:

The period between pulse  $(L \cdot K_0 + R')$  and pulse  $((L+1) \cdot K_0 + R')$  is constant, where  $L$ ,  $K_0$ ,  $R'$  are integers.

$$1 \leq R' \leq K_0,$$

( $L$  is a positive or negative integer).

From this, it is concluded that pulses that are  $K_0$  pulses apart are all equally spaced. The infinite pulse sequence is therefore broken down into groups of  $K_0$  pulses. Thus, if in each group the pulses are numbered,

$$1, 2, 3, \dots R', \dots (K_0-1), K_0,$$

Then, pulse  $R'$  can be associated with pulse  $R'$  in every group and will form a basic pulse sequence of constant period  $P/(2.K_0)$ . Hence, for each value of  $R'$  there is a pulse sequence which is identical except for a time displacement. The time displacement depends upon the state of modulation of the  $R^{\text{th}}$  pulse. The spectrum of the basic pulse spectrum is derived, then the time-shift theorem is applied to each pulse sequence generated by every value of  $R'$  in the group of  $K_0$  pulses. Finally the Superposition Theorem is applied over the range of  $R'$ . Fig. 4.1 illustrates the principle.

Let  $F_B(f)$  be the basic pulse spectrum of the pulse sequence of duration  $2K/P$ . This includes the pulse at  $t=0$ . The fundamental frequency component of this pulse group is given by equation (4.14).

Consider the  $R^{\text{th}}$  pulse in each group. The first  $R^{\text{th}}$  pulse occurs at time  $t_R$ . Hence, using the Time Shift Theorem, the spectrum generated,  $F_R(f)$ , by all the  $R^{\text{th}}$  pulses is,

$$F_R(f) = e^{-j2\pi f \cdot t_R} \cdot F_B(f) \quad \dots(4.15)$$

The total spectrum of every pulse is therefore given by the Superposition Theorem as  $F_T(f)$ , where:

$$F_T(f) = \sum_{R=1}^{K_0} F_R(f)$$

Therefore

$$F_T(f) = F_B(f) \cdot \sum_{R=1}^{K_0} e^{-j2\pi f \cdot t_R} \quad \dots(4.16)$$

Let the basic function be a sequence of delta pulses of period  $(\frac{2K_0}{P})$ , with a pulse coincident with the  $t=0$  sample.

Thus, basic function period =  $\frac{2K_o}{P}$ .

Therefore, basic function frequency =  $\frac{P}{2K_o}$ . ....(4.17)

Thus, from equations (4.12), (4.14), (4.17):

$$f_o = \frac{P}{2K_o} \quad \dots(4.18)$$

Thus, the lowest frequency component of the P.P.M. signal is the frequency of the basic function.

The basic function is defined,

$$F_B(t) = \sum_{Q=-\infty}^{+\infty} \delta\left(t - \frac{Q}{f_o}\right) \quad \dots(4.19)$$

Taking the Fourier Transform of equation (4.19)

$$F_B(f) = \int_{-\infty}^{+\infty} \left\{ \sum_{Q=-\infty}^{+\infty} \delta\left(t - \frac{Q}{f_o}\right) \right\} e^{-j2\pi ft} . dt$$

Rearranging the order of integration and summation and applying the Time Shift Theorem:

$$\text{Therefore, } F_B(f) = \sum_{Q=-\infty}^{+\infty} e^{-j2\pi f \frac{Q}{f_o}}$$

This has the spectrum:

$$F_B(f) = f_o \cdot \sum_{Q=-\infty}^{+\infty} \delta(f - Q \cdot f_o) \quad \dots(4.20)$$

Substituting  $F_B(f)$  from equation (4.20) into equation (4.16),

$$F_T(f) = \left[ f_o \sum_{Q=-\infty}^{+\infty} \delta(f - Q \cdot f_o) \right] \cdot \left[ \sum_{R=1}^{K_o} e^{-j2\pi ft_R} \right] \quad \dots(4.21)$$

Examination of equation (4.5) shows that,

$$t_M = -t_{-M} \quad \dots(4.22)$$

The pulse sequence is even. Hence, the Fourier series  $F_T(f)$  has Cosine terms only for the modulating function chosen. The summation of  $R'$  from  $1 \rightarrow K_0$  can therefore be expressed as:

$$\sum_{R=1}^{K_0} e^{-j2\pi ft_R} = \sum_{R=1}^{K_0} \cos(2\pi ft_R) - j \sum_{R=1}^{K_0} \sin(2\pi ft_R)$$

Therefore

$$\sum_{R=1}^{K_0} e^{-j2\pi ft_R} = \sum_{R=1}^{K_0} \cos(2\pi ft_R) \quad \dots(4.23)$$

$$\text{and } \sum_{R=1}^{K_0} \sin(2\pi ft_R) = 0 \quad \dots(4.24)$$

Thus equation (4.21) can be written,

$$F_T(f) = f_0 \cdot \left[ \sum_{Q=-\infty}^{+\infty} \delta(f - Q \cdot f_0) \right] \cdot \left[ \sum_{R=1}^{K_0} \cos(2\pi f \cdot t_R) \right] \quad \dots(4.25)$$

The  $\delta$  pulses that have been phase-modulated by the sine-wave input to generate the line spectrum of equation (4.25) are next converted to a standard pulse, as defined in the model equivalent. Each delta pulse is converted to a finite pulse of 2 units amplitude and duration  $1/P$ . Fig. (4.2) illustrates the conversion process.

Hence,

$$F_s(f) = \frac{2}{j2\pi f} \cdot \left[ F_T(f) - e^{j2\pi f/P} \cdot F_T(f) \right],$$

$$\text{Putting, } \frac{\sin(\frac{\pi f}{P})}{\frac{\pi f}{P}} = \text{Sinc}\left(\frac{\pi f}{P}\right),$$

Therefore,

$$F_s(f) = \frac{2}{P} \cdot e^{-j\pi f/P} \cdot \text{Sinc}\left(\frac{\pi f}{P}\right) \cdot F_T(f) \quad \dots(4.26)$$

Combining equations (4.25) and (4.26) to eliminate  $F_T(f)$ , subtracting a d.c. level of -1 to cancel the d.c. component of  $F_S(f)$  and finally rearranging, gives:

$$F_S(f) = \left[ \frac{2.f_o}{P} \sum_{Q=-\infty}^{+\infty} \sum_{R=1}^{K_o} e^{-j\pi Q f_o / P} \cdot \text{Sinc}\left(\frac{\pi.Qf_o}{P}\right) \cdot \text{Cos}(2\pi Q f_o \cdot t_R) \cdot \delta(f - Q f_o) \right] - \delta(f) \quad \dots(4.27)$$

It should be noted that,  $f = Q.f_o$ , since the frequency  $f$  is only evaluated at these values of  $Q.f_o$ .

The next process is to sample the standardised pulse-phase modulated pulses by a delta sifting function, the sampling rate being at the equivalent clock rate  $P$ . The sampling function takes the form,

$$f_s(t) = \sum_{M=-\infty}^{+\infty} \delta\left(t - \frac{M}{P}\right), \quad \dots(4.28)$$

The product of the P.P.M. standardised time signal and sifting function leads to a resultant spectrum evaluated through Convolution as,

$$\begin{aligned} F_{P2}(f) &= F_S(f) * \int_{-\infty}^{+\infty} f_s(t) e^{-j\omega t} dt, \\ &= F_S(f) * \int_{-\infty}^{+\infty} \left\{ \sum_{M=-\infty}^{+\infty} \delta\left(t - \frac{M}{P}\right) \right\} e^{-j\omega t} dt, \end{aligned}$$

Therefore

$$F_{P2}(f) = P \cdot \sum_{M=-\infty}^{+\infty} F_S(f - M.P) \quad \dots(4.29)$$

$F_{P2}(f)$  is the spectrum of the output-pulse sequence of the model when the pulses are in a delta format. Combining equations (4.29) and (4.27) to calculate the final spectrum:

Therefore,

$$F_{P2}(f) = 2 \cdot f_o \sum_{M=-\infty}^{+\infty} \sum_{Q=-\infty}^{+\infty} \sum_{R=1}^{K_o} e^{-j\pi \frac{(Qf_o - MP)}{P}} \cdot \text{Sinc} \left\{ \frac{\pi(Qf_o - MP)}{P} \right\} \cdot \text{Cos} \{ 2\pi(Qf_o - MP) \cdot t_R \} \cdot \delta(f - (Qf_o - MP)) \quad \dots(4.30)$$

\*Q≠0.

i.e. Putting Q≠0 is equivalent to subtracting  $\delta(f)$  in equation (4.27) when d.c. level of P.P.M. signal is zero.

The value of  $t_R$  is calculated from equation (4.6). Putting  $t_R = t_M$ , gives,

$$t_R = \frac{2 \cdot R'}{P} + \frac{2}{\omega_m} \sum_{N=1}^{\infty} \frac{1}{N} J_N \left( \frac{N \cdot D \cdot \omega_m}{P} \right) \cdot \text{Sin} \left( \frac{2NK_o \omega_m}{P} \right), \quad \dots(4.31)$$

If the time function is neither odd nor even, then the general spectrum, from equations (4.21), (4.30), becomes:

$$F_{P2}(f) = 2 \cdot f_o \sum_{M=-\infty}^{+\infty} \sum_{Q=-\infty}^{+\infty} \sum_{R=1}^{K_o} e^{-j\pi \frac{(Qf_o - MP)}{P}} \text{Sinc} \left\{ \frac{\pi(Qf_o - MP)}{P} \right\} \cdot e^{j2\pi(Qf_o - MP)t_R} \cdot \delta(f - (Qf_o - MP)), \quad \dots(4.32)$$

Equations (4.30) and (4.31) allow the complex Fourier Transform of the output pulse sequence to be calculated for a sine-wave input signal.

The analysis described, may be readily applied to a general periodic function. Equation (4.32) may be used for any periodic function whose fundamental frequency component is  $\omega_m$ , the same as the sine wave input just considered. The values of  $K_o$  and  $f_o$  are determined on the

basis of the fundamental component  $\omega_m$ , other upper harmonics not effecting the values. However, equation (4.31) is no longer applicable. It is therefore necessary to calculate the values of  $t_R$  over the range  $(1 \leq R \leq K)$ , by another method. A general procedure uses a digital computer as follows.

The computer uses equation (4.1) as an algorithm, evaluating  $x(t)$  at various instants over a period  $(1/f_0)$ . The analysis could follow a binary selective procedure to locate the P.S.Z.C.'s of  $x(t)$ . First,  $x(t)$  is evaluated at equally-spaced samples for a range of  $t$ , where,

$$0 \leq t \leq (1/f_0)$$

The sampling rate is made greater than twice the highest deviation frequency, i.e. greater than  $2P$ . Thus, it is possible to position a P.S.Z.C. to the nearest time slot by comparing samples, the time slots being of duration  $1/P$ . When the time slots containing P.S.Z.C.'s are known, each slot may be divided equally into two, and the P.S.Z.C. allocated to its appropriate section by comparing sample values. This process may be repeated until the desired accuracy of  $t_R$  is obtained.

Fig. 4.3 illustrates the binary selective procedure for obtaining a better approximation to the P.S.Z.C.'s locations.

If the transform of the integrated waveform  $S_2(f)$  is required, then:

$$S_2(f) = \frac{F_{P2}(f)}{j.2\pi f}, \quad \dots(4.33)$$

At this stage in the analysis, the conversion to a P.C.M. system is readily achieved by sampling the transform

$S_2(f)$  at or above the Nyquist rate. The sampling rate is a function of the delta-modulator clock rate  $P$ . The delta samples are then converted to finite pulses by a standard hold network similar to Fig. 4.2.

Hence, from equation (4.33) and (2.52):

$$S_{\text{PCM}}(f) = f_s \cdot \sum_{M_1=-\infty}^{+\infty} \frac{F_{P2}(f - Mf_s)}{j2\pi(f - Mf_s)}, \quad \dots(4.34)$$

Where the restrictions of equation (2.50) are applied.

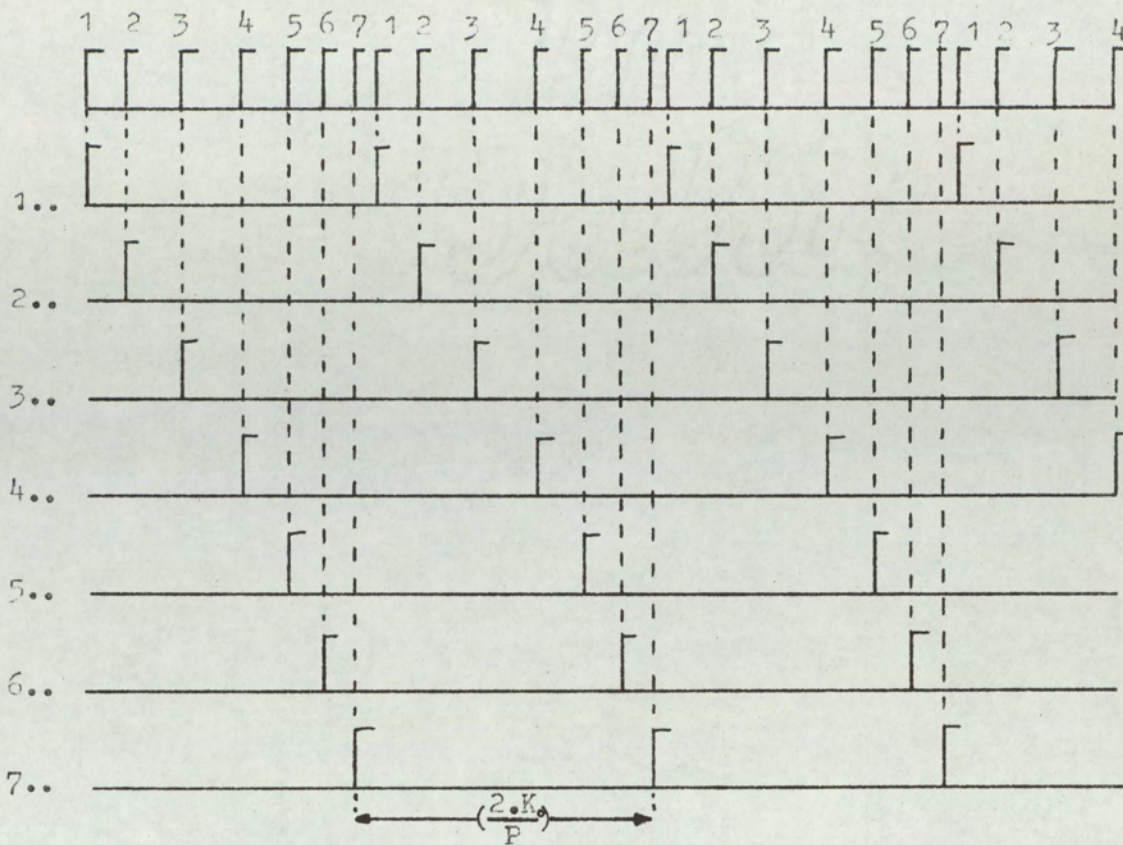


Fig.4-1. Pulse grouping of periodic pulse sequence.

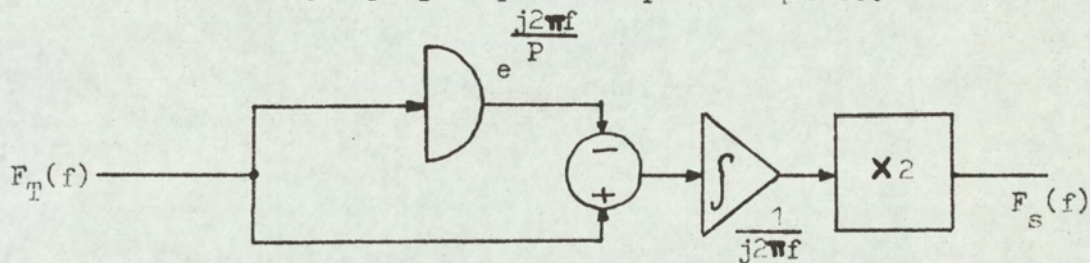
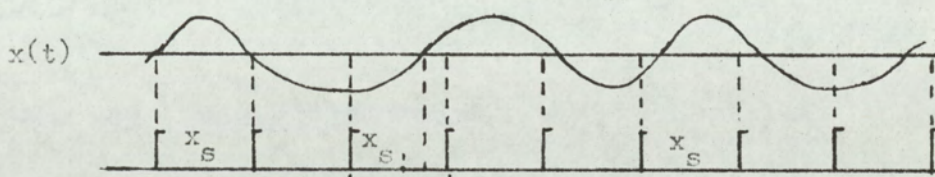


Fig.4-2. Standard pulse generator.



Example slot location.

At each clock sample, the time slot is divided into two. If a P.S.Z.C. is present, then it's position can be determined more accurately by further subdivision.

Fig.4-3. Location of  $t_R$  by binary slot division.

#### 4.2 Direct analysis of delta-modulation systems for ramp and sine-wave input signals. (13)

Although a ramp-input signal with superimposed sine wave is not practically realisable, except over finite periods, for delta-modulation. It is realisable when considering an equivalent delta-sigma modulator where it represents a constant d.c. level with superimposed sine wave.

13

It can be shown that an asymmetrical integrator (positive step-height is not equal to negative step-height) in a delta-modulator, is equivalent to a perfect integrator with a constant ramp input signal. The ramp input corrects for the integration asymmetry. Thus, when this asymmetry can be determined and the compensating ramp input calculated, it is necessary to add a ramp input to the perfect model to realise the practical system. A small d.c. offset with delta-sigma-modulation can also improve the coding threshold.

Let  $D_c$  be the slope of the ramp input and

$-D \cdot \sin(\omega_m t)$  the superimposed sinusoidal excitation.

Hence, 
$$D(t) = D_c \cdot t - D \cdot \sin(\omega_m t) \quad \dots(4.35)$$

Substituting for  $D(t)$  from equation (4.35) into equation (4.2),

therefore, 
$$2 \cdot M = P \cdot t_m - D_c \cdot t_m - D \cdot \sin(\omega_m t_m),$$

Rearranging,

$$2 \cdot M = (P - D_c) \cdot t_m - D \cdot \sin(\omega_m t_m) \quad \dots(4.36)$$

Hence, the addition of the ramp input modifies the mean rate of the P.S.Z.C.'s.

Hence, comparing equation (4.36) with equation (4.4) and modifying equations (4.5) and (4.12) gives:

$$t_m = \frac{2.M}{(P-D_c)} + \frac{2}{\omega_m} \sum_{N=1}^{\infty} \frac{1}{N} \cdot J_N \left( \frac{N.D.\omega_m}{(P-D_c)} \right) \cdot \text{Sin} \left( \frac{2.N.M.\omega_m}{(P-D_c)} \right), \quad \dots(4.37)$$

$$K_o = z \cdot \frac{(P-D_c)}{2.f_m} \quad \dots(4.38)$$

where, from equation (4.7),

$$t_K = \frac{2.K_o}{(P-D_c)} \quad \dots(4.39)$$

Using equations (4.37), (4.38), (4.39) in place of equations (4.5), (4.12) and (4.7), the analysis of the output spectrum may be determined as in section (4.1).

With superimposed slope modulation, the slope of the sinusoidal component must be reduced to prevent slope overload. Differentiating equation (4.35) and taking the maximum value,

$$\begin{aligned} \left. \frac{d}{dt} D(t) \right|_{\text{MAX}} &= D_c + \omega_m \cdot D, & D_c \text{ positive} \\ &= D_c - \omega_m \cdot D, & D_c \text{ negative} \\ \text{i.e. } \left. \frac{d}{dt} D(t) \right|_{\text{MAX}} &= |D_c| + |\omega_m \cdot D| \end{aligned}$$

The slope must not exceed the maximum slope, P, where P is the delta-modulator clock rate, and the step height is unity.

$$\text{Hence, } \{|D_c| + |\omega_m \cdot D|\} \leq P \quad \dots(4.40)$$

The infinite ramp input is not applicable to the P.C.M. system since the condition requires an infinite

signal range and P.C.M. has only a limited memory.

4.3 Direct analysis of delta-modulation system for ramp input. (13, 14)

To calculate the position of the P.S.Z.C.'s for the linear ramp input, put  $D=0$  in equation (4.35). Hence,

$$D(t) = D_c \cdot t \quad \dots(4.41)$$

$$\text{where, } |D_c| \leq P \quad \dots(4.42)$$

Hence, from equation (4.5),

$$t_m = \frac{2 \cdot M}{(P - D_c)} \quad \dots(4.43)$$

The P.S.Z.C.'s form a periodic function of fundamental frequency.

$$f_o = \frac{1}{\{t_{(m+1)} - t_m\}},$$

$$\text{therefore, } f_o = \frac{(P - D_c)}{2}, \quad \dots(4.44)$$

Hence, from equation (4.20),

$$F_B(f) = \frac{(P - D_c)}{2} \cdot \sum_{Q=-\infty}^{+\infty} \delta\left(f - Q \cdot \frac{(P - D_c)}{2}\right),$$

In this case,  $F_T(f) = F_B(f)$ , since the fundamental frequency is the actual pulse rate of the delta functions.

therefore,

$$F_T(f) = \left\{ \frac{P - D_c}{2} \right\} \cdot \sum_{Q=-\infty}^{+\infty} \delta\left(f - \frac{Q}{2} \cdot \{P - D_c\}\right) \quad \dots(4.45)$$

The spectrum  $F_{P2}(f)$  becomes,

$$F_{P2}(f) = \left( \frac{P - D_c}{P} \right) \cdot \sum_{M=-\infty}^{+\infty} \left[ \sum_{Q=-\infty}^{+\infty} e^{-j\pi \left( \frac{(Q - 2M)P - D_c Q}{2P} \right)} \cdot \text{Sinc} \left\{ \frac{\pi \left( (Q - 2M)P - D_c Q \right)}{2P} \right\} \right. \\ \left. \cdot \delta \left\{ f - \left( \frac{QP}{2} - \frac{QD_c}{2} - MP \right) \right\} - \delta(f - MP) \right] \quad \dots(4.46)$$

Equation (4.46) is the pulse spectrum of  $P_2(t)$  when the modulating signal is a linear ramp. Again there is no equivalent in the practical P.C.M. system.

4.4 High-band delta-modulation with low-frequency deviation, with application to spectral analysis of delta-modulation and P.C.M. system.

A delta-modulator operating at a clock rate of  $P$  (P.P.S.) is termed a low-band modulator, whereas a system operating at a higher pulse rate is termed a high-band modulator.

The model has described a system of phase modulation, where the carrier frequency deviates by a maximum frequency of  $(P/2)$  from the central carrier frequency  $P/2$ .

Such a modulation process produces a large number of side-bands of considerable power. Hence, calculations of the Fourier Transform are extremely complex for general functions. Initially, consideration is given to the integrated pulse waveform,  $S_2(t)$ , and an alternative method of generation is proposed. The waveform  $S_2(t)$  requires, that at the delta-modulator sampling instants, the integrated values of the pulse waveform are exposed. This was described in Chapter 3.

Let the clock rate  $b.P$  of the high-band delta-modulator be such that  $b$  is a positive integer. The high-band delta-modulator generates its integrated pulse waveform,  $S_H(t)$ . The waveform  $S_H(t)$  is sampled at the low clock rate,  $P$ , by a delta sampling function. There are two cases to consider.

Case 1:  $b$ . odd, positive integer.

By sampling  $S_H(t)$  by a delta sampling function,  $S_2(t)$  can be generated when  $b$  is an odd positive integer. It is important that the input-signal slope at no time exceeds slope overload condition of the low-band delta-modulator. Otherwise the sampled waveform changes may be greater than unity, assuming the high-band model has a unit-step output function. Consequently, the high-band modulator, whose input is made identical to the low-band modulator, is undermodulated.

The phase-modulated carrier of the high-band modulator, is obtained by modifying equation (3.12), such that,

$$x(t) = X.\text{Cos}\{\pi.(b.P.t + D(t))\}, \quad \dots(4.47)$$

Putting  $D(t)=P.t$  to generate maximum carrier deviation and so prevent overload of the low-band delta-modulator.

Therefore,

$$x(t) = X.\text{Cos}\{\pi.(b+1).P.t\},$$

i.e. the carrier deviation of the high-band model is  $\frac{P}{2}$ , but the centre frequency is  $\frac{bP}{2}$ . Hence the total deviation is only  $1/b$  of the maximum, under the stated loading conditions.

By making  $b$  large, the percentage deviation can be made small. Consequently, the analysis of the Fourier Transform of  $x(t)$  is simplified. Section 4.6 will extend this concept to provide an approximate solution for a general signal  $D(t)$ .

Case 2:  $b$ . even, positive integer.

For even  $b$ , the low-band samples are always on even levels; hence, the difference between two low-band samples is either zero or  $\pm 2$  units, providing that slope overload does not occur on the low-band system by undermodulating the high-band system, as before. Then each high-band sample has an error no greater than  $\pm 1$ ; similarly the low-band samples have the same error. However, since these sample values fall only on even levels, the P.C.M., quantised P.A.M., signal is generated where the quantisation step is of value 2 units, but the error is a maximum of  $\pm 1$ . This is the condition discussed in section (2.5). Hence, the delta-modulator centre frequency may be made large and the depth of modulation kept low. Then, by using even sampling, the P.C.M. system can be analysed. The same process is thus applicable to P.C.M. as for delta-modulation, the difference being in the even and odd sampling process. Both these sampling processes may be applied to the P.C.M. model of section 3.8. Thus, the P.C.M. model can generate the delta-modulated signal  $S_2(t)$  or the P.C.M. signal  $S_{PCM}(t)$ .

Fig. 4.6 shows a flow chart for basic direct calculations on the deltamodem model and P.C.M. model, for delta-modulation and P.C.M., P.A.M. quantised waveforms.

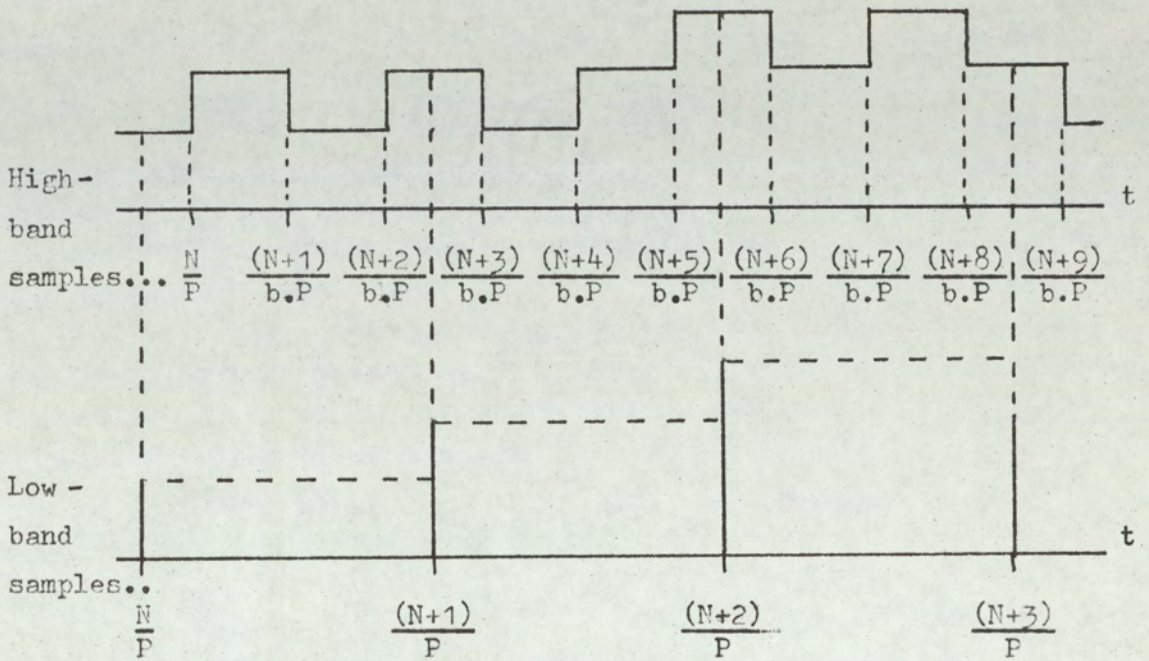


Fig.4-4. High-band to low-band conversion through sampling, for odd b.

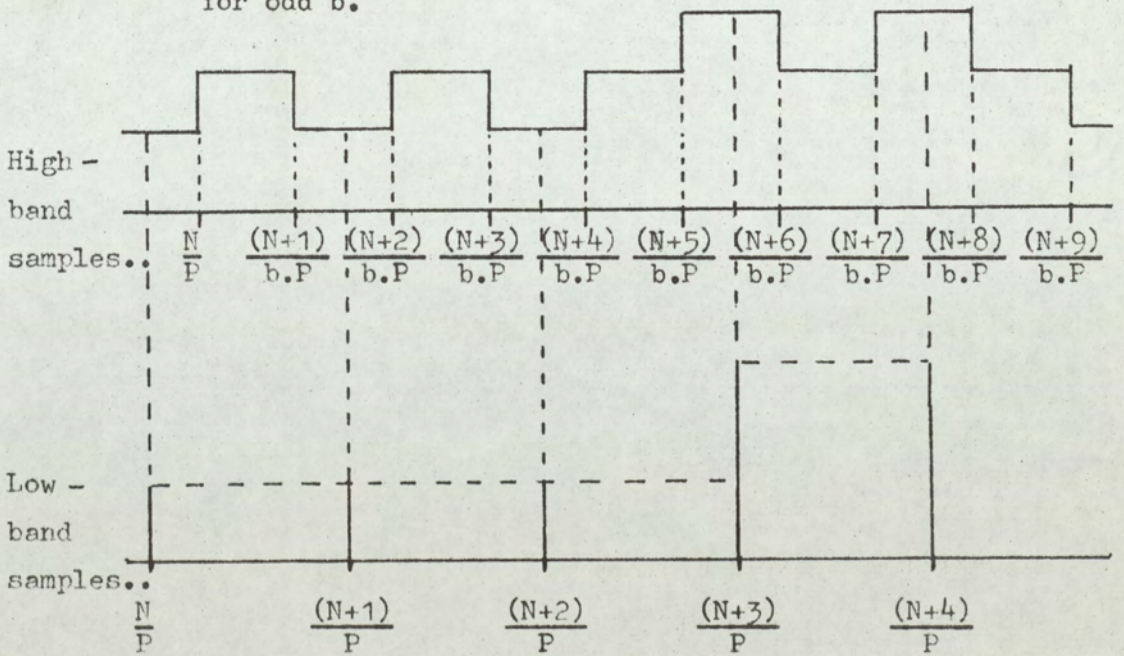
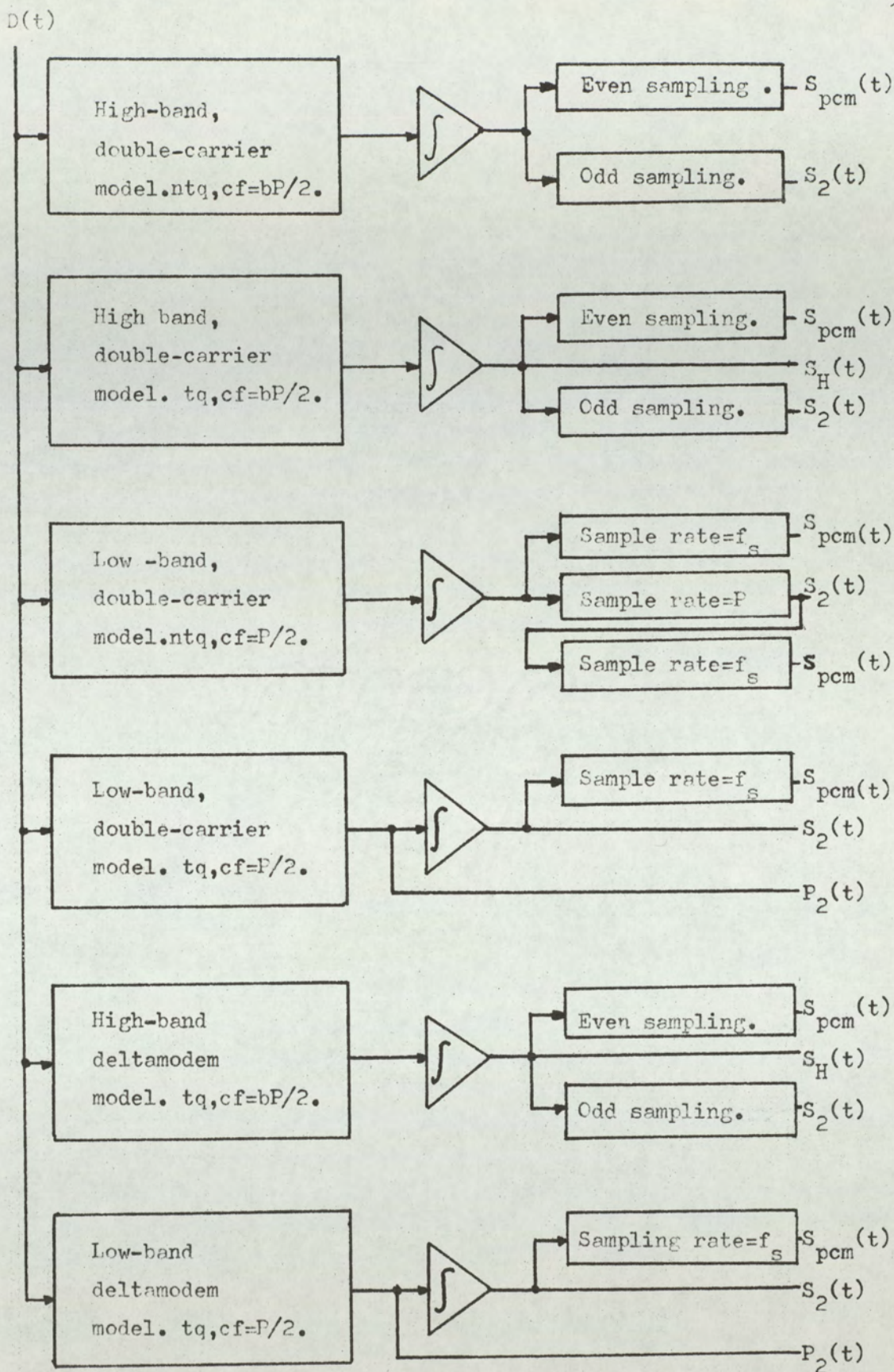


Fig.4-5. High-band to low-band conversion through sampling, for even b.



cf.... Centre frequency.      tq.... Time quantised.  
 ntq.... Not time quantised.

Fig.4-6. Flow chart of model systems for generating the P.A.M. signals of delta-modulation and pulse code modulation.

#### 4.5 Analytical determination of a P.P.M. waveform from a phase-modulated carrier

For spectral analysis, it is necessary to determine the relationship between the phase-modulated carrier,  $x(t)$  and the standard-pulse P.P.M. waveform, where the pulse duration is set at  $(1/b.P)$  secs., the sampling duration for the delta-modulator. The relationship is demonstrated by the schematic diagram of Fig. 4-7.

Observing the processes in Fig. 4-7, the relationship between  $f_p(t)$  the P.P.M. waveform and  $f(t)$  P.M. waveform is given by,

$$f_p(t) = \left[ \frac{f(t) - f(t-1/b.P)}{2} \right]^2 + \frac{f(t) - f(t-1/b.P)}{2} - 1,$$

Expanding,

$$f_p(t) = \frac{(f(t))^2}{4} - \frac{1}{2} f(t) \cdot f(t-1/b.P) + \frac{(f(t-1/b.P))^2}{4} + \frac{f(t) - f(t-1/b.P)}{2} - 1,$$

From Fig. 4-7,

$$(f(t))^2 = 1$$

$$(f(t-1/b.P))^2 = 1$$

$$\text{therefore } f_p(t) = \frac{1}{2} \left[ \{f(t) - f(t-1/b.P)\} - f(t) \cdot f(t-1/b.P) - 1 \right] \dots (4-48)$$

The conversion of  $x(t)$  to  $f(t)$  may be obtained by considering each harmonic of a square wave to be phase modulated. Thus, the expression for  $f(t)$  is an infinite series in terms of harmonics of  $x(t)$ .

$$\text{Put, } f(t) = \frac{2}{\pi} \sum_{M=-\infty}^{\infty} \frac{\text{Sin}\left(\frac{M\pi}{4}\right)}{M} \cdot e^{+j2\pi fMt}, \dots (4-49)$$

\* $M \neq 0$ ,

\* $M \neq 0$ ,

Equation (4-49) represents a square wave of fundamental frequency  $f$ . When the fundamental, corresponding to  $x(t)$ , equations (4-47), is phase modulated by  $D(t)$ , then,

$$2\pi \cdot f \cdot t = \pi \cdot (b \cdot Pt + D(t))$$

$$\text{Hence, } f(t) = \frac{2}{\pi} \cdot \sum_{\substack{M=-\infty \\ M \neq 0}}^{+\infty} \frac{\sin\left(\frac{M\pi}{4}\right)}{M} e^{j \pi M (b \cdot Pt + D(t))} \dots (4-50)$$

where,  $f(t) = x(t)$ , when  $|M| = 1$  and  $X = \frac{4}{\pi}$ ,

in equation (4-47).

Thus, if the instantaneous phase angle of  $x(t)$  is  $\theta$ , then the instantaneous phase angle of the  $M^{\text{th}}$  harmonic is  $(M\theta)$ .

Hence considering the infinite harmonics of  $x(t)$ . Equations (4-48) and (4-49) allow the time-domain solution of  $f_p(t)$  to be obtained.

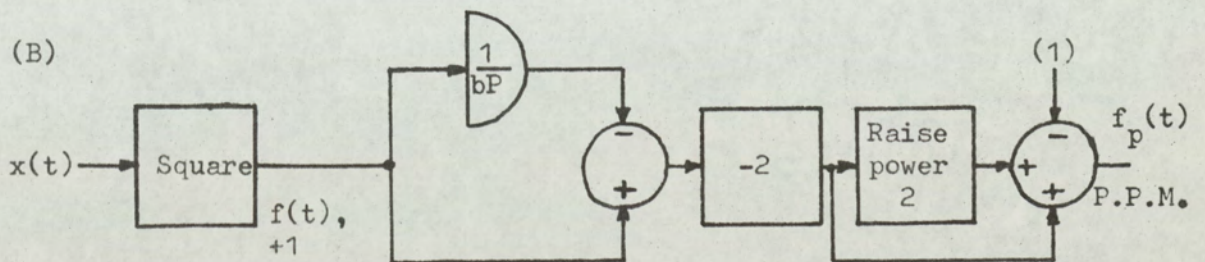
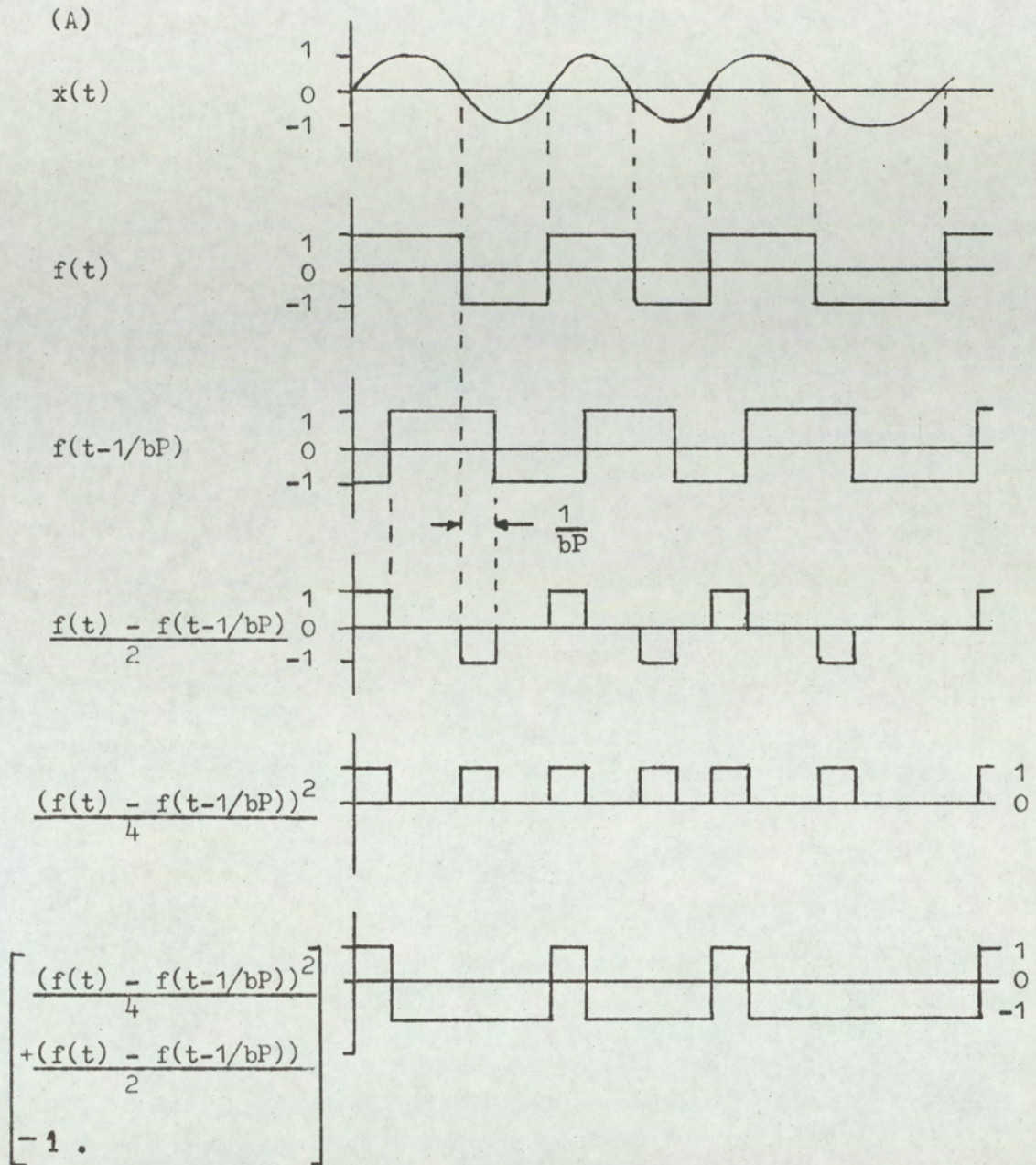


Fig.4-7. Conversion of  $x(t)$  to P.P.M. waveform  $f_p(t)$ .

(A)... Mathematical functions and waveforms of conversion.

(B)... System diagram of conversion process.

4.6 Application of high-band delta-modulation and analytical determination of P.P.M. signal to general spectral analysis.

It is possible to combine the signal transformations of equations (4-48) and (4-49) in a high-band delta-modulator and obtain expressions for a high-band, quantised P.A.M. waveform  $S_H(t)$ . Hence, by suitable sampling, the delta-modulation and P.C.M. waveforms  $S_2(t)$  and  $S_{PCM}(t)$  can be derived. The approach here, is to follow these processes in the frequency domain and determine the general spectra in terms of the spectrum of a high-band phase modulator with low deviation.

Fig.4-8 shows the calculation procedure.

Let  $f_p(f)$  be the Fourier Transform of  $f_p(t)$  and  $f(f)$  be the Fourier Transform of  $f(t)$ , then from equation (4-48),

$$f_p(f) = \frac{1}{2} \left[ \{ f(f) - e^{+j2\pi f/b.P} \cdot f(f) \} - \{ f(f) \} * \{ e^{j2\pi f/b.P} \cdot f(f) \} - \delta(f) \right], \quad \dots \quad (4-51)$$

If  $A_x(f)$  is the spectrum of the phase-modulated function  $x(t)$ , then the spectrum  $f(f)$  of the phase-modulated square wave is determined by extension of equation (4-50)

to give

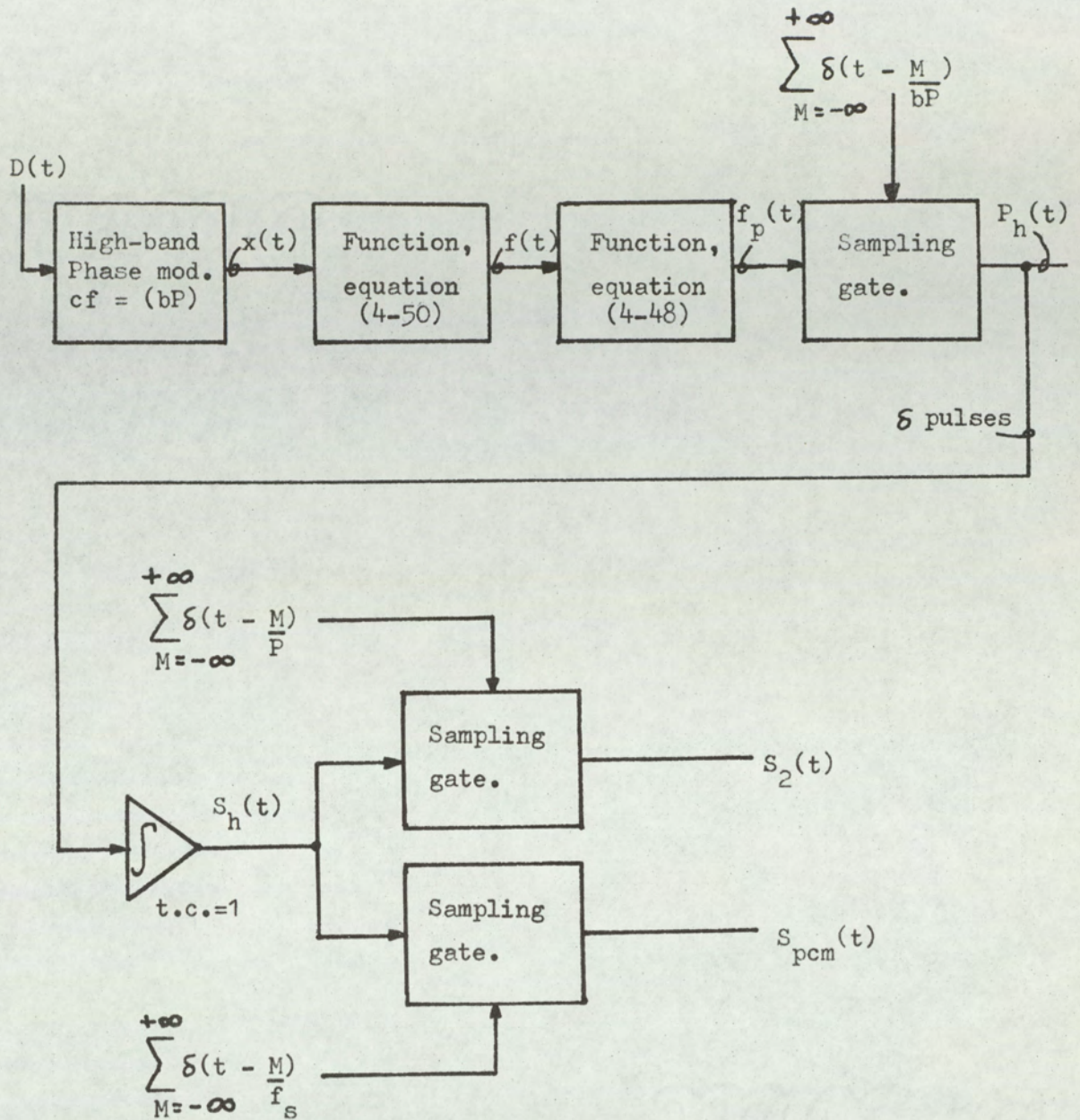
$$f(f) = \sum_{M=-\infty}^{+\infty} \frac{\text{Sin}\left(\frac{M\pi}{4}\right)}{M} \cdot A_x(Mf) \quad \dots \quad (4-52)$$

$M \neq 0,$

The advantage of making the high-band phase modulator of a high centre frequency, with low deviation, is in simplifying the spectrum  $A_x(f)$ . That is,  $A_x(f)$  is more easily determined, since the side bands decay more rapidly.

Finally,  $f_p(f)$  is sampled at the high-band clock rate  $b.P$  to determine the high-band output pulse waveform, which, after integration, yields the high-band, quantised P.A.M. spectrum  $S_H(f)$ . The sampling procedures of section 4.4 then complete the analysis.

Thus, an alternative approach is possible which does not depend upon the calculation of PSZC s. It allows the spectrum of the phase-modulated carrier  $x(t)$ , operating under low deviation, to be transformed through equations (4-52) and (4-51) and two sampling processes.



cf... centre frequency.

Fig.4-8. Calculation procedure for high-band delta-modulator using high-band phase modulator and the pulse converter of Fig.4-7.

#### 4.7 Model with generalised feedback and observations of stability of delta-modulators.

All delta-modulators using feedback, can be classified as unstable. However, in certain classes of modulator, the instability can be controlled by the modulating signal, so that the output pulse sequence efficiently carries modulation information. In a delta-modulator, the transfer function modifies the pulse output waveform and applies the signal to the modulator input. Consider the idling pattern condition for a delta-modulator. Fig.4-9 shows an idling modulator with the modulating signal removed.

A general linear transfer function modifies the phase and amplitude of the input signal. For the purpose of explanation, the phase and amplitude functions are considered separately though they are mutually dependent. In the forward path of the delta-modulator is a comparator. This can be considered as an amplifier of gain  $-A$  and an amplitude limiter. The amplifier gain can be included with the amplitude function  $|A_G(f)|$ , forming,

$$- A \cdot |A_G(f)| .$$

Since the forward loop functions as a comparator,  $A$  is large and, in the limit,  $A \rightarrow \infty$ . The significance is that the amplitude characteristic is destroyed. Hence, for a periodic idling pattern, only the fundamental frequency is detected, the output zero crossings being phase shifted by the phase function. Thus, the phase function determines the idling pattern, when the idling pattern is symmetrical and periodic. The phase functions represents delay; thus

as an initial discussion, the effect of loop delay on the idling pattern will be investigated. Fig. 4-10 represents the system for investigating the idling pattern.

In the following discussion the clock period is  $P$  (P.P.S.) and the output pulses are held for a time  $1/P$  secs. Assume, initially that the output of the modulator and delay **line** are at the '0' level, and that the **delay line** only contains a zero level. Thus, on the clock pulse  $P_1(t)$  goes high.  $T(f)$  seconds later, the output of the **delay line** goes high; then at the next clock pulse  $P_1(t)$  goes low.

From Fig. 4-11, it is clear that if  $N$  is a positive integer, for,

$$\left(\frac{N-1}{P}\right) < T(f) \leq \frac{N}{P}$$

then the half-cycle idling duration is  $\frac{N}{P}$

Hence, generally,  $\left(\frac{N-1}{P}\right) < T(f) \leq \frac{N}{P}$

then the idling pattern frequency =  $\frac{P}{(2.N)}$  .....(4-53)

The phase function,  $\phi_1(f)$ , of the general transfer function represents a frequency-dependent delay. Fig. 4-12 shows the relationship between the phase delay  $\phi_1(f)$  and the equivalent time delay  $T(f)$ ,  $T(f)$  being the frequency dependent delay.

$$\text{Hence, } -\frac{\phi_1(f)}{2\pi} = \frac{T(f)}{(1/f)},$$

$$\text{Therefore, } \phi_1(f) = -2\pi f \cdot T(f) \quad \text{.....(4-54)}$$

$$\text{Putting, } f = \frac{P}{(2N)},$$

$$\text{Therefore, } \phi_1 \left( \frac{P}{2N} \right) = -\pi \cdot \frac{P}{N} \cdot T \left( \frac{P}{2N} \right) \quad \dots\dots(4-55)$$

$$\text{Where, } \frac{(N-1)}{P} < T \left( \frac{P}{2N} \right) \leq \frac{N}{P},$$

$$\text{or, } \left\{ \frac{1}{2 \cdot f} - \frac{1}{P} \right\} < T(f) \leq \frac{1}{2 \cdot f},$$

Equation (4-55) states the phase delay for an idling pattern of frequency  $P/(2N)$ , when using a zero-order hold of duration  $1/P$ . The general delta-modulator was defined in terms of a delta-pulse sequence for the output waveform; thus the hold circuit can be included in the general feedback transfer function. Fig. 4-13 illustrates the hold circuit assumed at the output of Fig. 4-10 and Fig. 4-9.

The zero-order hold transfer functions,  $T_H(f)$ , can be written,

$$T_H(f) = \frac{1}{P} e^{-j\pi \cdot \frac{f}{P}} \cdot \text{Sinc} \left\{ \pi \cdot \frac{f}{P} \right\}, \quad \dots\dots(4-56)$$

Thus, the phase function of the hold network is given by,  $\phi_H(f)$ , where,

$$\phi_H(f) = -\pi \cdot \frac{f}{P} \quad \dots\dots(4-57)$$

Hence the total phase lag is given by the function  $\phi_1(f)$  and the function  $\phi_H(f)$ , where  $\phi_T(f)$  is the total phase-lag function, i.e.

$$\phi_T(f) = \phi_1(f) + \phi_H(f) \quad \dots\dots(4-58)$$

Substituting  $\phi_1(f)$  from equation (4-54) and  $\phi_H(f)$  from equation (4-57) in equation (4-58).

$$\phi_T(f) = -\pi f \left\{ 2 \cdot T(f) + \frac{1}{P} \right\}, \quad \dots\dots(4-59)$$

For efficient encoding, the idling pattern must always be at  $P/2$ , P.P.S., that is the idling pattern is,

... 010101...

Now it has been shown that for oscillation at a frequency  $f$  (where  $f$  is a sub-multiple of clock rate), that,

$$\left\{ \frac{1}{2 \cdot f} - \frac{1}{P} \right\} < T(f) \leq \frac{1}{2 \cdot f} ,$$

Hence,  $T(f) < \left\{ \frac{1}{2 \cdot f} - \frac{1}{P} \right\}$ , will not result in oscillations at the frequency  $f$ . However, the oscillation is at a frequency  $P/2$  hence,

$$T \left( \frac{P}{2} \right) \leq \frac{1}{P} ,$$

Applying these conditions for  $T(f)$  to the total phase-lag function of equation (4-59), gives

$$\phi_T(f) > - \pi \left\{ 1 - \frac{f}{P} \right\} , \text{ Condition 1.}$$

$$\text{and, } - \frac{3\pi}{2} < \phi_T \left( \frac{P}{2} \right) < - \frac{\pi}{2} , \text{ Condition 2.}$$

When the hold network is introduced, the limits on the additional transfer function  $\phi_1(f)$  can be stated:

$$\phi_1(f) > - \pi \left( 1 - \frac{2f}{P} \right) , \text{ Condition 3.}$$

$$- \pi < \phi_1 \left( \frac{P}{2} \right) < 0 , \text{ Condition 4.}$$

Conditions 1,2,3,4 ensure that in the idling state the only mode of oscillation is the  $P/2$  idling pattern. If these conditions were not met, then several natural modes of oscillation could result; the actual state depends on the state of excitation of the modulator and is thus indeterminate. In this case, the frequency of oscillation would not be uniquely defined and the encoding would be sub-optimum.

However, conditions 1,2,3,4 do require that the waveform

at the output of the transfer function, oscillates symmetrically about the comparator reference level. If this is not the case, then the idling pattern is not obtained for all phase delays in the range  $-\frac{3\pi}{2} \rightarrow \frac{\pi}{2}$ .

The three error waveforms shown in Fig.4-14 have undergone different phase delays by the transfer function in the feedback loop. On each error waveform, two reference levels have been indicated  $H, L$  representing two different comparator levels. It is clear that in the extreme cases of  $\pi/2$  and  $3\pi/2$ , the comparator can only operate satisfactorily if it is positioned at the mean of the periodic, idling error waveform. As the phase shift approaches  $\pi$ , the range over which satisfactory idling is obtained increases until at a delay of  $\pi$ , the reference level can be positioned anywhere over the signal range of the error waveform, allowing the modulator to always idle correctly.

Hence for ideal operation,

$$\phi_T \left( \frac{P}{2} \right) = \pi \quad \dots\dots(4-60)$$

Condition 1 still represents the condition for no oscillation and condition 3 applies for the system including a zero-order hold of duration  $1/P$  secs.

Thus, the phase margin limits can be explicitly defined. These are summarised below:

$$\phi_T \left( \frac{P}{2} \right) = \pi \quad \dots\dots(4-60)$$

$$\phi_1 \left( \frac{P}{2} \right) = \frac{\pi}{2} \quad \dots\dots(4-61)$$

For all other frequencies:

$$\phi_T (f) < \pi \left\{ 1 - \frac{f}{P} \right\} \quad \dots\dots(4-62),$$

$$\phi_1 (f) < \pi \left\{ 1 - \frac{2 \cdot f}{P} \right\} \quad \dots\dots(4-63),$$

The limiting phase functions are illustrated in Fig. 4-15, and Fig. 4-16. Note that they only apply at sub-multiples of the clock frequency and apply to idling stability.

When an input signal is applied to the delta-modulator the feedback network responds by generating many frequency components. If the modulation is efficient, then the largest components in the signal band should be related to the modulating function. The *deltamodem* model demonstrated that the signal information is initially carried by a pulse-phase modulated sequence then partially redistributed in time by the time quantisation. The time redistribution depends upon the position of the P.P.M. signal and the delta sampling during time quantisation; but it can lead to a delay of the information of between 0 and  $(1/P)$  secs. Any component which is applied to the input of the modulator (assuming it does not fall below the threshold) will be produced at the output with other frequency components due to quantisation distortion. Hence, it is necessary to ensure that the loop gain does not produce an unstable system. Fig. 4-17 is a modified second-order model system as shown in Fig. 3-11,C.

Frequency components may be injected either at the input port or at the quantisation noise port, however, the loop gain for any component must not produce instability.

Since  $S_2(t)$  and  $D(t)$  have a unity gain relationship at signal frequency, then,

$$e^{-j2\pi f/P} \cdot \frac{A(f)}{G} > -1; \quad \dots(4-64)$$

Note in the modulation process, the phase modulator effectively differentiates the input signal, however, during demodulation of the delta output pulses, the process is cancelled by the integrator.

From Fig. 3-10A for the second-order delta-modulator, the general feedback transfer function is  $A(f)$ . In terms of  $A(f)$  of Fig. 4-17 putting  $T_1 = 1$  sec,  $A_G(f)$  is given by:

$$A_G(f) = \frac{1}{j2\pi f} \left\{ 1 + \frac{A(f)}{G} \right\} \quad \dots(4-65)$$

From equation (4-64), the stability criterion is

$$\frac{A(f)}{G} > -e^{j2\pi f/P}$$

Hence substituting in equation (4-65) for  $\frac{A(f)}{G}$ , gives

$$A_G(f) > \frac{1}{j2\pi f} \left\{ 1 - e^{+j2\pi f/P} \right\}$$

Therefore,  $A_G(f) > -\frac{1}{P} \cdot e^{j\pi f/P} \cdot \text{Sinc} \left\{ \frac{\pi f}{P} \right\} \quad \dots(4-66)$

From equation (4-66), the phase margin is given by,

$$\phi_T(f) = \pi \left\{ 1 - \frac{f}{P} \right\} \quad \dots(4-67)$$

and  $|A_G(f)| < \left[ \text{Sinc} \left( \frac{\pi f}{P} \right) \right] \quad \dots(4-68)$

where  $|A_G(f)|$  is the maximum amplitude of a given frequency component.

Equations (4-67) and (4-68) apply to the total feedback network. It is interesting to observe that the stability conditions for the idling state is also the solution for the Nyquist stability criterion.

In delta-modulation networks, the general transfer function consists of either a single integrator or a double-integrator with a forward predictive loop.

The transfer function of the single integrator is

$$A_S(f) = \frac{1}{j2\pi f}, \quad \dots(4-69)$$

and for the double integrator, modifying equation (2-32) gives

$$A_D(f) = \frac{1}{j2\pi f} \left\{ 1 + \frac{1}{j2\pi f \cdot G} \right\} \quad \dots(4-70)$$

By comparing Fig. 4-16 and equations (4-69), the single integration function with hold network appears optimum at  $P/2$  and  $P/4$  and well within the limits of the phase margin at lower frequencies. Increasing the phase lag at  $P/2$  and  $P/4$  can generate a dual stable idling pattern of either 0101 or 00110011; this is readily observed in practice.

In all analogue networks, the hold circuit is required. However, it represents only a single clock-period store and thus its storage capability with respect to baseband signals is zero. However, it does introduce unnecessary phase shift, thus limiting the total storage capability of the feedback network. Thus, the digital methods of generation (which are capable of realising the

response of a transfer function without a hold network) have a greater phase margin, with enhanced performance and stability margin. The transfer function of equation (4.70) for double integration can be modified with respect to phase margin by changing the prediction  $G$ . The value of  $G$ , which is controlled by the type of modulator used, is calculated so that the phase response of the double integrator falls within the limits shown in either Fig. 4.16 or Fig. 4.15.

Consider the double-integrator network of Fig. 2.5A, together with equation (3.32). The phase shift of the network  $\phi_D(f)$  can be written:

$$\phi_D(f) = \pi - \tan^{-1}\{2\pi fGT_2\} \quad \dots(4.71)$$

For the digital system, where no hold network is used, Fig. 4.15 shows that

$$\phi_T\left(\frac{P}{4}\right) < \frac{3\pi}{4}$$

Hence, putting  $\phi_D(f) = \phi_T\left(\frac{P}{4}\right)$ ,  $f = \frac{P}{4}$  and solving equation (4.71), gives

$$G_T > \frac{2}{\pi} \cdot \frac{1}{P \cdot T_2} \quad \dots(4.72)$$

where  $G_T$  is the value of  $G$  evaluated for the system without a zero-order hold.

For the network using the hold of duration  $1/P$ , Fig. 4.16 shows that

$$\phi_1\left(\frac{P}{8}\right) = \frac{3\pi}{4},$$

Defining  $G_H = G$  for the hold circuit, then:

$$G_H > \frac{4}{\pi} \cdot \frac{1}{P \cdot T_2} \quad \dots(4.73)$$

For the system with the hold circuit a realistic solution for the quarter-clock-frequency idling pattern is not possible. Thus, the best solution to be found is one limiting the eighth-clock idling pattern  $P/8$ . Thus, with an analogue double-integration network using a hold circuit of duration  $1/P$ , two idling pattern modes

i.e. 0101 and 00110011

are possible. This infers that the quantisation noise can reach a higher power level. To stabilise the idling pattern,  $G$  would have to include a phase-advance network. The results (4.72), (4.73) compare favourably with the predictive theory which determined a value for  $G$  given by equation (2.34).

A double-integration network with a hold network can produce more quantisation noise than a double integration without a hold network. This can be of importance when the clock rate is only a few orders of magnitude higher than the highest modulating frequency. In such cases, a single-integrator system may give improved high-frequency noise performance, especially with high-frequency modulators which have their own inherent delay.

In section 2.6, it was stated that the single integrator and hold circuit were on the limit of stability with respect to a single idling pattern and that only a small delay was required to produce two possible idling patterns with an increase in quantisation error. Fig. 4.16 illustrates the phase margin, where the single integrator is represented by the dotted line, it is seen to be on the limit at  $P/4$  and at  $P/2$ . It is important that idling stability is observed as this controls the peak quantisation error which occurs.

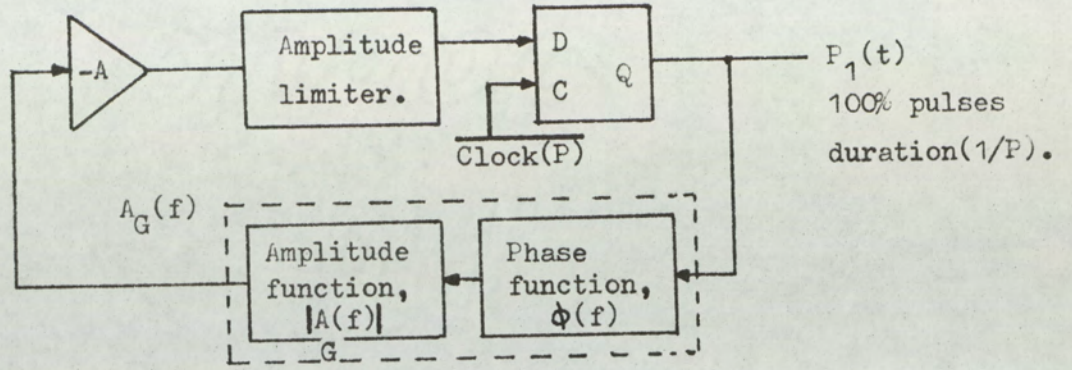


Fig.4-9. Idling delta-modulator.

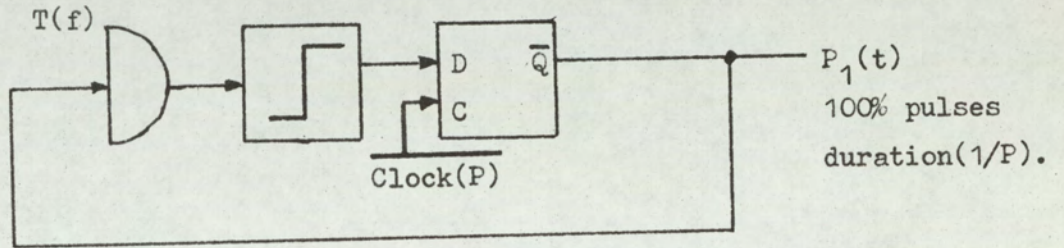


Fig.4-10. Idling pattern controlled by lumped-loop delay.

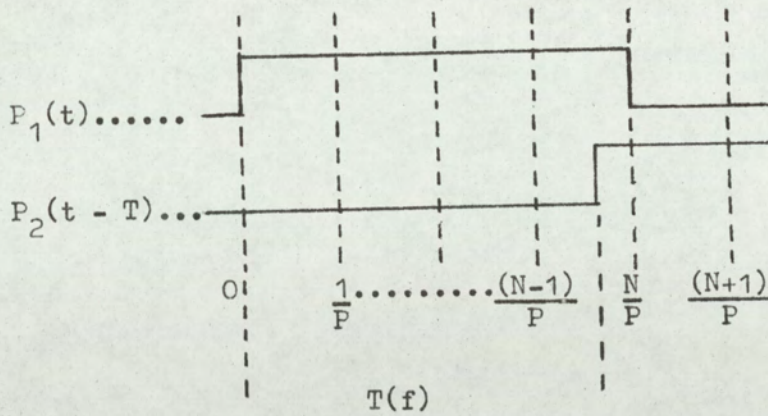


Fig.4-11. Half-cycle production of idling pattern.

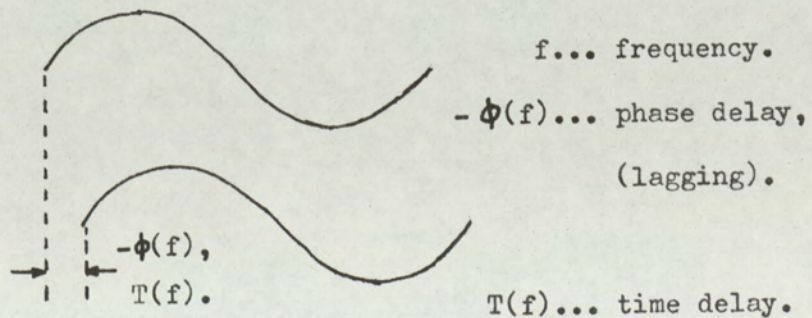


Fig.4-12. Time delay and phase delay at a frequency, f.

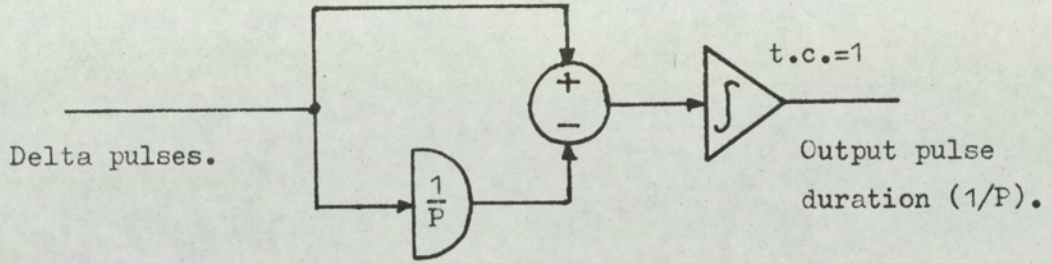


Fig.4-13. (1/P) duration hold network.

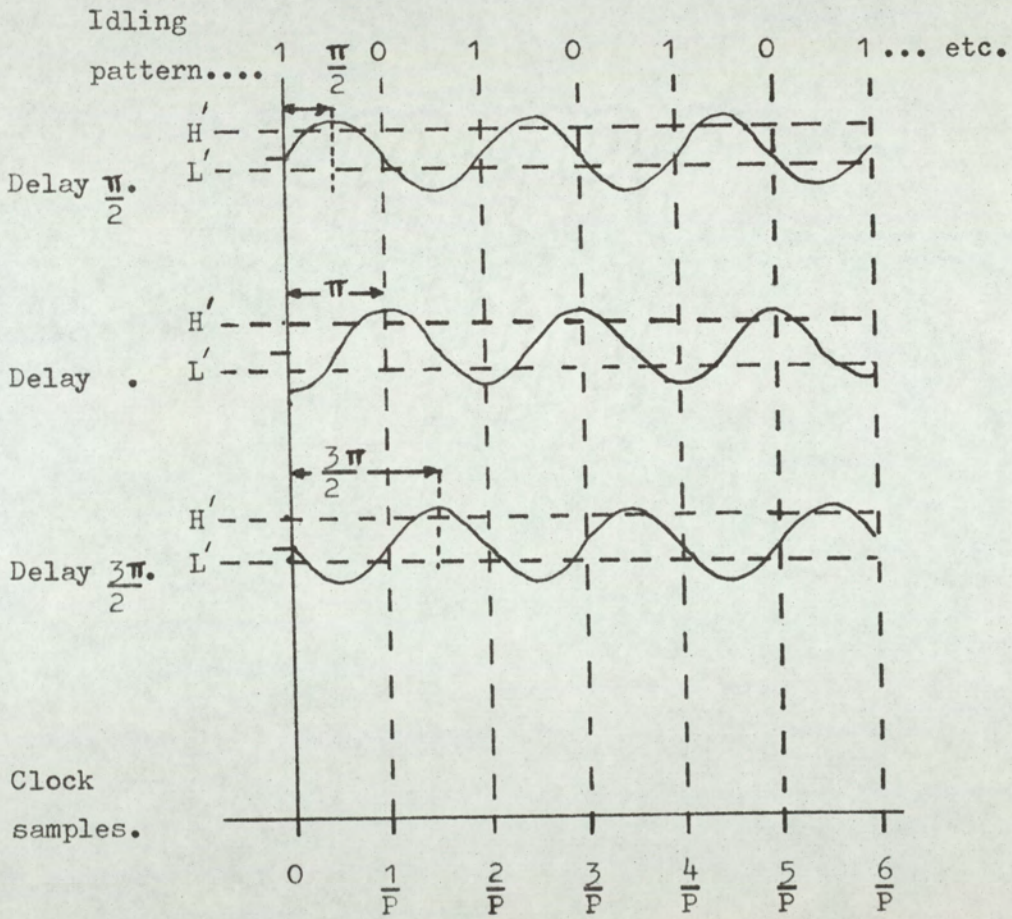


Fig.4-14. Three examples of phase delay for the fundamental frequency component of the  
 .... 1 0 1 0 ....  
 idling pattern.

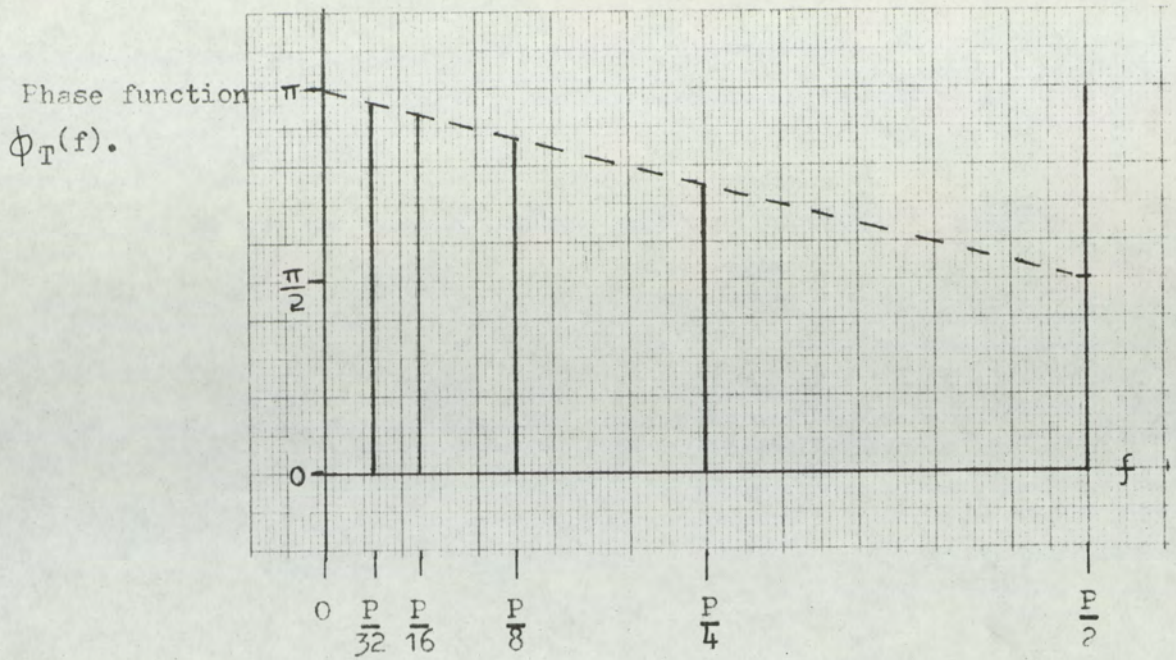


Fig.4-15. Variation of  $\phi_T(f)$  against frequency,  $f$ .

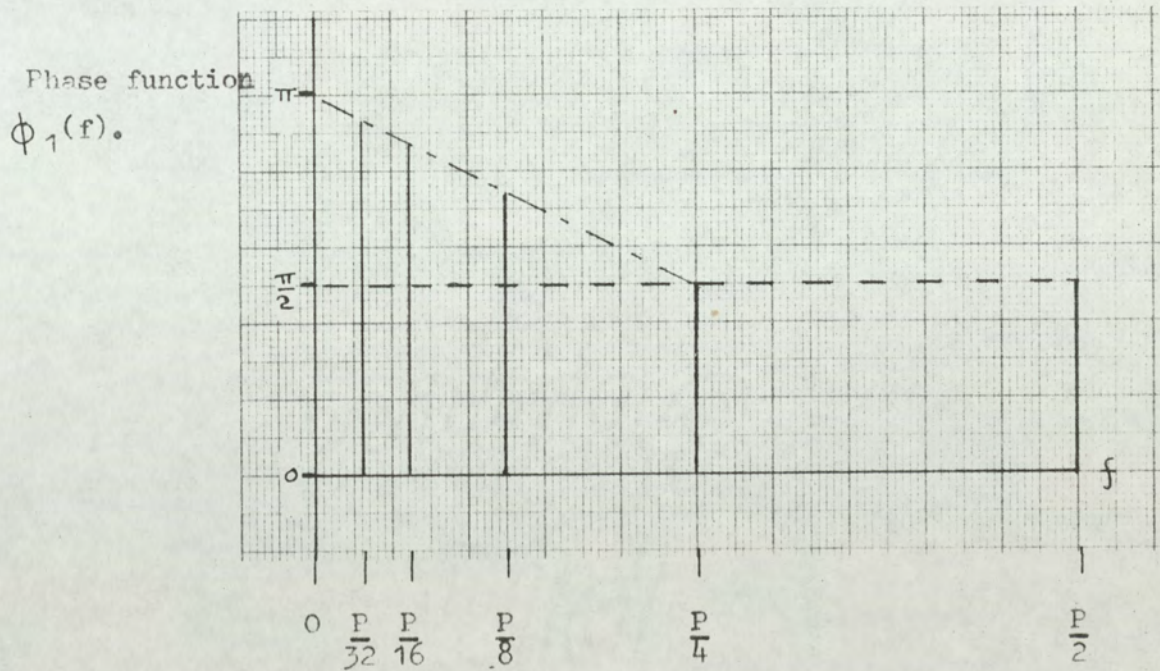
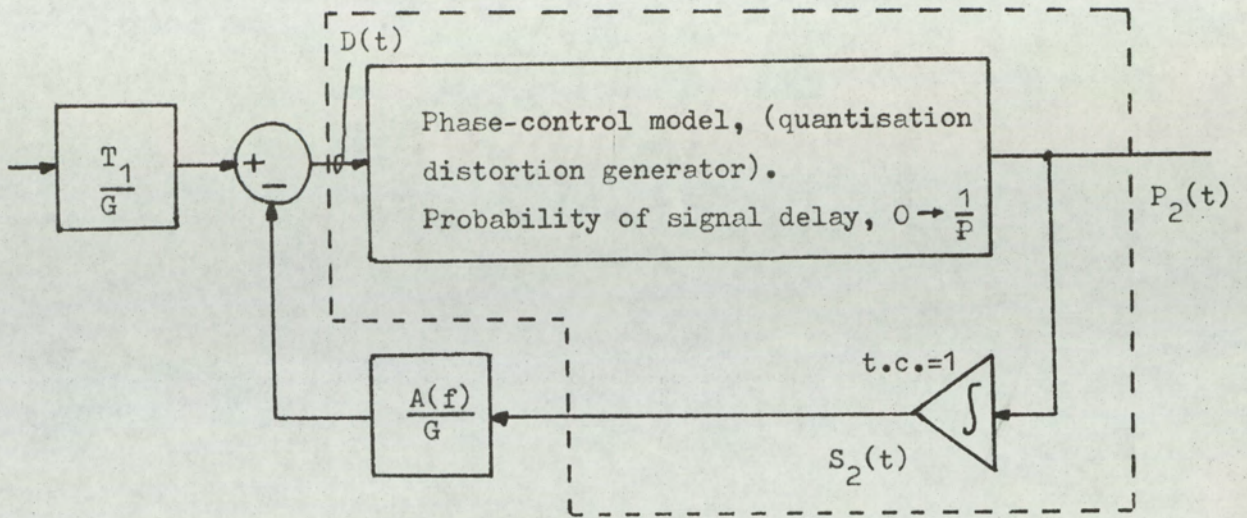
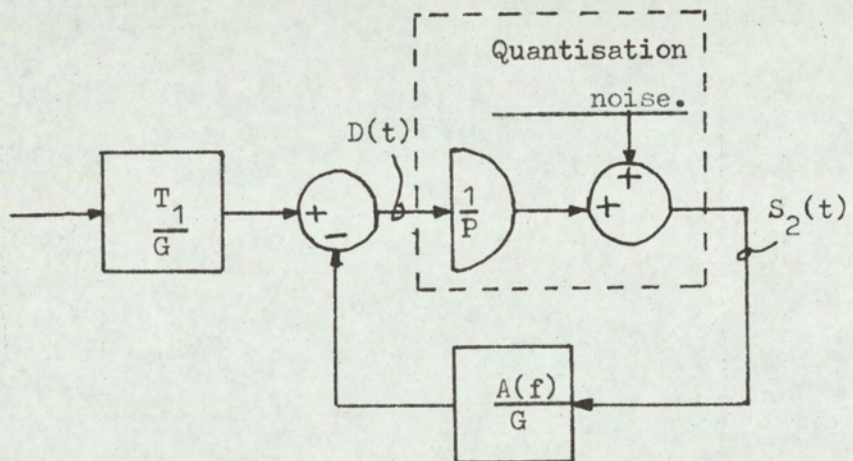


Fig.4-16. Variation of  $\phi_1(f)$  against frequency,  $f$ .



(A).....



(B)...

Fig.4-17. Modified second-order system for investigating low-frequency stability.

(A)... Second-order phase-control model indicating probable signal delay.

(B)... Linear, low-frequency equivalent model with maximum signal delay of  $(1/P)$ .

CHAPTER 5. ADAPTIVE DELTA-MODULATION WITH PULSE  
GROUPING TECHNIQUES.

5.1 Introduction to pulse grouping.

When a delta-modulator has zero input signal, the output pulse waveform is the idling pattern ...01010.... As the input signal rises positively, more '1' pulses are generated in the pulse sequence. In delta-modulation this change in pulse pattern is related to the modulating signal slope, while in delta-sigma modulation it is related to the amplitude. Once the input is non-zero, the idling pattern is destroyed and other pulse patterns appear. The first noticeable pattern is that of pair groupings of two '1's or two '0's, depending on the signal direction. As the signal becomes more positive the pair groupings become more common until a pulse pattern,

... 011011011 ...

is obtained. Further signal increase produces a further change in pulse grouping and triplet groupings become more common. A limiting condition is reached, where the pattern becomes,

... 0111011101110 ...

and the pattern then produces groups of four pulses on further signal increase. The pulse groupings will be classified as follows: the idling pattern is termed a

zero-order pulse group, the pulse pairs are a first-order pulse group, pulse triplets are second-order pulse groups, etc.

Since the pulse signals contain information as to the modulating signal, there is a predictable theory as to the pulse patterns generated. For this discussion, delta-sigma modulation will be described, although the results are equally applicable to delta-modulation. The input signal to the delta-sigma modulator is defined  $M(t)$  such that,

$M(t) = 1$ , output pulses all 1's.

$M(t) = 0$ , output pulses at idling pattern.

$M(t) = -1$ , output pulses all 0's.

To investigate the behaviour of various order pulses produced by d.c. modulating signals, a computer program was compiled which generated the pulse pattern of a single-integration delta-modulator with various d.c. excitations. The pulse sequence was evaluated over 1000 pulses for each d.c. input level. The levels were changed from zero to 1.00 in steps of 0.05. The output pulse waveform was observed at each input level. At each level, various order pulse groupings were observed and the number of each order groupings that occurred in the 1000 samples were recorded. The results were normalised by dividing by 1000; this gave a measure of the frequency of occurrence of the groups considered. Fig. 5.1 illustrates the results of the computer analysis.

Before continuing the discussion, an exact definition of a pulse group will be stated and the method of generating

such a group will be given.

Consider an  $N^{\text{th}}$  order group. To detect the presence of such a grouping, the pulses are observed in an  $(N+1)$  bit shift register. If the outputs of the register are  $Q_1, Q_2, \dots, Q_{(N+1)}$ , then a pulse group of order  $(N)$  is defined by the Boolean Expression,

$$N^{\text{th}} \text{ Order pulse group} = G_{+(N)} = Q_1 \cdot Q_2 \cdot Q_3 \cdot \dots \cdot Q_{(N)} \cdot Q_{(N+1)} \quad \dots(5.1)$$

This is a positive group since positive pulses are observed. For a negative  $N^{\text{th}}$  order grouping,

$$G_{-(N)} = \bar{Q}_1 \cdot \bar{Q}_2 \cdot \bar{Q}_3 \cdot \dots \cdot \bar{Q}_{(N+1)} \quad \dots(5.2)$$

Fig. 5.2 illustrates a system of a pulse group detector and illustrates the system with an example showing 1st, 2nd, 3rd and 4th order positive pulse groups.

The results of Fig. 5.1 indicate that there are precise threshold levels at which the various order pulse groupings commence. The results also indicate, that once a pulse group has occurred, the frequency of occurrence of that order of pulse group rises linearly with the modulating signal. Since the frequency of occurrence was measured over a finite pulse sequence, changes in modulating signal cause the frequency of occurrence to rise in steps, the step depending upon the group order and the number of pulses averaged. Thus, as the pulse group order becomes larger (keeping the total number of samples constant), then the step change becomes more coarse.

The next section determines the threshold level in terms of the modulating signal  $M(t)$ , for an  $N^{\text{th}}$  order pulse group.

## 5.2 Determination of threshold level of an $N^{\text{th}}$ order pulse group, for delta-sigma-modulations.

In chapter 3, delta-sigma modulation was demonstrated to be identical to time-quantised pulse-frequency modulation. This concept is used here to calculate the threshold level, for a delta-sigma-modulator, of an  $N^{\text{th}}$  order pulse group. In the model system, a carrier of frequency  $P/2$  is modulated in frequency by the delta-sigma modulator input signal  $M(t)$  to a maximum frequency deviation of  $P/2$ , corresponding to  $|M(t)|=1$ .

Thus the instantaneous frequency  $f$  may be defined in terms of  $P$  and  $M(t)$  by the relation

$$f = \frac{P}{2} + \frac{P}{2} \cdot M(t)$$

Therefore,  $f = \frac{P}{2} \cdot \{1 + M(t)\} \dots (5.3)$

A pulse group of order  $N$  occurs when  $(N+1)$  P.S.Z.C.'s fall in  $(N+1)$  consecutive time slots. For the threshold level defined  $m(N)$  for an  $N^{\text{th}}$  order system,  $M(t)$  must be the minimum value for this condition, which infers a minimum frequency deviation in the frequency-modulation model. The limiting condition for generation of an  $N^{\text{th}}$  order group is that when the time between the first and the last detected P.S.Z.C. is just equal to  $(N+1)$  time slots.

$(N+1)$  time slots occupy a duration  $\frac{(N+1)}{P}$ , since each slot is of duration  $1/P$ .

For the first and last P.S.Z.C. to just occupy a time  $\frac{(N+1)}{P}$ , the number of cycles of the frequency-modulated

carrier is  $N$ .

Therefore, period of f.m. carrier =  $(\frac{N+1}{P}) \cdot (\frac{1}{N})$

Therefore, frequency of f.m. carrier =  $(\frac{N}{N+1}) \cdot P$

Equating this frequency in equation (5.3) and substituting  $m(N) = M(t)$ , gives:

$$\frac{N}{(N+1)} P = \frac{P}{2}(1 + m(N))$$

Therefore,  $m(N) = (\frac{N-1}{N+1}) \dots (5.4)$

From equation (5.4),

$$m(1) = 0,$$

$$m(2) = \frac{1}{3},$$

$$m(3) = \frac{1}{2},$$

$$m(4) = \frac{3}{5}, \quad \text{etc.}$$

It can be seen that these results agree with the computer simulation, the results of which are illustrated in Fig. 5.1. Pulse group detection thus gives a very reliable measure of the depth of modulation of a delta-modulator, and is therefore very useful in adaptive systems.

The distribution of an  $N^{\text{th}}$  order pulse group sequence for  $1 \geq |M(t)| \geq m(N)$  is also required. Consider again the condition for  $(N+1)$  P.S.Z.C.'s to be distributed in  $(N+1)$  consecutive time slots, but that the number of cycles of f.m. carrier is  $\{N+\epsilon(N)\}$  where  $\epsilon(N)$  is a number related to the  $N^{\text{th}}$  order pulse group such that,

$$0 \leq \epsilon(N) \leq 1,$$

Thus,  $\{N + \epsilon(N)\}$  cycles of f.m. carrier occupy a time

$$\frac{(N+1)}{P}$$

Therefore, period of f.m. carrier =  $\left\{ \frac{(N+1)}{N + \epsilon(N)} \right\} \cdot \frac{1}{P}$

The frequency of f.m. carrier is

$$f = \left\{ \frac{N + \epsilon(N)}{(N+1)} \right\} \cdot P, \quad \dots (5.5)$$

Equating  $f$  in equations (5.5) and (5.3);

Therefore,

$$\left\{ \frac{(N + \epsilon(N))}{(N+1)} \right\} \cdot P = \frac{P}{2} \cdot \{1 + M(t)\},$$

Therefore,

$$\epsilon(N) = M(t) \cdot \frac{(N+1)}{2} - \frac{(N-1)}{2}, \quad \dots (5.6)$$

The frequency of occurrence of  $N^{\text{th}}$  order pulse groups is directly related to  $\epsilon(N)$ . When  $\epsilon(N)=1$ , the rate is  $P$  the clock rate, and when  $\epsilon(N)=0$ , only one group occurs and the rate is zero. Let the frequency of occurrence of  $N^{\text{th}}$  order pulse groups be  $f_N$ . The initial and final conditions are known and, from the computer results, the normalised frequency of occurrence suggests a linear relationship between  $f_N$  and  $M(t)$ . Thus from equation (5.6),  $f_N$  and  $\epsilon(N)$  are also linearly related. Hence, put

$$f_N = \epsilon(N) \cdot P \quad \dots (5.7)$$

The proposed model for pulse grouping distribution is therefore a frequency-modulated carrier commencing at zero frequency and rising to a rate  $P$  at peak modulation. The system is such that for the  $N^{\text{th}}$  order group,

for  $0 \leq |M(t)| < m(N)$

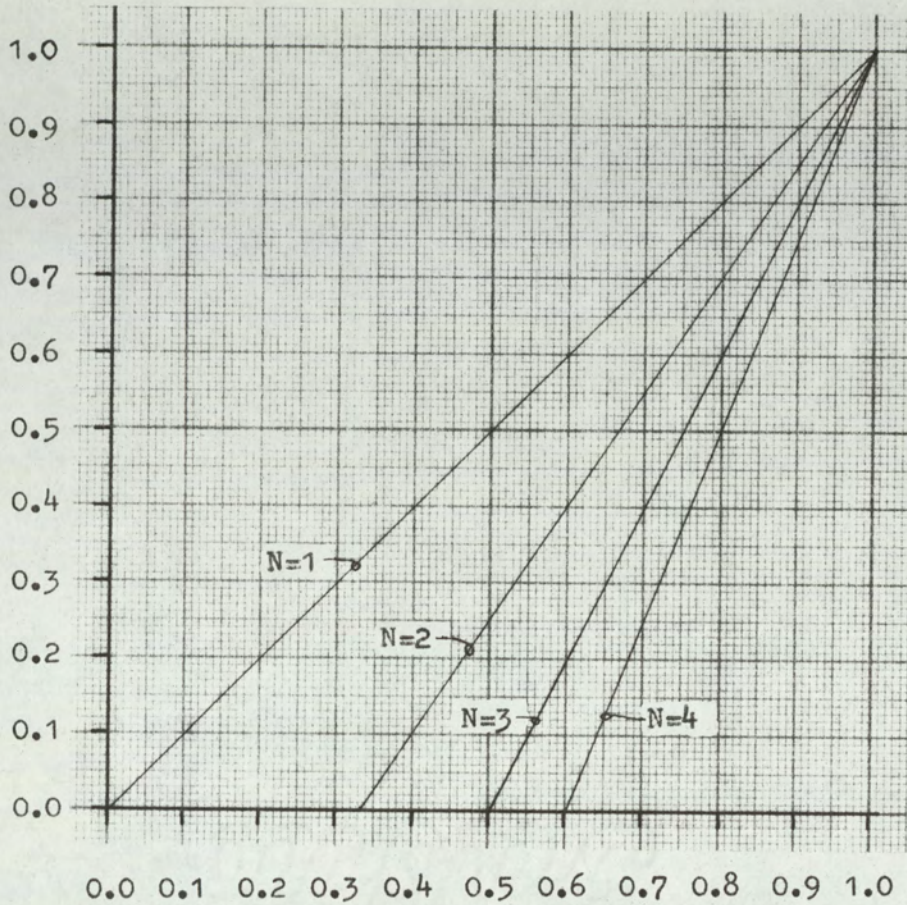
then  $f_N = 0$ .

and for  $m(N) \leq |M(t)| \leq 1$

then  $f_N = \epsilon(N) \cdot P$

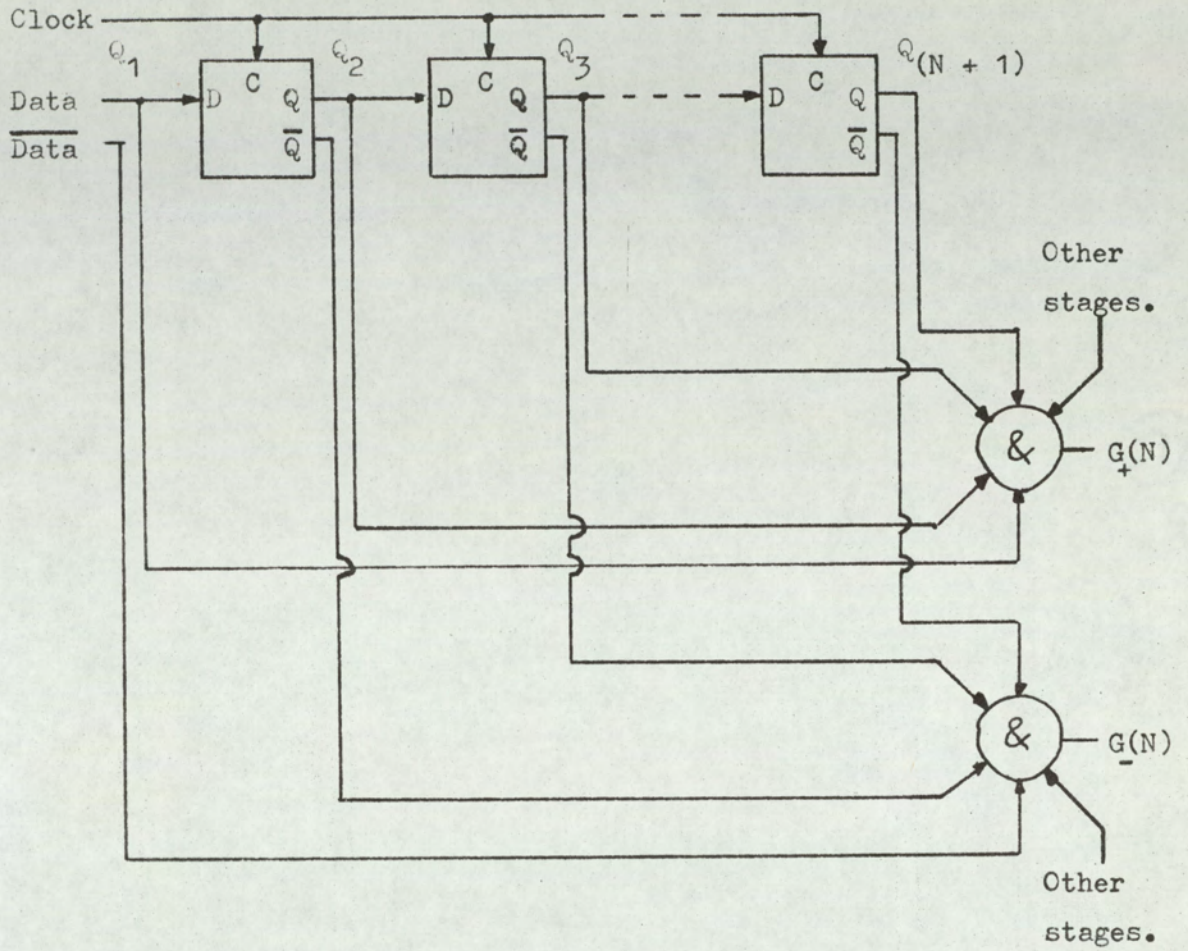
As in the previous model system, a reference point on the carrier is chosen which is related to the position of  $N^{\text{th}}$  order pulse groups. Again let the reference be the P.S.Z.C.'s of the frequency-modulated carrier. The P.S.Z.C.'s of the signal of frequency  $f_N$  are then time-slotted into time slots of length  $(1/P)$ . The model is identical, with respect to the time-slotting procedure, to the previous deltamodem model.

Frequency of occurrence of pulse groups of orders 1,2,3,4. (normalised).



Normalised input to delta-sigma modulator.

Fig.5-1. .... Pulse-group frequency of occurrence functions for d.c. input signals applied to a delta-sigma modulator.



Data.....	0	1	1	1	0	1	0	1	1	1	1	1	0	1	0	1
G <sub>+</sub> (1).....	0	0	1	1	0	0	0	0	1	1	1	1	0	0	0	0
G <sub>+</sub> (2).....	0	0	0	1	0	0	0	0	0	1	1	1	0	0	0	0
G <sub>+</sub> (3).....	0	0	0	0	0	0	0	0	0	0	1	1	0	0	0	0
G <sub>+</sub> (4).....	0	0	0	0	0	0	0	0	0	0	0	1	0	0	0	0
G <sub>+</sub> (5).....	0	0	0	0	0	0	0	0	0	0	0	0	0	0	0	0

Fig.5-2. Pulse group detection of order N with examples of detection of 1,2,3,4,5, order positive pulse groupings.

### 5.3 Suppressed-carrier delta-modulation.

In section 5.2, pulse grouping was discussed and the frequency of occurrence of an  $N^{\text{th}}$  order pulse group expressed as a function the modulating signal for a delta-sigma modulator. Fig. 5.1 illustrated the threshold phenomena associated with various group orders.

It is interesting to observe that the curve of frequency of occurrence versus modulating signal for the first-order group (group of two similar pulses) passes through the origin. Since the grouping is first order, the idling pattern is suppressed and the output during the idling pattern is a constant level. Fig. 5.3 represents a first order-system, its response and its integrated response to a typical pulse sequence.

The integrated first-order pulse sequence appears as a modified waveform of  $S_2(t)$ ; however, the 'carrier' component at one half the clock rate has been removed. A delta-modulator changes the phase of its  $P/2$  component on odd and even levels of  $S_2(t)$ . This can readily be seen by observing the idling pattern shown in Fig. 5.4.

The 1st-order system, as well as suppressing the half-clock-frequency component, also separates the positive signal from the negative signal, thus readily allowing a rectified waveform to be obtained.

Fig. 5.5 illustrates a 'full-wave' rectified signal extraction.

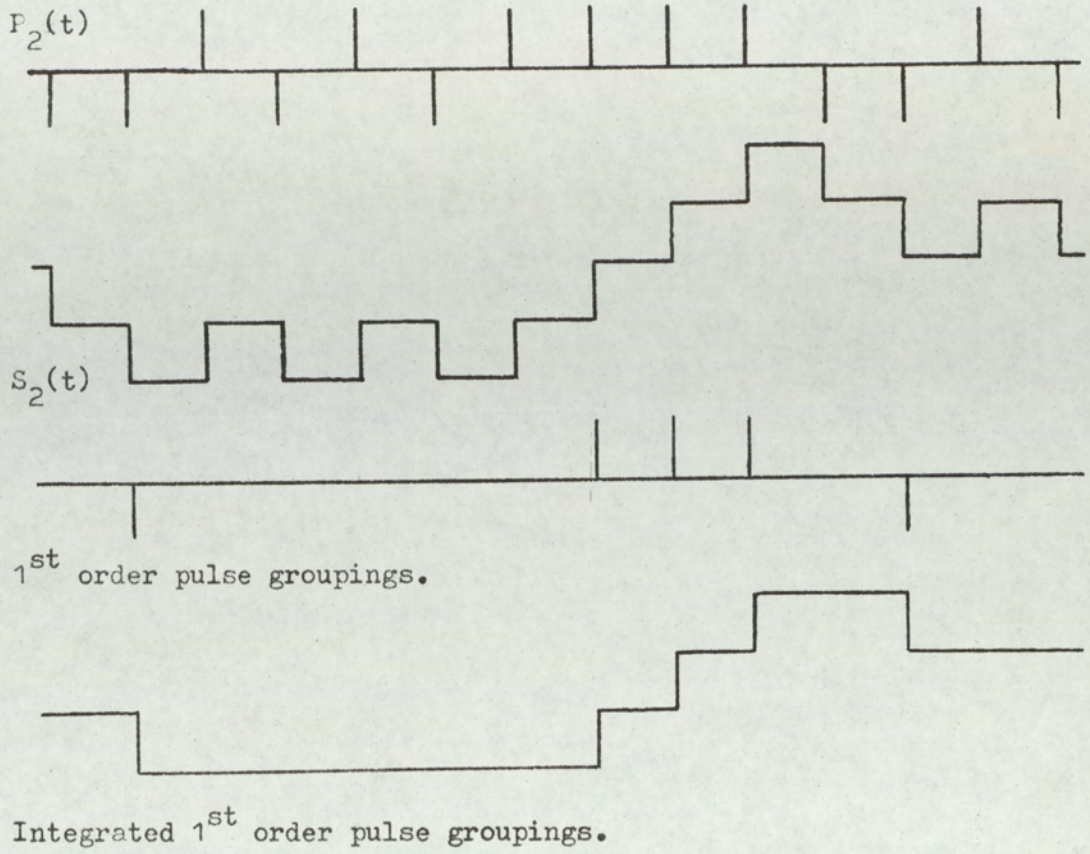


Fig.5-3. First-order pulse grouping with integration.

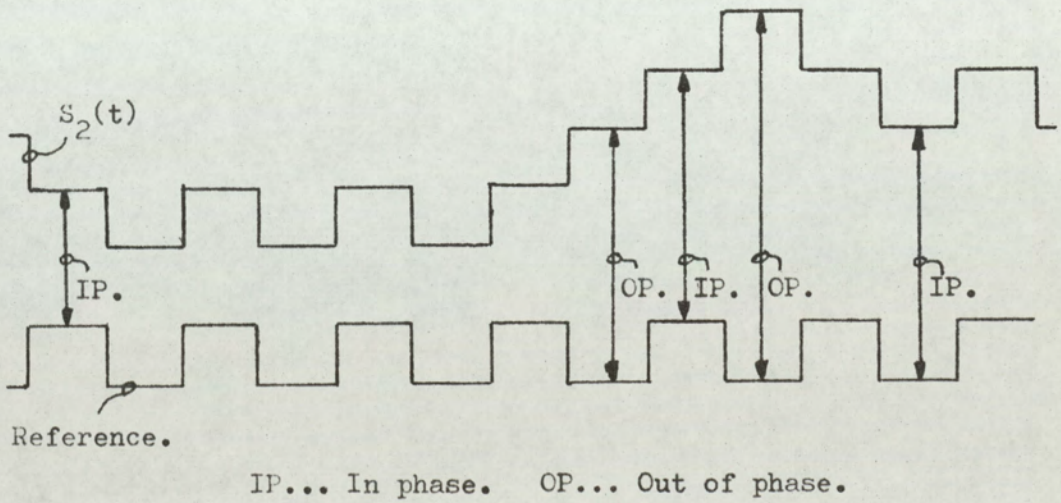


Fig.5-4. Change of phase of idling pattern with level of  $S_2(t)$ .

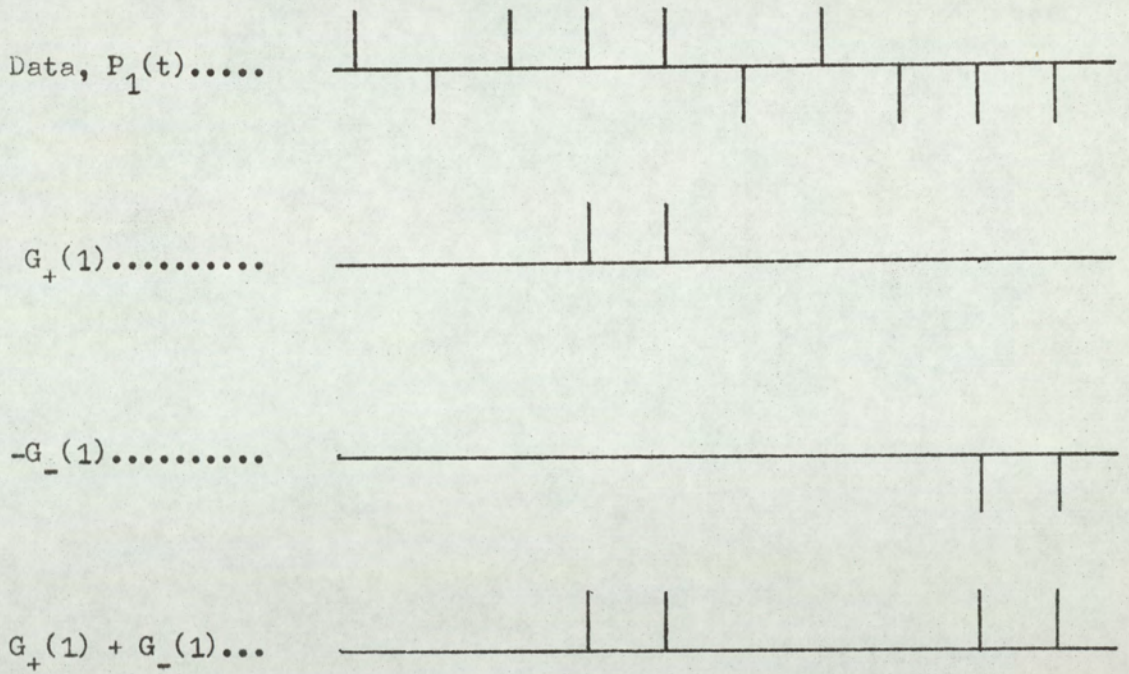
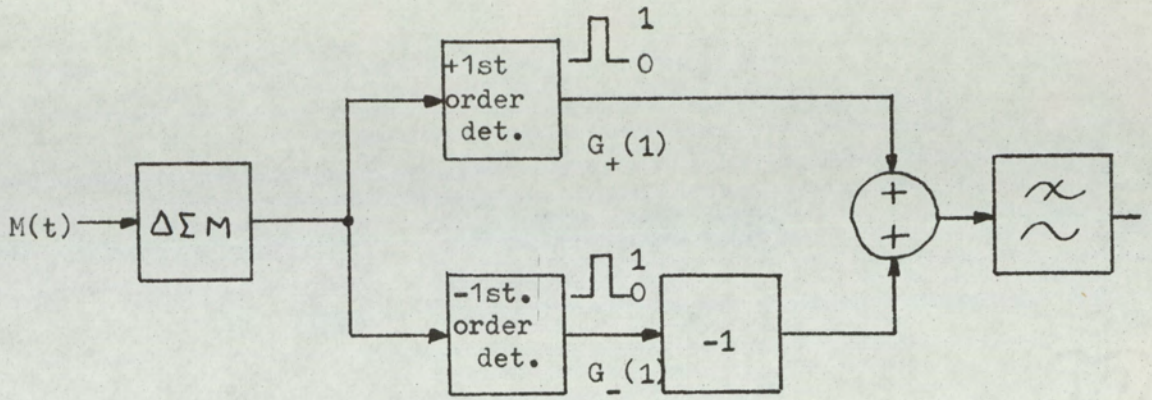


Fig.5-5. 'Full-wave' rectification using 1<sup>st</sup> order pulse groupings.

## 5.4 Basic adaptive system for delta-modulation.

(26, 27, 28, 29, 30, 31, 47, 48, 49)

This section deals with a basic adaptive loop that can be applied to television signals. The system is designed so that the high-frequency signals are fed directly to the modulator, but the low-frequency components are controlled so as not to overload the modulator. Fig. 5.6 illustrates the adaptive loop.

The modulator transfer-function for the adaptive loop, when  $\lambda'$  is the control signal, is

$$A_{M_a}(f) = \left\{ \frac{1+j\omega(RC)}{(\lambda'+1)+j\omega(RC)} \right\} \quad \dots(5.8)$$

The demodulator transfer function for the adaptive loop is

$$A_{D_a}(f) = \left\{ \frac{(\lambda'+1) + j\omega(RC)}{1+j\omega(RC)} \right\} \quad \dots(5.9)$$

Providing  $\lambda'$  tracks identically in both modulator and demodulator (a condition which can be ensured by identical control circuitry operating from the same pulse signal) then

$$A_{M_a}(f) \cdot A_{D_a}(f) = 1 \quad \dots(3.10)$$

Equation (5.10) holds providing that there are no transmission errors. It is also applicable when the delta-sigma-modulator is overloaded. Fig. 5.7 shows the transfer characteristic for static values of  $\lambda'$ , the control signal. Basically, as the low-frequency signal components increase in magnitude, their magnitude is attenuated by the RC feedback network. By correct choice of network, the high-frequency signal can be left unattenuated and the relative

gain of the input signal adjusted such that the high-frequency components give a reasonable depth of modulation.

The logic control signal can, in general, be formed by combinations of first, second (etc) order pulse groupings and the composite group signal approximately filtered.

The basic advantage of this approach to adaptive delta-modulation is that the modulator network is non-adaptive. It is thus simpler in design and can be optimised for operation at high pulse rates. In practice, it is virtually impossible to produce a wide-range adaptive modulator. The approach outlined here should allow the design of adaptive systems for delta-modulation at frequencies appropriate for television.

This type of adaptation also takes account of the improved noise performance with descending signal frequency that is obtainable with delta-sigma-modulation. That is, low frequency components may be under-modulated if it allows the high-frequency components to load the modulator more fully. Since also, the adaptive circuitry can operate in synchronism at both transmitter and receiver (neglecting propagation times), distortion generated at the transmitter is compensated for at the receiver.

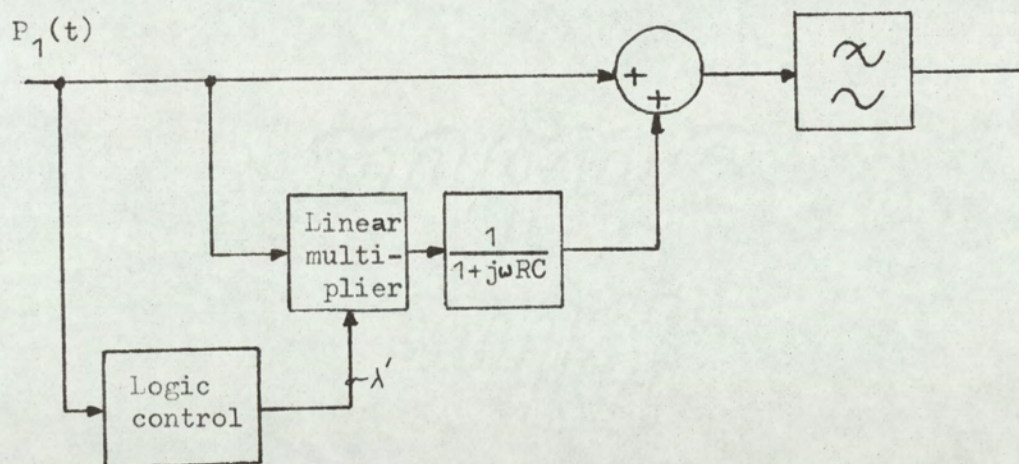
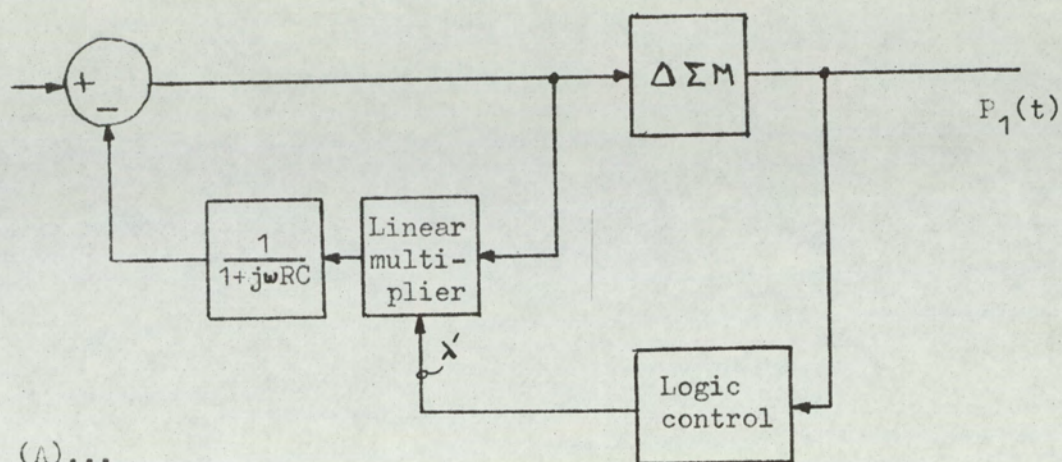


Fig.5-6. Adaptive control of delta-sigma modulator with external control network.

(A)... Encoder.

(B)... Decoder.

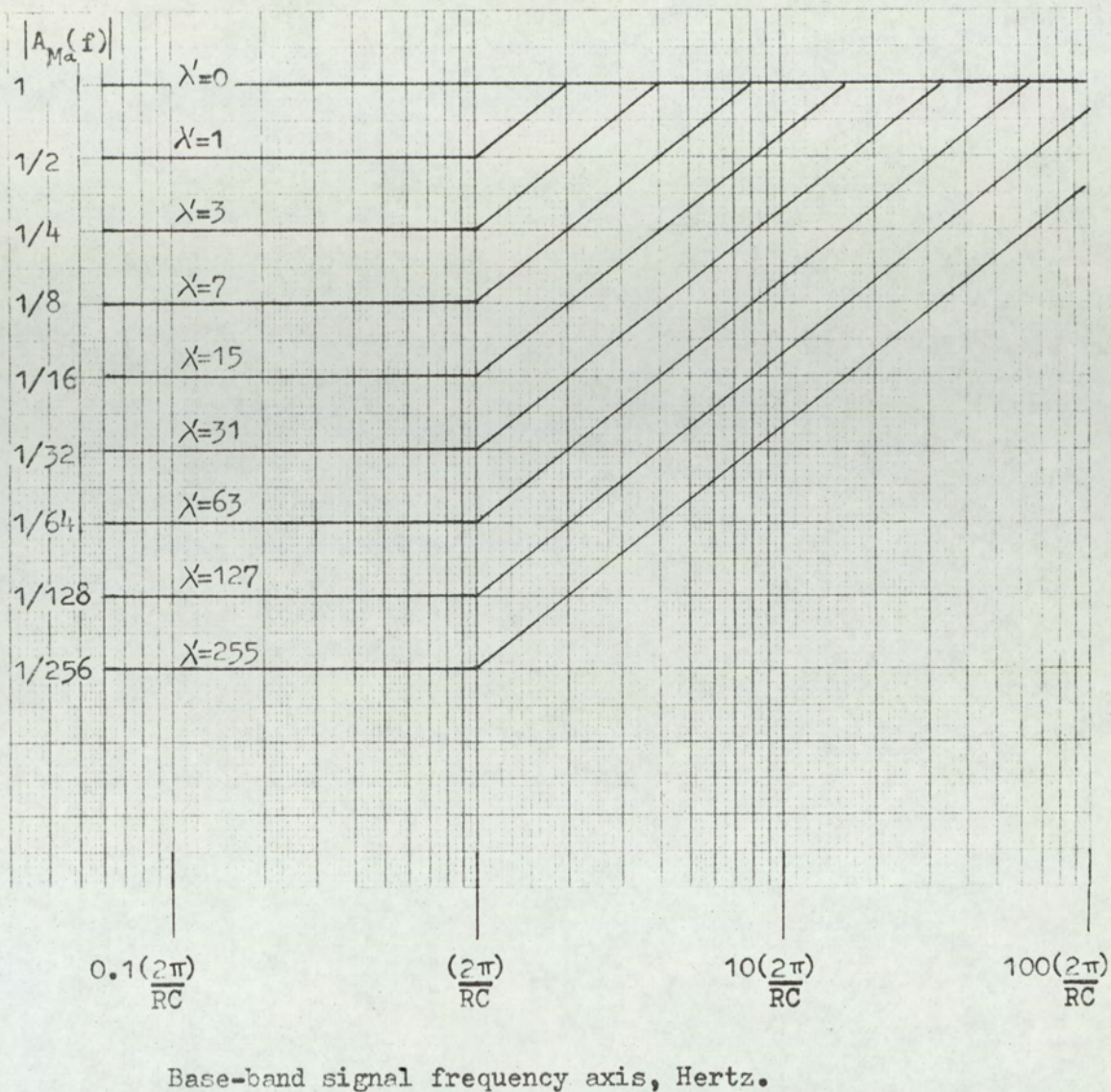


Fig5-7. Variation of the modulus of  $A_{M_a}(f)$ , for constant values of  $\lambda'$ , with signal frequency,  $f$ .

## 5.5 Instantaneous non-linear delta-modulation.

(32, 33, 34, 50, 51)

The companding system of section 5.4 involved an external control network with an analogue multiplier. Such a configuration involves considerable instrumentation difficulties. Since adaptive delta-modulation was not the objective of the research, the compander has only been dealt with in principle.

In the experiment with television, an adaptive delta-modulator operating on an instantaneous system was introduced, as this was more readily realised in practice.

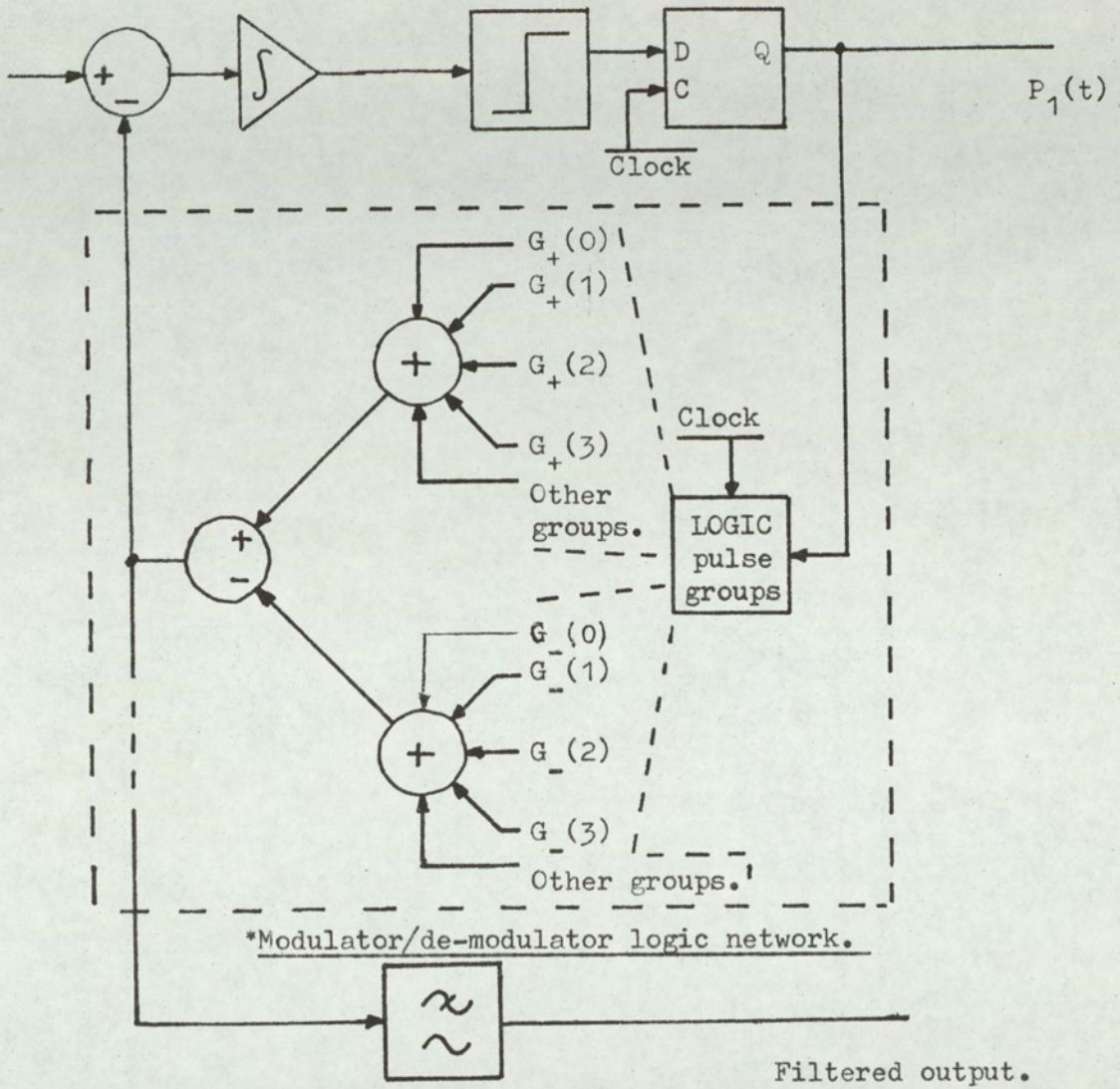
The principle is to adapt the pulse amplitude in the feedback network by observing various order pulse groupings, but combining the groupings by an addition network. Fig. 5.8 shows the basic configurations possible for a single-integration delta-sigma modulator.

Adaptive systems such as that of Fig. 5.8 are useful at high frequencies, since the network introduces the minimum of delay. By using a resistive network the output pulse sequence can be fed back to the input directly. The sequence is the zero-order pulse group and is shown in Fig. 5.8 as  $G_{+(0)}$ .

In the practical system, a single second-order adaption was used; the circuit details are given in a later section. The system is such that signals within  $\pm 1/3$  of peak (non-companded) delta-sigma modulation are not in any way effected. However, once the threshold  $m(2)$  is

exceeded, second-order pulse groupings become more frequent and the feedback signal effectively increases in amplitude, thus increasing the dynamic range. In terms of delta-modulation, the step height is adapted. If a pulse sequence containing a second-order group occurs, then the step height doubles in magnitude. Fig. 5.9 illustrates the process in terms of delta-modulation.

Computer results of this type of adaptation are dealt with in chapter (10).



\* Encoding and decoding control logic is identical.

Fig.5-8. Instantaneous adaptive delta-sigma modulator, using single integration.

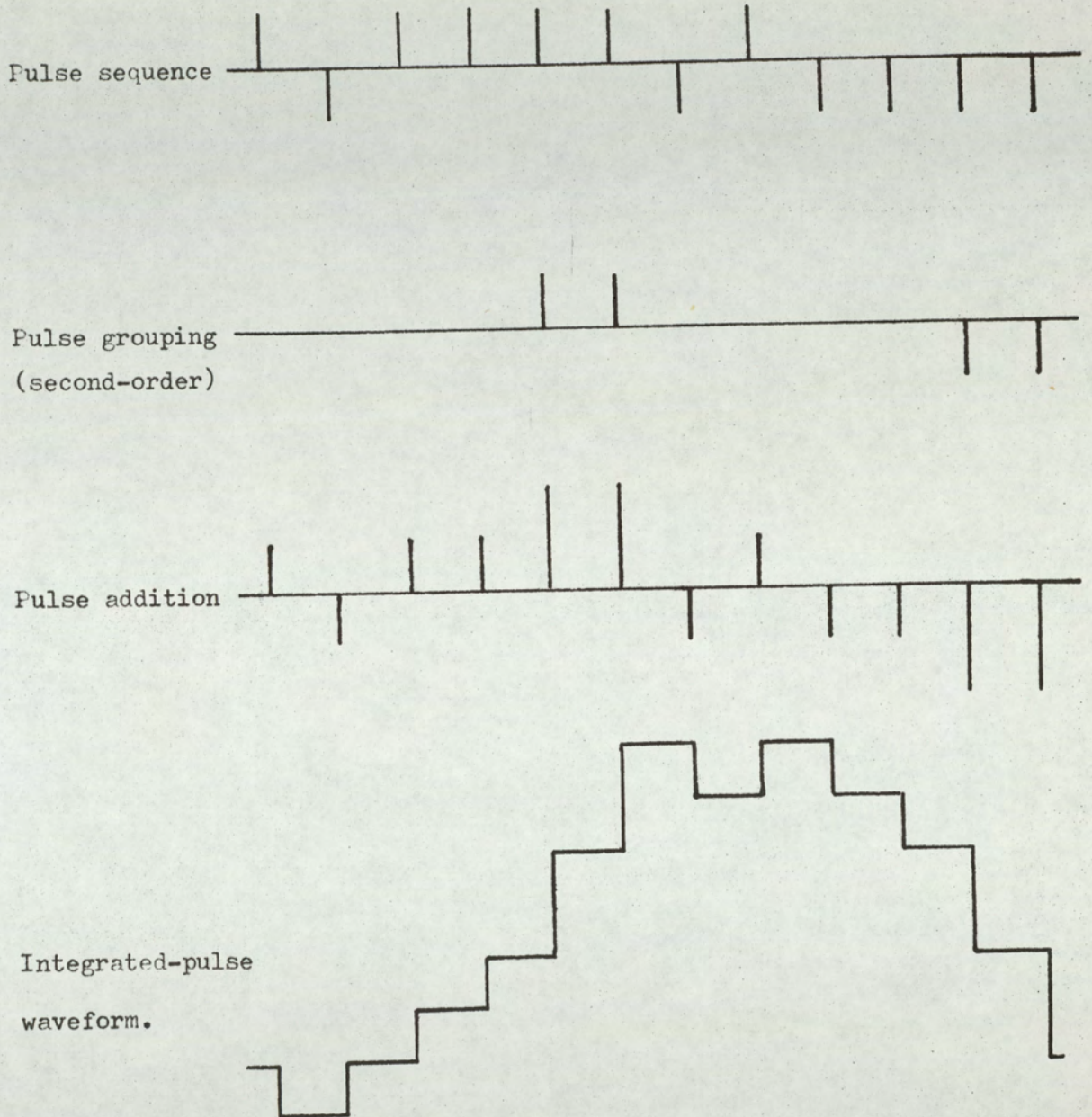


Fig.5-9 . Process of second-order adaptive companding.

CHAPTER 6. BASIC FUNDAMENTALS OF TELEVISION SYSTEMS.

## 6.1 Picture Structure and Bandwidth Requirements .

(52, 53, 54)

The purpose of the television system to be considered is the transmission, by one or more electrical signals, of a two-dimensional spatial sample of vision. The system is required to produce a two-dimensional image, at a remote receiver. The reconstructed image, when viewed by the human eye, must be a close approximation to the original image. The characteristics of the eye are of extreme importance and, as will be shown, allow considerable approximations to the image structure to be made with very little observable impairment, providing the image is viewed under specified conditions. The direct image is a two-dimensional projection of a three-dimensional scene, the boundary being finite and of a rectangular form. The direct image and indeed remote images, are viewed such that the image formed on the retina covers the <sup>61</sup>fovea. However, this condition is not rigid and a viewing distance of the order of four to ten times image height can be considered normal. The projected image, whether local or remote, will be referred to as the picture.

Since the eye is limited in resolution and the picture viewing conditions are defined, i.e. the reproduced image is not to be observed by a microscope or at very short distances, then the spatial bandwidth may be limited and made independent of absolute picture size.

The spatial bandwidth of the picture defines the spatial proximity that, say, a black dot and a white dot can be placed. Consider an array of black and white dots, the dot spacing being  $\Delta l$  and the dots lying on a straight line. The fundamental spatial frequency is then  $(1/2\Delta l)$  dots/unit length. If the spacing is the minimum that a system can reproduce,  $\Delta l_m$ , then, the spatial bandwidth,  $f_{s1}$ , is:

$$f_{s1} = \frac{1}{2\Delta l_m}, \quad \dots(6.1)$$

Let the vertical and horizontal spatial bandwidths be  $f_{vs}$ ,  $f_{hs}$  respectively. Since these bandwidths are finite, the picture can be sampled. In the systems considered here, the picture is divided into equally-spaced horizontal lines; thus the vertical bandwidth is constant over the whole picture area. Let the picture height be,  $L_v$ , and the width be,  $L_h$ , then if the system has  $N_1$  line samples,

$$f_{vs} = \frac{N_1}{(2 \cdot L_v)}, \quad \dots(6.2)$$

For a practical system,

$$f_{vs} = f_{hs}, \quad \dots(6.3)$$

since, generally, the eye resolution is similar in all planes.

From equation (6.2) and (6.3),

$$f_{hs} = \frac{N_1}{(2 \cdot L_v)}, \quad \dots(6.4)$$

The ratio of  $L_v$  to  $L_h$  is constant and is called the aspect ratio  $A_r$ , i.e.

$$A_r = \frac{L_h}{L_v}, \quad \dots(6.5)$$

The picture, however, is not temporally static; there are changes in picture structure with time. Thus, as well as spatial sampling, it is necessary to define the samples at various time instants. For simplicity, the samples are scanned. The process scans, with constant velocity, each line of the picture, line by line. Thus, for a monochrome picture, only one signal is generated, which is formed by the scanning process, the signal being proportional to the picture **luminance**. The bandwidth of the signal thus generated, is a function of scanning velocity and picture bandwidth. Fig. 6.1 illustrates a simple system, the scanning paths being indicated by arrows. The dotted lines represent fly-back periods in which the scan is suppressed.

The scanning signal bandwidth, for a given number of lines, is a compromise between horizontal, spatial bandwidth and picture scan rate. The rate at which the picture is scanned is primarily a function of subjective flicker and the ability for the picture to track moving scenes.

For the flicker caused by sequential scanning of the lines to be unobservable, the pictures must be completely scanned at a rate of about 50 pictures per second. This however, results in a rather high signal bandwidth, the bandwidth being raised basically to overcome the flicker effect. If the rate is reduced to 25 pictures per second, then the flicker is increased. However, the signal bandwidth is halved and the system

can still track moving scenes fairly accurately.

The system of 2:1 interlaced scanning may be introduced to offset the effect of flicker when the picture rate is reduced. The picture is divided into two fields, each field consisting of alternate sets of lines of the picture. Thus the system of Fig. 6.1 is decomposed into two fields, as shown in Fig. 6.2; the fields are designated 'ODD' and 'EVEN'.

For 2:1 interlacing, the field rate is twice the picture rate; thus, for a picture rate of 25, the flicker rate is 50. The system also improves the ability to track moving scenes, as the fields are temporally spaced.

Consider the scanning signal, of bandwidth,  $f_v$ . The time to scan a single line is:

$$\text{Time to scan a single line} = \frac{1}{N_1 \cdot P_r},$$

where  $P_r$  is the picture rate

$N_1$  the number of lines in the picture.

If the line to be scanned is a sequence of alternate black and white dots at the maximum spatial frequency  $f_{hs}$ , then the number of spatial cycles in a line of length  $L_h$  is  $(f_{hs} \cdot L_h)$ . Hence,

$$f_v = N_1 \cdot P_r \cdot L_h \cdot f_{hs},$$

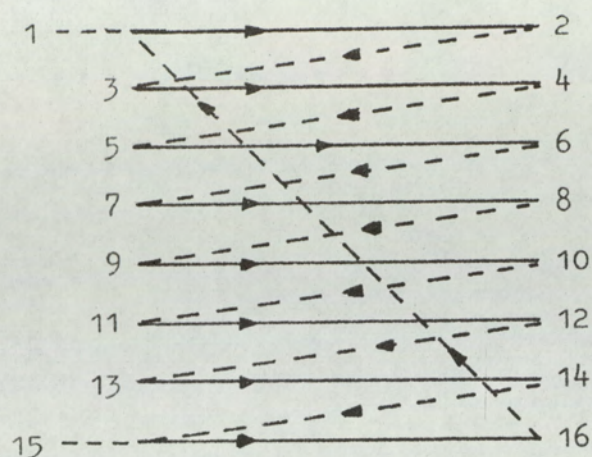
Eliminating  $f_{hs}$  from equation (6.4) and substituting for  $L_h/L_v$  from equation (6.5), then,

$$f_v = \frac{A_r \cdot P_r \cdot N_1^2}{2}, \quad \dots(6.6)$$

Thus the image is constructed by uniformly scanning an array of lines. For a monochrome image,

it is only necessary to read the luminance information during the scan and produce one electrical signal. When colour information is also required, more signal channels are needed; this is discussed in the next chapter.

The process of reading the image and converting the instantaneous samples to an electrical signal is immaterial to the present system. Only the form of signal generated and its relationship, spatially and temporally, to the scanned image is of importance, since it is the transmission and encoding of these signals that is of concern.



Scanning sequence... 1→2, 3→4, ..... 15→16, 16→1, 1→2,  
.....etc.

Fig.6-1. Simple linear scan line structure.

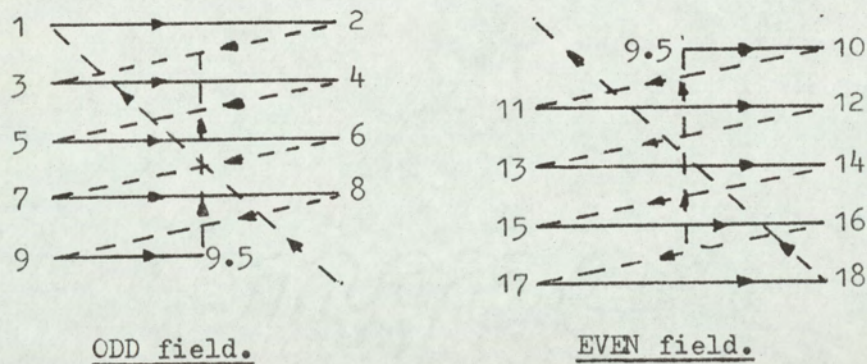


Fig.6-2. Two interlaced fields forming a single-picture scan.

## 6.2 Spatial and Temporal Identity

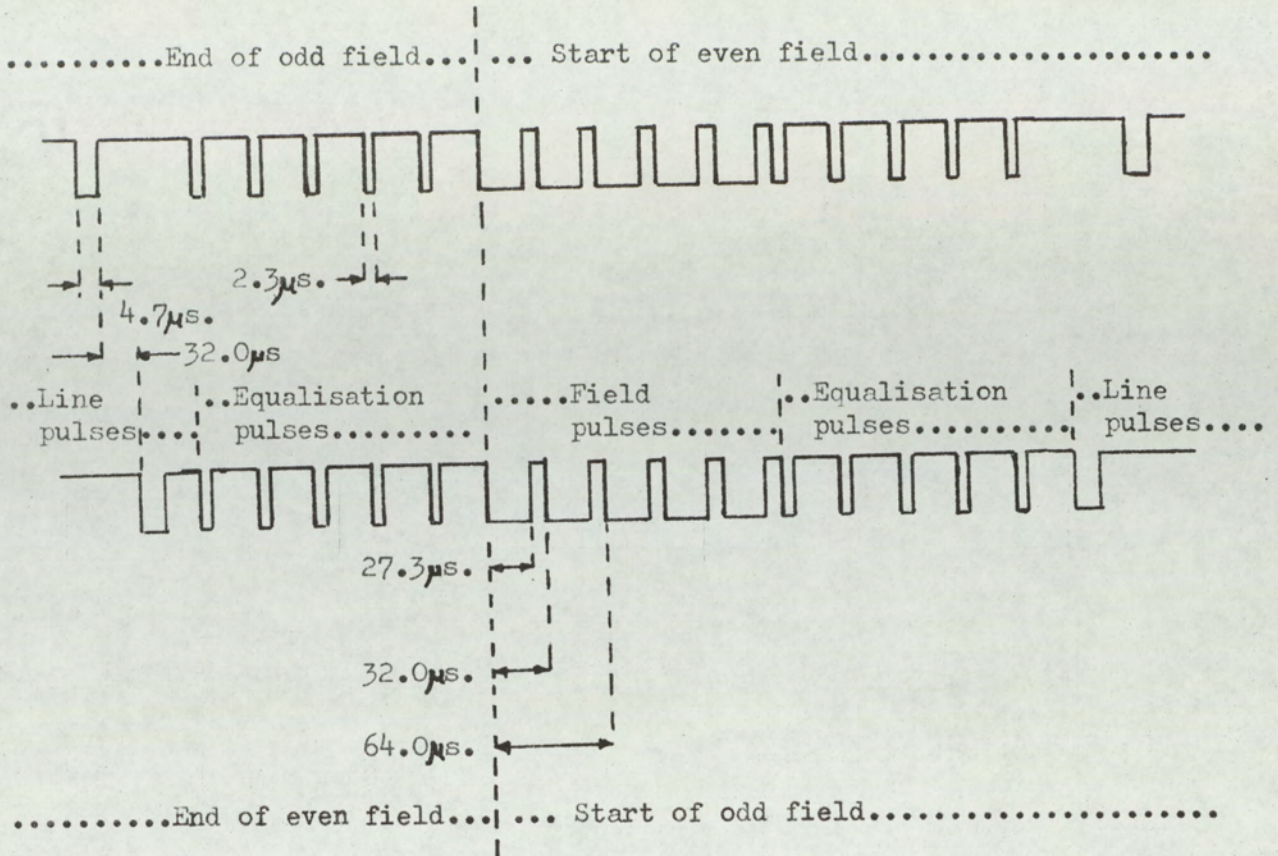
The signals generated by scanning define the picture. To reconstruct the image from the signals, it is necessary to relate instantaneous signal values to the appropriate spatial location on the image. Thus, it is necessary to scan the reconstructed image in synchronism with the original image scan, allowing for transmission delays. The scanning process is repetitive and the time to scan each line is identical. In order that the scanning processes are in synchronism, it is necessary to label the transmission signal so that the line and field can be identified. By introducing the synchronisation signals at the signal source, any transmission delays or subsequent storage, will maintain accurate spacial coordinates.

Synchronisation is established by introducing pulse patterns. The pulse patterns identify line commencement, field commencement and identify the field as 'odd' or 'even'. Fig. 6.3 illustrates the three synchronisation pulse patterns and pulse durations used in the C.C.I.R.\* 625 line-standard.

The initiation of each line is determined by a negative pulse of duration  $4.7 \mu\text{sec.}$ , the leading edge defining the commencement of the line. The line duration is  $64 \mu\text{sec.}$  Field detection is established by a series of five pulses of duration

\* Comité Consultatif International des Radiocommunications.

27.3  $\mu$ sec. at a rate of twice the line-repetition frequency. The phasing of these pulses establishes the field about to be transmitted. Since the field pulses contain a component at line frequency, line synchronisation can be maintained. In the C.C.I.R. system, the group of field pulses is preceded and followed by groups of five short-duration pulses, again at twice line frequency; their duration is 2.3  $\mu$ sec. These pulses are termed equalisation pulses. Their purpose is to simplify field-pulse detector circuits, since the field pulses are superimposed on the scanning signals or video signals. The line and field synchronisation pulses, trigger linear scan generators, which enable the video signals to be correctly positioned on the reconstructed image. Fig. 6.3 indicates the types of field pulse phasing, indicating 'odd' and 'even' fields. Basic system parameters are shown for later reference. Note that the field phasing is related to a component at twice line frequency; thus there is no discontinuity in the line-scan waveforms due to the displacement of the field pulses.



Line duration.....	64.0µs.
Line pulse duration.....	4-7µs. + 0.2µs.
Field pulse duration.....	27.3µs. + 0.2µs.
Equalisation pulse duration.....	2.3 + 0.1µs.
Number of lines per picture.....	625.
Interlace.....	2:1.
Picture rate.....	25 pictures per sec.
Field rate.....	50 fields per sec.

Fig.6-3. Synchronisation pulses and synchronisation parameters.

## 6.3 The Video Signal. (52, 53, 54)

The signal producing the brightness of the picture is termed the luminance signal. Its instantaneous value corresponds to the brightness of the scanned image at the point scanned at that time instant. Since the brightness range is limited between black and peak white, the range of the luminance signal is also limited. A precise voltage level can define black level and thus all intermediate grey tones up to peak white.

When the image is reconstructed, it is necessary to be able to relate the signal amplitude to a brightness level. For this purpose, a part of the line scan is transmitted at black level. The receiver can then sense black level and assess the picture brightness by comparing the instantaneous video amplitude to black level.

The luminance video signal is generally formed by a summation of the brightness component and the synchronisation pulses. The synchronisation pulses are positioned so that they lie below 'black level' and their amplitude is made an exact proportion of the black-to-peak-white signal voltage range. Thus, as well as providing synchronisation, the synchronisation pulses form a reference amplitude for setting the contrast ratio of the display system, which can be judged on a line-by-line basis. The system is useful for automatic circuitry to adjust the video signals in amplitude by measuring the

synchronisations pulse amplitude. The measured synchronisations pulse amplitude is compared with an inbuilt reference, hence, where a discrepancy occurs, the gain of the video-signal path can be adjusted.

When it is required to define the chromaticity, extra signals are necessary but their form depends upon system encoding. Specific details relating to chrominance are dealt with in chapter seven.

The standard presentation of the C.C.I.R. 625 line standard video signal is shown in Fig. 6.4. The 'front' and 'back porch', are levels transmitted at black level, and positioned before and after the synchronisation pulses. The 'front porch' is mainly a guard level which prevents a signal excursion from peak white to the tip of synchronisation pulse, which would complicate line synchronisation detection.

In the C.C.I.R. system there are twenty lines commencing at the first equalisation pulses, which are transmitted at black level, thus only 605 lines are used for active picture. It is seen in Fig. 6.4, that only about 52  $\mu$ sec. of each line contributes to the active picture and that about 12  $\mu$ sec. are occupied with synchronisation and black level transmission. Basically the 5.8  $\mu$ secs. of black level represent a periodical chopping of the video information. By virtue of the scanning structure, this chopping frequency can be made only a small fraction of the chopping rate required for a chopper

stabilised system. However, its effect is identical and it allows the video signal to pass through a.c. coupled circuits with exact d.c. restoration.

The luminance video-signal bandwidth can be calculated approximately from equation (6.6), putting,

$$A_r = \frac{4}{3}, \quad P_r = 25, \quad N_1 = 605$$

Hence,  $f_v \approx 6.1$  MHz

In practice, the video bandwidth is limited to 5.5MHz. The bandwidth of the video signals is directly related to the spatial bandwidth that is transmitted; thus in order to maintain picture definition, the video bandwidth must not be restricted.

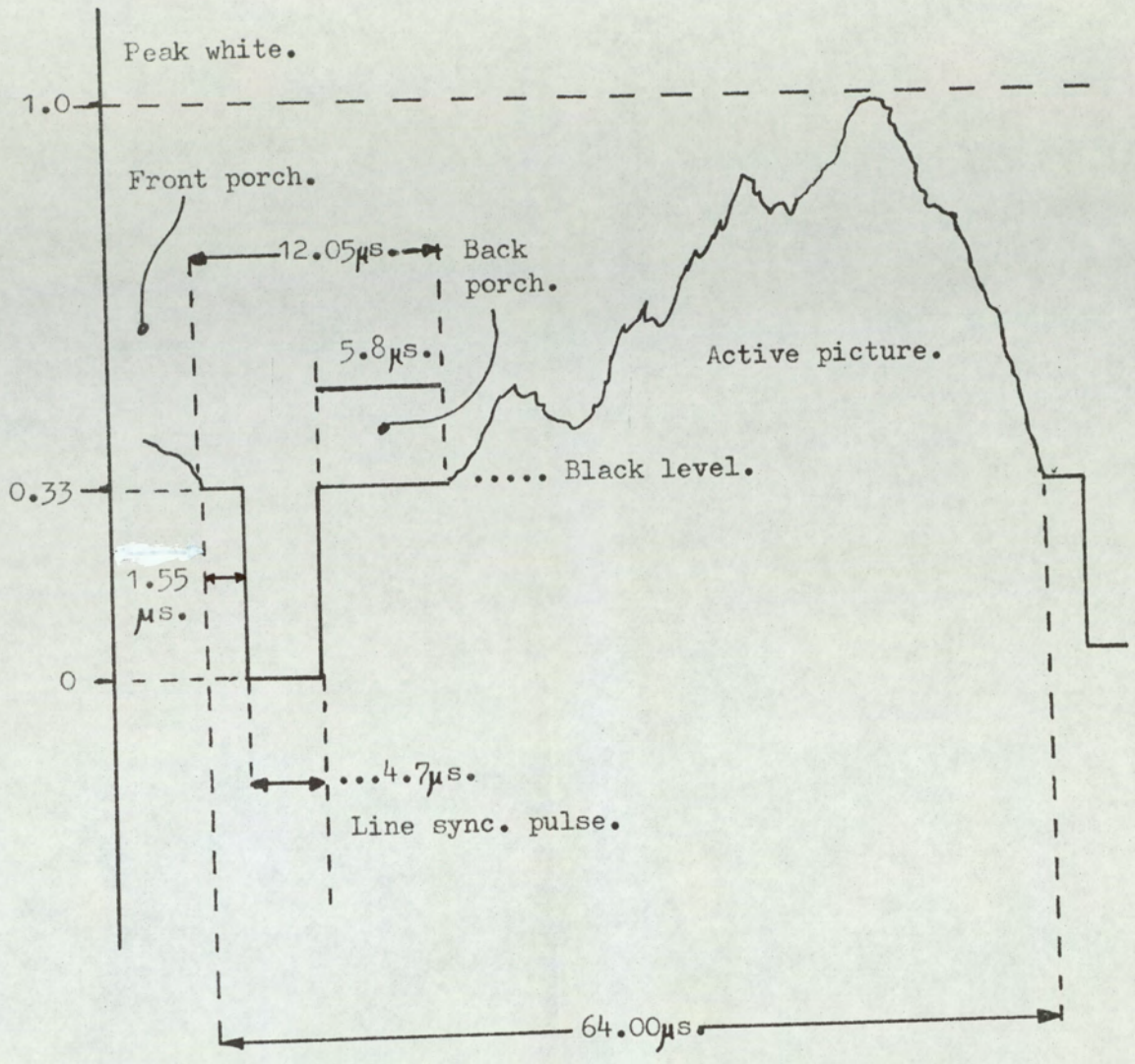


Fig6-4. C.C.I.R., 625 line-standard, luminance signal.

## 6.4 Gamma Correction (52, 53, 54)

With present-day display systems, the image intensity is not directly proportional to the control signal. Correction for this non-linearity is realised by introducing a complementary distortion characteristic. It has been found desirable to introduce the correction at the signal source of the television system by means of a predistortion called gamma correction. This saves each receiver terminal from having to correct for the non-linearity of its display; also the system introduces an instantaneous companding characteristic.

If  $E_L$  represents the luminance voltage, which is linearly related to the image brightness, then gamma correction generates a signal  $E'_L$ , where,

$$E'_L = E_L^{1/\gamma}, \quad \dots(6.7)$$

and,  $\gamma=2.2$ .

When a colour image is transmitted, the gamma correction process is applied to an array of signals. The signals to be presented to digital systems also have to be gamma corrected but, since the system maintains signal balance, the gamma correction characteristic is not modified.

CHAPTER 7.FUNDAMENTAL OF COLOUR WITH  
APPLICATION TO TELEVISION.

## 7.1 Introduction. (53, 54, 55)

The sensation of colour is of the mind and is a purely subjective phenomenon. The science of colour, colorimetry, must therefore be based upon subjective measurement, and is difficult to describe in absolute terms.

The foundation of colour theory stems from Newton's famous experiment in 1666, when he demonstrated that "white" light could be decomposed into a mixture of all pure colours, the visual colours of the spectrum of light. These colours are termed 'spectral colours'. It must be appreciated that the experimental interpretation of such decomposition is purely subjective; it is the result of stimulation of our visual senses.

Physicists have demonstrated that the excitation stimulus of colour is an electromagnetic wave structure; this result is basically Maxwell's Electromagnetic Theory of light'. The importance of this theory is that it develops the foundations of an objective study of the sensation of colour. The electromagnetic waves that stimulate visual perception are found to have wavelengths in the range, approximately, 400 to 700 n.m. Hence it is possible to assign the subjective, spectral colour to an objective scale of the wavelength of an electromagnetic wave.

Already it is possible to realise a colour reproduction system. A general colour is produced by an additive mixture of various wavelengths, the proportions of energy each wavelength being precisely known. The reproduction system must be capable of producing each wavelength of

the original and also of controlling the energy distributions to match the original components. In so doing, the exact colour will be reproduced. This system although exact, is extremely difficult to engineer. Hence it is necessary to examine more carefully the subjective characteristics of the eye and brain and determine what acceptable simplifications can be introduced.

Experience demonstrates that colour is extremely variable. A tomato appears red in sunlight, yet viewed under sodium vapour lighting it is black. Certain flowers are vivid in direct white light, yet when observed in the evening or when illuminated by an overcast sky, they seem much less vivid. It is the quality of the light or more specifically, the spectral distributions of the light energy; illuminating the objects, that produces the apparent change in colour. The other variable in the system is the eye, which together with the brain exhibits psychological and physiological characteristics. The latter are extremely complex and not, as yet, fully understood. However, the quality of the illuminant can readily be controlled by careful measurement and spectral filtering; thus only the visual sensors are variable.

A method that is used to define a particular colour from an objective point of view, is to determine the "spectral reflectance" of the object under test. When viewed under white light, (white being defined here as a constant-energy spectrum over the range of visual perception) the colour may be readily defined by determining the energy spectrum of the reflected light, the characteristic defining the "Spectral Reflectance". In practice, the object is scanned with a narrow band of light and the percentage of reflected light is measured

for a range of wavelengths. Thus a curve is generated of percentage reflected light against wavelength, which fully defines the colour of the object.

It can be seen that it is relatively simple to define an objective measurement of colour without bringing colour into the measurement. Such a measurement would then be applicable to any sensor that responds over the range in which the Spectral Reflectance is defined. However, the objective of the colour theory is to realise and engineer a colour television system, directed at homo-sapiens. Such a system must base its design parameters around the characteristics of the human eye and its association with the brain.

## 7.2. Trichromatic Visual Model. (53, 54)

During the seventeenth century, it was discovered that the eye possessed at least basic trichromatic characteristics. By trichromatic, it is inferred that a range of colours may be accurately matched, subjectively, by the addition of carefully proportioned amounts of three colour stimuli. By 1722, Jakob christoffel Leblan was using a form of trichromatic printing and in 1861 James Clerk Maxwell was successful in producing the first trichromatic photograph. It is interesting to observe that Maxwell's primary objective was not to demonstrate trichromatic colour photography but to demonstrate the trichromatic nature of colour vision. Maxwell demonstrated his findings during a Friday evening discourse at the Royal Institution, on the 17th May, 1861.

Maxwell's experiment is of extreme importance, as it is the basis of most present-day colour television and colour photographic systems. In principle, the experiment was achieved by producing three similar photographs of the given object, each photograph being taken through a different colour filter; in fact red, green and blue filters were used. The luminance of the three photographs were therefore proportional to red, green and blue components of the object. In the reproduction system, the slides were independantly illuminated by red, green and blue light and projected onto a screen in registration. The result realised a colour image where a fairly wide range of colours was reproduced.

Hence experiment shows that a wide range of colours may be accurately reproduced by a trichromatic system. This is a physiological

fact and not dependent upon any particular theory.

In recent years, much work has been directed at the mechanism of colour vision of the eye. Examinations of the light and image sensor, the retina, has determined that there are at two types of vision . These have been designated 'rod visions' and cone vision', the names being derived from their appearance when viewed under a microscope. It is a common experience that under low levels of illumination, colours appear very desaturated and vision is mainly in varying shades of grey. This vision is attributed to the 'rods', which are far more numerous on the retina. Such vision is observed to depend upon the bleaching of a substance called 'visual purple', contained in the 'rods'. Colour vision is attributed to the 'cones'. It is believed that there are three types of 'cone' sensors; each having different photosensitive pigments, responding to red, green and blue light. Experiment suggests **this** is possible, though not yet conclusive.

To engineer a practical colour reproduction system, it is necessary to know the relative sensitivities of the eye to the red, green and blue stimuli. Subjective experiments, and measurements of absorption of the pigments found in the 'cones', have been correlated to produce a set of curves that are said to be typical of the red, green and blue sensors of the eye. The sensitivity curves are designated  $\rho, \gamma, \beta$  and are plotted against the wavelength of light, as shown in Fig. 7.1, a,b.

Fig. 7.1 shows two sets of characteristics,

- (a) Indirect determination of probable sensitivity curves of eye
- (b) Curves of sensitivity determined from bleaching of pigments on human retina.

Figs. 7.1 (a) and (b) illustrate the basic sensitivity curves established by indirect measurement and pigment analysis respectively. The areas of the sensitivity curves are used for the determination of filter responses for the red, green and blue channels, the determination of optimum reproduction colours and, finally, in forming the basis of colour mixing.

In a trichromatic system, the aim is to reproduce the identical  $\rho, \gamma, \beta$  responses that were stimulated by the original image. Ideally, red light should only produce a  $\rho$  response, green light a  $\gamma$  response and blue light a  $\beta$  response. To do this, three filters of narrow bandwidth sample the light, producing red, green and blue responses, which define the red, green, blue channel responses. These channels, in a reproduction mode, then stimulate the  $\rho, \gamma, \beta$  sensors.

However, the  $\rho, \gamma, \beta$  sensitivity curves considerably overlap and it is impossible to excite each sensor independently; hence, there is interchannel crosstalk. There is no way in which the crosstalk can be overcome; yet in practice it proves not to be objectionable. Basically, the effect of cross talk is to desaturate

the colours. The original sensor produces three responses  $\rho_0, \gamma_0, \beta_0$ , which define the subjective colour impression on the object being observed. This process includes interchannel crosstalk, but a given object produces a unique  $\rho_0, \gamma_0, \beta_0$ , response. In the transmission system, it is possible to generate three red, green and blue channel responses, R,G,B such that:

$$R \propto \rho_0$$

$$G \propto \gamma_0$$

$$B \propto \beta_0$$

When the three channels R,G,B are converted to red, green and blue light, the quality being about that shown in the shaded regions of Fig. 7.1a, the light generates the required response  $\rho_0, \gamma_0, \beta_0$ . Also, to a lesser degree, R produces a green ( $\rho_G$ ) and blue ( $\rho_B$ ) response, G produces a red ( $\gamma_R$ ) and blue ( $\gamma_B$ ) response and B mainly a green response ( $\beta_G$ ); see Fig. 7.1 a,b.

Thus, the red, green and blue responses can be written:

$$\text{Red Response} = \rho_0 + \begin{array}{|l} \rho_G + \rho_B \end{array}$$

$$\text{Green Response} = \gamma_0 + \begin{array}{|l} \gamma_R + \gamma_B \end{array}$$

$$\text{Blue Response} = \beta_0 + \begin{array}{|l} \beta_G \end{array}$$

Desired Response	Interchannel crosstalk Response
---------------------	---------------------------------

The crosstalk components contribute additively at the  $\rho, \gamma, \beta$  sensors of the eye, the eye tending to integrate these components to white or grey. Hence, the effect of interchannel crosstalk on the reproduction system is to desaturate the original colour. The distortion introduced by the trichromatic system, which is a fundamental failing of the system, is to distort the saturation rather than the hue of the original colour. The effect only becomes noticeable when trying to match colours of high saturation, the pure spectral colours.

In colorimetry, an objective stimulus creates a subjective impression; thus standard terminology has been created to describe the subjective and objective. This is defined by, the British Standard 1611: 1953 and C.I.E. International Lighting Vocabulary, 1967.

Subjective Term	Objective Term	Definition
Hue Saturation	Dominant Wavelength Purity	Colour Measure of amount of white light mixed with colour.
Luminosity	Luminance	Measurement of energy creating brightness of colour or colours.
Lightness	Luminance Factor	Measurement of amount of reflected energy from object
Hue and Saturation	Chromaticity	

Colour television is based upon the trichromatic visual

model described. Subjectively, trichromatic colour mixing can reproduce most colours except colours of high saturation, however, even these, under certain conditions, can be matched in television by the concept of negative colour. It is evident that a continuous, spectral-energy distribution can be matched by a line spectrum consisting of three lines in the red, green and blue regions. Such spectral pairs although objectively dissimilar, can yield the same subjective response. The spectral pairs are termed 'metameric pairs' or 'metamers'.

In colorimetry, it is necessary to present data to determine conveniently what combinations of trichromatic stimuli produce a particular colour of a particular saturation: that is define the chromaticity.

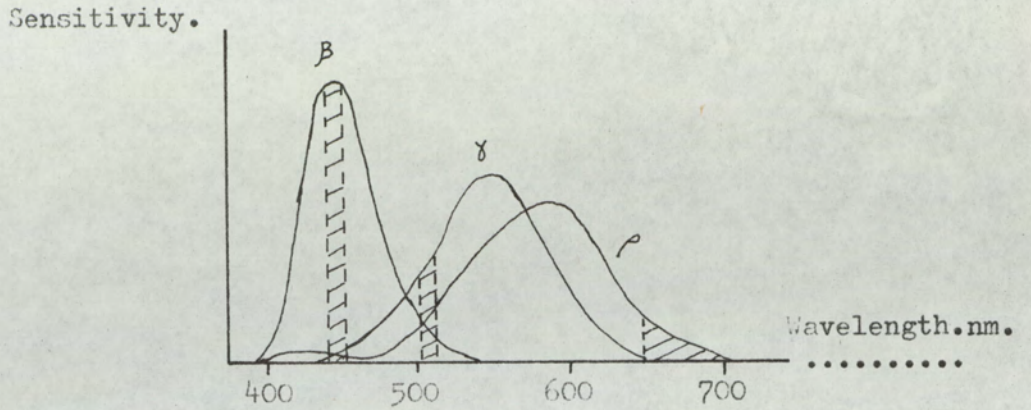


Fig.7-1(a).....

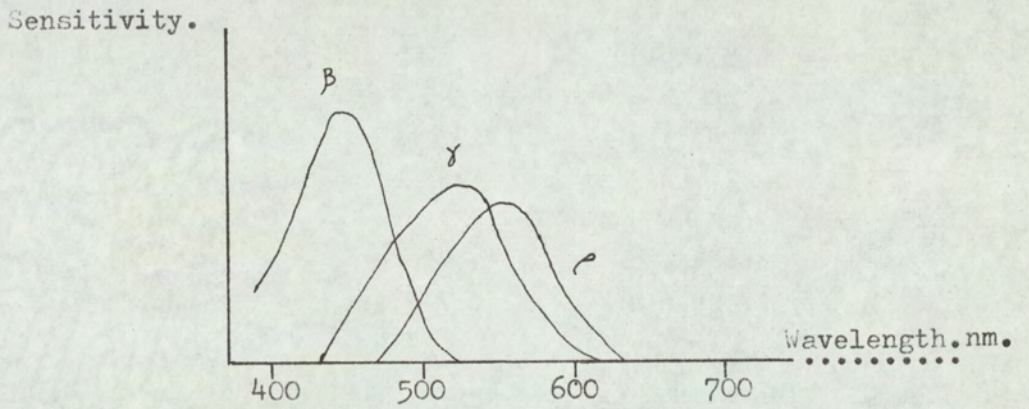


Fig.7-1(b).....

- Fig.7-1(a). Indirect determination of probable sensitivity curves of a human eye.
- Fig.7-1(b). Curves of sensitivity determined from bleaching of pigments on the human retina.

### 7.3 Colour-Matching Functions,

Let the three colour sources of the trichromatic system be designated R,G,B. For convenience, R,G,B are measured in energy units, though this is arbitrary and luminance units could equally be used. It is necessary to know what 'amounts' of R,G and B are necessary to match a colour of wavelength, value  $\lambda$ n.m. The colour match can conveniently be expressed as an identity. This is presented:

$$1.O(\lambda) \equiv \bar{r}_\lambda (R) + \bar{g}_\lambda (G) + \bar{b}_\lambda (B) \dots\dots \quad (7.1)$$

The identity reads: one unit of wavelength  $\lambda$  may be matched subjectively in colour by,  $\bar{r}_\lambda$  units of the stimulus (R),  $\bar{g}_\lambda$  units of the stimulus (G) and  $\bar{b}_\lambda$  units of the stimulus (B). The units may be energy units or luminance units.

Identity (7.1) holds for all the visual colours, providing the colour matching functions,  $\bar{r}_\lambda$ ,  $\bar{g}_\lambda$ , and  $\bar{b}_\lambda$ , can take negative values. If a colour cannot be matched by an additive trichromatic system, then an addition of a part of one primary to that colour, enables the combination to be matched by the other two primaries. The addition of the primary to the colour is said to be a negative quantity. In a television system, negative colour can be realised within certain bounds. If a highly saturated colour is to be added to a particular background colour, it is possible to reduce one of the primary stimuli. Providing that the resulting reduction in the primary stimulus is not negative, then negative colour is realisable in a practical system.

Identity (7.1) is a formal presentation of a metameric pair of spectra and is thus related to the sensitivity curves of the eye.

Experiment shows that the identity of (7.1) may be multiplied by a factor,  $k_N$ , where:

$$k_N(\lambda_N) \equiv k_N \bar{r}_{\lambda N} (R) + k_N \bar{g}_{\lambda N} (G) + k_N \bar{b}_{\lambda N} (B) \dots \quad (7.2)$$

Also, the mixing of several colours may be calculated on an additive basis as follows:

$$\sum_{N=0}^{\bar{N}} \{ k_N(\lambda_N) \} \equiv \sum_{N=0}^{\bar{N}} \{ k_N \cdot \bar{r}_{\lambda N} (R) \} + \sum_{N=0}^{\bar{N}} \{ k_N \cdot \bar{g}_{\lambda N} (G) \} + \sum_{N=0}^{\bar{N}} \{ k_N \cdot \bar{b}_{\lambda N} (B) \}, \dots \quad (7.3)$$

This identity is known as Grassman's Law.

The identity (7.3) may be generalised to a form:

$$k(c) \equiv R_c(R) + G_c(G) + B_c(B), \dots \quad (7.4)$$

where,  $k$  represents the resultant quantity of the resultant colour (C). The quantities  $R_c$ ,  $G_c$  and  $B_c$ , the amounts of the trichromatic stimuli, are termed 'tristimulus values'. The 'tristimulus values', the stimuli R,G,B and the luminance of the reference white form a complete specification for a colour, (C), in the trichromatic system.

The theory has been concerned only with components of discrete wavelengths. In practice, a colour is defined by an energy (or luminance) distribution  $E_\lambda$ .  $E_\lambda$  represents an objective definition of a colour (C). The tristimulus values,  $R_c$ ,  $G_c$ ,  $B_c$  are then defined by three integrals. The integrals represent the continuous relation between the identities (7.3) and (7.4). They are expressed:

$$R_C = \int E_\lambda \cdot \bar{r}_\lambda \cdot d\lambda, \quad \dots \quad (7.5)$$

$$G_C = \int E_\lambda \cdot \bar{g}_\lambda \cdot d\lambda, \quad \dots \quad (7.6)$$

$$B_C = \int E_\lambda \cdot \bar{b}_\lambda \cdot d\lambda, \quad \dots \quad (7.7)$$

Integrated over the visual spectrum.

In equations (7.5), (7.6) and (7.7), the colour matching functions represent the amounts of primary stimuli required to match the equal-energy spectrum. The colour matching functions, however, depend upon the primary stimuli chosen.

#### 7.4 Chromaticity Triangle.

It is possible to express the relationship between tristimulus values and chromaticity in the form of a map or colour triangle.

Consider  $k$  units of a colour ( $C$ ) to be matched by  $R_c$  units of stimulus ( $R$ ),  $G_c$  units of stimulus ( $G$ ) and  $B_c$  units of stimulus ( $B$ ).

This result was expressed in the colour matching equation (7.4).

The units of  $R_c, G_c$  and  $B_c$  are arbitrary; thus normalising the identity (7.4), gives:

$$\frac{k}{(R_c + G_c + B_c)} (C) \equiv \frac{R_c}{(R_c + G_c + B_c)} (R) + \frac{G_c}{(R_c + G_c + B_c)} (G) + \frac{B_c}{(R_c + G_c + B_c)} (B),$$

i.e.

$$\frac{k}{(R_c + G_c + B_c)} (C) \equiv r (R) + g (G) + b (B), \quad \dots \quad (7.8)$$

$$\text{where,} \quad r = \frac{R_c}{(R_c + G_c + B_c)}, \quad \dots \quad (7.9)$$

$$g = \frac{G_c}{(R_c + G_c + B_c)}, \quad \dots \quad (7.10)$$

$$b = \frac{B_c}{(R_c + G_c + B_c)}, \quad \dots \quad (7.11)$$

From equations (7.9), (7.10), (7.11), it follows by addition that:

$$r + g + b = 1, \quad \dots \quad (7.12)$$

$r, g$  and  $b$  represent chromaticity co-ordinates. It is possible to map  $g$  against  $r$  for a range of values of  $g$  and  $r$ . The resulting diagram is the colour triangle of Fig. 7.2. In colorimetry, it is usual to define a reference white ( $W$ ) and adjust the luminances of the matching stimuli

(R), (G), (B), such that equal amounts of  $r, g, b$  produce the reference white. The colours (R), (G), (B) and the reference white (W) are represented by the chromaticity co-ordinates  $g, r$ , as

Stimulus	Chromaticity Co-ordinates	
	$g$	$r$
(R)	0	1
(G)	1	0
(B)	0	0
(W)	$1/3$	$1/3$

The third co-ordinate,  $b$ , follows directly from equation (7.12)

The colour triangle of Fig. 7.2 has several useful properties. Consider two colours ( $C_1$ ) and ( $C_2$ ) of total luminance  $L_1$  and  $L_2$  respectively. The colours may be represented by the identities:

$$L_1(C_1) \equiv r_1(R) + g_1(G) + b_1(B), \dots \quad (7.13)$$

$$L_2(C_2) \equiv r_2(R) + g_2(G) + b_2(B), \dots \quad (7.14)$$

If,  $L_R, L_G, L_B$  are the photometric luminances of the trichromatic stimuli such that when added they produce the reference white, then:

$$L_1 = L_R \cdot r_1 + L_G \cdot g_1 + L_B \cdot b_1, \dots \quad (7.15)$$

$$L_2 = L_R \cdot r_2 + L_G \cdot g_2 + L_B \cdot b_2, \dots \quad (7.16)$$

Consider the colour ( $C_M$ ) formed by an additive mixture of  $M_1$  units of ( $C_1$ ) and  $M_2$  units of ( $C_2$ ). The resultant luminance of ( $C_M$ ) is  $L_M$ , hence:

$$L_M(C_M) \equiv M_1(C_1) + M_2(C_2) \dots \quad (7.17)$$

From identities (7.13) and (7.14),  $M_1(C_1)$  and  $M_2(C_2)$  can be calculated, thus from identity (7.17):

$$\begin{aligned} L_M(C_M) \equiv & M_1 \cdot \frac{r_1}{L_1}(R) + M_1 \cdot \frac{g_1}{L_1}(G) + M_1 \cdot \frac{b_1}{L_1}(B) \\ & + M_2 \cdot \frac{r_2}{L_2}(R) + M_2 \cdot \frac{g_2}{L_2}(G) + M_2 \cdot \frac{b_2}{L_2}(B) \\ & \dots (7.18) \end{aligned}$$

The sum of the coefficients of the identity (7.18) reduces to:

$$\text{Sum of coefficients} = \left[ \begin{array}{c} \frac{M_1}{L_1} + \frac{M_2}{L_2} \end{array} \right]$$

Dividing the identity (7.18) by the sum of the coefficients of the trichromatic stimuli, to determine the chromaticity co-ordinates  $r_M, g_M, b_M$ , of the colour mixture, gives:

$$r_M = \left[ \frac{\frac{M_1 \cdot r_1}{L_1} + \frac{M_2 \cdot r_2}{L_2}}{\frac{M_1}{L_1} + \frac{M_2}{L_2}} \right], \dots (7.19)$$

$$g_M = \left[ \frac{\frac{M_1 \cdot g_1}{L_1} + \frac{M_2 \cdot g_2}{L_2}}{\frac{M_1}{L_1} + \frac{M_2}{L_2}} \right], \dots (7.20)$$

$$b_M = \left[ \frac{\frac{M_1 \cdot b_1}{L_1} + \frac{M_2 \cdot b_2}{L_2}}{\frac{M_1}{L_1} + \frac{M_2}{L_2}} \right], \dots (7.21)$$

It follows by addition that,

$$r_M + g_M + b_M = 1, \dots (7.22)$$

The colours  $(C_1)$ ,  $(C_2)$  and  $(C_M)$  are represented on the chromaticity diagram, such as the diagram shown in Fig. 7.3. The position on the diagram of  $(C_M)$  in relation to  $(C_1)$  and  $(C_2)$  is set by equations (7.19), (7.20) and (7.21). The interpretation of these equations shows that  $C_M$  lies on a straight line joining  $(C_1)$  and  $(C_2)$ .

Consider the ratio, 
$$\left[ \frac{r_2 - r_M}{r_M - r_1} \right],$$

From equation (7.19):

$$(r_2 - r_M) = r_2 \cdot \left\{ \frac{M_1}{L_1} + \frac{M_2}{L_2} \right\} - \left\{ \frac{M_1 \cdot r_1}{L_1} + \frac{M_2 \cdot r_2}{L_2} \right\},$$


---


$$\left\{ \frac{M_1}{L_1} + \frac{M_2}{L_2} \right\}$$

Therefore,

$$(r_2 - r_M) = \frac{M_1 \cdot (r_2 - r_1)}{L_1 \cdot \left\{ \frac{M_1}{L_1} + \frac{M_2}{L_2} \right\}},$$

Similarly:

$$(r_M - r_1) = \frac{M_2 (r_2 - r_1)}{L_2 \left\{ \frac{M_1}{L_1} + \frac{M_2}{L_2} \right\}}$$

$$\text{Hence, } \left[ \begin{array}{c} r_2 - r_M \\ \frac{r_2 - r_M}{r_M - r_1} \end{array} \right] = \left[ \begin{array}{c} \frac{M_1}{L_1} \cdot \frac{L_2}{M_2} \\ L_1 \quad M_2 \end{array} \right], \dots \quad (7.23)$$

Similar expressions can be obtained for the g and b axis.

The full interpretation is that  $C_M$  lies on the line joining  $C_1$  and  $C_2$  and divides it in the ratio given by equation (7.23). This is termed "the Centre of Gravity Law of colour Mixing".

The advantages of the chromaticity diagram can be listed as follows:

- (a) The chromaticity diagram presents, in a concise form, the relationship of all colours to the chromaticity co-ordinates r,g,b.
- (b) The locus of the pure, spectral colours is convex, thus by joining the ends of the locus by a straight line, the closed surface contains all the visual colours. The area outside the closed surface represents co-ordinate values that are never required for colour matching.
- (c) The Centre of Gravity Law allows colour mixing to be readily achieved.
- (d) The Centre of Gravity Law automatically infers that two colours, when additively mixed, can reproduce all colours lying upon the straight connecting line.

- (e) Extending the Centre of Gravity Law to three colours infers that a range of colours can be produced by additive colour mixing. The range is limited to the colours contained in the closed surface formed by joining the colours, represented on the chromaticity diagram, by straight lines. The closed surface formed is a triangle, called a colour triangle. A television system using trichromatic stimuli, can reproduce all colours within the triangle.
- (f) All colours within the locus on the chromaticity diagram but not on the locus, are desaturated. The nearer the colour is placed to the reference white, the lower becomes the saturation. The Centre of Gravity Law implies, that if an amount of reference white is added to a pure colour, then the colour moves along a straight line joining reference white to the pure colour. Along this line only the saturation changes, the hue remaining constant.

The chromaticity diagram of Fig. 7.2 was defined for particular trichromatic stimuli (R), (G), (B). The diagram in fact corresponds to the stimuli defined by:

$$\begin{aligned} (R) &\equiv 650 \text{ nm} \\ (G) &\equiv 530 \text{ nm} \\ (B) &\equiv 460 \text{ nm} \end{aligned}$$

It is possible to define other reference stimuli and produce alternative chromaticity diagrams. Such diagrams contain the same information as that of Fig. 7.2. However, it is desirable to produce a diagram which has special properties. The chromaticity diagram, in terms of chromaticity co-ordinates (U), (V), (W) possesses the property

that constant, incremental steps across the diagram represent nearly constant changes in chromaticity. The (V) axis contains all the information relating to the relative luminance of colours. The diagram is related to the (R), (G), (B) system by linear transformation equations; thus, it retains the properties of chromaticity diagrams already discussed. Finally, the coefficients of (U), (V), (W) are all positive, the reference stimuli being "super-saturated" and lying outside the range of visible colours; they are, therefore, fictitious.

The (U), (V), (W) chromaticity co-ordinates representing (R), (G), (B), where (R), (G), (B) are the reference stimuli used in television are given by

	(u)	(v)	(w)
Red (R)	0.477	0.352	0.171
Green(G)	0.076	0.384	0.541
Blue(B)	0.152	0.130	0.718
White(W)	0.201	0.307	0.492

( $S_c$ ) is the 'equal-energy' reference white.

Table (7.1) (u), (v), (w) coefficients of (R), (G), (B), ( $S_c$ ) stimuli.

Fig. 7.4 shows the  $v, u$  plane of the (U), (V), (W) chromaticity diagram. On the diagram, the trichromatic stimuli and reference white, ( $S_c$ ), have been indicated. Also the locus of pure, spectral colours is shown. The television system, using these trichromatic stimuli, is capable of producing all colours within the triangle formed

by joining the co-ordinate points of (R), (G) and (B).

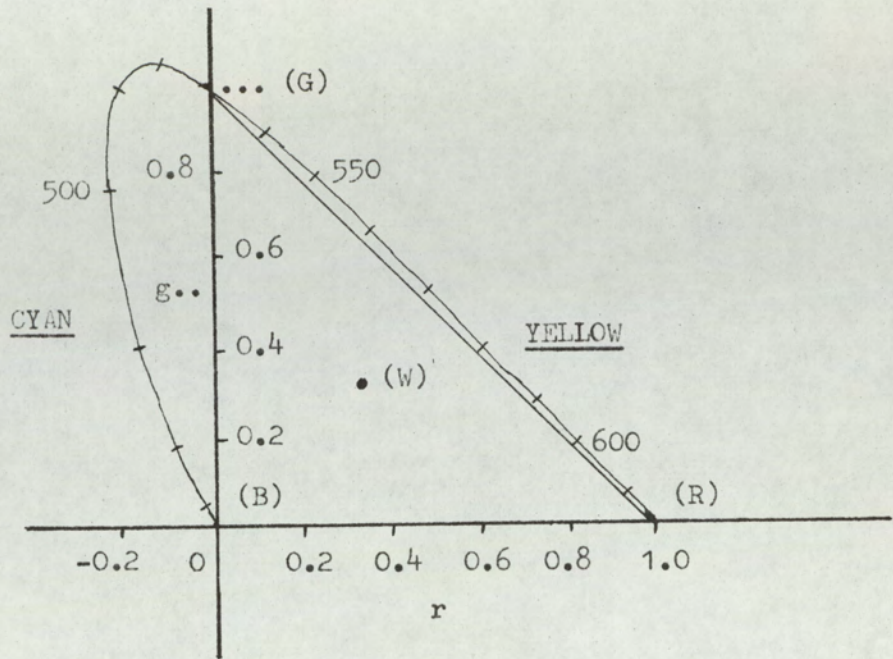


Fig.7-2. Colour triangle for  $g, r$ , coordinates in  $r, g, b$ , system.

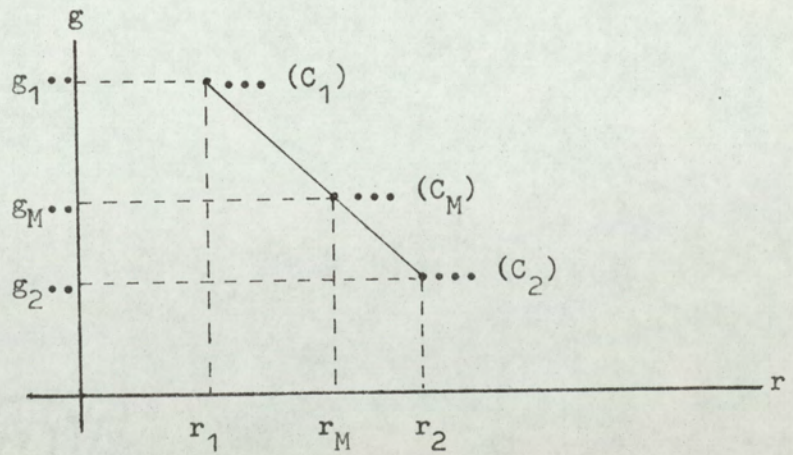


Fig.7-3. Position of  $(C_1)$ ,  $(C_2)$ ,  $(C_M)$ , on chromaticity diagram.

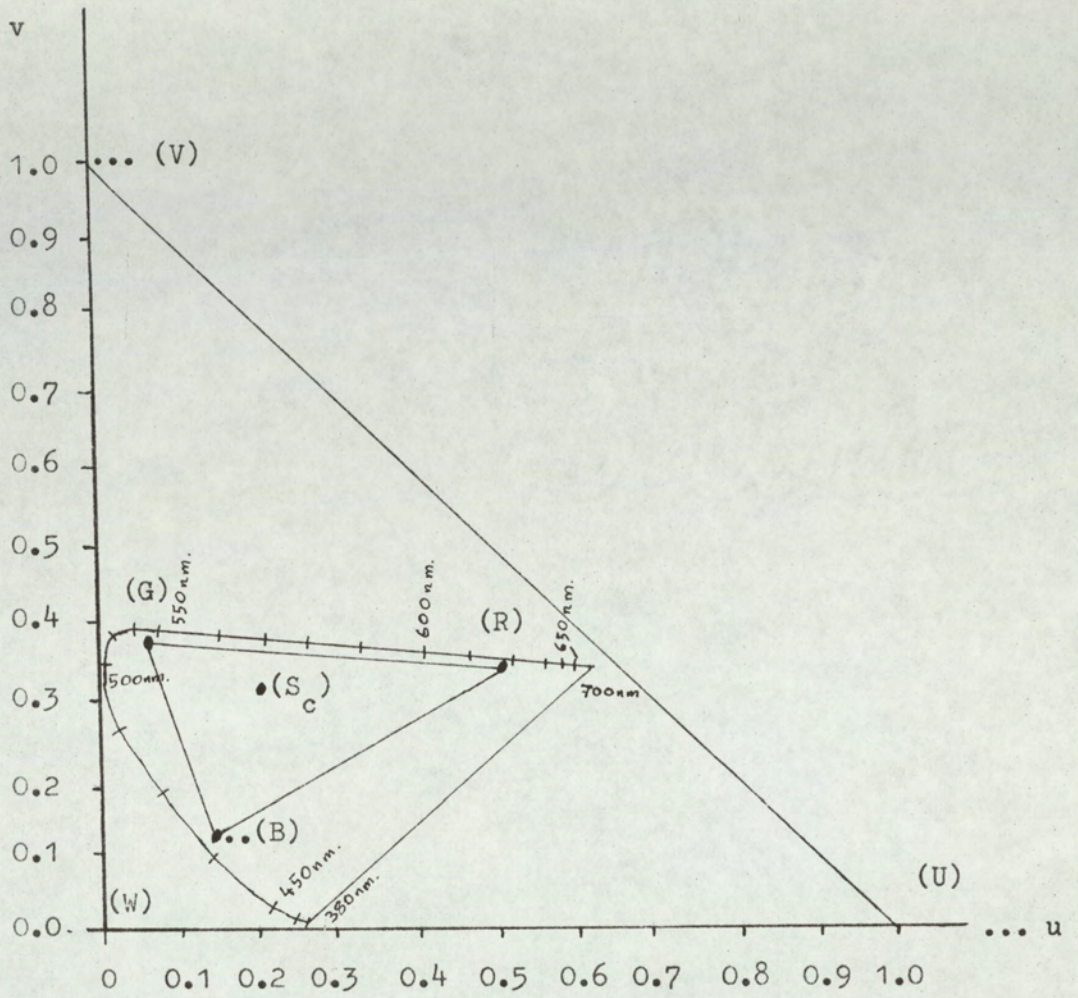


Fig.7-4. (U), (V), (W), chromaticity coordinate system.

## 7.5 Fundamentals of Colorimetry applied to Colour Television. (53, 54)

The colour television systems to be discussed, are based upon trichromatic colour matching. The systems are engineered to produce three registered images. Each image is produced in a similar manner to a monochrome television picture. However, one image is produced in red, the second in green and the third in blue. By controlling the relative image intensities of the simultaneously-scanned pictures, the instantaneous colour of the picture, during the scan, can be reproduced by additive colour mixing. Thus, three simultaneous signals are required to control the luminance and chrominance of the display device, when using trichromatic colour matching.

Initially, each signal corresponds, in format, to the video signal discussed in chapter 6; thus three, wide-band signals are reproduced. Examination of the human eye has revealed that fine detail of vision is detected mainly in luminance changes. This is due to a concentration of 'rod' receptors in the region called the fovea, which results in high-definition vision in this local area of the retina. The engineering implication of this fact is that the chromaticity information may be transmitted with reduced spatial resolution. Reduction of spatial resolution is realisable by two methods and, in practice, both may be implemented. The first is a reduction in horizontal spatial bandwidth, this, as will be shown, is achieved by band-limiting the chrominance signals. The second method is a reduction in the vertical, spatial bandwidth. The process of bandlimiting in the vertical is based on a line by line averaging technique. This, as discussed later, can lead to

a reduction of the number of signal channels required to define the colour image.

The picture reproduced by the television system consists basically of two superimposed images. The first corresponds almost exactly to the image produced by a monochrome television system; it is a high-definition picture described only in luminance. Superimposed, in register, over this luminance image is a lower spatial definition image, describing the chrominance information. In practice, the spatial bandwidth of the chrominance image may be reduced by at least one fifth and, for certain colours, this can be reduced even more. The result of this strategy, when observed by the eye, is that the reproduced image resembles very closely a high-definition trichromatic system, where each colour stimulus is independent and reproduced at full bandwidth.

Reduction of chrominance spatial resolution implies that considerable saving in the channel information capacity is possible. The development of the electrical signals necessary for presenting the complete colour-image structure are now considered. The treatment is general, so that various presentations are possible for digital encoding and spatial bandwidth reduction can be realised for the chrominance of the scanned image.

$R_C, G_C, B_C$  are the tristimulus values of the (R), (G), (B) reference stimuli used in the colour-system display. Let  $L_R, L_G, L_B$  be the luminances of the stimuli to generate the required reference white,  $S_C$ . Hence, the luminance  $L_C$  of a colour (C) is given by:

$$L_C = L_R \cdot R_C + L_G \cdot G_C + L_B \cdot B_C, \dots \quad (7.24)$$

The colour, (C), is given by the identity:

$$L_C (C_L) \equiv L_R \cdot R_C (R_L) + L_G \cdot G_C (G_L) + L_B \cdot B_C (B_L), \dots \quad (7.25)$$

where the L signifies the quantities are measured in luminance units.

Equations (7.5), (7.6), (7.7) showed that the tristimulus values were determined by integration of the colour matching functions. By producing suitable optical filters, the integration over the positive lobes of the colour matching functions may be obtained. Thus, electrical signals may be derived which are directly proportional to the tristimulus values. Let the three signals be  $E_R, E_G, E_B$  and  $\sigma$  be the constant of proportionality applicable to each signal channel, then:

$$E_R = \sigma \cdot R_C,$$

$$E_G = \sigma \cdot G_C,$$

$$E_B = \sigma \cdot B_C,$$

Applying these proportionalities to equation (7.24), it is possible to derive an electrical signal  $E_L$ , which is proportional to the total luminance of the tristimulus colour-match. Hence:

$$E_L = \sigma \cdot \{L_R \cdot E_R + L_G \cdot E_G + L_B \cdot E_B\}, \dots \quad (7.26)$$

To normalise the luminance values, put:

$$\sigma = \frac{1}{(L_R + L_G + L_B)}, \dots \quad (7.27)$$

Hence, defining luminosity coefficients  $\ell, m, n$  such that:

$$\ell = \sigma \cdot L_R, \dots \quad (7.28)$$

$$m = \sigma \cdot L_G, \dots \quad (7.29)$$

$$n = \sigma \cdot L_B, \dots \quad (7.30)$$

Summing the luminosity coefficients as defined by equations

(7.28), (7.29), (7.30) and substituting for  $\sigma$ , from equation (7.27), gives:

$$\ell + m + n = 1, \dots \quad (7.31)$$

Hence, the luminance signal,  $E_L$ , may be written:

$$E_L = \ell \cdot E_R + m \cdot E_G + n \cdot E_B, \dots \quad (7.32)$$

Thus the luminance and colour responses can be described in terms of electrical signals. However, it is necessary to know the luminosity coefficients  $\ell, m, n$  so that the luminance signal can be determined.

The reference white,  $S_C$ , is given when the tristimulus values are equal, i.e. put:

$$R_C = G_C = B_C = T_C,$$

From equations (7.24)

$$L_C = (L_R + L_G + L_B) \cdot T_C,$$

Substituting for  $L_C$  and normalising the identity (7.25), gives:

$$1.0 (S_{CL}) \equiv \frac{L_R}{(L_R + L_G + L_B)} (R) + \frac{L_G}{(L_R + L_G + L_B)} (G) + \frac{L_B}{(L_R + L_G + L_B)} (B),$$

Which, from equations (7.27), (7.28), (7.29) and (7.30), may be written:

$$1.0 (S_{CL}) \equiv \ell (R_L) + m (G_L) + n (B_L), \quad (7.33)$$

(note suffix L signifies luminance units).

In the (U), (V), (W) chromaticity-co-ordinate system, the relative luminance of colours is entirely contained in the (V) axis. Thus, from the table 7.1, which listed the (R), (G), (B) to (U), (V), (W) linear transformation equations, the relative luminances of the (R), (G), (B) stimuli can be written:

$$0.352 (R_L) \equiv 0.477 (U) + 0.352 (V) + 0.171 (W),$$

$$0.384 (G_L) \equiv 0.076 (U) + 0.384 (V) + 0.541 (W),$$

$$0.130 (B_L) \equiv 0.152 (U) + 0.130 (V) + 0.718 (W),$$

Transforming equations (7.33) to (U), (V), (W), co-ordinates:

$$\begin{aligned} 1.0(S_{CL}) &\equiv \frac{0.477}{0.352} \cdot \ell (U) + \ell (V) + \frac{0.171}{0.352} \cdot \ell (W) \\ &+ \frac{0.076}{0.384} \cdot m (U) + m (V) + \frac{0.541}{0.384} \cdot m (W) \\ &+ \frac{0.152}{0.130} \cdot n (U) + n (V) + \frac{0.718}{0.130} \cdot n (W), \\ &\dots\dots\dots \end{aligned} \quad (7.34).$$

Tables (7.1) also defines the location of  $S_C$ , such that in terms of luminance:

$$0.307 (S_{CL}) \equiv 0.201 (U) + 0.307 (V) + 0.492 (W)$$

Hence:

$$\begin{aligned} 1.0 (S_{CL}) &\equiv \frac{0.201}{0.307} (U) + 1.0 (V) + \frac{0.492}{0.307} (W), \\ &\dots\dots\dots \end{aligned} \quad (7.35)$$

Comparing coefficients of (U), (V), (W) in identities (7.34) and (7.35), three simultaneous equations in terms of  $\ell, m, n$  are obtained. Solving, gives:

$$\ell = 0.299, \quad \dots (7.36)$$

$$m = 0.587, \quad \dots (7.37)$$

$$n = 0.114 \quad \dots (7.38)$$

Hence, equation (7.32) becomes:

$$E_L = 0.299 \cdot E_R + 0.587 \cdot E_G + 0.114 \cdot E_B \quad \dots (7.39).$$

Having determined the coefficients  $\ell, m, n$ , it is possible to determine the transformation equations in terms of tristimulus values.

Hence for white,  $S_C$ , applying equation (7.33) and noting the form of equations (7.24), (7.25):

$$\ell \cdot R_C (R_L) + m \cdot G_C (G_L) + n \cdot B_C (B_L) \equiv R_C (R) + G_C (G) + B_C (B) \quad \dots (7.40)$$

Hence, it follows by comparing both sides of the identity:

$$\ell (R_L) = 1.0 (R) ,$$

$$m (G_L) = 1.0 (G) ,$$

$$n (B_L) = 1.0 (B) ,$$

Hence, substituting for  $\ell, m, n$  rearranging, and substituting in the (U), (V), (W) co-ordinate system, it follows:

$$0.352 (R_L) \equiv \frac{0.352}{0.299} (R) \equiv 0.477 (U) + 0.352 (V) + 0.171 (W),$$

therefore,

$$1.0 (R) \equiv 0.405 (U) + 0.299 (V) + 0.145 (W) ,$$

By similar analysis for G and B, the matrix equation is developed:

$$1.0 \begin{bmatrix} (R) \\ (G) \\ (B) \end{bmatrix} = \begin{bmatrix} 0.405 & 0.299 & 0.145 \\ 0.116 & 0.587 & 0.827 \\ 0.133 & 0.114 & 0.627 \end{bmatrix} \begin{bmatrix} (U) \\ (V) \\ (W) \end{bmatrix},$$

..... (7.41)

It can be seen, that in this equation, the (V) axis contains the relative luminosity coefficients of the tristimulus values. The equation readily allows transformations between (R), (G), (B) co-ordinates and (U), (V), (W) co-ordinates.

## 7.6 The Principle of Constant Luminance. (53, 54)

Section 7.5 showed that three simultaneous signals are required to define the luminance and chrominance information of a colour-television display unit. However, if  $E_R, E_G, E_B$  form the three signals, then a fourth signal,  $E_L$ , may be derived from them. This is the luminance component. The luminance signal requires to be transmitted at full system bandwidth, so as not to degrade the horizontal resolution. Thus, it is often desirable to transmit the luminance signal over the communication channel; this has the advantage of producing a compatible signal for a monochrome display. To define chromaticity, two other signals are necessary. However, the luminance is defined by  $E_L$ , thus the other two signals can be transmitted at reduced bandwidth, to limit the chrominance-image horizontal resolution. There is another advantage in transmitting a separate luminance signal. Let  $E_L, E_R, E_B$  be the transmitted signal and  $\Delta E_{LN}, \Delta E_{RN}, \Delta E_{BN}$  the instantaneous transmission impairments. Hence, the received signals are:

$$\begin{array}{l} E_L + \Delta E_{LN}, \\ E_R + \Delta E_{RN}, \\ E_B + \Delta E_{BN}, \end{array} \left. \begin{array}{l} ] \\ ] \\ ] \end{array} \right\} \begin{array}{l} \text{Full bandwidth} \\ \\ \text{Reduced bandwidth} \end{array}$$

The three signals applied to the display system are  $E_{Rd}, E_{Gd}, E_{Bd}$  are calculated from equations (7.32):

where,  $E_{Rd} = E_R + \Delta E_{RN}$ ,

$$E_{Gd} = \frac{1}{m} \{ E_L + \Delta E_{LN} \} - \frac{\ell}{m} \{ E_R + \Delta E_{RN} \} \\ - \frac{n}{m} \{ E_B + \Delta E_{BN} \},$$

$$E_{Bd} = E_B + \Delta E_{BN},$$

Applying the three display signals  $E_{Rd}$ ,  $E_{Gd}$ ,  $E_{Bd}$  to the display device, produces a resultant luminance signal  $E_{Ld}$ , where  $E_{Ld}$  is given by equation (7.32):

$$E_{Ld} = \ell \cdot E_{Rd} + m \cdot E_{Gd} + n \cdot E_{Bd}, \\ = \ell \{ E_R + \Delta E_{RN} \} + \{ E_L + \Delta E_{LN} \} - \ell \{ E_R + \Delta E_{RN} \} \\ - n \{ E_B + \Delta E_{BN} \} + n \{ E_B + \Delta E_{BN} \},$$

Therefore,  $E_{Ld} = E_L + \Delta E_{LN}, \dots\dots\dots$  (7.42)

Equation (7.42) shows that in the linear system, where  $E_L$  is linearly related to  $E_R$ ,  $E_G$  and  $E_B$ , then, if  $E_L$  is transmitted, the noise on the other two signals need only introduce chrominance errors. That is, the luminance is independent of  $\Delta E_{RN}$  and  $\Delta E_{BN}$ . This is the principle of constant luminance.

In practice, however, gamma correction can modify this principle so that errors occur. The effects are often small and can, in certain systems, be minimised. Usually, gamma correction only causes noticeable error in highly saturated colours.

## 7.7 Colour - Difference Signals

It is possible to separate the chrominance and luminance information by choosing a set of functions called 'colour-difference signals'.

Let the three colour-difference signals be  $D_R$ ,  $D_G$ ,  $D_B$ ; where,

$$D_R = \{ E_R - E_L \}, \quad (7.43)$$

$$D_G = \{ E_G - E_L \}, \quad (7.44)$$

$$D_B = \{ E_B - E_L \}, \quad (7.45)$$

$$\text{Now, } E_L = \ell \cdot E_R + m \cdot E_G + n \cdot E_B,$$

and from equations (7.31)

$$1 = \ell + m + n,$$

$$\text{also, } E_L = \ell \cdot E_R + m \cdot E_G + n \cdot E_B,$$

$$\text{Hence, } 0 = \ell \{ E_R - E_L \} + m \cdot \{ E_G - E_L \} + n \cdot \{ E_B - E_L \}$$

Substituting  $D_R, D_G, D_B$  from equations (7.43), (7.44) and (7.45) for the colour-difference signals, gives,

$$\ell \cdot D_R + m \cdot D_G + n \cdot D_B = 0, \dots \quad (7.46)$$

The total picture information required can be transmitted by the luminance signal  $E_L$  and two of the three colour-difference signals. If a picture with only luminance information is transmitted, then,

$$E_R = E_G = E_B = E_L,$$

$$\text{and } D_R = D_G = D_B = 0,$$

For the linear system, the colour-difference signals carry only the chrominance information; this is shown when the signals are represented on the chromaticity diagram. The colour-difference signals may be band-limited to reduce the chrominance resolution as required.

Consider the three signals  $D_R, E_L, D_B$ . These completely define the luminance and chrominance of the picture. It is possible to define three trichromatic stimuli,  $(C_R), (S_L), (C_B)$  corresponding to the signals  $D_R, E_L, D_B$  respectively. This assumes a linear relation between the tristimulus values and the electrical signals. Assuming linearity between tristimulus values and electrical signals  $k$  units of a colour  $(C)$ , as defined by equation (7.4), may be expressed as:

$$\begin{aligned} k(C) &\propto E_R (R) + E_G (G) + E_B (B) \\ &\equiv D_R (C_R) + E_L (S_C) + D_B (C_B), \end{aligned} \quad \dots\dots \quad (7.47)$$

$E_R, E_G, E_B$  and  $D_R, E_L, D_B$  are related by the equation:

$$E_R = 1.0.D_R + 1.0.E_L + 0.0.D_B, \dots \quad (7.48)$$

$$E_G = \frac{-\ell}{m} .D_R + 1.0.E_L + \frac{n}{m} .D_B, \dots \quad (7.49)$$

$$E_B = 0.0.D_R + 1.0.E_L + 1.0.D_B, \dots \quad (7.50)$$

Substituting for  $E_R, E_G, E_B$  from equations (7.48), (7.49), (7.50) in the colour identity (7.47), gives:

$$\begin{aligned}
k(C) &\propto \left\{ \begin{array}{l} \{1.0.D_R\} (R) \\ + \left\{ \frac{-\ell}{m} .D_R \right\} (G) \\ + \{0.0.D_R\} (B) \end{array} \right\} + \left\{ \begin{array}{l} \{1.0.E_L\} (R) \\ + \{1.0.E_L\} (G) \\ + \{1.0.E_L\} (B) \end{array} \right\} + \left\{ \begin{array}{l} \{0.0.D_B\} (R) \\ + \left\{ \frac{-n}{m} .D_B \right\} (G) \\ + \{1.0.D_B\} (B) \end{array} \right\} \\
&\equiv D_R(C_R) + E_L(S_C) + D_B(C_B), \quad \dots\dots (7.47a)
\end{aligned}$$

Comparing terms in  $D_R$ ,

$$\begin{aligned}
D_R \cdot \{1.0\} (R) + D_R \cdot \left\{ \frac{-\ell}{m} \right\} (G) + D_R \cdot \{0.0\} (B) \\
&\equiv D_R (C_R),
\end{aligned}$$

Hence,

$$1.0(C_R) \equiv 1.0 (R) + \frac{(-\ell)}{m} (G) + 0.0(B), \dots \quad (7.51)$$

Similarly for  $E_L$  and  $D_B$ ,

$$1.0 (S_C) \equiv 1.0 (R) + 1.0 (G) + 1.0 (B), \dots \quad (7.52)$$

$$1.0 (C_B) \equiv 0.0 (R) + \frac{(-n)}{m} (G) + 1.0 (B), \dots \quad (7.53)$$

It can be seen by substitution of identities (7.51), (7.52) (7.53) in identity (7.47a) that identity (7.47a) is correct. Thus, identities (7.51), (7.52) and (7.53) represent the location of  $(C_R)$ ,  $(S_C)$  and  $(C_B)$  in the  $(R), (G), (B)$  system. To convert to  $(U), (V), (W)$  the transformation matrix of equation (7.41) gives,

$$1.0 (C_R) \equiv 0.346 (U) + 0.000 (V) - 0.276 (W), \dots \quad (7.54)$$

$$1.0 (S_C) \equiv 0.653 (U) + 1.000 (V) + 1.599 (W), \dots \quad (7.55)$$

$$1.0 (C_B) \equiv 0.110 (U) + 0.000 (V) + 0.467 (W), \dots \quad (7.56)$$

Dividing each identity by the sum of the coefficients of (U), (V), (W) to determine the chromaticity co-ordinates, U,V,W, gives:

Stimulus	u	v	w
(C <sub>R</sub> )	4.981	0.000	-3.981
(S <sub>C</sub> )	0.201	0.307	0.492
(C <sub>B</sub> )	0.191	0.000	0.809

Table 7.2 Chromaticity co-ordinates u,v,w of (C<sub>R</sub>), (S<sub>C</sub>), (C<sub>B</sub>).

By construction of a suitable grid of lines on the chromaticity diagram, the changes in the stimuli (C<sub>R</sub>), (S<sub>C</sub>) (C<sub>B</sub>) can readily be observed. Hence, for a particular set of trichromatic stimuli, there location on the chromaticity diagram is extremely useful. This procedure is adopted in the television systems to be discussed in later chapters.

### 7.8 Systematic representation of chromaticity changes on the chromaticity diagram.

By drawing a set of straight lines through a reference stimulus, it is possible to observe changes in chromaticity due only to that stimulus. For illustration, the technique is applied to the (R),(G),(B) colour triangle of Fig. (7.2). The results obtained in one chromaticity diagram may readily be transformed, linearly, into another chromaticity diagram by suitable transformation equations.

Consider a straight line of slope  $s$  through the (R) stimulus, thus,

$$\begin{aligned} g &= s.(r-1), \\ &= s.(r-r-g-b), \end{aligned}$$

Therefore, 
$$\frac{g}{b} = \frac{-s}{(1+s)},$$

Thus, for a line drawn through the stimulus (R), the ratio of the  $g$  and  $b$  chromaticity co-ordinates is constant.

Applying equations (7.10) and (7.11), it follows that for a line of slope  $s$  drawn through the (R)stimulus, then,

$$\frac{G_C}{B_C} = \frac{-s}{(1+s)},$$

Similarly, it can be shown that for a line through the green stimulus (G), then

$$\frac{R_C}{B_C} = \text{constant},$$

and for a line through the blue stimulus,

$$\frac{R_C}{G_C} = \text{constant.}$$

A similar result follows for any choice of reference stimuli. Consider the reference stimuli formed by  $(C_R), (S_C), (C_B)$  in section (7.7); they are represented in the chromaticity diagram of Fig. 7.5.

In the linear system, the amounts of  $(C_R), (S_C), (C_B)$  are proportional to the electrical signals  $D_R, E_L, D_B$ .

Hence, it can be shown that:

1. Straight lines through  $(C_R)$  represent

$$\frac{(E_B - E_L)}{E_L} = \text{constant,}$$

2. Straight lines through  $(S_C)$  represent

$$\frac{(E_R - E_L)}{(E_B - E_L)} = \text{constant,}$$

3. Straight lines through  $(C_B)$  represent

$$\frac{(E_R - E_L)}{E_L} = \text{constant}$$

Fig. 7.6 shows the U,V,W chromaticity diagram with the positions of (R), (G) and (B) stimuli as indicated in Table 7.1; also the stimuli  $(C_R), (S_C)$  and  $(C_B)$  are shown. Consider the array

of lines that can be drawn from the reference ( $C_B$ ) that fall within the bounds of the colour triangle formed by the stimuli (R), (G), (B). It is necessary to calculate the ratio  $\frac{(E_R - E_L)}{E_L}$  for a particular line on the diagram. Fig. 7.6 shows that all lines through the point ( $C_B$ ), intersect the line joining the stimuli (R) and (G). It is therefore convenient to calculate the ratio  $\frac{(E_R - E_L)}{E_L}$  for points along the line joining (R) and (G); colours displayed on this line are mixtures of (R) and (G) only. Thus, in the electrical equivalent,  $E_B = 0$ . Thus the ratio may be expressed in terms of  $E_R$  and  $E_G$  only, if calculated on this line.

Consider the colour ( $C_{RG}$ ), being a mixture of (R) and (G) only. If the tristimulus values are linearly related to the electrical signals, then

$$(C_{RG}) \propto E_R (R) + E_G (G) + 0 (B),$$

Transforming to (U), (V), (W) co-ordinates by the transformation equation (7.41) gives:

$$\begin{aligned} (C_{RG}) \propto E_R \{0.405(U) + 0.299(V) + 0.145(W)\} \\ + E_G \{0.116(U) + 0.587(V) + 0.827(W)\}, \end{aligned}$$

Hence,

$$\begin{aligned} (C_{RG}) \propto \{0.405 \cdot E_R + 0.116 \cdot E_G\} (U) \\ + \{0.299 \cdot E_R + 0.587 \cdot E_G\} (V) \\ + \{0.145 \cdot E_R + 0.827 \cdot E_G\} (W), \end{aligned}$$

Dividing by the sum of the coefficients of (U), (V) and (W), the chromaticity co-ordinates  $u, v$  can be calculated as,

$$u = \frac{0.405 \cdot E_R + 0.116 \cdot E_G}{0.849 \cdot E_R + 1.530 \cdot E_G},$$

$$v = \frac{0.299 \cdot E_R + 0.587 \cdot E_G}{0.849 \cdot E_R + 1.530 \cdot E_G}$$

Rearranging,

$$\frac{E_R}{E_G} = -\frac{(1.530 \cdot u - 0.116)}{(0.849 \cdot u - 0.405)}, \quad \dots (7.57)$$

$u, v$  lie on the line joining (R) and (G), thus eliminating

$\frac{E_R}{E_G}$  and rearranging,

$$v = -0.079u + 0.389, \quad \dots (7.58)$$

Since  $E_B = 0$ , then,

$$E_L = l \cdot E_R + m \cdot E_G,$$

Thus, rearranging and substituting for  $E_L$ ,

$$\frac{(E_R - E_L)}{E_L} = \frac{1}{1 + \frac{m}{\left(\frac{E_R}{E_G}\right)}} - 1, \quad \dots (7.59)$$

Substituting for  $l, m, n$  from equations (7.36), (7.37), (7.38) and eliminating  $\frac{E_R}{E_G}$  by substitution from equation (7.57);

equation (7.59) can be written

$$\frac{(E_R - E_L)}{E_L} = \frac{-37.317.u + 2.829}{u - 4.951} - 1, \quad \dots (7.60)$$

From equations (7.58), (7.60) it is possible to construct a grid on Fig. 7.6, showing lines of constant  $\frac{(E_R - E_L)}{E_L}$ , and to calculate the ratio with respect to the position of the line on the chromaticity diagram. The construction is shown on the diagram Fig. 7.6.

A similar set of equations can be formed for lines drawn through  $(C_R)$ . In this case, the ratio  $\frac{(E_B - E_L)}{E_L}$  is calculated with respect to the chromaticity co-ordinates lying on the  $E_L$  line joining the (G) and (B) stimuli. The equations are developed as follows:

$(C_{GB}) \propto O(R) + E_G (G) + E_B (B)$ ,  
transforming from equation (7.41)

$$\begin{aligned} (C_{GB}) &\propto \{0.116.E_G + 0.133.E_B\} \quad (U) \\ &+ \{0.587.E_G + 0.114.E_B\} \quad (V) \\ &+ \{0.827.E_G + 0.627.E_B\} \quad (W), \end{aligned}$$

Calculating the chromaticity co-ordinates  $u, v$  by division of the sum of the coefficients and rearranging, it can be shown that

$$\frac{E_G}{E_B} = \frac{-(0.874v - 0.114)}{(1.530v - 0.587)}, \quad \dots (7.61)$$

$$u = -0.030.v + 0.192, \quad \dots (7.62)$$

Equations (7.61) and (7.62) only apply on the line joining (G) and (B). Now,  $E_R = 0$ , thus,

$$E_L = m.E_G + n.E_B,$$

Hence, 
$$\frac{(E_B - E_L)}{E_L} = \frac{1}{\frac{m.E_G + n}{E_B}} - 1,$$

Substituting for  $\frac{E_G}{E_B}$  from equation(7.61) and for the luminosity coefficients  $m, n$  from equations (7.37), (7.38), hence,

$$\frac{(E_B - E_L)}{E_L} = \frac{-5.513 v + 1.732}{v}, \quad \dots (7.63)$$

Thus from equations (7.62) and (7.63), the ratio of  $(\frac{E_B - E_L}{E_L})$  can be calculated along the line joining (G), (B).

Hence, a grid of straight lines passing through  $(C_R)$  may be drawn and the represented ratio  $(\frac{E_B - E_L}{E_L})$  calculated.

The grid is shown on Fig. 7.6

It follows by similar calculations that on the line joining (R) and (B) on the (U), (V), (W) diagram, where  $E_G = 0$ , that,

$$\frac{E_B}{E_R} = - \frac{(0.849u - 0.405)}{(0.874.u - 0.133)}, \quad \dots (7.64)$$

$$\text{and, } v = 0.682.u + 0.027, \quad \dots (7.65)$$

Equations (7.57), (7.58), (7.61), (7.62), (7.64), (7.65) are used in calculations in chapter 8.

$\frac{(E_B - E_L)}{E_L}$	v (G)→(B)	$\frac{(E_B - E_L)}{E_L}$	v (G)→(B)	$\frac{(E_R - E_L)}{E_L}$	u (R)→(G)
-1.000	0.384	3.500	0.191	-1.000	0.076
-0.500	0.346	4.000	0.182	-0.500	0.140
+0.000	0.314	4.500	0.173	+0.000	0.203
0.500	0.288	5.000	0.165	0.500	0.264
1.000	0.266	5.500	0.157	1.000	0.324
1.500	0.245	6.000	0.150	1.500	0.382
2.000	0.231	6.500	0.144	2.000	0.439
2.500	0.216	7.000	0.138	2.344	0.477
3.000	0.203	7.500	0.133		
		7.772	0.130		

Table 7.3 Ratios  $\left(\frac{E_B - E_L}{E_L}\right)$ ,  $\left(\frac{E_R - E_L}{E_L}\right)$  calculated for values of u,v on (U),(V),(W) chromaticity diagram.

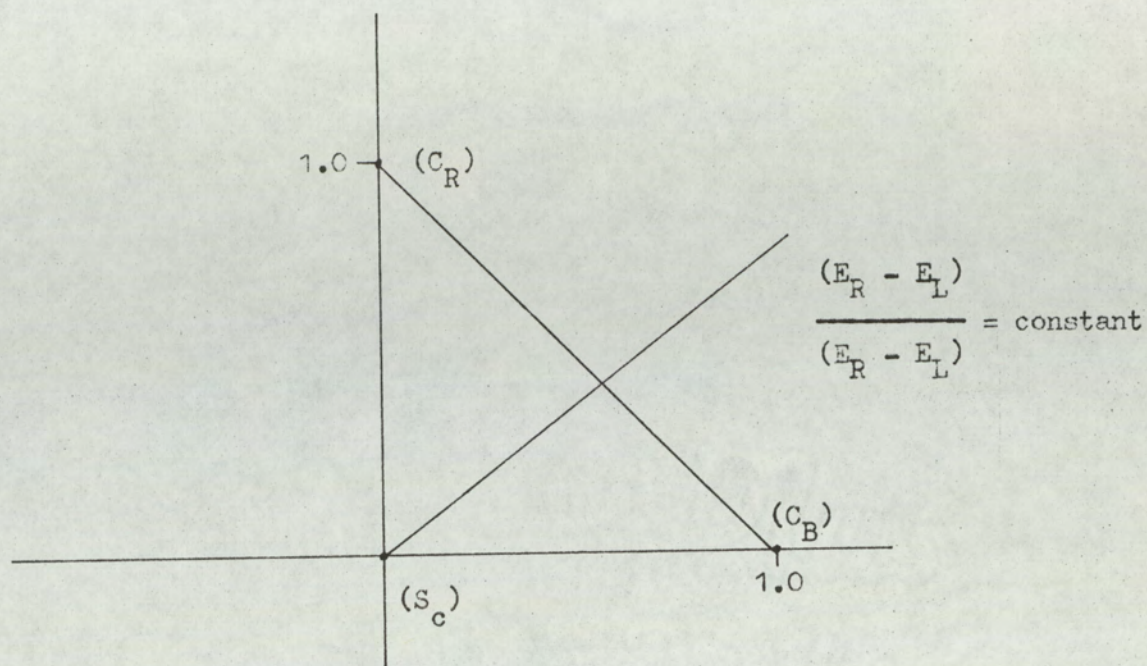


Fig.7-5. Colour triangle formed by stimuli  $(C_R)$ ,  $(C_B)$ ,  $(S_C)$ .

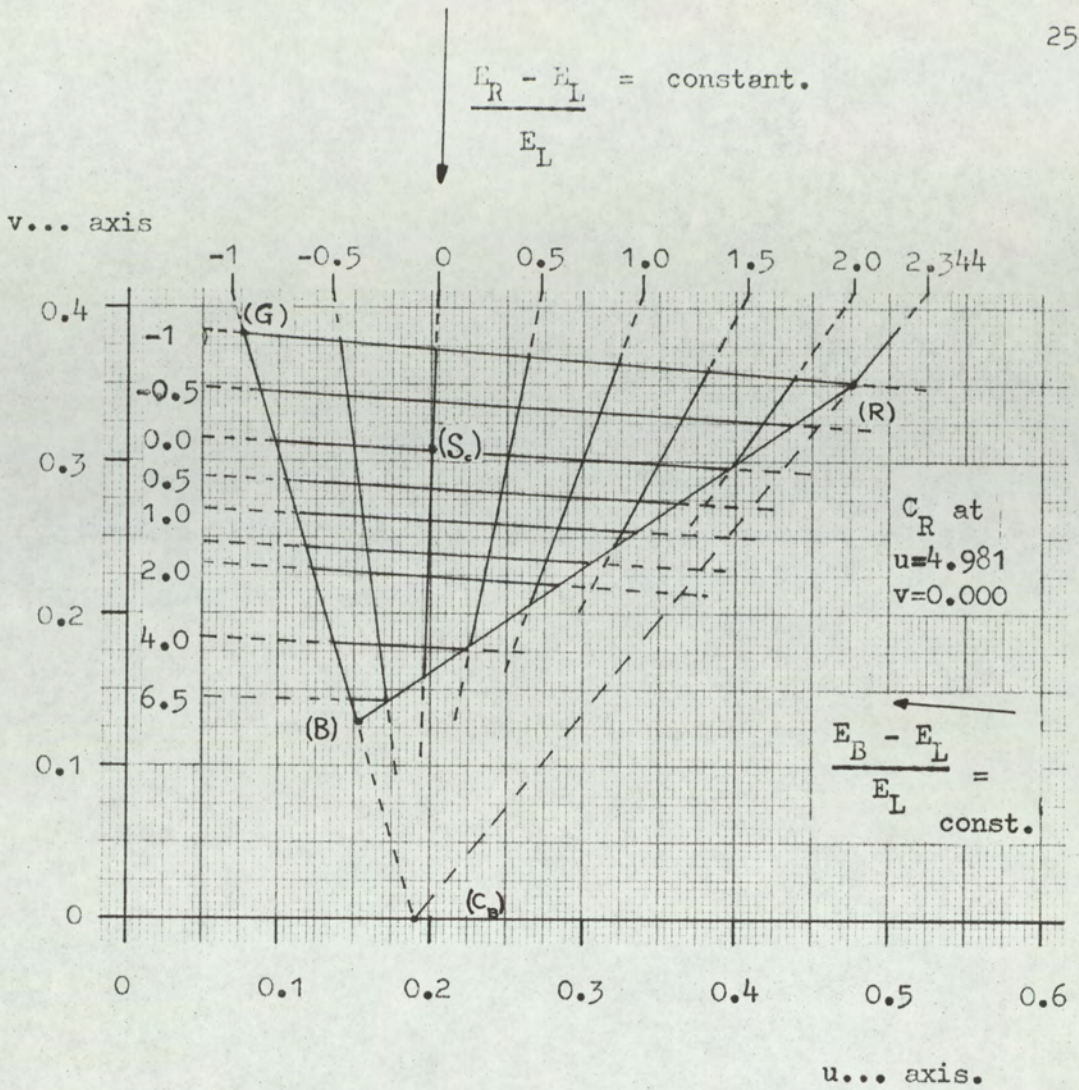


Fig.7-6 Chromaticity diagram showing location of (R), (G), (B), (C<sub>R</sub>), (S<sub>c</sub>), (C<sub>B</sub>) and ratios  $\frac{E_R - E_L}{E_L}$ ,  $\frac{E_B - E_L}{E_L}$  on (U), (V), (W) diagram.

CHAPTER 8.COLOUR ENCODING SYSTEMS.

## 8.1. Introduction.

Colour encoding systems can be categorised into two basic groups. The first group uses analogue encoding methods for introducing the chrominance informations. These include such systems as N.T.S.C., P.A.L., S.E.C.A.M., F.A.M., etc. Analogue colour-encoding methods, rely on picture redundancy contained within the luminance signal. It is also possible to digitally encode, directly, these composite video signals. However, such systems require adequate signal-to-noise ratio at high-frequencies in the base-band, together with linear gain and phase responses. Such digitally encoded signals, after demodulation, are compatible with commercial standard equipment. In the author's experimental equipment, the red, green and blue signals were obtained from a decoded, P.A.L - composite video signal. Section 8.2. describes the basic P.A.L. system as an example of analogue encoding and to express the limitations of the signals that were available for experimental operations. Detailed information of analogue encoding of chrominance signals is to be found in the literature.(53, 54)

Subsequent sections of this chapter deal exclusively with digital encoding techniques using pulse-compression and time-division-multiplex (t.d.m) techniques; this forms the second basic group. The advantage of direct digital encoding is that the high-frequency energy content of the video signal is minimised, thus allowing pre-emphasis networks to enhance the signal-to-noise ratio of the modulated signals. The distortions introduced by an analogue encoder are eliminated and with certain systems, the luminance signal may be extracted without

decoding the t.d.m. signal. The signal range of a monochrome signal is not as great as for an analogue-encoded composite video signal; thus, the signal-to-error noise ratio can be increased.

In present-day broadcast equipment, once the red, green and blue signals are generated they are immediately encoded in composite form so as to maintain signal balance accurately and to minimise transmission - line requirements. It is envisaged that a digital encoder would take the place of the analogue encoder; thus, signal balance would **again** be maintained and the number of highly-stable analogue circuits minimised.

## 8.2. The P.A.L. - encoded systems. (53, 54)

This section contains a brief description of the P.A.L - encoded system. Observation of the luminance signal of the standard C.C.I.R. 625 line television system shows that the spectral energy distribution is generally formed in groups of high energy separated by groups of relatively low energy. This spectral structure is developed through high adjacent-line correlation. Such correlation is developed by two processes. Firstly there is a spatial correlation of adjacent lines, since the picture does not generally, consist of random noise. Secondly there is a inter-line correlation formed by two successive pictures being, generally, extremely similar. Hence the frequency spectrum contains high-energy zones at multiples of line-frequency and picture-frequency. Thus, it may be concluded that there is a range of signals that can be superimposed upon the luminance signal. If the frequency distributions of the superimposed signal has energy groupings which fall within the low-energy regions of the luminance signal, then only low visibility interference is added to the viewed picture.

The process of modulation of the chrominance signals is to modulate a subcarrier in amplitude and phase; the carrier is suppressed. The chrominance signals  $D_R$  and  $D_B$  defined by equations (7 - 43) and (7 - 45) contain energy groups similar to the luminance signal, since they are also formed by the scanning process. It is possible to choose a subcarrier such that the energy spectra of the luminance and sub-carrier sidebands only partially interfere with the picture. Patterns with the lowest visibility appear to be generated, in the 625 line system, by a combination of quarter line offset and picture offset. The chosen signal is also not too complicated to generate, it is defined by,

$$f_{SC} = (284 - 0.25) \cdot f_L + P_R, \dots (8.1)$$

where,  $f_{SC}$  is the subcarrier frequency in Hz.  
 $f_L$  is the line repetition frequency.  
 $P_R$  is the picture repetition frequency.

In the 625 line, C.C.I.R. system.

$$f_L = 15625 \text{ Hz}, \quad P_R = 25 \text{ Hz}, \quad f_{SC} = 4433618.75 \pm 1 \text{ Hz}.$$

Two subcarriers of frequency  $f_{SC}$ , but with  $\pi/2$  phase difference, are each modulated by a colour-difference signal. The colour-difference signals chosen are  $D_R$  and  $D_B$ , being the smallest of the three signals,  $D_R$ ,  $D_G$ ,  $D_B$ . The two amplitude-modulated subcarriers are then superimposed, which results in a subcarrier modulated in amplitude and phase. In both modulation processes, the subcarrier is suppressed; thus only sideband information is generated. The sidebands of the modulator subcarrier are finally superimposed onto the luminance signals. For correct demodulation, a burst of subcarrier is introduced into the black-level interval of each line.

Consider now the modulation process of the P.A.L. system in closer detail. In Fig. 6.4, the signal range of the luminance and synchronization pulses was normalised to a value, one. However, when the modulated subcarrier is superimposed on the luminance signal, it is necessary to allow signal excursions of greater than one. In practice, the signal excursion is limited to a level of 0.333 above peak white (1.0), and 0.333 below black level (0.333). Thus, the subcarrier level never falls below the tip of the synchronization pulse.

For this limitation in amplitude swing, it is necessary to limit the excursions of the electrical colour-difference signals  $D_R$  and  $D_B$ . If  $E_V$  and  $E_u$  are electrical signals applied to the suppressed-carrier amplitude modulators, then they are defined by:

$$E_V = \frac{D_R}{1.14}, \quad \dots\dots\dots (8.2)$$

$$E_u = \frac{D_B}{2.03}, \quad \dots\dots\dots (8.3).$$

In practice, the signals  $E_V$  and  $E_u$  are small, since highly-saturated colours rarely occur.

The P.A.L. system is characterised by the phase of  $E_V$  being changed by  $\pi$  rad on alternate lines.

Hence, the composite signal of luminance and chrominance is defined by the equations:

$$E_{NC} = E_L + E_u \cdot \sin(2\pi f_{sc} \cdot t) + E_V \cdot \cos(2\pi f_{sc} \cdot t) \quad \dots\dots\dots (8.4).$$

$$E_{(N+1)C} = E_L + E_u \cdot \sin(2\pi f_{sc} \cdot t) - E_V \cdot \cos(2\pi f_{sc} \cdot t), \quad \dots\dots (8.5)$$

where,  $E_{NC}$  is the composite electrical signal on line N and  $E_{(N+1)C}$  is the composite electrical signal on line (N+1).

The signals described by equations (8.4) and (8.5) are assumed to be gamma corrected. The effects of gamma correction are treated fully in the literature. (53, 54)

Equations (8.4) and (8.5) show that, when the chrominance signals are small, then only a small sideband signal is added to the luminance; thus any visible patterning is small. Patterning is generally only visible in the region of highly-saturated colours.

The signals  $E_u$  and  $E_v$  produce quadrature modulation. Fig 8.1 illustrates the vector diagram formed. In the diagram, the angular position of the resultant vector defines the hue of the colour, while the magnitude of the vector defines the saturation.

The positions of the reference stimuli ( $C_R$ ), ( $S_C$ ), ( $C_B$ ) used in the P.A.L. system are discussed in section 7.8. The position of these stimuli are shown on the (u), (v), (w) chromaticity diagram of Fig 7.6. The grids drawn for constant  $\frac{E_R - E_L}{E_L}$  and  $\frac{E_B - E_L}{E_L}$  show the variation of the colour-difference signals with respect to changes in chromaticity.

When the P.A.L. encoded signal is transmitted in analogue form and during demodulation, phase distortion can produce changes in hue of the transmitted colour. However, in the P.A.L. system, the phase of the  $E_u$  signal is changed by  $\pi$  on alternate lines. Thus, with the assumption that the chrominance of adjacent lines is similar, then phase errors can be translated from resultant hue errors to saturation errors. The eye is far more tolerant of errors in saturation than to those of hue. Again, this process is described in the literature.

In demodulation, the chrominance information is extracted using a suitable band-pass filter and a notch-filter or comb-filter introduced in the luminance channel to minimise chrominance patterning. The phase of the  $E_u$  signal is corrected by a phase-inversion switch. To synchronise demodulation, the reference burst introduced in black-level is changed in phase on alternate lines according to the transmitted phase of  $E_u$ ; its transmitted phase is  $+\pi/4$  or  $-\pi/4$ .

The main effects of the P.A.L. system are therefore as follows:

- (a) Introduction of chrominance-subcarrier interference on the display.
- (b) Band-limiting of chrominance signal to 1.1 M H Z, thus affecting horizontal chrominance spatial frequency.
- (c) Limitation of vertical spatial frequency when using adjacent line averaging for correction of phase errors.
- (d) Requirement of linear phase and gain characteristics of signal-processing networks handling composite signal.
- (e) Adequate dynamic range at high frequencies to encode, without clipping, peak subcarrier amplitude.

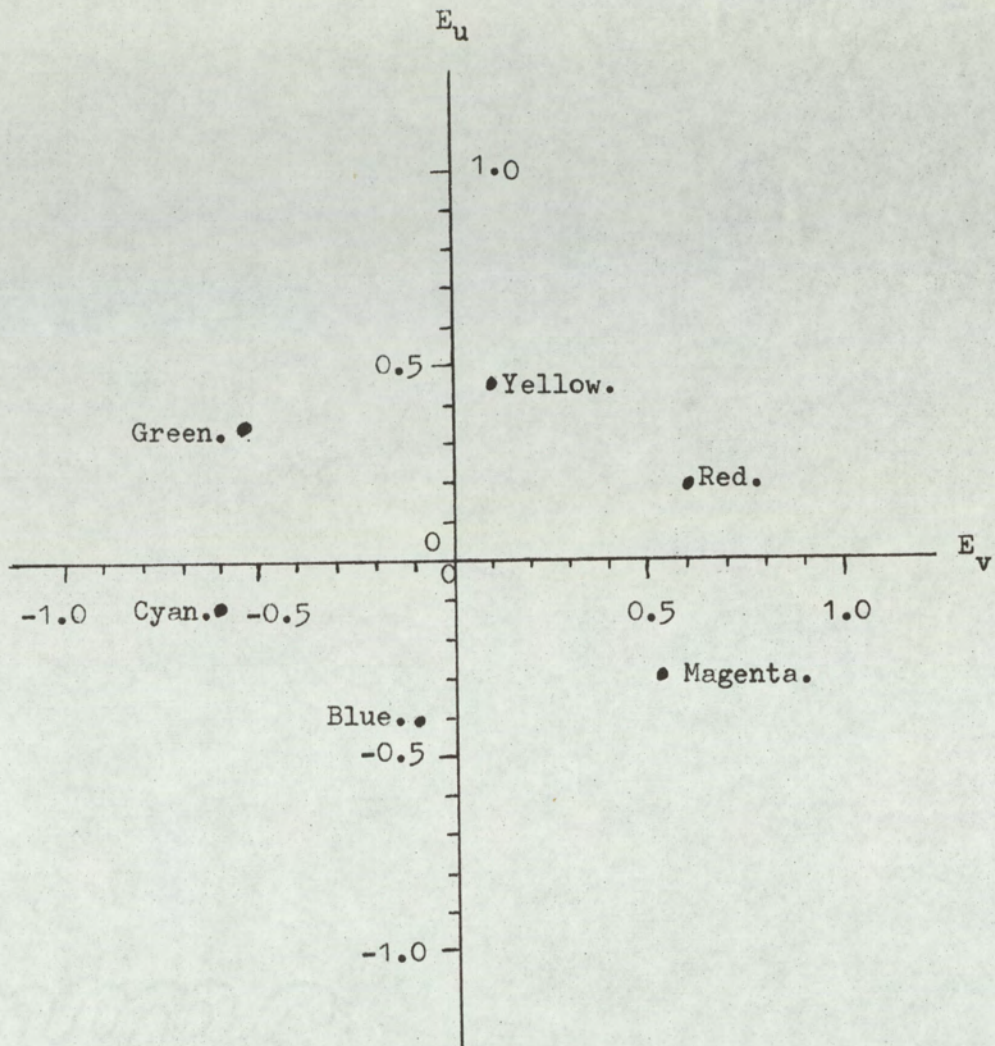


Fig.8.1. Vector presentation of chrominance with respect to phase and amplitude of the subcarrier of the quadrature modulation process.

- 8.3. Classification of basic digital-encoding techniques primarily for encoding colour-television signals using delta-sigma modulation. (6)

The digital-encoding systems can initially be classified into three basic groups:

- A. Systems using three channels.
- B. Systems using two channels.
- C. Systems using one channel.

By suitable time-division multiplex techniques and pulse-compression techniques, the following sub-divisions are formed on the basic groups A and B; these are A.1, A.2, B.1, B.2, respectively:

- A.1. Three wide-bandwidth channels combined using t.d.m.
- A.2. Two wide-bandwidth channels combined using t.d.m. and supplemented with a third low-bandwidth channel obtained using pulse-compression and redundancy in the video waveform.
- B.1. Two wide-bandwidth channels combined using t.d.m. The third channel is realised by using line-sequential switching and storage, thus reducing the vertical chrominance resolutions.
- B.2. A single wide-band channel and one low-bandwidth channel realised by using reduced resolution chrominance in both the vertical and horizontal directions and using pulse-compression for the second channel.

The systems to be described are designed to incorporate some of the following techniques:

1. Digital encoding of video signals using delta-sigma modulation with the possible inclusion of non-linear adaptation.
2. To use the digital technique of t.d.m.
3. To use the digital technique of pulse-compression.
4. To encode the luminance signal with maximum fidelity.
5. To use high-frequency, inter-channel averaging to minimise the luminance impairment.
6. To utilise the potentially rising signal-to-quantisation - noise ratio that is obtainable at lower frequencies using delta-sigma modulation.
7. To limit the chrominance horizontal resolution by effectively band-limiting the chrominance signals, nominally to  $1.1 \text{ M.Hz}$ .
8. To use adjacent-line averaging, thus limiting the vertical chrominance resolution with the aims of reducing the number of channels required to define the picture.
9. To produce a compatible luminance signal for driving a monochrome display without requiring complex decoding circuiting.
10. Minimisation of subjective picture impairment by non-equal weighting of the quantisation noise to the red, green and blue channels.
11. Incorporation of pre-emphasis networks to improve the high-frequency performance of the delta-sigma modulator.

12. Base-band analogue encoding to produce desired system performance.

The description of the systems applicable to the digital-encoding of colour television signals begins with t.d.m. and pulse-compression techniques. These are discussed in section 8.4 and 8.5 respectively.

#### 8.4. Multi-channel realisation through time-division-multiplexing (t.d.m). (18, 19, 21, 35)

The digital systems used for encoding high-quality colour pictures, require pulse rates in the order of 50 to 100 M.Hz. for transmission over suitable digital channels. In encoding the colour video signals, it is necessary to present to the display, after decoding, three simultaneous signals of red, green and blue. Thus, the digital channel and peripheral equipment, must be capable of transmitting multi-channel information. This is assuming that the chrominance has not been pre-encoded onto the video signal to form a composite signal, as described in section 8.2.

The simplest method of producing simultaneous channel transmission with a digital channel is to use t.d.m. Since the information over a digital channel is transmitted in discrete signal packages, it is possible to allocate, sequentially, signal packages to each channel required. It is convenient to allocate a single pulse to a signal package; however, with increased complexity it is possible to generate multi-pulse packages. In the colour television systems described, high-frequency signal averaging is used; this is described in section 8.6. Signal averaging necessitates a symmetrical channel distribution. Thus, when not using pulse-compression techniques, the t.d.m. systems are limited to a symmetrical channel allocation.

The three-channel t.d.m. system shown in Fig. 8.2A sequentially samples each of the three channels, designated  $A_3, B_3, C_3$ . Thus, in a group of three pulses, the first pulse is allocated to channel  $A_3$ ,

the second to channel  $B_3$  and the third to channel  $C_3$ . The sampling sequence is then repeated, hence generating a sequential and symmetrical t.d.m. system. It follows that each channel has identical coding capability.

The two-channel t.d.m. system, illustrated in Fig. 8.2B, is similar to the three channel system; however, the multiplex switch samples the two channels, designated  $A_2, B_2$ , alternately. Again, each channel carries equal information capacity, the channels being symmetrical and having identical format.

Other two and three channel multiplexing schemes are possible. It is possible to use a non-equal pulse allocation to the channels where one or two channels are of reduced bandwidth. However, it will be shown that with such schemes, high-frequency averaging cannot be used to enhance the luminance signal; thus only the symmetrical systems are considered.

To decode the t.d.m. system, it is necessary to introduce coding to identify the channel sequence. Also, in digital systems coding is necessary to define the line and field synchronisation.

In a practical system, decoding would be controlled by pulses generated from a phase-locked oscillator, the pulse being produced at the pulse rate of the digital channel. Such a system could present excellent short-term frequency stability. Hence, for durations of about one line period (64  $\mu$ .sec), a local pulse source is available for operation of regenerators and decoding systems. It would also allow the omission of t.d.m. frame reference signals during the active line period. Thus, if t.d.m. decoding was synchronised during the non-active line period, the synchronism would be maintained during the active picture.

However, before the t.d.m. can be brought into synchronism, line and field synchronisation must be obtained. Again, coding patterns during the non-active line period must be introduced. With coding patterns, there is always the probability of the code patterns occurring in the picture information periods; thus the pulse pattern chosen must have a low probability of **occurrence**. However, with line and field synchronisation, the parameters of synchronisation are known. It is therefore possible having once obtained a synchronisation lock, to predict exactly at what times the line and field synchronisation code patterns occur. Thus, the recognition circuits can be gated in and out during these intervals, minimising the probability of detecting a code in error. Basically, this system utilises picture synchronisation redundancy to enhance the synchronisation detection.

Complete systems synchronisation thus requires:

- (a) Phase-locked loop to lock onto pulse digit rate to produce control pulses and regeneration sample pulses.
- (b) Line-synchronisation detection to phase line frequency and decoding system with transmitter.
- (c) Field-synchronisation to position picture in correct phase for display.
- (d) t.d.m recognition pattern detection for detecting sequence of channels being transmitted, checked on a line-by-line basis.

The list (a) to (d) indicates the required order of detection, since each detection-network depends upon the operation of the preceding detection network.

t.d.m. synchronisation can be achieved basically in two ways. For detection, it is assumed that functions listed (a), (b), (c) are operating in synchronism so that the position of the t.d.m. code is accurately known and detection networks can be gated in accordingly. The first method is to introduce a code pattern in the digital channel so that the t.d.m. sequential switch may be phased. The second method encodes via the delta or delta-sigma-modulators different known signals onto each channel, which may then be detected by signal identification.

The various methods of total system synchronisation are not of direct relevance to the arguments being presented. The exact system design of the control networks depends upon the application. It is therefore assumed that synchronisation is achieved. The theory is

concerned only with the t.d.m and signal presentations using this system, together with minimisation of subjective impairment of television pictures when constraining the signals for transmission over the chosen t.d.m. system.

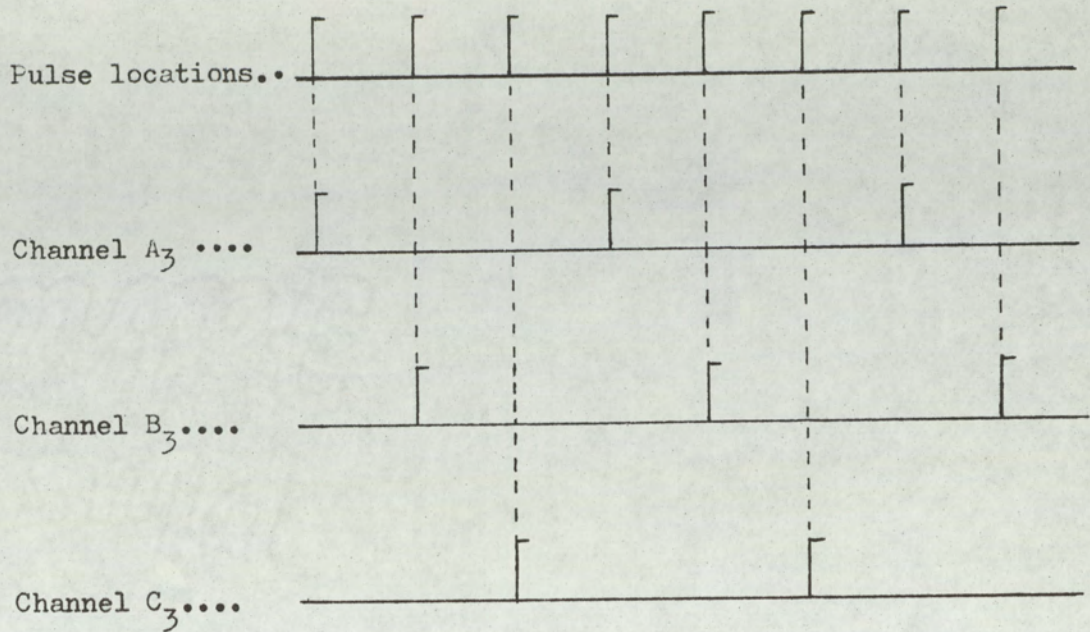


Fig8-2(a)...

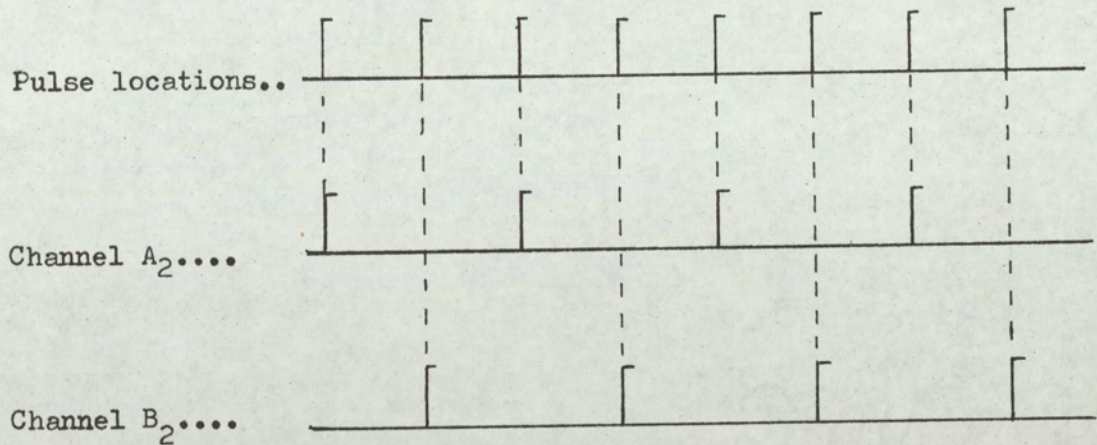


Fig.8-2(b)...

Fig.8-2(a). Symmetrical, three channel t.d.m. system.

Fig.8-2(b). symmetrical, two channel t.d.m. system.

### 8.5. Pulse-compression in digital encoder for colour-television systems.

Pulse-compression can be used to encode the chrominance information and realize an auxiliary, low-bandwidth channel. The auxiliary channel can be applied to two-channel and three-channel systems. In these systems the signals to be encoded are applied to the respective digital modulators. The auxiliary channel modulator, however, operates at a lower clock rate than the other channels. The high-bandwidth signal or signals are multiplexed, if necessary, directly and applied to the digital channel. However, the auxiliary signal is clocked into a shift register initially shifting at the same rate as the auxiliary channel digital modulator; the auxiliary signal is therefore temporarily stored; the procedure is shown in Fig.8.3. This modulation process operates only during the active period of the television line. At the end of the active-line period, the complete auxiliary line store is clocked at the higher, digital-channel pulse rate, into the digital channel. The speed of clocking is such that the auxiliary channel occupies just less than the line-blanking period, the period occupied by line synchronisation pulse and black level. In demodulation the reverse procedure applies. During the line blanking period, the pulse package of the auxiliary channel is clocked into a shift register at the pulse rate of the digital channel. In the following active-line period, the register, now operating at a lower clock rate, presents the auxiliary signal to the decoder at the same rate at which it was originally encoded. Thus, the low-bandwidth channel during transmission, occupies the time of the line-blanking period.

With such a system, the relationship of the encoding clock rates between the high-bandwidth and low-bandwidth channels must be exactly defined, as only certain clock ratios are possible. The chosen ratio depends upon the line structure and the bandwidth reduction of the auxiliary channel compared to the high-bandwidth channels.

The validity of this encoding method is that a signal whose bandwidth is restricted, may be encoded at a lower-pulse rate than a signal containing higher frequency components. Since in colour television, the chrominance signals can be band-limited, then they can be encoded at a lower pulse rate. In practice, the chrominance bandwidth is restricted to one fifth the luminance bandwidth. Thus, the encoding pulse rate of the chrominance signal may also be reduced to one fifth, providing the chrominance signal encoding accuracy produces impairment which is not subjectively objectionable.

The auxiliary channel pulse rate is calculated as follows:

Required line standard parameters for 625 line, C.C.I.R system,

Line duration,	64 $\mu$ sec.
Line-blanking duration,	12 $\mu$ sec (12.05 $\mu$ sec).
Active-line duration,	52 $\mu$ sec.

However, for a general analysis, let:

Line duration =	$y$ ,
Line-blanking duration =	$x$ ,
Digital channel clock rate =	$P$ ,
Auxilliary channel clock rate =	$\frac{P}{N_a}$ ,

where  $N_a$  is an integer expressing the ratio of the auxiliary channel clock rate to the digital channel (also encoder) clock rate.

Let  $R_a$  be the number of pulses in the active line to be compressed into the line-blanking period. and let  $\epsilon_p$  be the number of excess pulses required over the register store to completely fill the line blanking period at a clock rate of  $P$ .

Hence, the number of pulses stored,  $R_a$ , in the active line period of duration  $(y-x)$  is,

$$(y-x) \frac{P}{N_a} = R_a, \dots\dots\dots (8.1)$$

The number of pulses in the line blanking period is  $P.x$  and the number of stored pulses plus excess pulses is  $(R_a + \epsilon_p)$ .

Thus,

$$P.x = (R_a + \epsilon_p), \dots\dots\dots (8.2)$$

Substitution for  $R_a$  from equation (8.2) into equation (8.1), gives:

$$(y-x) \cdot \frac{P}{N_a} = P.x - \epsilon_p,$$

$$\text{Therefore, } P = \frac{N_a \cdot \epsilon_p}{x \cdot (1+N_a) - y}, \dots\dots\dots (8.3)$$

For a positive, non-infinite solution for  $P$ , then,

$$x \cdot (1+N_a) > y,$$

$$\text{i.e. } N_a > \frac{y}{x} - 1, \dots\dots\dots (8.4)$$

Rearranging equation (8.3) gives:

$$\epsilon_p = \frac{P \cdot \{ x \cdot (1+N_a) - y \}}{N_a}, \dots\dots\dots (8.5)$$

applying condition (8.4) and substituting for  $x$  and  $y$  gives the values:

$$y = 64 \mu \text{ sec}$$

$$x = 12 \mu \text{ sec}$$

From condition (8.4)

$$N_a > \frac{64}{12},$$

Therefore, since  $N_a$  is integer, for simple encoding,

$$N_a = 5, 6, 7, \dots \text{ etc.}$$

However, a bandwidth reduction of 5 is required for the chrominance signal,

Hence,

$$N_a = 5.$$

Substituting for  $N_a$ ,  $x, y$  in equation (8.5)

$$\epsilon_p = P \cdot \frac{8}{5}, \quad \dots \quad (8.6)$$

For an integer number of excess pulses,  $P$  must be a multiple of 5. The restrictions on  $P$  are imposed by  $x$  and  $y$ ; thus to modify the value of  $P$ , modifications in  $x$  and  $y$  are necessary.

In the pulse-compression process, the auxiliary signal undergoes a delay of one-line period. To correct for this the high-bandwidth signals must be delayed by one line. The delay is best introduced at the encoder, thus eliminating redundant use of delay networks at each receiving terminal. Delay may be either digital or analogue prior to encoding. Due to the large number of bits in the high-bandwidth channel, the analogue delay system is, at present, the most economical.

The compressed chrominance information contains only one channel. In a two-channel system, the chrominance information can be alternated between two channel sources, line by line. In this system, an address is required to identify the channel transmitted. The address is introduced as a pulse pattern during the time allocated for synchronisation. The synchronisation signal also forms a pulse pattern. However, once the system is in full synchronism, the chrominance signal transmitted can be estimated; thus the address pattern is then only used as a check on the system.

Consider the parameters of the system when the clock rate is 100 MHz:

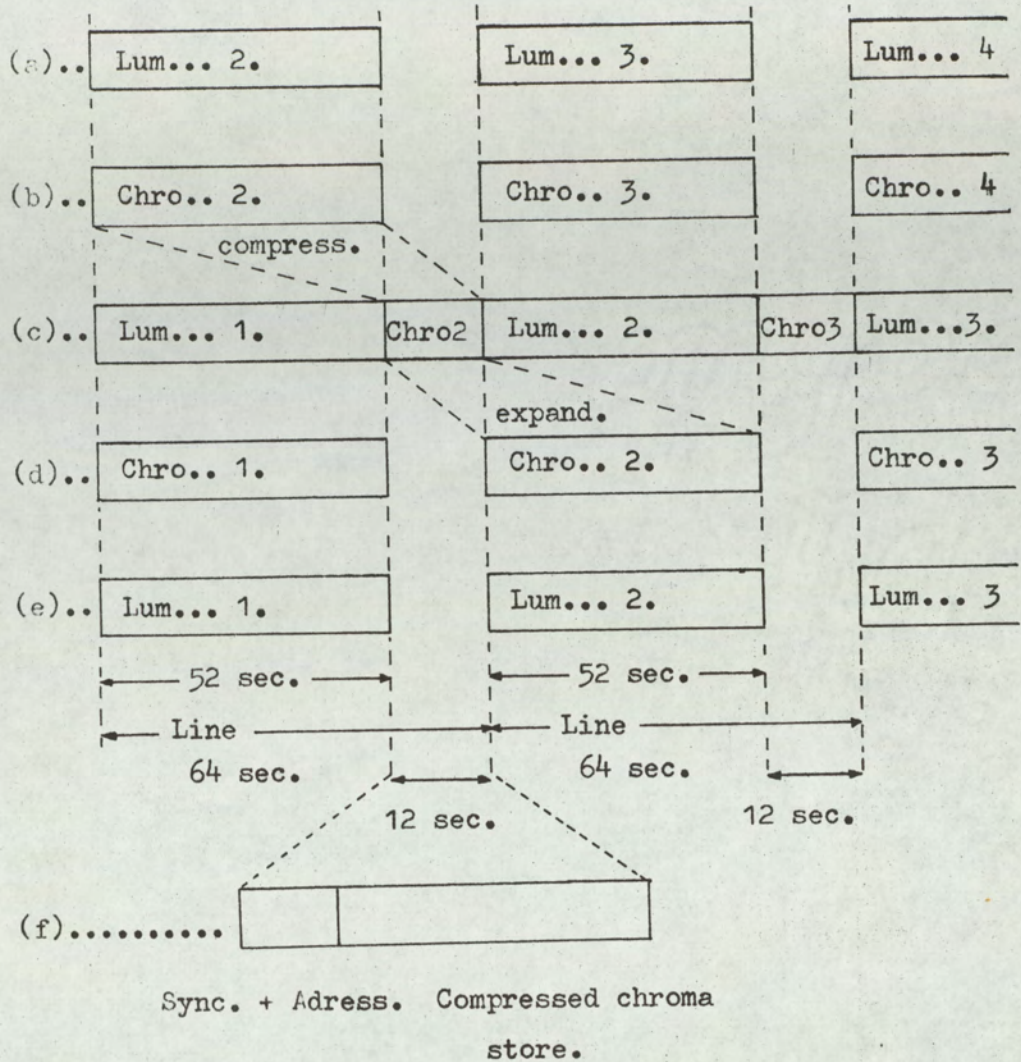
Substituting for  $y, x, P, N_a$ , from equation (8.1) then  $R_a$ , becomes

$$R_a = 1040 \text{ pulses.}$$

From equation (8.6),  $\epsilon_p$  is

$$\epsilon_p = 160 \text{ pulses.}$$

Hence, for a 100 MHz pulse rate, 160 pulses are available for synchronisation and address functions. also, to store the chrominance information in one line, 1040 bit register is required.



- (a)... Luminance digit sequence, lines 2,3,4.
  - (b)... Chrominance digit sequence, lines 2,3,4.
  - (c)... Delayed luminance and compressed chrominance in syncs.  
lines 1,2,3.
  - (d)... Pulse expanded chrominance.
  - (e)... Delayed luminance.
  - (f)... Expanded view of chrominance transmission period showing sub-period for synchronisation and line identification.
- } Correctly phased by only expanding chrominance.

Fig.8-3. Chrominance pulse-compression system.

### 8.6 High-frequency averaging of two or three simultaneous, multiplexed signals.

The red, green and blue signals that control the display device, carry the band-limited chrominance information. The upper chrominance bandwidth is set nominally at 1.1M.HZ. Thus, at frequencies over 1.1 M.HZ, each signal carries the same information.

Let:

$E_{RH}$	Frequencies > 1.1 M.HZ. in red signal.
$E_{RL}$	Frequencies < 1.1.M.HZ. in red signal.
$E_{GH}$	Frequencies > 1.1 M.HZ. in green signal.
$E_{GL}$	Frequencies < 1.1 M.HZ. in green signal.
$E_{BH}$	Frequencies > 1.1 M.HZ. in blue signal.
$E_{BL}$	Frequencies < 1.1 M.HZ. in blue signal.
$E_{LH}$	Frequencies > 1.1 M.HZ. in luminance signal.
$E_{LL}$	Frequencies < 1.1 M.HZ. in luminance signal.

Thus,

$$E_R = E_{RH} + E_{RL}, \quad \dots \quad (8.7)$$

$$E_G = E_{GH} + E_{GL}, \quad \dots \quad (8.8)$$

$$E_B = E_{BH} + E_{BL}, \quad \dots \quad (8.9)$$

$$E_L = E_{LH} + E_{LL}, \quad \dots \quad (8.10)$$

and

$$E_{LH} = \lambda E_{RH} + m. E_{GH} + n. E_{BH}, \dots \quad (8.11)$$

$$E_{LL} = \lambda E_{RL} + m. E_{GL} + n. E_{BL}, \dots \quad (8.12)$$

$$E_{LH} = E_{RH} = E_{GH} = E_{BH}, \dots \quad (8.13)$$

Equation (8-13) applies, since the high-frequency information is common to all signals because of the band-limited chrominance information. In delta-modulation, the high-frequency performance is severely limited by reduced signal to quantisation error noise. Hence, the highest possible pulse rate must be available to encode the signals with high-frequency content. In a symmetrical multiplex system, the pulse rate of each channel is limited. For a two-channel system, the channel pulse rate is one half the total pulse rate, while for a three channel system it is one third the total pulse rate. In encoding colour signals, it is only necessary to differentiate between signals at frequencies below 1.1 M.HZ. By suitable weighting the modulating signals applied to the t.d.m. system, it is possible to enhance the luminance performance by averaging between the two or three channels. That is, each channel, at high frequencies, carries an equal proportion of the luminance signal.

At low frequencies, the signal to quantisation noise is greater; thus chrominance noise (which is now differential-channel noise) is reduced. It is clear that the luminance will not be encoded as accurately as by a single delta-modulator encoder. However, by a symmetrical distribution of the luminance signal between channels, the encoding is considerably better than that of a single channel at one half or one third the total pulse rate. As well as simple averaging of the outputs of two or three delta-modulators, the samples are displaced in time. Thus, the luminance is sampled at the maximum clock rate of the channel, although the encoding is not as efficient as a single modulator. The noise performance improvement that is obtainable with this method depends upon the luminance weighting in each channel. If  $E_R$ ,  $E_G$ ,  $E_B$  were encoded directly, then the

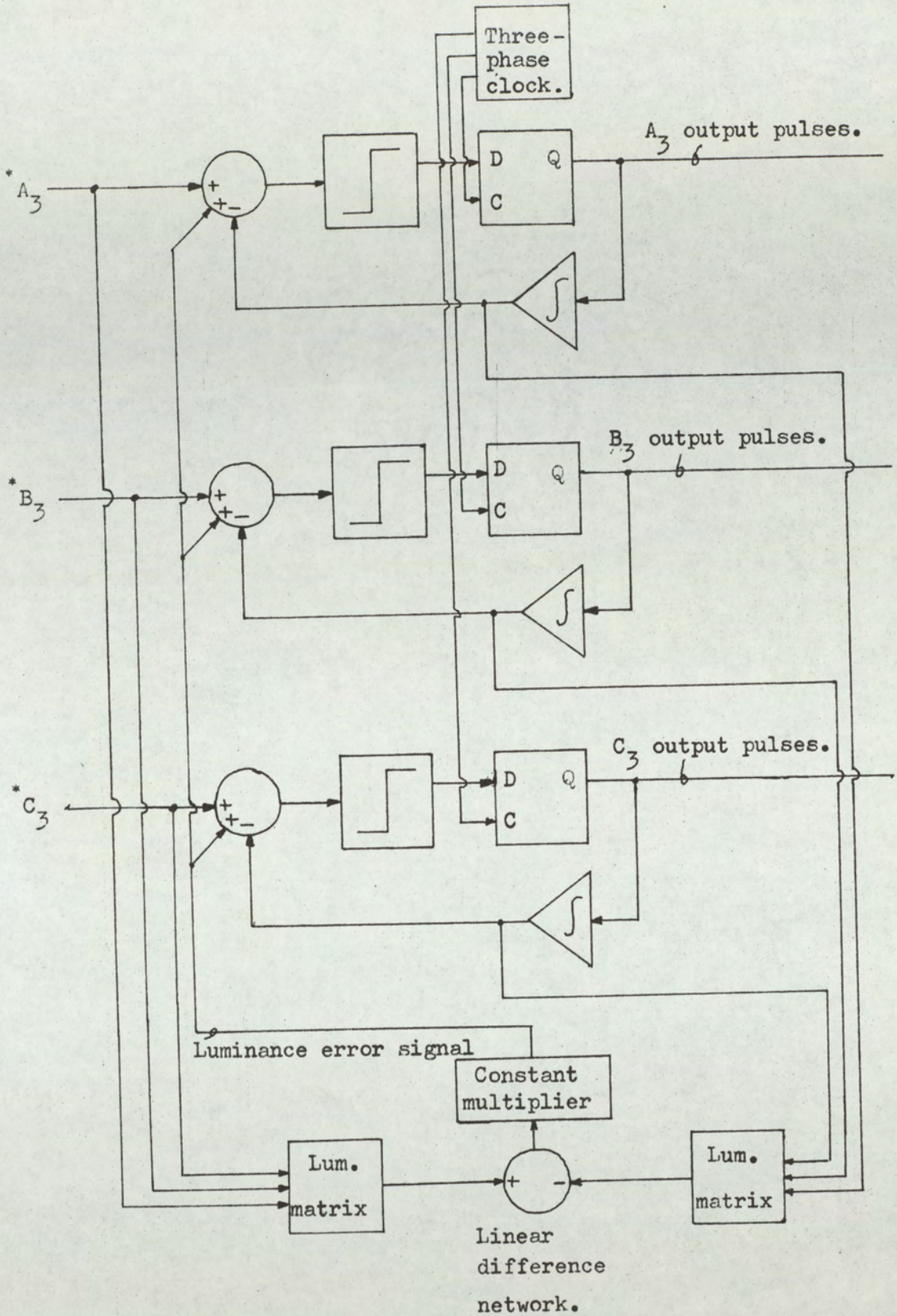
luminance would be distributed in accordance with the luminosity coefficients. Such a distribution would not encode the luminance to best advantage, although the chrominance noise would be minimum. By suitable weighting, it is possible to exchange chrominance noise and luminance noise. The exact distributions are discussed in the following sections.

Assume that a signal distribution is chosen such that the luminance is equally divided between the symmetrically multiplexed channels. The maximum improvement in luminance encoding that can be obtained, is when the luminance is directly encoded by a single modulator operating at the total pulse rate of the multiplexed channels. However, under such conditions the chrominance crosstalk would be 100%, so no meaningful red, green and blue signals would be available. Thus, a compromise is required in the exchange of luminance quantisation noise and chrominance quantisation noise.

The compromise may be achieved basically by two methods. However, the first method is the least efficient:

1. If a proportion of the luminance signal is added to each signal, so that luminance dominates the encoding of each channel, the luminance fidelity will rise. However, for frequencies above 1.1 M.HZ, the signals of each channel are identical; thus, this strategy can only effect performance below 1.1 M.HZ. In the limit, the system would consist of three modulators each encoding the same signal. This is not as efficient as a single modulator operating at the channel pulse rate.
2. The second method shown in Fig 8.4 involves coupling between the modulators. Again assume that the signal distribution gives

equal weighting to the luminance signal on each channel. From the two or three encoding signals, it is possible to determine another signal equal to the luminance. Similarly, from the decoded signals, prior to final filtering, a decoded luminance signal can be obtained. From these two signals a difference signal can be formed, which represents the luminance error signal. By adding a proportion of this error signal to each of the modulator error signals, the luminance encoding fidelity can be controlled. In the limit, when each error signal consisted only of the luminance error signal, then the modulators would operate as a single encoder and the luminance would be encoded with maximum fidelity.



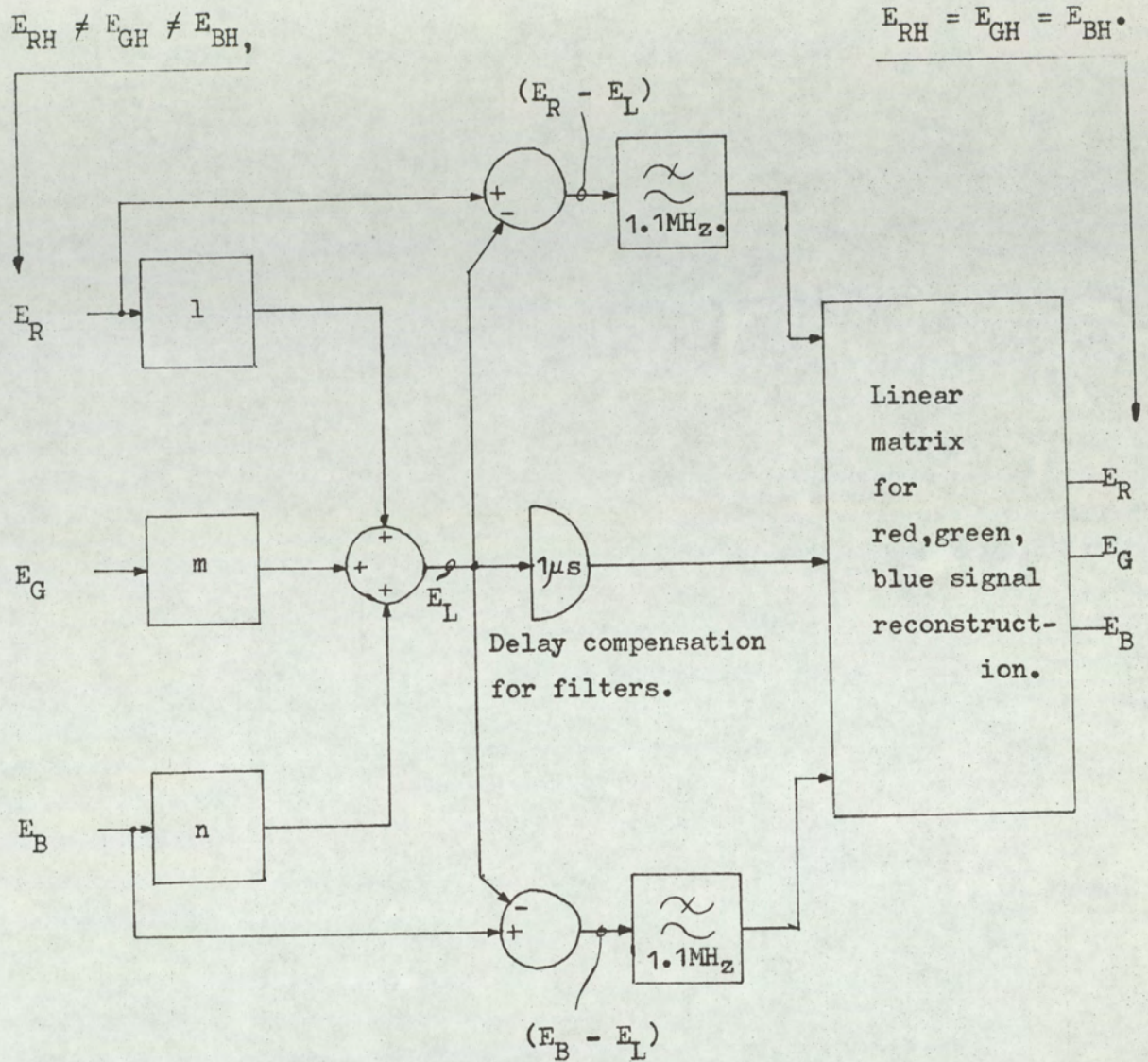
\* See section 8-8, system group A1.

Fig.8-4. Luminance error coupling to enhance luminance encoding performance in exchange for chrominance encoding accuracy.

### 8. 7. Chrominance band-limiting of $E_R$ , $E_G$ , $E_B$ signals.

In the systems to be discussed, it is generally assumed that equation (8-13) applies for frequencies above 1.1 M.Hz. This allows correct high-frequency averaging to be used and limits the chrominance resolution in the horizontal direction. It is therefore necessary to introduce a network prior to baseband encoding, which will mix the high-frequency components. If signals are derived from a P.A.L. type decoder, this function will have already been performed.

The basic network is shown in Fig 8.5. The luminance signal  $E_L$  is formed from an addition of the red, green and blue channels, using the weighting factors  $l, m, n$  derived from equation (7-32). The colour difference signals are formed and band-limited to reduce the chrominance resolutions. From these signals and a delay-compensated luminance signal, the signals  $E_R, E_G, E_B$  are reconstructed from a linear matrix. However, the colour-difference signals are (ideally) zero above 1.1 M.Hz; thus the high-frequency content of  $E_R, E_G, E_B$  are also equal (ie.  $E_L$ ).



Output such that: Output high-frequency components are mixed.

Fig.8-5. High-frequency addition network to limit chrominance resolution and make equal the high-frequency components of the video signals of  $E_R$ ,  $E_G$ ,  $E_B$ .

8.8. Baseband encoding of video signals for modulating three simultaneous delta-sigma-modulators, each channel being full bandwidth and symmetrical. (System group A1).

This section develops the format of the analogue signals for simultaneous modulating delta-sigma modulators. The channels are designated  $A_3$ ,  $B_3$ ,  $C_3$  in accordance with Fig.8.2A of section 8.4(the symmetrical t.d.m. system).

For the application of the principle of high-frequency averaging, it is necessary that each channel contributes an equal weighting to the luminance signal and that the sum of the three channels is at all times equal to the luminance signal. The equal weighting of the luminance to each channel applies for all frequencies above 1.1.M.Hz and for all frequencies when the chrominance information is zero. It is also necessary that each signal can fully modulate each delta-sigma modulator, when the overload limits are identical. That is, each channel must have the same peak-signal level and preferably that the three signals are equal for transmission of luminance only.

Consider the encoding sequence:

$$\begin{aligned} A_3' &= \ell \cdot E_R + (1-\ell) \cdot E_L, \\ B_3' &= m \cdot E_G + (1-m) \cdot E_L, \\ C_3' &= n \cdot E_B + (1-n) \cdot E_L, \end{aligned}$$

If  $A_{3H}'$ ,  $B_{3H}'$ ,  $C_{3H}'$ , are the respective high-frequency contents of  $A_3'$ ,  $B_3'$ ,  $C_3'$ , then

$$A_{3H}' = \ell \cdot E_{RH} + (1-\ell) \cdot E_{LH},$$

Applying equation (8,13) gives

$$A'_{3H} = E_{LH},$$

Similarly,

$$B'_{3H} = E_{LH}, \quad \text{and} \quad C'_{3H} = E_{LH}.$$

Thus, the high-frequency components of each channel add to form the high-frequency luminance signal.

Also,

$$\begin{aligned} A'_3 + B'_3 + C'_3 &= \ell \cdot E_R + m \cdot E_G + n \cdot E_B + 3 \cdot E_L \\ &\quad - \ell \cdot E_L - m \cdot E_L - n \cdot E_L, \end{aligned}$$

applying equations (7-31) and (7-32), then,

$$A'_3 + B'_3 + C'_3 = 3 \cdot E_L,$$

i.e. the three channels add to form the luminance signal.

The three equations for  $A'_3$ ,  $B'_3$  and  $C'_3$  show that each has a component of luminance added. However, the components are not equal and substituting the values for  $\ell, m, n$  from equations (7-36), (7-37), (7-38) shows that

$$(1-m) < (1-\ell), (1-n)$$

Thus,  $B'_3$  has the smallest luminance component. Adding a luminance component  $(m-1) \cdot E_L$  to each channel, gives

$$\begin{aligned} A_3 &= \ell \cdot E_R + (1-\ell) \cdot E_L + (m-1) \cdot E_L, \\ B_3 &= m \cdot E_G + (1-m) \cdot E_L + (m-1) \cdot E_L, \\ C_3 &= n \cdot E_B + (1-n) \cdot E_L + (m-1) \cdot E_L, \end{aligned}$$

Hence,

$$\begin{aligned} A_3 &= \ell \cdot E_R + (m-\ell) \cdot E_L, \\ B_3 &= m \cdot E_G, \\ C_3 &= n \cdot E_B + (m-n) \cdot E_L, \end{aligned}$$

Thus, when luminance only is transmitted, each channel adds to  $m \cdot E_L$ . Normalising the channels  $A_3, B_3, C_3$  to form  $A_{3n}, B_{3n}, C_{3n}$ , and rearranging, gives,

$$A_{3n} = \frac{\ell}{m} \cdot (E_R - E_L) + E_L, \dots\dots\dots (8-14)$$

$$B_{3n} = (E_G - E_L) + E_L, \dots\dots\dots (8-15).$$

$$C_{3n} = \frac{n}{m} \cdot (E_B - E_L) + E_L, \dots\dots\dots (8-16)$$

Inspection of equations (8-14), (8-15), (8-16) shows that the high-frequency components of each channel add to form the luminance, as do the low-frequency components when the chrominance information is zero. The equations show the luminance and chrominance components, the chrominance signals being expressed as colour-difference signals. Since the signals  $E_R, E_G, E_B, E_L$  are equal at high frequencies, the colour-difference components are zero. Thus, the form of the equations clearly expresses the luminance at high frequencies. The equations also give a method of chrominance resolution limiting, if the band-limiting discussed in section 8.7 has not been applied. In this case, the colour-difference signals are bandlimited and added to the luminance to form  $A_{3n}, B_{3n}, C_{3n}$  directly.

Adding the three signals  $A_{3n}, B_{3n}, C_{3n}$  gives,

$$\begin{aligned} A_{3n} + B_{3n} + C_{3n} &= \frac{\ell}{m} \cdot E_R + E_G + \frac{n}{m} \cdot E_B \\ &\quad + 2 \cdot E_L - \frac{\ell}{m} \cdot E_L - \frac{n}{m} \cdot E_L, \\ &= \frac{1}{m} \cdot \{ \ell \cdot E_R + m \cdot E_G + n \cdot E_B \} \\ &\quad + \frac{1}{m} \{ 2 \cdot m \cdot E_L - \ell \cdot E_L - n \cdot E_L \} \end{aligned}$$

Applying equations (7-31), (7-32) gives:

$$A_{3n} + B_{3n} + C_{3n} = 3 \cdot E_L, \dots\dots\dots (8-17).$$

Thus, the three channels **add** to form a multiple of the luminance signal. The luminance signal is symmetrically distributed between the three channels as discussed previously.

Since the red, green and blue signals are **not** equally weighted, the noise contribution of the delta-sigma modulators will not divide equally between these signals. Let,  $A_{3q}, B_{3q}, C_{3q}$  be the normalised, instantaneous quantisation noise-signals; the received signals,  $A_{3r}, B_{3r}, C_{3r}$  are then,

$$A_{3r} = A_{3n} + A_{3q}, \dots\dots\dots (8-18)$$

$$B_{3r} = B_{3n} + B_{3q}, \dots\dots\dots (8-19)$$

$$C_{3r} = C_{3n} + C_{3q}, \dots\dots\dots (8-20)$$

Equation (8-17) shows that the luminance and noise are given as,

$$E_L = \frac{1}{3} \cdot \{A_{3n} + B_{3n} + C_{3n}\} + \frac{1}{3} \cdot \{A_{3q} + B_{3q} + C_{3q}\}, \dots (8-21)$$

and are produced **equally** from all three channels.

Decoding red: From equation (8-14),

$$E_R = \frac{m}{l} \cdot A_{3n} + \frac{(l-m)}{l} \cdot E_L,$$

Substituting  $E_L$  from equation (8-17).

Therefore,

$$E_R = \frac{(l + 2 \cdot m)}{3 \cdot l} \cdot A_{3n} + \frac{(l - m)}{3 \cdot l} \cdot (B_{3n} + C_{3n}) \dots\dots\dots (8-22)$$

$$+ \frac{(l + 2 \cdot m)}{3 \cdot l} \cdot A_{3q} + \frac{(l - m)}{3 \cdot l} \cdot (B_{3q} + C_{3q})$$

Decoding green: From equation (8-15)

$$E_G = B_{3n} ,$$

Substituting equation (8-19) and changing to received voltage, therefore,

$$E_G = B_{3n} + B_{3q} , \dots\dots\dots (8-23)$$

Decoding blue: By comparing the symmetry of equation (8-16) with equation (8-14), then

$$E_B = \frac{(n + 2.m)}{3.n} \cdot C_{3n} + \frac{(n - m)}{3.n} \cdot (B_{3n} + A_{3n}) \dots\dots\dots (8-24)$$

$$+ \frac{(n + 2.m)}{3.n} C_{3q} + \frac{(n-m)}{3.n} \cdot (B_{3q} + A_{3q}),$$

Equations (8-22), (8-23) and (8- 24) calculate the decoded signals from the three multiplexed channels; they also indicate the noise contribution of each channel.

Consider the noise contribution of the red channel to the luminance of the red, i.e.  $\ell \cdot E_R$ . From equation (8-22), the red luminance noise is

$$\ell \cdot E_R \left| \begin{array}{l} \text{noise} \end{array} \right. = \ell \cdot \frac{\{A_{3q} + B_{3q} + C_{3q}\}}{3} + m \cdot \frac{\{2 \cdot A_{3q} - B_{3q} - C_{3q}\}}{3} \dots\dots\dots (8-25)$$

Similarly for the green luminance noise, from equation (8-23),

$$m \cdot E_G \left| \begin{array}{l} \text{noise} \end{array} \right. = m \cdot B_{3q} , \dots\dots\dots (8-26)$$

and the blue luminance noise, from equation (8-24), is

$$n.E_B \left| \begin{array}{l} \\ \text{Noise} \end{array} \right. = n \cdot \left\{ \frac{A_{3q} + B_{3q} + C_{3q}}{3} \right\} + m \cdot \left\{ \frac{2 \cdot C_{3q} - A_{3q} - B_{3q}}{3} \right\}$$

..... (8-27)

Equations (8-25), (8-26) and (8-27) show how the luminance noise is distributed among the three multiplexed signals  $A_{3n}$ ,  $B_{3n}$ ,  $C_{3n}$ . The three weighted noise signals add to form,

$$l.E_R \left| \begin{array}{l} \\ \text{Noise} \end{array} \right. + m.E_G \left| \begin{array}{l} \\ \text{Noise} \end{array} \right. + n.E_B \left| \begin{array}{l} \\ \text{Noise} \end{array} \right. = \frac{1}{3} \cdot \{ A_{3q} + B_{3q} + C_{3q} \}$$

.....(8-28)

It is necessary to observe, on the chromaticity diagram, how changes in the stimuli  $A_{3n}$ ,  $B_{3n}$ ,  $C_{3n}$  effect chromaticity. Thus reference stimuli ( $A_{3n}$ ), ( $B_{3n}$ ), ( $C_{3n}$ ) can be plotted on the (U), (V), (W) chromaticity diagram. Proceeding as in section (7.7) the coefficients  $l, m, n$  in the equations (8-22), (8-23) and (8-24) are obtained from equations (7-36), (7-37) and (7-38) and it is assumed that the noise signals  $A_{3q}$ ,  $B_{3q}$ ,  $C_{3q}$  are zero in these equations. Hence,  $E_R, E_G, E_B$  are given by,

$$\begin{aligned} E_R &= 1.6421 \cdot A_{3n} - 0.3211 \cdot B_{3n} - 0.3211 \cdot C_{3n}, \\ E_G &= 0.0000 \cdot A_{3n} + 1.0000 \cdot B_{3n} + 0.0000 \cdot C_{3n}, \\ E_B &= -1.3830 \cdot A_{3n} - 1.3830 \cdot B_{3n} + 3.7661 \cdot C_{3n}, \end{aligned}$$

Following the procedure of section 7.7 and writing the colour matching identities of ( $A_{3n}$ ), ( $B_{3n}$ ), ( $C_{3n}$ ) in terms of the (R), (G), (B) stimuli, gives:

$$1.0(A_{3n}) \equiv 1.6421 (R) + 0.0000 (G) - 1.3830 (B),$$

$$1.0(B_{3n}) \equiv -0.3211(R) + 1.0000 (G) - 1.3830 (B),$$

$$1.0(C_{3n}) \equiv -0.3211(R) + 0.0000 (G) + 3.7661 (B),$$

Converting from the (R), (G), (B) diagram to the (U), (V), (W) diagrams, using the transformation equation (7-41), gives:

$$1.0 (A_{3n}) \equiv 0.4812 (U) + 0.3333 (V) - 0.6290 (W),$$

$$1.0 (B_{3n}) \equiv -0.1979 (U) + 0.3333 (V) - 0.0867 (W),$$

$$1.0 (C_{3n}) \equiv 0.3709 (U) + 0.3333 (V) + 2.3147 (W),$$

Dividing each identity by the sum of the coefficients to determine the chromaticity coordinates of  $(A_{3n})$ ,  $(B_{3n})$ ,  $(C_{3n})$  in terms of (U), (V), (W) gives the results shown in Table 8.1.

Table 8.1. Chromaticity coordinates of  $(A_{3n})$ ,  $(B_{3n})$ ,  $(C_{3n})$ .

Stimulus	u	v	w
$(A_{3n})$	2.594	1.797	-3.391
$(B_{3n})$	-4.064	6.845	-1.780
$(C_{3n})$	0.123	0.110	0.767

To observe changes in the stimuli  $A_{3n}$ ,  $B_{3n}$ ,  $C_{3n}$ , the procedure developed in section 7.8 is applied.

Consider a family of straight lines drawn on the (U), (V), (W) chromaticity diagram and through the stimulus  $(A_{3n})$ . The lines represent,  $\frac{B_{3n}}{C_{3n}} = \text{constant}$ .

To determine the constant for each line, the ratio is evaluated on the straight line joining the stimuli (G) and (B); thus  $E_R = 0$ .

From equations (8-15), (8-16), the ratio is given by:

$$\frac{B_{3n}}{C_{3n}} = \frac{E_G}{\left\{ \frac{n}{m} \cdot E_B + \frac{(1-n)}{m} \cdot E_L \right\}}$$

Eliminating  $E_L$  using equation (7-32), putting  $E_R = 0$ , substituting for  $l, m, n$  from equations (7-36), (7-37), (7-38) and finally rearranging, gives:

$$\frac{B_{3n}}{C_{3n}} = \frac{\frac{E_G}{E_B}}{\left\{ 0.286 + 0.473 \cdot \frac{E_G}{E_B} \right\}}$$

Substituting for  $\frac{E_G}{E_B}$ , from equation (7-61), gives,

$$\frac{B_{3n}}{C_{3n}} = - \frac{(36.115v - 4.711)}{(v - 4.711)}, \dots\dots\dots (8-29)$$

The u coordinate is given by equation (7-62) i.e.

$$u = - 0.030 \cdot v + 0.192, \dots\dots\dots (7-62).$$

Note that u,v lie on the line joining (G) and (B).

Similarly for lines drawn through  $(B_{3n})$ , where  $\frac{C_{3n}}{A_{3n}} = \text{constant}$ .

Consider the evaluation of the ratio along the line joining (R) and (L), i.e.  $E_G = 0$ .

From equations (8-14) and (8-16) the ratio is given by;

$$\frac{C_{3n}}{A_{3n}} = \frac{\frac{n}{m} \cdot E_B + \frac{(1-n)}{m} \cdot E_L}{\frac{l}{m} \cdot E_R + \frac{(1-l)}{m} \cdot E_L}$$

Eliminating  $E_L$  using equation (7-32), putting  $E_G = 0$ , substituting for  $\ell, m, n$  from equations (7-36), (7-37), (7-38) and finally rearranging, gives:

$$\frac{C_{3n}}{A_{3n}} = \frac{0.2861 \cdot \frac{E_B}{E_R} + 0.2409}{0.0559 \cdot \frac{E_B}{E_R} + 0.6561},$$

Substituting equation (7-64) and rearranging,

$$\text{Therefore, } \frac{C_{3n}}{A_{3n}} = - \frac{0.062 \cdot u + 0.160}{u - 0.123}, \quad \dots (8-30)$$

The  $v$  coordinate is given by equation (7-65), i.e.

$$v = 0.682 \cdot u + 0.027, \quad \dots (7-65).$$

Note that  $u$  and  $v$  lie on the line joining (R) and (B)

Finally, the ratio  $\frac{A_{3n}}{B_{3n}}$  is calculated for lines

drawn through  $(C_{3n})$

The ratio is evaluated along the line joining (G) and (R).

From equations (8-14) and (8-15) the ratio is given by;

$$\frac{A_{3n}}{B_{3n}} = \frac{\frac{\ell}{m} \cdot E_R + \frac{(1-\ell)}{m} \cdot E_L}{E_G}$$

Eliminating  $E_L$  using equation (7-32), putting  $E_B=0$ , substituting for  $\ell, m, n$  from equations (7-36), (7-37) and (7-38) and finally rearranging, gives

$$\frac{A_{3n}}{B_{3n}} = 0.6561 \cdot \frac{E_R}{E_G} + 0.2880,$$

Substituting equation (7-57) and rearranging.

$$\text{Therefore, } \frac{A_{3n}}{B_{3n}} = \frac{-0.894 \cdot u - 0.048}{u - 0.477}, \quad \dots\dots\dots (8-31)$$

The  $v$  coordinate is given by equation (7-58).

$$v = -0.079 \cdot u + 0.389, \quad \dots\dots\dots (7-58)$$

Note that  $u$  and  $v$  lie on the line joining (G) and (R),

Equations (8-29), (8-30) and (8-31) allow the variations of two out of the three stimuli to be observed on the chromaticity chart when one stimulus is held constant. Fig 8-6 shows the family of lines drawn from each stimulus; the corresponding ratio of each line is indicated. The scale of the diagram is such that the stimuli  $A_{3n}$  and  $B_{3n}$  cannot be shown, however, the respective lines, when projected back, pass through these points on the chromaticity chart.

Table 8.2 lists the ratios evaluated for the  $A_{3n}$ ,  $B_{3n}$ ,  $C_{3n}$  signals, derived from equations (8-31), (8-30) and (8-29).

Table 8.2. Ratios  $\frac{A_{3n}}{C_{3n}}$ ,  $\frac{B_{3n}}{C_{3n}}$ ,  $\frac{C_{3n}}{A_{3n}}$  calculated for (u), (V), (W) chromaticity diagram.

$\frac{A_{3n}}{B_{3n}}$	u (G)→(R)	$\frac{B_{3n}}{C_{3n}}$	v (G)→(B)	$\frac{C_{3n}}{A_{3n}}$	u (R)→(B)
0.288	0.076	0.000	0.130	0.367	0.477
0.500	0.137	0.500	0.193	0.500	0.395
1.000	0.227	1.000	0.254	1.000	0.266
1.500	0.279	1.500	0.313	1.500	0.221
2.000	0.313	2.000	0.371	2.000	0.197
2.500	0.337	2.110	0.354	2.500	0.183
3.000	0.355			3.000	0.173
3.500	0.369			3.500	0.166
4.000	0.380			4.000	0.161
4.500	0.389			4.500	0.157
5.000	0.397			5.000	0.153
∞	0.477			5.118	0.152

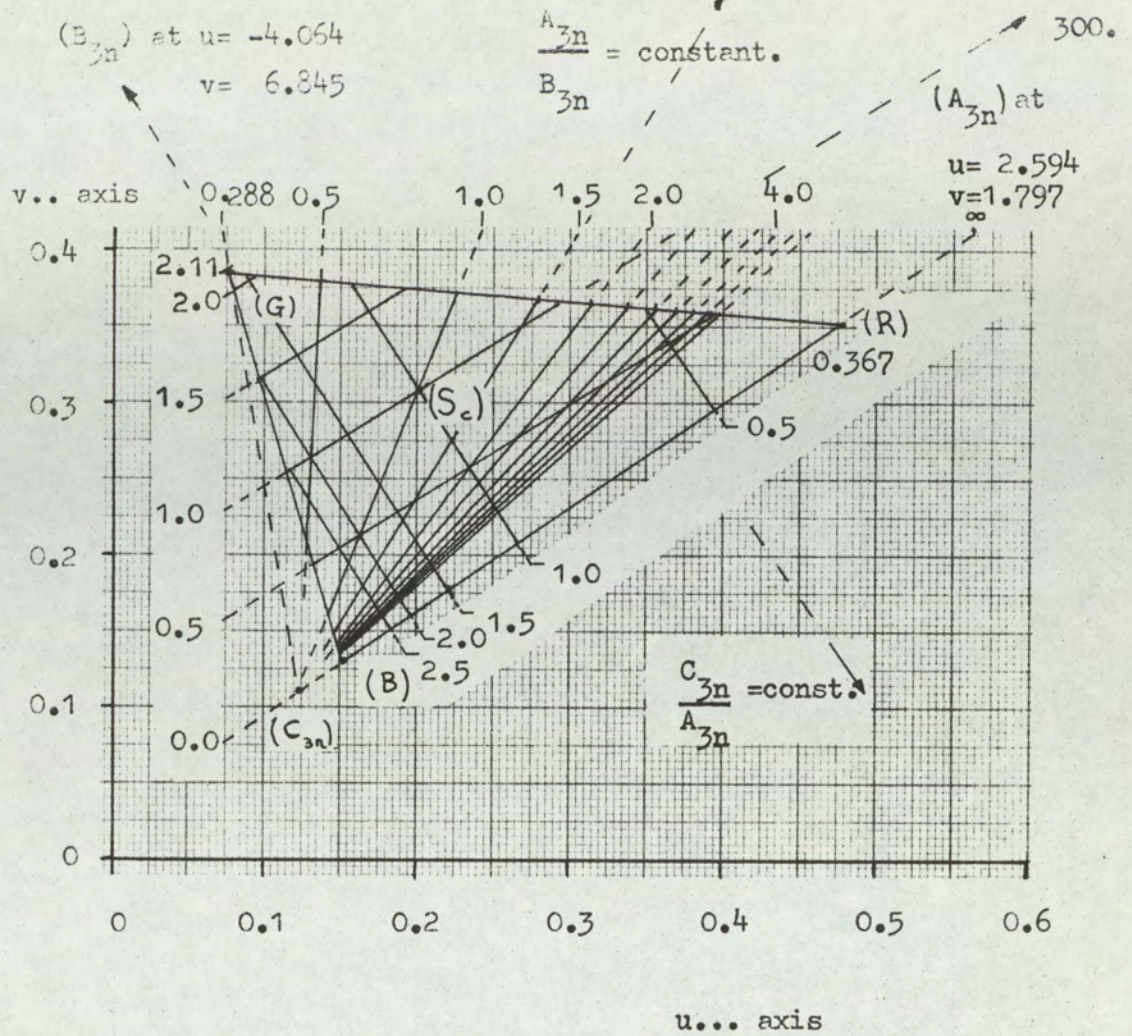


Fig.8-6. Chromaticity diagram for proposed three-channel system, using  $A_{3n}$ ,  $B_{3n}$ ,  $C_{3n}$ .

Switches operate in synchronism at line frequency.

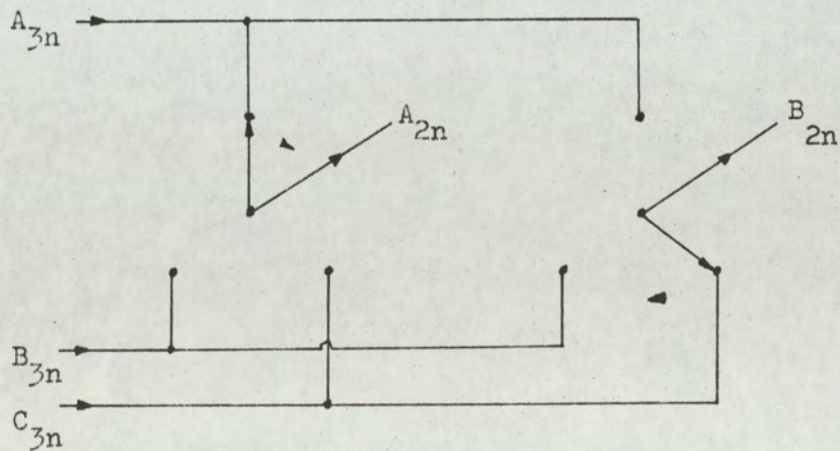


Fig.8-7. Sequential multiplexing for reducing 3 channels to 2 channels.

8.9 Three-channel encoding systems using two symmetrical t.d.m. channels and one low-bandwidth auxiliary channel.  
(System group A2)

If the number of channels in the symmetrical t.d.m system is reduced from three to two, then the luminance signal can be more accurately encoded. However, a third, low-bandwidth channel is available using the pulse compression technique developed in section 8.5. Thus for the low-frequency signals (i.e. chrominance signals) three simultaneous channels are available.

To enhance the luminance encoding, the t.d.m channels must contribute equally to the luminance signal at high frequencies and add together to form the luminance signal at all frequencies. Using this method, a luminance signal for driving monochrome displays is always available and t.d.m. synchronism is not required for decoding a monochrome signal.

In colour vision, the eye is least sensitive to changes in the blue region. This is reflected in the low luminosity coefficient of  $n = 0.114$ . Since the auxiliary time-compressed channel operates at a reduced pulse rate, the encoding is not as accurate. This is partially compensated for by reducing the bandwidth of the channel in the same ratio as the pulse-rate reduction. It is desirable that the auxiliary channel will not impair the luminance performance; thus the signal chosen for transmission is the blue colour-difference signal,  $(E_R - E_L)$ .

To allow the two channels in the symmetrical t.d.m system to add to form the true luminance signal, one or both of the signals must contain a component of the blue signal. There are several ways in which the signals can be defined; however, only

one method is discussed and is treated as an example. By combining the red and the blue signals, it is possible to match the true luminance of the two symmetrical t.d.m. channels more closely; thus this method is chosen. Let the two symmetrical t.d.m. channels of the three-channel systems be initially  $A'_{32}$ ,  $B'_{32}$ . Then

$$A'_{32} = \ell \cdot E_R + n \cdot E_B + (1-\ell-n) \cdot E_L,$$

$$B'_{32} = m \cdot E_G + (1-m) \cdot E_L,$$

As before, subtracting the smaller of the two true luminance contributions from both channels, i.e.  $(1-m)E_L$ , gives

$$A_{32} = \ell \cdot E_R + n \cdot E_B + (m-n-\ell) \cdot E_L,$$

$$B_{32} = m \cdot E_G$$

Normalising the two signals gives

$$A_{32n} = \frac{\ell}{m} (E_R - E_L) + \frac{n}{m} (E_B - E_L) + E_L, \quad \dots\dots\dots(8-32)$$

$$B_{32n} = (E_G - E_L) + E_L, \quad \dots\dots\dots(8-33)$$

The third channel of the three-channel system is  $C_{3a}$  and is carried in the auxiliary time slot.

Put,  $C_{3a} = (E_B - E_L),$

It is necessary to normalise the blue colour-difference signal. Applying equation (7-32) to eliminate  $E_L$ , gives

$$C_{3a} = (E_B \cdot (1-n) + \ell \cdot E_R + m \cdot E_G),$$

Now,  $(1-n) = (\ell+m)$ , from equation (7-31).

Thus,  $E_B = 1, E_R = E_G = 0$  gives the equal but opposite response to,  $E_B = 0, E_R = E_G = 1$ .

$$\text{Thus, } \left| C_{3a} \right|_{\text{MAX}} = (1-n),$$

Hence, if  $C_{3an}$  is the normalised channel of  $C_{3a}$ , then,

$$C_{3an} = \frac{1}{(1-n)} \cdot (E_B - E_L), \quad \dots \dots \dots (8-34).$$

Equations(8-32), (8-33), (8-34) define the transmission signals for the two channel and one **auxiliary**-channel system.

8.10. Two-channel encoding using two symmetrical t.d.m signals and reduced vertical-chrominance resolution.  
(System group B1)

By reduction of the vertical-chrominance resolution and the use of one-line stores, the required number of signal channels to transmit the picture can be reduced to two. The signals  $E_R, E_G, E_B$  are processed, as indicated in section 8.7, so the horizontal chrominance resolution is limited to one fifth the horizontal-luminance resolution. Thus, the vertical-chrominance resolution is about five times greater than the horizontal-chrominance resolution.

By averaging between successive lines of a field the vertical-chrominance resolution can be reduced. Such averaging applied to a 2:1 interlace system will reduce the vertical resolution by a factor of four. In practice, it is possible to use the same chrominance signal for two adjacent lines of a field. Thus, less chrominance information can be transmitted on a line, the information being stored for a line duration.

Consider a two-channel symmetrical t.d.m. encoding system. Again, there are many possible channel combinations, so the basic principles only are discussed.

There are two basic procedures that can be employed in encoding a two-channel system:

1. Sequential switching of three signals, taking two signals simultaneously.

The system defines three signals. The signals are then transmitted two at a time being symmetrically and sequentially selected; the method is indicated in Fig. 8-7

The multiplex switches are of  $\frac{2\pi}{3}$  radians phase differences and switch during the line-blanking period. For this method, the three channels  $A_{3n}$ ,  $B_{3n}$ ,  $C_{3n}$ , defined by equations (8-14), (8-15), (8-16) in section 8.8 are suitable. Since at high frequencies, averaging can be applied to enhance the luminance encoding. Since there are only two channels, the luminance degradation should not be as severe as with the three-channel system. However, pairs of signals selected by the multiplex switch, when added, do not form a true broadband luminance signal; thus special decoding techniques are required. With this method, phased multiplex detection is necessary for decoding the luminance signal.

During decoding, while any pair of signal is being transmitted, the third signal is held in a line store from the previous line. Initially, the three channels (one stored, two direct) are passed through 1.1 MHz low-pass filters. The three band-limited signals are then added together, thus forming (as shown in equation (8-17)) a low-bandwidth luminance signal. Note that this decoding does introduce an amount of low-frequency luminance averaging between lines. The luminance can then be subtracted from the three band-limited signals  $A_{3n}$ ,  $B_{3n}$ ,  $C_{3n}$  to expose the colour-difference signals shown in equations (8-14), (8-15) and (8-16).

Decoding is complex with this type of signal presentation, as it is difficult to produce the true luminance signal. The networks used have to be switched on a line-by-line basis, since different signal combinations are required for each of the three phases of multiplexing.

2. Sequential switching of signal pairs to produce true luminance.

A modification to the encoding signals can realise a system capable of transmitting true luminance; thus decoding is simplified.

Such a sequence is defined as follows:

Using equations (8-14), (8-15) (8-16) to define  $A_{3n}$ ,  $B_{3n}$ ,  $C_{3n}$ , then

$$\begin{aligned} \text{Line } N. \quad A_{2n} &= A_{3n}, \\ B_{2n} &= \frac{1}{2} \cdot \{ B_{3n} + C_{3n} \} \\ \\ \text{line } (N+1) \quad A_{2n} &= B_{3n} \\ B_{2n} &= \frac{1}{2} \cdot \{ C_{3n} + A_{3n} \} \\ \\ \text{line } (N+2) \quad A_{2n} &= C_{3n} \\ B_{3n} &= \frac{1}{2} \cdot \{ A_{3n} + B_{3n} \} \end{aligned}$$

Repeat sequence.

Noting that  $A_{2n}$ ,  $B_{2n}$  are transmitted symmetrically on a t.d.m. basis and applying equation (8-17) gives

$$\begin{aligned} A_{2n} + 2 \cdot B_{2n} &= A_{3n} + B_{3n} + C_{3n} \\ &= 3 \cdot E_L, \end{aligned}$$

Thus, the true luminance is determined at all times. The sequence of channels, as indicated, allows simpler decoding. In decoding, the signal carried on channel  $A_{2n}$  is delayed by one line; then, by subtracting one half this signal from channel  $B_{3n}$ , the composite signal can be separated.

Consider line N. On this line the available signals are:

$$\begin{array}{l}
 A_{3n} \\
 \frac{1}{2} \{ B_{3n} + C_{3n} \} , \\
 C_{3n} \left| \begin{array}{l} \\ \\ \text{delayed} \end{array} \right.
 \end{array}
 \left. \begin{array}{l} \\ \\ \end{array} \right\}
 \begin{array}{l}
 \text{Symmetrical t.d.m} \\
 \text{encoding} \\
 \\
 \text{Channel } A_{2n} \text{ from} \\
 \text{previous line.}
 \end{array}$$

At high frequencies  $B_{3n} = C_{3n}$ ; thus high frequency luminance is equally encoded over both t.d.m. channels. The signals can be band-limited; thus  $A_{3n}$ ,  $B_{3n}$ ,  $C_{3n}$  can be separated. Since the luminance is known, the colour-difference signals can be derived and  $E_R$ ,  $E_G$ ,  $E_B$  produced. Precise decoding details are not given here, as several variations are possible. The basic method, however, follows from the equation defining the transmission signals.

With this method, the luminance signal may be extracted without decoding the t.d.m. although channel  $B_{2n}$  carries the sum of two channels; thus the chrominance is less accurately encoded. The averaging is sequentially rotated between all channels combinations; hence averaging is symmetrically distributed.

Other channel combinations are possible, but they possibly require two line stores for decoding.

8-11 Two channel system using a single wide-bandwidth channel with auxilliary low-bandwidth channel. (C.I.S.S)  
(System group B2)

To encode the luminance signal by delta-sigma modulation, with the minimum of impairment, a single delta-sigma modulator operating at the transmission pulse rate is required. The transmission pulse rate represents the maximum pulse rate available in the system. In this section, a system is discussed which uses all the transmission pulses available in the active line for encoding the luminance signal. The chrominance signals are encoded at a low pulse rate and introduced into the auxilliary channel as discussed in section 8-5. Since only one channel is available in the auxilliary channel and the use of t.d.m. is undesirable due to the already reduced pulse rate, then the chrominance-vertical resolution must be reduced. By transmitting alternating chrominance signals on a line-by-line switching basis and using a line delay line in the decoder, the required chrominance information can be transmitted. Basically in this system, each of the two chrominance signals is used twice. The vertical-chrominance resolution is then reduced by this line-by-line averaging process. Since the lines are averaged between adjacent lines of a field, the averaging is actually introduced over four lines of a picture, due to the 2:1 interlaced system described in chapter 6. The vertical resolution of the chrominance is therefore reduced by a factor of four.

To illustrate the transmission sequence, consider the signals transmitted over three successive lines:

Let  $A_{2n}$  be the high band-width signal  
(transmitting luminance).

and  $B_{2an}$ ,  $C_{2an}$  the low band-width signals  
(transmitting chrominance).

The transmission sequence on lines  $N$ ,  $(N+1)$ ,  $(N+2)$  is  
therefore:

Line $N$	$A_{2n} _N$	,	$B_{2an} _N$
Line $(N+1)$	$A_{2n} _{(N+1)}$	,	$C_{2an} _{(N+1)}$
Line $(N+2)$	$A_{2n} _{(N+2)}$	,	$B_{2an} _{(N+2)}$
etc.			

The decoding sequence is given by:

Line $N$ .	$A_{2n} _N$	,	$B_{2an} _N$	,	$C_{2an} _{(N-1)}$
Line $(N+1)$	$A_{2n} _{(N+1)}$	,	$B_{2an} _N$	,	$C_{2an} _{(N+1)}$
Line $(N+2)$	$A_{2n} _{(N+2)}$	,	$B_{2an} _{(N+2)}$	,	$C_{2an} _{(N+1)}$
etc.					

By storing each chrominance signal in a one-line delay line, signals  $B_{2an}$ ,  $C_{2an}$  are simultaneously available. The instrumentation of decoding is discussed in detail in chapter 9.

The normalised luminance signal which is continually applied to the channel carrying  $A_{2n}$  during the active period is defined by equation (7-32). It is necessary to define the desired parameters for the chrominance signals, as follows:

1. The chosen signal should permit simple decoding when both channels are normalised, with the minimum of switching in the decoder and should preferably require equal channel gain.
2. The noise distribution between  $E_R$ ,  $E_G$  and  $E_B$  is such that when weighted by the luminosity coefficients the noise signals will be approximately of equal power. This infers that  $E_G$  has the least noise and  $E_B$  carries the most noise. This is a reasonable strategy, since the sensitivity of vision to change is most sensitive in the green, and least sensitive in the blue. (In colour systems such as the N.T.S.C system, the blue signal bandwidth is reduced more than the red and green.)
3. The principle of constant luminance must apply since a separate luminance signal is transmitted.

Consider combinations of the red and blue colour difference signals, where  $k_1$  and  $k_2$  are constants i.e.

$$B_{2an} = k_1 (E_R - E_L) + k_2 (E_B - E_L), \quad \dots (8-35)$$

$$C_{2an} = k_1 (E_R - E_L) - k_2 (E_B - E_L), \quad \dots (8-36)$$

This type of signal presentation is useful, since decoding is by means of a sum and a difference amplifier. A switched inverter is required as will be discussed in chapter 9 in the difference channel.

Assume that these two signals have been transmitted and that one is available at the output of a delay line; thus both are simultaneously available. Let the noise introduced by quantisation be respectively  $B_{2q}$  and  $C_{2q}$  for the channels  $B_{2an}$ ,  $C_{2an}$ .

Thus decoding:

(where  $E_{Rd}$ ,  $E_{Gd}$ ,  $E_{Bd}$ ,  $E_{Ld}$  are the decoded signals including noise)

$$(E_{Rd} - E_{Ld}) = \frac{1}{2 \cdot k_1} \cdot (B_{2an} + C_{2an}) + \frac{1}{2k_1} \cdot (B_{2q} + C_{2q}) \dots (8-37)$$

$$(E_{Bd} - E_{Ld}) = \frac{1}{2 \cdot k_2} \cdot (B_{2an} - C_{2an}) + \frac{1}{2k_2} \cdot (B_{2q} - C_{2q}), \dots (8-38)$$

From equation (7-46) and eliminating  $D_R$ ,  $D_G$ ,  $D_B$  from equations (7-43), (7-44) and (7-45),  $(E_{Gd} - E_{Ld})$  is given by,

$$(E_{Gd} - E_{Ld}) = -\frac{\ell}{m} (E_{Rd} - E_{Ld}) - \frac{n}{m} \cdot (E_{Bd} - E_{Ld}),$$

Thus, from equations (8-37), (8-38), eliminating  $(E_{Rd} - E_{Ld})$ ,

$(E_{Bd} - E_{Ld})$  gives,

$$(E_{Gd} - E_{Ld}) = -\frac{\ell}{m} \cdot \frac{1}{2 \cdot k} (B_{2an} + C_{2an}) - \frac{n}{m} \cdot \frac{1}{2 \cdot k_2} (B_{2an} - C_{2an}) \\ - \frac{\ell}{m} \cdot \frac{1}{2 \cdot k_1} (B_{2q} + C_{2q}) - \frac{n}{m} \cdot \frac{1}{2k_2} (B_{2q} - C_{2q}) \dots (8-39)$$

Let  $A_{2q}$  be the quantisation noise introduced during encoding the luminance signal. Thus,  $E_{Rd}$ ,  $E_{Gd}$  and  $E_{Bd}$  can be calculated from equations (8-37), (8-38) and (8-39).

$$\text{i.e. } E_{Ld} = A_{2q} + A_{2n}, \\ E_{Rd} = \frac{1}{2 \cdot k_1} (B_{2an} + C_{2an}) + \frac{1}{2 \cdot k_1} (B_{2q} + C_{2q}) + A_{2n} + A_{2q}, \\ E_{Gd} = -\frac{\ell}{m} \cdot \frac{1}{2 \cdot k_1} (B_{2an} + C_{2an}) - \frac{n}{m} \cdot \frac{1}{2 \cdot k_2} (B_{2an} - C_{2an}) + A_{2n} \\ - \frac{\ell}{m} \cdot \frac{1}{2 \cdot k_1} (B_{2q} + C_{2q}) - \frac{n}{m} \cdot \frac{1}{2 \cdot k_2} (B_{2q} - C_{2q}) + A_{2q}, \\ E_{Bd} = \frac{1}{2 \cdot k_2} (B_{2an} - C_{2an}) + \frac{1}{2 \cdot k_2} (B_{2q} - C_{2q}) + A_{2n} + A_{2q},$$

The luminance weightings of the signals  $E_R$ ,  $E_G$  and  $E_B$  are respectively  $l.E_R$ ,  $m.E_G$  and  $n.E_B$ .

Hence,

$$\text{Red luminance noise} = l \cdot \frac{1}{2 \cdot k_1} (B_{2q} + C_{2q}) + l \cdot A_{2q},$$

$$\text{Green luminance noise} = - l \cdot \frac{1}{2 \cdot k_1} (B_{2q} + C_{2q}) - n \cdot \frac{1}{2 \cdot k_2} (B_{2q} - C_{2q}) + m \cdot A_{2q},$$

$$\text{Blue luminance noise} = n \cdot \frac{1}{2 \cdot k_2} (B_{2q} - C_{2q}) + n \cdot A_{2q},$$

Note that,

$$\Sigma(\text{red} + \text{green} + \text{blue}) \text{ luminance noise} = A_{2q},$$

i.e. the principle of constant luminance applies.

The coefficients  $k_1$  and  $k_2$  are chosen such that the noise on the red, green and blue signals causes an equally disturbing effect on the display, the noise having a common source, i.e. the auxilliary channel. Since the noise  $A_{2q}$  effects only luminance, it may be disregarded when considering noise introduced by chrominance only.

The noise causing changes in luminance of each colour signal has two components. One component, a function of  $A_{2q}$ , affects only the luminance of the relevant picture. This noise is appropriately distributed among the three colour signals. The other component affects only chrominance. Although this component affects the luminance of a particular colour, the other two colours change so that the total luminance is unaltered and only the colour balance is disturbed.

By putting  $k_1 = \lambda.l, \dots\dots (8-40)$

$k_2 = \lambda.n, \dots\dots (8-41)$

where  $\lambda$  is a constant of proportionality,

then changes in the red luminance and blue luminance caused by  $(B_{2q} \pm C_{2q})$  are equal. Thus, the noise affects the subjective luminance of the red and the blue signals and approximately appears to be of equal visual impairment. Since the green luminance noise is equal but opposite to the sum of the red and blue luminance noise, then the net luminance change is zero. Substituting from equations (8-40) and (8-41) the chrominance noise expressions reduce to

Red luminance noise  $= \frac{1}{\lambda.2} (B_{2q} + C_{2q}) = l.\Delta E_{RN}$   
(component effecting chroma.only)

Green luminance noise  $= -\frac{1}{\lambda} \cdot B_{2q} = m.\Delta E_{GN}$   
(component effecting chroma.only)

Blue luminance noise  $= \frac{1}{\lambda.2} (B_{2q} - C_{2q}) = n.\Delta E_{BN}$   
(component effecting chroma.only)

Thus, assuming  $B_{2q}$  and  $C_{2q}$  have the same peak deviations (which is reasonable, since they are encoded by the same delta-sigma-modulator), then the luminance noise of each of red, green and blue channels has equal subjective impairment on chrominance.

Substituting equations (8-40) and (8-41) in equations (8-35) and (8-36) to eliminate  $k_1$  and  $k_2$ , then:

$B_{2an} = \lambda \cdot \{ l \cdot (E_R - E_L) + n \cdot (E_B - E_L) \} \dots\dots (8-42)$

$C_{2an} = \lambda \cdot \{ l \cdot (E_R - E_L) - n \cdot (E_B - E_L) \} \dots\dots (8-43)$

To permit a fixed gain in the decoder, the constant  $\lambda$  should be the same in both channels, as shown. It is necessary to investigate the peak excursions of the signals  $B_{2an}$ ,  $C_{2an}$  and choose  $\lambda$  for normalisation.

Eliminating  $E_L$ , by substitutions from equation (7-32), gives:

$$B_{2an} = \lambda \cdot \left[ \ell \cdot (1-\ell-n) \cdot E_R + m \cdot (-\ell-n) \cdot E_G + n \cdot (1-\ell-n) \cdot E_B \right]$$

$$C_{2an} = \lambda \cdot \left[ \ell \cdot (1-\ell+n) \cdot E_R + m \cdot (-\ell+n) \cdot E_G + n \cdot (-1-\ell+h) \cdot E_B \right]$$

Eliminating  $\ell, m, n$  from equations (7-36), (7-37), (7-38)

gives:

$$B_{2an} = \lambda \cdot \left[ 0.1755 \cdot E_R - 0.2424 \cdot E_G + 0.0669 \cdot E_B \right]$$

$$C_{2an} = \lambda \cdot \left[ 0.2437 \cdot E_R - 0.1086 \cdot E_G - 0.1351 \cdot E_B \right]$$

It is clear that the positive and negative excursions of  $B_{2an}$  and of  $C_{2an}$  are symmetrical about zero. i.e. for  $B_{2an}$  the sum of the positive coefficients equals the negative coefficient. Similarly, for  $C_{2an}$  the sum of the negative coefficients equals the positive coefficient.

Hence,

$$|B_{2an}|_{MAX} = 0.2424 \cdot \lambda ,$$

$$|C_{2an}|_{MAX} = 0.2437 \cdot \lambda ,$$

Putting  $\lambda = \frac{1}{0.2437} ,$

..... (8-40a)

Then the normalised equations for signals  $B_{2an}$  and  $C_{2an}$  become:

$$B_{2an} = 0.7201.E_R - 0.9947.E_G + 0.2745.E_B, \quad \dots (8-44)$$

$$C_{2an} = 1.0000.E_R - 0.4456.E_G - 0.5544.E_B, \quad \dots (8-45)$$

{ The equations (8-44), (8-45) are given to four figure accuracy for future calculations }.

Equation (8-44) could be normalised to unity; however, decoding is facilitated by presenting the signal as shown. Also, in terms of instrumentation, the difference is so small as to be negligible; it represents 0.5% undermodulation.

Examination of equation (8-44) shows that it is the green colour-difference signal.

Signal  $A_{2n}$ , from equation (7-39) is given by:

$$A_{2n} = 0.299.E_R + 0.587.E_G + 0.114.E_B, \quad \dots (8-46)$$

Equations (8-46), (8-44) and (8-45) define the transmission signals in terms of  $E_R$ ,  $E_G$ ,  $E_B$ . It is thus possible to locate the positions of stimuli ( $A_{2n}$ ), ( $B_{2an}$ ), ( $C_{2an}$ ) on the (U), (V), (W) chromaticity diagram.

Expressing  $E_R$ ,  $E_G$  and  $E_B$  in terms of  $A_{2n}$ ,  $B_{2an}$ ,  $C_{2an}$  from equations (8-46), (8-44) and (8-45) gives:

$$E_R = 1.0000.A_{2n} + 0.4074.B_{2an} + 0.4074.C_{2an},$$

$$E_G = 1.0000.A_{2n} - 0.4150.B_{2an} + 0.0000.C_{2an},$$

$$E_B = 1.0000.A_{2n} + 1.0684.B_{2an} - 1.0684.C_{2an},$$

Following the procedure of section 7-7 and writing the colour matching identities of ( $A_{2n}$ ), ( $B_{2an}$ ), ( $C_{2an}$ ) in terms of the (R), (G), (B) stimuli, gives:

$$1.0 (A_{2n}) \equiv 1.0000 (R) + 1.0000 (G) + 1.0000 (B),$$

$$1.0 (B_{2an}) \equiv 0.4074 (R) - 0.4150 (G) + 1.0684 (B),$$

$$1.0 (C_{2an}) \equiv 0.4074 (R) + 0.0000 (G) - 1.0684 (B),$$

Converting from the (R), (G), (B) diagram to the (U), (V), (W) diagram, using the transformation equation (7-41), gives:

$$1.0 (A_{2n}) \equiv 0.654 (U) + 1.000 (V) + 1.599 (W),$$

$$1.0 (B_{2an}) \equiv 0.2590(U) + 0.0000(V) + 0.3858(W),$$

$$1.0 (C_{2an}) \equiv 0.0229(U) + 0.0000(V) - 0.6108(W),$$

Dividing each identity by the sum of the coefficients to determine the chromaticity coordinates of  $(A_{2n})$ ,  $(B_{2an})$  and  $(C_{2an})$  in terms of (U), (V), (W) gives the results shown in Table 8.3.

Table 8.3 chromaticity coordinates of  $(A_{2n})$ ,  $(B_{2an})$ ,  $(C_{2an})$

Stimulus	u	v	w
$(A_{2n})$	0.201	0.307	0.492
$(B_{2an})$	0.402	0.000	0.598
$(C_{2an})$	-0.039	0.000	1.039

The signals  $B_{2an}$ ,  $C_{2an}$  only affect chromaticity. To observe the variations of these signals in terms of subjective chrominance, consider the families of lines drawn through the stimuli ( $B_{2an}$ ), ( $C_{2an}$ ), i.e. following the presentation discussed in section 7-8.

For the family of straight lines drawn on the (U), (V), (W) chromaticity diagram all passing through the location of stimulus ( $B_{2an}$ ), the lines represent,  $\frac{C_{2an}}{A_{2n}} = \text{constant}$ .

To determine the constant for each line, the ratio is evaluated on the straight line joining the stimuli (R) and (B), thus  $E_G = 0$ . From equations (8-45) and (8-46) and putting  $E_G = 0$ , thus,

$$\frac{C_{2an}}{A_{2n}} = \frac{1.0000 - 0.5544 \cdot \frac{E_B}{E_R}}{0.299 + 0.114 \cdot \frac{E_B}{E_R}}$$

Substituting for  $\frac{E_B}{E_R}$  from equation (7-64), gives;

$$\frac{C_{2an}}{A_{2n}} = \frac{8.174 \cdot u - 2.173}{1.000 \cdot u + 0.039}, \quad \dots (8-47)$$

$v$  is determined from equation (7-65) and is given by

$$v = 0.682 \cdot u + 0.027, \quad \dots (7-65)$$

$C_{2an}/A_{2n}$	$u$ (R)→(B)	$C_{2an}/A_{2n}$	$u$ (R)→(B)
3.344	0.477	- 0.500	0.248
3.000	0.443	- 1.000	0.233
2.500	0.400	- 1.500	0.219
2.000	0.365	- 2.000	0.206
1.500	0.334	- 2.500	0.194
1.000	0.308	- 3.000	0.184
0.500	0.286	- 3.500	0.174
0.000	0.266	- 4.000	0.165
		- 4.500	0.157
		- 4.863	0.152

Table 8-4. Ratio  $C_{2an}/A_{2n}$  calculated at values of  $u$ ,  $u$  being on (R), (B).

Similarly, for the family of straight lines drawn on the (U), (V), (W) chromaticity diagram and through the stimulus ( $C_{2an}$ ), the lines represent,  $\frac{B_{2an}}{A_{2n}} = \text{constant}$ .

To determine the constant for each line, the ratio is evaluated on the straight line joining the stimuli (G), (B); thus  $E_R = 0$ . From equations (8-44), (8-46), putting  $E_R = 0$  and normalising equation (8-44), then,

$$\frac{B_{2an}}{A_{2n}} = \frac{-1.0000 \cdot \frac{E_G}{E_B} + 0.2760}{0.587 \cdot \frac{E_G}{E_B} + 0.114}$$

Substituting for  $\frac{E_G}{E_B}$  from equation (7-61), gives:

$$\frac{B_{2an}}{C_{2an}} = \frac{-3.828 \cdot v + 0.815}{1.000 \cdot v}, \quad \dots\dots(8-48)$$

The corresponding value of u for values of v being on the line joining (G), (B) is given by equation (7-62) i.e.

$$u = -0.030 \cdot v + 0.192, \quad \dots\dots(7-62).$$

$B_{2an}/A_{2n}$	$v$ (G)→(B)	$B_{2an}/A_{2n}$	$v$ (G)→(B)
2.421	0.130	-0.500	0.249
2.000	0.140	-1.000	0.288
1.500	0.153	-1.500	0.350
1.000	0.169	-1.703	0.384
0.500	0.188		
0.000	0.213		

Table 8-5 Ratio  $B_{2an}/A_{2n}$  calculated at values of v, v being on (G), (B).

Fig 8-7 gives curves showing the relationship between the chrominance signals  $B_{2an}$ ,  $C_{2an}$  and the luminance signal  $A_{2n}$ . The grids of lines are seen to cover the (R), (G), (B) triangle

fairly uniformly, except in the blue region. However, the eye does not perceive detail in blue so readily; thus the blue signal can tolerate more noise at high frequencies than the red or green. The grids are somewhat more uniform than in the P.A.L system. Since the diagram approximately represents a constant chromaticity chart, a more uniform grid is advantageous. In the N.T.S.C. system, the chrominance signals are linearly transformed, so shifting the location of the reference stimuli and producing a more uniform grid than the P.A.L. The locations of  $(A_{2n})$ ,  $(B_{2an})$  correspond almost exactly to the stimuli  $(S_C)$  and  $(C_Q)$  of the N.T.S.C system. The location of  $(C_{2an})$  is, however, different from that of  $(C_I)$  and is located at about  $(-0.46)$  on the  $u$  axis. For comparison, the N.T.S.C signals are given by,

$$E_I = 0.596 \cdot E_R - 0.275 \cdot E_G - 0.321 \cdot E_B, \dots\dots (8-49)$$

$$E_Q = 0.212 \cdot E_R - 0.523 \cdot E_G + 0.312 \cdot E_B, \dots\dots (8-50)$$

The chosen chrominance signals facilitate decoding as well as distributing the quantisation noise evenly amongst the red, green and blue luminance levels.

Chapter 9 deals with the instrumentation of the colour system based on the parameters  $A_{2n}$ ,  $B_{2an}$ ,  $C_{2an}$ .

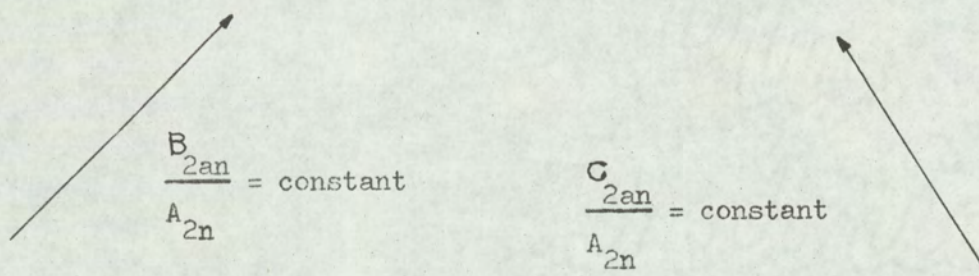
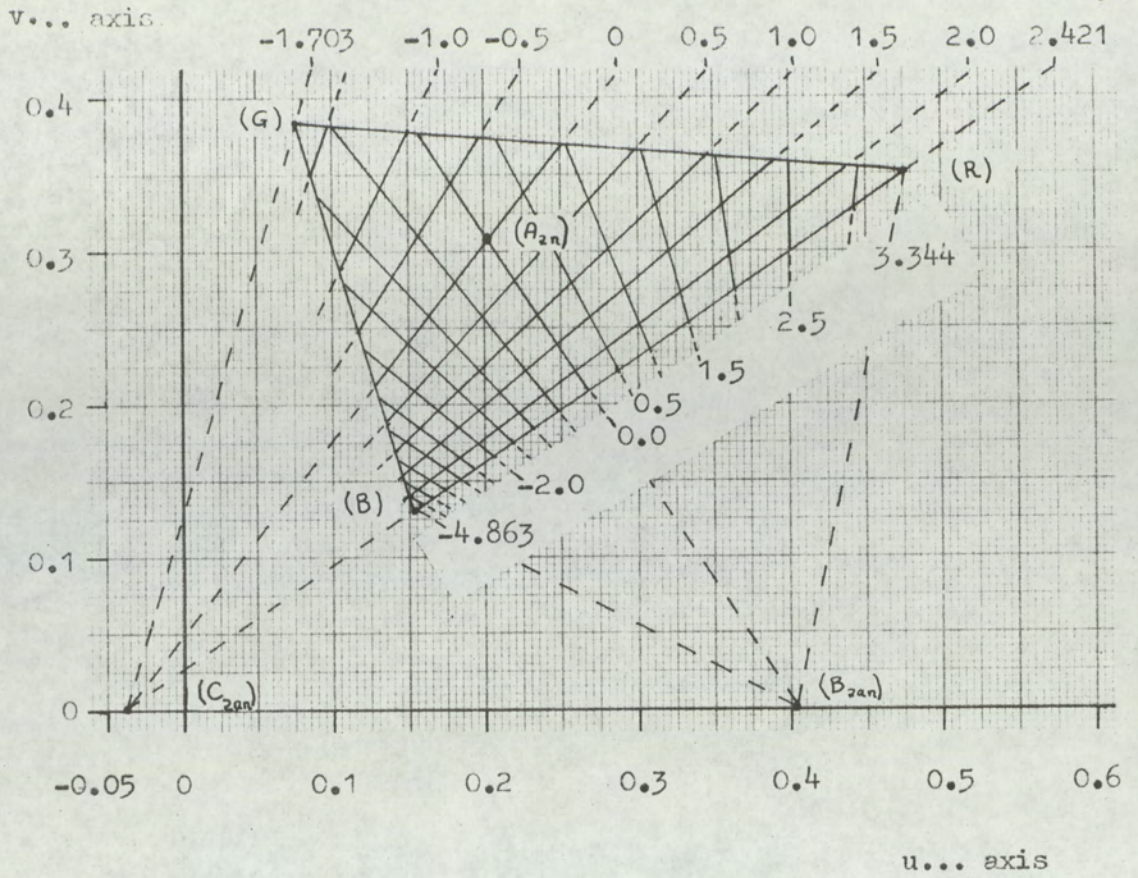


Fig.8-8. Chromaticity diagram for C.I.S.S., having channels A<sub>2n</sub>, B<sub>2an</sub>, C<sub>2an</sub>, displayed on u, v, w chart.

CHAPTER 9.INSTRUMENTATION OF DIGITAL ENCODING  
SYSTEM FOR COLOUR TELEVISION SIGNALS.

9.1 The 'Chrominance in Syncs, System ' (C.I.S.S.) developed in this chapter is based on the signal parameters defined in section 8.11, where a detailed discussion was given of a system of the two channel family. It was suggested that the chrominance signal could be inserted in **part** of the period occupied by line blanking. The system required the use of **pulse** compression techniques. The required pulse compression system was discussed in section 8.5

The process of pulse compression, if **performed** without error, does not in anyway modify the video signal. Thus, picture impairment is independent of pulse-compression. The system to be described here is a simulation of the C.I.S.S. encoder. The process of pulse compression is not performed. However, the video signals are encoded in all other respects to the requirements of the system; thus the impairment of the picture due to encoding can be simulated.

In the simulation, the encoded luminance and alternating chrominance signals are applied to two delta-sigma modulators. The modulator encoding luminance operates at the full system clock rate while the other modulator operates at one-fifth the clock rate. After digital modulation, the signals are immediately decoded by low-pass filters back to the required analogue form. The signals are now distorted by the quantisation process. Decoding the two signals to form the required signals of red, green and blue, is completed by analogue decoding circuits. In the analogue encoder and decoder, line sequential switching is performed, also black- level

clamping circuits (B.L.C.) operate. All pulse and control functions originate from a central control system which simultaneously controls the encoder and decoder. Consequently, synchronisation of encoder and decoder is simplified and address pulse sequences are not required. This simplification is legitimate, since picture impairment is not directly related to address sequences, providing the encoding and decoding systems are held in synchronism.

The main disadvantage with C.I.S.S. is that complex control systems are required and large ( 1000 bits +) high speed registers are used for the pulse compression. However, it is anticipated that with L.S.I. and M.S.I. circuits, these disadvantages could be minimised and compact encoder and decoder terminals designed.

In the system to be described, a facility for inverting the luminance and chrominance signals on alternate lines was introduced in order to try to minimise vertical contouring due to the delta-modulator encoders.

The reasons for selecting this system for further investigation are as follows:

- (a) Only a single channel, operating at the full system pulse rate is required for encoding the luminance signal. Thus, maximum fidelity of luminance encoding is obtainable.
- (b) Effective use of pre-emphasis and de-emphasis networks is possible, so enhancing the signal-to-error noise ratio of the delta-sigma modulators used for digitally encoding the chrominance and luminance signals.

- (c) The principle of constant luminance applies; this is described in section 7.6
- (d) The noise distribution among the chrominance signals is controlled; see section 8.11
- (e) A monochrome (luminance only) signal is directly available without complex decoding and does not depend upon high-frequency averaging of two or more multiplexed channels. The principle was discussed in section 8.6
- (f) There is no luminance-to-chrominance crosstalk as with analogue encoding methods. Such analogue encoding systems were discussed in section 8.2
- (g) The chrominance signal is completely stored in the line-blanking period, thus utilising redundant channel capacity.
- (h) Use can be made of reducing the vertical-chrominance resolution to minimise the required chrominance signals.
- (i) The choice of signals allows straight-forward analogue encoding and decoding systems to be designed.

Fig. 9.1 illustrates the basic system of analogue encoding, digital modulation, demodulation and analogue decoding. The system description is subdivided into five sections as follows:

Section 9.2	Analogue encoding systems
Section 9.3	Digital-control system
Section 9.4	Delta-sigma modulation and demodulation filters
Section 9.5	Analogue-decoder system
Section 9.6	Chopped filter for luminance and chrominance signals.

Composite waveform.

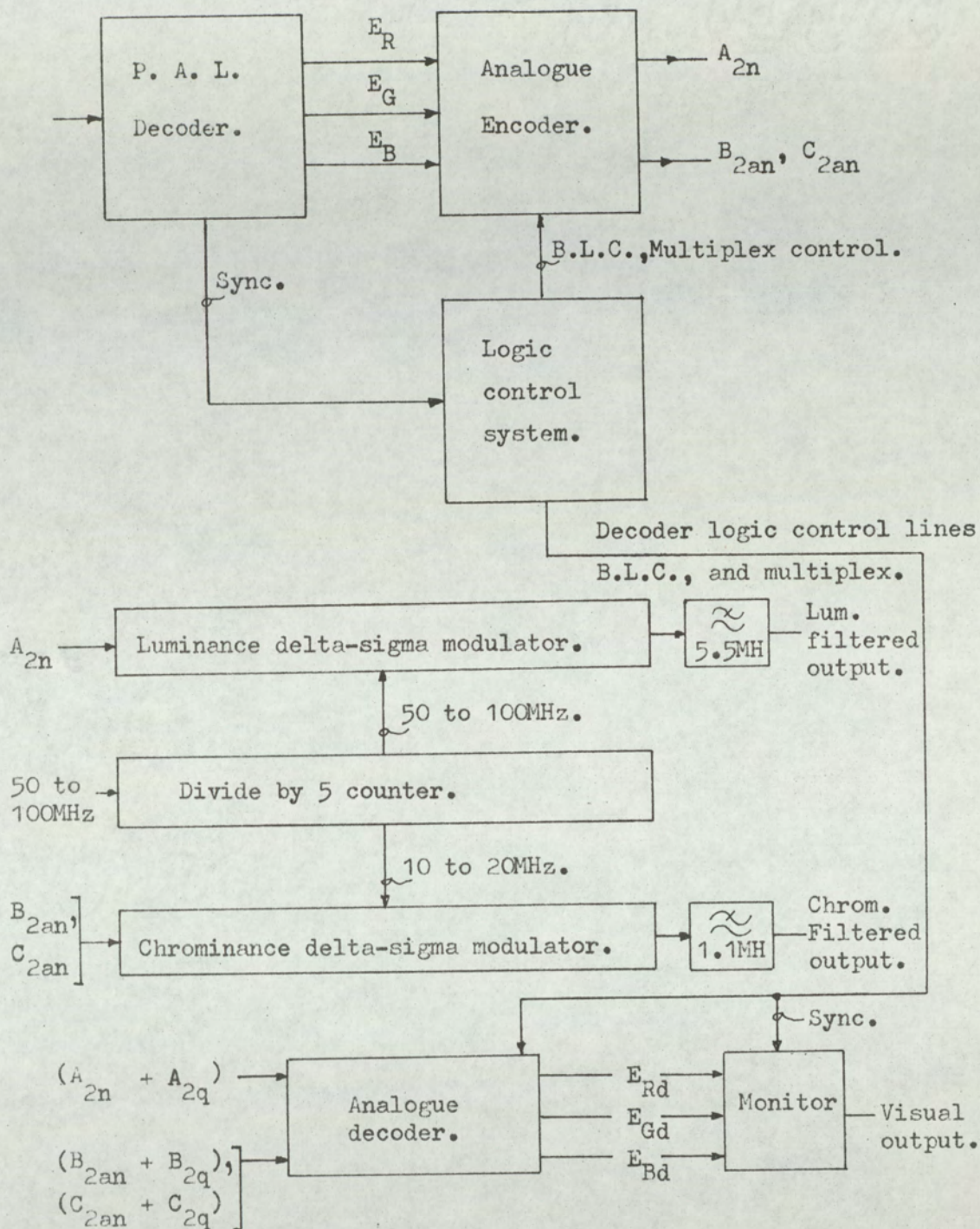


Fig.9-1. Basic encoding, modulation and decoding systems used in C.I.S.S. simulation.

## 9.2 The analogue encoder

The analogue encoder can be subdivided into four basic networks:

1. Transmission-signal matrices
2. Black level clamps, (B.L.C.)
3. Multiplex switcher
4. Pre-emphasis and line driver

### 1. Transmission signal matrices

The purpose of the transmission-signal matrices is to produce from the three video signals  $E_R, E_G, E_B$ , the signals  $A_{2n}, B_{2an}, C_{2an}$  as defined by equations (8.46), (8.44), (8.45) respectively. Also the matrices are required to produce  $-A_{2n}, -B_{2an}, -C_{2an}$ . The matrices in system form, are produced by high-gain differential input and differential output summing amplifiers. The form of the summing amplifiers allows both positive and negative summing functions. Consider the summing amplifier of Fig. 9.2. The amplifier is treated generally; thus it is applicable to all differential summing amplifiers used in the system.

For input and output suffix 1,

$$\frac{E_{i1} - e_1}{R_1} = \frac{e_1 - E_{o1}}{R_2}$$

and for input and output suffix 2

$$\frac{E_{i2} - e_2}{R_1} = \frac{e_2 - E_{o2}}{R_2}$$

where

$E_{i1}$  input signal to input 1

$E_{i2}$  input signal to input 2

$e_1, e_2$  differential inputs of high gain amplifier

$E_{o1}$  output signal of output 1

$E_{o2}$  output signal of output 2

$R_1, R_2$  input and feedback resistors

Rearranging and subtracting the two equations, gives,

$$\frac{1}{R_1} (E_{i1} - E_{i2}) - \left\{ \frac{1}{R_1} + \frac{1}{R_2} \right\} (e_1 - e_2) = \frac{-1}{R_2} (E_{o1} - E_{o2}),$$

But, for the high gain amplifier,

$$\frac{E_{o1} - E_{o2}}{e_{i1} - e_{i2}} = -A,$$

where A is the amplifier gain.

Hence, eliminating  $(e_{i1} - e_{i2})$ , gives,

$$(E_{i1} - E_{i2}) = \frac{-R_1}{R_2} \cdot (E_{o1} - E_{o2}) - \frac{1}{A} \left\{ 1 + \frac{R_1}{R_2} \right\},$$

Hence,

$$\frac{E_{o1} - E_{o2}}{E_{i1} - E_{i2}} = \frac{-1}{\frac{R_1}{R_2} + \frac{1}{A} \left( 1 + \frac{R_1}{R_2} \right)}, \quad \dots (9.1)$$

If  $A \gg 1$ , then,

$$\frac{E_{o1} - E_{o2}}{E_{i1} - E_{i2}} = \frac{-R_2}{R_1}, \quad \dots (9.2)$$

The amplifier shown in Fig. 9.2 is symmetrical about both pairs of input and output terminals; thus,

$$E_{o1} = -E_{o2}, \quad \dots (9.3)$$

Hence, the amplifier produces an inverted output signal.

It is possible to apply this network to generate  $A_{2n}$ ,  $B_{2an}$ ,  $C_{2an}$ .

To generate  $A_{2n}$ :

The modified summing amplifier used to produce  $A_{2n}$  is shown in Fig. 9.3.

The three input signals  $E_R, E_G, E_B$ , are applied to a resistive summing network formed by  $R_3, R_4, R_5$ , the level of each signal being set by a preset potentiometer.  $R_3, R_4, R_5$  are chosen such that,

$$\frac{1}{R_1} = \frac{1}{R_3} + \frac{1}{R_4} + \frac{1}{R_5}, \quad \dots (9.4)$$

Thus, the combination of signals  $E_R, E_G, E_B$ , together with a suitable choice of resistors  $R_3, R_4, R_5$  is exactly equivalent to a signal  $E_L$ , defined by equation (7.39) applied across a single resistor of value  $R_1$ . Assume that the preset potentiometers are set at minimum attenuation; then using equations (9.4) and (7.39) and equating currents in the equivalent network, as shown as  $i$  in Fig. 9.3, gives:

$$i = \frac{E_L}{R_1} = \frac{E_R}{R_3} + \frac{E_G}{R_4} + \frac{E_B}{R_5}$$

Thus, applying equation (7.39),

$$E_L = \frac{R_1}{R_3} E_R + \frac{R_1}{R_4} E_G + \frac{R_1}{R_5} E_B$$

Putting  $\frac{R_1}{R_3} = 0.299,$

$$\frac{R_1}{R_4} = 0.587,$$

$$\frac{R_1}{R_5} = 0.114,$$

Therefore,  $R_3 = 3.344.R_1, \dots (9.5)$

$$R_4 = 1.703.R_1, \dots (9.6)$$

$$R_5 = 8.772.R_1, \dots (9.7)$$

In the network shown in Fig. 9.3, one differential input is maintained zero potential i.e.  $E_{i2} = 0$ . Also, the gain with respect to ground is required and not the differential output. Hence, the gain is one half that indicated by equation (9.2) i.e. applying equations (9.3) and eliminating  $E_{o2}$ , gives:

$$\frac{E_{o1}}{E_{i1}} = \frac{-1}{2} \cdot \frac{R_2}{R_1}$$

But  $E_L = E_{i1}$  and substituting equation (7.39) for  $E_L$ , gives:

$$\frac{E_{o1}}{(0.299E_R + 0.587E_G + 0.114E_B)} = \frac{-R_2}{2.R_1} \dots (9.8)$$

Thus, the summing amplifier gain can be calculated from equation (9.8) by specifying  $R_1$  and  $R_2$ . The values  $R_3$ ,  $R_4$ ,  $R_5$  then follow directly from equations (9.5), (9.6) and (9.7). The preset gain controls in each signal path allow the balance of  $E_R$ ,  $E_G$  and  $E_B$  to be precisely set.

The summing amplifier for producing the signal  $A_{2n}$  can, with modification, be used to produce the signals  $B_{2an}$ ,  $C_{2an}$ . Signal addition and subtraction are required for these two summing amplifiers; thus both inputs are used. For channel  $B_{2an}$ ,  $E_R$  and  $E_B$  are grouped to the positive input, since equation (8.44) requires that positive amounts of these signals be added to a negative contribution from  $E_R$ . Similarly, equations (8.45), requires that  $E_G$  and  $E_B$  are grouped to the negative input. The exact proportions of  $E_R, E_G, E_B$  to produce  $B_{2an}$  and  $C_{2an}$  are set according to equations (8.44) and (8.45) by preset controls. The grouped inputs of both amplifiers are given equal weighting and are set at  $2.R_1$ ; thus the amplifiers remain symmetrical.

The input groupings are shown in the two equations for the transfer functions of the amplifiers. The equation forms are similar to equation (9.8).

For the  $B_{2an}$  summing network:

$$\frac{E_{O1}}{(0.5 E_R - 1.0 E_G + 0.5 E_B)} = \frac{-R_2}{2.R_1}, \quad \dots \quad (9.10)$$

and for the  $C_{2an}$  summing network:

$$\frac{E_{O1}}{(1.0 E_R - 0.5 E_G - 0.5 E_B)} = \frac{-R_2}{2.R_1} \quad \dots \quad (9.11)$$

Equations (9.10), (9.11) assume that the presets are fully advanced, thus introducing no attenuation.

The complete signal matrixing network for  $A_{2n}$ ,  $B_{2an}$ ,  $C_{2an}$  is shown in Fig. 9.4. Circuit diagrams for these networks are shown in appendix 1.

## 2. Black-level clamps, (B.L.C.)

It is necessary to bring each of the video signals to a common d.c. level before multiplexing (at line rate) can be performed. In section 6.3, the significance of the black-level period was discussed. Black-level clamping can be achieved by introducing, during the black-level period, a low-impedance path to ground in an a.c.-coupled stage. The capacitor in the coupling thus acts as a memory element to store the d.c. level. This clamping procedure applies equally to luminance and chrominance signals. It is necessary both for multiplexing and for maintaining the video signals within the active signal range of the delta-sigma modulators. It is clear that if there was a d.c. offset between, say, chrominance signals transmitted on successive lines, then false chrominance information would be transmitted. This offset could be removed at the decoder, but this requires added circuit complexity.

The black-level clamps system, which is introduced into each of the six channels shown in Fig. 9.4, is illustrated in principle in Fig. 9.5. Further circuit details are given in Appendix 1.

During black-level, the output of the low output-impedance drive amplifier remains constant. A pulse is applied to the gate of the F.E.T. which switches from a high resistance (several megohms) to a low resistance (about  $50\Omega$ ). The source of the F.E.T. is connected to

ground; thus, the drain, over a period of several lines, tends to zero during the black-level clamping period. By introducing a high-impedance load to the capacitor during the remaining line period, the charge on the capacitor is stored. Thus, d.c. level is maintained. The high input impedance buffer amplifier is given a d.c. level control to compensate for d.c. offsets between channels prior to multiplexing.

The signal  $B_{e1}$  is applied to the clamping pulse during the black-level period.

### 3. Multiplex switcher

It is necessary to select the required signal for transmission and to select the signal using a fast switch capable of transmitting analogue signals. The system contains four chrominance signals (positive and negative) and two luminance signals (positive and negative). Each signal is applied to an F.E.T. switch as shown in Fig. 9.6. The signals are then combined to a common node via a protection resistor. These resistors protect the circuitry should two F.E.T.'s be simultaneously on, either by system malfunction or during switching transients.

The gate of each F.E.T. is driven from a pulse generator. The logic signals are  $C_{c1}, C_{c2}, C_{c3}, C_{c4}$  for the chrominance control signal and  $L_{c1}, L_{c2}$  for the luminance control signals. A signal of '1' represents that the F.E.T. switch is on and a '0' that the switch is off. Circuit details of the pulse generator are given in appendix 2, where, the discrete logical circuitry is described. The function of the control logic for driving the

multiplex switches is given in section 9.3.

All F.E.T's are driven by a pulse drive circuit, details are given in Appendix 2 .

#### 4. Line drivers and pre-emphasis networks

The line driver amplifiers provide  $75\Omega$  source impedances for driving the transmission lines which connect the encoder to the two delta-sigma modulators. The amplifiers also provide facilities for gain adjustment, d.c. level control and pre-emphasis. The amplifier is shown in Fig. 9.7.

The transfer function  $T_L(f)$  of the line-drive amplifier, assuming a high-gain amplifier, is given by:

$$T_L(f) = 1 + \frac{R_3}{Z_1}, \quad \dots (9.12)$$

$$\text{where, } Z_1 = R_1 \cdot \frac{\{1 + j2\pi f c_1 R_2\}}{\{1 + 2\pi f (R_1 + R_2)\}}, \quad \dots (9.13)$$

From equations (9.12) and (9.13), eliminating  $z$ , gives,

$$T_L(f) = \frac{(1 + \frac{R_3}{R_1}) \cdot (1 + j 2\pi f c_1 \frac{R_1 R_2 + R_2 R_3 + R_3 R_1}{R_1 + R_3})}{(1 + j 2\pi f c_1 R_2)}, \quad \dots (9.14)$$

The pre-emphasis characteristics chosen for the luminance and chrominance channels are shown in Fig. 9.7a. Since the delta-sigma modulators are amplitude dependent, excessive over-shoot

on fast-rising signals is undesirable. The pre-emphasis networks were chosen by observing the signal rise times when the encoder was driven from a Philips colour-bar generator and P.A.L. decoder. The value of  $C_1$  in the pre-emphasis network was chosen to give the best rise time with the minimum of over-shoot, for both luminance and chrominance signals. It is anticipated, however, that superior results would be obtainable with an adaptive filter of the form described in section 5.4.

Circuit details of the line drive amplifiers are given in appendix 1.

The complete analogue encoder is shown in Fig. 9.8, both analogue inputs and outputs are indicated together with logic inputs.

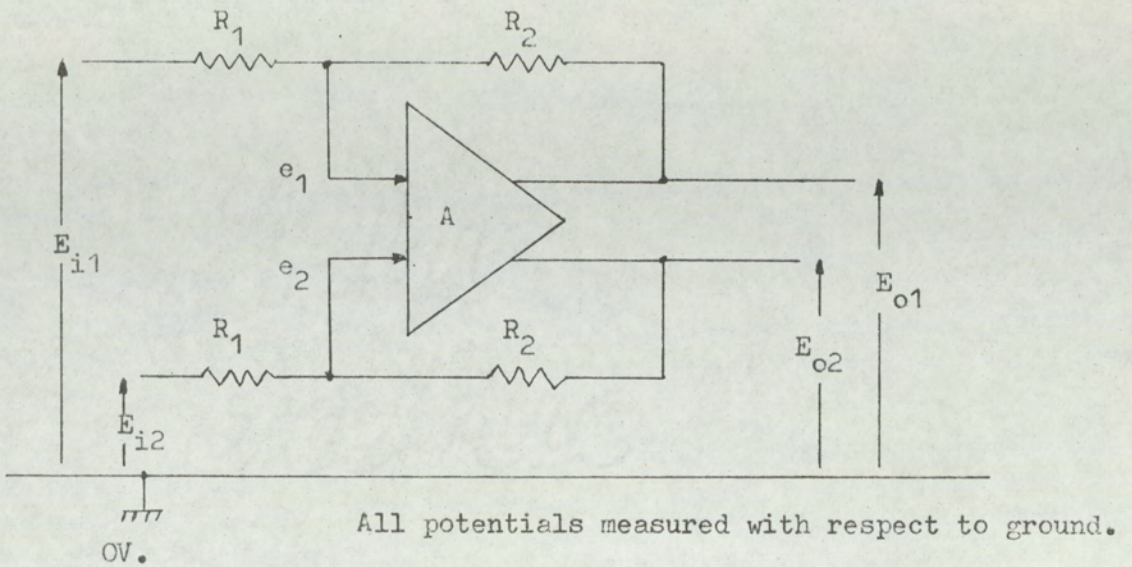


Fig.9-2. Differential summing amplifier.

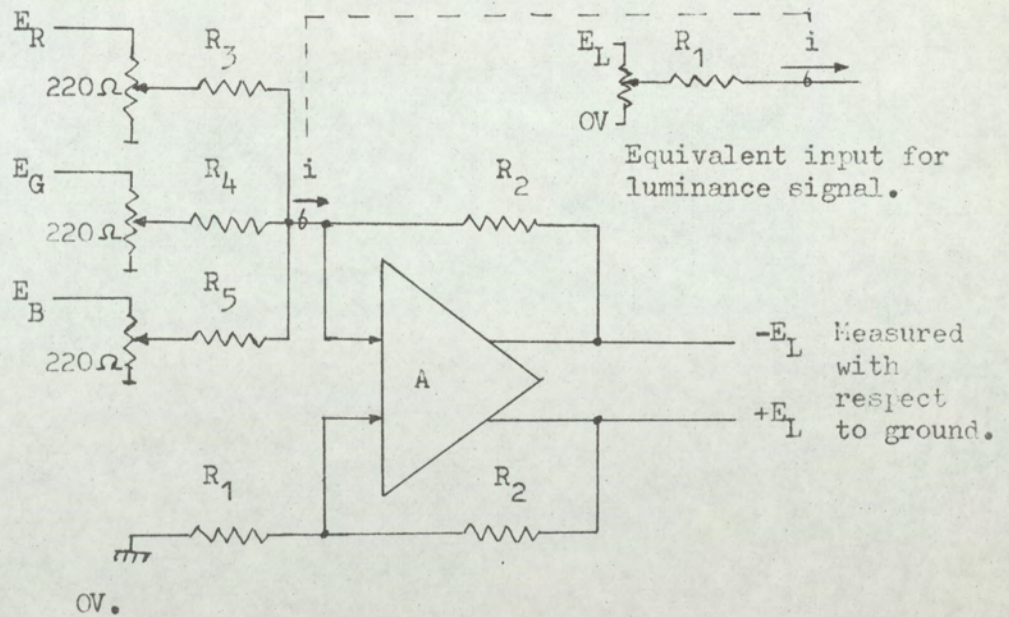


Fig.9-3. The summing amplifier for generating  $A_{2n}$ .

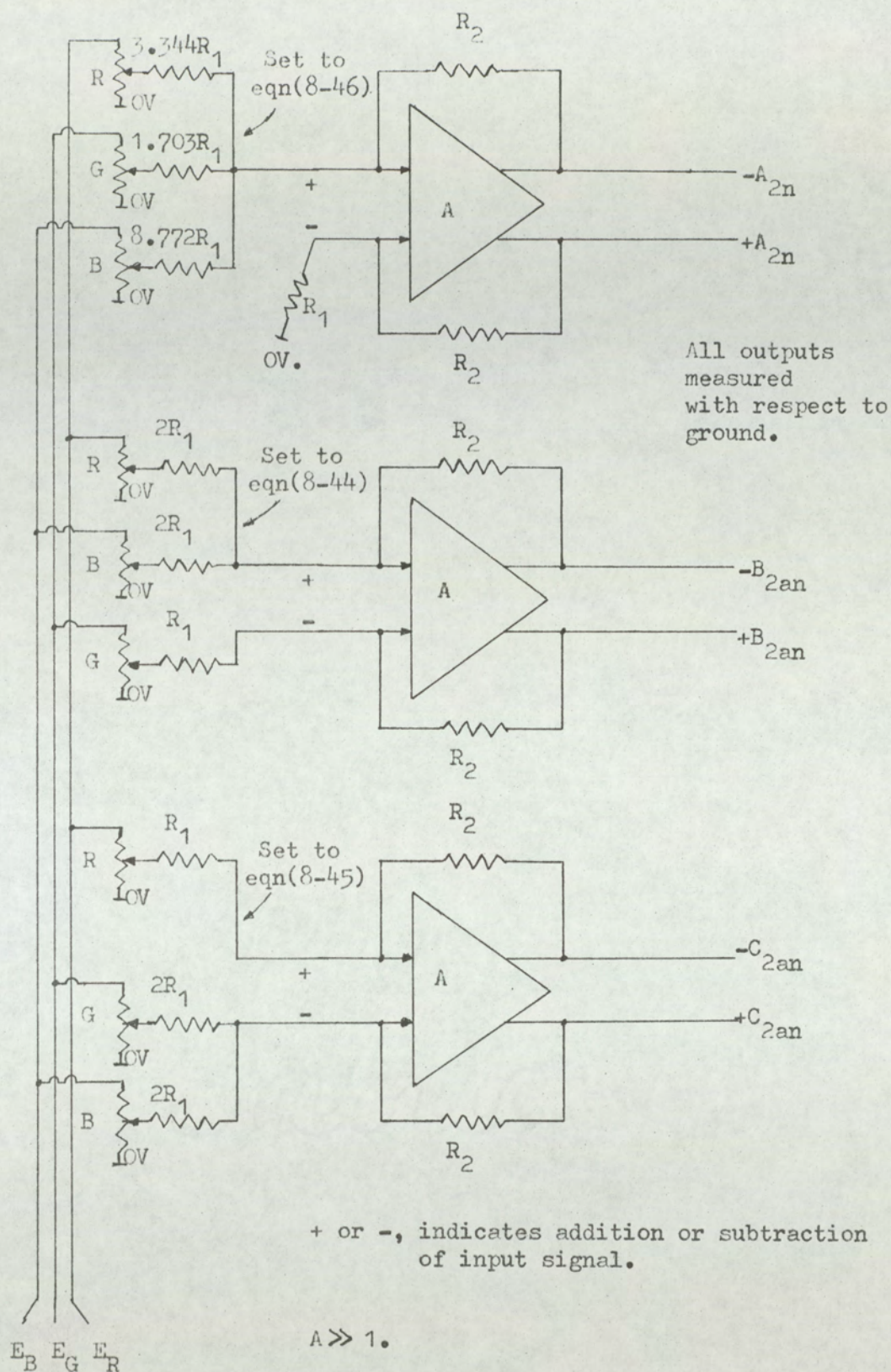


Fig.9-4. Signal matrixing to form  $A_{2n}$ ,  $-A_{2n}$ ,  $B_{2n}$ ,  $-B_{2n}$ ,  $C_{2n}$ ,  $-C_{2n}$  from signals  $E_R$ ,  $E_G$ ,  $E_B$ .

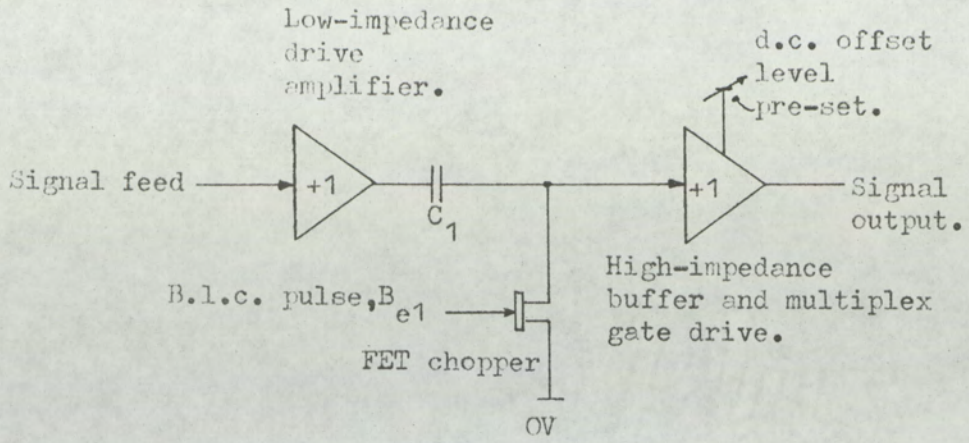
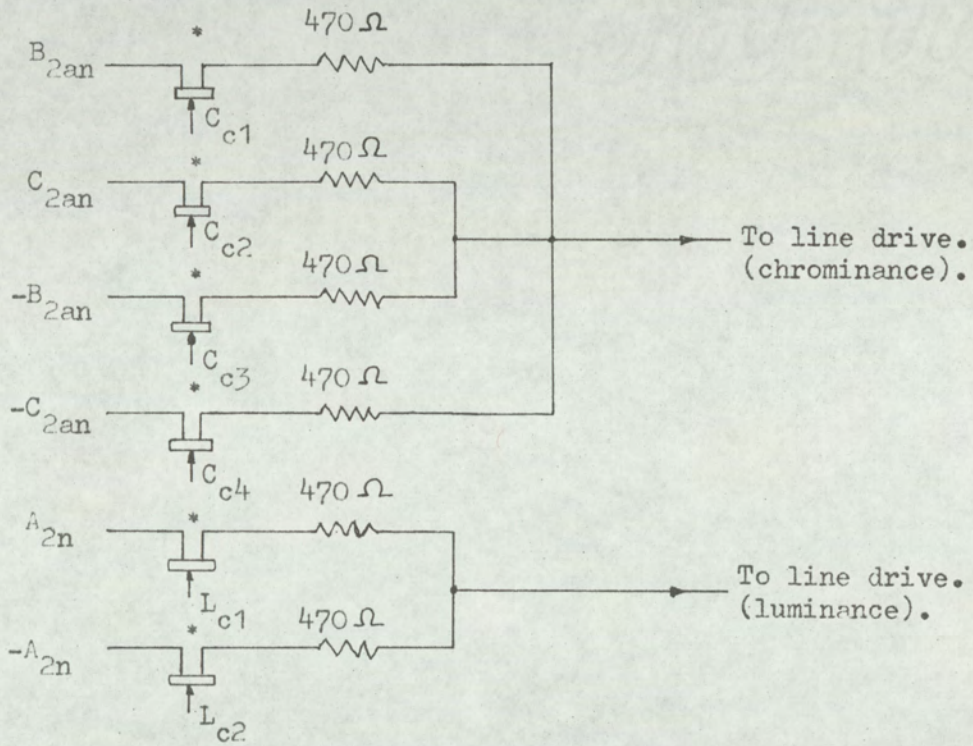


Fig.9-5. Black-level clamp network.



\* All FET's driven by pulse generator, given in Appendix 2.

Fig.9-6. Multiplex switcher for chrominance and luminance channels.

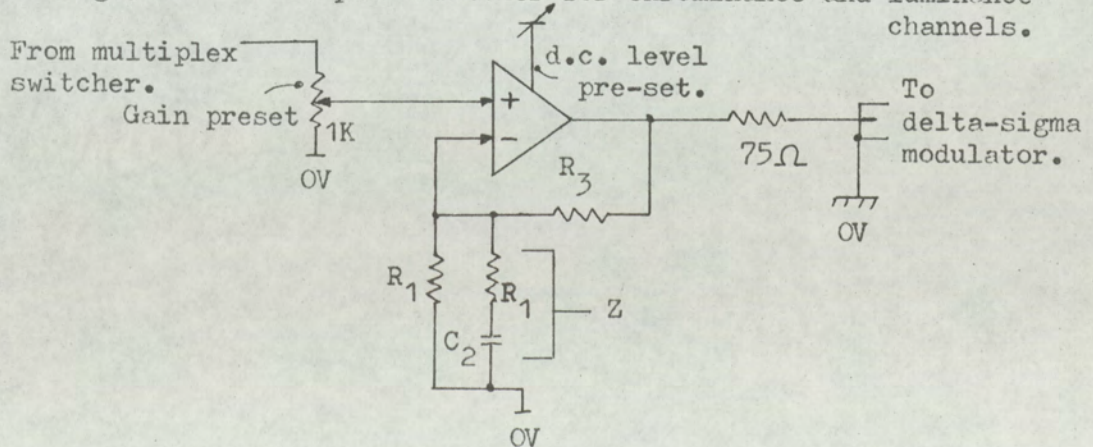
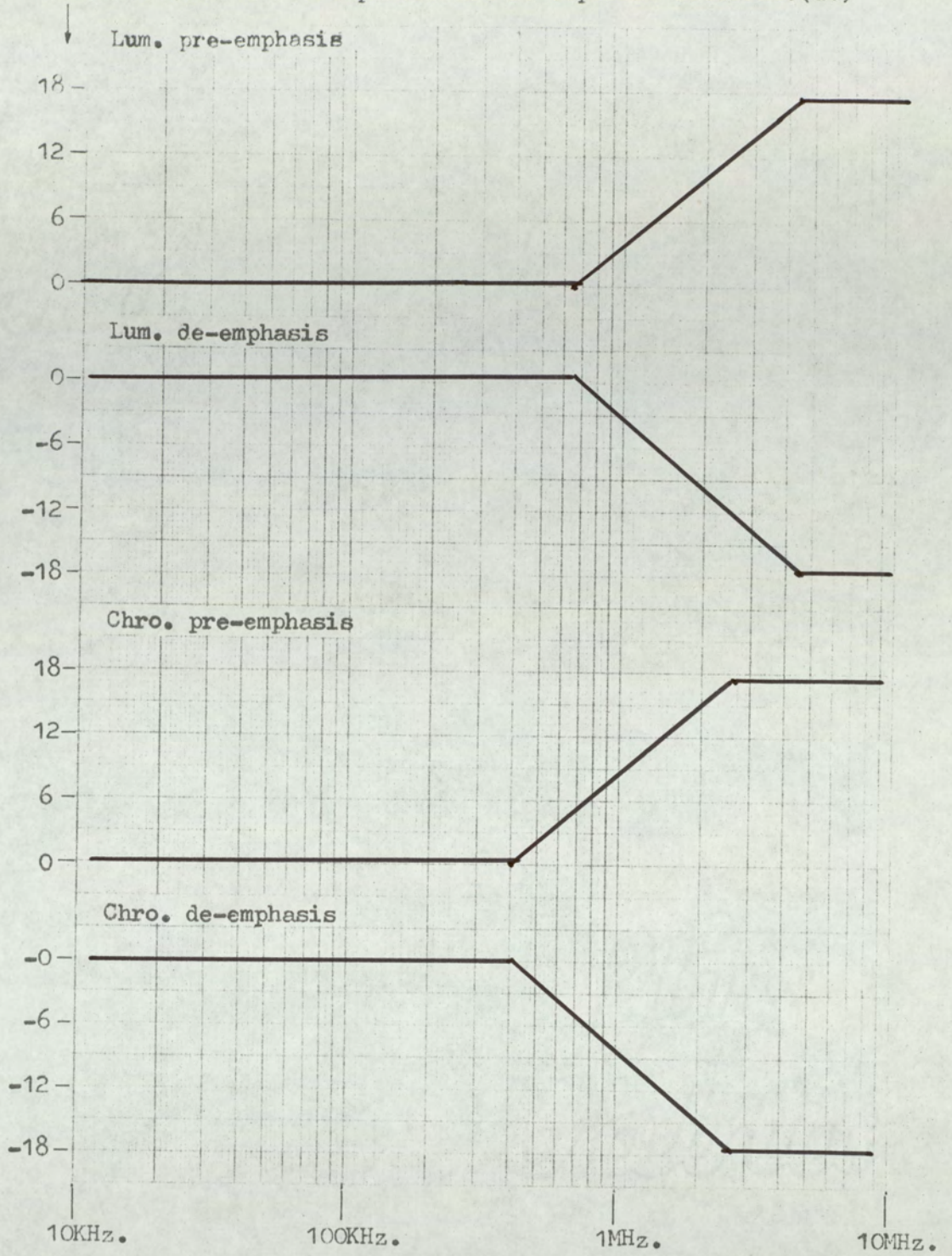


Fig.9-7. Line-drive amplifier for luminance and chrominance channels, with pre-emphasis network.



Base-band signal frequency, Hertz.

Fig.9-7(a). Pre-emphasis and de-emphasis characteristics for luminance and chrominance channels.

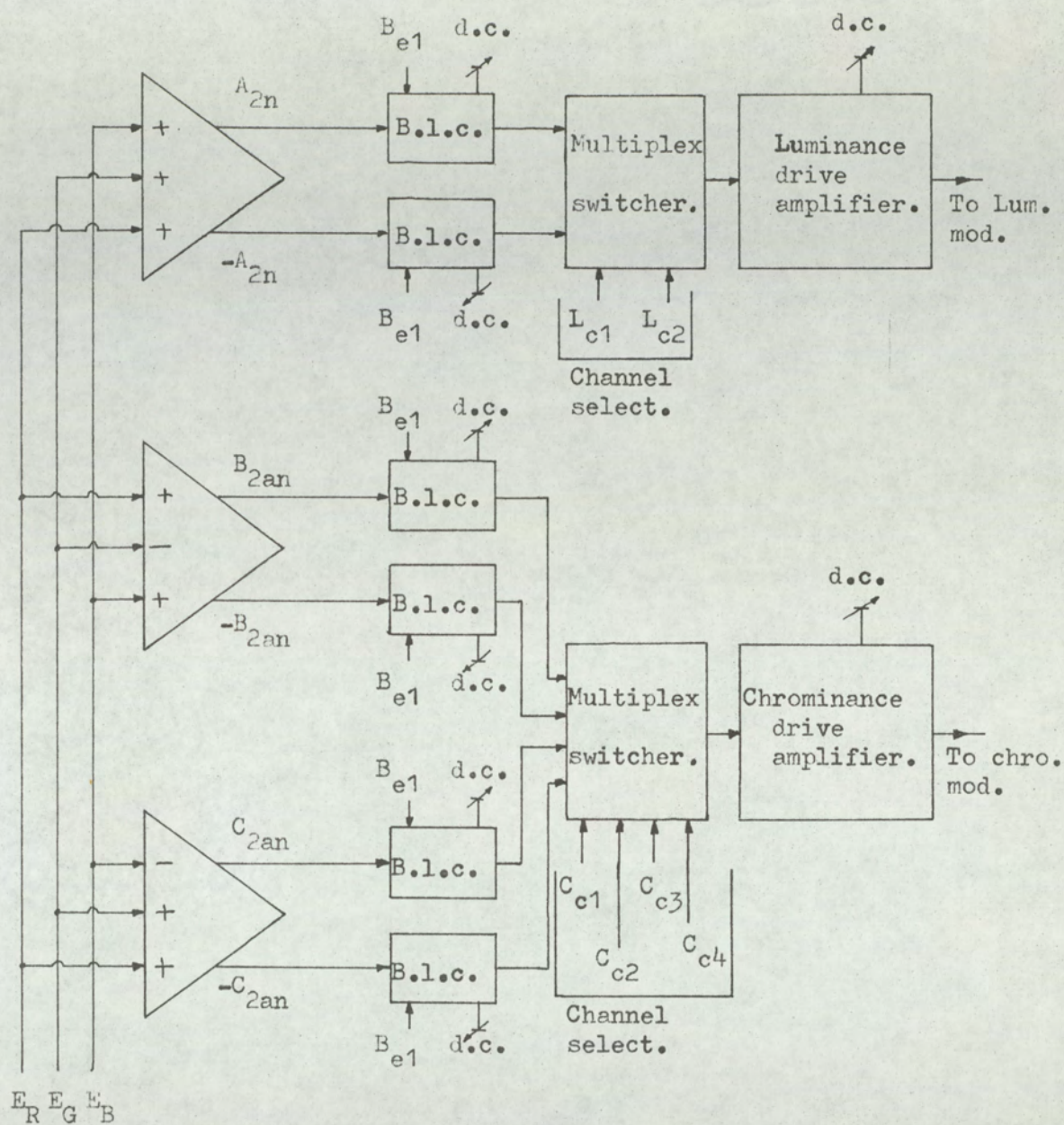


Fig.9-8. Complete analogue encoder (excluding digital control).

### 9.3 The digital control system

The control pulses for multiplexing, de-multiplexing, black-level clamping and synchronisation pulse sources are developed in the digital control system. Fig. 9.9 illustrates the pulses and signals which form the inputs and outputs of the digital control.

The digital control can be sub-divided into four basic groups:

1. Synchronisation and clock generation
2. Black-level clamping system
3. Encoder multiplex control signals for luminance and chrominance channels.
4. Decoder multiplex control signals for luminance and chrominance channels.

The designations of the pulses in Fig. 9.9 are as follows:

(w.r.t. Fig. 9.9)

$B_{e1}$	encoder B.l.c. source
$C_{l1}$	clock pulse
$B_{l+}, B_{l-}$	luminance decoder B.l.c. pulses
$B_{c1}, B_{c2}$	chrominance decoder B.l.c. pulses
$S_y$	multiplex synchronisation pulse
$L_{c1}, L_{c2}$	encoder, luminance, multiplex control pulses
$C_{c1}, C_{c2}, C_{c3}, C_{c4}$	encoder, chrominance, multiplex control pulses
$L_D$	luminance, decoder, de-multiplex control pulses
$C_{D1}, C_{D2}$	chrominance, decoder, de-multiplex control pulses
$C_t$	clock detection signal.

## 1. Synchronisation and clock generation

A line and field synchronisation pulse separator is provided so that t.t.l. logic level pulses are available for driving auxiliary equipment. The pulses can also form the basis of the clock  $c_{l1}$  for driving the control unit. It is necessary that all multiplex switching functions are executed during the line-blanking period. The leading edge of each line pulse thus produces a useful reference for triggering the multiplex control sequences. Circuit details are given in Appendix 2, which shows the circuits of the discrete logic functions.

## 2. Black-level clamping systems

Fig. 9.10 shows the black-level clamping for the encoder system. Six B.l.c. pulses are required; however, all pulses are in phase and can therefore be generated from a common source. Since the B.l.c. pulses are required during black level, the clamping pulses can be triggered from the trailing edge of the line synchronisation pulses. An inhibit pulse is introduced for most of the active line to prevent the B.l.c. pulse generator from being spuriously triggered during the active picture. The B.l.c. synchronisation inhibit pulse is removed for about  $12 \mu \text{ sec}$  in each line, the period being activated by the system clock. The system was initially designed to operate from either a positive or negative clock source; thus, the inhibit pulse generator can be initiated by either a positive or a negative edge. Since the field synchronisation pulses are greater than  $12 \mu \text{ sec}$ , the B.l.c. does not trigger during the five field pulses of each field.

In the encoder, the B.l.c. pulses are produced from a monostable, the output swing being from about -6V to +6V. Thus, with a suitable diode coupling the B.L.C., F.E.T. choppers can be driven directly.

Fig. 9.11, shows the system of B.l.c. clamping in the decoder. In the decoder, four B.l.c. pulses are required. Initially, both the luminance and chrominance B.l.c. trigger pulses are delayed to compensate for the luminance and chrominance filters used to decode the delta-sigma modulators. The chrominance and luminance channels require different trigger delays due to the difference in signal delay of the chrominance and luminance filters. The luminance decoder (as will be shown in section 9-5) requires two parallel channels. In one mode of system operation, the B. l.c. pulses are alternated, at line rate, between the two luminance channels. Thus, the B.l.c. pulses for the luminance are split and are controlled by the luminance de-multiplex control signal  $L_D$  and combined by an AND function.

The chrominance section of the decoder requires two B.l.c. pulses, one before and one after the delay-line store. To allow for the delay introduced by the filters of the delay-line circuit, a  $\mu$ sec monostable is introduced as compensation. All monostables in the decoder are SN74121N, of the Texas TTL family; further description will therefore not be given as the system operation is shown in Fig. 9.10.

The logic outputs of the B.l.c. generator system are not compatible with the FET choppers. Appendix 2 describes a suitable interfacing circuit; the logic is not inverted by this circuit.

3. Encoder multiplex control signals for luminance and chrominance channels.

The chrominance multiplex control system is considered first, The coding sequence is as follows:

$$C_{C1} = 1, \quad \text{then channel } B_{2an} \text{ is open}$$

$$C_{C2} = 1, \quad \text{then channel } C_{2an} \text{ is open}$$

$$C_{C3} = 1, \quad \text{then channel } -B_{2an} \text{ is open}$$

$$C_{C4} = 1, \quad \text{then channel } -C_{2an} \text{ is open}$$

Note that only one channel can be open at any given time.

Four different operating modes have been defined for the chrominance channel. Thus, two bits of information are required to store the operating mode. Let the store be binary and let the two signals  $F_{C1}, F_{C2}$  be the store outputs; hence,

Mode 1

$$F_{C1} = 0, F_{C2} = 0$$

$$C_{C1} = C_{C2} = C_{C3} = C_{C4} = 0, \text{ always}$$

Mode 2

$$F_{C1} = 1, F_{C2} = 0$$

$$C_{C1} = 1, 0; C_{C2} = 0, 1 \text{ i.e. alternating line by line}$$

$$C_{C3} = C_{C4} = 0, \text{ always}$$

Mode 3

$$F_{C1} = 0, F_{C2} = 1$$

$$C_{C3} = 1, 0; C_{C4} = 0, 1 \text{ i.e. alternating line by line}$$

$$C_{C1} = C_{C2} = 0, \text{ always}$$

Mode 4

$$F_{C1} = 1, F_{C2} = 1$$

$$C_{C1} = 1,0,0,0, ; C_{C2} = 0,1,0,0, ;$$

$$C_{C3} = 0,0,1,0, ; C_{C4} = 0,0,0,1, ;$$

in sequence.

It can be seen in the sequences for each mode of operation, that the longest sequence is that of mode 4, which operates over four successive lines. A binary counter to the base four is required. Let the outputs of the counter be  $Y_C$  and  $X_C$ . The counting sequence is shown in the following truth table, together with the data inputs  $Y_D, X_D$  to give the next count "D" type bistables are used in the counter.

$X_C$	$Y_C$	$X_D$	$Y_D$
0	0	1	0
1	0	0	1
0	1	1	1
1	1	0	0

The Boolean expressions for the counter are,

$$X_D = \bar{X}_C \quad \dots (9.15)$$

$$Y_D = (\bar{X}_C \cdot Y_C) + (X_C \cdot \bar{Y}_C),$$

Therefore,

$$Y_D = \frac{\bar{X}_C \cdot Y_C}{(\bar{X}_C \cdot Y_C) + (X_C \cdot \bar{Y}_C)} \quad \dots (9.16)$$

Fig. 9.11 illustrates the counter system and the logic functions are derived from equations (9.15) and (9.16).

From the data supplied, it is possible to determine the Boolean expressions for the conditions that the multiplex control signals are at the 1 level. Observing the truth table and corresponding states of  $F_{C1}$ ,  $F_{C2}$ , then:

Mode 1

No expressions, control signals always zero.

Mode 2

$$C_{C1} = \bar{X}_C \cdot F_{C1} \cdot \bar{F}_{C2},$$

$$C_{C2} = X_C \cdot F_{C1} \cdot \bar{F}_{C2},$$

Mode 3

$$C_{C3} = \bar{X}_C \cdot \bar{F}_{C1} \cdot F_{C2},$$

$$C_{C4} = X_C \cdot \bar{F}_{C1} \cdot F_{C2},$$

Mode 4

$$C_{C1} = \bar{X}_C \cdot \bar{Y}_C \cdot F_{C1} \cdot F_{C2},$$

$$C_{C2} = X_C \cdot \bar{Y}_C \cdot F_{C1} \cdot F_{C2},$$

$$C_{C3} = \bar{X}_C \cdot Y_C \cdot F_{C1} \cdot F_{C2},$$

$$C_{C4} = X_C \cdot Y_C \cdot F_{C1} \cdot F_{C2},$$

Thus combining the expressions for  $C_{C1}$ ,  $C_{C2}$ ,  $C_{C3}$ ,  $C_{C4}$  and symmetrically transforming to NAND logic, gives,

$$C_{C1} = \bar{X}_C \cdot F_{C1} \cdot \bar{F}_{C2} + \bar{X}_C \cdot \bar{Y}_C \cdot F_{C1} \cdot F_{C2}$$

Therefore,

$$C_{C1} = \overline{\overline{X_C \cdot F_{C1} \cdot \overline{F_{C2}}}} \cdot \overline{\overline{X_C \cdot \overline{Y_C} \cdot F_{C1} \cdot F_{C2}}}, \quad \dots (9.17)$$

$$C_{C2} = X_C \cdot F_{C1} \cdot \overline{F_{C2}} + X_C \cdot \overline{Y_C} \cdot F_{C1} \cdot F_{C2},$$

therefore,

$$C_{C2} = \overline{\overline{X_C \cdot F_{C1} \cdot \overline{F_{C2}}}} \cdot \overline{\overline{X_C \cdot \overline{Y_C} \cdot F_{C1} \cdot F_{C2}}}, \quad \dots (9.18)$$

$$C_{C3} = \overline{\overline{X_C \cdot \overline{F_{C1}} \cdot F_{C2}}} + \overline{\overline{X_C \cdot Y_C \cdot F_{C1} \cdot F_{C2}}}$$

therefore,

$$C_{C3} = \overline{\overline{X_C \cdot \overline{F_{C1}} \cdot F_{C2}}} \cdot \overline{\overline{X_C \cdot Y_C \cdot F_{C1} \cdot F_{C2}}}, \quad \dots (9.19)$$

$$C_{C4} = \overline{\overline{X_C \cdot \overline{F_{C1}} \cdot F_{C2}}} + \overline{\overline{X_C \cdot Y_C \cdot F_{C1} \cdot F_{C2}}}$$

therefore,

$$C_{C4} = \overline{\overline{X_C \cdot \overline{F_{C1}} \cdot F_{C2}}} \cdot \overline{\overline{X_C \cdot Y_C \cdot F_{C1} \cdot F_{C2}}} \quad \dots (9.20)$$

Fig. 9.12 illustrates the logic systems derived from the equations (9.17), (9.18), (9.19), (9.20) for producing  $C_{C1}, C_{C2}, C_{C3}, C_{C4}$ .

The mode of operation is set by  $F_{C1}, F_{C2}$ . In the system this information was stored digitally by two set-reset bistables. Let  $R_{C1}, R_{C2}$  be the respective reset inputs,  $S_{C1}, S_{C2}$  the set inputs and  $F_{C1}, F_{C2}$  the stored outputs. The logic operation is such that:

$R_{C1} = 1, S_{C1} = 1,$  then output stored,

$R_{C1} = 0, S_{C1} = 1,$  then  $F_{C1} = 0,$

$R_{C1} = 1, S_{C1} = 0,$  then  $F_{C1} = 1,$

$R_{C1} = 0, S_{C1} = 0,$  output indeterminate

Similarly for  $R_{C2}, S_{C2}, F_{C2}.$

The modes of operation are set by four, non-latching, push-to-make switches. When the switches are not operated then:

$$R_{C1} = R_{C2} = S_{C1} = S_{C2} = 1,$$

and the outputs  $F_{C1}, F_{C2}$  remain stored.

Let the four switches be called,  $S_{F1}, S_{F2}, S_{F3}, S_{F4}.$  The switches are normally at zero and when activated they produce a level 1 at the contacts.

Thus, to store the required signals  $F_{C1}, F_{C2},$  the input information to each store for each operating mode is given by:

#### Mode 1

$$S_{F1} = 1, \text{ then } F_{C1} = 0, F_{C2} = 0$$

$$\text{thus } R_{C1} = 0, \quad S_{C1} = 1,$$

$$R_{C2} = 0, \quad S_{C2} = 1,$$

#### Mode 2

$$S_{F2} = 1, \text{ then } F_{C1} = 0, F_{C2} = 0,$$

$$\text{thus, } R_{C1} = 1, \quad S_{C1} = 0$$

$$R_{C2} = 0, \quad S_{C2} = 1,$$

Mode 3

$$S_{F3} = 1, \text{ then } F_{C1} = 0, F_{C2} = 1,$$

$$\text{thus } R_{C1} = 0, S_{C1} = 1,$$

$$R_{C2} = 1, S_{C2} = 0,$$

Mode 4

$$S_{F4} = 1, \text{ then } F_{C1} = 1, F_{C2} = 1$$

$$R_{C1} = 1, S_{C1} = 0,$$

$$R_{C2} = 1, S_{C2} = 0,$$

The conditions for  $R_{C1}$ ,  $R_{C2}$ ,  $S_{C1}$ ,  $S_{C2}$  each to be at, are given by,

$$R_{C1} = S_{F2} + S_{F4} + (\bar{S}_{F1} \cdot \bar{S}_{F2} \cdot \bar{S}_{F3} \cdot \bar{S}_{F4}),$$

$$R_{C2} = S_{F3} + S_{F4} + (\bar{S}_{F1} \cdot \bar{S}_{F2} \cdot \bar{S}_{F3} \cdot \bar{S}_{F4}),$$

$$S_{C1} = S_{F1} + S_{F3} + (\bar{S}_{F1} \cdot \bar{S}_{F2} \cdot \bar{S}_{F3} \cdot \bar{S}_{F4}),$$

$$S_{C2} = S_{F1} + S_{F2} + (\bar{S}_{F1} \cdot \bar{S}_{F2} \cdot \bar{S}_{F3} \cdot \bar{S}_{F4}),$$

$$\text{Put, } N_C = \overline{(\bar{S}_{F1} \cdot \bar{S}_{F2} \cdot \bar{S}_{F3} \cdot \bar{S}_{F4})},$$

$$\text{then } R_{C1} = \frac{S_{F2} \cdot S_{F4} \cdot N_C}{\bar{S}_{F1} \cdot \bar{S}_{F2} \cdot \bar{S}_{F3} \cdot \bar{S}_{F4}}, \quad \dots (9.21)$$

$$R_{C2} = \frac{S_{F3} \cdot S_{F4} \cdot N_C}{\bar{S}_{F1} \cdot \bar{S}_{F2} \cdot \bar{S}_{F3} \cdot \bar{S}_{F4}}, \quad \dots (9.22)$$

$$S_{C1} = \frac{S_{F1} \cdot S_{F3} \cdot N_C}{\bar{S}_{F1} \cdot \bar{S}_{F2} \cdot \bar{S}_{F3} \cdot \bar{S}_{F4}}, \quad \dots (9.23)$$

$$S_{C2} = \frac{S_{F1} \cdot S_{F2} \cdot N_C}{\bar{S}_{F1} \cdot \bar{S}_{F2} \cdot \bar{S}_{F3} \cdot \bar{S}_{F4}}, \quad \dots (9.24)$$

Fig. 9.13 illustrates the logic system for storing the mode of operation. The switch  $S_{F1}$ , was modified by introducing a function  $C_t$  using an AND gate. When  $C_t = 0$ , the system reverts to the mode 1. A circuit, shown in Appendix 2, senses the presence of the clock pulse (or synch pulse); should the clock fail, then after a few seconds,  $C_t = 0$ . Also, when the system is initially switched on,  $C_t = 0$ . The circuit location is illustrated in Fig. 9.13.

A facility is included for inverting the clock  $C_2$  to the counter, as illustrated in Fig. 9.11. Fig 9.14 shows the network together with the internal and external clock driving circuits. In the tests run on the system, the clock source was derived directly from the output of the synchronisation pulse separator, Fig. 9.12, 9.13.

The luminance multiplex control system is similar to that of the chrominance multiplex control system. The same counter (as shown in Fig 9.11) is used, although (due to the simplified format of the luminance multiplexing) only the output  $X_C$  is required. Again four modes of operation of the luminance channel exist; thus, the storage system illustrated in Fig. 9.13 is applicable for the luminance channel. The network of Fig. 9.13 is duplicated for the luminance channel and will not be described again. However, the storage output signals, for the luminance channel are designated  $F_{L1}, F_{L2}$ .

The luminance coding sequence is as follows:

From Fig. 9.6, it can be seen that,

$L_{C1} = 1$ , then channel  $A_{2n}$  is open

$L_{C2} = 1$ , then channel  $-A_{2n}$  is open

Note that only one channel can be open at any given time;  
hence:

Mode 1

$$F_{L1} = 0, \quad F_{L2} = 0,$$

$$L_{C1} = L_{C2} = 0,$$

Mode 2

$$F_{L1} = 1, \quad F_{L2} = 0,$$

therefore,

$$L_{C1} = 1, \quad L_{C2} = 0,$$

Mode 3

$$F_{L1} = 0, \quad F_{L2} = 1,$$

therefore,

$$L_{C1} = 0, \quad L_{C2} = 1,$$

Mode 4

$$F_{L1} = 1, \quad F_{L2} = 1,$$

therefore

$$L_{C1} = 0, 1, \quad L_{C2} = 1, 0, \quad \text{i.e. alternating line by line.}$$

It is possible to determine the Boolean expressions that give  $L_{C1}, L_{C2}$  the value 1. i.e.

Mode 1

No expression, control signals always zero

Mode 2

$$L_{C1} = F_{L1} \cdot \overline{F_{L2}},$$

Mode 3

$$L_{C2} = \overline{F_{L1}} \cdot F_{L2},$$

Mode 4

$$L_{C1} = X_C \cdot F_{L1} \cdot F_{L2},$$

$$L_{C2} = \overline{X_C} \cdot F_{L1} \cdot F_{L2},$$

Thus, combining the expressions for  $L_{C1}, L_{C2}$  and symmetrically transforming to NAND logic, gives:

$$L_{C1} = F_{L1} \cdot \overline{F_{L2}} + X_C \cdot F_{L1} \cdot F_{L2}$$

therefore,

$$L_{C1} = \overline{\overline{F_{L1}} \cdot \overline{F_{L2}}} \cdot \overline{\overline{X_C} \cdot \overline{F_{L1}} \cdot \overline{F_{L2}}}, \quad \dots (9.25)$$

$$L_{C2} = \overline{\overline{F_{L1}} \cdot F_{L2}} + \overline{\overline{X_C} \cdot F_{L1} \cdot F_{L2}},$$

therefore,

$$L_{C2} = \overline{\overline{\overline{F_{L1}} \cdot F_{L2}} \cdot \overline{\overline{X_C} \cdot F_{L1} \cdot F_{L2}}}, \quad \dots (9.26)$$

The logic systems obtained from equations (9.25) and (9.26) are shown in Fig. 9.15.

In order to synchronise an external system to the counter in the multiplex control logic, an external synchronisation signal  $S_y$  is provided. This provides a pulse output when  $X_c = Y_c = 0$ .  $S_y$  is defined by the equation,

$$S_y = \bar{X} \cdot \bar{Y} \cdot C_{L2}, \quad \dots (9.27)$$

and is shown in Fig. 9.15

The operating mode of both the luminance control and the chrominance control are indicated by lamps. Fig. 9.17 illustrates the circuit and Table 9.1 the logic combinations for each operating mode.

	Luminance	Chrominance
Mode 1	$M_L = \bar{F}_{L1}$ $N_L = F_{L2}$	$\bar{F}_{C1}$ $F_{C2}$
Mode 2	$M_L = \bar{F}_{L1}$ $N_L = F_{L2}$	$F_{C1}$ $F_{C2}$
Mode 3	$M_L = \bar{F}_{L1}$ $N_L = F_{L2}$	$\bar{F}_{C1}$ $F_{C2}$
Mode 4	$M_L = F_{L1}$ $N_L = F_{L2}$	$F_{C1}$ $F_{C2}$

Table 9.1. Logic combinations for lamp indications.

#### 4. Decoder multiplex control signals for luminance and chrominance channels

Section 9.5 reveals that the de-multiplexing is realised by switched inversion. The luminance channel has only one inversion sequence; the chrominance channel has two inversion sequences. The inversions are always operated during the Line blanking period; thus any switching transients are not visible.

The switching functions of the decoder have to be delayed compared with the multiplex switching of the encoder; otherwise the switching would appear on the right-hand side of the display. The delay is due to the filters in the luminance and chrominance-pulse demodulators. The compensating delay which is introduced into the decoder logic control channels, positions the inversion switching within the line synchronising pulse. The positioning is not critical, as switching generally takes less than  $1 \mu \text{ sec}$ .

The decoding logic extracts the control pulses required for decoding from the signals  $C_{C1}, C_{C2}, C_{C3}, C_{C4}, L_{C1}, L_{C2}$ , forming the decoder control pulses  $C_{D1}, C_{D2}, L_D$ . Three simultaneously clocked single-stage shift registers driven by a delayed clock then produce the required delayed control pulses,  $C_{DD1}, C_{DD2}, L_{DD}$ .

The primary chrominance control pulse  $C_{D1}$ , is given by:

$$C_{D1} = C_{C3} + C_{C4} ,$$

therefore,

$$C_{D1} = \overline{C_{C3}} \cdot \overline{C_{C4}} , \quad (9.28)$$

The secondary chrominance control pulse  $C_{D2}$ , is given by:

$$C_{D2} = C_{C2} + C_{C4} ,$$

Therefore:

$$C_{D2} = \overline{\overline{C_{C2}} \cdot \overline{C_{C4}}} , \quad (9.29)$$

The luminance signal  $L_D$  is given by:

$$L_D = L_{C2} , \quad (9.30) .$$

The significance of equations (9.28), (9.29), (9.30) is given in section 9.5, where the analogue decoder is discussed.

The shift register delay and logicrealisation of equations (9.28), (9.29) and (9.30) are given in Fig. 9.17; also the generation of  $C_{DD1}$ ,  $C_{DD2}$ ,  $L_{DD}$  is shown.

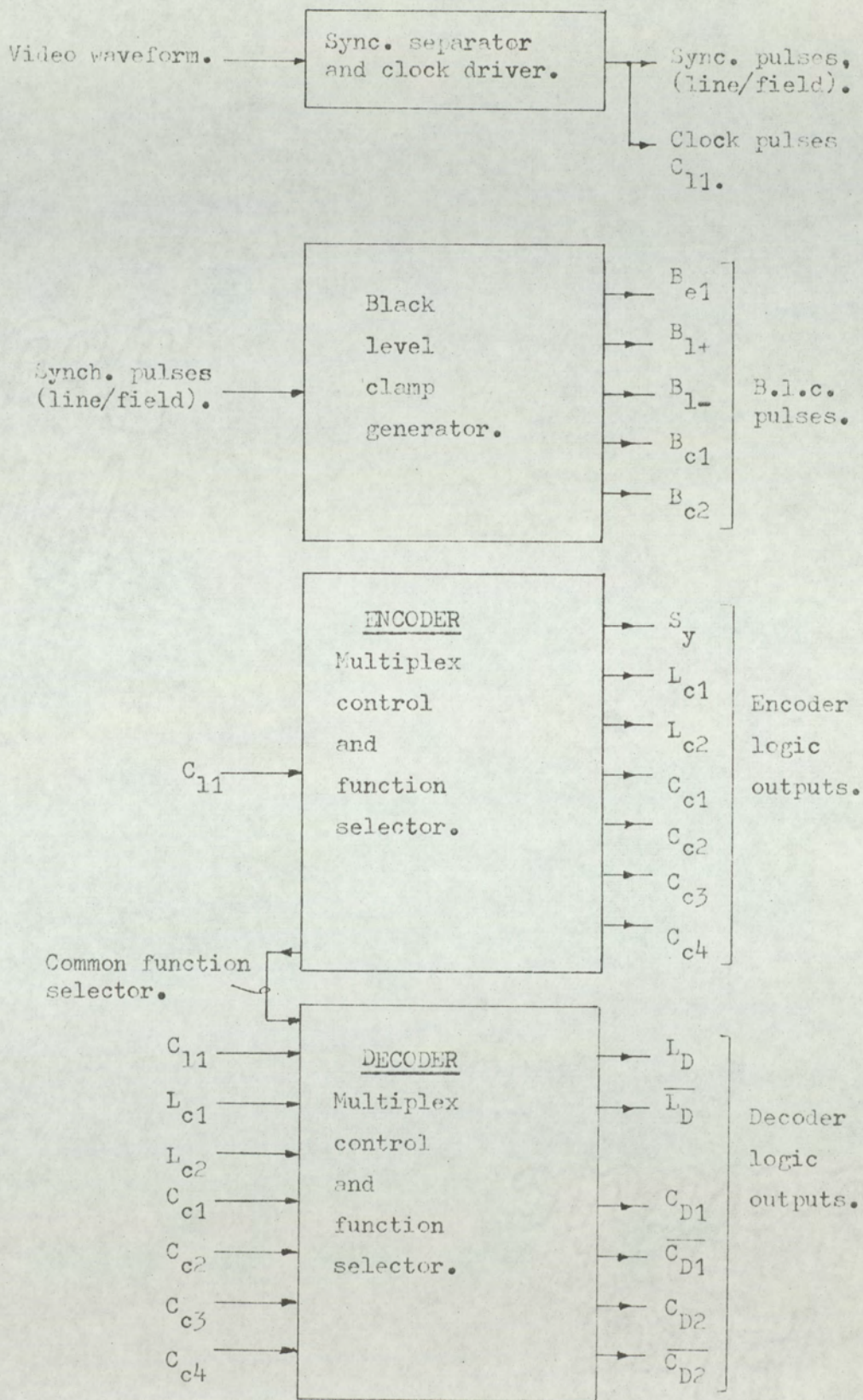


Fig.9-9. Digital control system.

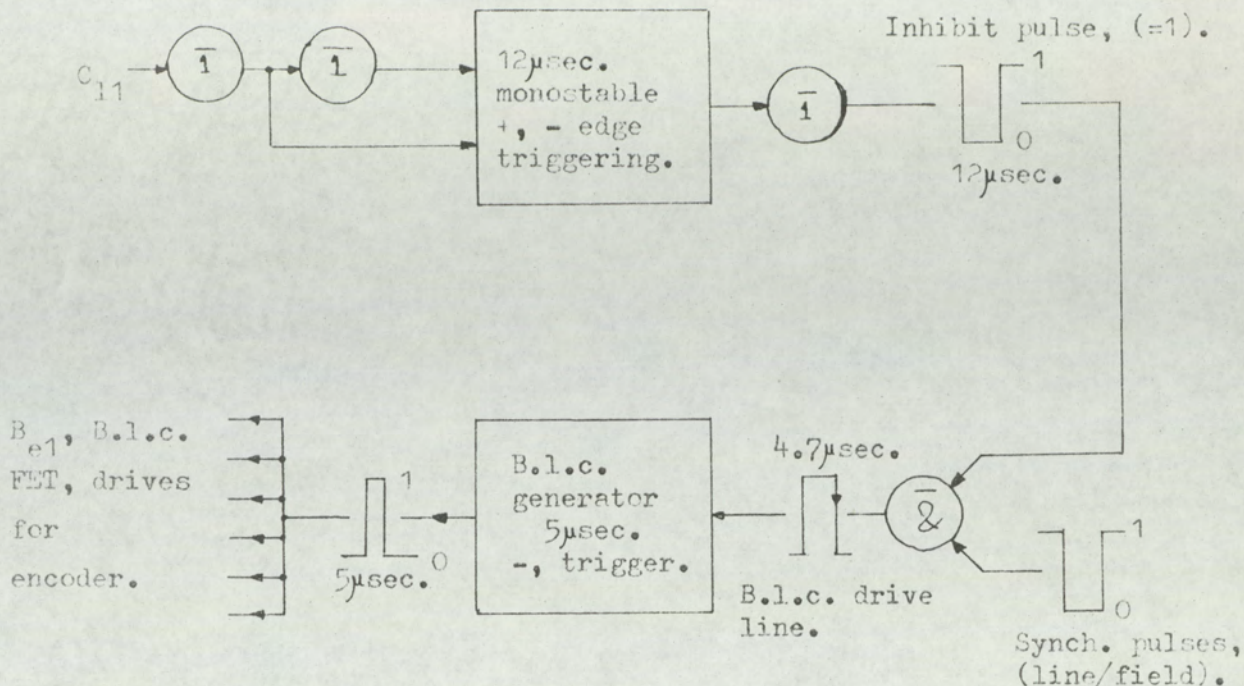


Fig.9-10(a). Encoder B.l.c. generation.

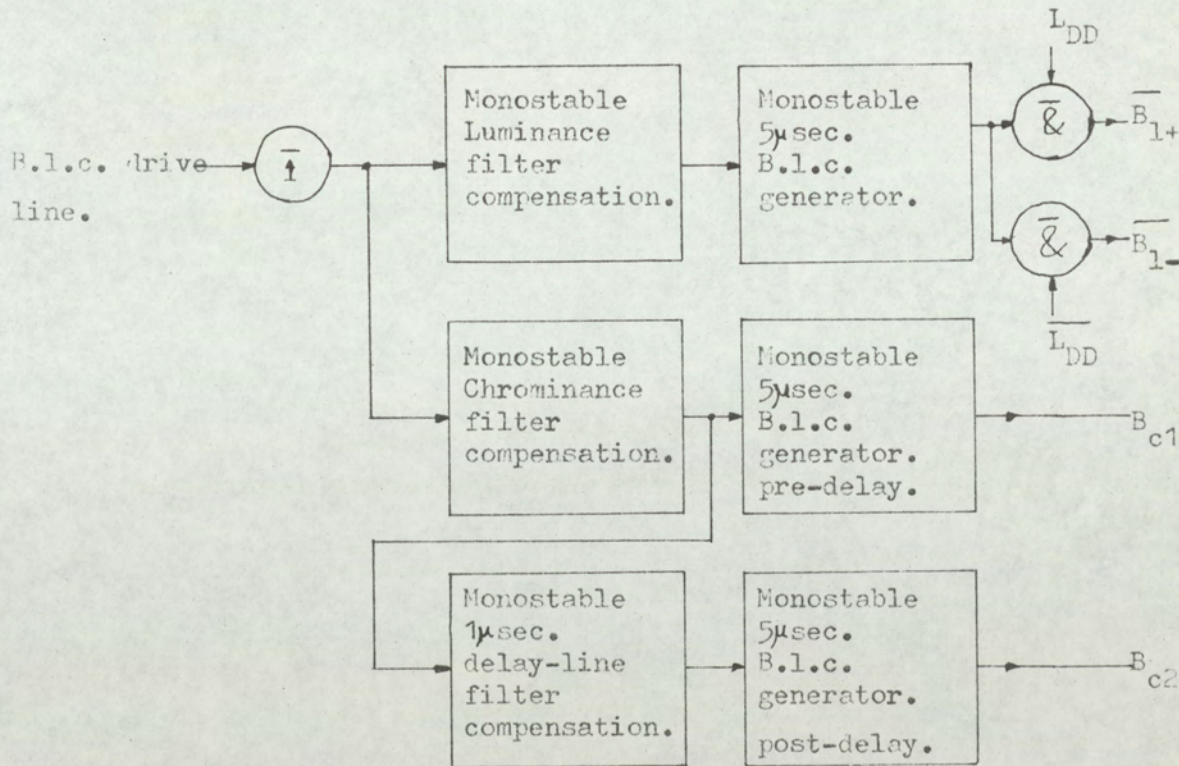


Fig.9-10(b). Decoder B.l.c. generation.

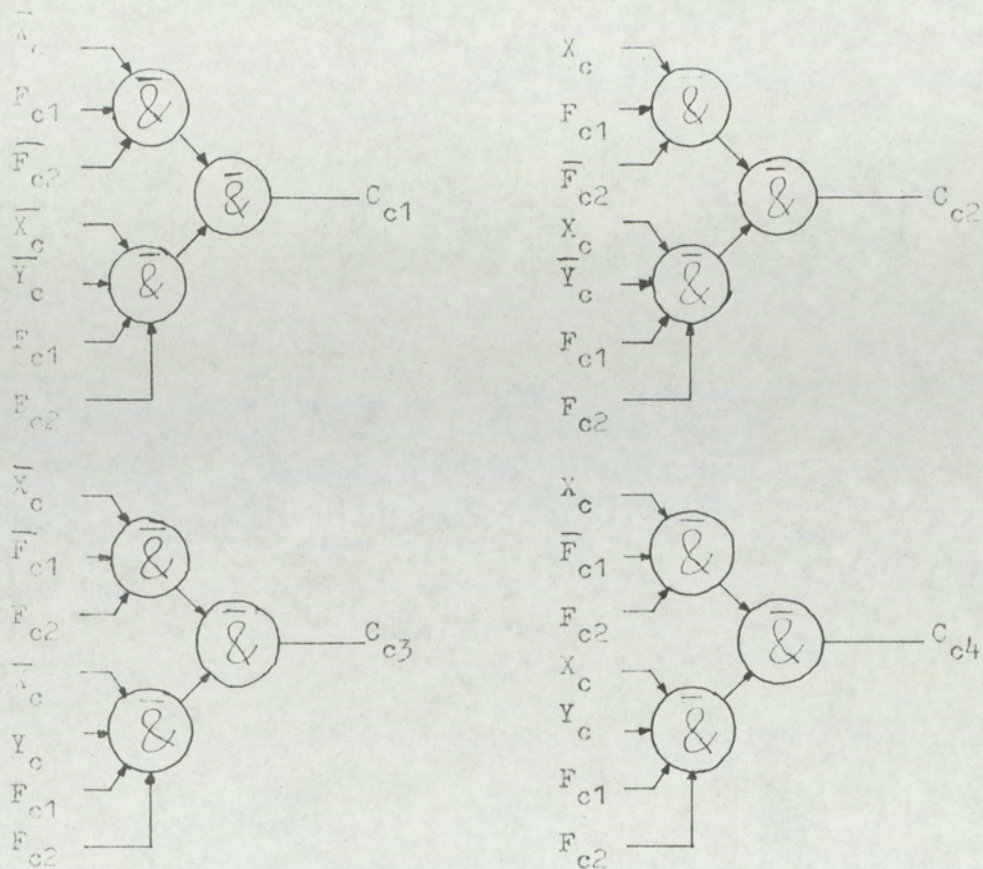
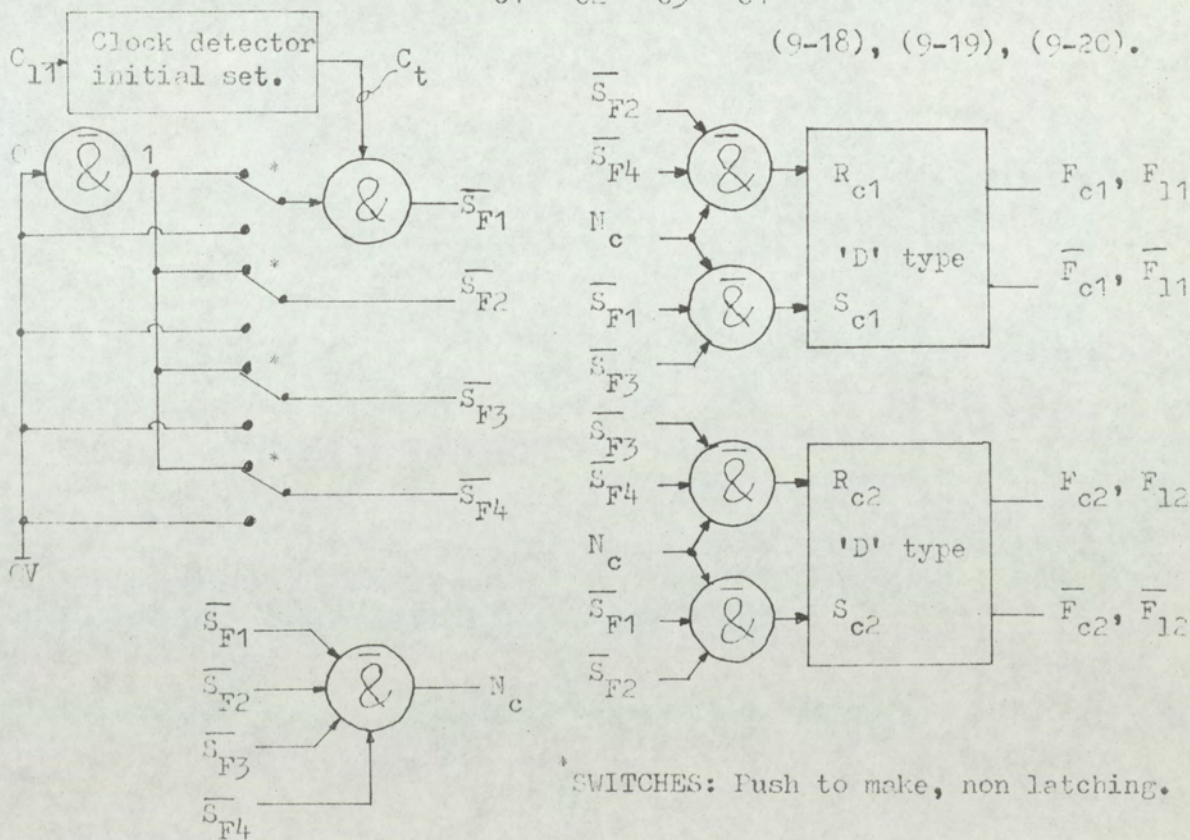


Fig.9-12. Production of  $C_{c1}$ ,  $C_{c2}$ ,  $C_{c3}$ ,  $C_{c4}$  from equations (9-17), (9-18), (9-19), (9-20).



SWITCHES: Push to make, non latching.

Fig.9-13. Switch and mode storage logic. (Applicable for luminance and chrominance channels).

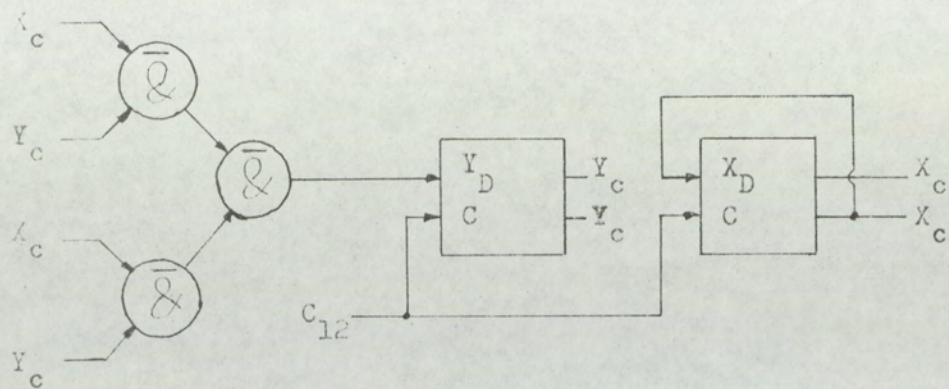


Fig.9-11. Counter for multiplex control.

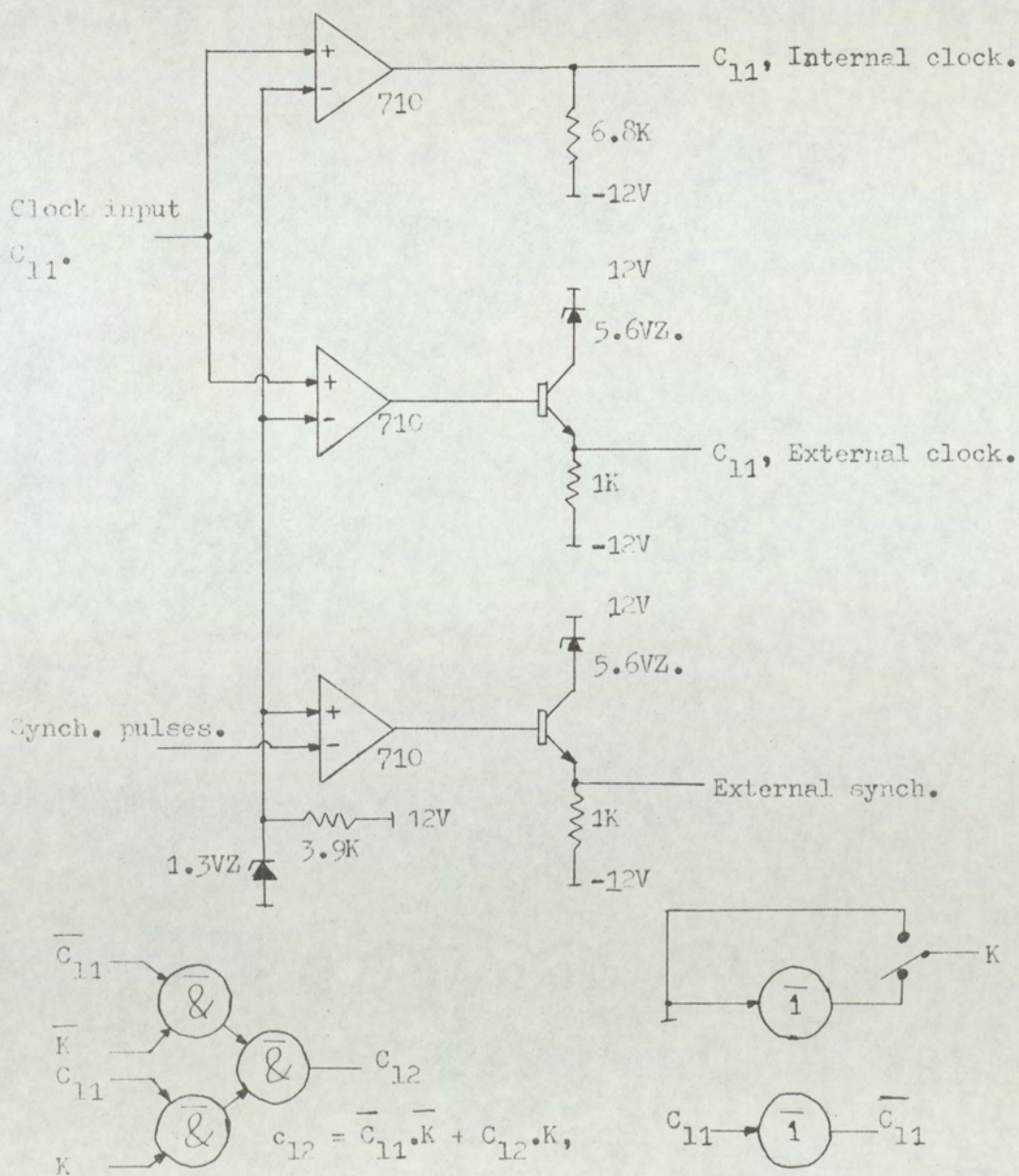


Fig.9-14. Clock inversion, clock and synch. distribution.

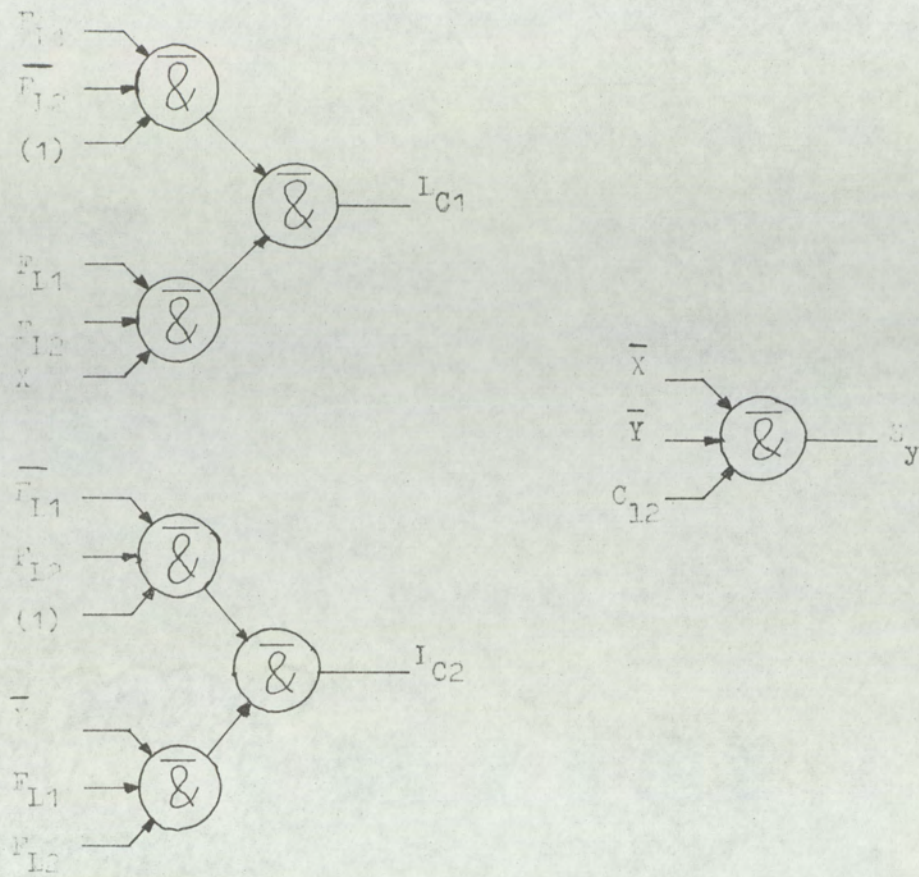


Fig. 9-15. Luminance multiplex logic and synch. pulses.

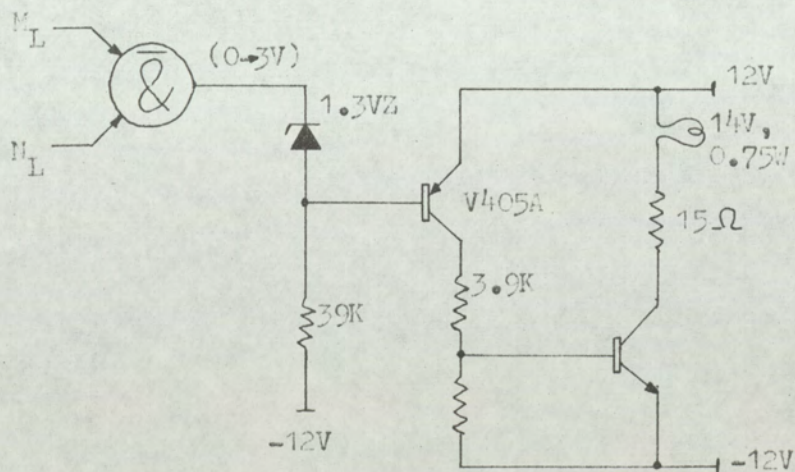


Fig. 9-16. Indicator-lamp circuit showing logic inputs.

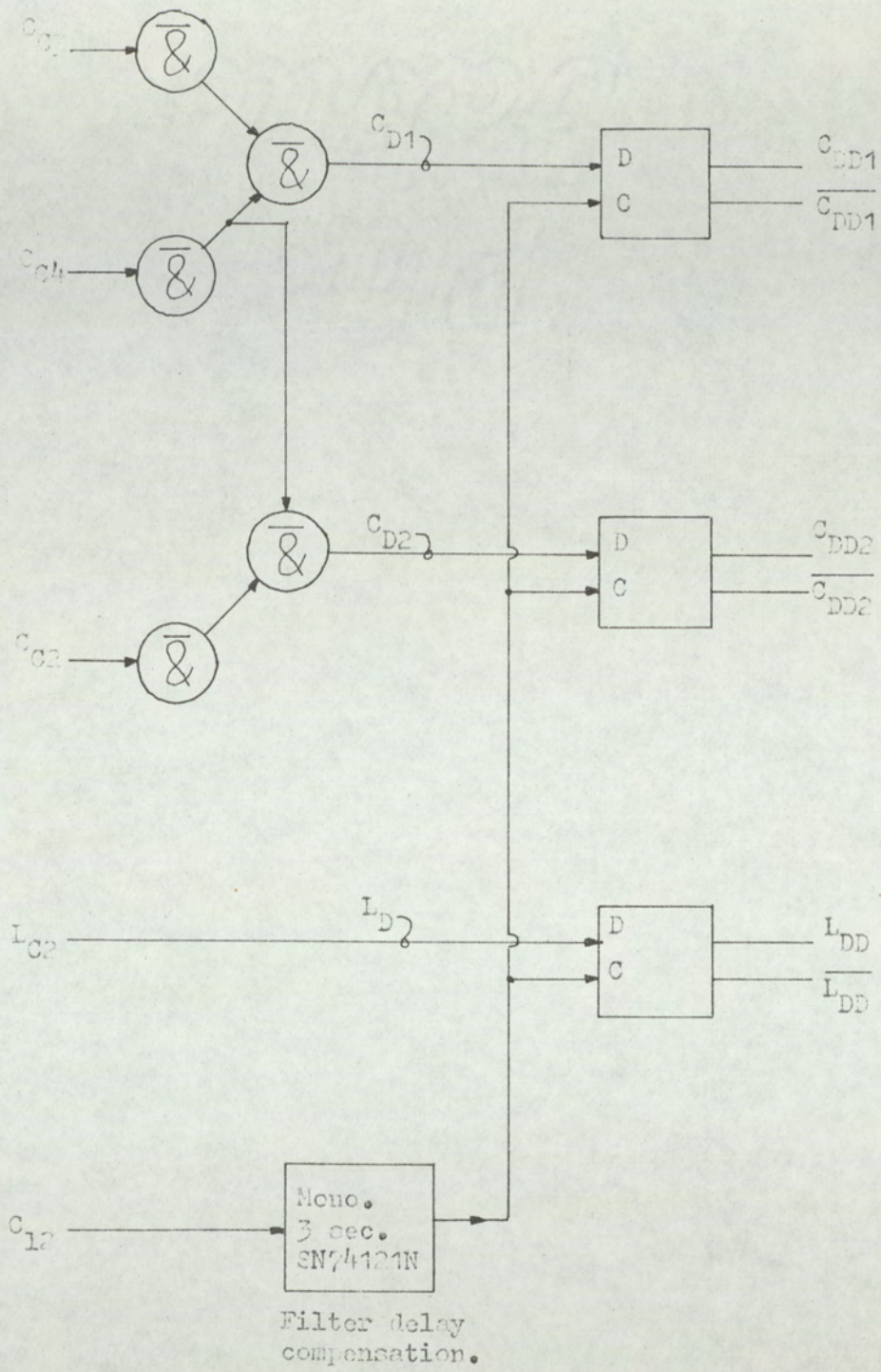


FIG.9-17. Pulse control system for decoder.

#### 9.4 Delta-sigma modulators and demodulators

The delta-sigma modulators used in the C.I.S.S. are of the analogue feedback type with RC integration networks in the forward paths of their closed loops. These modulators were chosen since the total loop delay was low. The storage element is a Motorola MECL III 'D-type' bistable. Experiment showed that the data input of this device exhibited a sensitive threshold, thus making it suitable as a level-detecting device. Since the bistable performs the functions of both storage and level detection, the loop delay is minimised. The pulse rise time of these devices is of the order of one nanosecond. Full details can be found in the literature.

In the system, two delta-sigma-modulators are used. One operates as the luminance encoder, the clock rate being of the order of 50 to 100 MHz. The luminance modulator uses second-order pulse-height adaptation in the feedback path; this is discussed in section 5.5. The other delta-sigma modulator operates over a pulse range of 10 to 20 MHz and encodes the chrominance signals. The pulse rate of the chrominance modulator is one fifth of the luminance modulator. The basic system is illustrated in Fig. 9.1

The divide by 5 logic circuit was obtained from the Motorola data and is illustrated in Fig. 9.18. In this network, the low-input-impedance bistables are used; thus external 'pull-down' resistors on the data and clock inputs are unnecessary.

The luminance and chrominance delta-sigma modulators are shown in Fig. 9.19. In all systems, the wiring was kept short. The devices were mounted on non-conductive board with copper wire (22 swg) used for the short interconnections. The input and output sockets were positioned close to the devices to minimise reflection. The devices used as the level detectors, were the high-input-impedance version of the data-input bistable.

The modulators both use resistive summing network. The resistance values are made small to offset loading effects of the D input and the capacitance for the integrator was chosen by experiment. In the luminance modulator a shift register and two three-input AND/NAND gates are used to detect the second-order positive and negative pulse groups.

The outputs of these gates are summed with the zero-order pulse group obtained from the first bistable. The summing networks are formed by three equal-valued resistive networks. The resistors chosen for the network producing the output pulses has an output impedance of approximately  $75\Omega$ . The pulse output represents the decoded output and is not the digital output  $P_1(t)$ , which is the zero-order pulse group of the first bistable. Thus, the output can be decoded directly by low-pass filtering without introducing second-order pulse group detection.

The filters used for low-pass filtering of the pulse waveforms for the chrominance and luminance digital signals were of B.B.C. design. The luminance filter was

L.P. Link, 5.8 MHz

FL4/512/185

The chrominance filter was built from a B.B.C. design,

75Ω 1.1 MHz Filter,

circuit R34599 A4.

The position of the filters in the system is shown in Fig 9.1.

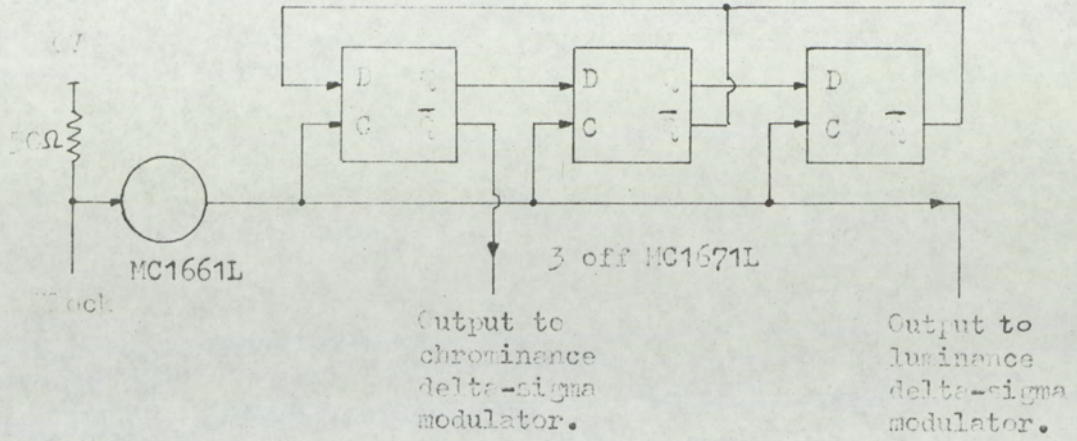


Fig. 9-18. Motorola 5 logic for MECL 3 system.

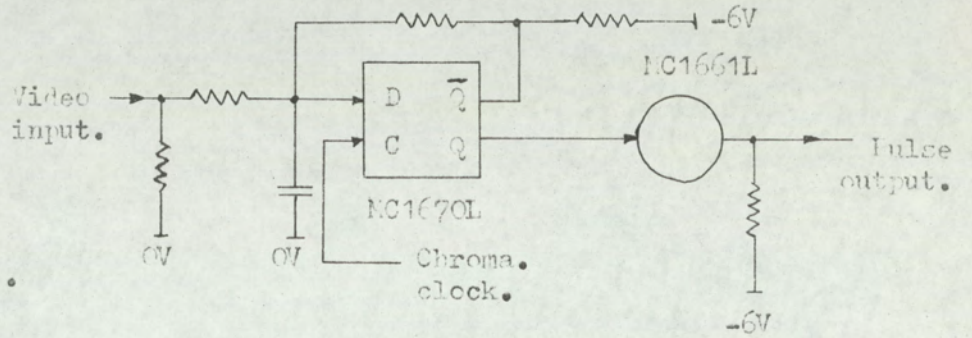


Fig. 9-19(a).

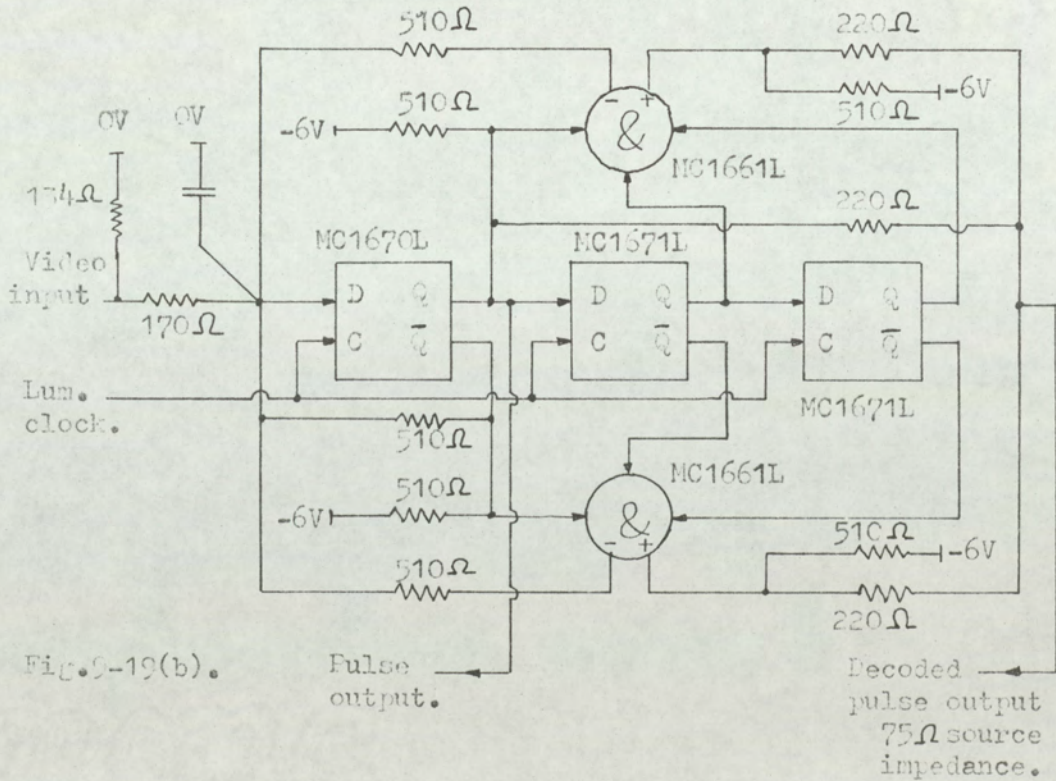


Fig. 9-19(b).

Fig. 9-19(a). Chrominance delta-sigma modulator.

Fig. 9-19(b). Luminance delta-sigma modulator with 2nd order pulse grouping.

### 9.5. Analogue decoder system

The analogue decoder accepts the demodulated pulse waveforms from the luminance and chrominance delta-sigma modulators, together with control and B.L.C. pulses. From these signals, the decoder reconstructs the red, green and blue signals  $E_{rd}$ ,  $E_{gd}$ ,  $E_{bd}$  to drive the display device. (Suffix d indicates that the signals include transmission noise, and have the chrominance information averaged in the vertical).

The decoder can be subdivided into three subgroups:

1. Luminance channel processing.
2. Chrominance channel processing.
3. Final signal matrixing.
1. Luminance channel processing.

The luminance channel has to amplify the demodulated luminance signal, de-emphasise the signal, introduce black-level clamping and perform de-multiplexing. In modes 1,2,3 for the luminance signal, no dynamic system switching is involved; the network is fixed. However, in mode 4, when the transmission sequence is:

$$\dots A_{2n}, -A_{2n}, A_{2n}, -A_{2n}, \text{ etc } \dots$$

Then a switched inversion process is necessary operating at line frequency. Thus, the gain of the channel in mode 4 alternates from positive to negative on successive lines, the switching being performed during the line synchronisation pulse. The switching network is designed to minimise changes in d.c level on successive lines; thus two parallel sub-channels are introduced to allow independent control of d.c levels.

The luminance channel also has a delay line of 1  $\mu$ sec introduced to compensate for the differential delay in the luminance and chrominance channels due to the low-pass filters.

The luminance channel is shown in Fig 9-20. The circuits of the amplifiers used are given in appendix 1. The amplifiers are designed around a single high-gain stage; the external components shown in Fig.9-20 produce the required operations.

The stages are as follows:

#### Input amplifier

The input amplifier is driven from a low-resistance potentiometer to adjust the input signal level. The potentiometer (in conjunction with a parallel resistor) provides a line termination of 75 $\Omega$ . The gain of the amplifier is set at (+4) and a d.c level control can set the output d.c. level for differing input d.c. levels. The stage, using a 75 $\Omega$  series resistor, provides the drive for the compensating delay line.

#### Delay Line

The delay line is a 1  $\mu$ sec passive network, it is loaded by a 75 $\Omega$  resistor for matching. The line is a Matthey Printed Products Limited, silver-star delay line, capable of propagating the full luminance band-width.

#### Buffer Amplifier

The buffer amplifier provides a high-impedance load for the delay; it has a gain of 4.

### De-emphasis Network.

The transfer function of the luminance de-emphasis network is:

$$A_{de}(f) = \frac{1}{1+j2\pi f(T_{Ld})} \quad , \dots \dots \dots (9-31)$$

The network compensates for the pre-emphasis network introduced in the encoder, as expressed by equation (9-14). The de-emphasis characteristic is shown in Fig 9-7a, complementing the pre-emphasis characteristic.

### Low-output-impedance buffer

A low-output-impedance buffer responds to the voltage across the de-emphasis capacitor, the amplifier having a high input impedance. The amplifier drives two parallel B.L.C circuits.

### B.L.C circuits.

The operation of each B.L.C. circuit is identical to that described in section 9-2,2. However, two parallel circuits are provided, the operation depending on the operating mode of luminance channel. When  $A_{2n}$  is transmitted, then  $L_{dd}$  and  $B_{\ell+}$  are activated. Similarly, when  $-A_{2n}$  is transmitted then  $\overline{L_{dd}}$  and  $B_{\ell-}$  control the function. Finally, in mode 4 when  $A_{2n}$ ,  $-A_{2n}$ , etc, is transmitted the system switches between the two operating conditions. This always produces  $-A_{2n}$  at the final output, whether the system is operating in mode 2,3 or 4. The use of two circuits allow differences in black level between successive lines to be eliminated, when operating in the alternating mode 4, D.C level controls are provided on both B.L.C. outputs.

### Switched inverter stage

The inverter stage operates as a unity-gain amplifier. However, depending upon whether  $L_{(M)} = 1$  or  $0$ , the gain of the amplifier is respectively  $-1$  or  $+1$ . The two equivalent forms of the amplifier are shown in Fig 9-20. The changeover period, which is in the line sync. pulse, takes in the order of  $1 \mu\text{sec}$ . The output of the switched inverter applies the luminance signal to the final matrixing network.

#### 2. Chrominance channel processing.

The chrominance channel can be sub-divided into two sections. The first section is similar to the luminance channel, except that the delay line stage is omitted. This section is shown in Fig 9-21. Only a single black-level clamp circuit is used. The switched inverter is similar to the luminance channel but, since it only has one input, channel switching is omitted. The switched inverter inverts the gain of the channel, depending on whether mode 2 or 3 is in operation. In mode 4, the gain changes every two lines, since in this mode the transmission sequences is:

$$\dots B_{2an}, C_{2an}, -B_{2an}, -C_{2an} \dots$$

Thus, when switching is applied the output becomes:

$$\dots B_{2an}, C_{2an}, B_{2an}, C_{2an} \dots$$

The logic drives from the decoder were discussed in section 9-3,4.

The transfer function of the chrominance de-emphasis network is given by:

$$A_{dc}(f) = \frac{1}{1+j2\pi f(T_{cd})}, \quad \dots\dots (9-32)$$

As with the luminance de-emphasis, the characteristics of pre-emphasis and de-emphasis are shown in Fig 9-7a. In the chrominance channel, the de-emphasis buffer has a gain of 4; thus the input channel gain is potentially 16. Details of the amplifier circuit used in each stage are given in appendix 1. The primary B.L.C pulse is shown as  $B_{c1}$  in Fig 9-21.

The second stage of the decoder incorporates the one-line, delay-line store and performs the sum and difference functions to obtain the colour-difference signals. The system is shown complete in Fig.9-22.

The system stages are as follows:

#### Delay line and amplifier

The output of the primary decoder drives an active delay circuit. The delay circuit stores one line of chrominance signal by having a delay of 64  $\mu$ sec, the line period. The chrominance signal is carried on an amplitude-modulated carrier, the frequency being at colour-subcarrier. Details of the delay line, modulator and demodulator are given in appendix 3. The overall attenuation of the delay line and processing circuits is 0.14.

#### Balanced amplifier.

The balanced amplifier is also driven from the primary decoder and produces a differential output. The function of the differential output is to produce signals for operating linear addition and subtraction functions.

### Filter networks.

Two parallel low-pass filters are used to filter out frequency components above chrominance base-band; these frequency components are primarily generated by the delay-line modulators. The filters are sixth-order Butterworth, details are given in appendix 4. The filters also include a resistive summing network, both being driven by the output of the delay line. However, as shown in Fig. 9-22, the differential output of the amplifier in parallel with the delay line, feeds a positive signal to one summing junction and an inverted signal to the other junction. Thus, the output of the filters represent the sum and the difference of successive lines of chrominance. The resistive addition network includes a series, preset control for balancing and the sum and difference functions. The filters are introduced after addition and subtraction as the inclusion of the filter in the delay line output would have produced a delay in excess of 64  $\mu$ sec. Thus, two filters are required.

### Black-level clamps.

The black-level clamp circuits are similar to those discussed in section 9.2,2. However, the driver stage provides a gain of 3 and the high-input-impedance buffer has a gain of 2. The input-signal level to each black-level clamp circuit is controlled by a preset potentiometer. Both B.l.c choppers operate simultaneously the drive being the delayed drive  $B_{C2}$ , section 9.3, Fig. 9-10.

### 3. Final signal matrixing.

The network of the signal matrixing system is shown in Fig. 9-23. The network has a switched unity-gain inverter in the

difference channel and a linear addition matrix for producing the signals  $E_{Rd}$ ,  $E_{(d)}$ ,  $E_{Bd}$ .

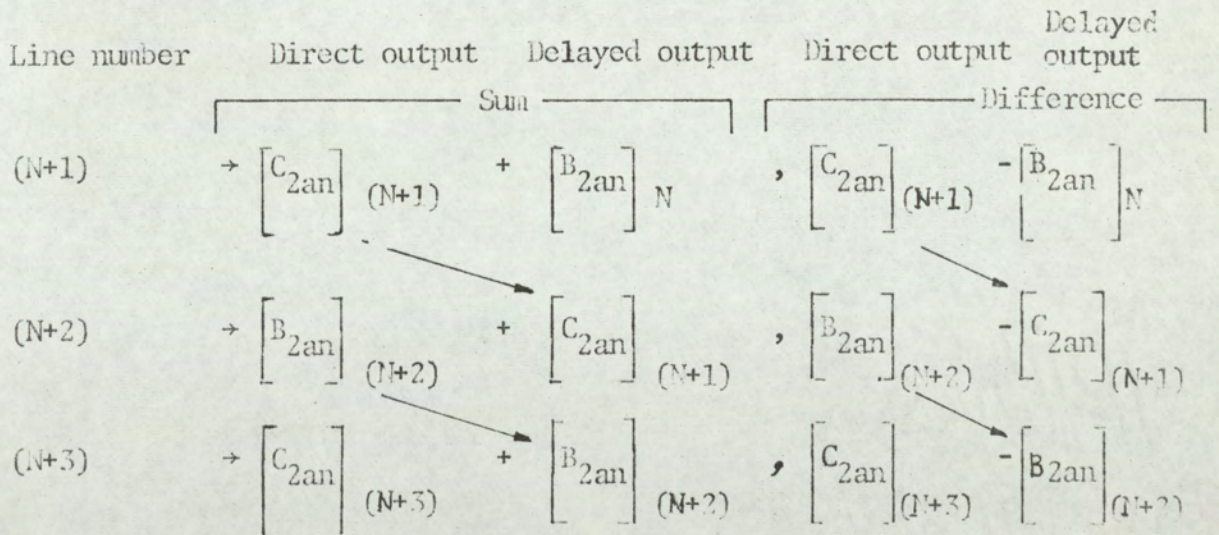
The secondary de-multiplexing switch operates as follows:

The output of the primary decoder, Fig. 9-21 produces chrominance signals, which alternate on successive lines to produce the transmission sequence:

$$\dots\dots [B_{2an}]_N [C_{2an}]_{(N+1)}, [B_{2an}]_{(N+2)} [C_{2an}]_{(N+3)}, \dots$$

The bracket N i.e.  $[ \dots ]_N$ , represents the signal actually transmitted on the  $N^{th}$  line.

The line-alternating chrominance signal then passes through the delay line and sum and difference channels, thus using each chrominance signal twice. The output of the sum and difference channels is as follows:



etc.

From the above sequence, the polarity of the sum signal is seen to remain constant at all times; however, the difference signal alternates in polarity line-by-line. Thus, the functions of the secondary de-multiplexing switch is to invert the gain of the difference

channel on successive lines. Switching, therefore, occurs at line rate and is the same for operating nodes 2,3,4. The output of the two channels are adjusted so that the sum and difference signals are:

$$\text{Sum} = (B_{2an} + C_{2an}),$$

$$\text{Difference} = (B_{2an} - C_{2an}).$$

The decoding is as follows:

Putting decoded values  $E_{Rd}$ ,  $E_{Gd}$ ,  $E_{Bd}$ ,  $E_{Ld}$  in equations (8-35) and (8-36), the sum channel is given by:

$$(B_{2an} + C_{2an}) = 2 \cdot k_1 (E_{Rd} - E_{Ld}).$$

Similarly, the difference signal is:

$$(B_{2an} - C_{2an}) = 2 \cdot k_2 (E_{Bd} - E_{Ld}),$$

Thus, rearranging and eliminating  $k_1$  and  $k_2$  from equations (8-40), (8.41), gives:

$$(E_{Rd} - E_{Ld}) = \frac{1}{2 \cdot \lambda \cdot \ell} (B_{2an} + C_{2an}),$$

$$\text{and } (E_{Bd} - E_{Ld}) = \frac{1}{2 \cdot \lambda \cdot n} (B_{2an} - C_{2an}),$$

From equation (7-46), eliminating  $D_R$ ,  $D_G$ ,  $D_B$  using equations (7-43), (7-44), (7-45) gives:

$$(E_{Gd} - E_{Ld}) = - \frac{\ell}{m} (E_{Rd} - E_{Ld}) - \frac{n}{m} (E_{Bd} - E_{Ld})$$

Thus, substituting for  $(E_{Rd} - E_{Ld})$  and  $(E_{Bd} - E_{Ld})$  gives:

$$(E_{Gd} - E_{Ld}) = - \frac{1}{2m\lambda} \cdot \{ (B_{2an} + C_{2an}) + (B_{2an} - C_{2an}) \}.$$

Hence, eliminating  $\ell, m, n$  using equations (7-36), (7-37) and (7-38) and  $\lambda$  using equation (8-40a), the colour-difference signals in terms of the transmission signals are:

$$(E_{Rd} - E_{Ld}) = 0.407 \cdot (B_{2an} + C_{2an}), \quad \dots\dots\dots(9-33)$$

$$(E_{Gd} - E_{Ld}) = - 0.208 \cdot \{ (B_{2an} + C_{2an}) + (B_{2an} - C_{2an}) \}, \quad \dots\dots\dots(9-34)$$

$$(E_{Bd} - E_{Ld}) = 1.069 \cdot (B_{2an} - C_{2an}), \quad \dots\dots\dots(9-35).$$

The green colour difference signal can be extracted by switching the green colour difference always to the channel carrying  $B_{2an}$  (either the direct or delayed signal). However, the simplest decoding is obtained, without switching, by using a simple addition of the sum and difference signals. Thus, the secondary de-multiplex switch effectively forms the channel selection for green.

The decoded luminance  $E_{Ld}$  (as discussed in section 9-5 and Fig 9-20) is added to the red, green and blue colour-difference signals. Thus  $E_{Rd}$ ,  $E_{Gd}$ , and  $E_{Bd}$  are formed as:

$$E_{Rd} = E_{Ld} + (E_{Rd} - E_{Ld}).$$

Therefore,

$$E_{Rd} = E_{Ld} + 0.407 (B_{2an} + C_{2an}), \quad \dots\dots\dots (9-36)$$

Similarly,

$$E_{Gd} = E_{Ld} - 0.208 \cdot \{ (B_{3an} + C_{2an}) + (B_{2an} - C_{2an}) \}, \dots\dots (9-37)$$

and

$$E_{Bd} = E_{Ld} + 1.069 \cdot (B_{2an} - C_{2an}), \quad \dots\dots\dots (9-38).$$

The channels carrying the signals  $(B_{2an} + C_{2an})$  and  $(B_{2an} - C_{2an})$  are adjusted to have a signal range of -1 volt to +1 volt. Thus, to produce the normalised output voltage range when  $B_{2an}$ ,  $C_{2an}$  have signal ranges of -1 volt to +1 volt, amplification

is required in the sum and difference channels. This amplification is introduced at the final matrix. It is necessary since the luminance signal  $E_{Ld}$  has a one volt signal range, not including the synchronisation pulse.

The peak signal excursion of the sum and difference channels can be determined by substituting for  $B_{2an}$ ,  $C_{2an}$  from equations (8-44) and (8-45).

Thus,

$$(B_{2an} + C_{2an}) = 1.7201 \cdot E_{Rd} - 1.4403 \cdot E_{Gd} - 0.2799 \cdot E_{Bd},$$

$$(B_{2an} - C_{2an}) = -0.2799 \cdot E_{Rd} - 0.5491 \cdot E_{Gd} + 0.8289 \cdot E_{Bd},$$

Since the sum and difference channels are adjusted to have the same gain, then the gain coefficient, which is common to both channels is 1.7201, the coefficient of  $E_{Rd}$  for the sum channel; this represents the peak signal excursion of  $(B_{2an} + C_{2an})$ .

Thus, the decoding equations become:

$$E_{Rd} = E_{Ld} + \overbrace{(0.407 \cdot 1.7201)}^{0.700}, (B_{2an} + C_{2an})^*, \dots \quad (9-36a)$$

$$E_{Gd} = E_{Ld} - \overbrace{(0.208 \cdot 1.7201)}^{0.358} \cdot \{(B_{2an} + C_{2an})^* + (B_{2an} - C_{2an})^*\} \dots \quad (9-37a)$$

$$E_{Bd} = E_{Ld} + \overbrace{(1.069 \cdot 1.7201)}^{1.839} \cdot (B_{2an} - C_{2an})^*, \dots \quad (9-38a)$$

\* indicates the signals have been reduced by a factor 1.7201 to limit the peak excursion of  $(B_{2an} + C_{2an})$  from -1 volt to +1 volt. This is only a design requirement and is not fundamental to the system.

The resistance values shown in Fig 2-23 for the final matrixing are calculated from the coefficients shown in equations

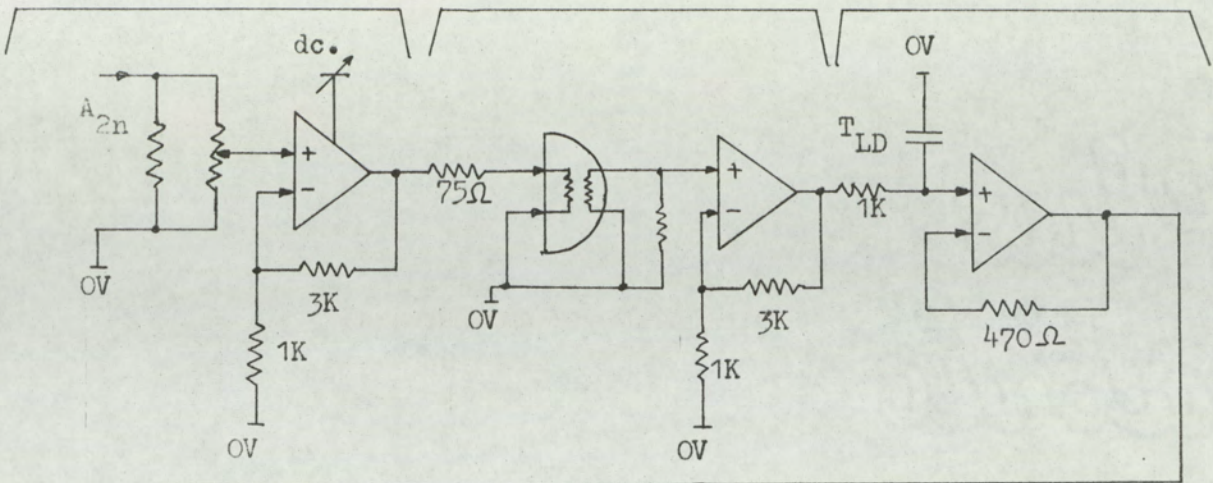
(9-36a), (9-37a), (9-38a). With a feedback resistor of 5.6 K in the virtual-earth amplifier, the colour-difference channel input resistors for the red, green and blue colour-difference signals are respectively, 8.00K $\Omega$ , 15.64K $\Omega$ , 3.06K $\Omega$ .

A facility was provided for re-introducing the synchronisation pulses in the output waveforms  $E_{Rd}$ ,  $E_{Gd}$ ,  $E_{Bd}$ .

X4, amplifier  
d.c. level set.

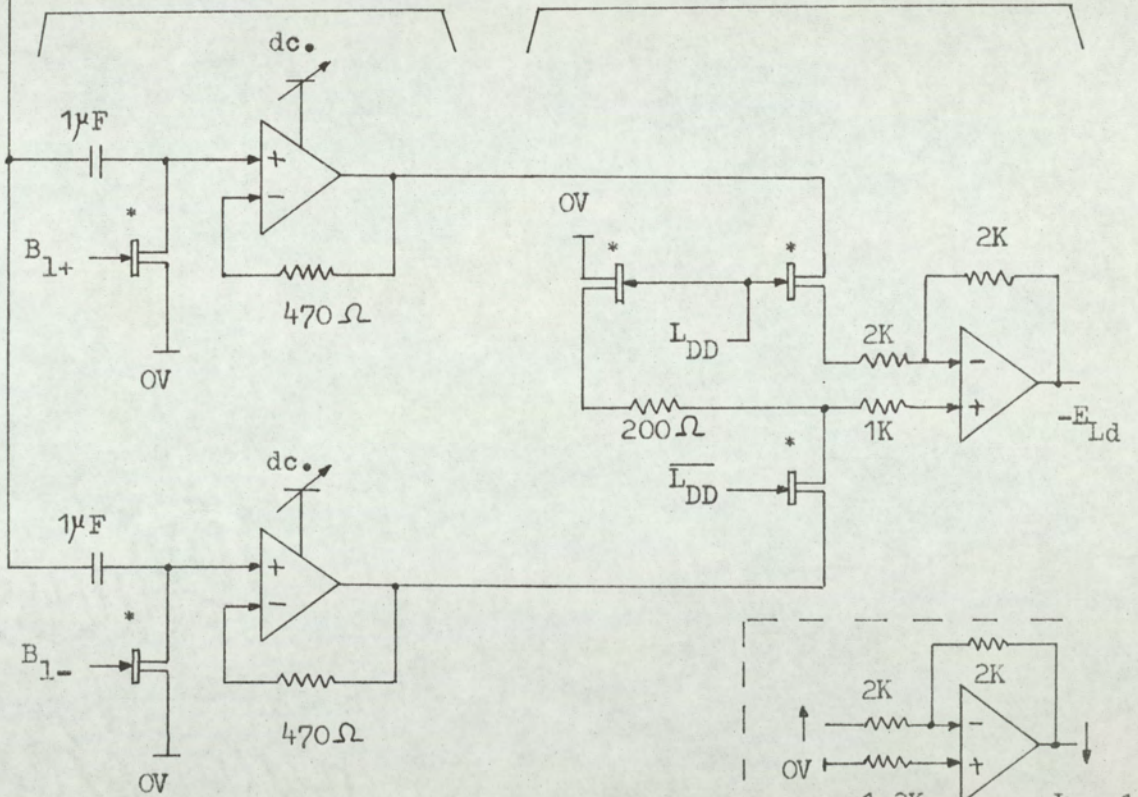
1 sec. delay-line  
X4, amplifier.

De-emphasis network  
B.l.c. driver stage.

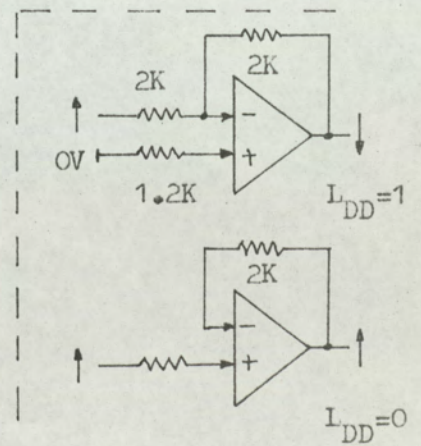


B.l.c. chopper, buffer.

Switched inverter.

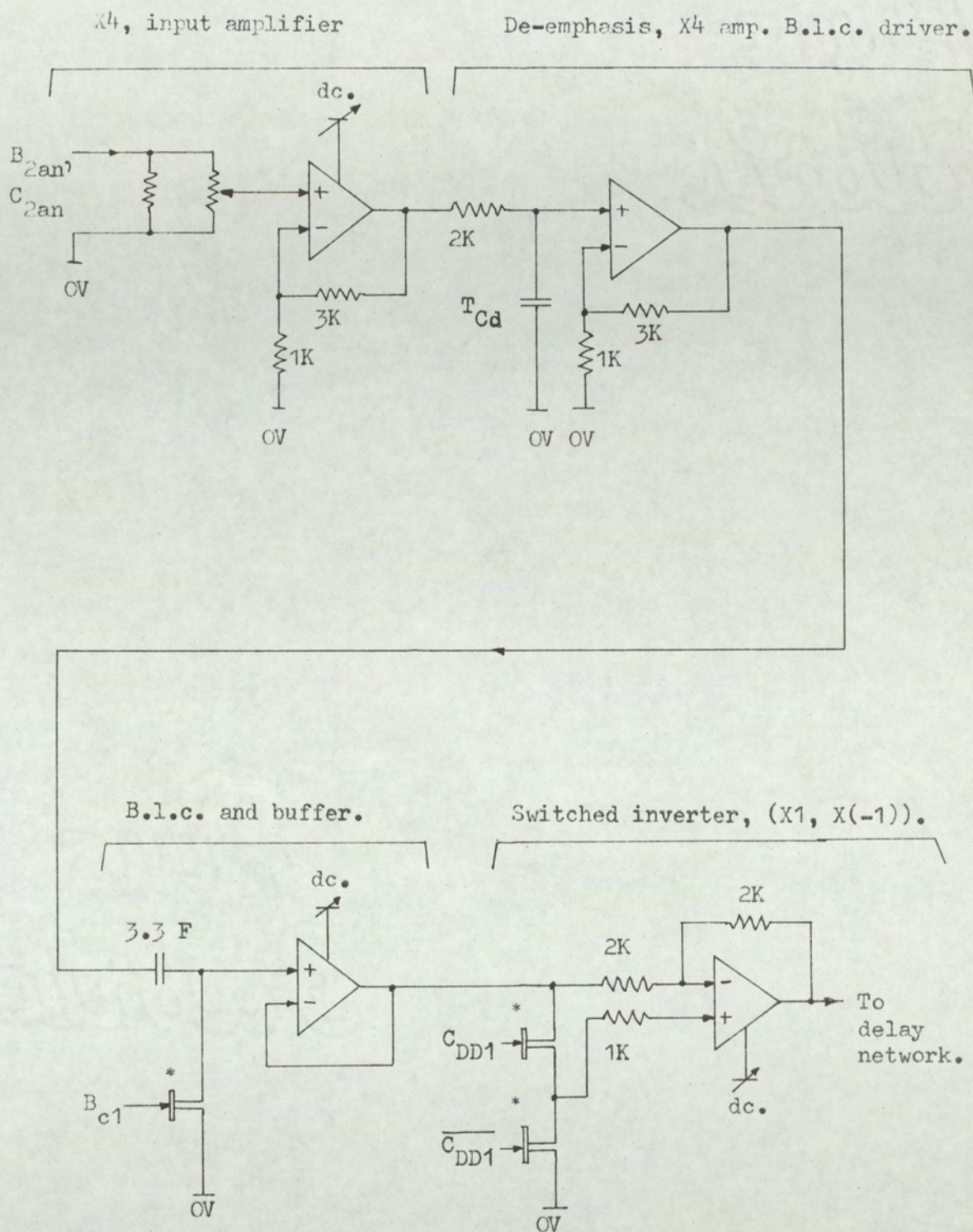


\* All FET's driven from pulse generators, (details in appendix 2).



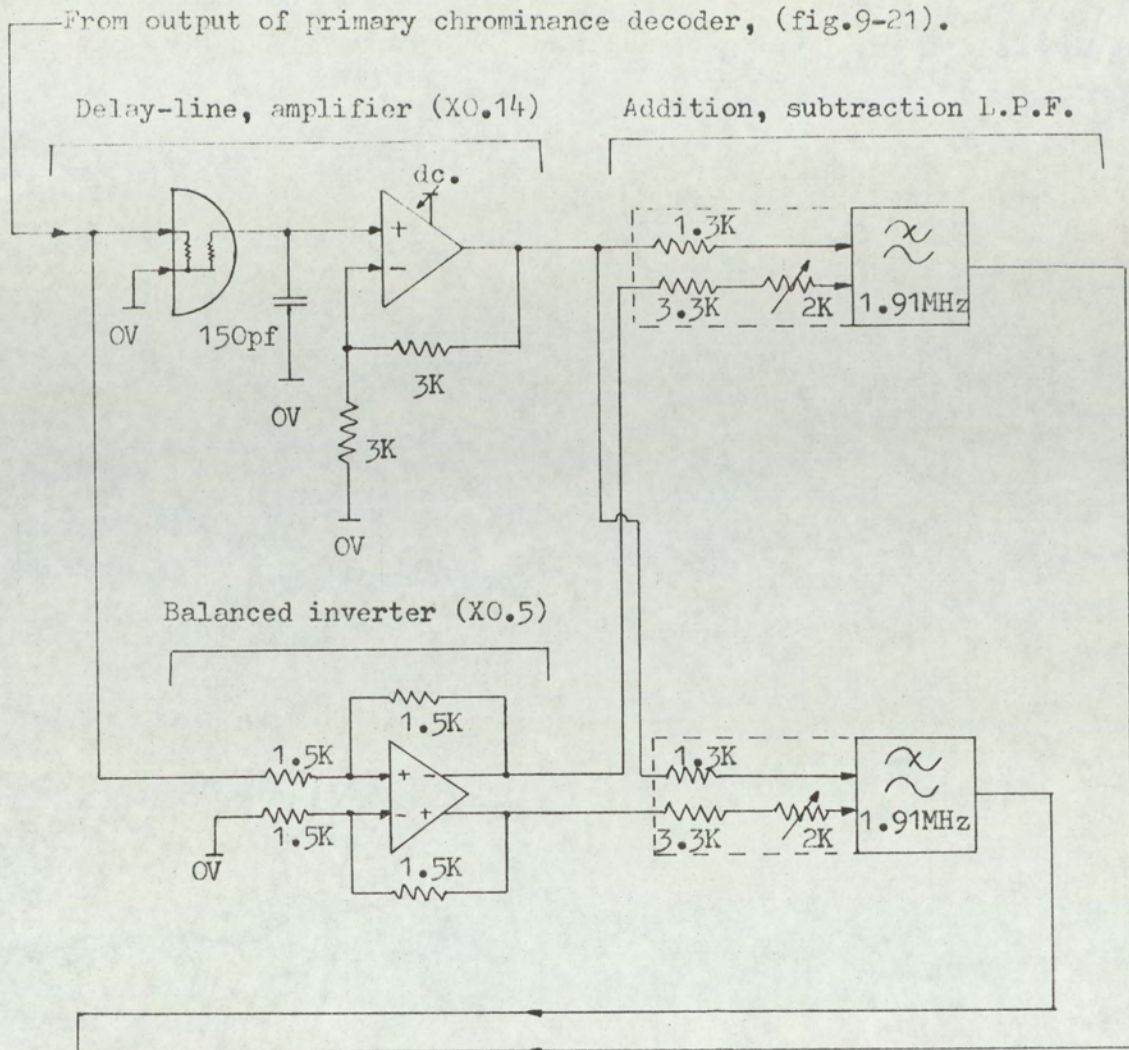
Equivalent network of inverting stage.

Fig.9-20. Luminance-channel decoder.



\* All FET's are driven from pulse generators,  
 details are given in appendix 2.

Fig.9-21. Primary chrominance decoding.



\* All FET's driven from pulse generators, (details appendix 2)

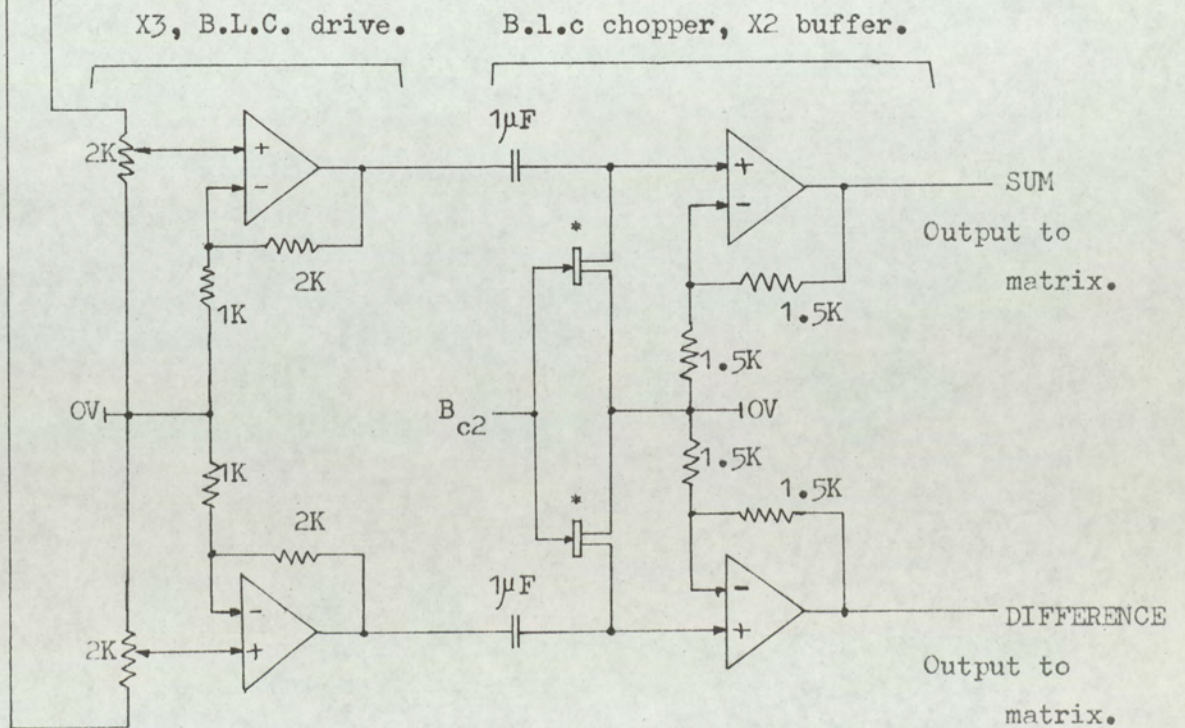


Fig.9-22. Chrominance-channel delay, sum and difference.

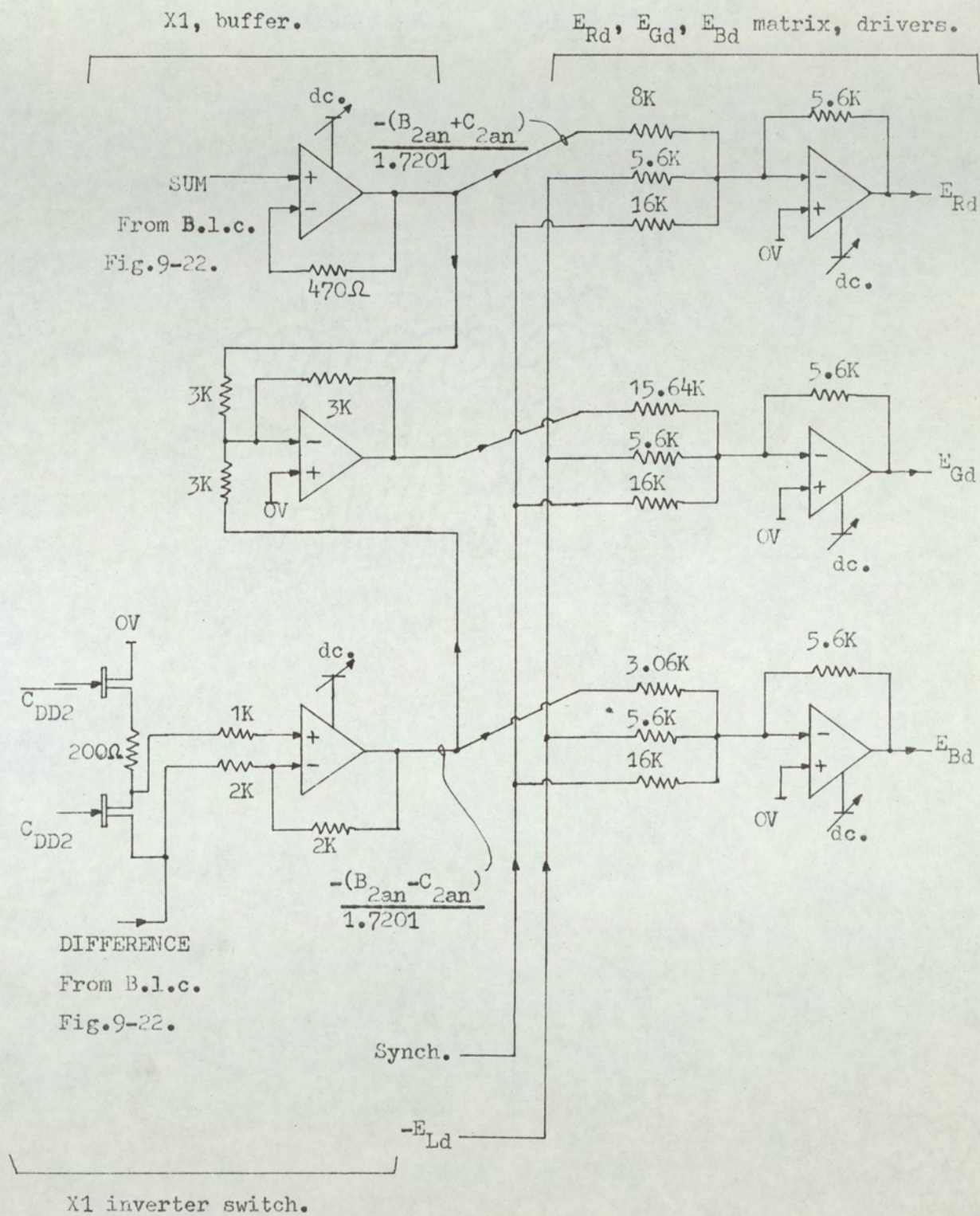


Fig.9-23. Final signal matrixing.

### 9.6 Chopped filtering of luminance and chrominance signals.

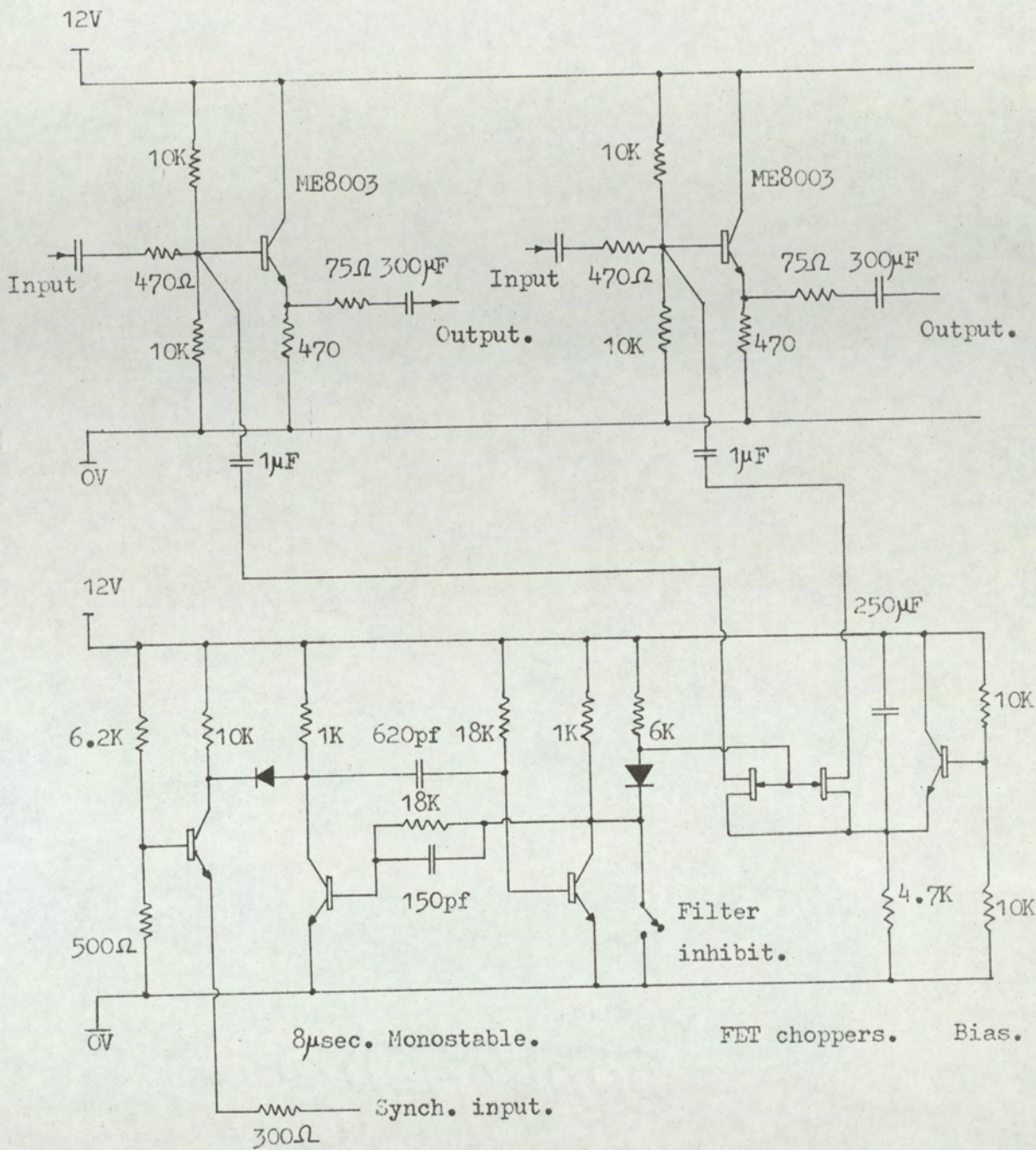
Quantisation noise introduced during the black-level period of the luminance and chrominance signals, can increase the visual picture impairment. This impairment is due to the black-level clamp circuits being perturbed by noise on the signal and causing the effective d.c. level of the picture to change line by line.

To minimise this effect, a chopped filter was introduced between the delta-sigma modulators and low-pass filters. The filter is effectively an RC network with a FET switch in the capacitor lead. The network is shown in Fig 9-24. The capacitor is switched into circuit for about 8  $\mu$ sec during the black level. The capacitor is large, thus voltage changes from line to line can only change by small amounts. The FET's are driven from a monostable which is triggered from the trailing edge of the synchronisation pulses (positive going pulses). The duration of the monostable is about 8  $\mu$ sec. The chopper circuit effectively clamps the black level at a constant voltage, the voltage level being determined by an average over several lines. The synchronisation pulse source was obtained from the external synchronisation source described in Fig. 9-14, section 9-3.

The complete circuit is shown in Fig 9-24 for reference.

Luminance filter.

Chrominance filter.



Diodes..... OA200.

Fig.9-24. Luminance and chrominance chopped filters.

CHAPTER 10. COMPUTER PROGRAMMING AND COMPARATIVE SIMULATION.

## 10.1 Deltamodem model and delta-modulator comparative simulation.

During the development of the deltamodem model, a comparative simulation was performed. In the simulation, algorithms were developed which performed exactly the functions of the model and a delta-modulator.

The program was written to demonstrate the feasibility of the model for performing a delta-modulator function. At this stage in development, the model had not been rigorously proved; thus it was necessary to produce an accurate working system to show that there was equivalence between the two systems. The program demonstrated the exactness of the model by producing two identical pulse sequences when both systems were excited by the same input signal. In the systems, the integrated pulse waveforms were produced by addition. A '1' pulse was given a weighting  $+\pi$  while a '0' pulse was given a weighting  $-\pi$ , thus simplifying the integration. The computer program as well as a practical systems verification, produced a method which, through analysis, has produced a rigorous basis for equivalence. The program is therefore presented as an essential stage in the development of the model analysis as well as demonstration of the model's exactness.

The program is presented in its original form, since once equivalence had been demonstrated, further computer program development was considered unnecessary. As a result of the order of model development, the initial conditions given in the program are not the same as those given in chapter 3; however, the initial conditions are compatible.

In both the deltamodem model and the delta-modulator systems, the step height of the demodulating integrators were normalised to  $\pi$  units. The choice of  $\pi$  was obtained from the algorithm for the model. The clock rate of the model and delta-modulator was the same for both systems; also the input signals were made identical. Thus, with correct choice of initial conditions, equivalence was demonstrated by the generation of identical pulse waveforms for both systems. The program incorporated both systems, thus allowing the results to be printed out simultaneously to aid comparison.

The basic operations of the program is given as well as the program structure. The program is written in ALGOL and was executed on an I.C.L. 1900 machine.

The discussion of the program commences with further detail on the relation of P.S.Z.C's to initial conditions, the error distribution being chosen to give minimum error-signal power.

Fig. 10-1a shows the relationship of P.S.Z.C to the idling pattern when the input signal is zero and constant. The phase-modulated carrier, as used in section 3.3,B is a cosine function.

In Fig. 10-1 the quantisation error is minimum since the input signal is zero and the idling pattern is,

$$\dots - 0.5, 0.5, -0.5, 0.5, \dots$$

i.e. averaging to zero and having minimum power.

If the modulating input signal increased to a value of just less than 0.5 and stayed constant, then the phase of carrier would advance by  $\pi/2$ , similarly, if the input decreased to just greater than -0.5 and stayed constant, then the phase would retard by  $\pi/2$ . These two

conditions are shown in Fig. 10-1 B and 10-1 C.

The diagrams Fig 10-1,a,b, c are all compatible, where the input modulating signal, carrier phase and idling pattern are all closely related and inter-dependant. Any change in the initial conditions of the system must be arranged so that the basic system operation is unaltered. Hence, equation (3.3) states,

$$s_1(t) = D(t) - q(t),$$

thus,

$$s_2(t) + 0.5 = \{D(t) + 0.5\} - q(t)$$

therefore,

$$s_2(t) + 0.5 = D_s(t) - q(t) \dots\dots\dots (10.1)$$

where,  $D_s(t) = D(t) + 0.5, \dots\dots\dots (10.2)$

Hence, shifting the initial condition of the integrator by 0.5, requires that the input be shifted by 0.5 to keep the system identical to that of section 3.3. Thus, the phase of the carrier is advanced by  $\pi/2$ .

The delta-modem program was written with an assymetrical idling pattern, the integrator assuming a level (equivalent to) of +1 in the first time slot ( $0 \rightarrow 1/P$ ).

The algorithm for the delta-modem model corresponds to a modification of equations (3-12), which states:

$$x(t) = X \cos \{ \pi (P.t + D(t)) \} , \dots (3.12)$$

As shown, shifting the integrator initial conditions by + 0.5 is equivalent to advancing the phase by  $\pi/2$ . Thus, writing  $x(t)$  in terms of  $\theta$ , the phase-modulated function used in the computer program, gives:

$$M = X_0 \cos \left\{ \pi (P \cdot t + D(t)) - \frac{\pi}{2} \right\},$$

putting  $X = 1$  and rearranging, then,

$$M = \text{SIN} \{ \pi (P \cdot t + D(t)) \},$$

The program is arranged such that  $M$  is evaluated in the main program loop at clock instants. Thus the  $N^{\text{th}}$  clock sample, where  $P$  is the clock rate, occurs at a time

$$t = \frac{N}{P},$$

thus,

$$M = \text{SIN} \{ \pi (N + D(t)) \},$$

therefore,

$$M = \text{SIN} \{ \pi \cdot N + (\pi \cdot D(t)) \},$$

In the program,  $AI = \pi \cdot D(t)$ ,

therefore,

$$M = \text{SIN} \{ \pi \cdot N + AI \}, \quad \dots \dots \quad (10-3).$$

However, in the program  $AI$  was treated as the input signal thus the modulator was undermodulated by a factor of  $1/\pi$ . This was realised by increasing the step height from 1, as in chapter 3, to a value  $\pi$ . The value  $AI$  was also used in the delta-modulator program; thus the step height was made  $\pi$ .

In the delta-modem program, it was necessary to detect the P.S.Z.C's of  $M$ . For P.S.Z.C detection,  $M$  was evaluated at ten equally spaced time intervals over each clock period. Thus, by comparing adjacent samples, a P.S.Z.C could be detected. If a P.S.Z.C was detected, then the information was stored until the end of the clock sample, at which time a '1' or '0' pulse was produced at the output of the delta-modem. The store was then emptied.

By repeating this procedure over each clock interval the output pulse pattern was developed.

The delta-modulator simulation was based on section 3.3A. At each clock sample, the input signal was compared with the locally accumulated store output. If the comparison was positive, then the output pulse was  $-\pi$  and if the output was negative, then the output pulse was  $+\pi$ . The output pulses were then summed to form the locally integrated output.

The input signal AI to both systems was identical and given by:

$$AI = \frac{5}{8} \cdot PRF \sum_{Q=2}^9 \text{SIN} \left[ \frac{1}{PRF \cdot 10} \cdot \frac{Q}{2} \right], \dots (10.4)$$

In the program,  $PRF = 55$  Equation (10-4) shows that the lowest frequency component of the modulating signal was 1/550 Hz.

The print-out produced the output pulse sequences, locally integrated outputs, error signals and input modulating signal at each clock sample, for both the deltamodem model and delta-modulator. The output signals were found to be identical for both systems at all sample instants.

```

'BEGIN'
'REAL' K,WM,N,AI,M,PI,X,S,WHI,KI,L;
'INTEGER' PRF, R,PQ;
'ARRAY' C,A,P,D,CI,P1,D1 |1: 1000|;
SELECTOUTPUT (O); SELECTINPUT (O);
WI: = 2 * 3.1415927/10;
PRF: = 55;
K: = WM/PRF;
KI: = 1;
'FOR' L:=1.5 'STEP' 0.5'UNTIL' 5 'DO'
KI: = KI + L;
S: = 5*PRF/KI;
PO: = M:=0;
N: =1;
P [1] := 3.141 5927;
A [1] := C [1] := D [1] :=0;
P1 [1]: = 3.1415927;
CI [1]: = D1 [1] = 0;
D1 [1] := D [1] := 3.1415927;
DELTA:
'FOR' R: = 1 'STEP' 1 'UNTIL' 10 'DO'
'BEGIN'
M = 0;
N: = N + 0.1;
N: = N-1;
AI: = SIN (K * N);
'FOR' L: = 1.5 'STEP' 0.5 'UNTIL' 5 'DO'
AI: = AI + SIN (k * N * L);

```

```

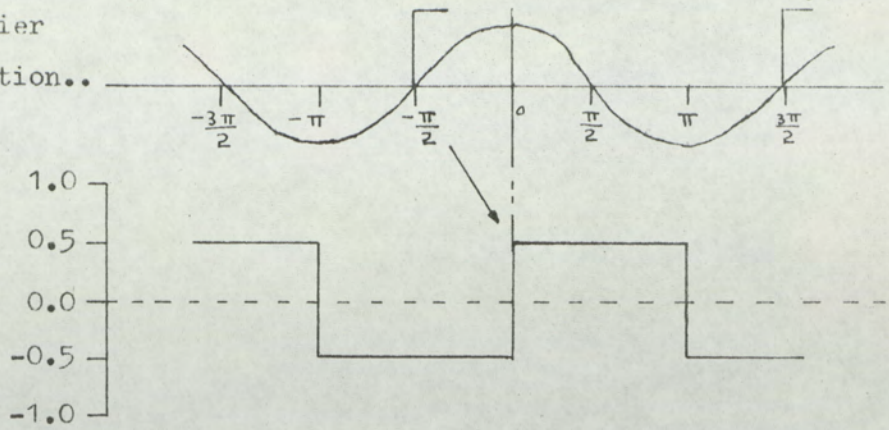
AI: = S * AI;
A: = SIN (N * 3.1415927 + AI);
N: = N+1;
'IF' AI < 0 'THEN'
'BEGIN'
'IF' AI 'GE' 0 'THEN' PO: = 1;
'END'; 'END';
A [N] : = AI;
'IF' PO = 1 'THEN' P [N] : = 1 'ELSE' P [N] : = -1;
P [N] : = P [N] * 3.1415927;
PO = 0;
D [N] : = D [N-1] + P [N];
X: = A [N] - D [N];
C [N] : = X;
'IF' N < 0999 'THEN' 'GOTTO' DELTA:
'FOR' N: = 2 'STEP' 1 'UNTIL' 998 'DO'
'BEGIN'
'IF' (A[N] - D1 [N-1]) 'GE' 0 'THEN'
P1 [N] : = 3.1415927 'ELSE' P1[N] : = 3.1415927;
D1 [N] : = D1 [N-1] + P1[N];
C1 [N] : = A [N] - D1 [N];
'END';
'FOR' R:=1 'STEP' 1 'UNTIL' 998 'DO'
'BEGIN'
PRINT (P1[R] ,1,6); SPACE (1);
PRINT (P[R],1,6); SPACE (1);

```

```
PRINT (A [R], 2,6); SPACE (1);  
PRINT (D1 [R], 2,6); SPACE (1);  
PRINT (D [R], 2,6); SPACE (1);  
PRINT (C1 [R], 2,6); SPACE (1);  
PRINT (C [R], 2,6); NEWLINE (1);  
'END'; 'END';
```

---

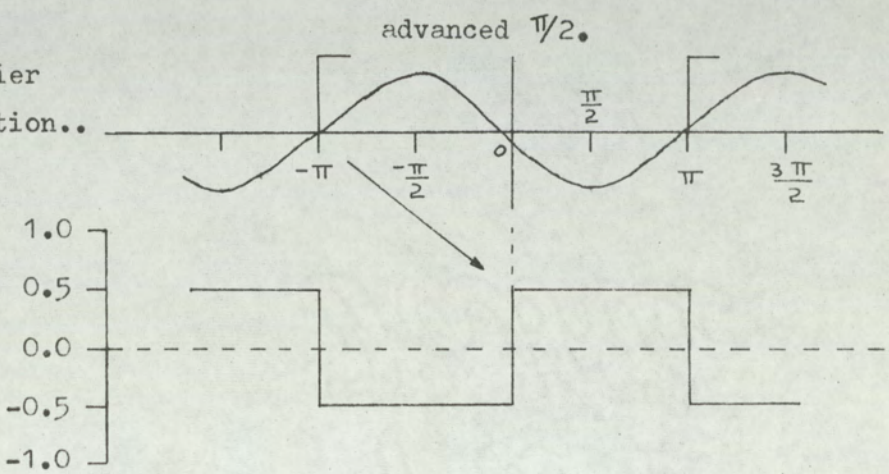
Phase-modulated carrier  
with p.s.z.c. indication..



Idling  
pattern.....

Fig.10-1(a).

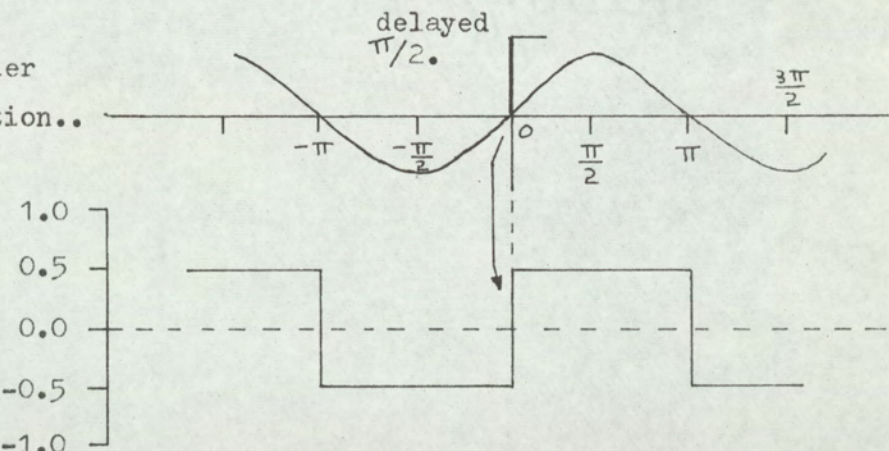
Phase-modulated carrier  
with p.s.z.c. indication..



Idling  
pattern.....

Fig.10-1(b).

Phase-modulated carrier  
with p.s.z.c. indication..



Idling  
pattern

Fig.10-1(c).

- Fig.10-1(a). Symmetrical idling pattern with p.s.z.c.'s correctly placed for symmetrical error.
- Fig.10-1(b). Carrier advanced by  $\pi/2$  due to input of just less than 0.5, assuming initial conditions as in Fig.10-1(a).
- Fig.10-1(c). Carrier retarded by  $\pi/2$  due to input of just greater than -0.5, assuming initial conditions as in Fig.10-1(a).

10-2. Delta-modulator simulation using a non-recursive filter to approximate the response of a RC integrator.

The feasibility of using a non-recursive filter in the feedback loop of a delta-modulator, as discussed in section 2.8, was determined by computer simulation. The input signal to the delta-modulator was made the sum of two sine waves. During the execution of the program, the output pulse pattern was generated, together with the input signal, the integrated output and the error signal, at each sample. The matrix representing the weighting coefficients of the non-recursive filter was also displayed. It was therefore possible to examine the operations of the delta-modulator, and to check the feasibility of operation of this system.

The simulation was performed as follows:-

The shift register of the non-recursive filter was simulated using a 250-element one-dimensional matrix array. The matrix stored the pulse pattern over 250 samples, the pulse being stored as either +1 or -1. After the execution of a sample, the pulse sequence was sequentially transferred along the matrix, thus simulating the shifting of the register. The weighting coefficients used in the filter were also stored in a 250-element one-dimensional matrix. The coefficient distribution of the elements was made exponential, the time constant being set **at unity**.

Integration at each sample was performed by weighting the pulses stored in the pulse storage matrix and adding the resultant weightings. In the delta-modulation simulation, the integrated pulse waveform was compared with the input signal at that instant and a decision made at the sample as to the pulse generated, i.e.

1 or 0. Thus, repeating the sequence the pulse waveform is computed.

The input signal used in the simulation was given by,

$$AI = 10\left\{\sin\left[\frac{2\pi t}{3}\right] + \sin\left[0.9\frac{2\pi t}{3}t\right]\right\} \dots(10-5)$$

The pulse waveform was evaluated over 1000 samples, the P.R.F being set at 50 P.P.S. Results showed that over the sequence, the maximum error was 1.847959 occurring near the commencement of modulation, where the signal **slope** was maximum. However, the error was usually less than or near to 1. The error function showed correlation with signal **slope** in that when the signal **slope** was positive the error was usually positive; similarly when the signal **slope** was negative the error was more **generally** negative. The simulation showed that the performance was similar to a delta-modulator with an RC integrator and that this type of generation of a delta-modulator pulse waveform is feasible.

The program is as follows:

```
'BEGIN'
'ARRAY' C [0: 250];
'INTEGER' 'ARRAY' P [0: 1000];
'REAL' AI, S,K,K1,F,E,W1;
'INTEGER' R,L,PRF;
SELECTINPUT (0); SELECTOUTPUT (0);
W1:=2*3.1415927/3;
PRF:= 5 0;
K: = W1/PRF;
K1: = 0.9*K;
C[0]: = 1;
```

```

'FOR' R:=1 'STEP' 1 'UNTIL' 250 'DO'
C [R ]: = EXP (-R/PRF);
'FOR' R:=0 'STEP' 2 'UNTIL' 250 'DO'
P[R] : = 1;
'FOR' R: = 1 'STEP' 2 'UNTIL' 249 'DO'
P [R] : = -1;
'FOR' R:=0 'STEP' 1 'UNTIL' 1000 'DO'
'BEGIN'
AI: = 10* (SIN (K*R) + SIN (K1+R));
F: = 0;
'FOR' L: = 0 'STEP' 1 'UNTIL' 250 'DO'
F: = F + C [L] + P [L] ;
E: = AI - F;
'FOR' L: = 250 'STEP' -1 'UNTIL' 1 'DO'
P [L] : = P [ L-1];
'IF' E 'GE' 0 'THEN' P [ 0]: = 1 'ELSE' P [0]: = -1;
PRINT (P [1],1,0); SPACE (3);
PRINT (AI,2,6); SPACE (1);
PRINT (F,2,6); SPACE (3);
PRINT (E,2,6); SPACE (3);
'IF' R < 251 'THEN' PRINT (C[R] ,1,6);
NEWLINE (1);
'END'; 'END';

```

---

### 10.3 Simulation of instantaneous, non-linear delta-modulation

A delta-modulator is described in section 5.5 which used pulse grouping techniques to perform non-linear adaptation. The general structure of this class of delta-modulator is shown in Fig. 5.11 and Fig. 10.2. A computer program was written which simulated exactly the non-linear delta-modulator and evaluated the signal-to-quantisation error ratio for a range of input signals.

Two types of non-linear delta-modulator were simulated. The first used a 'second order only' pulse group detection. The pulse group weighting was 1 or -1, depending on whether the group was '111' or '000'. The second delta-modulator used second and third order group detection. The weighting for both groups was made equal to either 1 for '111' or '1111' pulse sequences or equal to -1 for '000' or '0000' pulse sequences.

The signals applied to the two delta-modulators were single **sine - wave** functions of various amplitudes and frequencies. The range of signal frequencies was given by:

$$\text{modulating signal frequencies} = \left[ 0.01 \cdot 2^N \right]_{N=0}^9 \text{ Hz., ... (10.6)}$$

Thus, from equation (10.6), the range of modulating frequencies is from 0.01 Hz to 5.12 Hz. In the program, the clock rate of the delta-modulator was made 50Hz and 100Hz. The maximum modulating signal amplitude for a single integrations non-adaptive delta-modulator depends upon the signal frequency and system clock rate. The signal amplitude was thus classified by a slope loading factor, when examining a single integration system. Hence, a signal of value 1 represents a sine wave which fully loads the single integrator delta-modulator.

The range of signal amplitudes for each signal frequency was 0.2 to 2.8 in steps of 0.2.

In both delta-modulator systems, the zero-order pulse group, i.e. the output pulse sequence 0101, was given a weighting of either -1 for a 0 pulse or +1 for a 1 pulse. However, the sum of the second and third order pulse groups (see Fig. 10.2) were attenuated by a factor  $H[R]$ , where  $H[R]$  was constant for a given signal evaluation. However,  $H[R]$  could take values ,

$$H[R] = 0.0, 0.2, 0.4, 0.6, 0.8, 1.0$$

Thus the effects of varying amounts of adaptation could be investigated. Each input signal was evaluated at each value of  $H[R]$ .

The program operation is described by Fig. 10.2. The program was readily modified to either the third and second order systems or second-order-only system.

In the program,  $P_0[R] \dots P_4[R]$  could have values -1 or +1. Pulse groups were detected by summing directly the outputs of the register. For example, consider the third-order pulse group detector.

$$P_0[R] + P_1[R] + P_2[R] + P_3[R] = 4$$

then the output of the comparator was 1.

$$\text{If } P_0[R] + P_1[R] + P_2[R] + P_3[R] = -1,$$

then the output of the comparator was -1. Otherwise the output remained zero. In Fig. 10.2, the comparator for detecting levels  $> 3$  or  $< -3$  are shown separately, since the program used separate statements for these functions.

The results of the program are shown in Figs 10.3 to 10.14; they are discussed in section 10 - 5.

```

'BEGIN'
'REAL' D,S,W1,W2,W3, DD,P,F;
'INTEGER' M,R,G;
'ARRAY' I1,H,DC,SN [0:10];
'ARRAY' PLX [0:10];
'INTEGER' 'ARRAY' PO,P1,P2,P3,P4,P5,PL2,PL3,PL4,PL1,PL5,I21,I2[0:10];
SELECTOUTPUT (0);
P:=100; (or 50)
'FOR' G:=0 'STEP', 'UNTIL' 9 'DO'
'BEGIN'
F:=(0.01)*(2↑G);
PRINT (P,3,6); SPACE (6);
PRINT (F,3,6); NEWLINE (2);
'FOR' R:=0 'STEP' 1 'UNTIL' 5 'DO'
'BEGIN'
H[R] := R* 0.2;
PRINT (H[R] ,3,6); SPACE (6);
'END'; NEWLINE (4);
'FOR' W3 = 0.2 'STEP' 0.2 'UNTIL' 3 'DO'
'BEGIN'
S:=W3;
PRINT (S,3,6); NEWLINE (1);
W1: = 6.2831854 * F/P;
S:= S/W1;
W2: = 10/(LN(10));
DD: = 0;
'FOR' R:= 0 'STEP' 1 'UNTIL' 5 'DO'
'BEGIN'
I2 [R]: = I1 [R] : = 0;
PO[R]: = P2[R]: = -1;

```



```

I1 [R] := I1 [R] + PO [R] + H [R] * (I21 [R]);
DC [R] := DC [R] + (D - I1 [R])2;
'END';

DD := DD + D*D;
'END';

'FOR' R: = 0 'STEP' 1 'UNTIL' 5 'DO'
'BEGIN'

SN [R] := W2* (LN(DD/DC [R]));
PRINT (SN [R],3,6); SPACE (6)
'END';      NEWLINE (2);
'END';      PAPERTHROW ;
'END'; 'END';

```

---

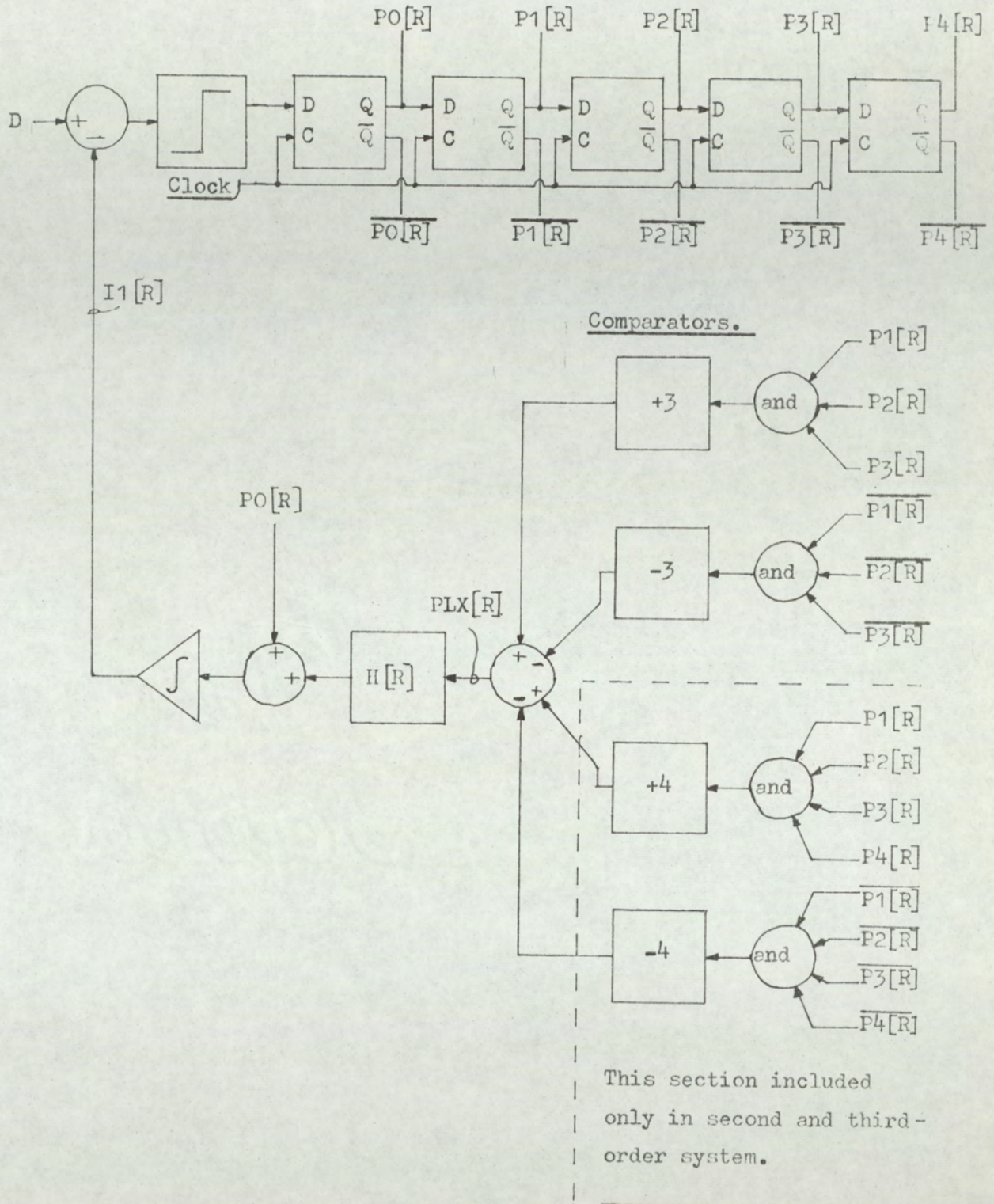


Fig.10-2. Adaptive delta-modulator presented for computation.

10.4 Delta-modulator simulation to determine relationships between pulse groups and slope of the modulating signal.

The results shown in Fig. 5.1 were determined by the program presented in this section. The program simulated a perfect single-integration delta-modulator and allowed 1st, 2nd, 3rd and 4th order pulse group detection. Over the range of samples evaluated the total number of pulse groups in each order pulse group was recorded. Each recorded value was divided by the total number of samples; thus the mean rate of occurrence of each pulse group was determined. This process was repeated for each of a range of input signals.

The input signal at each evaluation was a ramp of constant slope. The range of slopes was from 0.01 to 1.00 in steps of 0.01; a slope of 1.00 represented full loading of the delta-modulator. Hence, it was possible to relate the mean rate of occurrence of pulse groups of order 1,2,3,4 to the normalised signal slope.

The evaluation was repeated for various numbers of samples, the range of samples being:

$$\text{number of samples} = \begin{bmatrix} 2^N \\ 0 \end{bmatrix} \begin{matrix} 10 \\ 0 \end{matrix}, \quad \dots \quad (10.7)$$

The results shown in Fig.5.1 were taken when  $N = 10$ ; thus the number of samples was 1024, using 1024 samples the evaluation of the rate of occurrence of pulse groups could be determined to a fine degree of accuracy. The results agreed with the predicted threshold level determined in section 5.2. The results showed that, for signals above the pulse-group threshold level, the mean rate of occurrence of pulse groups is directly proportional to the slope of the modulating signal.

The program is as follows:-

```

'BEGIN'
'REAL' M,D,K1,K2,K3,K4,E1,E2,E3,E4;
'INTEGER' R,L,PO,P1,P2,S,X1,X2,X3,X4,
          C,A,P3,P4;
'ARRAY' Y1,Y2,Y3,Y4 [ 1:100 ] ;
SELECTOUTPUT (0);
'FOR' c:=0 'STEP' 1 'UNTIL' 10 'DO'
'BEGIN'
E1:=E2:=E3:=E4:=0;
A:= 2 ↑ c;
PRINT (A,5,0); NEWLINE (1);
'FOR' M:= 0.01 'STEP' 0.01 'UNTIL' 1.01 'DO'
'BEGIN'
PRINT (M,1,2); SPACE (6);
L:=100*M;
Y1 [L] := M;
Y2 [L] := 1.5*M-0.5;
Y3 [L] := 2*M - 1;
Y4 [L] := 2.5*M - 1.5;
'IF' Y2 [L] < 0 'THEN' Y2 [L] := 0;
'IF' Y3 [L] < 0 'THEN' Y3 [L] := 0;
'IF' Y4 [L] < 0 'THEN' Y4 [L] := 0;
PO:= P2:= P4:= -1;
P1:=P3:= +1;
S:=0;
X1:=X2:=X3:=X4:=0,
'FOR' R:=0 'STEP' 1 'UNTIL' A 'DO'
'BEGIN'
D:=R*M;
P4:=P3;

```

```

P3:=P2;
P2:=P1;
P1:=P0;
'IF' (D-S) 'GE' 0 'THEN' PO:= 1 'ELSE' PO:=-1;
S:= S + PO;
'IF' (PO + P1) = 2 'THEN' X1:=X1 +1;
'IF' (PO + P1 + P2) = 3 'THEN' X2:= X2 + 1;
'IF' (PO + P1 + P2 + P3) = 4 'THEN' X3:= X3 + 1;
'IF' (PO + P1 + P2 + P3 + P4) = 5 'THEN' X4:= X4:=X4+1;
'END'

K1:= X1/A;
K2:= X2/A;
K3:= X3/A;
K4:= X4/A;
E1:= (K1 - Y1 [L] ) ↑ 2 + E1;
E2:= (K2 - Y2 [L] ) ↑ 2 + E2;
E3:= (K3 - Y3 [L] ) ↑ 2 + E3;
E4:= (K4 - Y4 [L] ) ↑ 2 + E4;
PRINT (K1,1,8); SPACE (3);
PRINT (K2,1,8); SPACE (3);
PRINT (K3,1,8); SPACE (3);
PRINT (K4,1,8); NEWLINE (1);
'END'

E1:=SQRT (E1/100);
E2:=SQRT (E2/100);
E3:=SQRT (E3/100);
E4:=SQRT (E4/100);
PRINT (E1,3,6); SPACE (3);
PRINT (E2,3,6); SPACE (3);

```

```
PRINT (E3,3,6); SPACE (3);  
PRINT (E4,3,6); NEWLINE (3);  
'END'; 'END';
```

---

The program also allowed a mean-square error term to be calculated from the calculated mean rate of occurrence of pulse groups and the ideal mean rate of occurrence of pulse groups. The latter is obtained when the number of samples over which the average is taken tends to infinity. The mean rate of occurrence of each pulse group was calculated for signals having a slope ranging from 0.00 to 1.00 in steps of 0.01. The mean rate of occurrence of pulse groups was calculated at each signal slope. The accuracy of the calculation depended on the number of sample points; thus an error term can be calculated, the magnitude of which is a function of the number of samples. By summing the square of the errors and dividing the total number of signals (i.e. 100) the mean-square error term is obtained. This process was repeated for various numbers of samples as given by equation (10.7). The results are shown in Table 10.1.

Number of samples in average				
	<u>MEAN-SQUARE ERROR VALUES</u>			
	1st order pulse group	2nd order pulse group	3rd order pulse group	4th order pulse group
1	0.573018	0.476705	0.414367	0.371988
2	0.573018	0.468772	0.414367	0.371988
4	0.241402	0.308824	0.405216	0.366060
8	0.112278	0.131210	0.155584	0.182603
16	0.054701	0.062328	0.070611	0.079353
32	0.027179	0.030349	0.034500	0.037526
64	0.013247	0.014684	0.016370	0.017511
128	0.006624	0.007460	0.008053	0.008818
256	0.003369	0.003772	0.004183	0.004655
512	0.001606	0.001837	0.002000	0.002259
1024	0.000848	0.000933	0.001041	0.001141

Table 10.1. Mean-square error terms between calculated mean rates of occurrence of pulse groups and ideal mean rates of occurrence of pulse groups, for varying sample numbers.

## 10.5

## Computer results for instantaneous adaptation.

The results of the program section 10.3 are drawn out on the set of graphs Fig. 10.3 to Fig. 10.14 inclusive. The results show that, for all systems increasing the amount of adaptation results in an improved dynamic range of the system, although the signal-to-quantisation-noise ratio remains about constant under peak loading conditions. The peak loading of the delta-modulator for a given amount of adaptation may be determined by considering the peak-signal slope which can be encoded. The peak positive signal slope is realised when the transmission sequences is a continuous sequence of '1' pulses such that (referring to section 10.3, Fig. 10.2),

$$P_0 [R] = P_1 [R] = P_2 [R] = P_3 [R] = P_4 [R] = 1.$$

Thus, for the second and third order system:

$$PLX [R] = 2;$$

Thus, assuming a unit-step height for the delta-modulator without adaptation, then the step height with an amount  $H [R]$  of adaptive signal is given by:

$$\text{Step height} = 1 + 2 H [R],$$

If the pulse rate is  $P$  (P.P.S.), then the peak-signal slope is:

$$\text{Peak-signal slope} = P \{ 1 + 2.H [R] \},$$

Substituting in equation (2.21), and taking the maximum slope, therefore:

$$(2\pi f) \cdot \bar{D}_f = P \cdot \{ 1 + 2.H [R] \}$$

In section 10.3,  $D$  represented the normalised input signal referred to the delta-modulator without adaptation. Thus, put,

$$D = \frac{\bar{D}_f}{P} (2\pi f),$$

$$\text{hence, } D_{2,3} = 1 + 2.H [R] , \dots \quad (10.7)$$

$$\text{Similarly, } D_2 = 1 + H [R] , \dots \quad (10.8)$$

where  $D_{2,3}$  is the normalised modulating signal referred to the system with second and third-order adaptation and  $D_2$  is the normalised modulating signal for the second-order only system.

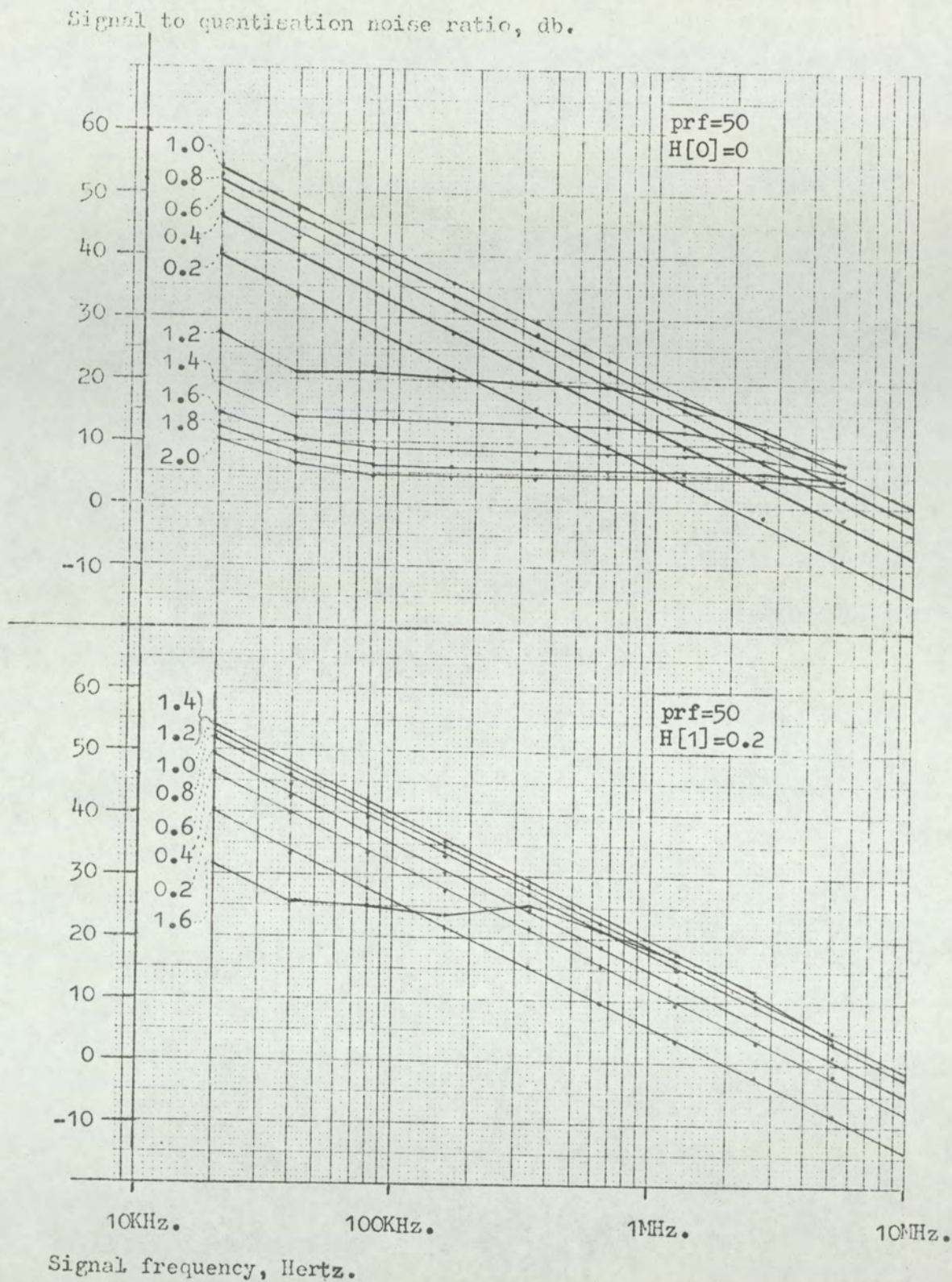
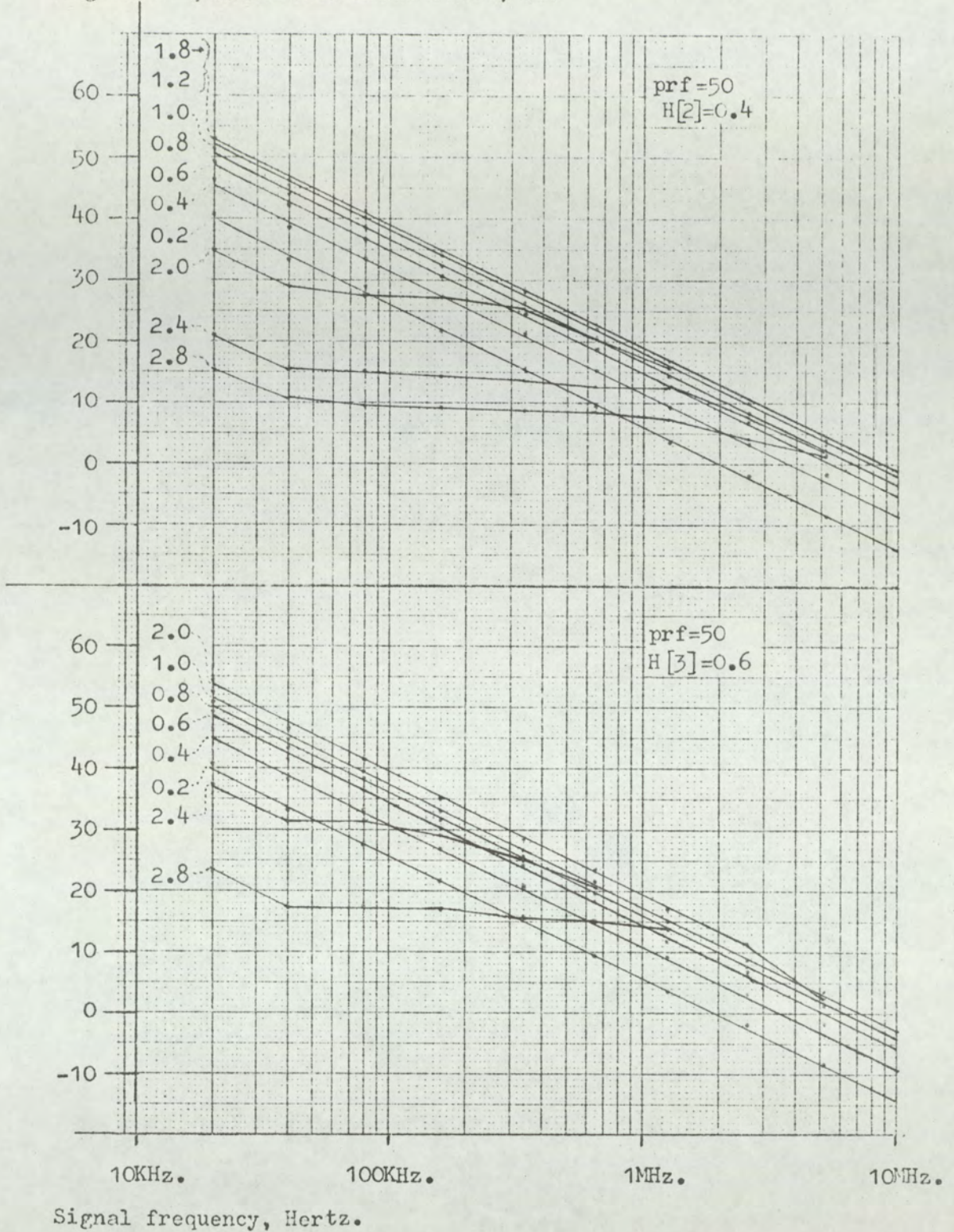


Fig.10-3. Signal to quantisation noise ratios for a delta-modulator against frequency with  $D$  as parameter and clock pulse rate constant. The delta-modulator has second and third-order adaptation. prf. = 50,  $H[0] = 0$ ,  $H[1] = 0.2$ .

\*  $D$ , is normalised modulating signal, single sine wave.

Signal to quantisation noise ratio, db.

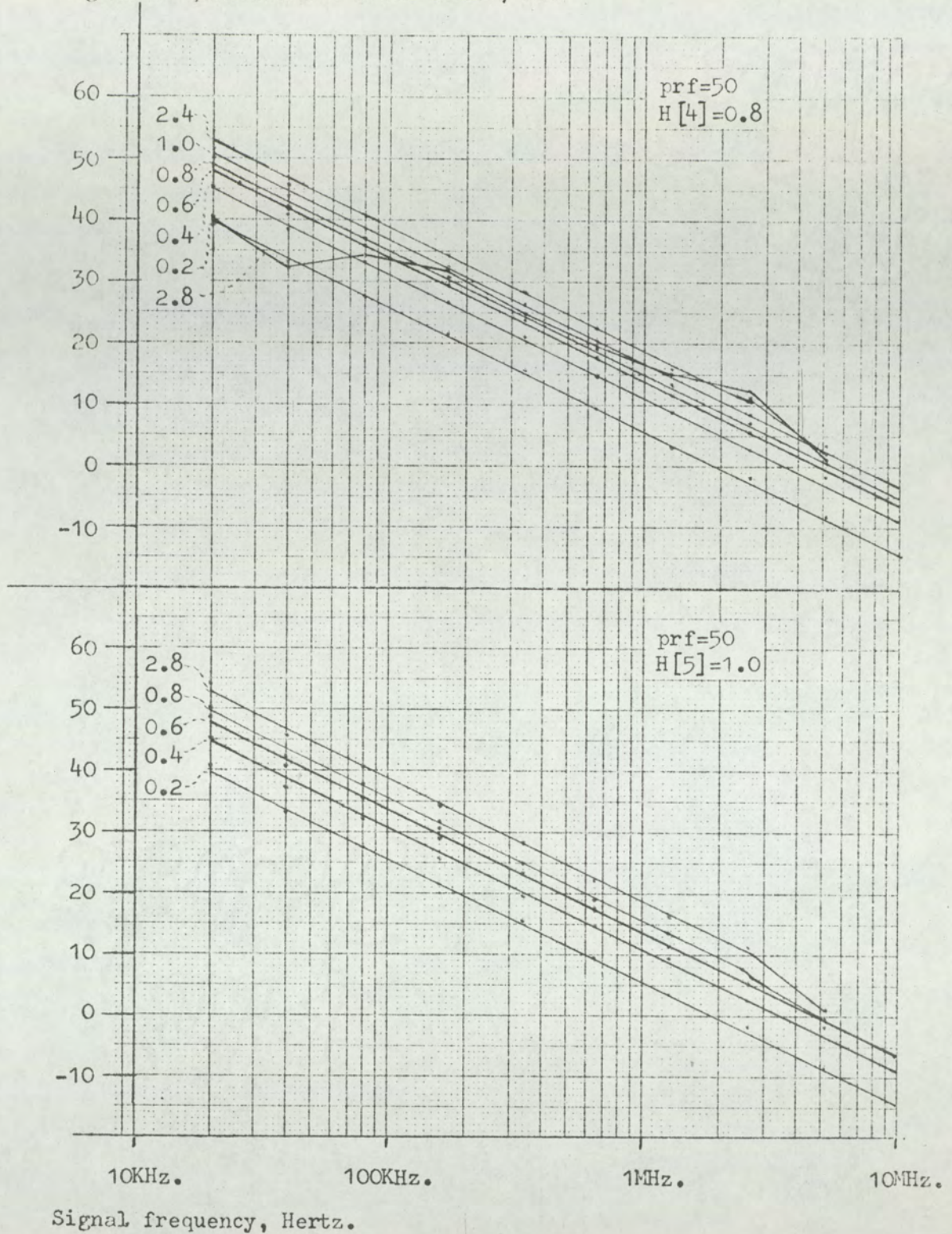


Signal frequency, Hertz.

Fig.10-4. Signal to quantisation noise ratios for a delta-modulator against frequency with  $D^*$  as parameter and clock rate constant. The delta-modulator has second and third-order adaptation.  $\text{prf} = 50$ ,  $H[2] = 0.4$ ,  $H[3] = 0.6$ .

\*  $D$ , is normalised modulating signal, single sine wave.

Signal to quantisation noise ratio, db.



Signal frequency, Hertz.

Fig.10-5. Signal to quantisation noise ratios for a delta-modulator against frequency with  $D^*$  as parameter and clock rate constant. The delta-modulator has second and third-order adaptation.  $\text{prf.} = 50$ ,  $H[4] = 0.8$ ,  $H[5] = 1.0$ .

\*  $D^*$ , is normalised modulating signal, single sine wave.

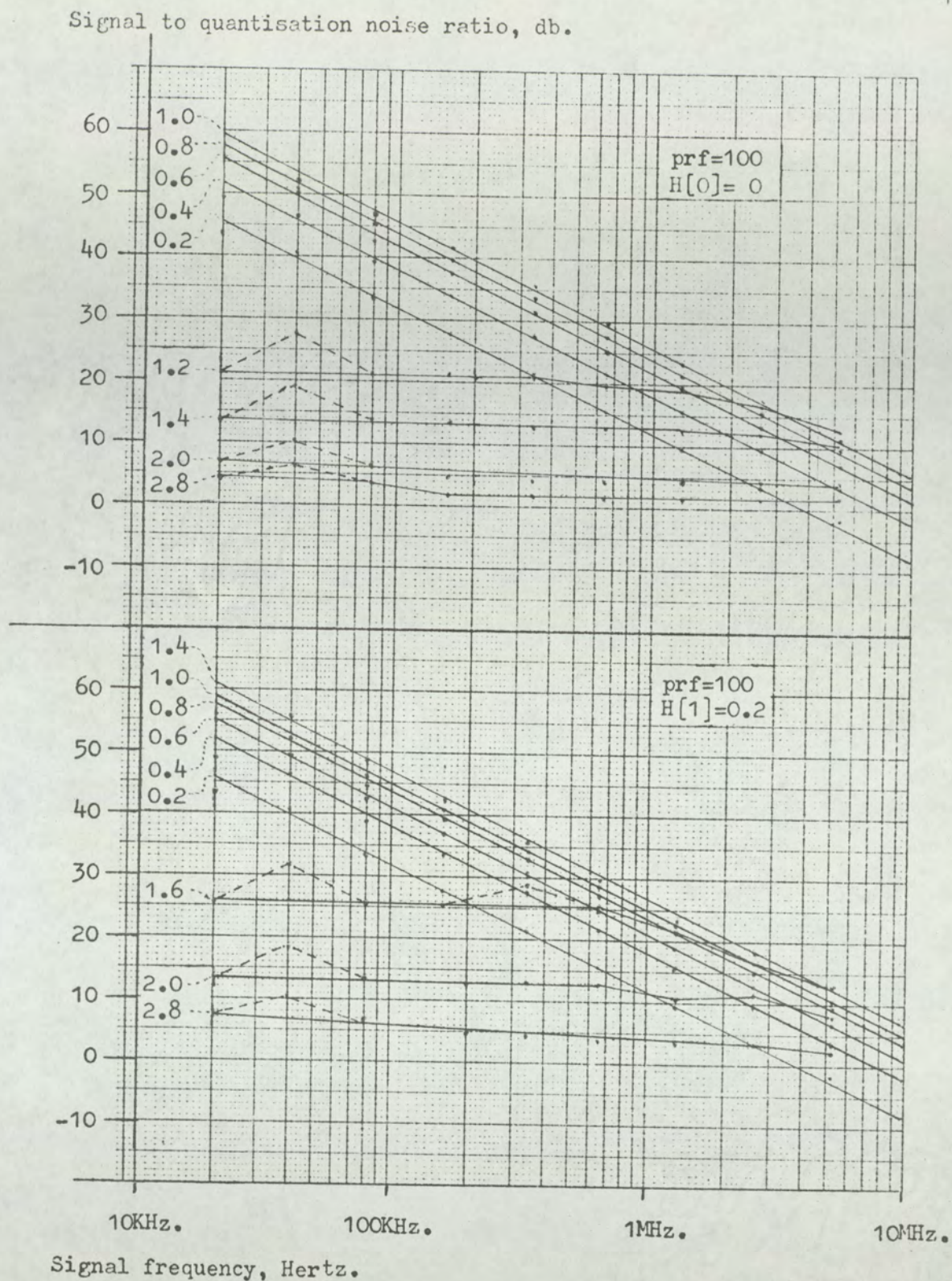


Fig.10-6. Signal to quantisation noise ratios for a delta-modulator against frequency with  $D^*$  as parameter and clock pulse rate constant. The delta-modulator has second and third-order adaptation. prf. = 100,  $H[0] = 0$ ,  $H[1] = 0.2$ .

\*  $D^*$  is normalised modulating signal, single sine wave.

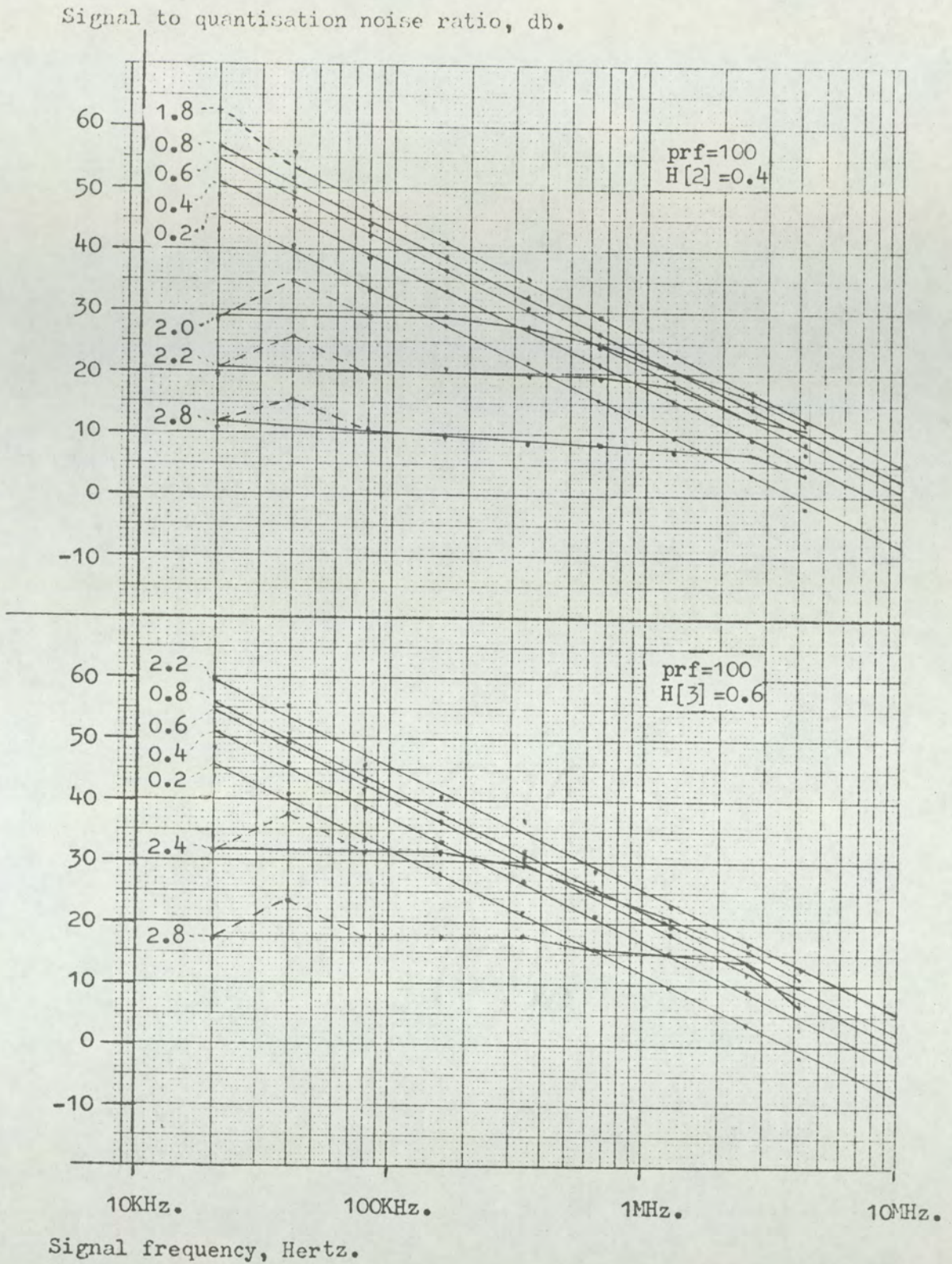
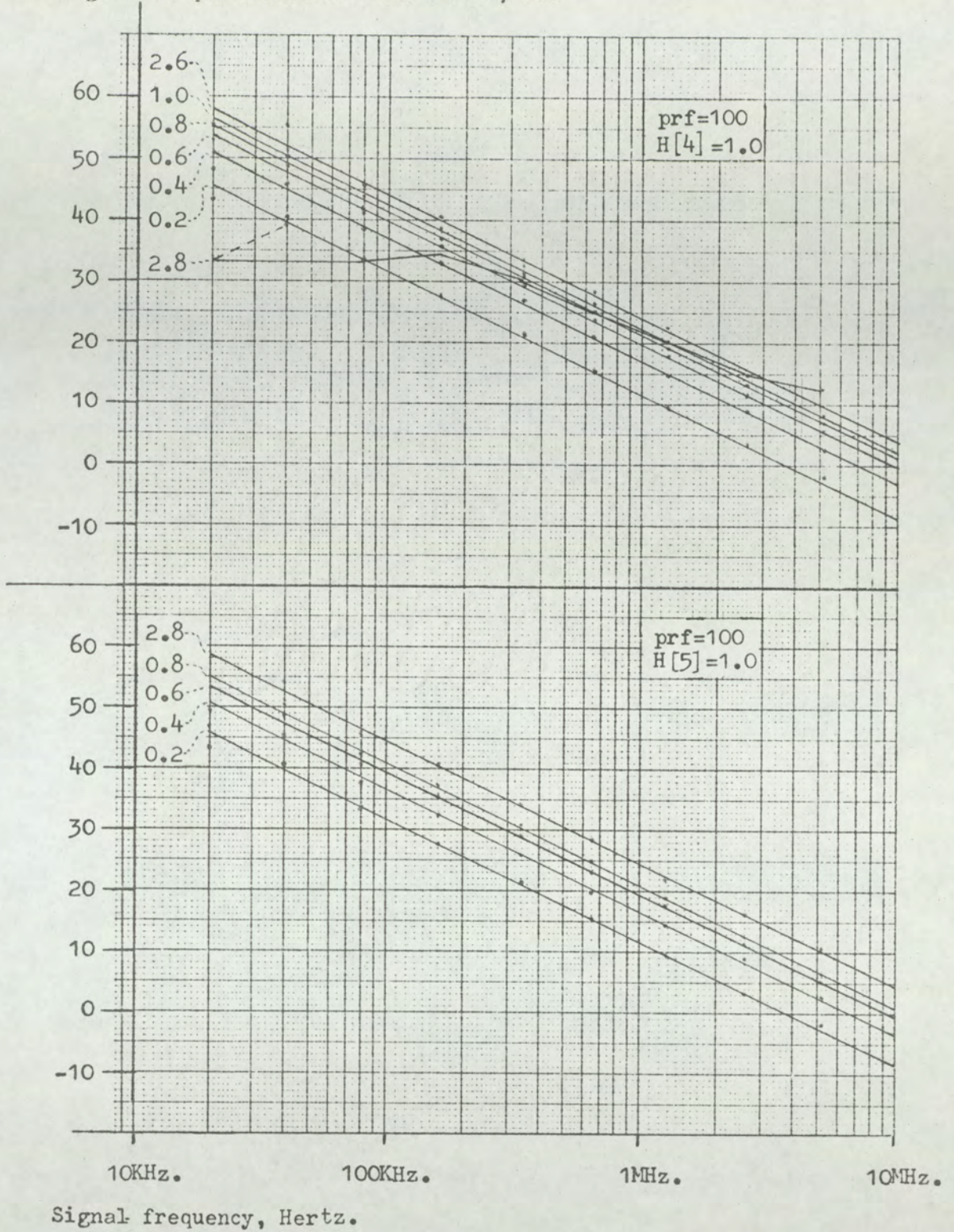


Fig.10-7. Signal to quantisation noise ratios for a delta-modulator against frequency with  $D^*$  as parameter and clock pulse rate constant. The delta-modulator has second and third-order adaptation. prf. = 100,  $H[2] = 0.4$ ,  $H[3] = 0.6$ .

\*  $D$ , is normalised modulating signal, single sine wave.

Signal to quantisation noise ratio, db.

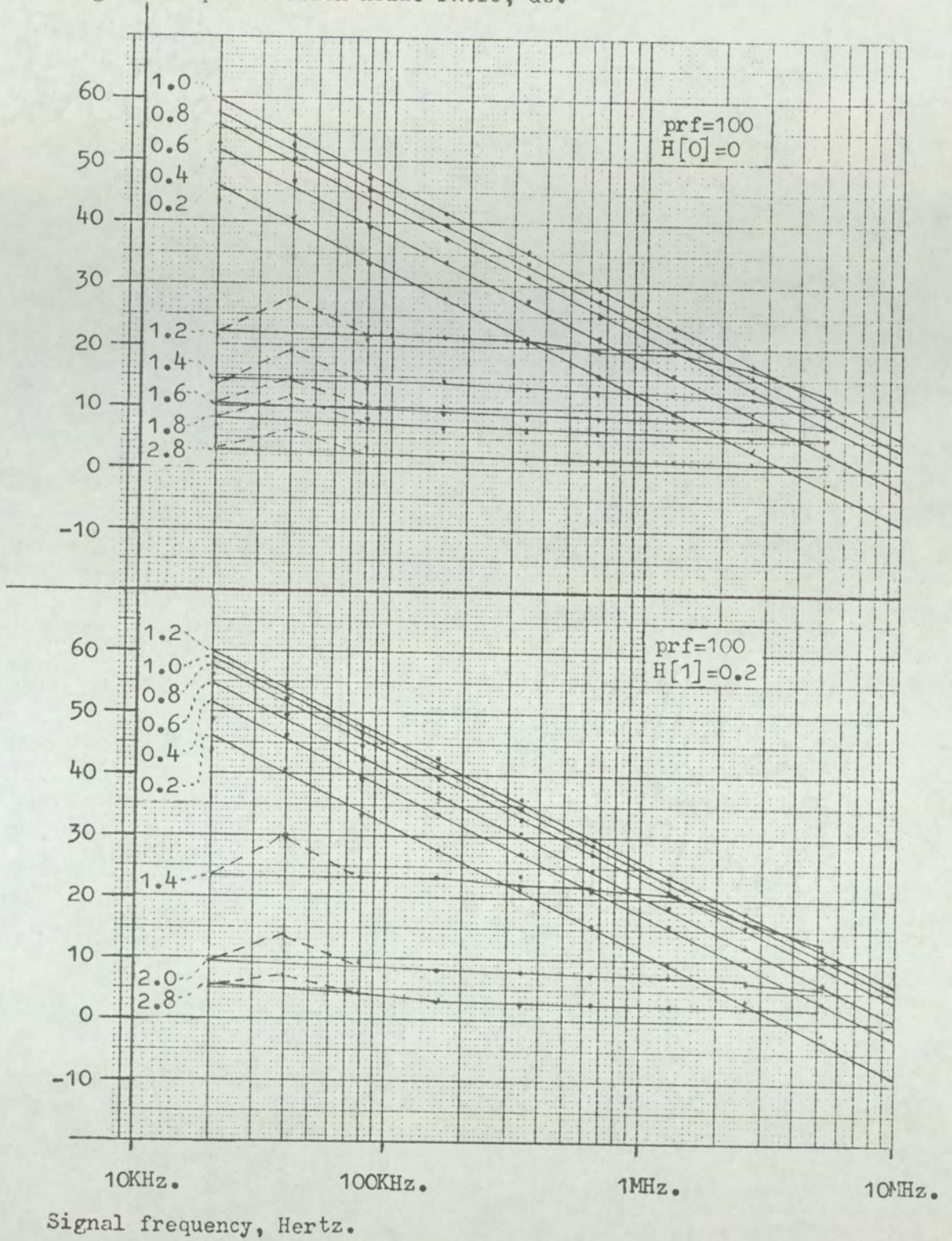


Signal frequency, Hertz.

Fig.10-8. Signal to quantisation noise ratios for a delta-modulator against frequency with  $D$  as parameter and clock pulse rate constant. The delta-modulator has second and third-order adaptation.  $prf. = 100, H[4] = 0.8, H[5] = 1.0.$

\*  $D$ , is normalised modulating signal, single sine wave.

Signal to quantisation noise ratio, db.



Signal frequency, Hertz.

Fig. 10-9. Signal to quantisation noise ratios for a delta-modulator against frequency with  $D$  as parameter and clock pulse rate constant. The delta-modulator has second-order only adaptation.  $prf. = 100, H[0] = 0, H[1] = 0.2.$

\*  $D$ , normalised modulating signal, single sine wave.

Signal to quantisation noise ratio, db.

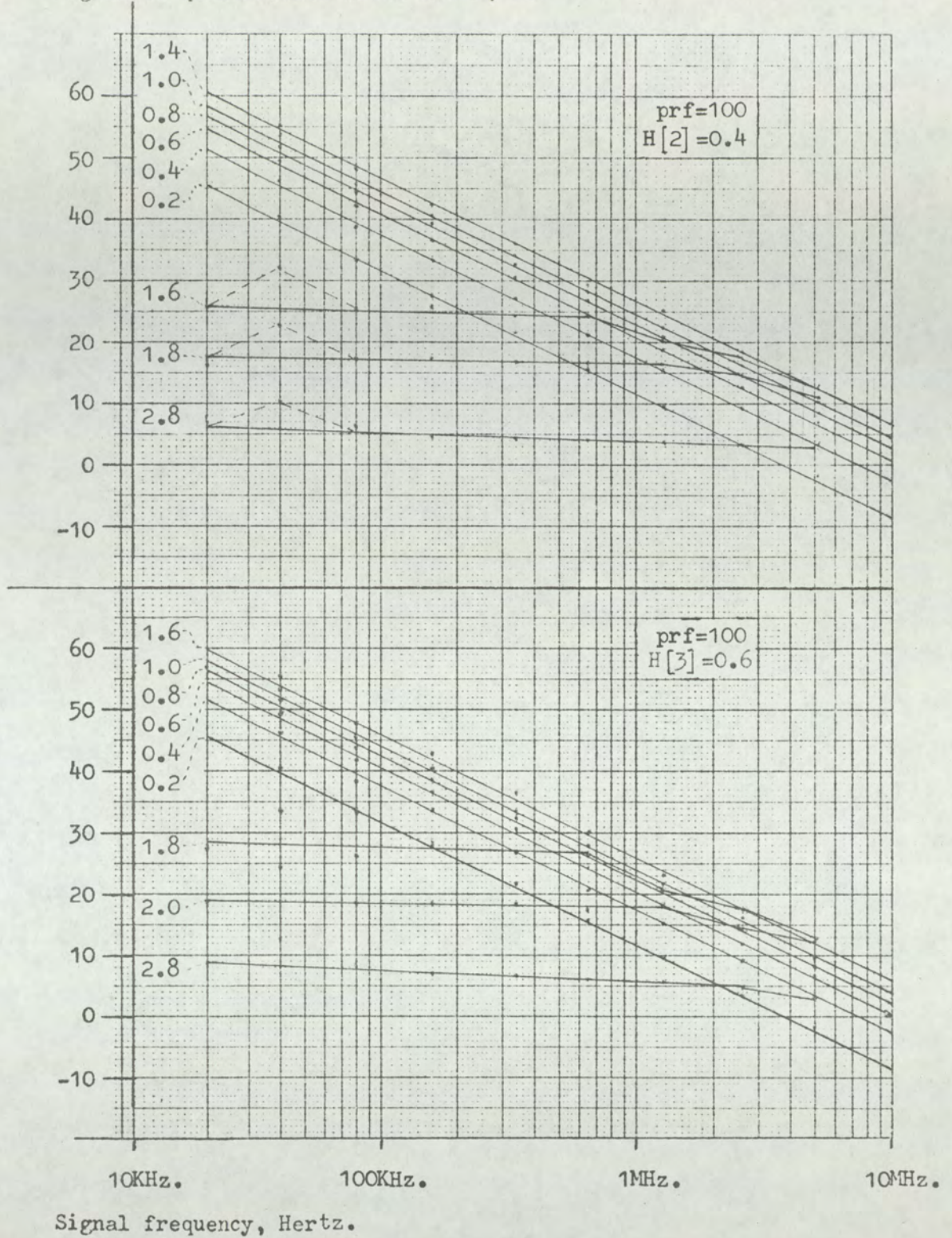


Fig.10-10. Signal to quantisation noise ratios for a delta-modulator against frequency with  $D$  as parameter and clock pulse rate constant. The delta-modulator has second-order only adaptation.  $\text{prf.} = 100$ ,  $H[2] = 0.4$ ,  $H[3] = 0.6$ .

\*  $D$ , normalised modulating signal, single sine wave.

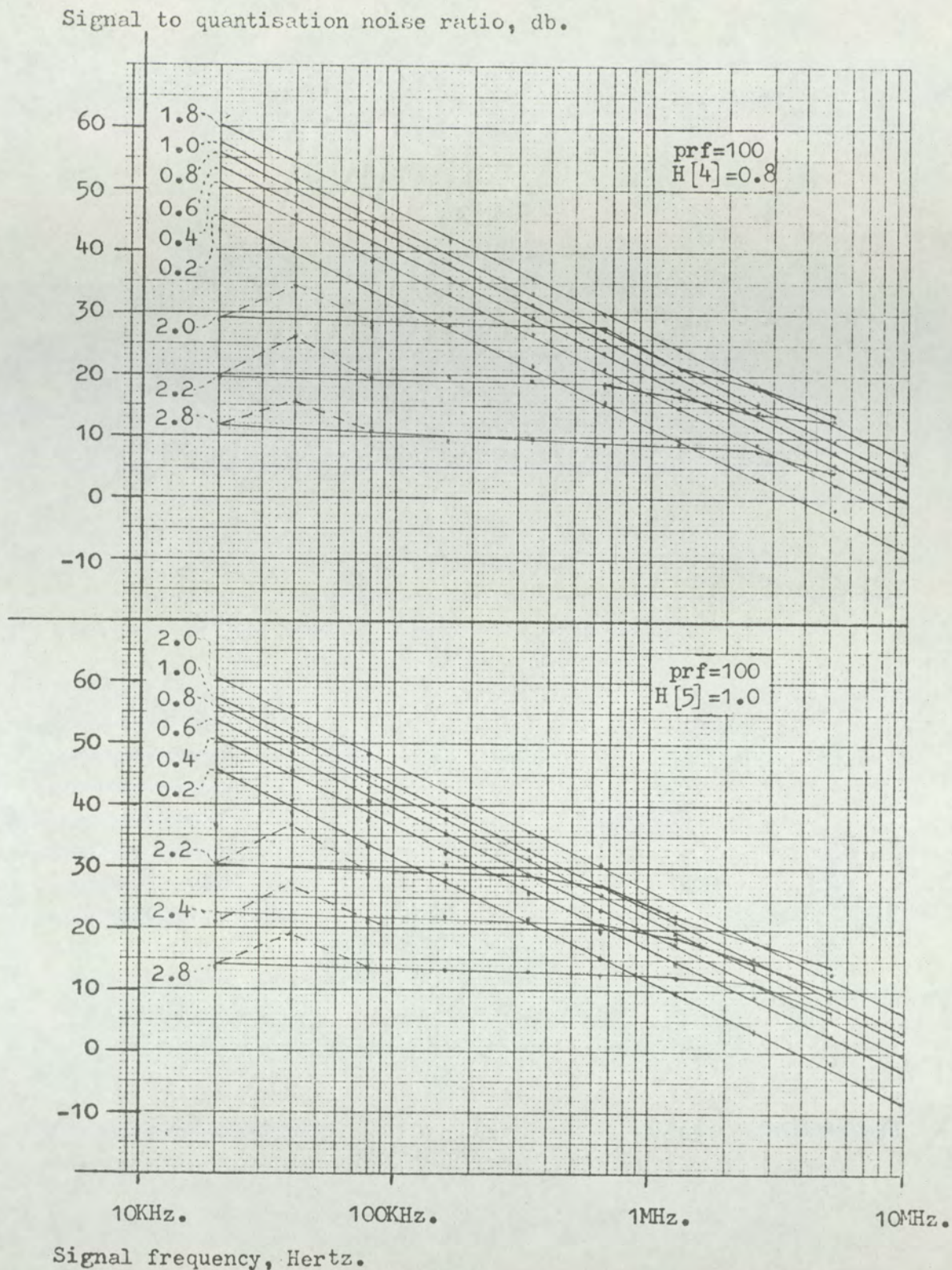
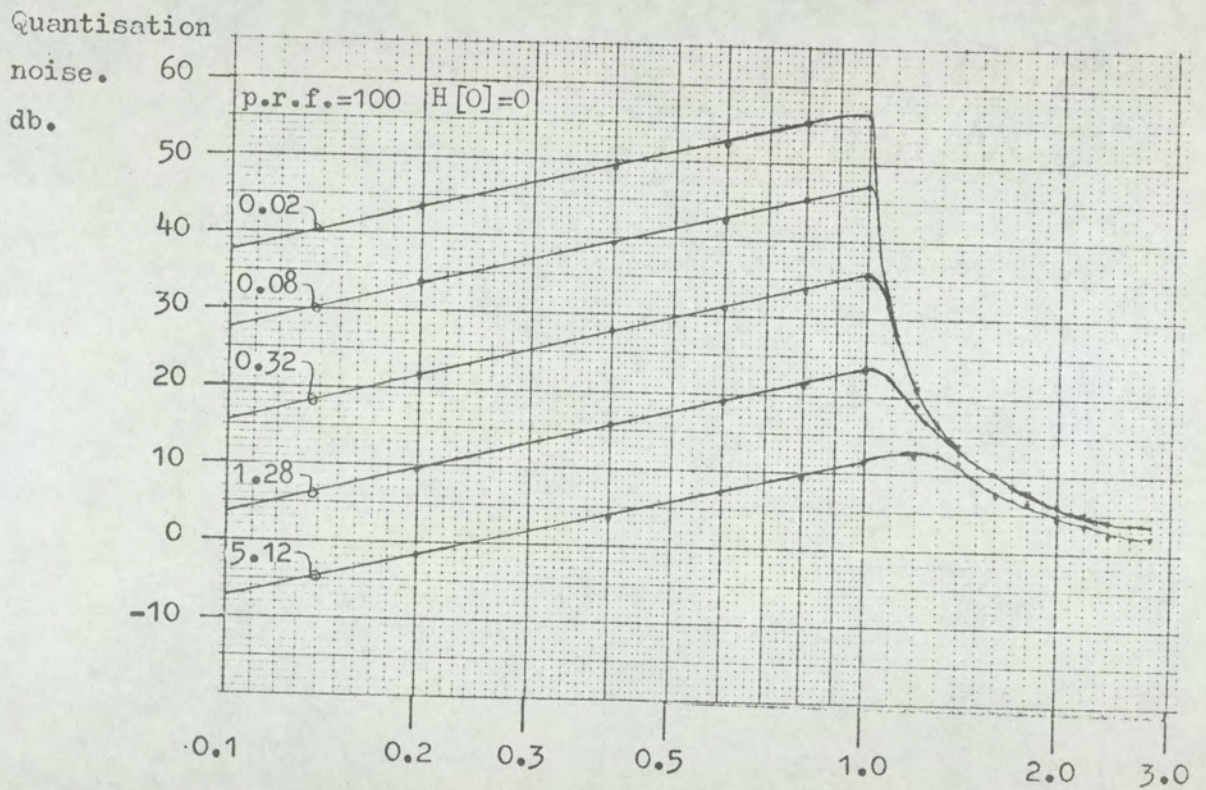
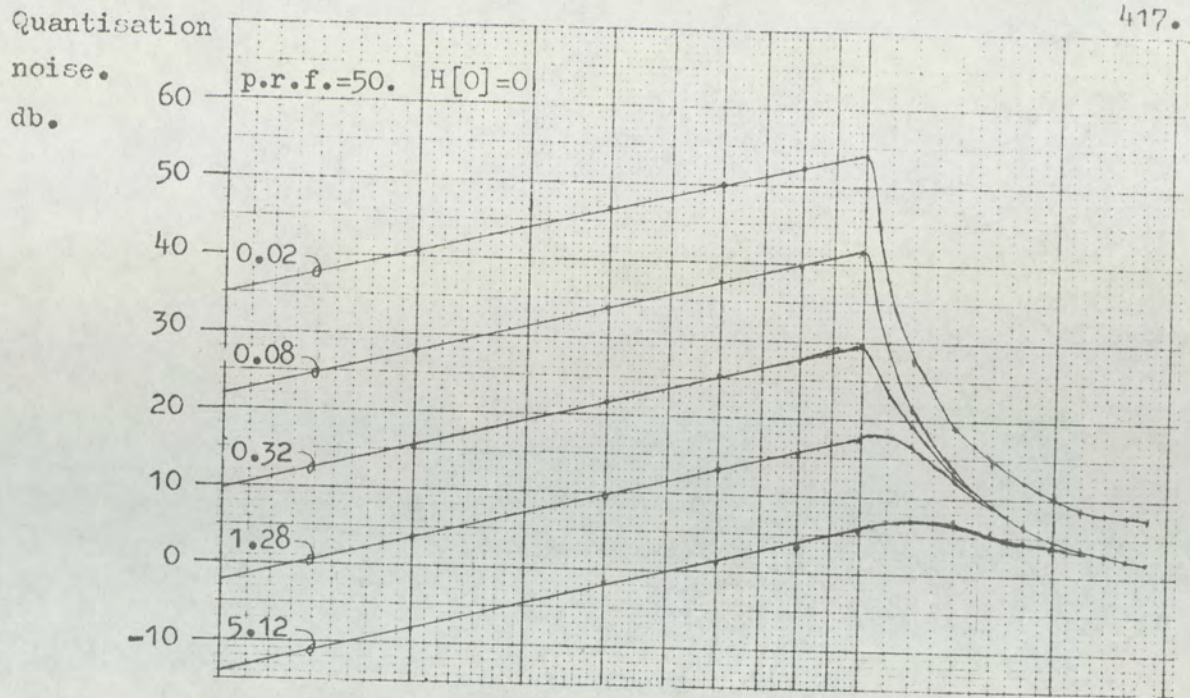


Fig.10-11. Signal to quantisation noise ratios for a delta-modulator against frequency with  $D$  as parameter and clock pulse rate constant. The delta-modulator has second-order only adaptation. prf. = 100,  $H[4] = 0.8$ ,  $H[5] = 1.0$ .

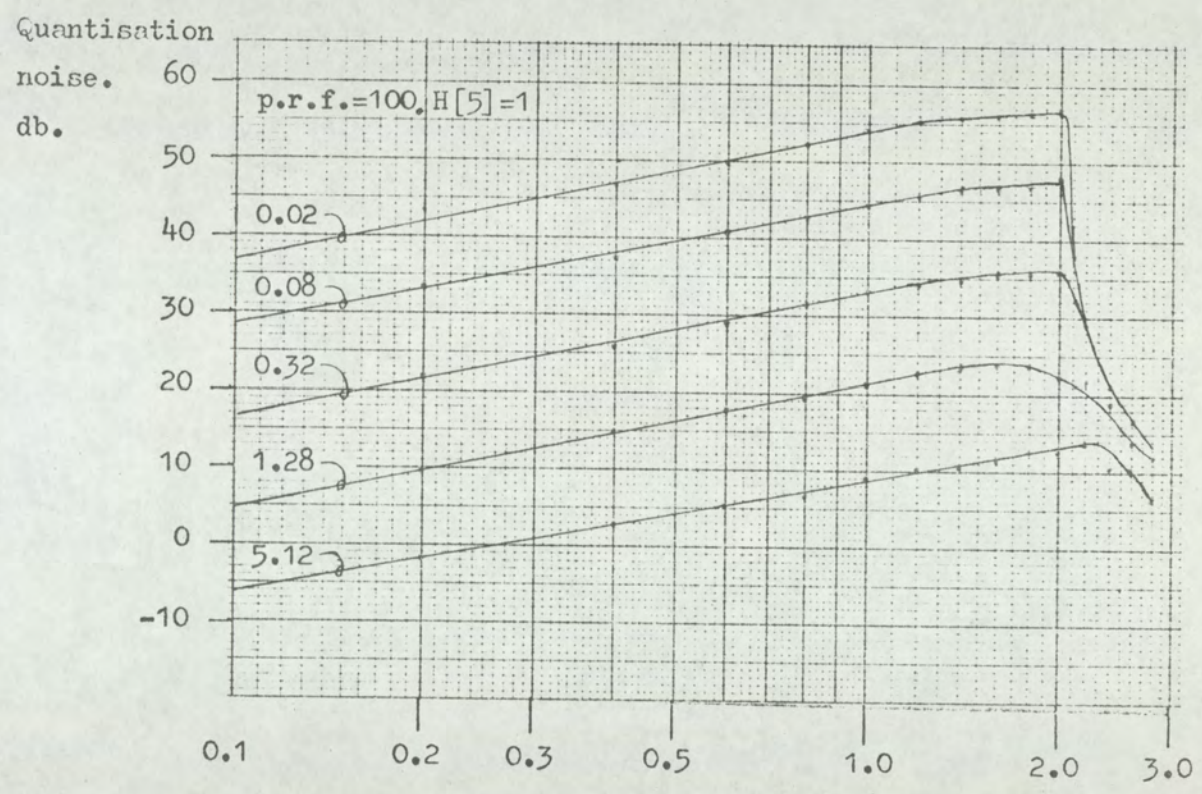
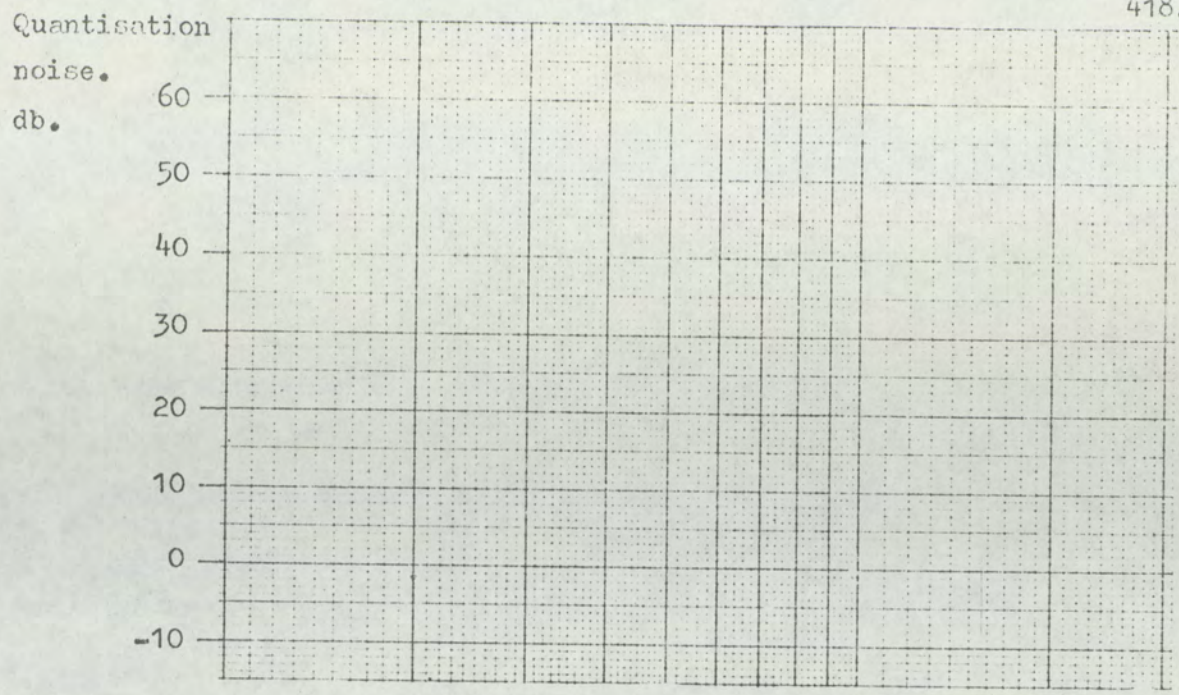
\*  $D$ , normalised modulating signal, single sine wave.



Normalised modulating signal, single sine wave.

(1.0 represents 100% loading of a single-integration, delta-modulator without adaptation.)

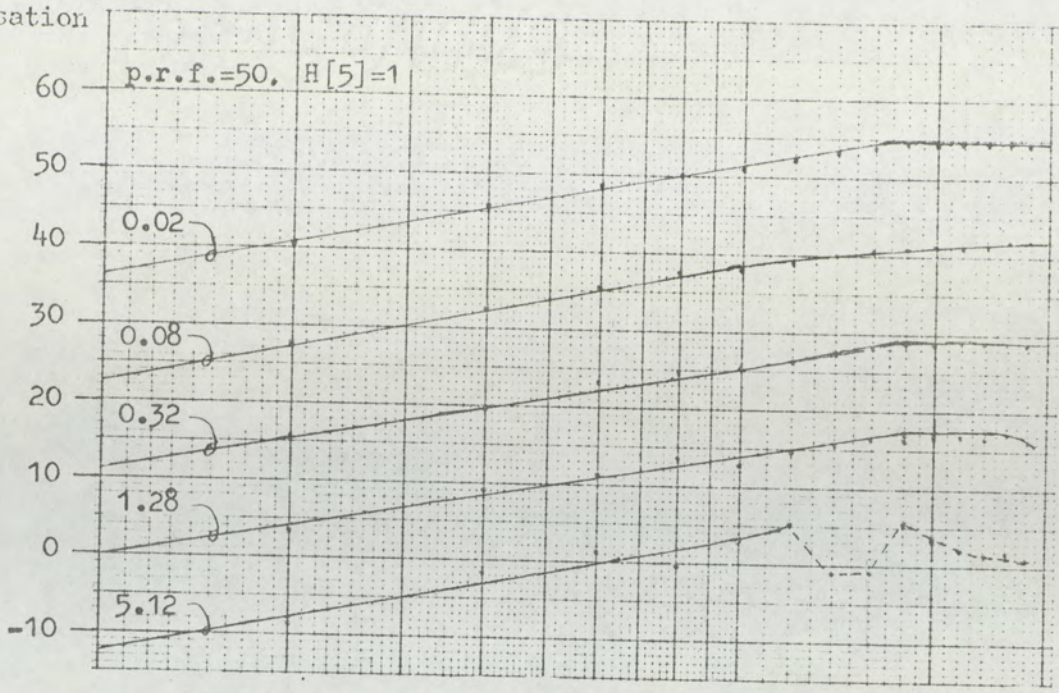
Fig.10-12. Signal to quantisation noise ratio against modulating signal showing constant frequency contours. Clock frequencies of 50, and 100 units. No adaptation applied to single-integration delta-modulator.



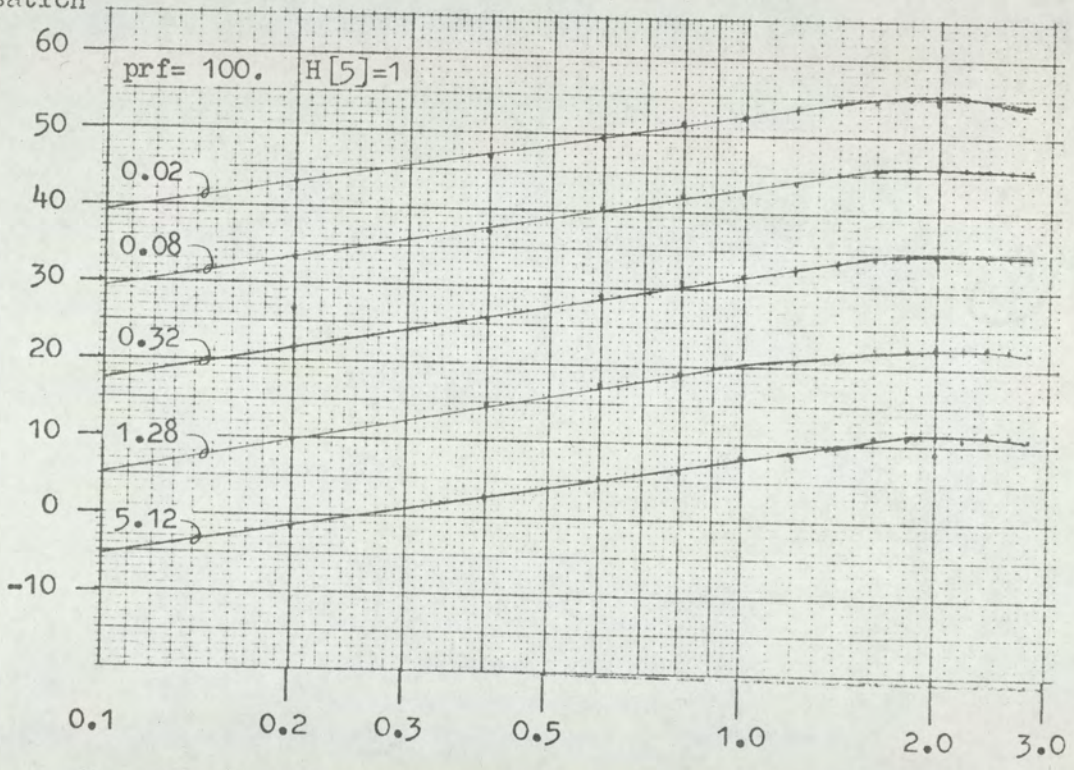
Normalised modulating signal, single sine wave.  
 (1.0 represents 100% loading of a single-integration, delta-modulator without adaptation.)

Fig.10-13. Signal to quantisation noise ratios against modulation depth for single-integration delta-modulator with second-order only adaptation. (clock pulse rate constant at 100 units.) Contours of constant frequency.

Quantisation  
noise.  
db.



Quantisation  
noise.  
db.



Normalised modulating signal, single sine wave.

(1.0 represents 100% loading of a single-integration, delta-modulator without adaptation.)

Fig.10-14. Signal to quantisation noise ratios against modulation depth for single-integration delta-modulation with second and third-order adaptation. (Clock pulse rates 50 and 100 units.) Contours of constant frequency.

## CHAPTER 11. EXPERIMENTAL RESULTS.

### 11.1 Objective waveform tests and results. (60)

The C.I.S.S system, the instrumentation of which was described in chapter 9, was subjected to a series of waveform tests to ascertain its performance capability. The tests were designed to examine the system bandwidth, channel linearity and **inter-channel crosstalk** under various modulation conditions.

For bandwidth testing a '2T' pulse and bar waveform was used, from which a K-rating could readily be determined. Theoretical analysis of pulse and bar testing can be found in the literature. The measurement equipment used for these tests were:

2T,T, pulse and bar generator,

Marconi Instruments Ltd.

Generator Waveform 11B (S.No.210308/20.)

Solatron Oscilloscope Type CD814-2/NS 3.

S.No.111211, No. 8A.

Standard K-rating.

The results of the '2T' pulse and bar tests are shown in Figs 11-6 (b) and (c). The waveforms show a slight fall in the high-frequency response. The K-rating was approximately 3 when the modulators were switched out of circuit, falling to 4 when the modulation were switched in and the signal encoded at a rate of 100 kHz. The **trailing** edge of the '2T' pulse shows considerable ringing, this being slightly exaggerated when the luminance delta-

sigma modulator was operating. The ringing represented the greatest error on the '2T' pulse, with a k-rating exceeding 4. The ringing on the **trailing** edge is due mainly to the luminance low-pass filter **accentuated** by errors in the pre-emphasis and de-emphasis networks.

The C.I.S.S. was used in conjunction with the vision signal circuitry of the Pye display monitor type which also supplied the P.A.L. decoding facilities. Thus, the above K-ratings include the monitor circuits which supplies the vision signals  $E_R, E_G, E_B$  from the composite input signal. Since the '2T' pulse generator supplied no chrominance information,

$$E_R = E_G = E_B$$

The '2T' pulse therefore tested only the luminance circuitry. However, '2T' testing of the independent channels  $E_R, E_G, E_B$  is unsuitable due to the restricted bandwidth of the chrominance channel.

The effects of non-linearity and overshoot on the luminance channel with and without pulse modulation was investigated by a series of staircase and **sawtooth** (linear ramp) waveform. These waveforms were obtained from the following equipment:

Generator Waveform 10<sub>c</sub>, (M k A)

Marconi Instruments Ltd.,

S.No. 55170/42.

The results of the staircase waveform applied to the luminance channel only is shown in Figs. 11-1, (a), (b) (c) and Fig. 11-6 (a). The waveforms show no pulse overshoot or ringing effects.

However, examination of Figs 11-1 (b) and (c) show clearly the non-linear encoding affects of the luminance delta-sigma modulator. The effect is seen to be a displacement of the amplitude levels in the staircase. The non-linearity is accentuated at the lower pulse rate of 50MHz, as shown in Fig. 11-1(c), where the increased quantisation noise can readily be observed as a blurring of the waveform.

Non-linearity in the luminance encoder is also well illustrated by using a **sawtooth** waveform, as shown in Figs. 11-5(a), (b) and (c). Fig 11-5 (c) clearly shows that the non-linearity increases at reduced pulse rates. The waveforms show also that the non-linear effect covers medium to large picture areas, this being indicated by the plateaus in the waveform. This suggests that increasing, effectively, the effective time constant of the integrator would be advantageous. However, this was not possible in the present design of h.f. delta-sigma modulator, due to diminished amplitude of the integrated error signal.

The effect on non-linearity of the luminance encoder was also investigated with the presence of superimposed, chrominance sub-carrier signal of constant amplitude and phase. The superimposed sub-carrier was added to both the staircase and the **sawtooth** waveforms by means of the facility provided by the  $10_C$  waveform generator. The results are shown in Figs. 11-3 (a), (b), (c), (d), (e), (f) and Figs 11-4 (a), (b), (c), (d), (e), (f). A differential-gain test set was used to determine the amplitude modulation of the subcarrier component due to the C.I.S.S both with and without digital encoding.

The differential gain test set used was,

Measuring set, No.43B, S.No.057

Link Electronics, differential-gain and phase set.

The waveforms Figs 11-3 (b),(c) and Figs 11-4 (b), (c) show that in the low greys, the linear vision signal circuits introduce in excess of 10% differential gain distribution. Introducing the delta-sigma modulators causes severe changes in differential gain. This effect is predictable, since the encoding accuracy of the pulse modulator falls with rising signal frequency, thus the quantisation error is high at the sub-carrier frequency. Comparing waveforms Fig.11-3(e) and Fig.11-4(e) and waveforms Fig.11-3(f) and Fig 11-4 (f), considerable similarity can be observed. Thus, the finite steps of the staircase waveform only cause minor changes in the differential gain profiles of the luminance encoder. The presence of sub-carrier does, however, improve the encoding of the luminance signal. This is best observed by comparing the signal envelope of Fig.11-4 (d) with the staircase waveform of Fig.11-1 (b) and similarly for Fig 11-5 (b) and Fig 11-4 (d). This encoding improvement could usually be observed on true picture signals by comparing pictures with and without the presence of the chrominance sub-carrier. The effect of the presence of sub-carriers was investigated in other tests to be described.

The tests described so far have used only the luminance channel, although it should be noted that chrominance channel was still in circuit. The chrominance channels were tested for independent channel response and for inter-channel crosstalk. These tests used the staircase and the sawtooth waveforms. Initially, the staircase waveform was applied to each of the three channels in turn. The staircase waveform, for each channel, was examined without

digital encoding, with digital encoding at 100MHz and no sub-carrier and finally encoded at 100 MHz with the presence of sub-carrier. The red, green and blue channel responses are shown on traces, Fig.11-1 (d),(e),(f); Figs.11-2 (a),(b),(c) and Figs 11-2 (d),(e),(f) respectively. The traces clearly show that the green channel is most accurately encoded, then red and finally the blue channel. This is due to the weighting of the red, green and blue channels when forming the chrominance signals. The traces also show how the presence of sub-carrier can improve the encoding accuracy of each channel, making the step height of each encoded signal almost equal. Since the blue channel effectively has most amplification in the decoding circuits, the effect of ringing in the low-pass filter can be observed on the blue staircase signal, even without encoding.

A similar series of tests were performed using the sawtooth waveform without sub-carrier. These tests were applied at encoding rates of 100 MHz and 50MHz, since the sawtooth waveform is more revealing as to the non-linearity in the dynamic range of the system. Figs.11-5(d), (e),(f) show the red, green and blue channel responses when encoded at 100 MHz, while Figs 11-7(d),(e),(f) repeat the same tests at 50MHz. The tests at 50MHz clearly illustrate the weighting of coding accuracy between the red, green and blue channels and show the blue-channel encoding to be extremely poor on this test.

Finally, inter-channel crosstalk was examined. This set of tests used the staircase waveform. Basically, equal proportions of the staircase signal were applied to two out of the three channels, and the output of the third channel was recorded; thus three tests were required. The three tests were performed under two conditions,

modulation switched out and encoded at 100 MHz. The traces are shown in Figs. 11-6 (d), (e), (f) and Figures 11-7 (a), (b), (c) respectively. The trace of Fig. 11-6 (f) reveals that the system was not correctly adjusted, as the waveform displayed a small rising slope. Since it is only possible to differentiate between signals below 1.1 MHz., the transition points on the staircase signal can clearly be seen. The transitions represent high-frequency information in the luminance channel and therefore appear at the output of the system. The non-linear distortions in the encoding process accentuate the steps on the staircase, as would be expected; these are clearly evident in Figs. 11-7 (a), (b), (c).

In this series of tests it was necessary, for testing the chrominance circuits, to choose a set of test signals that were periodic with a fundamental component at line frequency (neglecting field synchronisation which in this instance was omitted). This was because of the nature of encoding the chrominance, since the vertical chrominance resolution was limited by signal averaging. Thus, it was not possible to make sine-wave tests independently on each channel. This also was not possible because line synchronisation information was necessary for correct system operation.

Finally, it is stressed that the system was not deliberately adjusted to give optimum inter-channel crosstalk and colour-balance responses prior to all tests (other than the d.c. level of the signal applied to the luminance and chrominance delta-sigma modulators). This system had been accurately adjusted approximately one month before the tests. The tests thus indicate that the system was stable and that no major re-alignment was necessary.

- Fig.11-1...(a). Staircase input signal with zero chrominance, monitored on green output with modulators switched out.
- (b). Staircase input signal with zero chrominance monitored on green output, encoded at 100MHz.
- (c). Staircase input signal with zero chrominance, monitored on green output, encoded at 50MHz.
- (d). Staircase input signal to red channel only, monitored on red output, with modulators switched out.
- (e). Staircase input signal to red channel only, monitored on red output, encoded at 100MHz.
- (f). Staircase input signal with sub-carrier to red channel, monitored on red output, encoded at 100MHz.
- Fig.11-2...(a). Staircase input signal to green channel only, monitored on green output, with modulators switched out.
- (b). Staircase input signal to green channel only, monitored on green output, encoded at 100MHz.
- (c). Staircase input signal with sub-carrier to green channel, monitored on green output, encoded at 100MHz.
- (d). Staircase input signal to blue channel only, monitored on blue output, with modulators switched out.
- (e). Staircase input signal to blue channel only, monitored on blue output, encoded at 100MHz.
- (f). Staircase input signal with sub-carrier to blue channel, monitored on blue output, encoded at 100MHz.
- Fig.11-3...(a). Ramp and sub-carrier input signal with zero chrominance, monitored on green output, with modulators switched out.
- (b). Differential gain profile derived from the waveform in Fig.11-3(a).
- (c). As in Fig.11-3(b) but with 10% gain shift.
- (d). Ramp and sub-carrier input signal with zero chrominance, monitored on green output, encoded at 100MHz.

(e). Differential gain profile derived from the waveform in Fig.11-3(d).

(f). As Fig.11-3(e) but encoded at 50MHz.

Fig.11-4...(a). Staircase and sub-carrier input signal with zero chrominance, monitored on green output, with modulators switched out.

(b). Differential gain profile derived from Fig.11-4(a).

(c). As in Fig.11-4(b) but with 10% gain shift.

(d). Staircase and sub-carrier input signal with zero chrominance, monitored on green output, encoded at 100MHz.

(e). Differential gain profile derived from the waveform in Fig.11-4(d).

(f). As in Fig.11-4(e) but encoded at 50MHz.

Fig.11-5...(a). Ramp input signal, zero chrominance, monitored on green output, with modulators switched out.

(b). As in Fig.11-5(a) but encoded at 100MHz.

(c). As in Fig.11-5(a) but encoded at 50MHz.

(d). Ramp input to red channel only, monitored on red output and encoded at 100MHz.

(e). Ramp input to green channel only, monitored on green output and encoded at 100MHz.

(f). Ramp input to blue channel only, monitored on blue output and encoded at 100MHz.

Fig.11-6...(a). Staircase input signal to system, zero chrominance, modulators switched out.

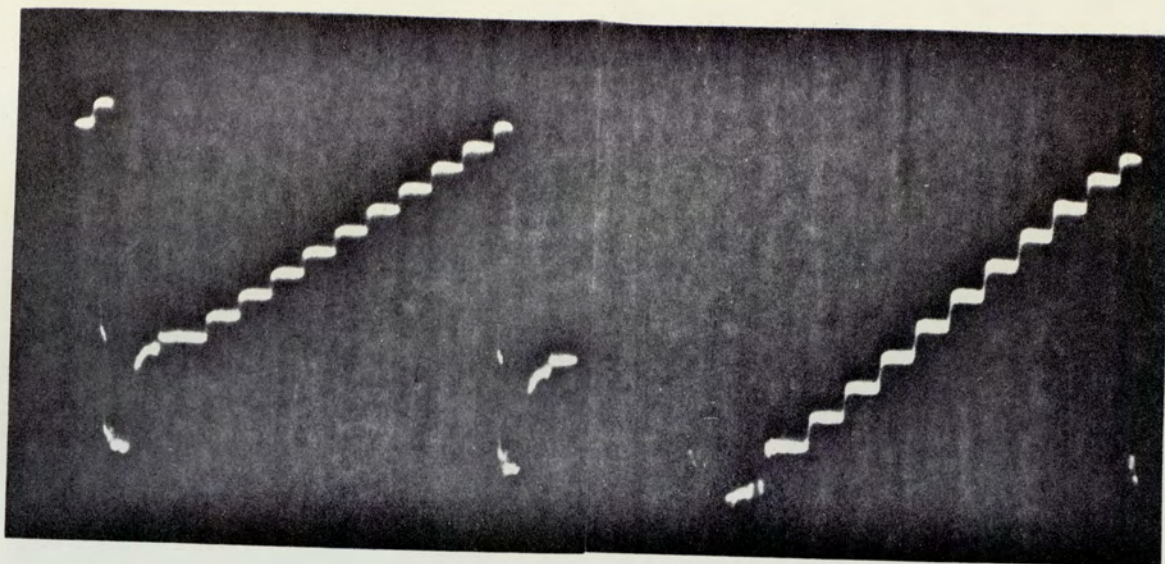
(b). 2T pulse drive, zero chrominance and modulators switched out, monitored on green output.

(c). As in Fig.11-6(b), but encoded at 100MHz.

- (d). Staircase input signal to green and blue channels monitored on red output, modulators switched out.
- (e). Staircase input signal to red and blue channels, monitored on green output, modulators switched out.
- (f). Staircase input signal to red and green channels monitored on blue output, modulators switched out.

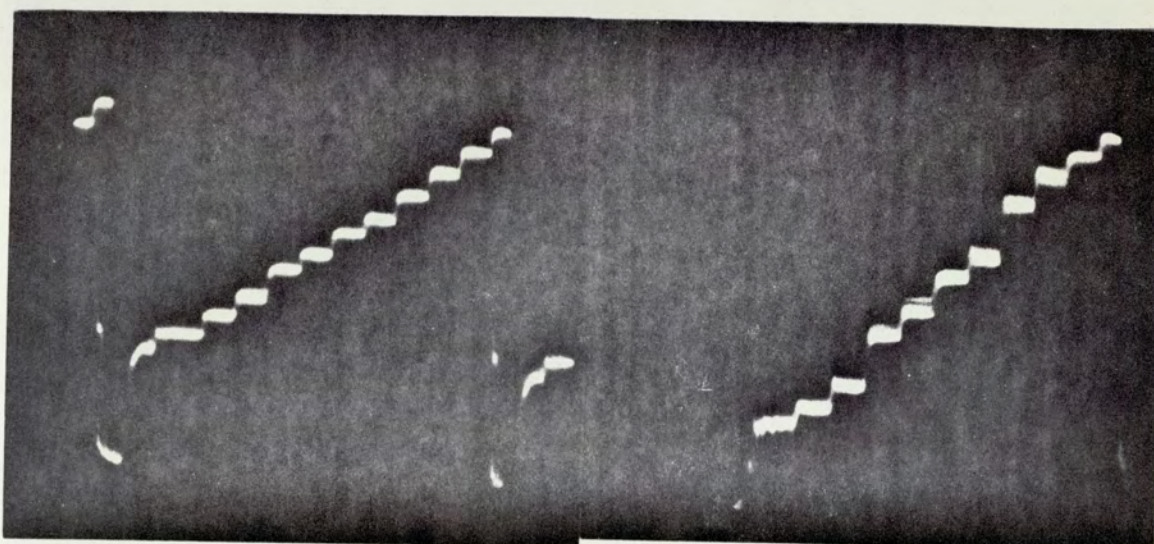
Fig.11-7...(a). Staircase input signal to green and blue channels monitored on red output and encoded at 100MHz.

- (b). Staircase input signal to red and blue channels monitored on green output and encoded at 100MHz.
- (c). Staircase input signal to red and green channels monitored on blue output and encoded at 100MHz.
- (d). Ramp input to red channel only, monitored on red output and encoded at 50 MHz.
- (e). Ramp input to green channel only, monitored on green output and encoded at 50MHz.
- (f). Ramp input to blue channel only, monitored on blue output and encoded at 50MHz.



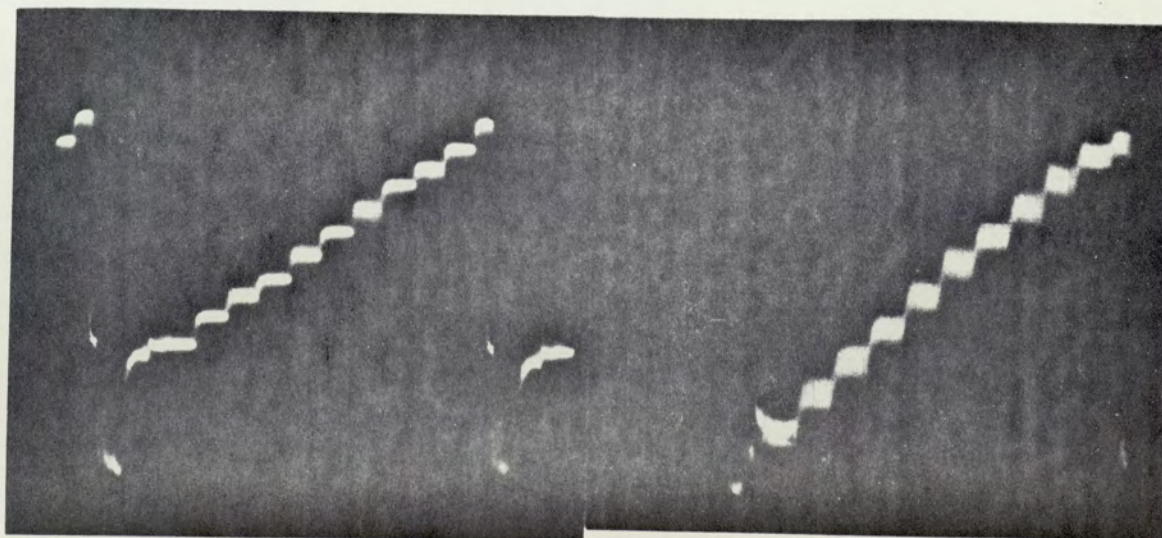
(a)...

(d)...



(b)...

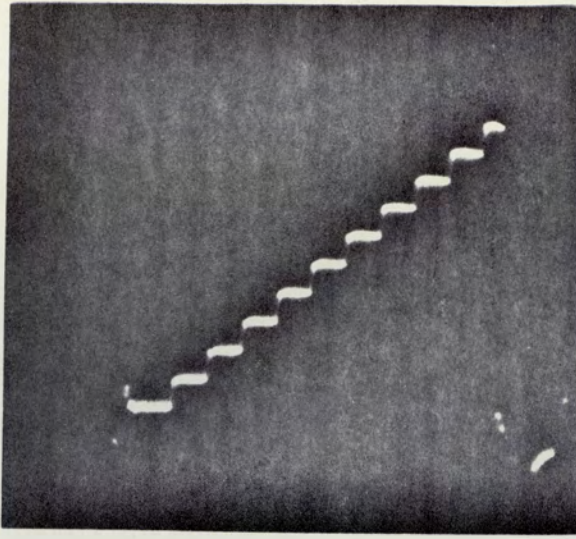
(e)...



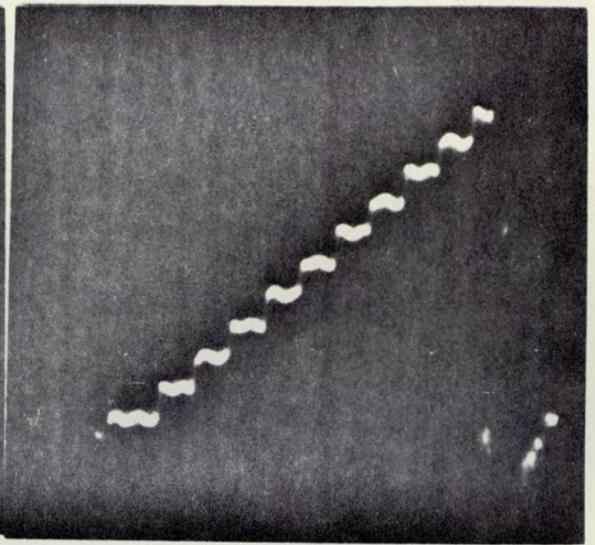
(c)...

(f)...

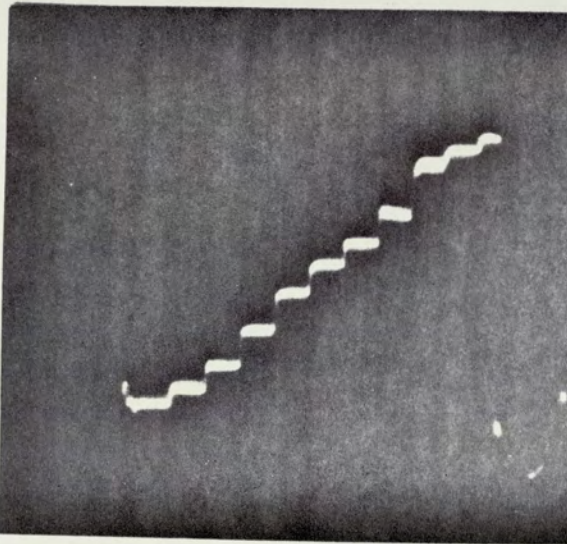
Fig.11-1. System test waveforms and performance record.  
(see page426 for list of sub-captions).



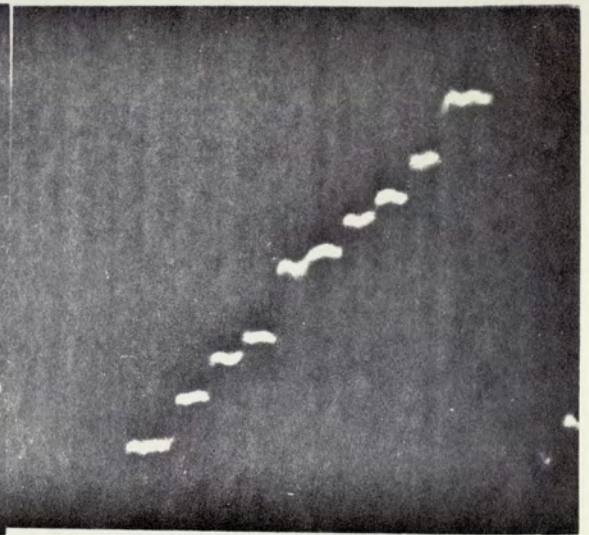
(a)...



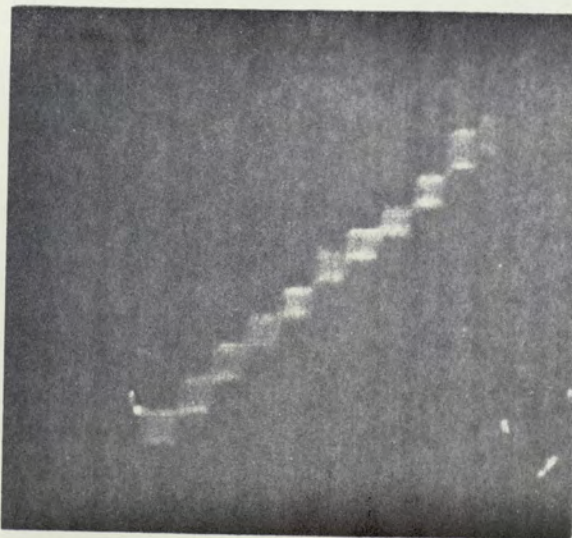
(d)...



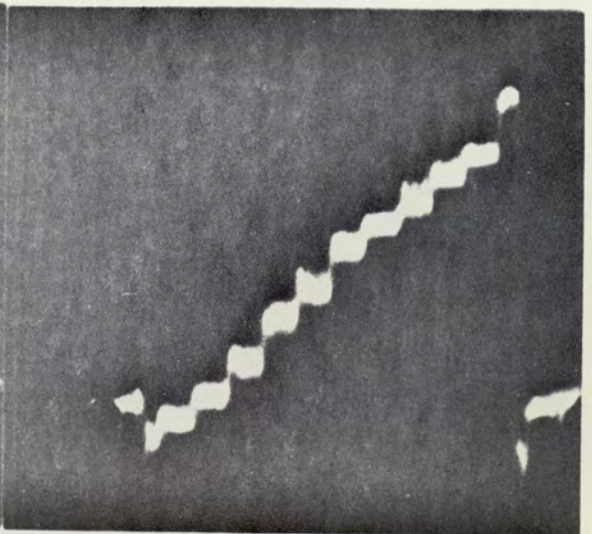
(b)...



(e)...



(c)...



(f)...

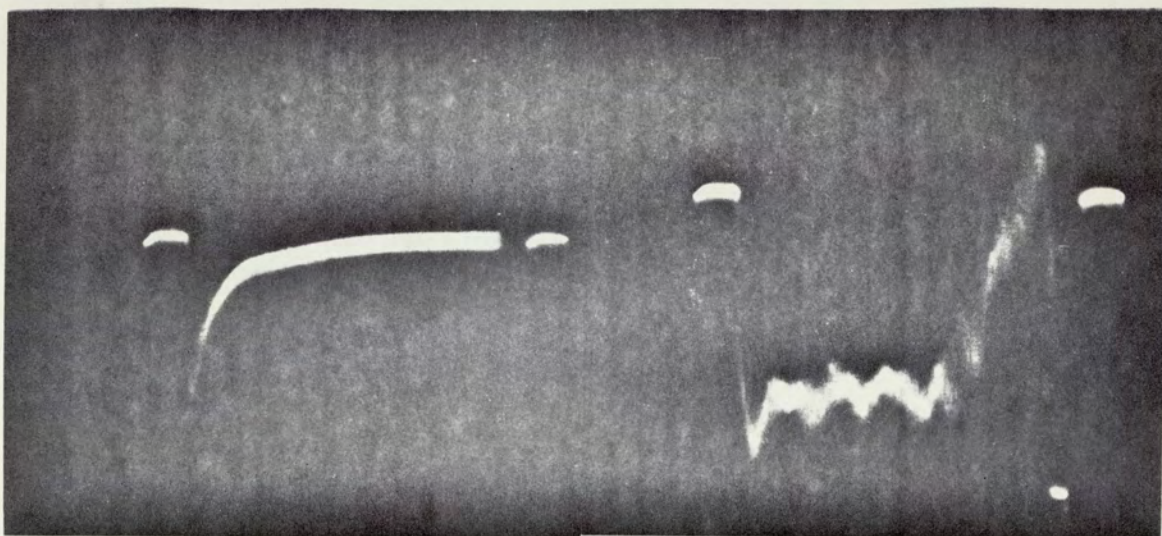
Fig.11-2. System test waveforms and performance record.

(see page 426 for list of sub-captions).



(a)...

(d)...



(b)...

(e)...

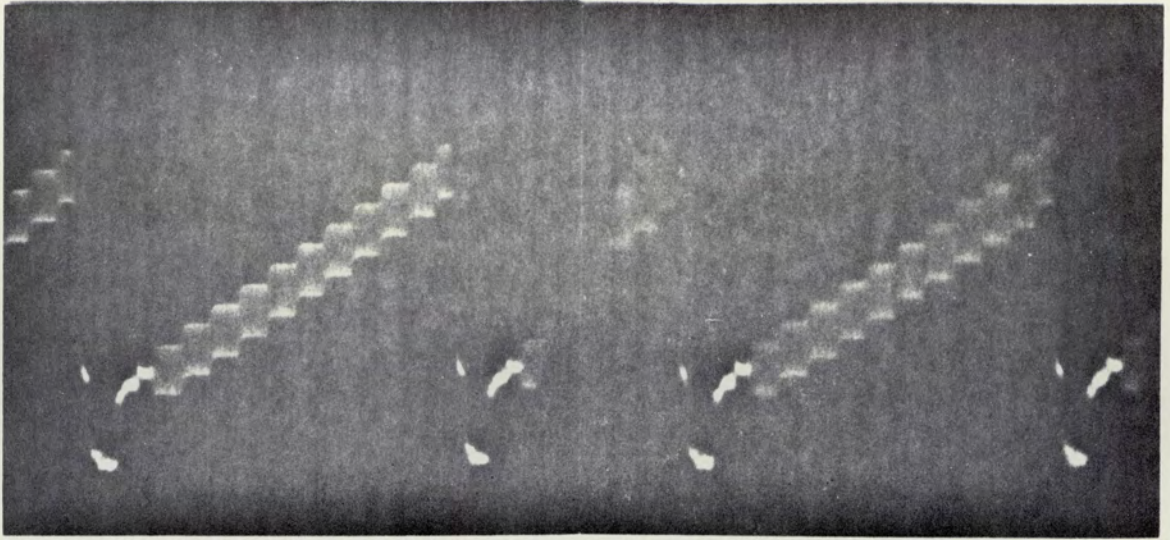


(c)...

(f)...

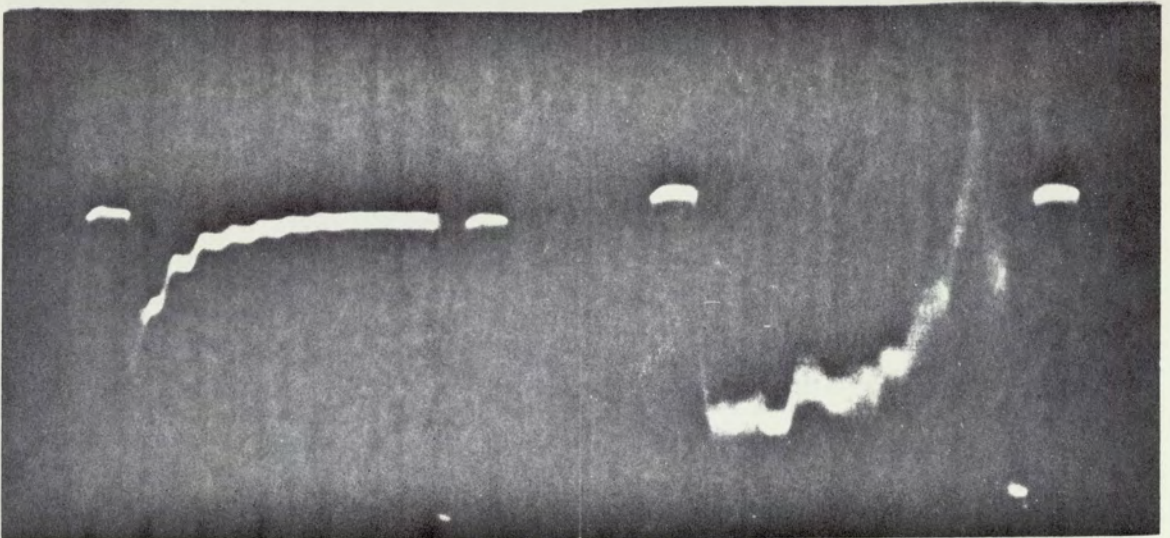
Fig.11-3. System test waveforms and performance record.

(see page 426 for list of sub-captions).



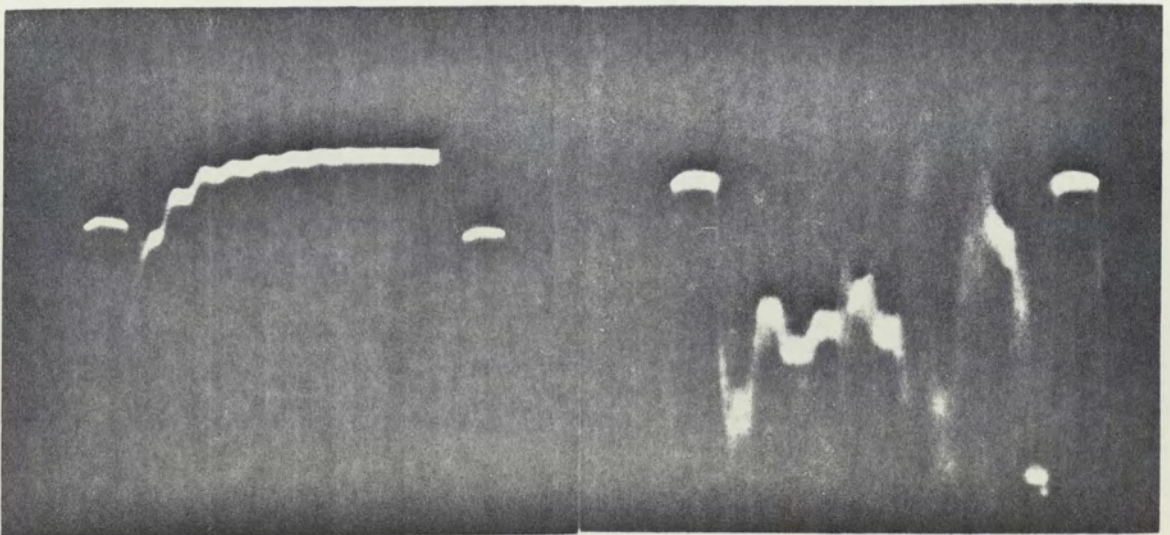
(a)...

(d)...



(b)...

(e)...

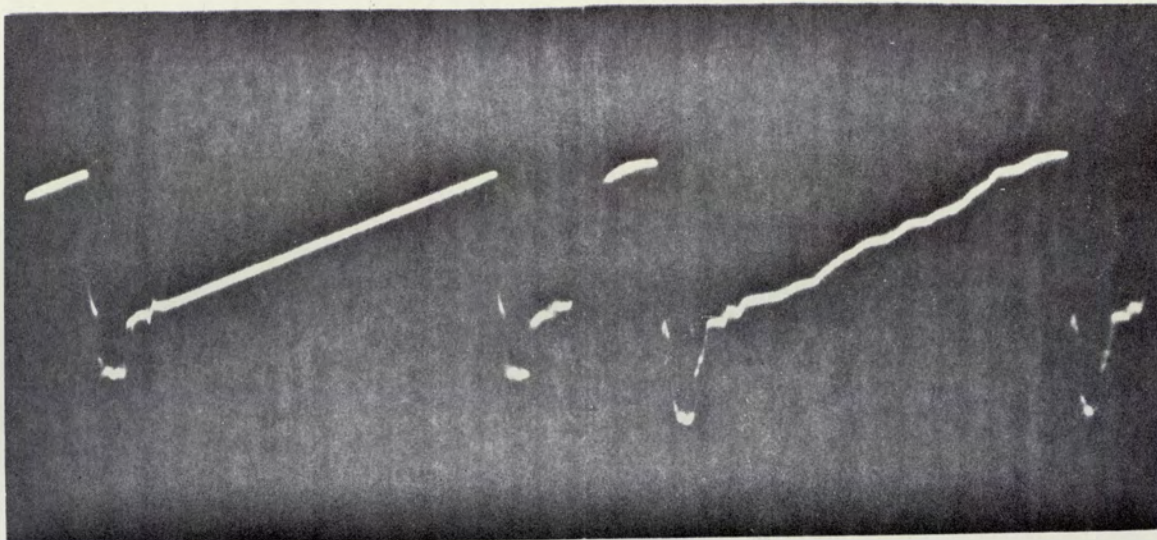


(c)...

(f)...

Fig.11-4. System test waveforms and performance record.

(see page 427 for list of sub-captions).



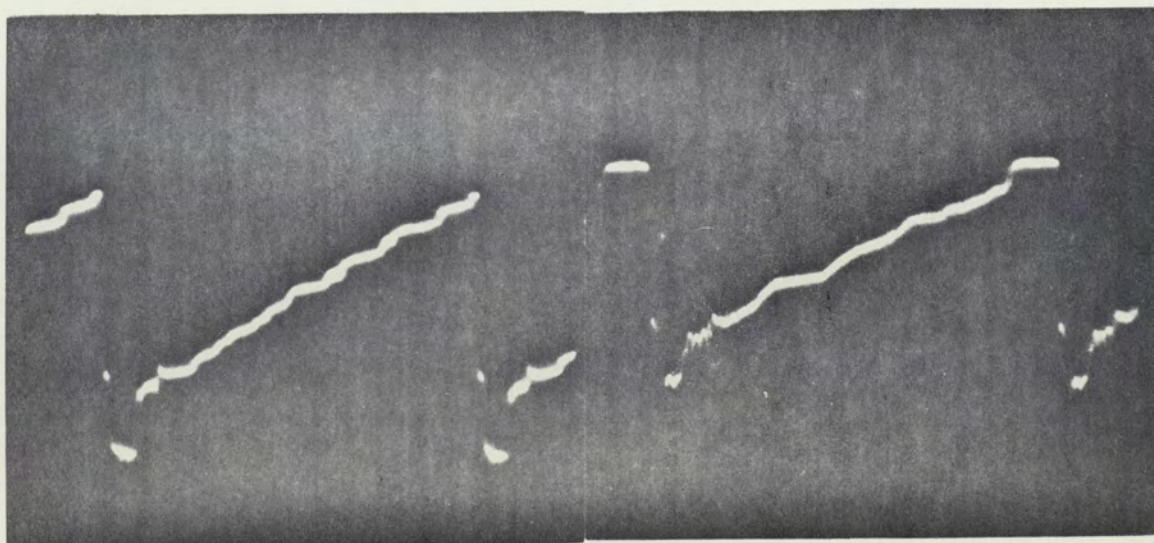
(a)...

(d)...



(b)...

(e)...

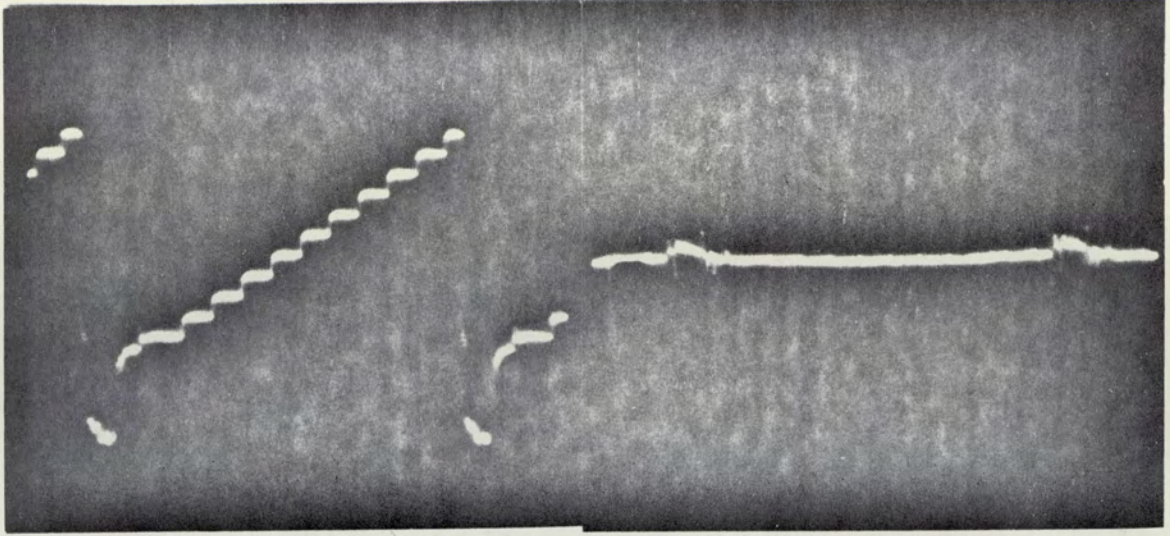


(c)...

(f)...

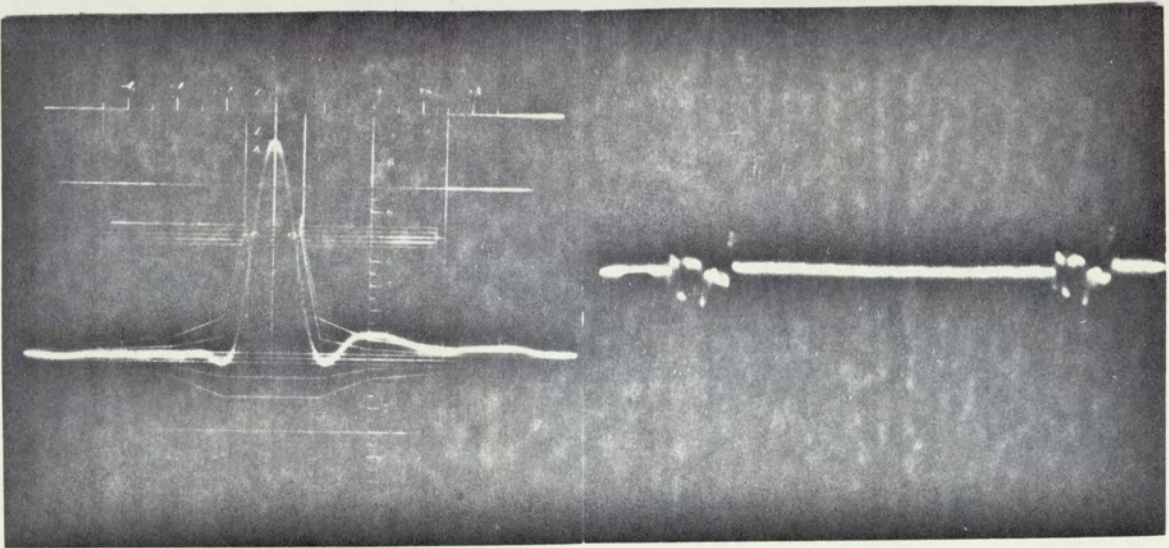
Fig.11-5. System test waveforms and performance record.

(see page 427 for list of sub-captions).



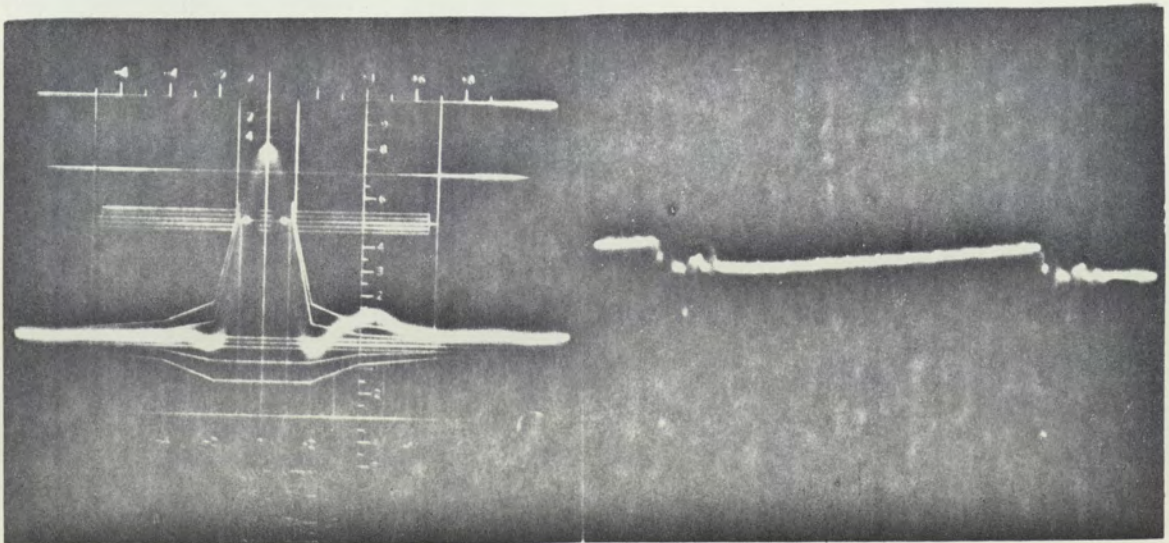
(a)...

(d)...



(b)...

(e)...

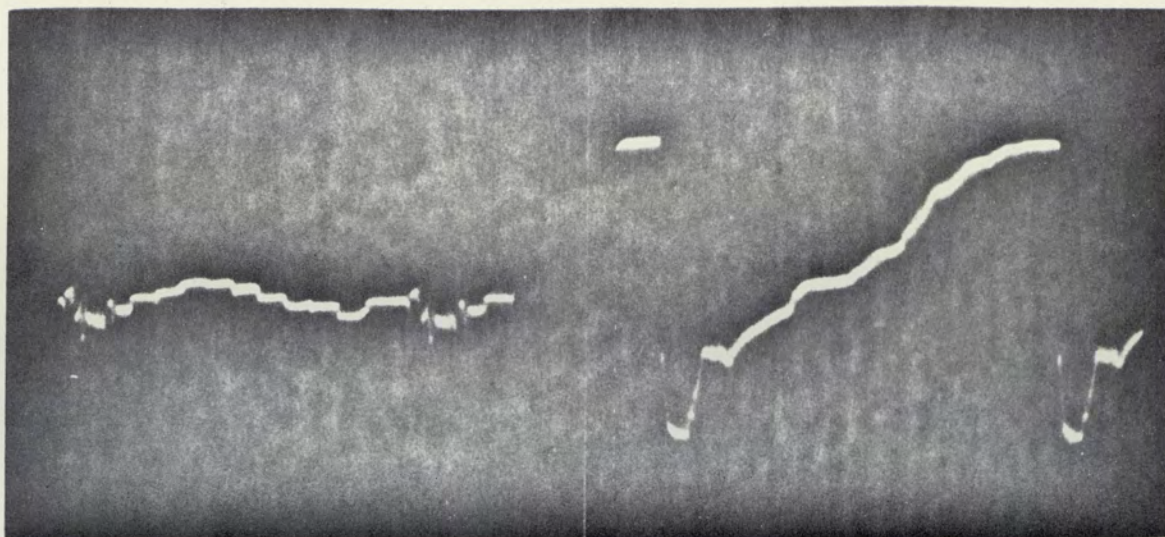


(c)...

(f)...

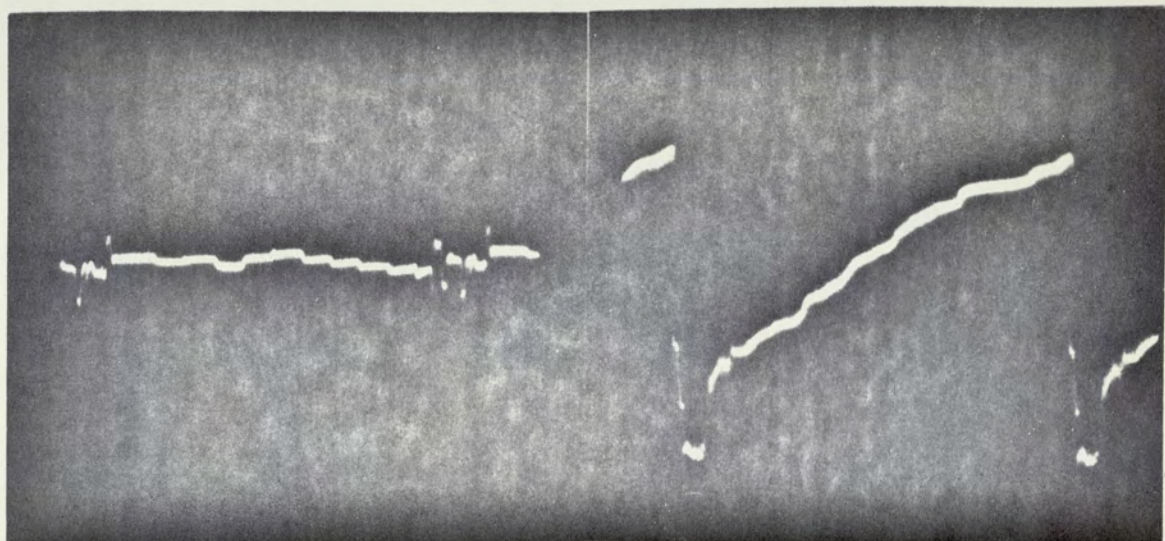
Fig.11-6. System test waveforms and performance record.

(see page 427 for list of sub-captions).



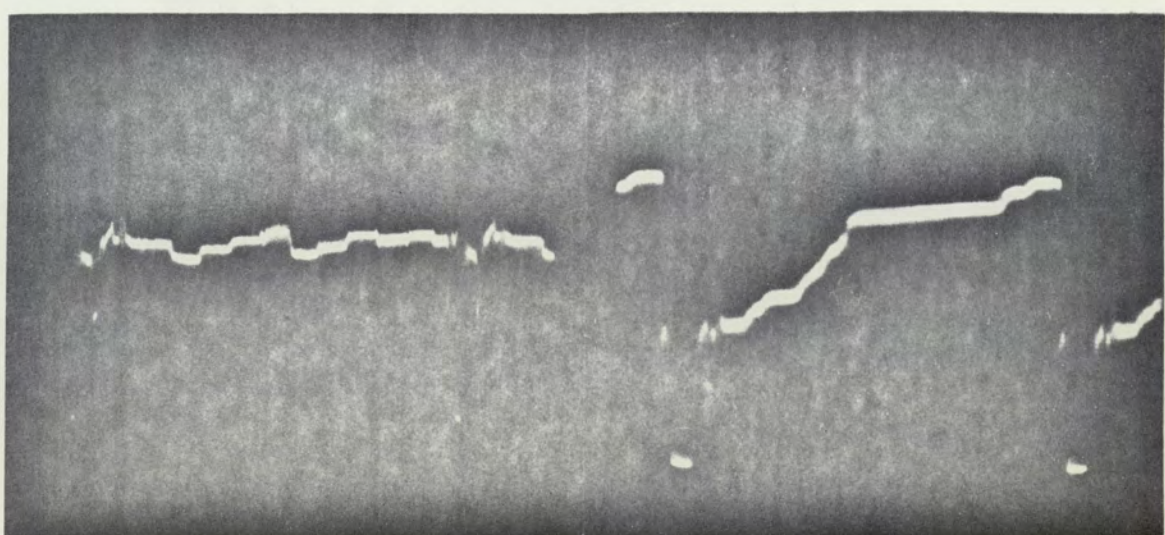
(a)...

(d)...



(b)...

(e)...



(c)...

(f)...

Fig.11-7. System test waveforms and performance record.  
(see page 428 for list of sub-captions).

## 11.2 Objective picture tests and results.

A series of photographs were made of the display on the colour monitor. The images chosen were a set of colour pictures (motionless) which were broadcast by the I.T.A. network forming part of their daily trade test programme. The results of these tests are shown Fig 11.9 to Fig. 11.17 inclusive. Fig. 11.9 to Fig. 11.13 include five groups of four pictures. The first picture, (a) in each group, is without digital encoding but through the analogue circuitry; the second picture, (b), is with digital encoding at 100MHz, the third picture (c), with digital encoding at 50MHz and finally the fourth picture, (d), with encoding at 18-25 MHz. (The tolerance on the latter pulse rate is due to the frequency not being accurately determined in the time available to record the display.)

When pictures are obtained from a t.v. display, considerable difficulty can be experienced in obtaining the correct exposure and colour balance. The photographs presented were carefully balanced for colour by the printer. However, photographs in sets I(a), (b) and sets (c), (d) were taken on different occasions and printed independently; thus considerable differences in colour balance and contrast can be observed.

Generally, difference between the direct signals and the signals encoded at 100 MHz (20MHz chrominance) are extremely small, being mainly small changes in saturation. However the photographs fail to show the low-noise effects in the form of moderate-level streaking in horizontal bands across the picture. This effect, although not generally disturbing at normal viewing distances was noticeable. On reducing the pulse rate to 50MHz (10MHz chrominance), chrominance

distortion become more objectionable, especially in the dark red, magentas and blues. Also, changing the d.c. level of the chrominance signal by small amounts (prior to the chrominance delta-sigma modulator) could produce changes in hue, especially in the red regions. At this frequency, the 'granular' back-ground noise of the picture had deteriorated although it was still at an acceptable level. However, introduction of the second-order adaptive delta-sigma modulator and pre-emphasis/de-emphasis networks improved the performance considerably. On monochrome pictures, contouring was observable at 50MHz, although the presence of chrominance information improved this defect.

At the lower pulse rate (18 to 25MHz), although luminance information was observable, the chrominance was either absent or highly distorted. Thus with the present system, results at these low pulse rates were not considered to be of practical use. The photographs in Figs 11.14 to Fig 11.17 show pictures encoded at 50MHz and at the lower rate (18 to 25MHz).

The two pictures shown in Fig 11.8 illustrate the effect of the non-linearity of the luminance delta-sigma modulator. The photographs Fig 11.8(a) corresponds to Fig 11.5(a), while Fig. 11.8(b) corresponds to Fig 11.5(b). The effect, although visible, is generally only objectionable under strict test conditions, such as sawtooth waveform testing. For normal picture signals, the effect is marked by noise and other detail to which the eye cannot give an accurate reference.

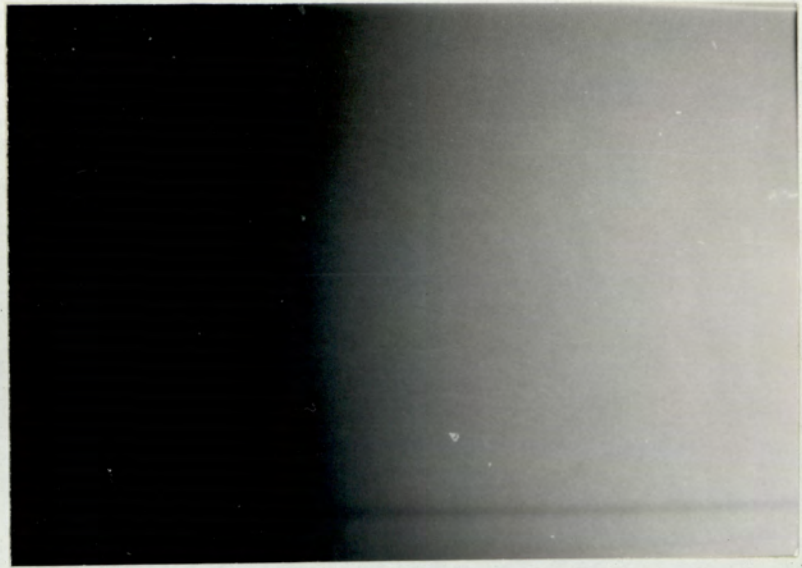


Fig.11-8(a). Ramp input to C.I.S.S.,luminance drive only,delta-sigma modulators switched out.



Fig.11-8(b). Ramp input to C.I.S.S.,luminance drive only,delta-sigma modulators switched in. (encoding rate (100MHz.)).



Fig.11-9(a). Through C.I.S.S., delta-sigma modulators switched out.



Fig.11-9(b). Through C.I.S.S., delta-sigma modulators switched in, encoding rate 100MHz.



Fig.11-9(c). Through C.I.S.S., delta-sigma modulators switched in, encoding rate 50 MHz.



Fig.11-9(d). Through C.I.S.S., delta-sigma modulators switched in, encoding rate 18  $\rightarrow$  25 MHz.



Fig.11-10(a). Through C.I.S.S.,delta-sigma modulators switched out.



Fig.11-10(b). Through C.I.S.S.,delta-sigma modulators switched in, encoding rate 100 MHz.



Fig.11-10(c). Through C.I.S.S.,delta-sigma modulators switched in, encoding rate 50 MHz.



Fig.11-10(d). Through C.I.S.S.,delta-sigma modulators switched in, encoding rate 18 → 25 MHz.



Fig.11-11(a). Through C.I.S.S.,delta-sigma modulators switched out.



Fig.11-11(b). Through C.I.S.S.,delta-sigma modulators switched in, encoding rate 100 MHz.



Fig.11-11(c). Through C.I.S.S.,delta-sigma modulators switched in, encoding rate 50 MHz.



Fig.11-11(d). Through C.I.S.S.,delta-sigma modulators switched in, encoding rate 18 → 25 MHz.

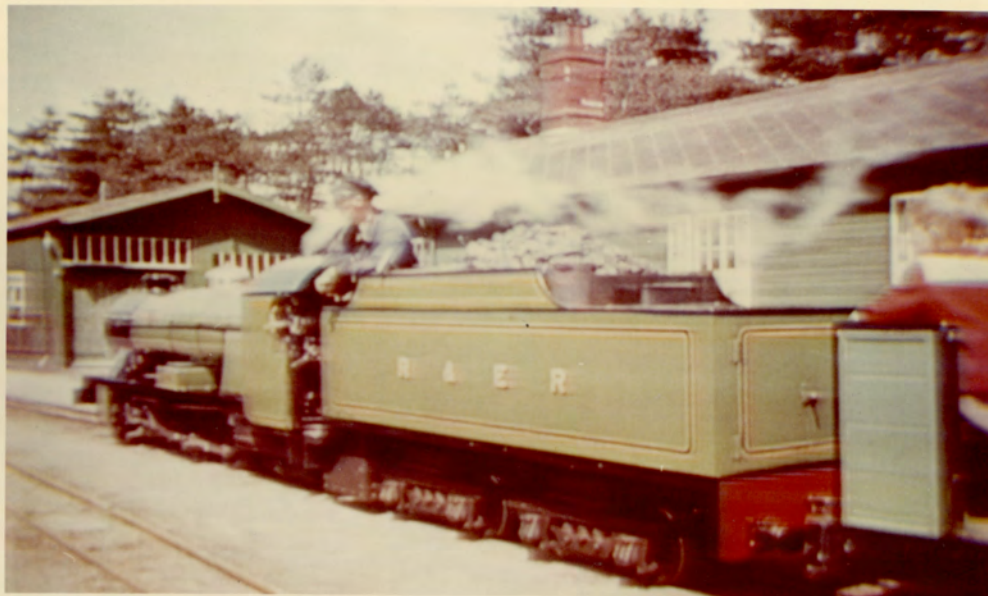


Fig.11-12(a). Through C.I.S.S.,delta-sigma modulators switched out.



Fig.11-12(b). Through C.I.S.S.,delta-sigma modulators switched in, encoding rate 100 MHz.



Fig.11-12(c). Through C.I.S.S.,delta-sigma modulators switched in, encoding rate 50 MHz.

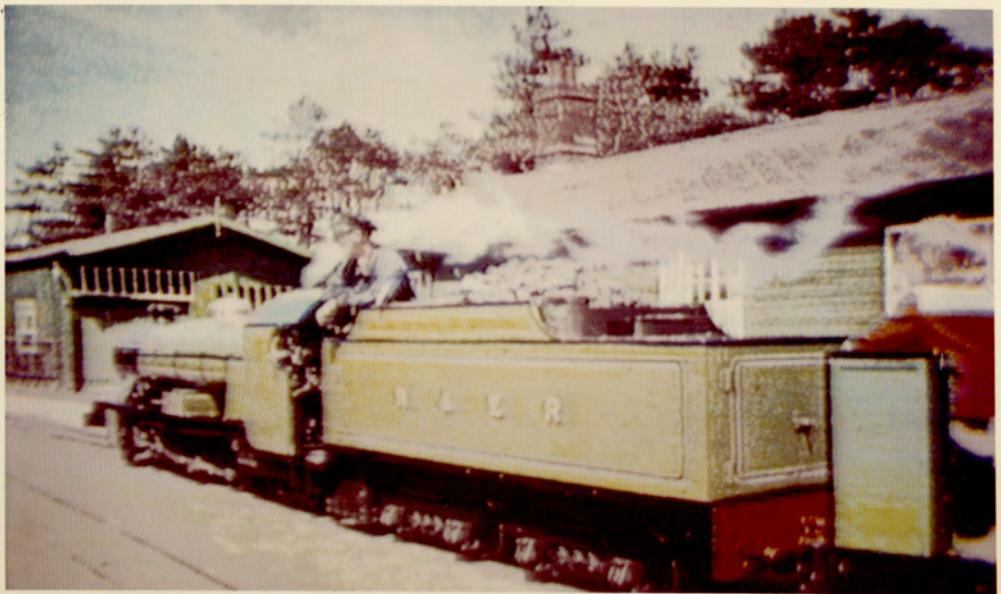


Fig.11-12(d). Through C.I.S.S.,delta-sigma modulators switched in, encoding rate 18 → 25 MHz.



Fig.11-13(a). Through C.I.S.S.,delta-sigma modulators switched out.



Fig.11-13(b). Through C.I.S.S.,delta-sigma modulators switched in, encoding rate 100 MHz.



Fig.11-13(c). Through C.I.S.S.,delta-sigma modulators switched in, encoding rate 50 MHz.



Fig.11-13(d). Through C.I.S.S.,delta-sigma modulators switched in, encoding rate 18 → 25 MHz.



Fig.11-14(a). Through C.I.S.S.,delta-sigma modulators switched in, encoding rate 50 MHz.



Fig.11-14(b). Through C.I.S.S.,delta-sigma modulators switched in, encoding rate 18 → 25 MHz.



Fig.11-15(a). Through C.I.S.S.,delta-sigma modulators switched in, encoding rate 50 MHz.

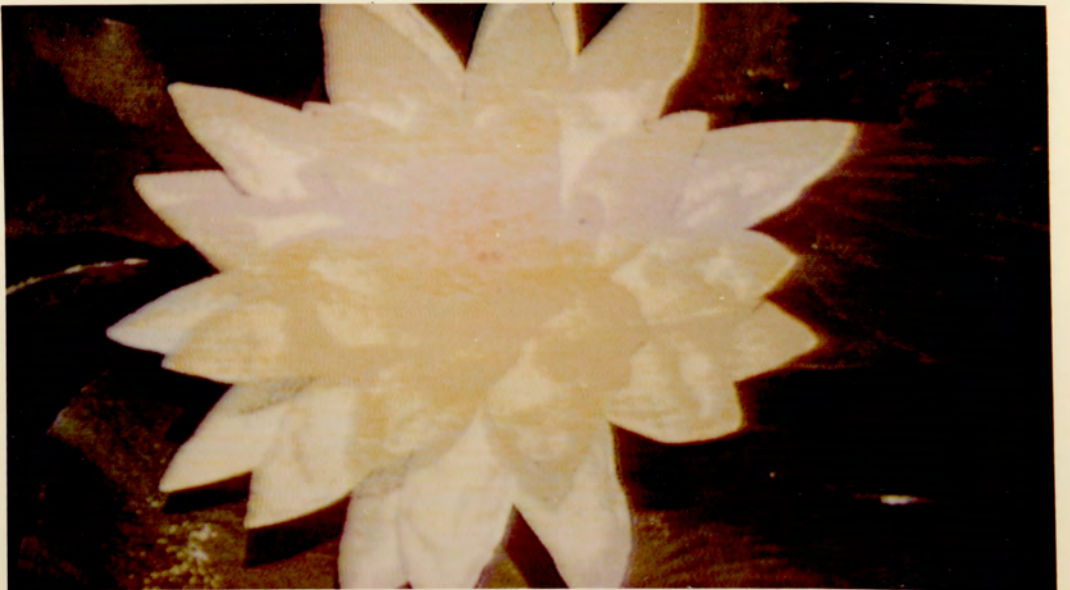


Fig.11-15(b). Through C.I.S.S.,delta-sigma modulators switched in, encoding rate 18 → 25 MHz.



Fig.11-16(a). Through C.I.S.S.,delta-sigma modulators switched in, encoding rate 50 MHz.



Fig.11-16(b). Through C.I.S.S.,delta-sigma modulators switched in, encoding rate 18 → 25 MHz.



Fig.11-17(a). Through C.I.S.S.,delta-sigma modulators switched in, encoding rate 50 MHz.



Fig.11-17(b). Through C.I.S.S.,delta-sigma modulators switched in, encoding rate 18 → 25 MHz.

### 11.3 Subjective tests and results. (62)

To obtain a measure of the subjective performance of the C.I.S.S. system, a varied panel of viewers was used to assess the picture quality. The objective was to obtain a measure of picture impairment due to digital encoding using delta-sigma modulation. Judgement was made using a series of eleven colour pictures displayed on the picture monitor. Nine of these colour pictures were those used in the tests of section 11.2 and displayed in Fig 11.9 to Fig 11.17. The viewers were required to make their judgement on a comparison between two versions of the same picture. The first picture was processed by the C.I.S.S. but excluded the luminance and chrominance delta-sigma modulators, while the second included the digital encoding system. By switching directly between the two pictures, judgement could be made by comparison. Two sets of comparisons were performed. The first compared on uncoded picture with a picture encoded at 100MHz pulse rate. The second made the comparison between the uncoded picture and a picture encoded at 50MHz.

The tests were performed in a darkened room at a viewing distance approximately six to eight times picture height. Each test consisted of a series of viewing sessions with groups of two or three viewers. Each picture was shown for approximately twenty seconds with about five comparisons displayed for each picture. A set of motionless pictures was chosen since it allowed amore accurate comparison to be made than is possible with pictures in motion. Thus, each image could be studied in detail.

Judgement was made on a standard E.B.U. impairment scale. <sup>62</sup>

The scale is as follows,

Table 11.1 E.B.U. impairment scale

GRADE	E.B.U. IMPAIRMENT SCALE
1.	Imperceptible
2.	Just perceptible
3.	Definately perceptible but not disturbing
4.	Somewhat objectionable
5.	Definately objectionable
6.	Unusable

Each viewer was asked to interpret the scale according to his or her own judgement. This condition was imposed to prevent any unnecessary conditioning or biasing by the implanting of ideas, thus defeating the objective of an independant opinion of impairment.

The results of the two sets of tests are shown in Fig.11.8 and Fig. 11.19. Fig. 11.18 refers to the 100MHz bit rate comparison while Fig. 11.19 refers to the 50MHz test. The two sets of results represent the normalised frequency of occurrence of each grade for each picture (i.e. the number of times each grade occurs for each picture. Figs. 11.18,11.19 also show the mean rate of occurrence of each grade averaged over the eleven pictures, (i.e. for each grade, the total number of times of occurrence of that grade was summed over the eleven pictures and then divided by the total number of samples) The results of this averaging were graphically displayed for each of the two comparison groups, and are shown in Fig. 11.18,19 under

'average result'.

The results suggest that for the 100MHz pulse rate the E.B.U. grading was about grade 2.23 while for the 50MHz pulse rate, the grading was about 2.82. The mean grading figures were obtained by taking moments, considering the total occurrence of each grade as the weight of that grade for the two tests.

During the tests, the main comments were concerned with the low-frequency noise (streaking) and changes in hue and saturation. In general, the photographs also display this change. At 50MHz, a distortion on highly-saturated reds became noticeable as the red tended to magenta. This effect was caused by overloading in the chrominance channel; it could usually be minimised by careful adjustment of the chrominance d.c. level applied to the chrominance delta-sigma modulator. The main objection to noise was in the low-luminance red, through magenta to the blue regions, where the effect was generally objectionable. It was noted, that the low-frequency noise was less objectionable at the lower pulse rate although granular noise was more evident. The effect is thought to be due to encoding errors formed by excessive loop delay and diminished error-voltage amplitude.

It can be stated that, in general, the viewers' opinion of the C.I.S.S. simulation was encouraging. The comments suggested that the errors were not objectionable and that pictures of lower quality than produced by C.I.S.S. were in many cases considered satisfactory.

Finally it must be emphasised that the test were performed from signals received off the air and that transmission noise masked some of the effects of digital modulation.

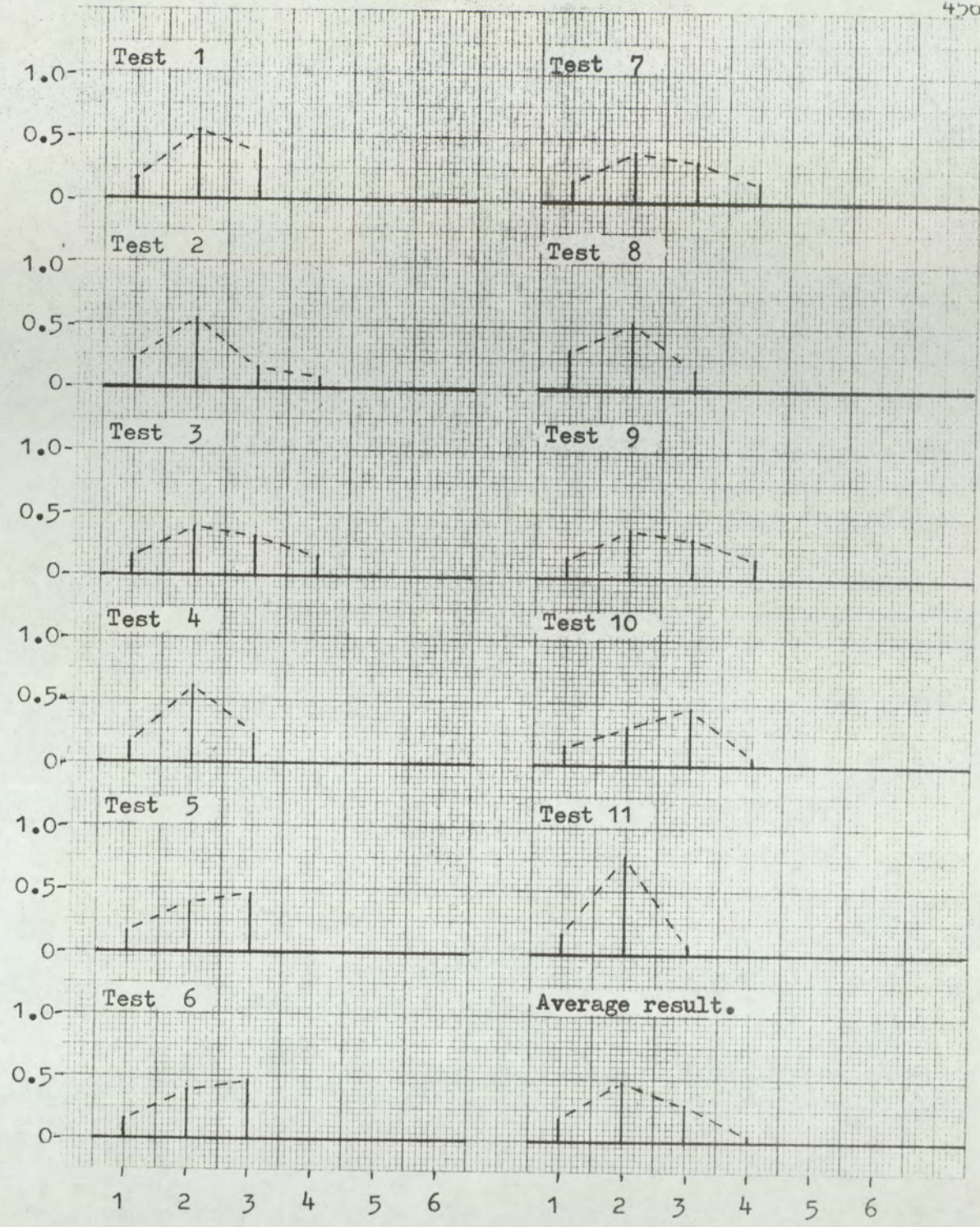


Fig.11-18. Results of subjective tests, encoding rate 100MHz.

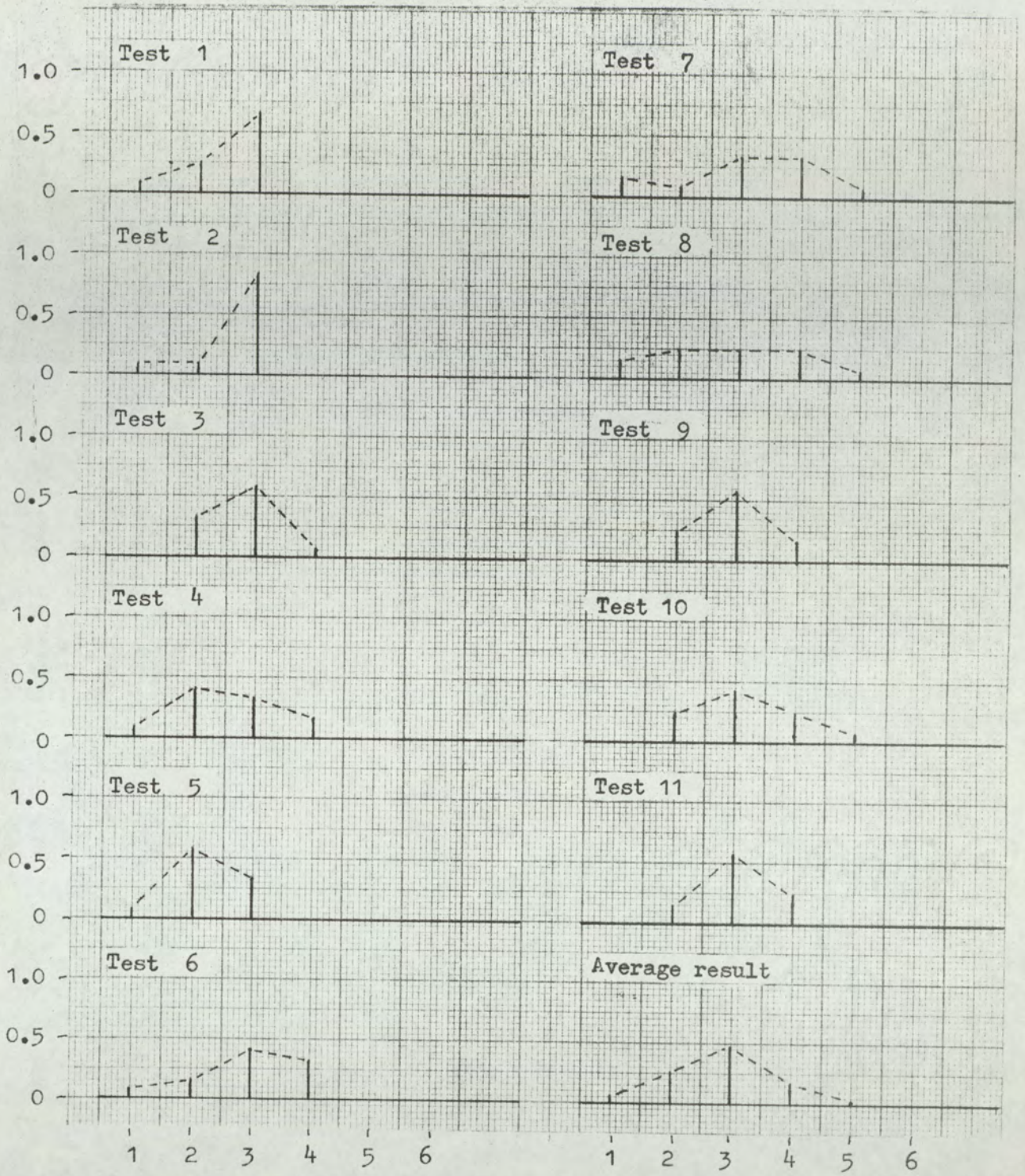


Fig.11-19. Results of subjective tests, encoding rate 50MHz.

## CHAPTER 12 CONCLUSIONS

### 12.1 Theoretical analysis of digital encoding.

Delta-modulation is the basic digital encoding method for encoding analogue signals into a digital pulse sequence. From delta-modulation it is possible to derive many of the sequential forms of digital encoder. In the thesis, the single, ideal-integrator delta-modulator was chosen as the central element for related forms of pulse modulator. It was shown (3.5, 3.6) by the use of feedback around the ideal delta-modulator that RC integration and higher-order integration can be produced. Also, rearrangement of the transfer function in the feedback path and the forward path of the delta-modulator can produce delta-sigma modulation and a hybrid delta/delta-sigma modulator (2.3, 2.4). Hybrid delta/delta-sigma modulation can provide pre-emphasis at the input signal of a delta-sigma modulator without using an external preemphasis network with the encoder.

The relationship of delta-modulation and P.C.M. was also derived (2.5). This relationship again uses the single-integrator delta-modulator as a central element, but requires a sample-and-hold network after the delta-modulator. Thus, although the basic delta-modulator represents a redundant form of digital encoding, it can represent a method of P.C.M. encoding with inherently less redundancy.

Thus, by analysing the performance and requirements of the single-integrator delta-modulator, the theory can be extended to these related modulation techniques. In chapter 3, the thesis systematically develops a method of analysis of delta-modulation. The theory shows that there is an exact relationship between delta-modulation and time-quantised phase-modulation. Similarly, the relationship is shown for delta-sigma

modulation and time-quantised frequency modulation, the two pairs of processes being linked by an integral relationship. Two basic forms of analysis are given, one in terms of a "single carrier" (3.3), the other in terms of a "double carrier" (3.4). The "double-carrier" model illustrates the reciprocal relationship between the positioning of '1' and '0' pulses and produces a '+1' and '-1' pulses without introducing a d.c. level shift of the standard pulse. However, both systems are identical in performance. In order that slope overload could be simulated it was necessary to precede the model with a predictive slope-overload function (3.7). Since a separate slope-overload network was used, it was possible to show that the slope-overload distortion could be considered in isolation from the delta-modulator.

Quantisation distortion using the basic model for a general signal whose Fourier Transform was known, was still complicated. This was due to the large number of side-band components generated by the phase (or frequency) modulators. The effects of side-band generation can be reduced by minimising the carrier-frequency deviation. Thus, "high-band" delta-modulation (4.4) was introduced. Basically, this represented an identical system but operating at a much higher clock rate. Hence, if the integrated step height remains constant and the maximum signal amplitude is not increased, then the deviation is effectively reduced. The integrated pulse waveform formed at the model output can readily be converted to a lower-rate, sampled signal by a correctly timed sampling process. This method exchanges the phase modulation side-band components for spectrum sampling.

It is concluded that the model discussed in chapters 3 and 4 forms a powerful foundation for analysing pulse-modulation systems. As an example, chapter 4 develops the spectral components for a basic sinusoidal and ramp modulating function. The spectrum is shown to be a

complex array of line components. However, a general method of analysis is also presented (4.4,4.5,4.6). Thus, if the Fourier Transform of the modulating signal is known, then the Fourier Transform of the sampled, amplitude-quantised signal can be derived.

It should also be possible to extend the theory to non-linear encoding systems, since a linearly-quantised encoder preceded by a non-linear function is identical to a non-linear encoder. In such systems (e.g. non-uniform step height P.C.M.) non-linearity is used to enhance the low-level signal encoding.

The theory is considered fundamental to the analysis of digital pulse modulation processes which can be derived from the single-integrator delta-modulator. The theory was verified both by computer simulation and by experiment.

## 12.2 Design of Delta-Modulators

In chapter 3, the parameters affecting the performance of the delta-modulator were discussed. This was supported by a development of the stability criteria for the delta-modulator encoder, (4.6).

It was shown that the modulus of the transfer function in the feedback path dictated the required frequency distribution of the modulating signal. This was developed from the consideration of slope overload (2.2). Within limits, therefore, the transfer function could be designed by considering the energy spectrum of the modulating function.

By extending the theory developed in chapters 3 and 4, it was shown in section 4.6 that the stability of the delta-modulator control loop depends mainly upon the phase response of the closed loop. Fig. 4.15, and Fig. 4.16 show the loop phase response which must not be exceeded; this is to prevent several modes of idling pattern from occurring. Equation 4.67 gives the bounds on the phase response of a delta-modulator. The analysis used the ideal phase-control model with a closed loop (Fig. 4.17). The phase-control model represents a stable network where the modulating signal is encoded and then decoded by the integrator. By virtue of the sampling process, this signal can be delayed up to one clock period duration. The analysis assumed the worst case delay and applied the Nyquist stability criterion. The phase-control model with external feedback can represent higher-order encoding functions (section 3.6, Fig. 3.10).

To maintain stability and to prevent the error exceeding the quantisation step (in general the quantisation step is signal dependent, equation 2.29) the loop delay must be minimised, (Fig. 2.14). In

analogue delta-modulator encoders (2.7,4.7), the effects of finite-duration output pulses were shown to introduce unnecessary phase delay. Sections 2.8,2.9 show that by digital techniques, the phase delay around the closed loop can be minimised by effectively simulating a delta-pulse response. Two types of digital encoder were presented, the first using a non-recursive filter, the second an UP/DOWN counter. The advantage of the first encoder is high speed performance, while the second can also operate as a P.C.M. encoder (2.5) by sampling the number held in the binary store at the required rate.

In developing the practical delta-modulator encoder for television signals, the major problem was the comparison of the error signal. The problem was solved by using a Motorola MECL III 'D' type bistable, type MCL670L (Fig. 9.9). In the delta-modulator, the 'D' input was found suitable for use as a comparator. Any attempt to introduce a comparator resulted in a drastic reduction of the maximum pulse rate. The modulator used finite pulses and a single RC integrator.

If an active integrator was introduced, the maximum encoding pulse rate was reduced due to the increase in loop delay. It was therefore found necessary to limit the integrator to a simple resistor-capacitor network to permit encoding digit rates in excess of 50 MHz, as a result, the noise power below the turnover frequency of the integrator remained constant; this severely limited the performance of the encoder.

### 12.3 Adaptive Delta-Modulation

In order to achieve the maximum performance of a delta-modulator, it is necessary that the modulator is adequately loaded by the modulating signal. This is especially true for the higher modulating frequencies. With delta-sigma modulation, especially for television signals where the high-frequency power is often low, pre-emphasis is necessary with subsequent de-emphasis at the receiver. Thus, an improvement in signal to quantisation noise is achieved.

The principle becomes more effective if the amount of pre-emphasis can be controlled, depending upon the high-frequency power of the modulating signal. The principle of an adaptive transfer function is developed in section 5.4. It is shown that an identical network can be used at the encoder and at the decoder (Fig. 5.6). Thus complementary action is obtained and the de-emphasis network is controlled in sympathy with the pre-emphasis network. If the control signals are obtained directly from the transmitted pulse sequence then, providing no transmission errors occur, identical tracking is possible.

With delta-modulation, the low-frequency performance is often more than adequate, whereas the high-frequency performance is not. Hence, as the high-frequency power of the modulating signal rises, low frequency components may be attenuated simultaneously with the increasing high-frequency components. Thus more signal amplitude is available for the higher frequencies. This performance can readily be achieved with combinations of adaptive-transfer functions.

An improvement in performance of the delta-sigma modulator used

for encoding the luminance signal (Fig. 9.19b) was obtained by using an instantaneous adaptive system (5.5). The advantage of this system was in the practical realisation of a delta-modulator without increasing the loop delay. The encoder used pulse-group detection of order two, (5.1,5.2). This provided a 6db improvement in the dynamic range of the delta-modulator. Fig. 5.1 shows that a second-order pulse group has a normalised threshold level of  $1/3$ . This allows signals below this level to remain un-adapted, with the advantage of a smaller quantisation-step height.

Chapter 5 considers pulse-grouping techniques in general. By applying the theory developed for the frequency-control model in chapters 2 and 3, the threshold levels could readily be calculated. The results for first, second, third and fourth-order pulse groups are shown in Fig. 5.1. The theory of pulse grouping represents a natural corollary of the general theory. The results enable the distribution of pulse groups to be examined, both in terms of their threshold level (equation 5.4) and their distribution in time. The latter can be studied by developing a frequency-modulation model similar to that of chapter 3. In this model the carrier is again signal dependent, but has a frequency of zero at the threshold level or below, rising to the frequency equal to the clock rate at full modulation. By time-slotting the positive zero crossings of the frequency-modulated carrier the position of a pulse group of a given order can be located.

It is clear, therefore, that as the order of the pulse group becomes high, the encoding accuracy of the high-order pulse group becomes poor. Therefore, a delta-modulator (or delta-sigma modulator) that uses several orders of pulse groups requires a higher pulse rate.

This permits the higher frequencies to be encoded with the same improvement in dynamic range as the lower frequencies.

## 12.4 Computer Simulation.

At several stages, computer programming was used to verify the fundamentals postulated by the theory and to perform exact calculations with respect to quantisations noise performance and adaptive systems.

The first program (10.1) was used to verify the theory developed in chapter 3 for the basic delta-modulator model. The results of the program proved conclusively that the theory was a true representation of a delta-modulator system. The program basically simulated a delta-modulator and a delta-modulator model. The two systems were given identical initial conditions and subjected to the same modulating signal. The modulating signal was represented by the sum of eight sine waves of different frequencies. When the two systems were evaluated over 999 samples, at no instant did the two output waveforms differ.

The second program (10.2) represented a direct simulation of a non-recursive filter simulating the response of a simple resistor-capacitor integrator. The array of coefficients of the filter were stored in a one-dimensional matrix. The program verified that this system performed as a delta-modulator.

The final two programs were concerned with adaptive delta-modulation (10.3) and analysis of pulse groups for ramp inputs of differing slope (10.4). The program discussed in section 10.3 produced curves for non-band-limited signal-to-quantisation-noise ratios for differing modulation depths and signal frequencies. These curves were produced for adaptive delta-modulators with different degrees of adaptation. The results are shown in Fig. 10.3

to Fig 10-14. The results clearly show that as the degree of adaptation is increased, the dynamic range of the modulator is increased, but the signal-to-quantisation-noise ratio for a given signal level (below a normalised level of 1) is only increased by a small amount. The noise characteristic is such that from a modulation depth of zero to one, the signal-to-quantisation-noise ratio rises (at about 6db per octave) with increasing modulation depth. However, once the signal level exceeds the normalised level 'one', then the signal-to-quantisation-noise ratio remains almost constant for increasing signal level, until the slope-overload criterion as described by (equation 11.1 for second and third-order pulse groupings and equation 11.12 for second-order only pulse groupings) is exceeded.

However, the advantages of the adaptive delta-modulator presented lie not only in the improvement in dynamic range, but also in the ease with which the system can be implemented at high pulse rates. Fig. 9.19(b) illustrates the luminance encoder which used second-order only adaptation.

The theory developed in chapter 5 for calculation of pulse-group threshold levels agree precisely with the equation 5.4. The results also indicate the relationship between the rate of occurrence of pulse groups and the depth of modulation. These two parameters are linearly related between the threshold level and full modulation. This was calculated for d.c. modulating signals (applied to a delta-sigma modulator) the rate of occurrence being calculated by counting pulse groups over 1000 samples. The same result can be obtained by counting the number of cycles of an appropriately frequency-modulated carrier (equation 5.7, section 5.2).

## 12.5 Digital and analogue signal encoding for colour television

Chapters 6 and 7 are mainly devoted to the development of basic television theory and of colour theory. The objective of the colour theory was to develop sets of equations to enable the signals of various systems to be presented in terms of chromaticity. The basic techniques for manipulating signals in relation to chromaticity were discussed. In chapter 8, these techniques were applied directly to the sets of signals developed.

Chapter 8 discusses various families of encoding, section 8.3 listing the families that were considered. It was shown that, in order to encode the luminance signal accurately, then the minimum number of channels is required. An important consideration for decoding systems is that the true luminance signal can readily be obtained. This both simplifies decoding and allows a monochrome display to be readily obtained.

The signals of a three-channel system (equations 8.14, 8.15, 8.16) were developed which used high-frequency averaging to enhance luminance performance (8.6, 8.7). These signals were applied to a symmetrical t.d.m. system shown in Fig. 8.2A. This system did not use any vertical-chrominance averaging and allowed the simultaneous extraction of the red, green and blue signals. The signals used in this system were translated onto the chromaticity diagram (Fig. 8.6). Since each signal carries luminance information, the signals lie above the  $u$  axis of the chromaticity diagram.

Section 8.5 discussed a method, using pulse compression, for inserting a line of chrominance signal into the line-blanking period. This method was used in a three-channel encoder (8.9). The active line

period was occupied by two symmetrical t.d.m. channels and the third channel was transmitted via the auxiliary channel (8.5). This method improved the luminance encoding, since the luminance was now divided between only two channels. Section 8.10 used chrominance averaging and transmitted all the colour information on only two channels. Two basic methods were discussed. However, the latter method has the advantage that the two channels when summed together, form the true luminance signal at all times.

The final system, called "chrominance in syncs" (C.I.S.S.), was developed as a practical system which used only a single channel for luminance encoding with the auxiliary channel for chrominance encoding. The luminance signal was encoded to its maximum fidelity since only one encoder was used. The chrominance signals, which were of lower bandwidth, were transmitted alternately line by line over the lower-pulse-rate auxiliary channel. Thus, this system made best advantage of all the signal space available in a line.

Obviously, the logic control and digital store required for pulse compression are a disadvantage. However, it is envisaged that, with the introduction of large high-speed registers on large scale integration (L.S.I.), this will present no major problem. It was primarily because of the cost of constructing a large register that only a simulation of the C.I.S.S. was investigated. However, the signal impairment introduced by C.I.S.S. could readily be produced by eliminating the pulse-compression process.

The chromaticity represented by the signals defined for C.I.S.S. is given in Fig. 8.8. The signals were defined by equations 8.44 and 8.45. The grid structure shown in Fig. 8.8 covers the colour triangle with reasonable uniformity. The diagram was constructed by

the techniques developed in chapter 7.

## 12.6 Experimentation and subjective assessment of C.I.S.S.

Chapter 9 described the practical development of the C.I.S.S. simulation. The encoders for this system were discussed in sections 12.2 and 12.3. One of the primary advantages of a basic delta-modulator is that decoding is achieved with a linear-filter network. With the instantaneous adaptive delta-modulator it is necessary to examine pulse grouping; however, demodulation is still straightforward.

The system constructed used pre-emphasis with the corresponding de-emphasis in both the luminance and chrominance channels; this produced considerable improvement in signal-to-quantisation-noise ratio. The use of pre-emphasis with delta-sigma modulation is analogous to using pre-emphasis with a frequency modulator. When a simple 6db/octave rise is introduced the two processes are converted, at high frequencies, to delta-modulation and phase modulation respectively.

The method of choosing the pre-emphasis time constant was as follows. The output of the chrominance-encoder channel was observed when the input to the encoder was a colour-bar waveform in which the chrominance bandwidth was limited to 1.1 Mhz. The time constant of the pre-emphasis was then adjusted so that the maximum signal rise time without over-shoot was obtained. This was considered optimum (for a simple pre-emphasis network), since the delta-sigma modulator was sensitive to amplitude overload.

The system was tested by a series of waveform tests - (section 11.1). Also photographs were made of a set of test

slides after processing by C.I.S.S. (11.2). Finally, the system was judged by a panel of viewers (11.3). The subjective assessments were made using the E.B.U. impairment scale. The assessment at a pulse rate of 50MHz was 2.82, while at 100 MHz the assessment was 2.23.

One of the main system defects was the introduction of low-frequency noise. This, however, is a fault of the design of the delta-sigma modulators and is not a fundamental limitation. If the transfer function of the encoder can be improved, yet high-frequency encoding efficiency maintained, then superior results can be achieved.

## 12.7 Assessment of the research and future objectives

The results derived from the research programme are extremely encouraging. By theoretical analysis, it has been shown that digital pulse modulation systems can be analysed exactly by well-defined, mathematical techniques. The theory shows also the development of the quantisation-noise spectrum and gives information on delta-modulator designs.

It has been clearly demonstrated that delta-modulation can be used for encoding television waveforms and that high-speed encoders are practical and inexpensive. Also, instantaneous adaptation in the modulator design can yield significant improvement in dynamic range at all modulating frequencies and yet is simple to implement.

Several methods of encoding colour-television signals have been investigated and described in relation to their effect on chromaticity. It is hoped that the ideas, both theoretical and practical, will stimulate further interest in this field. The objective is clearly the development of an economical, high-performance digital encoding system which is free of the distortions introduced by sub-carrier encoding techniques. Using digital encoding, a simplified decoding system is then possible when only the luminance signal is required.

The success of delta-modulation depends clearly on the development of adaptive equalisers for controlling the power spectrum of the modulating signal. Methods of producing such systems have been described, yet much work is still necessary to

realise their optimum form.

It is necessary that the performance of the delta-sigma modulator encoder, especially at the lower frequencies be improved. The modulators used to date are not satisfactory for very high performance. A possible method for implementing a high-performance delta-sigma modulator is by producing a system based on the theory of chapter 3. A wide deviation frequency modulator in conjunction with a logical time quantiser can realise a system operating correctly in excess of 100MHz pulse rate. The frequency modulator can be realised by using a U.H.F. frequency modulator and a frequency translator network.

An interesting corollary of the theory developed in chapters 3 and 4 is proposed. Present-day P.C.M. digital to analogue converters require analogue networks of precision accuracy to enable conversion to be achieved. It is now possible to design a system that uses only a digital filter and a single analogue filter. Basically, a digital filter re-constructs the delta-modulator pulse waveform from a knowledge of the P.C.M. samples. This is the inverse process of section 2.5. The delta-modulator pulse sequence is now applied to the analogue filter, where decoding is completed. The system is fairly complex, yet it has inherent long-term stability and eliminates all but the absolutely essential analogue circuitry.

ACKNOWLEDGEMENTS.

The time, discussion and continued interest of my supervisors, Professor J. E. Flood and Mr. T. Scott, without whose help and guidance this thesis would not have reached completion, is gratefully acknowledged.

The financial support of the British Broadcasting Corporation in the form of a research studentship, together with the continued interest of members of the B.B.C. research staff, is greatly appreciated. In particular, my thanks are given to Mr. E. Rout, Dr. B. Moffat and Mr. J.D. Esler.

Finally, I would also like to thank Dr. G.K. Steel for his interest and constructive discussion during the research programme.



- 10.. H. Van de Weg, Quantisation Noise of a Single- Integration Delta-Modulation System with an N- Digit Code, Philips Res. Rep. 8, p.367, 1953.
- 11.. J. B. O' Neal, A Bound on Signal-to-Quantisation Noise Ratios for Digital Encoding Systems, Proc. I.E.E.E., Vol, 55, No. 3, p. 287, March 1967.
- 12.. L. A. Zetterberg, A Comparison between Delta and Pulse Code Modulation, Ericsson Technics 11, No.1, p. 95, Jan. 1955.
- 13.. J. E. Iwersen, Calculated Quantisation Noise of Single- Integration Delta-Modulation Coders, B.S.T.J., Vol. 48, No.7, p.2359, Sept. 1969
- 14.. R. R. Laane, Measured Quantisation Noise Spectrum for Single-Integration Delta-Modulation Coders, B.S.T.J., Vol. 49, No. 2, p. 159, Feb. 1970.
- 15.. R. R. Laane and B. T. Murphy, Delta-Modulation Codec for Telephone Transmission and Switching Applications, B.S.T.J., Vol. 49, No. 6, p. 1013, July/August 1970.
- 16.. F. K. Bowers, Assymmetric Delta-Modulation System, U.S. Patent 2-817-061, applied for June 7<sup>th</sup> 1955, issued Dec. 17<sup>th</sup>, 1957.
- 17.. F. B. Johnson, Calculated Delta-Modulator Performance, I.E.E.E. Trans. on Audio and Electro-acoustics, Vol. AU-16, p.121, March 1968.
- 18.. P. F. Panter, Modulation, Noise and Spectral Analysis, Mc Graw-Hill Book Co., 1965.
- 19.. J. A. Betts, Signal Processing, Modulation and Noise, E.U.P. Science and Technology Series 1970.

- 20.. F. K. Bowers, What Use is Delta Modulation to the Transmission Engineer ?, A.I.E.E. Trans., Vol. 76, pt.1, p. 142, May 1957.
- 21.. J. Mc. Kibbin, and J. B. M. Straliding, The Use of Delta Modulation in Pulse Transmission Systems, Electrical Eng. Trans. (Institute of Engineers, Australia), p. 35, March 1970.
- 22.. D. J. Goodman, The Application of Deltamodulation to Analog-to-P.C.M. encoding, B.S.T.J., Vol. 48, No. 2, p.321, Feb. 1969.
- 23.. H. Inose and Y. Yasuda, J. Murakami, A Telemetering System by Code Modulation- $\Delta\Sigma$  Modulation, I.R.E. Trans. PGSET 8, p. 204, Sept. 1962.
- 24.. H. Inose and Y. Yasuda, A Unity Bit Coding Method by Negative Feedback, Proc. I.E.E.E., Vol. 51, p.1524, Nov. 1963.
- 25.. J. C. Balder and C. Kramer, Video Transmission by Delta Modulation Using Tunnel Diodes, Proc. I.R.E., Vol. 50, p. 428, April 1962.
- 26.. Dolby Laboratories Inc., 346 Clapham Road, London S.W.9, (01-720-1111)
- 27.. B. Lane, Tape Recording Survey, Wireless World, Vol. 77, No. 1433, p. 563, Nov. 1971.
- 28.. A. Tomozawa and H. Kaneko, Companded Delta Modulation for Telephone Transmission, Proc. of the National Electronics Conference, Vol. 22, p. 463, 1966.

- 29.. J. M. Brown and S. J. Brolin,  
Companded Delta Modulation for Telephony,  
NEREM RECORD - 1966.
- 30.. J. A. Betts,  
Adaptive Delta Modulation for Telephony,  
Electronics Letters, Vol. 6, No. 11,  
p. 336, 28<sup>th</sup> May 1970.
- 31.. A. A. Cartmale and R. Steele,  
Calculating the Performance of Syllabically  
Companded Delta- Sigma Modulators,  
Proc. I.E.E., Vol. 117, No. 10, p. 1915,  
Oct. 1970.
- 32.. M. R. Winkler,  
High Information Delta Modulation,  
I.E.E.E., International Conv. Rec. pt. 8,  
p. 260, 1963.
- 33.. M. R. Winkler,  
Pictorial Transmission with H.I.D.M.,  
I.E.E.E., International Conv. Rec., pt. 1,  
p. 285, 1965.
- 34.. N. S. Jayant,  
Adaptive Delta Modulation with a One-Bit  
Memory, B.S.T.J., Vol. 49, No. 3, p. 321,  
March 1970.
- 35.. J. Brown and E. V. D. Glazier,  
Telecommunications, Science Paperbacks  
SP 43, 1964, Chapman and Hall Ltd.
- 36.. F. W. Arter,  
Simple Delta Modulation System,  
Proc. I.R.E. (Australia), p. 517,  
Sept. 1962.
- 37.. A. Lender and M. Kozuch, Single-Bit Delta Modulation System,  
Electronics, p. 125, Nov. 1961.

- 38.. C. J. Dalton, Delta Modulation for Sound Distribution:  
A General Survey, The B.B.C. Research  
Department, Rept. No. 1971/12, UDC 621.376.5.
- 39.. W. M. Goodall, Television by Pulse Code Modulation,  
B.S.T.J., Vol. 30, p.33, Jan. 1951.
- 40.. P. C. J. Hill, Hybrid P.C.M. - An Experimental Video  
System, Electronics Letters, Vol. 5,  
No. 16, p. 352, Aug. 7<sup>th</sup> 1969.
- 41.. W. T. Bisignani, G. P. Richards and J. W. Whelan,  
The Improved Gray Scale and Coarse - Fine  
P.C.M. Systems, Two New Digital T.V.  
Bandwidth Reduction Techniques,  
Proc. I.E.E.E., Vol. 54, No. 3, p.376,  
March 1966.
- 42.. W. M. Goodall, Telephony by Pulse Code Modulation,  
B.S.T.J., Vol. 16, No. 3, p. 395, July 1947.
- 43.. Y. Nakamura and H. Kaneko,  
Delta Modulation Encoder, NEC Research  
and Development, No. 1, 621.376.56:621.382,  
p. 46, Oct. 1960.
- 44.. C. M. Rader and B. Gold, Digital Filter Design Techniques in the  
Frequency Domain, Proc. I.E.E.E., Vol. 55,  
No. 2, p. 149, Feb. 1967.
- 45.. C. A. Halijak and J. S. Tripp,  
A Deterministic Study of Delta Modulation,  
I.R.E. International Conv. Rec., pt. 8,  
p. 247, 1963.
- 46.. J. E. Flood and M. J. Hawksford,  
Exact Model for Delta-Modulation Processes,  
Proc. I.E.E.E., Vol. 118, p. 1155, 1971.

- 47.. P. A. Wing, Adaptive Delta Modulation,  
Electronic Letters, Vol. 5, p. 191,  
May 1<sup>st</sup>, 1969.
- 48.. J. A. Greefkes and F. de Jager,  
Continuous Delta Modulation,  
Philips Res. Repts., p. 233, 1968.
- 49.. J. E. Abate, Linear and Adaptive Delta Modulation,  
Proc. I.E.E.E., Vol. 55, No. 3, p. 298,  
March 1967.
- 50.. C. M. B. Newton, Delta Modulation with Slope Overload  
Prediction, Electronic Letters, Vol. 6,  
No. 9, p. 272, 30<sup>th</sup> April 1970.
- 51.. I. Childs, Adaptive 2nd Order Delta-Modulation System  
with 1- Bit Memory, Electronics Letters,  
Vol. 7, No. 11, p. 295, 3<sup>rd</sup> June 1971.
- 52..
- 53.. P. S. Carnt and G. B. Townsend,  
Colour Television, Vol. 1, Iliffe Books Ltd.,  
1961.
- 54.. R. G. W. Hunt, The Reproduction of Colour, Fountain  
Press, 1967.
- 55.. R. C. Teevan and R. C. Birney (editors),  
Colour Vision, D. Van Nostrand Company Inc.,  
1961.
- 56.. C. F. Teacher, Digital Colour Television Techniques,  
Philco Corporation, Blue Bell, Pa,  
(Ladecolor.)
- 57.. R. D. Ramsay, Synchronisation of Digital Communication  
Networks, The Institute of Engineers,  
(Australia), Elec. Eng. Trans., March 1970.

- 58.. R. A. Bruce,  
Optimum Pre-emphasis and De-emphasis  
Networks for Transmission of Television  
by P.C.M., I.E.E.E. Trans. on Communication  
Technology, p.91, Sept. 1964.
- 59.. R. Steele,  
Pulse Delta Modulators - Inferior  
Performance but Simpler Circuitry,  
Electronics Engineering, p.75,  
Nov. 1970.
- 60.. L. E. Weaver,  
Sine Squared Pulse and Bar Testing in  
Colour Television, B.B.C. Engineering  
Monograph, No. 58, pt. 1 and 2, p. 1,  
August 1965.
- 61.. Z. L. Budrikis,  
On the Channel Capacity of the Human Sense  
of Vision, Proc. I.R.E.E. Australia,  
p. 228, April 1964.
- 62.. A. Brown,  
Subjective Assessment of Multiple  
Co - Channel Television Interference,  
B.B.C. Res. Rept. No. RA-26, 1968.

Appendix 1ANALOGUE CIRCUITRY

Fig. A1-1 illustrates the amplifier which was used to form the input matrix for the three channels  $A_{2n}$ ,  $B_{2an}$ ,  $C_{2an}$ , as shown in Figures 4-3, 9-4. In the system (C.I.S.S.) three of these amplifiers were used, but with different feedback; the feedback was discussed in section 9-2.

The amplifier is basically a two-stage, current-steering, differentially-coupled amplifier using d.c. coupling. The differential operation allows addition and subtraction of input signals and a differential output is available. In the second-differential stage, a partially-common collector load resistor is used. This improves the balance between each half of the differential stage and lowers the source impedance to the emitter follower output stage. The two differential stages each have a current source feeding the common emitters, thus enhancing common-mode rejection and increasing amplifier gain. The two current sources are stabilised by zener diodes. In the amplifier, resistors are kept to low values to minimise the effects of stray capacitance and thus improve high-frequency performance.

The amplifier stages are formed around three basic amplifier designs, with the exception of the differential amplifier shown in Fig. 9-22. The various gains that are required by these amplifiers are set by the external feedback resistors. The external resistors are shown in the system design in Chapter 9, together with the stage gains. The three basic amplifiers are shown in Figures A1-2, A1-3, A1-4.

These amplifiers have an emitter-coupled pair of transistors to obtain high-frequency performance. The load resistor of the second transistor is a current source, thus producing a high-gain stage. The amplifiers of Fig. A2-3 and A2-4 have an a.c. decoupled potentiometer connecting the emitters; this allows a d.c. shift of the output voltage. These amplifiers are used as follows:

	Diagram reference	Amp. reference
Input signal matrixing	9-2,9-3,9-4,9-8,	A1-1
B.L.C. drivers	9-5,9-8,9-20	A1-2
B.L.C. hi-z buffers	9-5,9-8,9-20,9-21,A1-3	
Line drivers	9-7,9-8,9-20 9-22,	A1-4
Decoder input stage , luminance	9 - 20	A1-3
Decoder input stage chrominance	9-21	A1-3
Luminance inverter stage	9-20	A1-3
Chrominance primary inverter	9-21	A1-3
Delay line output amp.	9-22	A-3
Balanced inverter	9-22	A1-5
Butterworth filter	9-22	A1-6
Secondary chrominance inverter and buffer	9-23	A1-3
Green difference amp.	9-23	A1-2
Output stages	9-23	A1-4

In certain amplifiers, minor modifications were introduced depending upon circuit requirements.



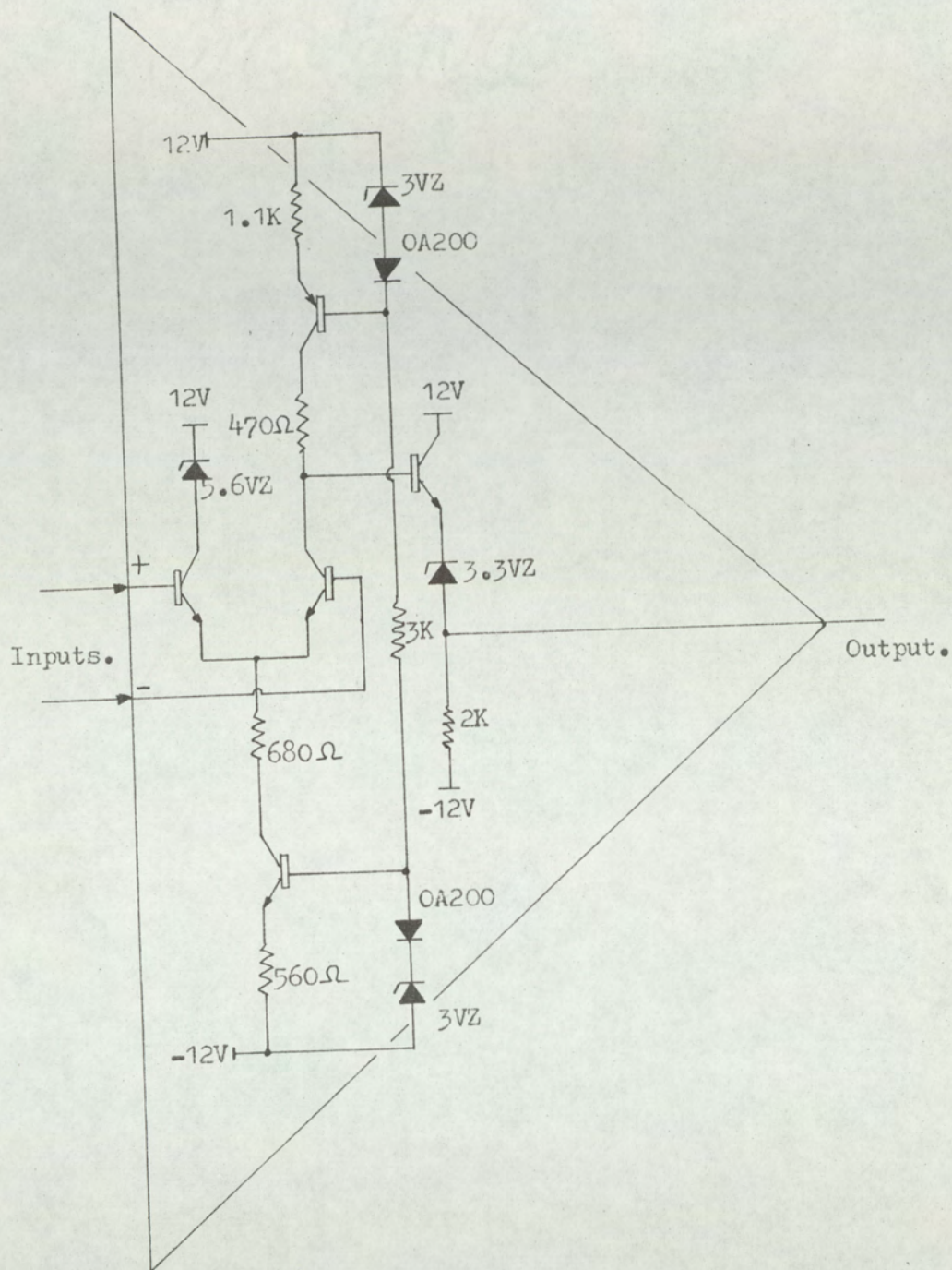


Fig.A1.2. High-gain, high-frequency amplifier module  
with no d.c. shift control.

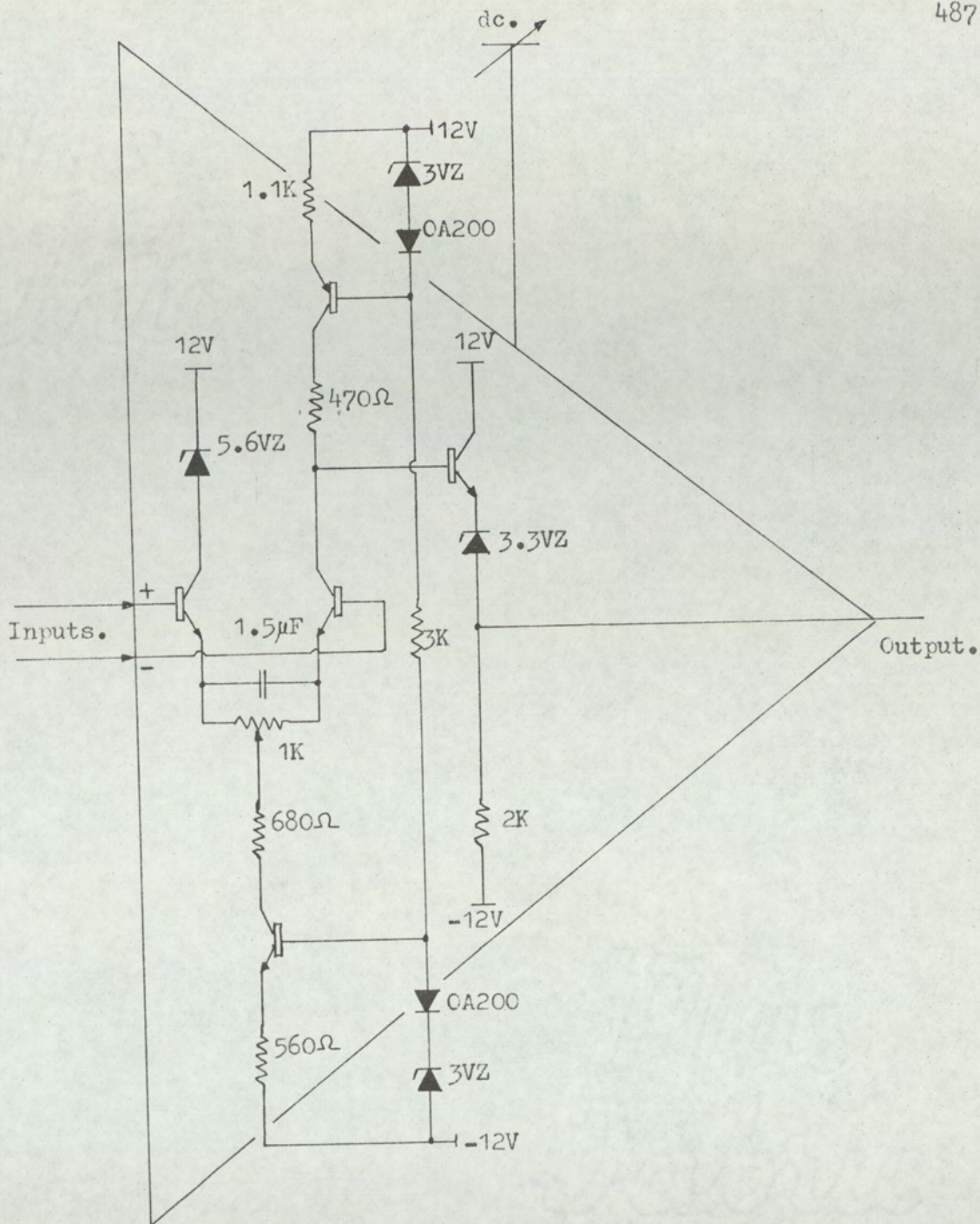


Fig.A1-3. High-gain, high-frequency amplifier module  
with d.c. level shift.

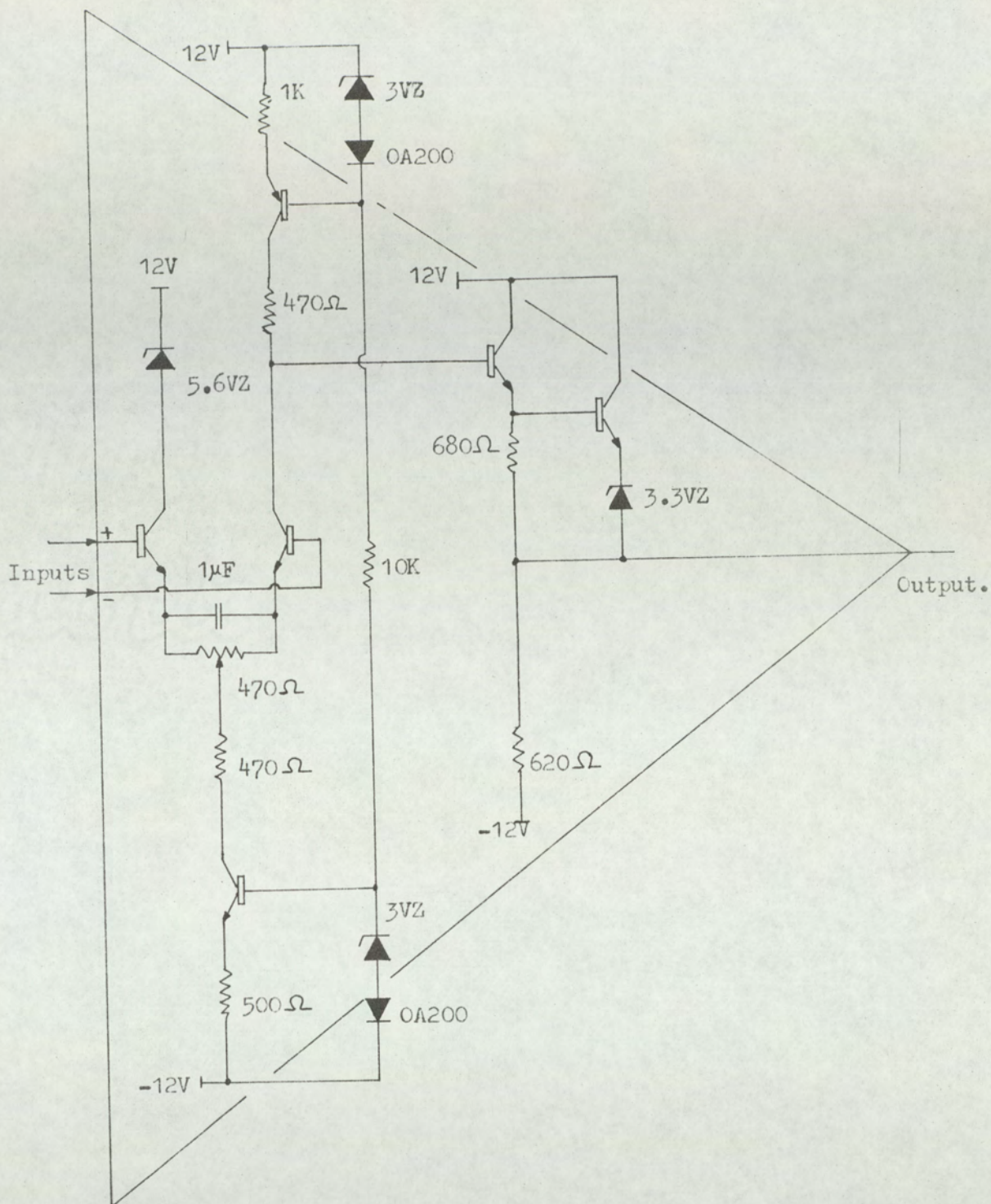


Fig.A1-4. High-gain, high-frequency line driver and delay-line driver amplifier, with d.c. shift.

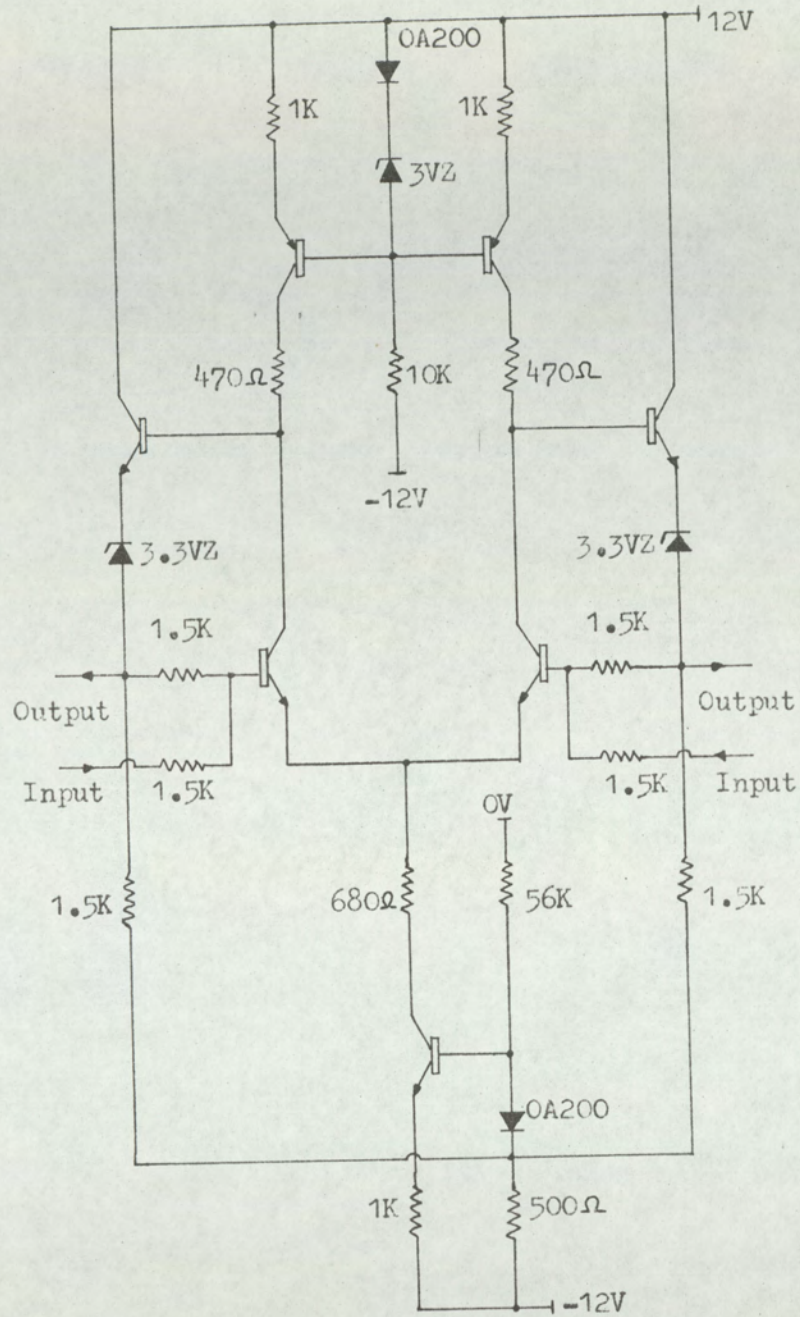


Fig.A1.5. Differential input/output amplifier for sum and difference channels.

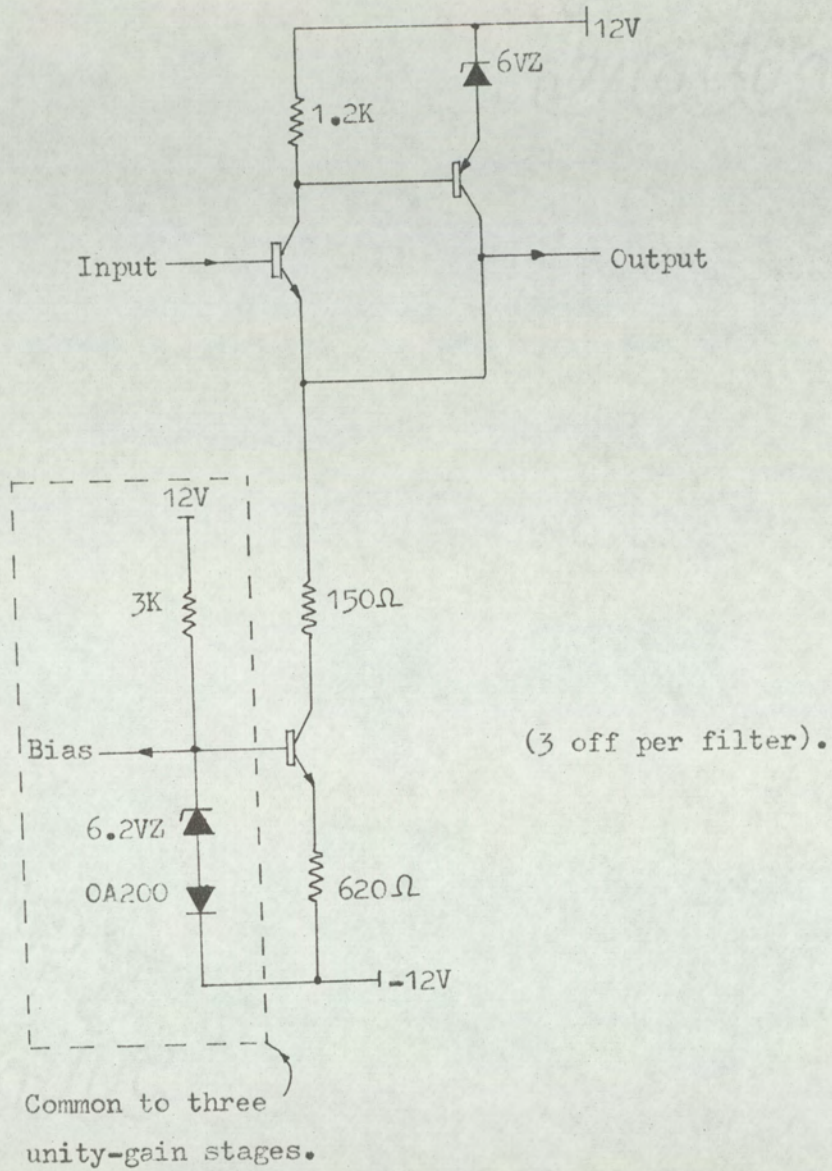


Fig.A1-6. Unity-gain amplifier for Butterworth filters.

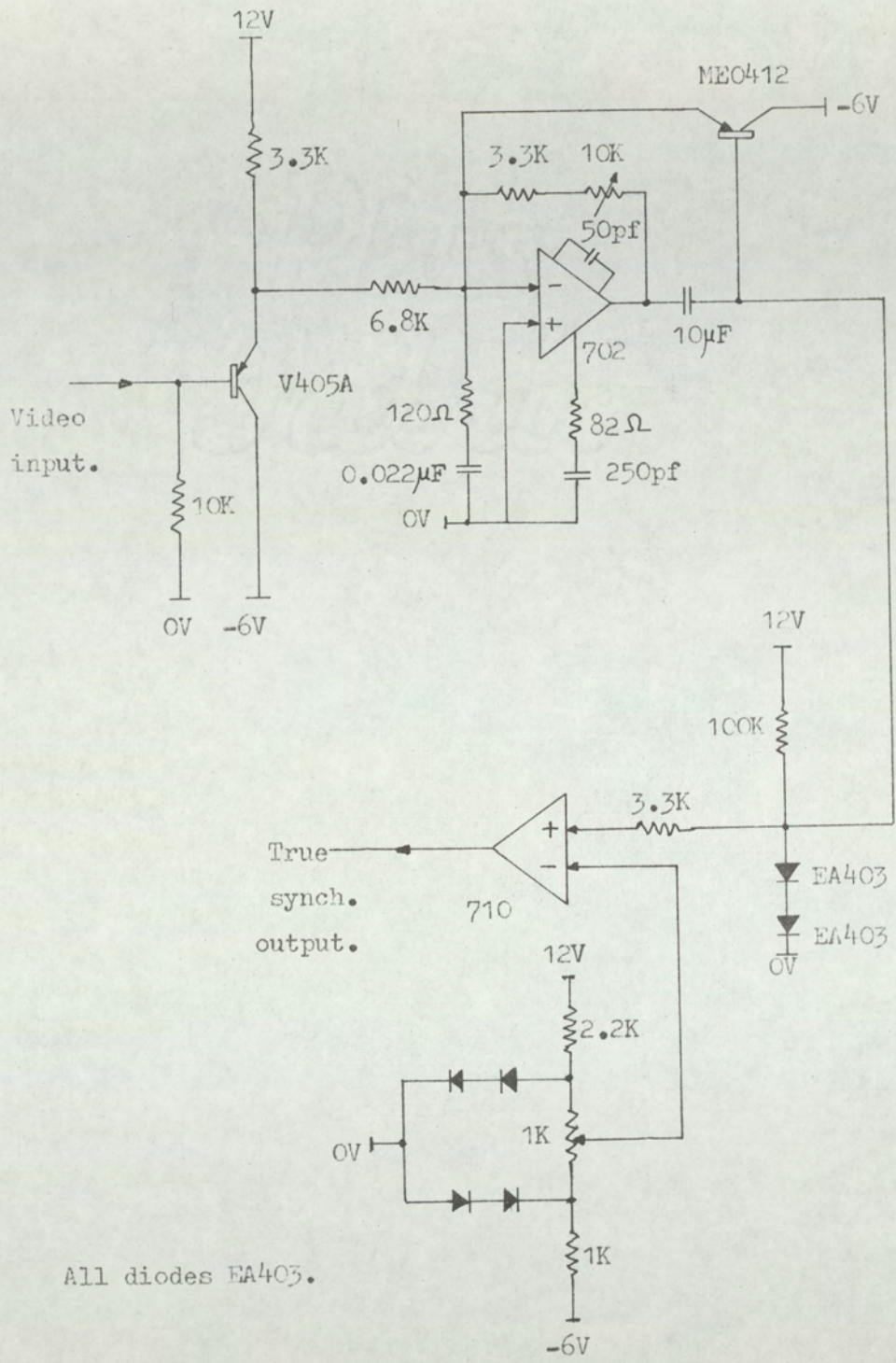
Appendix 2DIGITAL CIRCUITRY

In this appendix the discrete-component digital circuits are shown. The following table relates the circuit diagram to the system discussed in Chapter 9.

	Figure reference	Circuit diagram
Synchronisation pulse separator	9-9	A2-1
Initial set-up and clock detector	9-9,9-13,	A2-2
Encoder B.L.C. generator and F.E.T. driver	9-5,9-8,9-9,9-10,	A2-3
*F.E.T. driver stage	9-6,9-8,9-9,9-10, 9-20,9-21,9-22, 9-23,	A2-4

\* The T.T.L. Logic is interfaced to the F.E.T. circuits by the circuit shown in Fig. A2-2.

Details of the initial set-up and clock detector function are given in section 9-3-3.



All diodes EA403.

Fig.A2-1. Synchronisation pulse separator and clock source.

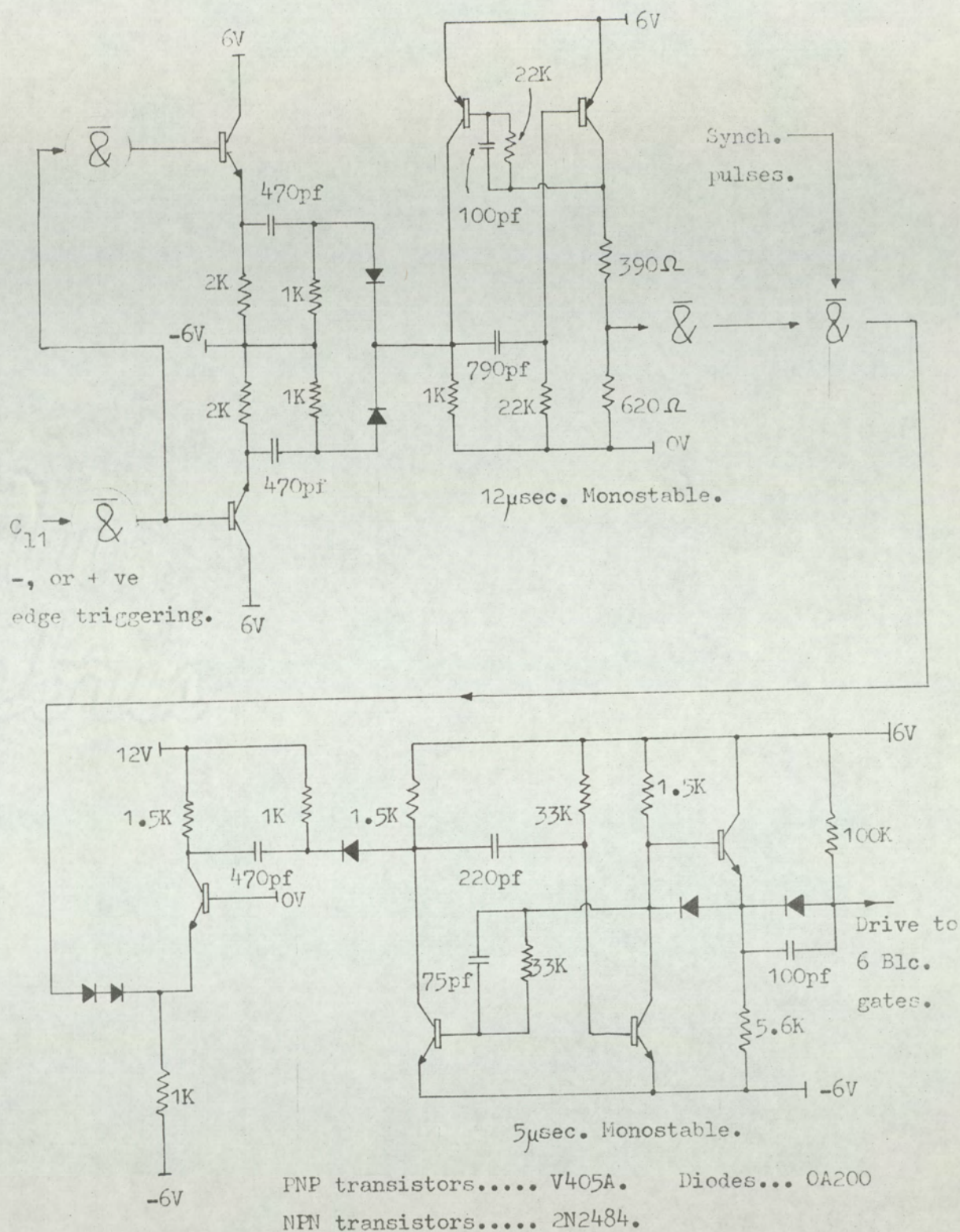


Fig.A2-2. B.l.c. generator for encoder, including FET drive.

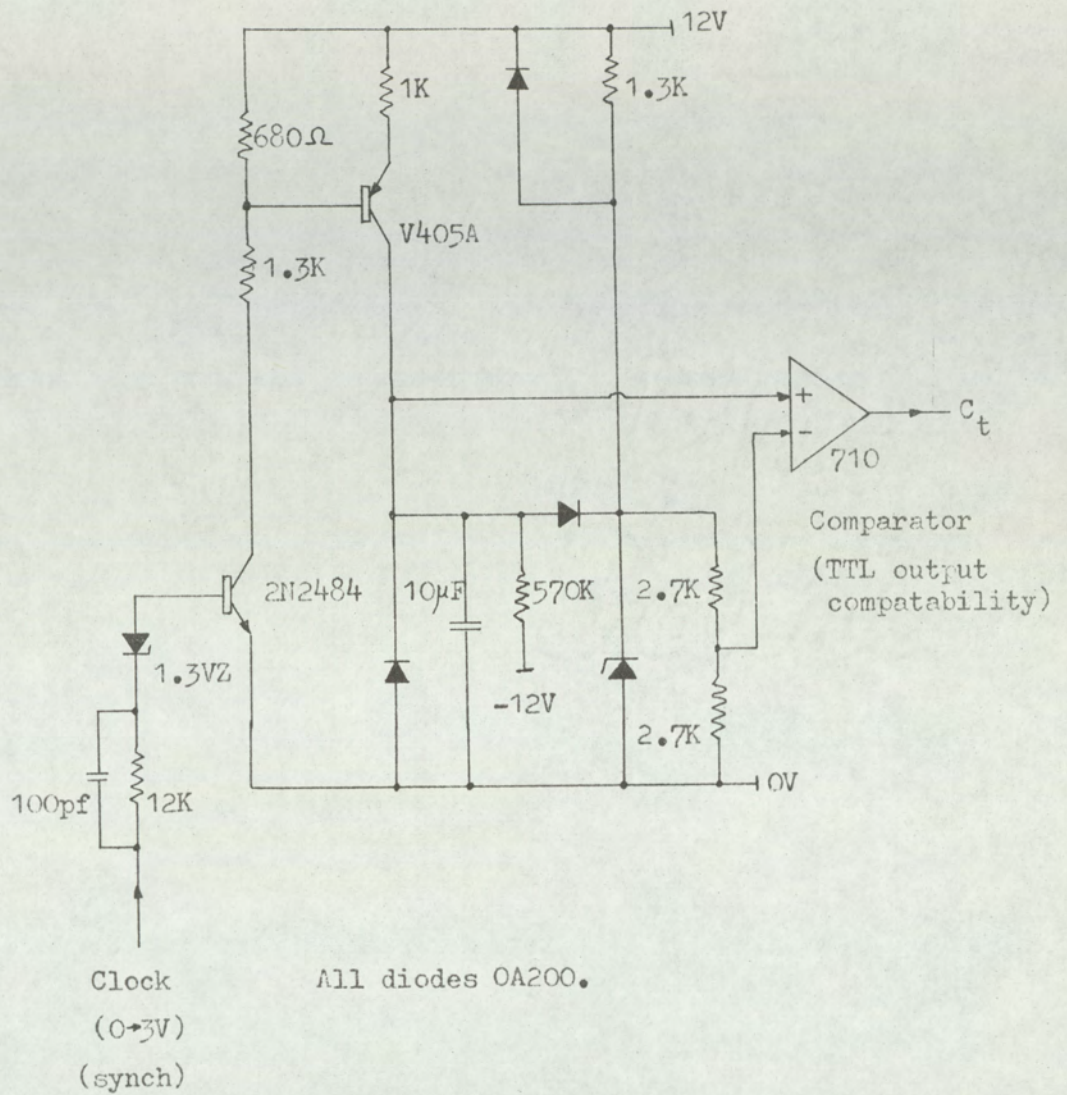


Fig.A2.3. Initial set-up and clock detector.

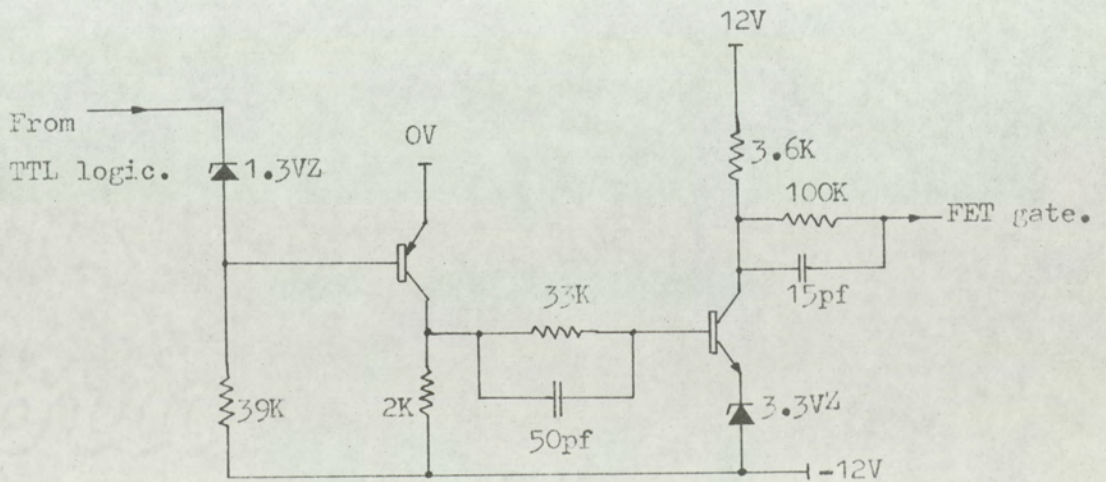


Fig.A2-4. FET gate drive stage.

CHROMINANCE DELAY SYSTEM

In the C.I.S.S. simulation, a one-line chrominance delay was required for decoding. The function of the delay system was discussed in section 9-5-2 and was shown in Fig. 9-22.

The delay function was formed by a Mullard DL 20 chrominance delay line. The basic specification is given in Fig. A3-1. Operation of this delay lines requires modulation centred about a frequency of 4.433619 MHz. Since the chrominance bandwidth did not exceed 1.1 MHz, simple double side-band amplitude modulation was used with a carrier of 4.433619 MHz (nominal). The carrier component simplified the demodulation process, allowing a suitable reference circuit. This function was necessary to allow correct d.c. restoration and control of the phase of all demodulated frequency components.

The local reference oscillator used a crystal in a controlled-gain, positive-feedback loop, shown in Fig. A3-2(b). The output of the oscillator was squared by the circuit in Fig. A3-2(b) to provide a square-wave, push-pull output for the product switching modulator of Fig. A3-3. The oscillator frequency, nominally 4.433619 MHz, was adequately stable to maintain all side-bands within the pass-band of the DL20 delay line. The DL20 delay line was driven by the product modulator, being fed (as shown in Fig. A3-3) from the collectors of two transistors. This produced an accurate drive impedance of  $400\Omega$ . Modulation was performed by switching the two drive transistors alternately at 4.433619 MHz and controlling the emitter current, by current steering, to be proportional to the chrominance signal. The pass-band of the delay line effectively selected only those sidebands symmetrically

distributed about 4.433619 MHz.

The output of the delay-line drove two circuits. The first was a differential switch, Fig. A3-4(a), which produced a push-pull square-wave signal at the centre frequency of 4.433619 MHz. The second circuit was a balanced, product demodulator, Fig. A3-4(b), which was switched by the differential switch of Fig. A3-4(a). When this demodulator is correctly balanced, it produces the base-band signal together with harmonic components. However, the side-band components and centre frequency associated with the 4.433619 MHz carrier are almost completely suppressed, thus the first set of harmonic components of appreciable power are associated with the second harmonic of 4.433619 MHz. This system effectively improves filtering by reducing visible interference components.

## GENERAL

The assembly consists of a glass delay element, with appropriate transducers and matching transformers, mounted on a chassis plate and enclosed by a plastic cover. The input impedances presented are  $100\Omega$  or  $400\Omega$ , selected by choice of connections, or the user's own transformers can be externally connected between pins 1 & 4 and 5 & 8. The output transformer is bifilar wound to provide balanced output voltages.

## ELECTRICAL DATA

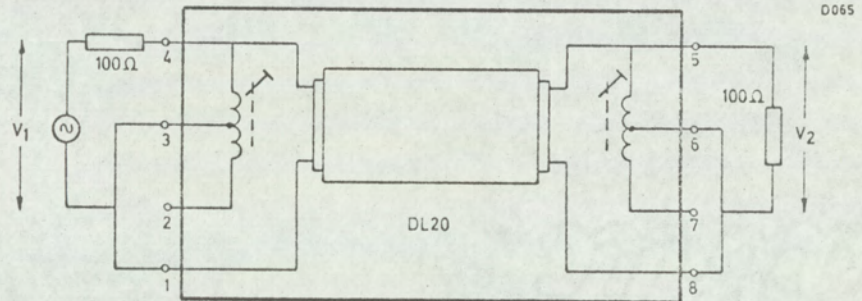
Phase delay time ( $f \approx 4.433619$ )	63.943	$\mu\text{s}$
Accuracy of adjustment	$\pm 5$	ns
Insertion loss ( $f_{\text{nom}}$ , $T_{\text{amb}} = 25^{\circ}\text{C}$ )	$11 \pm 3$	dB
Bandwidth (to -3dB points), minimum	3.43 to 5.23	MHz
Operating temperature range	-20 to +70	$^{\circ}\text{C}$
Input transformer ratio	4:1	
Maximum input (referred to $100\Omega$ input terminals)	10	V p-p
Unwanted reflections (at 3 $\tau$ )	>22	dB below
(others)	>27	1 $\tau$ signal

## Temperature stability

$\Delta$  Measured whilst heating from  $20^{\circ}\text{C}$  to  $50^{\circ}\text{C}$  linearly over a period of three hours,  $\Delta$  plus two hours at  $50^{\circ}\text{C}$ . Deviations are quoted with respect to the values at  $25^{\circ}\text{C}$ .

Phase delay, maximum	$\pm 5$	ns
Insertion loss, maximum	$\pm 0.3$	dB
Asymmetry of coils ( $f_{\text{nom}} \frac{V_0}{V_2}$ )	<0.05	

## CIRCUIT DIAGRAM



## MOUNTING

The unit is intended for direct insertion into printed wiring boards, fixing by means of the 4 lugs provided. Additionally, two holes are provided for mounting by two M3 screws as an alternative method of fixing.

Fig.A3-1. Specification of DL-20 delay line.

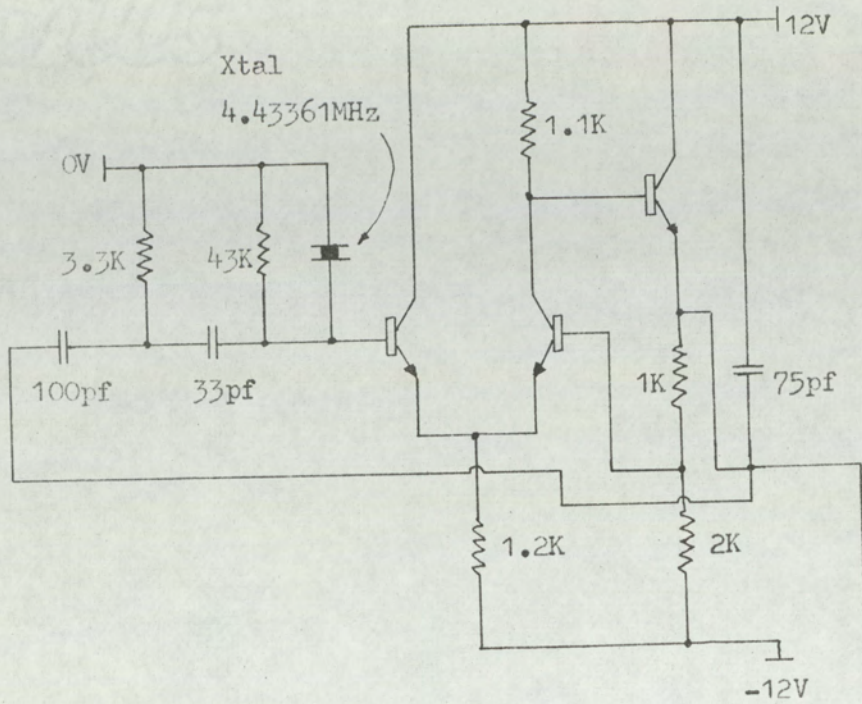


Fig.A3-2.(a). Crystal oscillator.

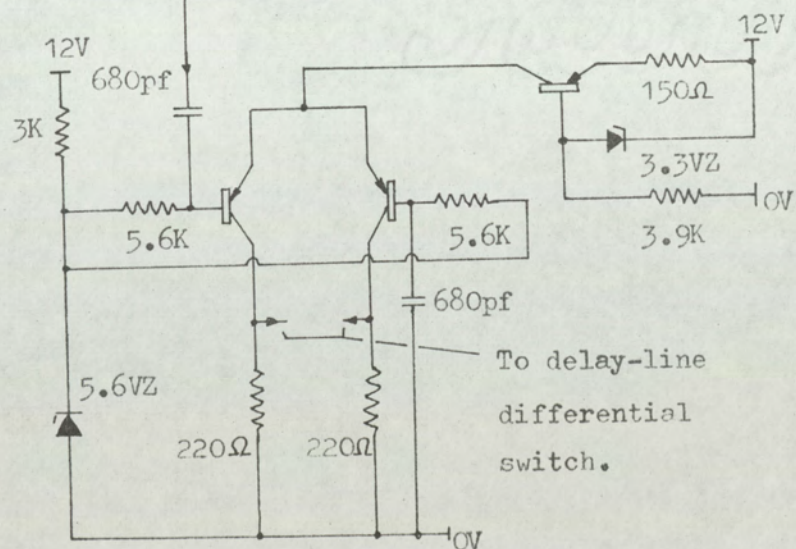


Fig.A3-2(b). Waveform squaring circuit.

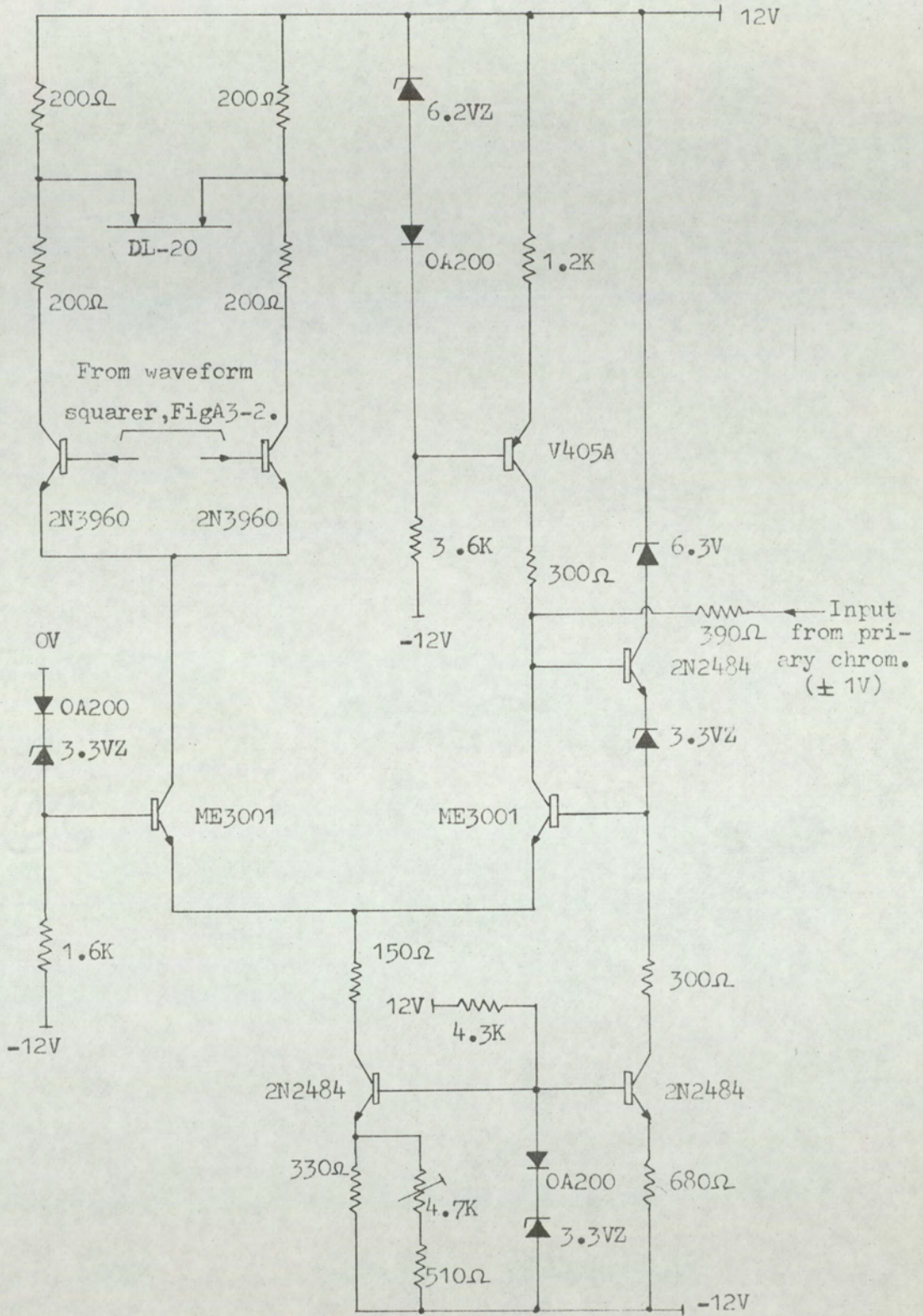
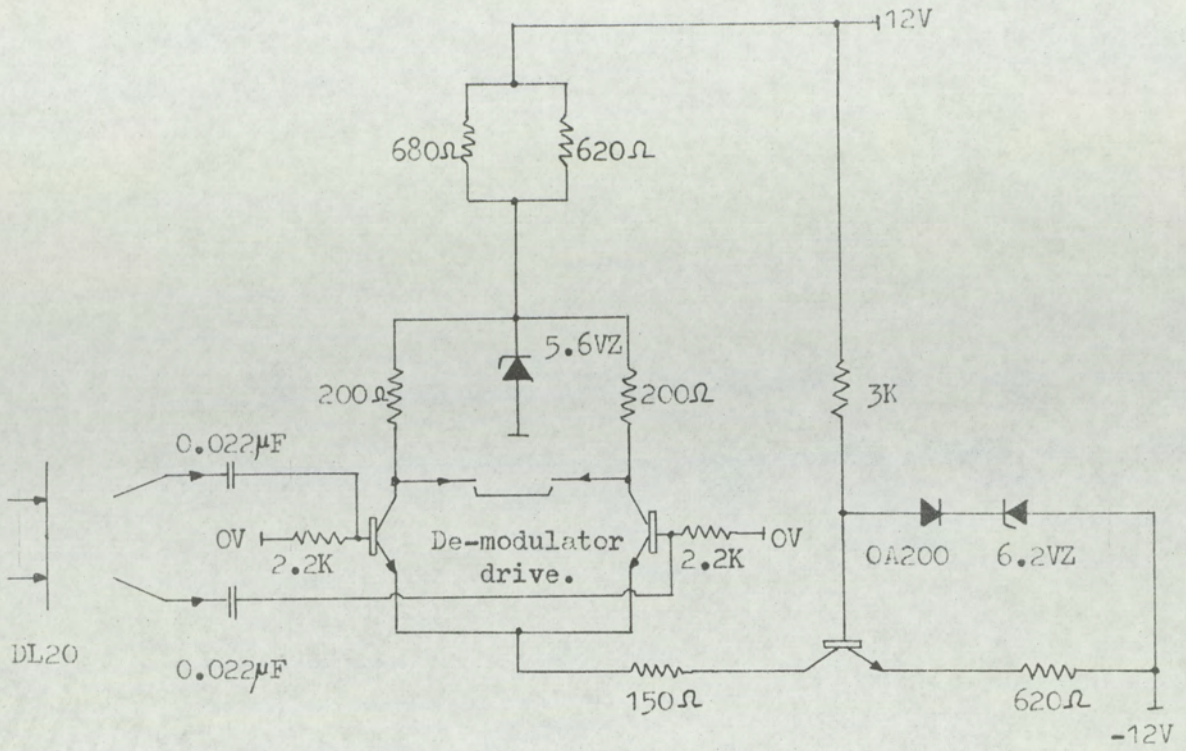
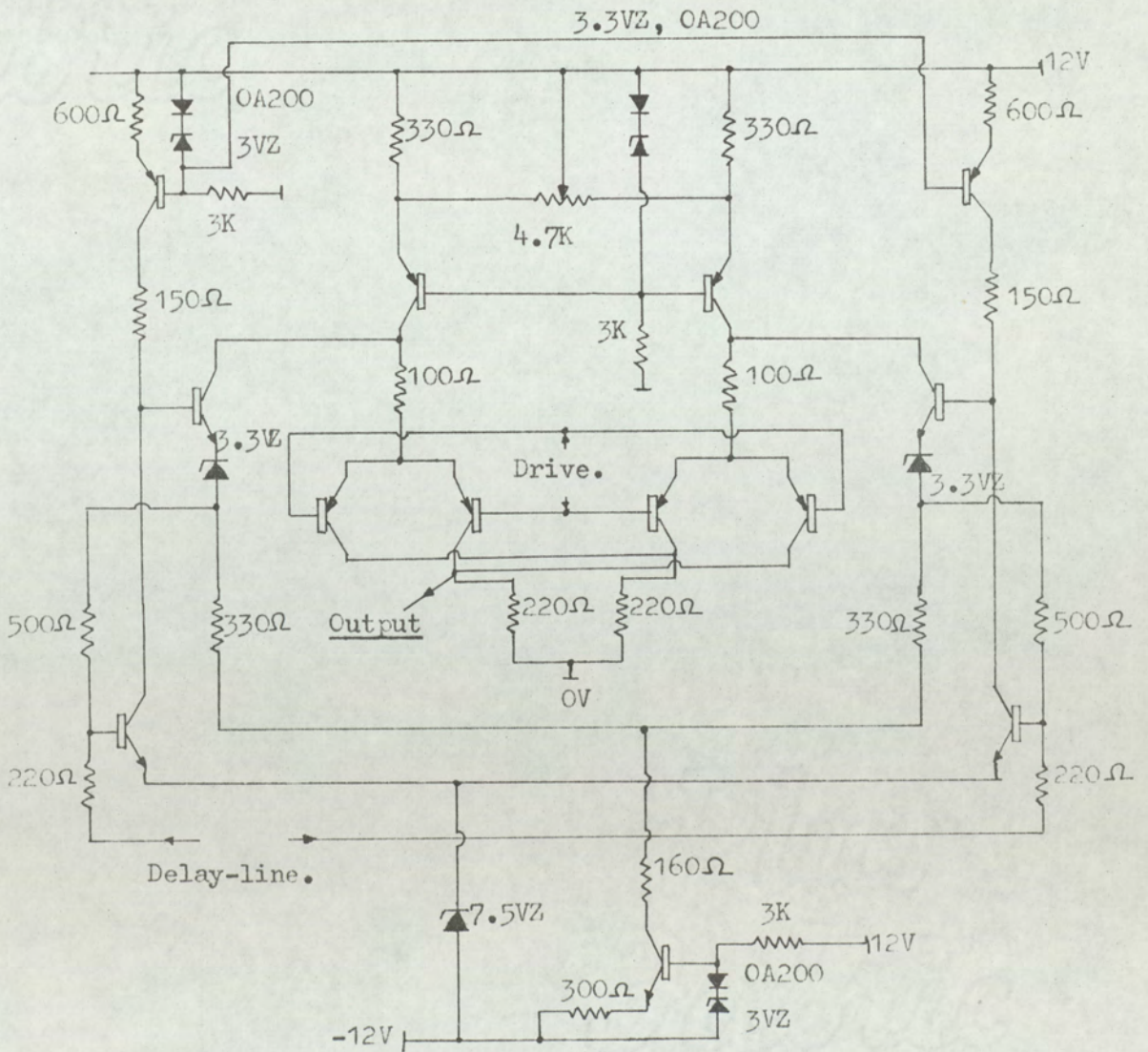


Fig. A3-3. Delay-line modulator.



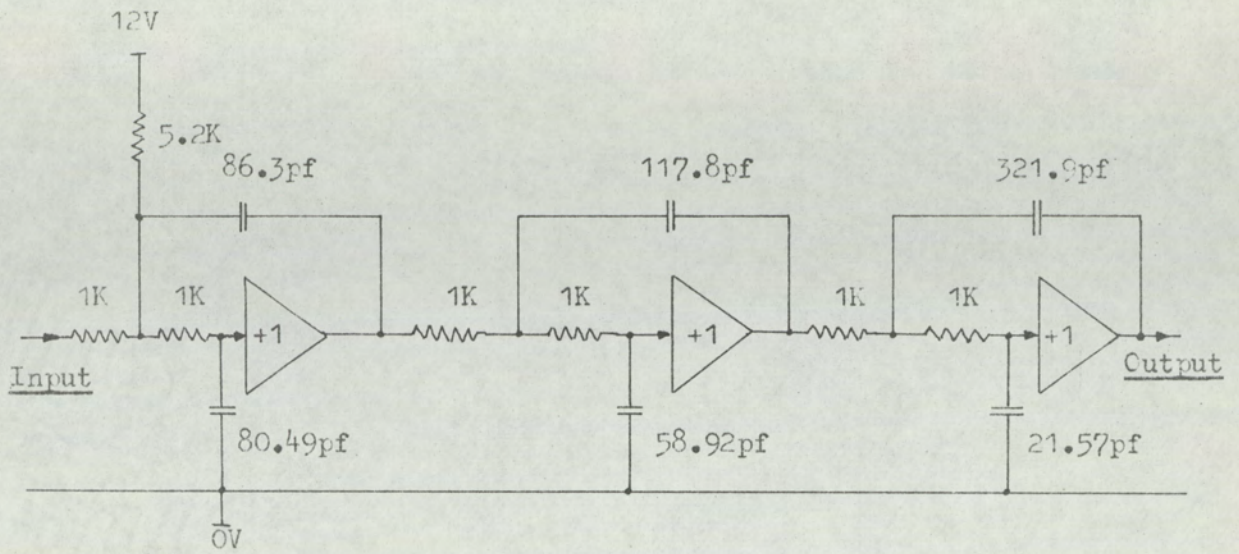
FigA3-4(a). De-modulator switching generator.



FigA3-4(b). Balanced product de-modulator.

APPENDIX A4Active Filters for Chrominance Demodulation

Final filtering of the output of the delay-line demodulator was performed by two sixth-order Butterworth filters. The position of these filters is shown in the system in Fig. 9-22. The normalised filter circuit is shown in Fig. A4-1. The filters use a set of identical unity-gain amplifiers, as shown in Fig. A4-2. The amplifiers are designed to have a high input impedance and a low output impedance. To ensure these conditions at h.f. a three transistor amplifier circuit was used using 100% feedback. The cut-off frequency was chosen to be  $6/\pi$  MHz; thus non-linear phase error distortion over the chrominance-signal pass-band is small. A relatively high cut-off frequency was permissible, since the demodulator suppressed much of the side-band signals at 4.4433619 MHz. The impedance level of the filter was chosen to be 1 K $\Omega$ . The denormalised capacitance values are shown in Fig. A4-1. Further design information can be found in reference .



Cut-off frequency.....  $\frac{6}{\pi}$  MHz.

Impedance level ..... 1K

Fig.A4-1. Sixth - order Butterworth filter.

Supporting Paper:      Exact Model for Delta-Modulation Processes.

J. E. Flood and M. J. Hawksford,

Proc. I.E.E., Vol. 118, p. 1155, 1971.

# PROCEEDINGS

THE INSTITUTION OF ELECTRICAL ENGINEERS

Volume 118

## Electronics

### Exact model for delta-modulation processes

Prof. J. E. Flood, D.Sc., C.Eng., F.I.E.E., and M. J. Hawksford, B.Sc.

*Indexing terms: Delta modulation, Modelling*

#### Abstract

A mathematical model is described which generates a pulse waveform identical to that of a single-integrator delta modulator, provided that the input signals to the latter do not cause slope overloading. The model uses analogue techniques of angle modulation and sampling to generate time- and amplitude-quantised signals, thus readily lending itself to exact analysis. The delta-modulation process is treated in a general manner that is equally applicable to delta-entry and sigma-entry systems. By this means, a central delta modem is defined which includes both pulse modulation and local decoding (prior to final filtering) of the pulse waveform. The model formulation is such that it is equivalent to the delta modem. The equivalence of the delta modem and model is proved analytically. It has also been verified by simulation on a digital computer and demonstrated experimentally. The model can be extended to simulate a double-integration network, provided that the necessary prediction is included. The model can also be extended to represent pulse-code modulation, because a linearly quantised p.c.m. signal can be obtained by suitable sampling of the output of a delta modulator.

#### List of symbols

$A(\omega)$  = transfer function of second integrator in double-integration process  
 $C$  = number of digits in binary code of p.c.m. system  
 $D(t)$  = instantaneous signal level, at time  $t$ , to delta modulator  
 $D_{max}$  = maximum amplitude of  $D(t)$ , when  $D(t)$  is sinusoidal  
 $d$  = sampling delay time in p.c.m. model  
 $E(t)$  = error signal in quantisation process at time  $t$   
 $f$  = signal frequency  
 $f_c$  = maximum signal frequency  
 $G$  = constant multiplier  
 $H$  = sampling rate of p.c.m. model  
 $K$  = constant, in phase-modulation process  
 $M$  = number of complete rotations of the phase of the phase-modulated carrier from zero time to  $N$ th sample  
 $N$  =  $N$ th sample in delta-modulation and model process  
 $N_{N1}$  = number of negative pulses in delta-modulation process from zero time to  $N$ th sample  
 $N_{N2}$  = number of negative pulses in model process from zero time to  $N$ th sample  
 $N_{P1}$  = number of positive pulses in delta-modulation process from zero time to  $N$ th sample  
 $N_{P2}$  = number of positive pulses in model process from zero time to  $N$ th sample  
 $N_S$  = Nyquist sampling rate  
 $P$  = delta-modulator and model-clock rate  
 $P_c$  = p.c.m.-system pulse rate  
 $P_1(t)$  = pulse pattern of delta-modulation process  
 $P_2(t)$  = pulse pattern of model process  
 $R$  = positive integer  
 $r$  = small positive number

$R_S$  = signal range in delta-modulation and p.c.m. processes  
 $S_1(t)$  = accumulated output of local integrator in delta modulation  
 $S'_1(t)$  = remote accumulated output, including transmission errors in delta-modulation process  
 $S_2(t)$  = accumulated output of local integrator in model process  
 $S'_2(t)$  = remote accumulated output, including transmission errors, in model process  
 $s(t)$  = normalised signal input to delta-sigma modulator and frequency-controlled model  
 $t$  = time  
 $T_1$  = time constant of first integrator in double-integration process  
 $x$  = instantaneous amplitude of phase-modulated sinusoid  
 $X$  = amplitude of phase-modulated sinusoid  
 $\delta$  = general delta pulse  
 $\phi$  = excess phase having range  $0-2\pi$   
 $\Phi(t)$  = phase function in phase-modulation process  
 $\omega$  = angular frequency

#### 1 Introduction

In the study of delta modulation ( $\Delta M$ ) and of p.c.m., the analysis of the noise structure generated by these modulation processes becomes tedious to describe mathematically owing to quantisation errors. It is useful to consider the possibility of alternative equivalent systems which lend themselves more readily to analysis.

Usually, textbook treatments<sup>1</sup> compare analogue-modulation methods to digital-modulation methods. However, they stress the differences between all analogue methods on the one hand and all digital methods on the other. Thus, similarities and equivalences between certain analogue and digital methods are overlooked.

Consider single-integration delta modulation<sup>2</sup> with a perfect integration process, i.e. infinite memory. If the input signal

Paper 6516 E, first received 19th January and in revised form 2nd July 1971

Prof. Flood is Head of, and Mr. Hawksford is with, the Department of Electrical Engineering, University of Aston in Birmingham, Sumpner Building, 19, Coleshill Street, Birmingham B4 7PB, England

PROC. IEE, Vol. 118, No. 9, SEPTEMBER 1971

remains constant, the output-pulse pattern is a sequence of equal amplitude and area pulses, but of alternating sign. Increasing the input signal causes an increase in the rate of 1 pulses, and a reduction in the rate of 0 pulses. Decreasing the input signal causes the opposite effect. It should be noted that the total rate of 1 and 0 pulses together is a constant, being the clock rate of the modulator. The difference between the rate of 1 pulses and the rate of 0 pulses is proportional to the slope of the input signal. Thus, the modulation process can be seen to be similar to a form of discrete-pulse-phase modulation, since, in pulse-phase modulation (p.p.m.), the rate of pulses is also proportional to the slope of the modulating signal.

Similarly, the relationship between pulse-frequency modulation and delta-sigma<sup>3</sup> modulation ( $\Delta\Sigma M$ ) can be argued, since the only difference between the phase-controlled and the frequency-controlled system is the position of the integration process. In pulse-frequency modulation (p.f.m.), a positive modulation signal results in an output pulse rate greater than the unmodulated pulse rate, and a negative modulating signal results in an output pulse rate less than the unmodulated pulse rate. In  $\Delta\Sigma M$ , the rate of transmission of 1 pulses is similarly greater than the unmodulated rate when the modulating signal is positive, and less than the unmodulated rate when the modulating signal is negative.

In p.p.m. and p.f.m., the output pulses are not constrained to fixed time slots, whereas in  $\Delta M$  and  $\Delta\Sigma M$  they are constrained by the clock pulse generator to discrete equispaced intervals. The similarities between the analogue and the digital methods would become even greater if the p.p.m. and p.f.m. signals were quantised by controlling the timing of their output pulses to coincide with the 'clock' pulses.

The object of this paper is to show that models derived from p.p.m. and p.f.m. can generate exactly the pulse trains produced by  $\Delta M$  and  $\Delta\Sigma M$ . These models should be of use in analysing the structure of quantisation noise generated by digital modulation processes.

## 2 Model for single-integration delta-modulation process

Fig. 1A shows a block schematic diagram of both a delta modulator and a delta-sigma modulator. With the switches  $Sw_A$  and  $Sw_B$  set in position 1, a delta-entry modulator is represented, and with the switches in position 2, a delta-sigma-entry modulator is represented. It can readily be appreciated that the overall operation of the two systems is identical except for the transposition of the linear integration process between the input and output stages. A scaling factor  $P$  is introduced at the sigma entry, and this, together with an integrator having unit time constant, generates a signal of slope  $P$  when the normalised sigma-entry input signal is a maximum. This corresponds to the delta modulator having an

input signal of maximum slope. The value of this slope is also  $P$ , because, when the delta modulator generates a continuous train of pulses at the clock rate  $P$ , integration of this pulse train results in a signal increasing with slope  $P$ . Whichever system is employed, the operation of the central delta modulator remains unaltered.

The proposed model for representing the above system is shown in Fig. 1B.

(a) The input signal  $D(t)$  to the delta modulator is used to phase-modulate a sinusoidal carrier of frequency  $P/2$  to a maximum frequency deviation of  $\pm P/2$  (block A, Fig. 1B).

(b) The phase-modulated carrier is converted to a naturally sampled p.p.m. signal (block B). The zero crossings of the phase-modulated carrier at which the phase-modulated carrier has a positive slope define the position of the leading edge of the standard pulse (block C). The standard pulses, thus generated, form the p.p.m. signal. The length of these pulses is exactly  $1/P$ , and the height is of magnitude 2.

A d.c. level of magnitude 1 is subtracted from the above pulse waveform as shown in Fig. 2B.

The waveform generated thus swings from  $-1$  to  $+1$ .

(c) The p.p.m. signal is now quantised by 'time slotting'. The time axis is divided into equally spaced time slots of duration  $1/P$ , where  $P$  is the equivalent delta-modulator clock rate. If the leading edge of a standard pulse occurs within a time slot, a 1 pulse is generated at the end of the time slot. If no leading edge occurs, a 0 pulse is generated. Thus, a series of discrete pulses is generated. This time slotting, illustrated in Fig. 2 by traces *b*, *c* and *d*, is made equivalent to a sampling process.

The length of the standard pulse is made identical to the duration of a time slot, hence, the length is  $1/P$ . If leading edge of a standard pulse falls within a time slot, the standard pulse is in a '1' state at the end of that time slot. The end of the time slot defines the sampling point in an equivalent delta-modulation process: thus the p.p.m. signal is sampled by a delta sampling pulse at this instant. If a standard pulse is present, then a  $+\delta$  output occurs. If no pulse is present, i.e. a leading edge has not occurred within the time slot, then the sample output is  $-\delta$ .

Thus, an output pulse train  $P_2(t)$  is generated (Fig. 1B) which corresponds to the pulse train  $P_1(t)$  in Fig. 1A, where the positions of the delta samples coincide with the 'clock' positions of the delta modulator.

## 3 Analytical demonstration of equivalence

### 3.1 Assumptions made

The following assumptions are made:

(a) Integration processes are perfect, so that there is no leakage. This is valid, since digital integration can be performed to a high degree of accuracy.

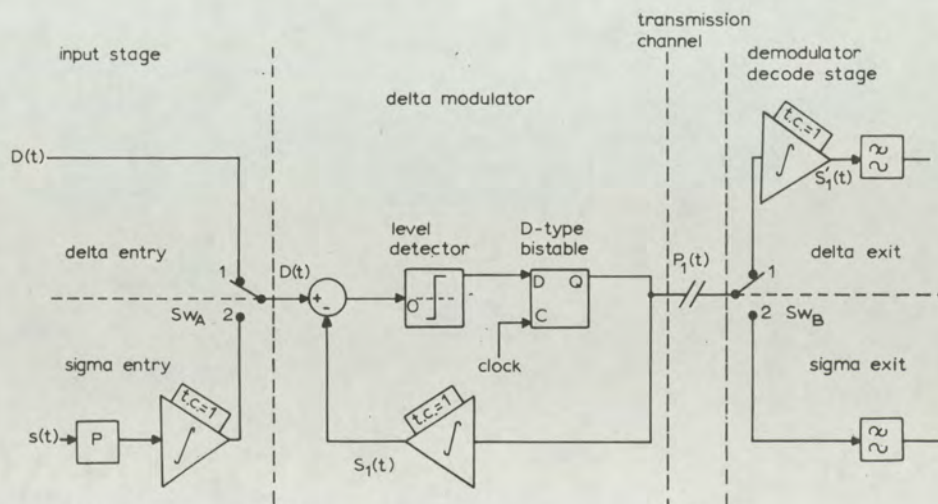


Fig. 1A  
Generalised structure for  $\Delta M$  and  $\Delta\Sigma M$  digital process

(b) In the delta modulator of Fig. 1A, the comparator performance is such that

- error  $\geq 0$ , comparator output high
- error  $< 0$ , comparator output low.

(e) At no time does the input signal exceed the overload conditions.

(f) If there are no error pulses in the transmission channel, similar waveforms are present at the sending and receiving terminals of Figs. 1A and 1B; i.e.

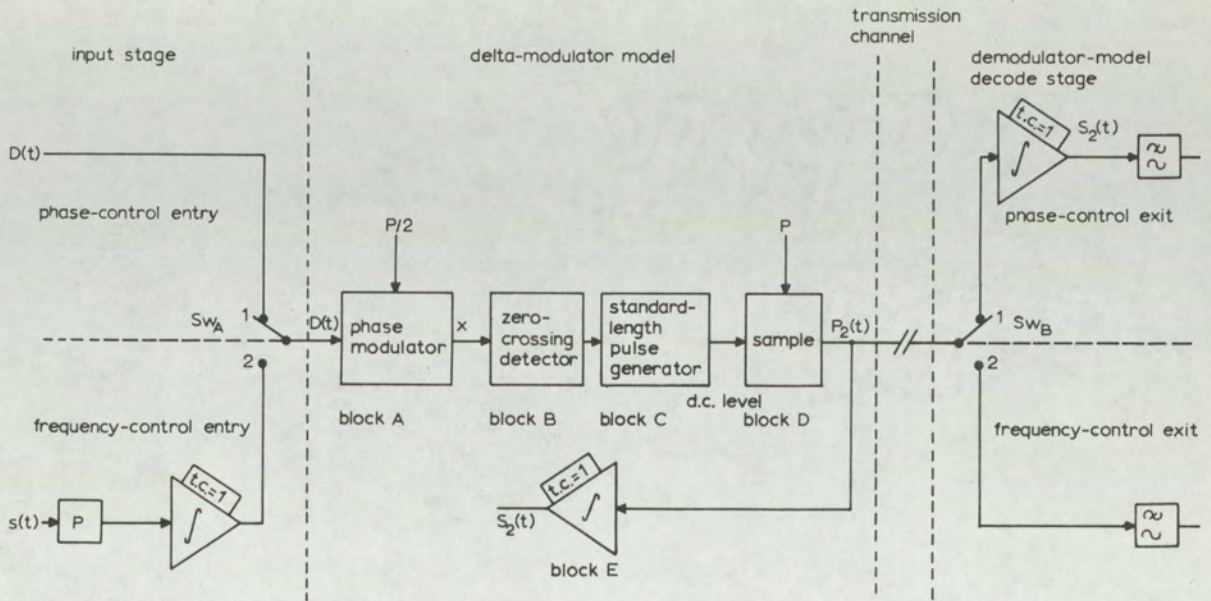


**Fig. 1B**  
Generalised model for  $\Delta M$  and  $\Delta \Sigma M$

(c) In the sampling process of the model of Fig. 1B, if the positive-slope zero crossing coincides with the delta sampling function, then a 1 pulse appears at the output of the model. This is compatible with (b).

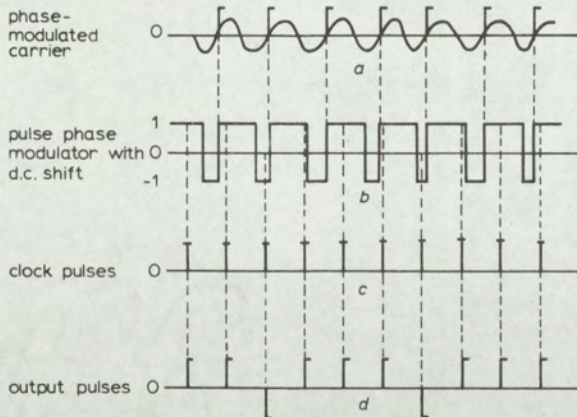


**Fig. 2**  
Waveforms in model process  
 a P.P.M. signal formed from a phase-modulated carrier  
 b P.P.M. with standard pulse of length  $1/P$  enabling time slotting of the leading edge to the nearest clock-pulse position, where p.r.f. is  $P$   
 c Clock pulses  
 d Time-slotted version of the p.p.m. which corresponds to the output pulse pattern  $P_2(t)$

(d) The initial conditions of the pulse-summing integrators in both the model and the delta modulator are set at  $+0.5$  during the first time slot, so that

$$S_1(t) = S_2(t) = 0.5$$

for  $0 \leq t < 1/P$

The initial conditions of the remaining integrators are set at zero for  $t = 0$ .

It is also assumed that all input modulating signals to both model and delta modulator are initially zero at  $t = 0$ . Thus, at commencement of processing, the systems will not be overloaded.

$$S_1(t) = S'_1(t)$$

$$S_2(t) = S'_2(t)$$

Since, in general, this does not occur, the analysis is only concerned with the delta modem. A locally decoded output prior to filtering is observed, thus allowing transmission errors to be ignored.

(g) The time slot associated with the  $N$ th sample is defined over the interval

$$\frac{(N-1)}{P} < t \leq \frac{N}{P}$$

### 3.2 Delta-modem feedback network

This system is described with reference to Fig. 1A. If the pulse-rate is  $P$ , (p.p.s.), the sampling points are spaced at intervals of  $(1/P)$  s.

Consider the conditions at the  $N$ th sample. The input signal is given by

$$D(t) = D\left(\frac{N}{P}\right) \dots \dots \dots (1)$$

Since the modulator at no time goes into slope overload, the output  $S_1(t)$  must lie within  $\pm$  one quantisation step of  $D(t)$ ; i.e.

$$S_1(t) = D(t) - E(t) \dots \dots \dots (2)$$

where  $-1 < E(t) < 1$ .

This assumes that the quantisation step is normalised to 1. That is, since  $P_1(t)$  is composed of  $\delta$  functions, and since all integrators have unit time constants, the output  $S_1(t)$  changes by steps of 1.

Hence, at time  $t$ , where

$$t = \lim_{r \rightarrow 0} \left[ \frac{N}{P} + r \dots \dots \dots (3) \right]$$

$$S_1\left(\frac{N}{P}\right) = D\left(\frac{N}{P}\right) - E\left(\frac{N}{P}\right) \dots \dots \dots (4)$$

The initial condition on the integrator is set during the first time slot ( $N = 1$ ), so that

$$S_1\left(\frac{N}{P}\right) = 0.5$$

Thus,  $S_1(t)$  can oscillate symmetrically about zero if  $D(t) = 0$ . The pulse at  $t = 0$  is not included in the count.

If, at time  $t$ , there have been  $N_{P1}$  positive pulses and  $N_{N1}$  negative pulses,

$$S_1\left(\frac{N}{P}\right) = N_{P1} - N_{N1} + 0.5 \quad \dots \quad (5)$$

$$\text{and } N = N_{P1} + N_{N1} \quad \dots \quad (6)$$

At the instant just after sampling, the error is within  $\pm 1$ . The pulse pattern  $P_1(t)$  is uniquely defined, since each pulse is generated by reference to the error at that sampling point.

### 3.3 Delta-modem model

This system is shown in Fig. 1B. Block A, the first stage of the model, is a phase modulator, modulating a carrier function of frequency  $P/2$ , where  $P$  is the delta modulator p.r.f.

A general expression for this carrier is

$$x = X \cos \{ \pi P t + \Phi(t) \} \quad \dots \quad (7)$$

where  $\Phi(t)$  is a linear function of the input signal  $D(t)$ . Put

$$\Phi(t) = K D(t) \quad \dots \quad (8)$$

The signal  $D(t)$  must be constrained so that the frequency deviation does not exceed  $\pm P/2$  ( $2\pi$ ). This restriction is in accordance with the slope overload criterion, and, to keep the phase rotation of eqn. 7 positive or zero,

$$\left| \frac{d}{dt} \Phi(t) \right|_{\max} = \frac{P}{2} (2\pi) \quad \dots \quad (9)$$

$$\text{i.e. } \left| K \frac{d}{dt} D(t) \right|_{\max} = \frac{P}{2} (2\pi) \quad \dots \quad (10)$$

The maximum slope of  $D(t)$  is given when the delta modulator of Fig. 1A is producing either all 1 or all 0 pulses. Thus, assuming unit step height,

$$\left| \frac{d}{dt} D(t) \right|_{\max} = P \quad \dots \quad (11)$$

Substituting eqn. 11 into eqn. 9 gives

$$\begin{aligned} \left| K \frac{d}{dt} D(t) \right|_{\max} &= K \left| \frac{d}{dt} D(t) \right|_{\max} \\ &= KP \\ &= \frac{P}{2} (2\pi) \end{aligned}$$

Hence,  $K = \pi$ .

Substituting  $K$  into eqn. 8, and, subsequently,  $\Phi(t)$  into eqn. 7, gives

$$x = X \cos [\pi \{ P t + D(t) \}] \quad \dots \quad (12)$$

The phase-modulated carrier is now converted to a naturally sampled p.p.m. signal by observing the positive-going zero crossings of  $x$  which occur whenever the phase of  $x$  passes through  $(-\pi/2 + 2M\pi)$ ;  $M$  is a positive integer, being the  $M$ th positive zero crossing from  $t = 0$ .

At time  $t$ , defined by eqn. 3, let the number of complete positive rotations of the phase of  $x$  be  $M$ , and let  $\phi$  be the excess phase. Then,

$$\phi + (2M\pi - \pi/2) = \pi(Pt + D(t)) \quad \dots \quad (13)$$

where  $0 \leq \phi < 2\pi$ .

At time  $t$ ,  $N$  samples have occurred. Thus, substituting from eqn. 3 into eqn. 13,

$$\left(\frac{\phi}{\pi}\right) + 2M - 0.5 = P\left(\frac{N}{P}\right) = D\left(\frac{N}{P}\right)$$

therefore,

$$(2M - 0.5) + \left(\frac{\phi}{\pi}\right) = N + D\left(\frac{N}{P}\right) \quad \dots \quad (14)$$

Again,  $N_{P2}$  positive pulses have occurred, and  $N_{N2}$  negative pulses have occurred.

Also, set an initial condition of  $+0.5$  during the  $N = 1$  time slot to bring the model initially into alignment with the delta modulator. Therefore,

$$S_2\left(\frac{N}{P}\right) = N_{P2} - N_{N2} + 0.5 \quad \dots \quad (15)$$

$$\text{But, } N = N_{P2} + N_{N2} \quad \dots \quad (16)$$

Thus, eqns. 15 and 16 generate

$$S_2\left(\frac{N}{P}\right) = N_{P2} - (N - N_{P2}) + 0.5$$

Therefore,

$$S_2\left(\frac{N}{P}\right) = 2N_{P2} - N + 0.5 \quad \dots \quad (17)$$

In eqn. 14,  $M$  represents the number of positive rotations of the phase of  $x$ , excluding the rotation in the  $N = 0$  time slot. Since the signal does not exceed slope overload, all the rotations of the phase are detected, and pass through the sampling process. Since each complete rotation is represented by a positive pulse,

$$M = N_{P2} \quad \dots \quad (18)$$

Substituting from eqn. 18 into eqn. 14, and rearranging,

$$2N_{P2} - N + 0.5 = D\left(\frac{N}{P}\right) - \left(\frac{\phi}{\pi}\right) + 1$$

Thus, substituting into eqn. 17 gives

$$S_2\left(\frac{N}{P}\right) = D\left(\frac{N}{P}\right) + \left(-\frac{\phi}{\pi} + 1\right) \quad \dots \quad (19)$$

The error term is  $\left(-\frac{\phi}{\pi} + 1\right)$ , since  $0 \leq \phi < 2\pi$ , and, hence,  $0 \leq \frac{\phi}{\pi} < 2$  and  $-1 \leq \left(1 - \frac{\phi}{\pi}\right) < 1$ .

Thus, eqn. 19 states that the accumulated output at the  $N$ th sample is equal to the modulating signal to an accuracy of  $\pm 1$ . This is identical to the delta modulator.

Since eqn. 19 holds for all integer values of  $N$ , a unique pulse pattern  $P_2(t)$  is generated.

Hence, with the appropriate choice of initial conditions for the model and delta-modulator integrator and of the initial phase of the phase-modulated carrier,

$$S_1\left(\frac{N}{P}\right) = S_2\left(\frac{N}{P}\right)$$

and, consequently,

$$P_1\left(\frac{N}{P}\right) = P_2\left(\frac{N}{P}\right)$$

for  $N = 1, 2, 3$  etc. . . .

Since the modulating signal  $D(t)$  and the accumulated signal in both processes are identical at each sampling point, the error signal is also identical. Consequently, both systems generate the same noise structure.

Thus, time-quantised pulse-phase modulation is in every way identical to delta modulation with a single integrator, providing correct initial conditions are observed and slope overloading does not occur.

If switches  $Sw_A$  and  $Sw_B$  in Figs. 1A and 1B are in position 2, an integrator is introduced at the input of both the delta

modulator and the model. A multiplier  $P$  is also introduced so that the magnitude of the input signal can be independent of the system parameters, i.e.

$$|s(t)|_{max} = 1$$

Thus, the required slope of  $D(t)$  is controlled by the multiplier  $P$ .

In the model of Fig. 1B the input signal to the phase modulator is

$$D(t) = P \int_0^t s(t) dt \quad (20)$$

The input signal thus controls the frequency of the carrier  $x$  instead of its phase. In the system of Fig. 1A, insertion of the integrator converts the system from a delta modulator to a delta-sigma modulator. Thus, delta-sigma modulation is exactly equivalent to a time-quantised pulse-frequency modulation process.

The model is thus applicable either to delta modulation or delta-sigma modulation. The only limitation is that slope overloading for  $\Delta M$  and amplitude overloading for  $\Delta \Sigma M$  are not represented. These effects may be included by adding suitable limiters at the inputs to the model.

The model should be useful for analysing quantising noise in  $\Delta M$  systems. The quantising noise generated by the sampling process in the model causes considerable overlap of the sidebands about the sampling harmonics. This explains why the idle-channel noise spectra observed by Iwersen<sup>4</sup> and Laane<sup>5</sup> appear to be phase modulated. It should also be noted that noise is added to the baseband signal prior to quantising due to sideband distortion in the angle-modulation system.

#### 4 Method of simulating double integration with prediction, using model

Fig. 3A shows a double-integration delta modulator with a prediction network. Prediction is established by

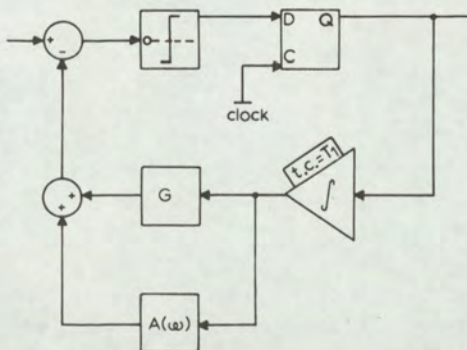


Fig. 3A Double-integration delta modulation with prediction

summing a fraction  $G$  of the first integral to the output of the second integrator whose transfer function is  $A(\omega)$ . On rearranging the loop, the equivalent network of Fig. 3B is

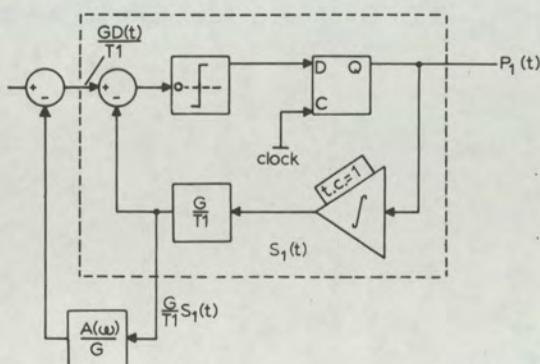


Fig. 3B Equivalent networks to Fig. 3A

obtained. Here the first integrator time constant has been normalised, and this is compensated for by a multiplying factor  $1/T_1$ .

In Fig. 3B, a single-integrator delta modulator is shown. The signals  $D(t)$ ,  $P_1(t)$ ,  $S_1(t)$  refer to the equivalent signals as shown in Fig. 1A. It is, therefore, possible to replace the feedback network, shown within the dotted lines, by the model equivalent, as illustrated in Fig. 4A. The input weighting factor  $T_1/G$ , scales the signal so that equivalence is obtained. Since  $A(\omega)$  is a linear network, the network can be simplified to that shown in Fig. 4B.

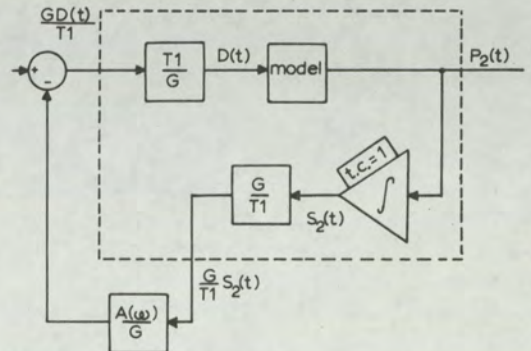


Fig. 4A Equivalent double-integration system using model

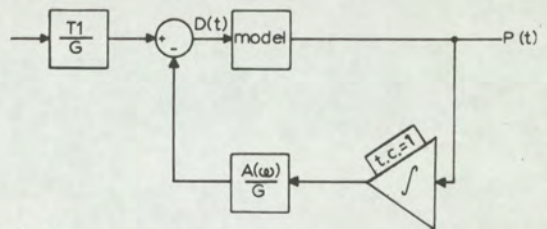


Fig. 4B Simplified representations of system model

The application of the model to the double-integration process reveals that, whereas the single-integration system can be realised on open loop, the double integration requires feedback control. This is one of the factors contributing to the improved noise performance available with this system. Here, the pulse step is adapted by a linear network, the degree of adaption being under feedback control. It is also of interest to note that, for an equivalent system to exist, prediction is essential. In practice, this is always used, as the double-integration system is unstable without prediction.

The model should prove useful in allowing a study to be made of the nature of  $A(\omega)$  necessary for the stability criteria to be met. The feedback loop also explains why the noise spectrum with double integration is more continuous than that of the single-integration modulator when encoding simple periodic functions. The model generates a wideband line spectrum for a sinusoidal input. The feedback path integrates this spectrum and feeds its many components back to the modulator input; thus, the modulator has a wideband input signal which results in a nearly continuous output spectrum. The buildup of the spectrum could alternatively be realised by an iterative open loop.

#### 5 Extension of model to p.c.m. with uniform quantisation

It has been shown that, at each sampling point of the delta modulator output (i.e.  $S_1(t)$  at intervals  $1/P$ ), the decoded signal is quantised to within  $\pm 1$  step height of the modulating signal  $D(t)$ , providing that the slope of  $D(t)$  does not cause an overload condition.

Hence, for delta modulation,

$$|\text{error}|_{\Delta M} \leq 1 \text{ (step height)}$$

In a delta modulator, the quantised output from the integrator is limited to a certain amplitude range, which is a function of signal frequency and the modulator 'clock' rate. (Assume a mean signal level of zero.) It is a characteristic of delta modulation that the amplitude range increases with decreasing signal frequency, having a theoretical infinite range at d.c. and a minimum range at the highest frequency component  $f_c$ .

In comparison, however, p.c.m. has a 'flat' signal-amplitude/frequency characteristic, handling the same amplitude range at d.c. as at the highest frequency component  $f_c$ . Thus, in order that a delta modulator may encode the same signal as a p.c.m. system, it is necessary that the amplitude range at the highest frequency  $f_c$  be greater than, or equal to, the signal range in the p.c.m. system.

In a p.c.m. system, the encoding accuracy is to within one-half of a quantisation step.

Hence, for p.c.m.,

$$|\text{error}|_{p.c.m.} < 0.5 \text{ (quantisation step)}$$

To make the  $\Delta M$  and p.c.m. processes compatible, the quantisation step of the p.c.m. is made twice that of the delta-modulator step height. Hence, in p.c.m., the quantisation step is designated a value, 2.

If at the zero sample of a delta modulator the integrator output is at an even level, it is observed that at even samples of the delta modulator the integrator output is at an even level, and on odd samples it is on odd levels. To convert the  $\Delta M$  integrated output to the quantised p.a.m. signal of p.c.m., the  $\Delta M$  output is sampled at the Nyquist (or greater) rate by delta pulses which are coincident with the  $\Delta M$  samples. Also, by sampling at even  $\Delta M$  samples, only even levels are generated for the p.a.m. signal. These coincide with the p.c.m. quantisation levels. Thus, there is a requirement that the  $\Delta M$  'clock' rate be a positive, even, integer multiple of the Nyquist sampling rate (or higher rate if used).

In practice, this method of generating p.c.m. can be used as a p.c.m. encoder.<sup>6,7</sup> It is arranged in the  $\Delta M$  that integration is performed by an up/down counter and digital/analogue converter. At each Nyquist sample, the number stored in the counter, excepting the smallest digit, forms the p.c.m. pulse pattern, which is then transmitted over the next sample interval.

Consider the required parameters for a  $\Delta M$  to perform the encoding of a signal which is compatible with a p.c.m. system, where

$$\begin{aligned} \text{quantisation step of } \Delta M &= 1 \\ \text{quantisation step of p.c.m.} &= 2 \end{aligned}$$

Let

$$D(t) = D_{max} \cos(2\pi ft) \quad \dots \quad (21)$$

For a unit quantisation step, the maximum value of  $D$  (to avoid slope overload) for a given pulse rate  $P$  and signal frequency is

$$D_{max} = \frac{P}{2\pi f} \quad \dots \quad (22)$$

If the maximum frequency to be encoded is  $f_c$ , the total signal range of  $D(t)$  is  $2D_{max}$ . Therefore the total signal range is

$$R_S = \frac{P}{\pi f_c} \quad \dots \quad (23)$$

In a p.c.m. system, the maximum-signal-amplitude/frequency response is flat.

Thus, if  $R_S$  is the signal range of the p.c.m. system, and  $f_c$  is the highest frequency component, for the delta modulator to be able to define completely the signal range without overload,

$$\frac{P}{\pi f_c} \geq R_S$$

$$\text{i.e. } P \geq \pi f_c R_S \quad \dots \quad (24)$$

The Nyquist sampling rate  $N_S$  for the p.c.m. system is given by

$$N_S = 2f_c \quad \dots \quad (25)$$

In practice, a higher sampling rate  $H$  is used, where

$$H \geq N_S \quad \dots \quad (26)$$

A further condition is imposed as previously discussed, i.e.

$$\frac{P}{H} = 2R \quad \dots \quad (27)$$

where  $R$  is a positive integer.

If, in the p.c.m. system, a  $C$  digit code is used,

$$R_S = 2 \times 2^C \quad \dots \quad (28)$$

Thus, the p.c.m. pulse rate  $P_c$  is given by

$$P_c = HC \quad \dots \quad (29)$$

Since in the  $\Delta M$  quantisation procedure the error is only within  $\pm 1$  at a time  $t$  defined by eqn. 3, the sampling at the rate  $H$  must be such that it occurs with a fixed delay  $d$  after the time  $t$ , as shown in Fig. 5B. Since the  $\Delta M$  clock interval is  $1/P$ , it is clear that

$$d < 1/P$$

which corresponds to the condition in eqn. 27.

Thus, the addition of the sampling process (shown in Figs. 5A and B) on the integrator output of a  $\Delta M$  followed by

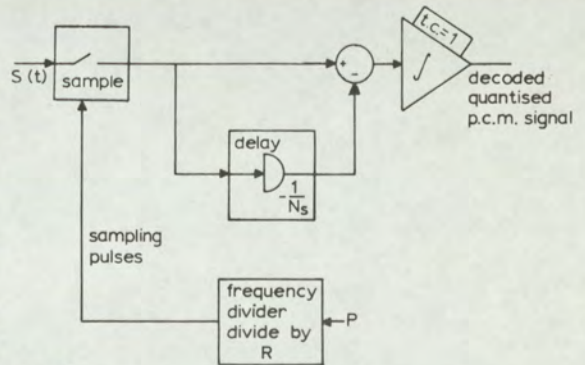


Fig. 5A  
Extension of model to p.c.m.

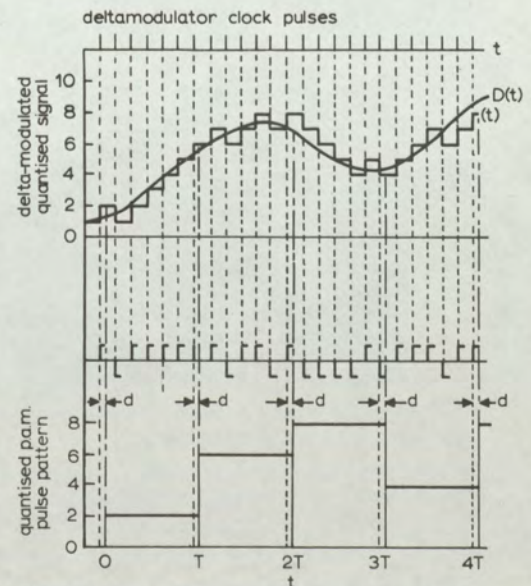


Fig. 5B  
Waveforms in buildup of p.c.m. by a delta-modulator encoder

a sample and hold circuit allows the spectral structure of a p.c.m. system to be analysed. Since the model described has been shown to be equivalent to  $\Delta M$ , this procedure holds equally for both the  $\Delta M$  and  $\Delta \Sigma M$  method.

## 6 Computer simulation and experimental work

The theory was checked by simulating a delta modulator and the model on a digital computer. The output signals were compared when each system received the same input signal.

The delta modulator was simulated by noting the error at each pulse and generating an output pulse accordingly. The integrated output was simulated by adding these output pulses, giving 0 pulses a weight of  $-1$ .

The model was simulated by generating the values of a phase-modulated carrier and noting the zero crossings having positive slope. The instantaneous value of the carrier was evaluated at ten equally spaced intervals during every time slot. On comparing the values in the sequence, a crossing could be detected, and was followed by the generation of a 1 pulse at the end of the time slot. The integrator output was again simulated by addition of the output pulses.

Operation of these systems was simulated for an input signal consisting of the sum of eight sinusoids of equal amplitudes but different frequencies. At each sample of the input signal, the output signals of the delta modulator and the model and the error signals were computed. This was carried out for a sequence of 999 samples, and at no time was there any difference between the outputs of the two systems.

In addition to the computer simulation, an experimental demonstration was carried out. A  $\Delta\Sigma$  system model, as shown in Fig. 1b, was constructed. A carrier of 200 kHz was frequency-modulated to a maximum deviation of  $\pm 5$  kHz. Modulation with a second carrier of 205 kHz was used to shift the central frequency down to 5 kHz, thus producing a 5 kHz carrier modulated to a maximum deviation of  $\pm 5$  kHz. This frequency-modulated carrier was squared and applied to a time quantiser using t.t.l. integrated logic circuits.

The time quantiser consisted of two counters, each counting up to four. One counter was driven by the f.m. waveform and the other by a train of 10 kHz clock pulses via an inhibit gate. When the two counters produced coincident outputs, the clock pulses were inhibited. When the f.m. waveform crossed zero with positive slope, the counter driven by it counted 'one'. This opened the inhibit gate, causing the clocked counter also to count 'one' and reach the same count. Since the frequency of the f.m. waveform did not exceed the clock pulse rate, the two counters could track, and output pulses were produced whenever the counters were not coincident, and thus a time-quantised output signal was provided.

The output waveform from this model was compared on an oscilloscope with that from a conventional delta-sigma modulator using a single integrator. When both systems had the same input signal, consisting of a sinewave of frequency within the range 50–500 Hz, they produced similar output pulse trains.

## 7 Conclusions

A model has been developed which describes the behaviour of single-integration delta modulation and delta-sigma modulation. It has been shown that delta modulation

is equivalent to a process of time-quantised pulse-phase modulation and delta-sigma modulation is equivalent to a process of time-quantised pulse-frequency modulation. The model can also be inserted in a suitable network so that a double-integration network is obtained.

The most important result of this analysis is that the single-integration delta modulator does not require feedback. Until now, the feedback feature of delta modulation has been considered a fundamental concept of this pulse-modulation technique. As a result, it has been almost impossible to obtain an exact analysis for this process. The properties of the model, however, invalidate this previous assumption, and equally demonstrate that delta modulation can be readily analysed using the well established mathematics of Fourier analysis and sampling. Only when double integration is used is the feedback path essential. Even here, the networks are linear and consequently the same mathematics apply, although the problem is somewhat more complex.

The model does not only have theoretical application. It can provide a practical method of delta modulation. Severe difficulties are encountered in designing conventional delta modulators using clock rates of the order of 100 MHz, which are required for the transmission of television signals. A system using time-quantised angle modulation should be easier to design for these high digit rates.

The model has also been extended to represent pulse-code modulation with uniform quantisation. The p.c.m. signal is generated by sampling the  $\Delta M$  quantised signal at the Nyquist rate, using a zero-order hold circuit.

## 8 Acknowledgments

The financial support of the British Broadcasting Corporation, in the form of a research studentship, together with the continued interest of members of the BBC research staff, is greatly appreciated.

The co-operation of J. Hodgson and D. Arrowsmith in the design and construction of the demonstration model is gratefully acknowledged.

## 9 References

- 1 PANTER, P. F.: 'Modulation, noise and spectral analysis' (McGraw-Hill, 1965)
- 2 DE JAGER, F.: 'Delta modulation, a method of p.c.m. transmission using the 1-unit code', *Philips Res. Rep.*, 1952, 7, p. 442
- 3 INOSE, H. L., and YASUHIKO YASUDA, Y.: 'A unity bit coding method by negative feedback', *Proc. Inst. Elec. Electron. Eng.*, 1963, 51, pp. 1524–1535
- 4 IWERSEN, J. E.: 'Calculated quantisation noise of single integration delta modulation coders', *Bell Syst. Tech. J.*, 1969, 48, pp. 2359–2389
- 5 LAANE, R. R.: 'Measured quantising noise spectrum for single integration delta modulation coders', *ibid.*, 1970, 49, pp. 191–195
- 6 MCKIBBIN, J., and STRADLING, J. B. M.: 'The use of delta modulation in pulse transmission systems', *Inst. Eng. Aust. Elec. Eng. Trans.*, 1970, 6, pp. 35–39
- 7 GOODMAN, D. J.: 'The application of delta modulation to analog-to-p.c.m. encoding', *Bell Syst. Tech. J.*, 1969, 48, pp. 321–343